frontiers | Research Topics

The cycling of biogenic elements and their microbial transformations in marine ecosystems

Edited by
Feng Chen, Junfu Dong and Li Jianlon

Published in
Frontiers in Marine Science

FRONTIERS EBOOK COPYRIGHT STATEMENT

The copyright in the text of individual articles in this ebook is the property of their respective authors or their respective institutions or funders. The copyright in graphics and images within each article may be subject to copyright of other parties. In both cases this is subject to a license granted to Frontiers.

The compilation of articles constituting this ebook is the property of Frontiers.

Each article within this ebook, and the ebook itself, are published under the most recent version of the Creative Commons CC-BY licence. The version current at the date of publication of this ebook is CC-BY 4.0. If the CC-BY licence is updated, the licence granted by Frontiers is automatically updated to the new version.

When exercising any right under the CC-BY licence, Frontiers must be attributed as the original publisher of the article or ebook, as applicable.

Authors have the responsibility of ensuring that any graphics or other materials which are the property of others may be included in the CC-BY licence, but this should be checked before relying on the CC-BY licence to reproduce those materials. Any copyright notices relating to those materials must be complied with.

Copyright and source acknowledgement notices may not be removed and must be displayed in any copy, derivative work or partial copy which includes the elements in question.

All copyright, and all rights therein, are protected by national and international copyright laws. The above represents a summary only. For further information please read Frontiers' Conditions for Website Use and Copyright Statement, and the applicable CC-BY licence.

ISSN 1664-8714
ISBN 978-2-8325-5772-3
DOI 10.3389/978-2-8325-5772-3

About Frontiers

Frontiers is more than just an open access publisher of scholarly articles: it is a pioneering approach to the world of academia, radically improving the way scholarly research is managed. The grand vision of Frontiers is a world where all people have an equal opportunity to seek, share and generate knowledge. Frontiers provides immediate and permanent online open access to all its publications, but this alone is not enough to realize our grand goals.

Frontiers journal series

The Frontiers journal series is a multi-tier and interdisciplinary set of open-access, online journals, promising a paradigm shift from the current review, selection and dissemination processes in academic publishing. All Frontiers journals are driven by researchers for researchers; therefore, they constitute a service to the scholarly community. At the same time, the *Frontiers journal series* operates on a revolutionary invention, the tiered publishing system, initially addressing specific communities of scholars, and gradually climbing up to broader public understanding, thus serving the interests of the lay society, too.

Dedication to quality

Each Frontiers article is a landmark of the highest quality, thanks to genuinely collaborative interactions between authors and review editors, who include some of the world's best academicians. Research must be certified by peers before entering a stream of knowledge that may eventually reach the public - and shape society; therefore, Frontiers only applies the most rigorous and unbiased reviews. Frontiers revolutionizes research publishing by freely delivering the most outstanding research, evaluated with no bias from both the academic and social point of view. By applying the most advanced information technologies, Frontiers is catapulting scholarly publishing into a new generation.

What are Frontiers Research Topics?

Frontiers Research Topics are very popular trademarks of the *Frontiers journals series*: they are collections of at least ten articles, all centered on a particular subject. With their unique mix of varied contributions from Original Research to Review Articles, Frontiers Research Topics unify the most influential researchers, the latest key findings and historical advances in a hot research area.

Find out more on how to host your own Frontiers Research Topic or contribute to one as an author by contacting the Frontiers editorial office: frontiersin.org/about/contact

The cycling of biogenic elements and their microbial transformations in marine ecosystems

Topic editors

Feng Chen — University of Maryland, College Park, United States
Junfu Dong — Shandong University, China
Li Jianlon — Shandong University, China

Citation

Chen, F., Dong, J., Jianlon, L., eds. (2024). *The cycling of biogenic elements and their microbial transformations in marine ecosystems*. Lausanne: Frontiers Media SA. doi: 10.3389/978-2-8325-5772-3

Table of contents

05 Editorial: The cycling of biogenic elements and their microbial transformations in marine ecosystems
Junfu Dong, Fang Wang and Qianying Chen

08 Effects of selective RNA processing and stabilization enzymes on carbon sequestration by photosynthesis of *Synechococcus* sp. PCC7002
Jinyu Chen, Daixi Liu, Yafei Wang, Shaoyu Wang and Ranran Huang

20 Enhanced production of highly methylated brGDGTs linked to anaerobic bacteria from sediments of the Mariana Trench
Zhiyu Zeng, Wenjie Xiao, Fengfeng Zheng, Yufei Chen, Yuanqing Zhu, Jiwei Tian and Chuanlun Zhang

32 Connecting coastal wetland microbial community characteristics with soil physicochemical properties across an estuarine salinity and vegetation gradient in Mobile Bay, AL, USA
Eric A. Weingarten, Carina M. Jung, Fiona H. Crocker, Marissa L. Kneer, Nia R. Hurst, Mark A. Chappell, Jacob F. Berkowitz and Karl J. Indest

51 Blue carbon in sediment from Sanggou Bay: composition, burial flux and its response to human activities
Shu Yang, Qian Yang, Xianli Song, Wei Zhou, Jihua Liu, Xiandong Qi, Junfeng Chen, Jun Huang, Bin Li and Yao Sun

61 Overestimation of microbial community respiration caused by nitrification, and the identification of keystone groups associated with respiration
Lianbao Zhang, Wei Zhou, Yanwei Wang, Yeping Liu, Junfeng Chen, Bin Li, Bei Su and Hui Song

74 Unraveling sources of cyanate in the marine environment: insights from cyanate distributions and production during the photochemical degradation of dissolved organic matter
Rui Wang, Jihua Liu, Yongle Xu, Li Liu and Kenneth Mopper

88 Temporal variations of biological nitrogen fixation and diazotrophic communities associated with artificial seaweed farms
Pengbing Pei, Muhammad Aslam, Chunyou Yang, Peilin Ye, Xiao Ke, Zhanhua Liang, Tangcheng Li, Weizhou Chen and Hong Du

105 Unveiling the eutrophication crisis: 20 years of nutrient development in Zhanjiang Bay, China
Haorui Liang, Junxiao Zhang, Jibiao Zhang, Peng Zhang, Xue Deng, Jiyu Chen, Zhiliang Wang, Chao Long, Chuqian Lu, Di Wang and Yuzhao Liang

121 Characterizing spatio-temporal variations of dimethyl sulfide in the Yellow and East China Sea based on BP neural network
Wen-Ning Guo, Qun Sun, Shuai-Qi Wang and Zhi-Hao Zhang

134 Interspecific differences in ecological stoichiometric characteristics of invertebrates and their influencing factors from the Beibu Gulf, China
Caiguang Wang, Liangliang Huang, Bin Kang, Liang Zhu, Hao Liu, Shuwen Zhao, Yanan Cheng, Asfandyar Shahab and Yunrong Yan

144 Niche differentiation in microorganisms capable of using alternative reduced nitrogen sources studied across depth and between oxic and anoxic ocean regions
Paulina Huanca-Valenzuela, Jacob A. Cram and Clara A. Fuchsman

frontiers | Frontiers in Marine Science

TYPE Editorial
PUBLISHED 26 November 2024
DOI 10.3389/fmars.2024.1514108

Check for updates

OPEN ACCESS

EDITED AND REVIEWED BY
Stelios Katsanevakis,
University of the Aegean, Greece

*CORRESPONDENCE
Junfu Dong
jfdong@sdu.edu.cn

RECEIVED 20 October 2024
ACCEPTED 04 November 2024
PUBLISHED 26 November 2024

CITATION
Dong J, Wang F and Chen Q (2024) Editorial: The cycling of biogenic elements and their microbial transformations in marine ecosystems.
Front. Mar. Sci. 11:1514108.
doi: 10.3389/fmars.2024.1514108

COPYRIGHT
© 2024 Dong, Wang and Chen. This is an open-access article distributed under the terms of the Creative Commons Attribution License (CC BY). The use, distribution or reproduction in other forums is permitted, provided the original author(s) and the copyright owner(s) are credited and that the original publication in this journal is cited, in accordance with accepted academic practice. No use, distribution or reproduction is permitted which does not comply with these terms.

Editorial: The cycling of biogenic elements and their microbial transformations in marine ecosystems

Junfu Dong[1,2]*, Fang Wang[3] and Qianying Chen[3]

[1]School of Life Sciences, Shandong University, Qingdao, Shandong, China, [2]Observation and Research Station of Bohai Strait Eco-Corridor, Ministry of Natural Resources (MNR), Qingdao, China, [3]Institute of Marine Science and Technology, Shandong University, Qingdao, China

KEYWORDS

biogenic elements, microbial community, spatiotemporal distribution, nutrient transformations, biogeochemical processes

Editorial on the Research Topic
The cycling of biogenic elements and their microbial transformations in marine ecosystems

Introduction

The cycling of the major biogenic elements -carbon, nitrogen, and sulfur- has diversified life on Earth. Marine ecosystems, which cover 71% of the Earth's surface, contribute substantially to element cycling. Phytoplankton, zooplankton, and microorganisms are the main forces driving major biogenic element cycling in this ecosystem. In the Anthropocene, global warming, atmospheric sedimentation, eutrophication, ocean acidification, and hypoxia have caused many changes in the cycling. It is therefore of great interest to take a comprehensive look at these changes.

This Research Topic aimed to explore groundbreaking studies on the cycling of biogenic elements and their microbial transformations in marine ecosystems, offering insights into the complex interactions between microbial communities, carbon sequestration, and the biogeochemical processes that shape our oceans. In the Research Topic setup phase, we focused on 1) the impacts of global climate change on the spatiotemporal distribution patterns, migration and transformation processes of marine biogenic elements, 2) the role of microorganisms on the transformations of biogenic elements in marine ecosystems, 3) the responses of microbial communities to global changes in marine ecosystems, and 4) the interactions between biogenic elements and microorganisms facing global climate change that can be efficiently linked to the cycling of biogenic elements and their microbial transformations in marine ecosystems.

The cycling of biogenic elements and their microbial transformations in marine ecosystems

In the marine ecosystem, almost all the energy source ultimately comes from phytoplankton, which is called photosynthesis. Chen et al. explored the post-transcriptional regulatory mechanism of selective RNA processing and stabilization (SRPS) in Synechococcus sp. PCC7002. In this study, the researchers found that the inactivation of SRPS enzymes significantly influences photosynthesis by affecting growth rate, pigment content, and the expression of key protein complex subunits involved in photosynthesis. The second study, by Wang R. et al., focused on the photochemical transformation of marine dissolved organic matter (DOM), particularly phytoplankton-derived DOM, highlighting the role of cyanate as a potential energy and nitrogen source for marine microbes. The third study, by Zeng et al., focused on the microbial transformation of biogenic elements in anaerobic areas. The study contributes to our understanding of the role of microorganisms in the transformation of biogenic elements in marine ecosystems and the implications for paleo-temperature or pH reconstructions. This Research Topic also included a comparison of microbial community respiration (MCR) methods between apparent oxygen utilization (AOU) and electron transport system (ETS) (Zhang et al.). This study indicated that oxygen consumption induced by nitrification causes the overestimation of MCR in the fall when evaluated from AOU. This research underscores the importance of considering the role of key microbial groups in the global carbon cycle. The above studies have focused on carbon transformation, highlighting the pivotal role of photochemistry and microorganisms in the cycling of biogenic elements.

For nitrogen cycling, this Research Topic contained the study by Huanca-Valenzuela et al., which focused on Diazotrophs, bacteria capable of biological nitrogen fixation. This study presented the metabolic versatility of marine microorganisms, using different nitrogen sources (such as urea and nitrate) between oxic and anoxic regions, by employing a multi-faceted approach. Another study, by Pei et al., explored the spatiotemporal distribution patterns of diazotrophic communities on *Gracilariopsis lemaneiformis*, which varied significantly among different cultivation periods and surroundings. This study underscores changes in nitrogenase activity and *nifH* gene abundance, which were influenced by environmental factors such as nutrient availability and temperature.

For sulfur cycling, Guo et al. showed that dimethyl sulfide (DMS) concentrations in the Yellow and East China Seas are positively correlated with Chl-a and sea surface temperature, but negatively correlated with sea surface salinity, highlighting the pivotal role of phytoplankton photosynthesis in sulfur cycling. We appreciate the innovative use of artificial intelligence to address the challenge of data scarcity in marine DMS observations.

Given the importance of microbes, our Research Topic also included their spatiotemporal distribution patterns. Weingarten et al. described the microbial diversity along an estuarine salinity gradient in the Mobile Bay estuary. They discovered that vegetation type, soil horizon, and salinity strongly influence microbial-soil relationships, with forested wetlands displaying distinct microbial biomes compared to other wetland types. Wang C. et al. uncovered the ecological stoichiometry of invertebrates in the Beibu Gulf, revealing significant interspecific differences in their elemental

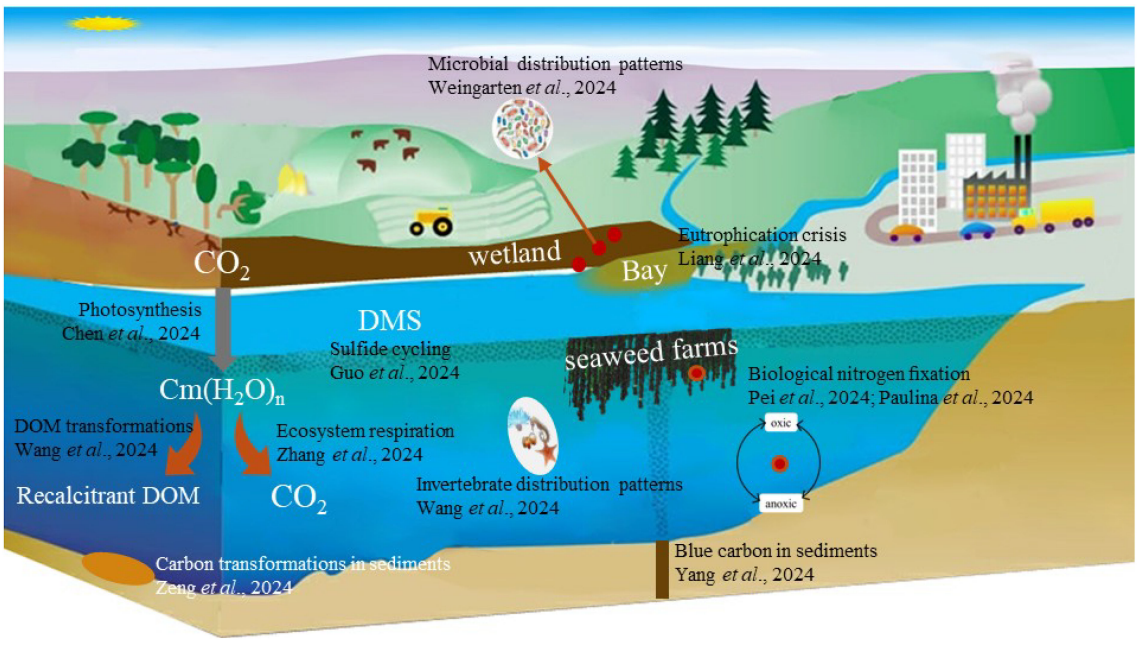

FIGURE 1
The schematic diagram of this Research Topic. DOM, dissolved organic matter; DMS, dimethyl sulfide.

composition and the influence of body size and food sources on these traits, highlighting the role of invertebrates in the biogeochemical cycling of nutrients and the potential impact of environmental changes on their growth and homeostasis.

The health of our oceans and their carbon sink function are the frontiers of marine science. In our Research Topic, Liang et al. provided a comprehensive analysis of nutrient dynamics and eutrophication in Zhanjiang Bay over two decades. Their study identified the main contributors to eutrophication and the impact of hydrodynamics and terrestrial inputs on nutrient concentrations, offering valuable insights for effective environmental management. They highlight the importance of considering local conditions, environmental factors, and ecological stoichiometry in managing and conserving marine ecosystems. The findings presented in this work not only advance our scientific knowledge but also provide a foundation for developing strategies to mitigate the impacts of eutrophication and promote the sustainable use of marine resources. Yang et al. investigated the composition of blue carbon in the sediments of a special type of marginal sea. The research reveals that sea-sourced carbon accounts for approximately 23% of the total carbon content in the sediments. The study also examined long-term changes in the blue carbon burial fluxes, which have been significantly affected by human aquaculture activities.

Perspectives

We thank all the researchers who have contributed and devoted their attention to this Research Topic. This Research Topic underscores the importance of cycling biogenic elements in the construction of the marine ecosystem, in addition to their biogeochemical transformations (Figure 1). However, further research is needed to address: 1) the multi-level responses of biogenic element cycling to global changes and anthropogenic disturbances, ranging from molecular to ecosystem scales; 2) long-term, continuous monitoring of biogenic element cycling in representative regions; 3) systemic biogeochemical processes in biogenic element cycling; 4) evaluation criteria for marine carbon sinks integrated with model forecasting; and 5) multi-omics and multidisciplinary approaches in the age of artificial intelligence (AI). All of the above are the innovative research being conducted in the field and serve as a foundation for future studies aimed at unraveling the mysteries of our oceans.

Author contributions

JD: Writing – original draft, Writing – review & editing. FW: Writing – review & editing. QC: Writing – review & editing.

Funding

The author(s) declare that financial support was received for the research, authorship, and/or publication of this article. This work was supported by the Ocean Negative Carbon Emissions (ONCE) Program, the National Natural Science Foundation of China (32101298), and the opening foundation of the Observation and Research Station of Bohai Strait Eco-Corridor, MNR, grant No. BH202305.

Conflict of interest

The authors declare that the research was conducted in the absence of any commercial or financial relationships that could be construed as a potential conflict of interest.

Publisher's note

All claims expressed in this article are solely those of the authors and do not necessarily represent those of their affiliated organizations, or those of the publisher, the editors and the reviewers. Any product that may be evaluated in this article, or claim that may be made by its manufacturer, is not guaranteed or endorsed by the publisher.

frontiers | Frontiers in Marine Science

TYPE Original Research
PUBLISHED 03 July 2023
DOI 10.3389/fmars.2023.1223060

Check for updates

OPEN ACCESS

EDITED BY
Junfu Dong,
College of Life Sciences, Shandong University, China

REVIEWED BY
Jianhua Fan,
East China University of Science and Technology, China
Yi Xin,
Hainan University, China

*CORRESPONDENCE
Ranran Huang
huangrr@sdu.edu.cn

RECEIVED 16 May 2023
ACCEPTED 14 June 2023
PUBLISHED 03 July 2023

CITATION
Chen J, Liu D, Wang Y, Wang S and Huang R (2023) Effects of selective RNA processing and stabilization enzymes on carbon sequestration by photosynthesis of *Synechococcus* sp. PCC7002. *Front. Mar. Sci.* 10:1223060. doi: 10.3389/fmars.2023.1223060

COPYRIGHT
© 2023 Chen, Liu, Wang, Wang and Huang. This is an open-access article distributed under the terms of the Creative Commons Attribution License (CC BY). The use, distribution or reproduction in other forums is permitted, provided the original author(s) and the copyright owner(s) are credited and that the original publication in this journal is cited, in accordance with accepted academic practice. No use, distribution or reproduction is permitted which does not comply with these terms.

Effects of selective RNA processing and stabilization enzymes on carbon sequestration by photosynthesis of *Synechococcus* sp. PCC7002

Jinyu Chen[1], Daixi Liu[2], Yafei Wang[1], Shaoyu Wang[1] and Ranran Huang[1]*

[1]Institute of Marine Science and Technology, Shandong University, Qingdao, China, [2]School of Pharmaceutical Sciences, Shandong University, Jinan, China

Synechococcus is one of the most abundant prokaryotic photosynthetic organisms on Earth and plays a key role in oceanic carbon fixation and transformation. To improve the photosynthetic efficiency of *synechococcus*, a post-transcriptional regulatory mechanism - Selective RNA Processing and Stabilization (SRPS) was considered. We inactivated the SRPS-enzymes, executor of the SRPS mechanism, to explore their regulation rule of photosynthetic carbon fixation efficiency in *Synechococcus*. The results showed that the inactivation of SRPS-enzymes mainly affected the growth rate or growth phase. It significantly alters the photosynthetic oxygen evolution rate, pigment content, chlorophyll fluorescence, carbon and nitrogen content, as well as the composition and biological activity of the dissolved organic matter derived from *Synechococcus* (SOM). Inactivating SRPS-enzymes results in an increase in the expression level of most subunits of the Cytochrome b6-f complex, while the expression levels of most subunits of PSI, PSII, RuBisCO, and NDH decrease. All SRPS-enzymes are involved in the expression regulation of basilic protein complexes in photosynthesis, such as PSI, PSII, Cytochrome b6-f complex, ATP synthase, and RuBisCO. Our results indicate that the inactivation of SRPS-enzymes have a significant influence on carbon sequestration by photosynthesis of *Synechococcus* sp. PCC7002.

KEYWORDS

***Synechococcus* sp. PCC 7002, selective RNA processing and stabilization (SRPS), photosynthetic carbon fixation, dissolved organic matter derived from *Synechococcus* (SOM), splice site**

1 Introduction

Excessive emissions of greenhouse gases have increased the atmosphere's ability to trap heat, resulting in a strengthening of the greenhouse effect and adverse changes to global climate. CO_2 is the most significant component of greenhouse gases, with concentrations in the atmosphere surpassing 400 ppm and emissions continuing to break records. To address climate issues and achieve carbon peaking and carbon neutrality, there is a need to increase efforts to reduce and store carbon. Part of the CO_2 generated by human activity remains in the atmosphere, while another portion is absorbed by the ocean and terrestrial ecosystems. The majority of the absorbed CO_2 enters the carbon cycle through autotrophic and heterotrophic processes.

The total area of the ocean accounts for about 70.8% of the Earth's surface area, and it is the foundation of all life. It absorbs approximately 1/4 of the CO_2 generated by human activities (Le Quéré et al., 2018). The ocean stores carbon through mechanisms such as the biological pump (BP), carbonate counter pump (CCP), microbial carbon pump (MCP), and solubility pump (Li et al., 2022), and the stored forms of carbon mainly include carbonate ions (eg, dissolved inorganic carbon, DIC), dissolved organic carbon (DOC), particulate organic carbon (POC), and biogenic organic carbon (BOC) (Jiao et al., 2014). More than 95% of the organic matter in the ocean exists in dissolved form, known as dissolved organic matter (DOM), and the carbon storage of ocean DOM accounts for about 93% of the total carbon on Earth (Swallow, 1963). It plays an important regulatory role in global climate change and CO_2 concentration changes, and is an important part of the carbon cycle on Earth and the world's largest carbon sink. DOC is a component of DOM, and the inert dissolved organic carbon (RDOC) pool accounts for more than 90% of the total DOC storage, making the CO_2 equivalent absorbed by marine and terrestrial ecosystems similar (Häder et al., 2007).

In the ocean, phytoplankton absorb DIC through photosynthesis and convert it into organic matter within their cells (Geider and La Roche, 2002). DOM is then released through active excretion, passive diffusion, or cell lysis and is transferred up the food chain in the form of POC. Ultimately, this POC is exported to the deep sea and plays a crucial role in the ocean's biological carbon sequestration/storage function (Falkowski, 2012). Marine microalgae, which are important representatives of phytoplankton, form the basis of the BP that sequesters carbon. Compared to land-based photosynthetic organisms, microalgae have a fast cell reproduction rate and high biomass production, with less than 1% of the biomass of land-based photosynthetic organisms being able to fix half of the annual CO_2 emissions into organic matter. In summary, marine microalgae can use CO_2 as a carbon source and convert it into organic matter through photosynthesis using sunlight as an energy source (Ibrahim et al., 2020), thus aiding in carbon sequestration.

Photosynthesis is the unique and important characteristic of autotrophic organisms that use light as their energy source. Cyanobacteria are the most abundant group of photosynthetic microorganisms on Earth (Hoover et al., 2005), with a simple structure and a cell wall structure and composition similar to Gram-negative bacteria. However, they have photosynthetic units similar to eukaryotic chloroplast (Carr and Whitton, 1982), which are almost directly or indirectly affected by photosynthesis. The cytoplasm contains carboxysomes and genetic material, the former is an organelle formed by polyhedral proteins to contain RuBisCO and participate in efficient carbon concentrating mechanism (CCM), which enrich CO_2 around RuBisCO and thus increase the photosynthetic carbon fixation efficiency of cyanobacteria (Ducat et al., 2011; Durall and Lindblad, 2015). Photosynthesis is achieved through the participation of two photosynthetic systems (Photosystem I, PS I; Photosystem II, PS II), using light energy to convert inorganic matter such as CO_2 and water into organic matter while producing oxygen. Key players in this process include PS I, PS II, the Cytochrome b6-f complex, ATP synthase, RuBisCO, and NADH dehydrogenase.

The PSII is a photosynthetic membrane protein that functions as the primary reaction center in light reactions. It consists of: (1) Core antenna proteins: A core antenna protein composed of two pigment protein complexes, chlorophyll protein 47 (CP_{47}) and chlorophyll protein 43 (CP_{43}), which surround P680 chlorophyll. These complexes are encoded by the *psbB* and *psbC*. (2) Light harvesting pigment protein complex II (LHCII): A complex of light-harvesting pigment proteins known as LHCII. (3) PSII reaction center: composed of D_1 and D_2 proteins (encoded by the *psbA* and *psbD*) and cytochrome b559. This reaction center is responsible for receiving light energy and facilitating electron transfer (Barber et al., 1997). (4) Oxygen-evolving complex peripheral proteins (Buchanan et al., 2015).

The Cytochrome b6-f complex is composed of 8 subunits, 13 transmembrane helices, and 7 tightly bound cofactors per monomer. Among these cofactors, three are involved in electron transfer: cytochrome f (Cyt f): encoded by the *petA*. 2Fe-2S iron-sulfur protein. Cytochrome b6 (CytB6): encoded by the *petB*. The presence of the cytochrome b6-f complex allows for the transfer of electrons between reduced plastoquinone (PQ) and oxidized plastocyanin (PC) (Wollman et al., 1999).

PSI is a pigment-protein complex that consists of the primary electron donor P700, primary electron acceptors A0 and A1, and three iron-sulfur proteins (ferredoxins, Fd) encoded by the *psaA*, *psaB*, and *psaC*. It catalyzes the transfer of electrons through a series of electron carriers, including PC (plastocyanin), from the cytochrome b6-f complex to Fd, ultimately leading to the generation of NADPH, which provides reducing power for the subsequent dark reactions. Simultaneously, the oxidized form of P700 (P700+) receives electrons from the cytochrome b6-f complex and PC, completing the electron flow between PSII and PSI.

ATP synthase is involved in both cellular respiration and cellular photosynthesis. It is composed of a membrane-embedded hydrophobic portion called CF0 and a membrane-exposed hydrophilic portion called CF1. CF1 is responsible for driving the phosphorylation of ADP to ATP. It contains two crucial subunits, CF1-α and CF1-β, which are encoded by the *atpA* and *atpB*, respectively.

Cyanobacteria, perform a process called photophosphorylation, where they utilize light energy to synthesize ATP through photosynthesis. The respiratory chain in cyanobacteria consists of

four enzyme complexes and two mobile electron carriers. The final enzyme complex in this chain is the cytochromeC oxidase complex (COX), which is responsible for transferring electrons from cytochrome C to molecular oxygen. The COX complex is composed of multiple subunits, including ndhA, ndhB, ndhC, ndhD, ndhD1, ndhD2, and ndhE, among others.

In prokaryotes, genes encoding translation protein complexes and related functions are often organized in the form of operons (Koonin, 2009). When encoding protein complexes in operon form, a certain proportion of protein subunits are expressed, but there is a conflict between the equimolar transcription abundance required for each gene in the protein complex under the operon structure and the non-equimolar protein abundance required for functional performance. Selective RNA processing and stabilization (SRPS) (Rochat et al., 2013), a post-transcriptional regulatory mechanism in prokaryotes, can solve this conflict. Previously, our laboratory has depicted the stoichiometric regulatory model of SRPS in *Escherichia coli*. The effectiveness of several SRPS elements was validated by using a dual-fluorescence reporter system. At the same time, analysis of published dRNA-seq data from pure-cultured marine microbes revealed that multiple operons may be potentially regulated by SRPS. Taking the *Prochlorococcus* marinus strMIT9313 (Voigt et al., 2014) as an example, a total of 32 protein complexes were found to be regulated by SRPS, including photosystems, plastocyanin, and photoinhibitory proteins, providing a strong signal that SRPS is widely present in known cultured marine microbes.

Given the important role of *Synechococcus* in marine biogeochemical cycles and synthetic biology, this study focuses on the SRPS enzyme (Table S1) from the model *Synechococcus* sp. PCC7002 (hereinafter referred to as PCC7002) to explore how it affects the growth rate, chlorophyll fluorescence, carbon and nitrogen decomposition, and expression of key protein complex subunits involved in photosynthesis (Table S2) through a series of pure-culture experiments after inactivating SRPS-enzymes.

2 Materials and methods

2.1 Strains and culture conditions

Single colony was picked from the ultra-clean bench and inoculated into a small conical flask containing fresh culture medium that had been preheated at 450°C in a muffle furnace for 5 hours to remove carbon. Kanamycin (Kan) antibiotic was added as required, with a final concentration of 50 μg mL^{-1}. The cultivation conditions were set at an average light intensity of 200 μmol m^{-2} s^{-1}, a temperature of 30°C, and a rotational speed of 200 rpm. The culture was shaken on a shaker for approximately three weeks until it reached the exponential phase with an OD_{730} of 4 ± 0.2, and then it was used as the seed liquid. The initial inoculum concentration was OD_{730} = 0.05. The seed liquid was transferred to sterile centrifuge tubes and centrifuged at 4000 rpm for 20 minutes to collect the algal cells. The cells were then resuspended in fresh A+ liquid medium (Sevens and Porter, 1980) and inoculated into conical flasks that had been preheated at 450°C in a muffle furnace for 5 hours to remove carbon. Each mutant strain was supplemented with a fixed amount of kanamycin (50 μg mL^{-1}).

2.2 Construction of PCC7002 mutants

The plasmid pJET1.2/blunt and the *kanamycin* fragment were kindly provided by a senior colleague in the laboratory. The gene fragment of SRPS-enzymes was obtained by PCR using the extracted PCC7002 genomic DNA as a template. Fragments of 1000 bp upstream and downstream of the gene segment of SRPS-enzymes in PCC7002 were selected and copied into the Snap Gene software. The target gene segment and regions suitable for primer design were marked. Using Snap Gene software, the SRPS-enzymes gene segment was replaced with the *kanamycin* segment. Then, it was combined with the pJET1.2/blunt vector, and suitable primers (Table S4) were designed for the connecting region. Obtaining gene fragments through PCR and plasmid reconstruction. When the OD_{730} of WT reaches around 5.0, 5 mL of algal culture is collected and centrifuged at 4000 rpm for 10 minutes. Then, 1 mL of fresh culture medium is added and concentrated fivefold. The mixture is combined with 300 ng of plasmid, sealed with a membrane and tightly closed with a lid. It is then placed in a conical flask on a light shaker and cultured for 24 hours. The next day, a sterile microporous membrane is placed on A+ solid medium without kanamycin (Kan). Spread 200 μL of a ten-fold diluted culture evenly on the microporous membrane and incubate for 48 hours. Transfer the microporous membrane to A+ solid medium containing kanamycin (50 μg mL^{-1}). Keep it in a light incubator for approximately two weeks, and single colonies will start to appear. Verify through PCR and send the products of PCR for sequencing.

2.3 Growth curve determination

The cell density in the culture of PCC7002 was monitored by a UV-visible spectrophotometer (UV-1800, Shimadzu, Japan). 1 mL of culture was taken from all culture bottles and the OD_{730} (Perez et al., 2016) was measured. The growth curve was determined by pre-experiments and recorded. μ_{max} was calculated by equation (Mou et al., 2018):

$$\mu_{max} = [LN(OD_{730t}) - LN(OD_{730t_0})] / (t - t_0)$$

Where OD_{730t} and OD_{730to} are the cell densities at time t and t_0, respectively.

2.4 Photosynthetic oxygen evolution rate determination

2 mL of algal solution was taken from exponential stage (OD730 = 4.0 ± 0.2) and dark-treated for 30 min. During the experiment, the light intensity was set to 0, 50, 100, 200, 400, and 600 μmol m^{-2} s^{-1}, with corresponding processing times were 3, 2, 2, 2, 2, and 2 min, respectively. The change in oxygen concentration during the light-dark period was observed, and a section with a

stable slope (around 1 min) was selected to obtain the oxygen evolution rate.

2.5 Measurement of pigment content

2 mL of algal culture was taken from lag phase (OD_{730} = 0.5 ± 0.2), exponential phase (OD_{730} = 4.0 ± 0.2), and decline phase (OD_{730} = 10.0 ± 0.2), which were collected by GF/F filter membranes (Whatman, diameter 25 mm). Then, 5 mL of 90% (v/v) acetone solution prepared with Milli-Q water was added, and the mixture was thoroughly mixed and immediately stored in the dark at 4°C for 12 h to extract the pigments. The next day, the sample was centrifuged at 4000 rpm for 10 min, and the supernatant was carefully pipetted into a quartz cuvette with a path length of 1 cm. The pigment content was determined by using 90% acetone solution as a blank reference and conducting baseline calibration. The mass concentrations of Chlα and Car were calculated using the Jeffrey spectrophotometric method (Parsons et al., 1984) based on Equations:

$$[\mathbf{Chl\alpha}] = [\mathbf{11.85\times(A664-A750)-1.54\times(A647-A750)-0.08\times(A630-A750)}]$$

$$[\mathbf{Car}] = [\mathbf{7.6\times(A480-A750)-1.49\times(A510-A750)}]$$

Where unit is μg mL^{-1}, A_{480}, A_{510}, A_{630}, A_{647}, A_{664}, and A_{750} represent the absorbance at 480, 510, 652, 665, and 750 nm, respectively.

2.6 Chlorophyll fluorescence measurement

2 mL of algal solution from each sample was taken at the exponential phase, and the algae were dark-treated for 30 min so that the fluorescence yield was at its lowest. The samples were then exposed to a series of light intensities of 0, 36, 82, 142, 220, 321, 452, 622, and 843 μmol m^{-2} s^{-1} for 18 s, 63 s, 152 s, 197 s, 242 s, 302 s, 391 s, 481 s, and 571 s, respectively, and rapid light curves (RLC) were measured. Using the method of Demmig-Adams (Demmig-Adams and Adams, 1994) and the formula (Webb et al., 1974) Y=Pm*[1-exp(-x/E_k)], a series of parameters including rETR, Ek, α and Fv/F_M (Genty et al., 1989) were determined by fitting the RLC. To ensure the accuracy of the data, the OD_{730} of the algae should be controlled at ≤ 2, and if necessary, all samples should be diluted proportionally with medium A+.

2.7 Carbon and nitrogen contents measurement

For carbon and nitrogen content measurement, GF/F filter membranes were used to filter the sample and then left in concentrated hydrochloric acid for 12 hours to remove inorganic carbon in the sample. Then, the sample was dried at 60°C for 24 hours, weighed, wrapped in cut tinfoil (burned at 450°C in a Muffle furnace for 5 hours), and the POC and PON content of algal cells were measured using an elemental analyzer (EA3000, ECA classic, NC Tecnologes, Italy).

2.8 DOM absorption and fluorescence measurements

Collect 5 mL of algal liquid at lag phase, exponential phase, and decline phase in a brown bottle. Dilute the collected algal liquid and filter it using a glass fiber filter membrane (Martínez-Pérez et al., 2017) under vacuum filtration (pressure< 0.04 MPa) into a new brown bottle. The dilution factor is 18-fold, and store it at -20°C.

Use Milli-Q water as a blank reference and place it in the sample compartment to perform the zero and baseline initialization operations. The default excitation (Ex) and emission (Em) slit widths are set to 1.0 nm, and the scanning range is set from 250 to 700 nm. Take a small amount of the test sample and rinse it twice in a quartz cuvette with an optical path length of 1 cm. After discarding the rinse solution, add the sample for measurement (each sample is measured three times, and the average value is taken). By peak detection and calculation, roughly compare the peak data present in all samples, and correct using the average absorbance coefficient between 575 and 600 nm. The formula for calculating the absorption coefficient of CDOM is as follows (Bricaud et al., 1981):

$$\mathbf{aCDOM(\lambda) = 2.303 \star ACDOM(\lambda) / L}$$

In the formulas provided, λ represents the actual wavelength, aCDOM(λ) and ACDOM(λ) represent the CDOM absorption coefficient and sample optical density at the wavelength λ, respectively. L represents the optical path length, and the unit is unified as meters (m). The value of the absorption coefficient is influenced by the dilution factor of the sample. In this study, the final calculated result needs to be multiplied by the dilution factor of the sample, which is 18. The spectral slope (S) is obtained by fitting a nonlinear least squares program within the ranges of 275 to 295 nm ($S_{275-295}$) and 350 to 400 nm ($S_{350-400}$). The formula (Blough, 2002) for calculating the spectral slope is as follows:

$$\mathbf{aCDOM(\lambda) = aCDOM(\lambda 0)exp[S((\lambda 0-\lambda))]}$$

where λ_0 is a reference wavelength.

The instrument is equipped with a 150 W xenon lamp, and the photomultiplier tube voltage is set to 600 V. The excitation and emission slit widths are both set to 10 nm. The excitation wavelength is set to 250-550 nm, and the emission wavelength is set to 250-600 nm. The scanning speed is set to 1200 nm min^{-1}. The data is processed using the drEEM 0.6.3 toolbox in MATLAB 2021a, utilizing the PARAFAC method for component analysis (Murphy et al., 2013). The dilution procedure of the samples includes the corresponding toolbox processing. Prior to analysis, the Raman correction program in the drEEM toolbox is used to remove the fluorescence data corresponding to Rayleigh scattering and Raman scattering. All fluorescence data is expressed in Raman Units (RU) for the calculation of HIX (Ohno, 2002) and BIX (Huguet et al., 2009).

2.9 Quantitative real-time PCR

10mL of algae cells were collected in the exponential phase and quickly frozen in liquid nitrogen. Grind the cells and use Trizol to rupture the cells. Use the EZ-10 Total RNA Mini-Preps Kit to obtain high-quality RNA. Measure the concentration of RNA using Nanodrop and Qubit 4 instruments (Thermo Fisher) and check the integrity of the extracted RNA. The Prime ScriptTM RT reagent Kit with gDNA Eraser (TaKaRa, China) was used to remove genomic DNA, and the SYBR® Premix Ex Taq™ II kit (TaKaRa, China) was used for reverse transcription and cDNA synthesis.

2.10 Data analysis

All data were derived from three biological duplicate samples from the same batch in the same growing environment. Two-way ANOVA was used to compare the significant differences between samples, and Pearson correlation coefficients were used to characterize the correlations between different indicators. The mean and standard deviation were partially displayed, and the significance level was set to $p \leq 0.05$.

3 Results

3.1 Effects of SRPS-enzymes on the growth

3.1.1 Growth curve

The mutant strains PCC7002Δ*rnj* and PCC7002Δ*III-2,3*, showed a delay of about 2 days in the lag phase compared to the wild-type (WT) (Figure 1). It was predicted that the inactivation of SRPS-enzymes caused changes in part of the metabolic pathway, which is not conducive for algae cells to adapt to the environment and slows down cell division. These three mutant strains showed similar growth trends in exponential and stable phases, all of which

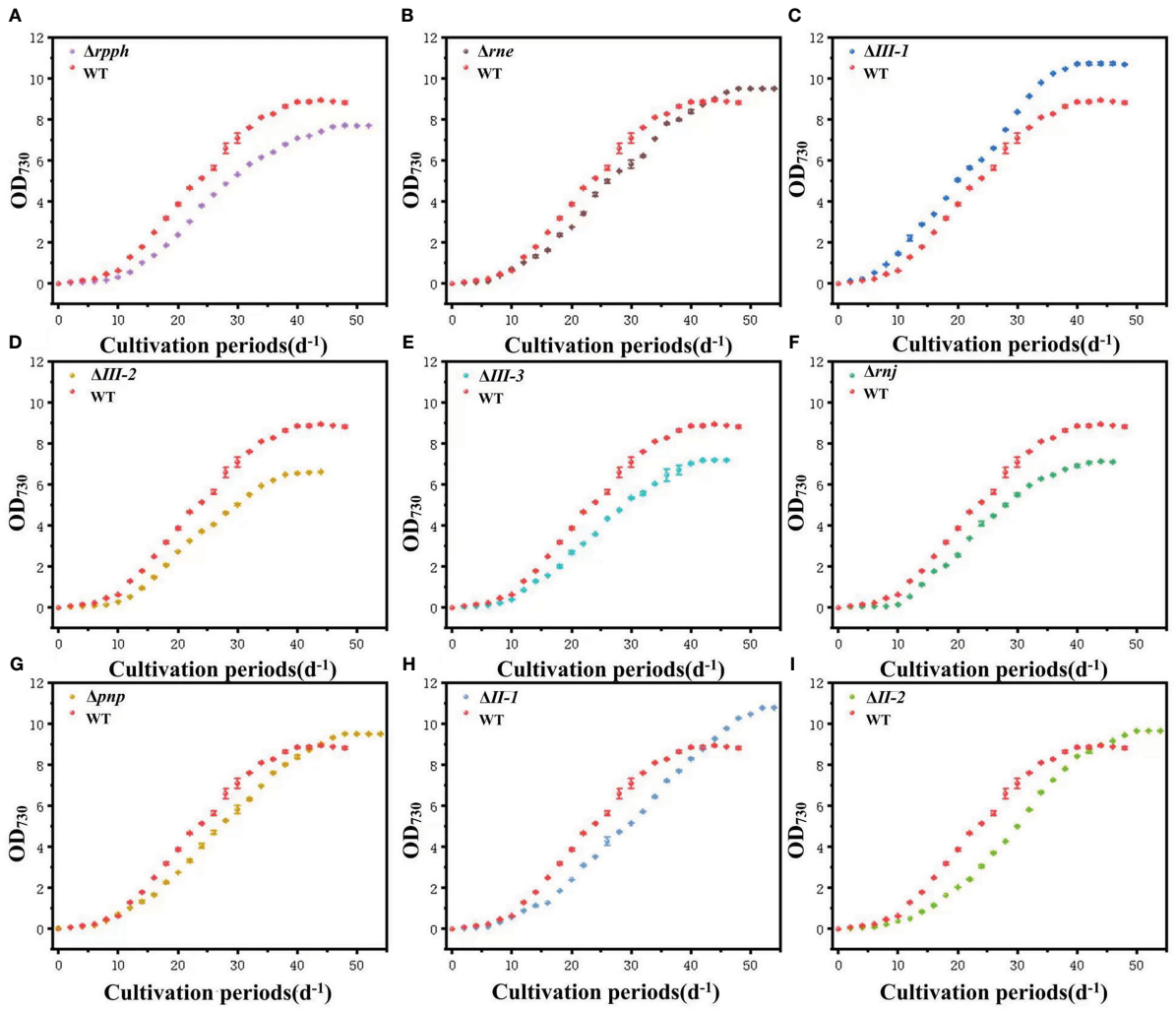

FIGURE 1
Changes of cell density of SRPS-enzymes mutants in PCC7002 relative to WT. **(A)** PCC7002Δ*rpph*; **(B)** PCC7002Δ*rne*; **(C)** PCC7002Δ*III-1*; **(D)** PCC7002Δ*III-2*; **(E)** PCC7002Δ*III-3*; **(F)** PCC7002Δ*rnj*; **(G)** PCC7002Δ*pnp*; **(H)** PCC7002Δ*II-1*; **(I)** PCC7002Δ*II-2*.

were significantly lower than those of WT. After the mutation of SRPS-enzymes expression gene, the growth curve in the exponential phase was more gentle than that of WT. WT reached the growth peak after being cultured for 44 days and the final OD_{730} was 8.83 ± 0.05. The cumulative cell density reached the maximum, and the number of algae cells began to decrease after 46 days, entering the decline phase. PCC7002Δ*rnj* and PCC7002Δ*III-2,3* entered the stable phase at day 40, and the final OD_{730} was 7.11 ± 0.02, 6.63 ± 0.01, and 7.19 ± 0.12, respectively, which were significantly lower than that of WT (paired test, P< 0.05). PCC7002Δ*III-1* was the only strain that outperforms WT throughout the entire growth stage. The duration of the three phases was similar to that of WT, but the final OD_{730} was 10.69 ± 0.23, which was 21% higher than that of WT. RppH was speculated to have pyrophosphohy drolase activity. The lag phase of PCC7002Δ*rpph* mutant strain was delayed by about 2 days compared to WT, and the growth state throughout the exponential phase was also relatively smooth. The time to enter the decline phase was delayed by 6 days compared to WT, but the duration was shortened by almost half.

As shown in Figure 1, mutants of the endonuclease RNaseE and the exonucleases RNaseII and PNPase showed similar growth trends, with no significant difference in growth rates during the lag phase compared to WT, except for a significantly shortened delay period in PCC7002Δ*II-2*. After entering the exponential phase, the growth rate of PCC7002Δ*II-1* was relatively stable and close to that of WT, while the growth curve of PCC7002Δ*II-2* showed a dramatic increase in the middle of the exponential phase, with a growth rate significantly higher than that of WT, followed by a slowdown in the late stage. It was speculated that the inactivation of RNaseII-2 reduces the efficiency of assembly of the protein complex involved in photosynthesis, which slows down or temporarily blocks the transfer rate of products (such as electrons, H^+ and ATP) between continuous biochemical reactions. When the accumulation of substrate was sufficient, efficient photosynthesis occurs, thus increasing the growth rate. After the substrate was exhausted, the growth rate slows down. When the substrates were consumed, the growth rate slows down. The duration of the exponential phase of the four mutant strains was extended by about 8 days, and the final OD_{730} of the three mutant strains except PCC7002Δ*II-1* was about 9.52, significantly different from that of WT (Paired test, P< 0.05).

3.2 Chlorophyll fluorescence

3.2.1 Relative electron transfer rate (rETR)

rETR of PSII varied with the change of light intensity during the exponential phase (Figure 2). In the measurement range of 0-600 μmol m^{-2} s^{-1}, compared with WT, the variation trend of rETR and photosynthetic oxygen evolution rate was basically consistent in PCC7002Δ*rnj*, PCC7002Δ*rpph*, PCC7002Δ*II-2*, PCC7002Δ*III-2,3*, and PCC7002Δ*pnp*. However, in PCC7002Δ*III-1* and PCC7002Δ*II-1*, this change was completely opposite. At the same time, PSII of algal cells has strong regulatory ability to weak light because when the light intensity was less than or equal to 100 μmol m^{-2} s^{-1}, most photosynthetic electron gates were in an open state, and rETR increases rapidly with the change of light intensity. However, rETR in PCC7002Δ*rne* and PCC7002Δ*pnp* does not change or decrease under weak light conditions. These data once again prove that inactivating SRPS-enzymes may affect the overall expression of carbon assimilation process-related protein complexes in the photosynthetic system, thereby cutting off the connection between the light reaction and the dark reaction.

3.2.2 Light saturation point (E_K)

E_K is an important manifestation of algal cell photosynthetic capacity. Its numerical value reflects the maximum demand for assimilation force of carbon assimilation process-related protein complexes in the photosynthetic system. The stronger the carbon assimilation capacity, the more assimilation force is needed, and the higher the light saturation point is (Yang and Zou, 2005). Meanwhile, a larger E_K value corresponds to stronger resistance of algal cells to strong light, indicating broad adaptability to light intensity. The E_K value of WT was 208.63 ± 1.36 μmol $m^{-2}s^{-1}$. Except for PCC7002Δ*III-1* (226.27 ± 2.01 μmol $m^{-2}s^{-1}$) and PCC7002Δ*rne* (183.22 ± 0.92 μmol $m^{-2}s^{-1}$) (Figure 3A), the E_K values were consistent with the photosynthetic oxygen evolution rate (Figure S3), PCC7002Δ*II-2* (219.77 ± 1.13 μmol $m^{-2}s^{-1}$) > WT > PCC7002Δ*rpph* (180.97 ± 1.13 μmol $m^{-2}s^{-1}$) > PCC7002Δ*II-1* (179.91 ± 0.51 μmol $m^{-2}s^{-1}$) > PCC7002Δ*rnj* (159.73 ± 1.68 μmol $m^{-2}s^{-1}$) > PCC7002Δ*III-3* (153.43 ± 1.37 μmol $m^{-2}s^{-1}$) > PCC7002Δ*III-3* (140.51 ± 2.73μmol $m^{-2}s^{-1}$) > PCC7002Δ*pnp* (64.67 ± 1.71 μmol $m^{-2}s^{-1}$).

3.2.3 Efficiency of electron transport (α)

The α represents the rate at which algae cells transfer electrons down the electron transport chain under actual light intensity, and its numerical value reflects the light tolerance and adaptability of algal cells (Figure 3B) (YE and Zhao, 2009). Therefore, the efficiency of photosynthetic electron transfer was consistent with the efficiency of photosynthesis of algal cells. The α of PCC7002Δ*II-2* and PCC7002Δ*III-1* was significantly improved compared to WT (Figures 2, 3, S4).PCC7002Δ*rpph* (0.0999 ± 0.0022) and PCC7002Δ*rne* (0.1479 ± 0.0305) were significantly lower than WT (Paired test, P.< 0.05), which was consistent with rETR and photosynthetic oxygen evolution rate (Figure S4).

3.2.4 Maximum photochemical efficiency of photosystem II (Fv/F_M)

F_V/F_M, reflecting the photosynthetic yield of PS II. By analyzing the F_V/F_M of different SRPS-enzymes mutant strains in three different periods (Figure 4), it can be found that the inactivation of the exonuclease RNaseII-1 has the greatest impact on F_V/F_M in algal cells, especially during the exponential phase, which should increase the values of PCC7002Δ*II-1* in terms of photosynthetic oxygen evolution rate, α, and even growth rate. However, all results were contrary to expectations (Figures 2, S1, S4).

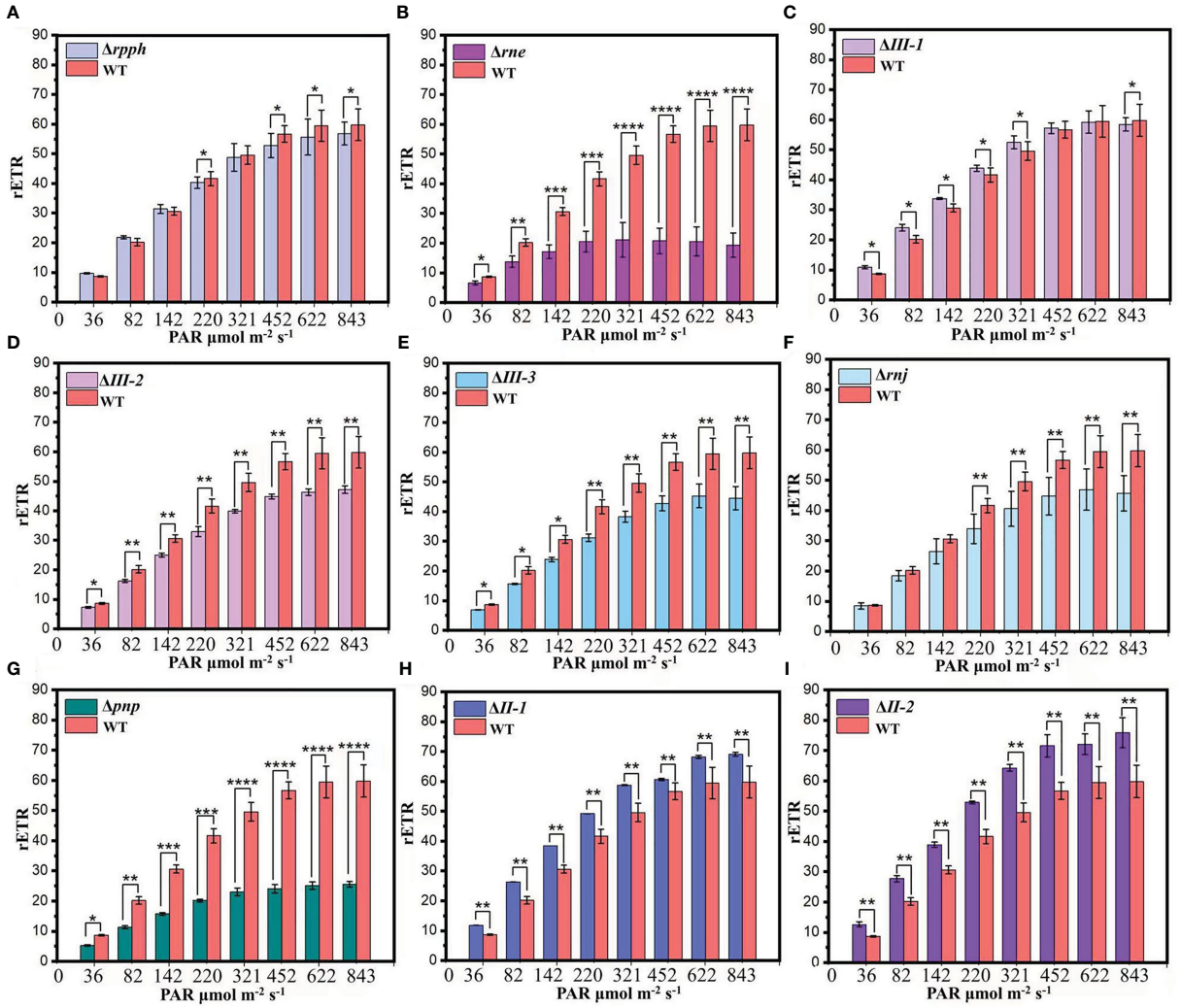

FIGURE 2
rETR in SRPS-enzymes mutants and WT at the exponential phase. **(A)** PCC7002Δ*rpph*; **(B)** PCC7002Δ*rne*; **(C)** PCC7002Δ*III-1*; **(D)** PCC7002Δ*III-2*; **(E)** PCC7002Δ*III-3*; **(F)** PCC7002Δ*rnj*; **(G)** PCC7002Δ*pnp*; **(H)** PCC7002Δ*II-1*; **(I)** PCC7002Δ*II-2*. *, p< 0.05 (two-way ANOVA); **, p< 0.01 (two-way ANOVA); ***, p< 0.001 (two-way ANOVA); ****, p< 0.0001 (two-way ANOVA).

3.3 Carbon and nitrogen content

3.3.1 Carbon content

Knockout of the endonuclease RNase III-1 and the exonuclease RNase II-1 significantly increased POC (Figure 5A). Compared to WT ($6.04 \times 10^4 \pm 286$ μmol L^{-1}), PCC7002Δ*III-1* and PCC7002ΔII-1 exhibited POC degradation of $8.83 \times 10^4 \pm 686$ μmol L^{-1} and $7.08 \times 10^4 \pm 294$ μmol L^{-1}, respectively, representing a 46% and 17% increase. Among the other five mutants excluding PCC7002Δrne, POC showed varying degrees of reduction compared to WT, particularly PCC7002Δ*III-2*, which decreased by 17% to $5.03 \times 10^4 \pm 1254$ μmol L^{-1}. These results are consistent with the μ_{max} values shown in Supplementary Figure 1. In PCC7002Δ*rne*, there is no correlation observed between POC and several common chlorophyll fluorescence parameters. This provides further validation for the hypothesis regarding the regulation of photosynthetic protein complex expression by the SRPS-enzymes.

3.3.2 Nitrogen content

Nitrogen is an important macroelement for the growth and primary production of marine phytoplankton. Limitation or deficiency of nitrogen can affect the growth and intracellular physiological metabolism of phytoplankton (Ying and Weiwei, 2020). Regarding PON (Figures 5B, C), the majority of enzyme knockouts have a promoting effect on PON compared to WT, although the magnitude of the changes is not significant. For example, the most significant increase in PON degradation is observed in PCC7002Δ*rnj* ($2.61 \times 10^4 \pm 1486$ μmol L^{-1}), which is only a 21% increase compared to WT ($1.18 \times 10^4 \pm 49$ μmol L^{-1}). Conversely, the most pronounced inhibition is seen in PCC7002Δ*III-3* ($0.98 \times 10^4 \pm 79$ μmol L^{-1}), resulting in a 17% decrease. In cyanobacterial cells, nitrogen assimilation metabolism is connected to photosynthetic carbon metabolism through 2-oxoglutarate (2-OG), which serves as a central node in the TCA cycle (Muro-Pastor et al., 2005). Therefore, the differential changes

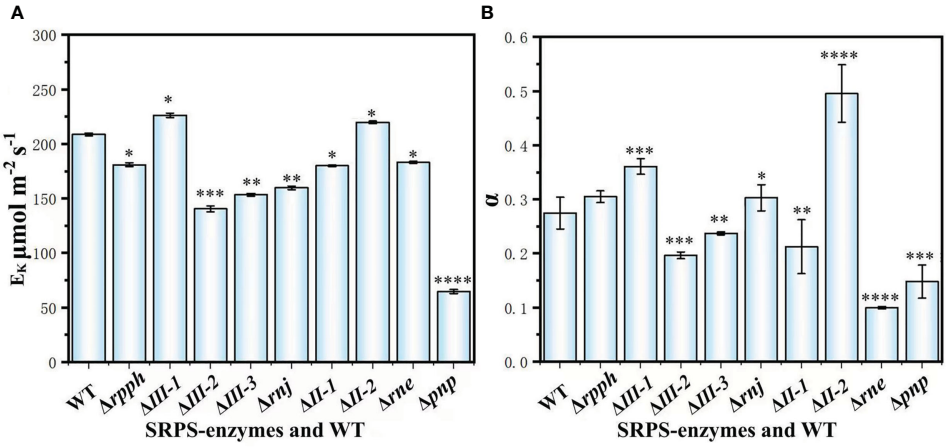

FIGURE 3
Chlorophyll fluorescence parameters in SRPS-enzymes mutants and WT during the exponential phase. **(A)** E_K; **(B)** α. *, p< 0.05 (two-way ANOVA); **, p< 0.01 (two-way ANOVA); ***, p< 0.001 (two-way ANOVA); ****, p< 0.0001 (two-way ANOVA).

in POC and PON suggest the involvement of the SRPS-enzymes in the internal regulatory mechanisms.

3.4 Quantitative real-time PCR

Using *RnpA* as the reference gene (Szekeres et al., 2014), the ΔΔCt method was used to calculate the relative expression level of the target gene: relative expression level of the target gene = $2^{-\Delta\Delta Ct}$ (Livak and Schmittgen, 2001), where $\Delta\Delta Ct = \Delta Ct_{Gene} - \Delta Ct_{Control}$, and ΔCt_{Gene} = Ct value of the target gene - Ct value of the internal reference gene in the same sample, $\Delta Ct_{Control}$ = Ct value of the target gene in the control group - Ct value of the internal reference gene.

From the comprehensive analysis of Figure 6, it can be found that mutations in all SRPS-enzymes regulate the expression of subunits of the key protein complex involved in photosynthetic carbon fixation. (1) It was known that *ndhD1* was responsible for coding the crucial subunit of the last protein complex (COX) in the respiratory chain, and its expression was decreased in all SRPS-enzymes mutant strains, which was consistent with the results of varying degrees of μ_{max} increase in most strains. (2) The inactivation of SRPS-enzymes promotes the expression of the subunit encoding gene *petA* in the Cytochrome b6-f complex, which differs from the changes in rETR and α. (3) In the expression of the remaining subunits, the vast majority showed a decrease, and only the expression levels of *psaB* and *psaC* in PCC7002Δ*III-1*, PCC7002Δ*II-1*, PCC7002Δ*II*-2, PCC7002Δ*rne* and PCC7002Δ*pnp*, *atpA* in PCC7002Δ*III-1*, PCC7002Δ*II-2*, PCC7002Δ*rne*, and PCC7002Δ*III-3*, PCC7002Δ*II-2* were significantly higher than in WT (paired test, P< 0.05).

4 Discussion

The SRPS mechanism is an important post-transcriptional regulatory mechanism in prokaryotes, and the SRPS-enzymes that play a major role mainly participates in regulating the expression of protein complexes or catalyzing consecutive biochemical reactions. Through a series of experiments, this study proves that the SRPS-enzymes in PCC7002 had a significant impact on the efficiency of photosynthetic carbon fixation and the expression of subunits of

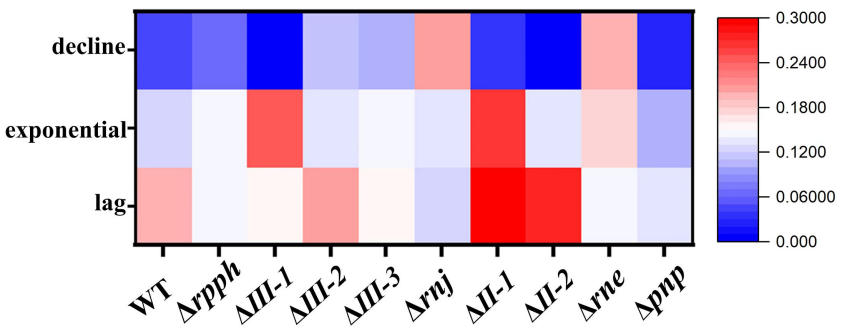

FIGURE 4
Changes in F_V/F_M in all algal solutions during the lag, exponential and decline phase. All mutants show a significant difference in F_V/F_V compared to WT: ****, p< 0.0001 (two-way ANOVA).

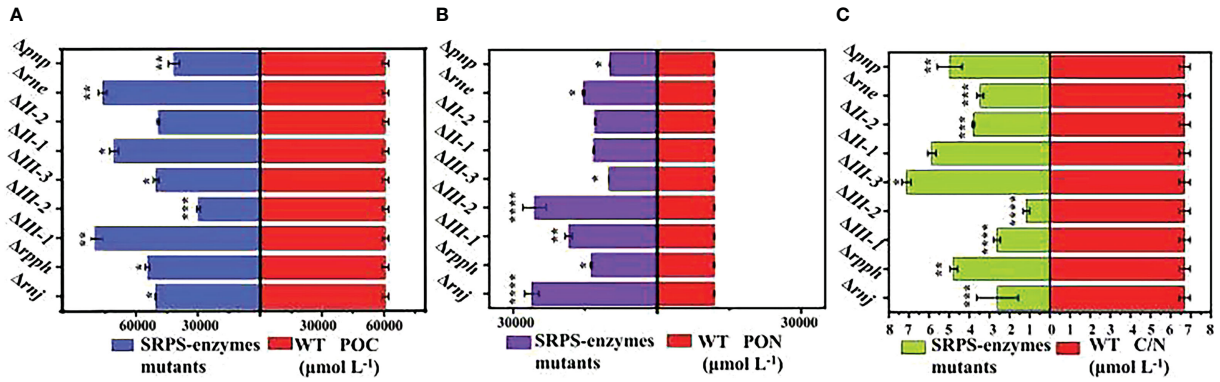

FIGURE 5
(A) Changes in POC in SRPS-enzymes mutants and WT during the exponential phase. **(B)** Changes in PON in SRPS-enzymes mutants and WT during the exponential phase; **(C)** Changes in C/N in SRPS-enzymes mutants and WT during the exponential phase. *, p< 0.05 (two-way ANOVA); **, p< 0.01 (two-way ANOVA); ***, p< 0.001 (two-way ANOVA); ****, p< 0.0001 (two-way ANOVA).

key photosynthetic protein complexes. However, there was no unified rule found from the comprehensive analysis of all parameter, and some experimental results were inconsistent with existing research conclusions. Based on this, we speculate on the regulation mechanism of SRPS-enzymes, which also lays the foundation for the precise analysis of SRPS molecular mechanisms in PCC7002.

The inactivation of SRPS-enzymes mainly affects the growth rate or changes the growth phase, and most of the nine mutant strains (except PCC7002Δ*II-1*) exhibit decrease in μ_{max}, while only PCC7002Δ*II-2* and PCC7002Δ*III-1* exhibit increase (Figure S1). Inactivting endonuclease genes mostly reduces the content of photosynthetic pigments (Figures S2, S3), mainly by shortening the growth phase, while the mutations of exonuclease genes mainly promote the content of photosynthetic pigments, prolonging their growth phase. Regarding changes in E_k, inactivating SRPS-enzymes mainly exhibits inhibitory effects, which were consistent with the changes in photosynthetic oxygen evolution rate and rETR after inactivating SRPS-enzymes under strong light conditions (PAR ≥ 100 μmol m^{-2} s^{-1}).

Knockout of the endonuclease RNase III-1 and the exonuclease RNase II-1 significantly increased POC (Figure 5). Compared to WT ($6.04 \times 10^4 \pm 286$ μmol L^{-1}), PCC7002ΔIII-1 and PCC7002ΔII-1 exhibited POC degradation of $8.83 \times 10^4 \pm 686$ μmol L^{-1} and $7.08 \times 10^4 \pm 294$ μmol L^{-1}, respectively, representing a 46% and 17% increase. Among the other five mutants excluding PCC7002Δrne, POC showed varying degrees of reduction compared to WT, particularly PCC7002ΔIII-2, which decreased by 17% to $5.03 \times 10^4 \pm 1254$ μmol L^{-1}. These results are consistent with the μ_{max} values shown in Supplementary Figure 1. In PCC7002Δrne, there is no correlation observed between POC and several common chlorophyll fluorescence parameters. This provides further validation for the hypothesis regarding the regulation of photosynthetic protein complex expression by the SRPS-enzymes.

Regarding PON (Figures 5B, C), the majority of enzyme knockouts have a promoting effect on PON compared to WT, although the magnitude of the changes is not significant. For example, the most significant increase in PON degradation is observed in PCC7002Δrnj ($2.61 \times 10^4 \pm 1486$ μmol L^{-1}), which is only a 21% increase compared to WT ($1.18 \times 10^4 \pm 49$ μmol L^{-1}). Conversely, the most pronounced inhibition is seen in PCC7002ΔIII-3 ($0.98 \times 10^4 \pm 79$ μmol L^{-1}), resulting in a 17% decrease. In cyanobacterial cells, nitrogen assimilation metabolism is connected to photosynthetic carbon metabolism through 2-oxoglutarate (2-OG), which serves as a central node in the TCA cycle (Muro-Pastor et al., 2005). Therefore, the differential changes in POC and PON suggest the involvement of the SRPS-enzymes in the internal regulatory mechanisms.

Mutations in the exonucleases (RNaseII and PNPase) led to a significant increase in S_R value, while the effect of mutations in endonucleases on S_R value is not consistent (Figure S5). Specifically, the knockdown of RNaseE led to an increase in S_R value, while the S_R values of PCC7002Δ*III-1*, PCC7002Δ*III-2*, and PCC7002Δ*III-3* all showed a decrease. Inactivation of all exonucleases, including RNaseJ, significantly increased the biological activity of SOM, while the three homologues of the endonuclease RNaseIII showed a consistent trend of significantly decreasing SOM biological activity, opposite to the effect of PCC7002Δ*pnp*. A higher HIX value indicates a higher degree of FDOM humification. BIX is generally used to indicate biological activity, FDOM sources, etc (Huguet et al., 2009). and can characterize the relative content of humic-like and protein-like components in FDOM. A higher BIX value means a higher relative content of humic-like components and higher biological activity of DOM (Zhang et al., 2022). HIX of PCC7002Δ*III-2* was consistently higher than that of other algal strains (Figure S6), possibly because the inactivation of RNaseIII-2 caused the onset of the decline phase to come earlier, and more SOM was released. In contrast, PCC7002Δ*III-1*, which had the highest μ_{max}, has always been in a vigorous growth state, so the humification degree of SOM has always been at its lowest. PCC7002Δ*rne*, which had a significantly increased μ_{max}, had a significantly higher BIX value than WT, consistent with S_R (Figures S1, S5, S7), indicating that the growth rate can have a significant impact on the biological activity of SOM.

Inactivating SRPS-enzymes results in an increase in the expression level of most subunits of the Cytochrome b6-f complex, while the

10.3389/fmars.2023.1223060

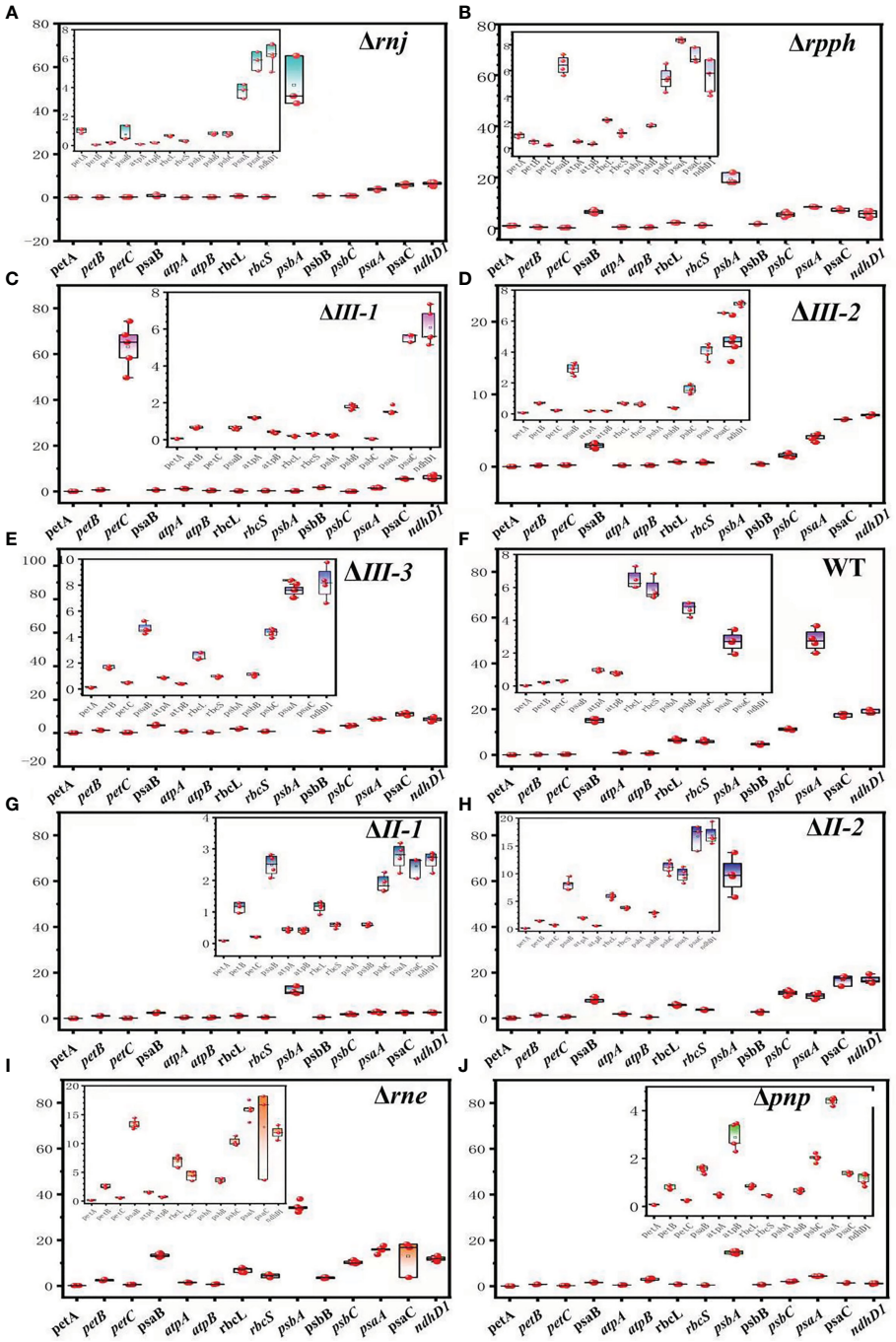

FIGURE 6
Expression of key protein complex subunits in SRPS-enzymes mutants and wild strain at the exponential phase. **(A)** PCC7002Δ*rnj*; **(B)** PCC7002Δ*rpph*; **(C)** PCC7002Δ*III-1*; **(D)** PCC7002Δ*III-2*; **(E)** PCC7002Δ*III-3*; **(F)** WT; **(G)** PCC7002Δ*II-1*; **(H)** PCC7002Δ*II-2*; **(I)** PCC7002Δ*rne*; **(J)** PCC7002Δ*pnp*.

expression levels of most subunits of PSI, PSII, RuBisCO, and NDH decrease. Only the mutation of RNaseE did not change the expression levels of *psaA, B, psbB, C, atpB, and rbcL*. Additionally, inactivating SRPS-enzymes mainly had a promoting effect on F_V/F_M, which was inconsistent with changes in chlorophyll fluorescence, growth rate, and gene expression levels. We speculate that (1) the splite sites of SRPS-enzymes are mainly located in several expressed genes of the Cytochrome b6-f complex, such as *petA, petB*, and *petC*. Similarly, RNaseIII-1, RNaseE, and RNaseII-2 also had splite sites in *atpA*, while RNaseIII-2 and RNaseII-2 had splite sites in *psbA*. In several subunits of PSI and PSII transcription, there are higher minimal folding free energy (MFE) near the splite sites of SRPS-enzymes, which was more conducive to SRPS-enzymes recognition and cleavage. (2) There are stable stem-loops near the splite sites of rppH in *petC* and *psbA*, near the splite site of RNaseII-2 in *psbC* and *psaC*, near the splite sites of RNaseE in *psaB, C, psbB, C, rbcL*, and *atpB* transcripts.

5 Conclusion

SRPS-enzymes in PCC7002 had a significant impact on the efficiency of photosynthesis and the expression of subunits of key photosynthetic protein complexes. The inactivation of SRPS-enzymes mainly affects the growth rate or changes the growth phase. In E_k, photosynthetic oxygen evolution rate and rETR, inactivating SRPS-enzymes mainly exhibits inhibitory effects (PAR ≥ 100 μmol m^{-2} s^{-1}). Additionally, inactivating SRPS-enzymes mainly had a promoting effect on F_V/F_M. The expression levels of *ndhD1* decreased in all mutant strains. The knockout of SRPS-enzymes had a promoting effect on the expression of the subunit encoding gene *petA* in the cytochrome b6-f complex. For the expression of the remaining protein subunits, the majority decreased, with only *psaB* and *psaC* in PCC7002Δ*III-1*, PCC7002Δ*II-1*, PCC7002Δ*II-2*, PCC7002Δ*rne*, and PCC7002Δ*pnp*, and the expression of *atpA* in PCC7002Δ*III-1*, PCC7002Δ*II-2*, and PCC7002Δ*rne* significantly higher than WT (Paired test, $p < 0.05$).

Author contributions

JC and DL performed the experiments, analyzed the data, and wrote the manuscript. YW and SW contributed to the investigation and data curation. RH designed the experiments and analyzed the data. All authors contributed to the article and approved the submitted version.

Funding

This work was supported by the National Natural Science Foundation of China [grant numbers 32170065, 31970113], the Key Research and Development Program of Shandong Province (2020ZLYS04).

Acknowledgments

The authors thank Yunhong Zhang, Xin Guo, Wei Zhao, Yue Meng, and Yueyue Li from Shandong University for sampling assistance and equipment assistance.

Conflict of interest

The authors declare that the research was conducted in the absence of any commercial or financial relationships that could be construed as a potential conflict of interest.

Publisher's note

All claims expressed in this article are solely those of the authors and do not necessarily represent those of their affiliated organizations, or those of the publisher, the editors and the reviewers. Any product that may be evaluated in this article, or claim that may be made by its manufacturer, is not guaranteed or endorsed by the publisher.

Supplementary material

The Supplementary Material for this article can be found online at: https://www.frontiersin.org/articles/10.3389/fmars.2023.1223060/full#supplementary-material

References

Barber, J., Nield, J., Morris, E., Zheleva, D., and Hankamer, B. (1997). The structure, function and dynamics of photosystem two. *Physiologia Plantarum* 100 (4), 817–827. doi: 10.1111/j.1399-3054.1997.tb00008.x

Blough, N. V. (2002). Chromophoric DOM in the coastal environment. *Biogeochem. Mar. Dissolved Organic Matter* 509–546. doi: 10.1016/B978-012323841-2/50012-9

Bricaud, A., Morel, A., and Prieur, L. (1981). Absorption by dissolved organic matter of the sea (yellow substance) in the UV and visible domains. *Limnol. Oceanogr.* 26 (1), 43–53. doi: 10.4319/lo.1981.26.1.0043

Buchanan, B. B., Gruissem, W., and Jones, R. L. (2015). *Biochemistry and molecular biology of plants* (Hoboken: John Wiley & Sons Inc.).

Carr, N. G., and Whitton, B. A. (1982). Cyanobacteria: Current perspectives. *The Biology of Cyanobacteria* 19, 1–8.

Demmig-Adams, B., and Adams, W. I. (1994). Capacity for energy dissipation in the pigment bed in leaves with different xanthophyll cycle pools. *Funct. Plant Biol.* 21 (5), 575–588. doi: 10.1071/PP9940575

Ducat, D. C., Way, J. C., and Silver, P. A. (2011). Engineering cyanobacteria to generate high-value products. *Trends Biotechnol.* 29 (2), 95–103. doi: 10.1016/j.tibtech.2010.12.003

Durall, C., and Lindblad, P. (2015). Mechanisms of carbon fixation and engineering for increased carbon fixation in cyanobacteria. *Algal. Res.* 11, 263–270. doi: 10.1016/j.algal.2015.07.002

Falkowski, P. (2012). Ocean science: the power of plankton. *Nature* 483 (7387), S17–S20. doi: 10.1038/483S17a

Geider, R. J., and La Roche, J. (2002). Redfield revisited: variability of c [ratio] n [ratio] p in marine microalgae and its biochemical basis. *Eur. J. Phycol.* 37 (1), 1–17. doi: 10.1017/S0967026201003456

Genty, B., Briantais, J.-M., and Baker, N. R. (1989). The relationship between the quantum yield of photosynthetic electron transport and quenching of chlorophyll fluorescence. *Biochim. Biophys. Acta (BBA)-General Subj.* 990 (1), 87–92. doi: 10.1016/S0304-4165(89)80016-9

Häder, D.-P., Kumar, H., Smith, R., and Worrest, R. (2007). Effects of solar UV radiation on aquatic ecosystems and interactions with climate change. *Photochem. Photobiol. Sci.* 6 (3), 267–285. doi: 10.1039/b700020k

Hoover, R. B., St. Amand, A., Levin, G. V., Hoover, R. B., Jerman, G. A., Rozanov, A. Y., et al. (2005). Morphology and elemental composition of recent and fossil cyanobacteria. *Astrobiology and Planetary Missions* 590603, 1–10. doi: 10.1117/12.624854

Huguet, A., Vacher, L., Relexans, S., Saubusse, S., Froidefond, J.-M., and Parlanti, E. (2009). Properties of fluorescent dissolved organic matter in the gironde estuary. *Organic Geochem.* 40 (6), 706–719. doi: 10.1016/j.orggeochem.2009.03.002

Ibrahim, F. G., Torre, R. M., Moya, B. L., and de Godos Crespo, I. (2020). "Carbon dioxide capture from carbon dioxide–rich gases by microalgae," in *From biofiltration to promising options in gaseous fluxes biotreatment* (Elsevier), 373–396. doi: 10.1016/B978-0-12-819064-7.00018-2

Jiao, N., Robinson, C., Azam, F., Thomas, H., Baltar, F., Dang, H., et al. (2014). Mechanisms of microbial carbon sequestration in the ocean–future research directions. *Biogeosciences* 11 (19), 5285–5306. doi: 10.5194/bg-11-5285-2014

Koonin, E. V. (2009). Evolution of genome architecture. *Int. J. Biochem. Cell Biol.* 41 (2), 298–306. doi: 10.1016/j.biocel.2008.09.015

Le Quéré, C., Andrew, R. M., Friedlingstein, P., Sitch, S., Pongratz, J., Manning, A. C., et al. (2018). Global carbon budget 2017. *Earth System Sci. Data* 10 (1), 405–448. doi: 10.5194/essd-10-405-2018

Li, J., Gong, P. H., and Guan, C. T. (2022). Research progress on fishery carbon sinking associated with marine ranching. *Prog. Fishery Sci.* 43 (05), 142–150. doi: 10.19663/j.issn2095-9869.20220118002. L.M.D.

Livak, K. J., and Schmittgen, T. D. (2001). Analysis of relative gene expression data using real-time quantitative PCR and the 2(-delta delta C(T)) method. *Methods* 25 (4), 402–408. doi: 10.1006/meth.2001.1262

Martínez-Pérez, A. M., Nieto-Cid, M., Osterholz, H., Catalá, T. S., Reche, I., Dittmar, T., et al. (2017). Linking optical and molecular signatures of dissolved organic matter in the Mediterranean Sea. *Sci. Rep.* 7 (1), 3436. doi: 10.1038/s41598-017-03735-4

Mou, S., Li, G., Li, H., Li, F., Shao, Z., Li, J., et al. (2018). Differential physiological responses of the coastal cyanobacterium synechococcus sp. PCC7002 to elevated p CO 2 at lag, exponential, and stationary growth phases. *Sci. China Earth Sci.* 61, 1397–1405. doi: 10.1007/s11430-017-9206-5

Muro-Pastor, M. I., Reyes, J. C., and Florencio, F. J. (2005). Ammonium assimilation in cyanobacteria. *Photosynthesis Res.* 83, 135–150. doi: 10.1007/s11120-004-2082-7

Murphy, K. R., Stedmon, C. A., Graeber, D., and Bro, R. (2013). Fluorescence spectroscopy and multi-way techniques. PARAFAC. *Anal. Methods* 5 (23), 6557–6566. doi: 10.1039/c3ay41160e

Ohno, T. (2002). Fluorescence inner-filtering correction for determining the humification index of dissolved organic matter. *Environ. Sci. Technol.* 36 (4), 742–746. doi: 10.1021/es0155276

Parsons, T. R., Maita, Y., and Lalli, C. M. (1984). *A manual of chemical and biological methods for seawater analysis*. Oxford: Pergamon Press (1984). 173 p.

Perez, A. A., Liu, Z., Rodionov, D. A., Li, Z., and Bryant, D. A. (2016). Complementation of cobalamin auxotrophy in synechococcus sp. strain PCC 7002 and validation of a putative cobalamin riboswitch *In vivo*. *J. Bacteriol.* 198 (19), 2743–2752. doi: 10.1128/JB.00475-16

Rochat, T., Bouloc, P., and Repoila, F. (2013). Gene expression control by selective RNA processing and stabilization in bacteria. *FEMS Microbiol. Lett.* 344 (2), 104–113. doi: 10.1111/1574-6968.12162

Sevens, S. E., and Porter, R. (1980). Transformation in agmenellum quadruplicatum. *Proc. Natl. Acad. Sci. USA* 77 (1), 6052–6056. doi: 10.1073/pnas.77.10.6052

Swallow, M. (1963). *The Sea: ideas and observations on progress in the study of the seas*. Interscience Publishers 90 (14), 554.

Szekeres, E., Sicora, C., Dragos, N., and Druga, B. (2014). Selection of proper reference genes for the cyanobacterium synechococcus PCC 7002 using real-time quantitative PCR. *FEMS Microbiol. Lett.* 359 (1), 102–109. doi: 10.1111/1574-6968.12574

Voigt, K., Sharma, C. M., Mitschke, J., Joke Lambrecht, S., Voss, B., Hess, W. R., et al. (2014). Comparative transcriptomics of two environmentally relevant cyanobacteria reveals unexpected transcriptome diversity. *ISME J.* 8 (10), 2056–2068. doi: 10.1038/ismej.2014.57

Webb, W. L., Newton, M., and Starr, D. (1974). Carbon dioxide exchange of alnus rubra: a mathematical model. *Oecologia* 17, 281–291. doi: 1007.00345747/bf28308943

Wollman, F.-A., Minai, L., and Nechushtai, R. (1999). The biogenesis and assembly of photosynthetic proteins in thylakoid membranes. *Biochim. Biophys. Acta (BBA)-Bioenergetics* 1411 (1), 21–85. doi: 10.1016/S0005-2728(99)00043-2

Yang, X.-H., and Zou, Q. (2005). Photosynthetic characteristics and chlorophyll fluorescence in level of cotton plants grown in full light and 40% dunlight. *Acta Phytoecologica Sin.* 29 (1), 8–15. doi: 10.17521/cjpe.2005.0002

YE, Z.-p., and Zhao, Z.-h. (2009). Effects of shading on the photosynthesis and chlorophyll content of bidens pilosa. *Chin. J. Ecol.* 28 (01), 19.

Ying, L., and Weiwei, J. (2020). Effects of nitrogen limitation time on growth, total lipid content, and fatty acid composition of halochlorococcum sarcotum and nannochloris oculata. *Mar. Sci.* 44 (2), 45–55. doi: 10.3389/fmars.2019.00095

Zhang, J., Liu, J., Liu, D., Chen, X., Shi, Q., He, C., et al. (2022). Temperature rise increases the bioavailability of marine synechococcus-derived dissolved organic matter. *Front. Microbiol.* 13, 838707. doi: 10.3389/fmicb.2022.838707

frontiers | Frontiers in Marine Science

TYPE Original Research
PUBLISHED 18 August 2023
DOI 10.3389/fmars.2023.1233560

Check for updates

OPEN ACCESS

EDITED BY
Junfu Dong,
Shandong University, China

REVIEWED BY
Mengyuan Wang,
Sun Yat-sen University, China
Ronnakrit Rattanasriampaipong,
Texas A and M University, United States

*CORRESPONDENCE
Fengfeng Zheng
zhengff@sustech.edu.cn
Chuanlun Zhang
zhangcl@sustech.edu.cn

†These authors have contributed equally to this work and share first authorship

RECEIVED 02 June 2023
ACCEPTED 21 July 2023
PUBLISHED 18 August 2023

CITATION
Zeng Z, Xiao W, Zheng F, Chen Y, Zhu Y, Tian J and Zhang C (2023) Enhanced production of highly methylated brGDGTs linked to anaerobic bacteria from sediments of the Mariana Trench. *Front. Mar. Sci.* 10:1233560. doi: 10.3389/fmars.2023.1233560

COPYRIGHT
© 2023 Zeng, Xiao, Zheng, Chen, Zhu, Tian and Zhang. This is an open-access article distributed under the terms of the Creative Commons Attribution License (CC BY). The use, distribution or reproduction in other forums is permitted, provided the original author(s) and the copyright owner(s) are credited and that the original publication in this journal is cited, in accordance with accepted academic practice. No use, distribution or reproduction is permitted which does not comply with these terms.

Enhanced production of highly methylated brGDGTs linked to anaerobic bacteria from sediments of the Mariana Trench

Zhiyu Zeng[1,2†], Wenjie Xiao[1,3†], Fengfeng Zheng[1,2*], Yufei Chen[1,2], Yuanqing Zhu[2,4], Jiwei Tian[5] and Chuanlun Zhang[1,2,4*]

[1]Shenzhen Key Laboratory of Marine Archaea Geo-Omics, Department of Ocean Science and Engineering, Southern University of Science and Technology, Shenzhen, China, [2]Southern Marine Science and Engineering Guangdong Laboratory (Guangzhou), Guangzhou, China, [3]Department of Biology, HADAL, Nordcee & DIAS, University of Southern Denmark, Odense M, Denmark, [4]Shanghai Sheshan National Geophysical Observatory, Shanghai, China, [5]Key Laboratory of Physical Oceanography, Ministry of Education, Ocean University of China, Qingdao, China

Branched glycerol dialkyl glycerol tetraethers (brGDGTs) are bacterial membrane lipids that are widely used in terrestrial paleoclimatic reconstructions. Recent studies have reported that brGDGTs can also be produced by marine bacteria. However, the environmental factors influencing marine-derived brGDGTs and their source organisms remain largely unknown. Here, we investigated the distribution and composition of brGDGTs and a suite of their putative derivatives called overly branched GDGTs (obGDGTs) in the Mariana Trench core sediments (water depth 8300 m, core length 320 cm), as well as the composition of bacterial communities. The ratio of the branched over isoprenoid tetraethers (BIT) was 0.03-0.21 (average 0.07; SD = 0.04; n = 21) and the ratio ΣIIIa/ΣIIa of brGDGTs was 0.93-7.47 (average 3.39; SD = 1.73; n = 21), which support the *in situ* production of brGDGTs. Co-occurrence network analysis revealed that a total of 33 types of bacteria at the order level (e.g., Armatimonadota DG-56, Proteobacteria Rhodospirillales, Chloroflexi SAR202_clade) were closely related to the distribution of brGDGTs and obGDGTs, which could be potential sources for these compounds. The abrupt increase in brGDGT and obGDGT concentrations in deeper oxygen-depleted sediments and their good correlations with anaerobic bacterial abundances suggest that these brGDGTs and obGDGTs may be produced by anaerobic bacteria residing in the anoxic sediments. Considerable variation in the degrees of methylation and cyclization of brGDGTs (obGDGTs) under different redox conditions indicate that sediment oxygen levels may have a profound impact on the presence and abundance of brGDGTs and obGDGTs, which should be considered when applying them for paleo-temperature or pH reconstructions. This study shows that brGDGTs and obGDGTs obtained from the Mariana Trench were probably produced by a variety of bacterial phyla indigenous in the hadal ocean, which are different from Acidobacteria commonly considered to be major terrestrial sources of brGDGTs.

KEYWORDS

branched GDGTs, overly branched GDGTs, *in situ* production, anaerobic bacteria, Mariana Trench

1 Introduction

Molecular biomarkers preserved in sedimentary archives provide valuable information on changes in paleoenvironments and climates (Summons et al., 2022). A suite of bacterial cell membrane lipids called branched glycerol dialkyl glycerol tetraethers (brGDGTs) are among these biomarkers that are ubiquitously distributed in virtually all ecosystems, including soils, peats, rivers, lakes, and marine environments (Tierney and Russell, 2009; Schouten et al., 2013; Günther et al., 2014; Zheng et al., 2016). BrGDGTs consist of two alkyl chains bound by ether bonds to two glycerol moieties, which are distinguished by the number and position of methyl branches and cyclopentane rings on the alkyl chains (Sinninghe Damsté et al., 2000; De Jonge et al., 2013). Several proxies based on brGDGT compositions, such as the Branched over Isoprenoid Tetraether (BIT) index (Hopmans et al., 2004; De Jonge et al., 2015) and the Methylation and Cyclization of Branched Tetraether (MBT and CBT) indexes (Weijers et al., 2007a), have been developed and widely employed to estimate organic carbon source, temperature and soil pH in modern and ancient geological settings (Weijers et al., 2007b; Wang et al., 2013; Wang et al., 2014; Yang et al., 2014; Sun et al., 2016; Wang et al., 2016; Zheng et al., 2016).

Despite widespread applications of brGDGTs in paleoclimatic research, their source organisms remain elusive. The stereochemistry of the glycerol units in brGDGTs points to a bacterial rather than archaeal origin (Sinninghe Damsté et al., 2000). Based on environmental studies in soils and peats, the phylum Acidobacteria was assumed to be the most likely biological sources of brGDGTs (Weijers et al., 2006; Weijers et al., 2009). This hypothesis was subsequently supported by the detection of abundant *iso*-diabolic acids, as brGDGT precursor lipids in strains of acidobacterial subgroups 1 and 3, and the identification of trace amount of brGDGT-Ia in two subgroup 1 cultures (Sinninghe Damsté et al., 2018).

Halamka et al. (2021) reported that oxygen limitation triggers brGDGT production in at least one subgroup 1 strain and confirmed the biosynthesis of three brGDGT compounds. More recently, Chen et al. (2022) and Halamka et al. (2023) identified another brGDGT-producing Acidobacterium (*Candidatus Solibacter usitatus*), and found that it can make a large portion of its cellular membrane out of structurally diverse brGDGTs. These studies are of great significance for understanding the mechanism of brGDGT-based proxies under laboratory conditions. Chen et al. (2022) specifically identified C5 methylated brGDGTs-producers by screening the homologs of archaeal tetraether synthase (Tes), which was initially proposed by Zeng et al. (2022) as a key protein responsible for synthesizing archaeal isoprenoid GDGTs. This approach offers a viable means of identifying potential brGDGTs producers in environmental samples. However, the structural variation of brGDGTs in diverse environments is much greater than that observed in the acidobacterial cultures, indicating that other phyla of bacteria could be possible brGDGT-producers (Liu et al., 2012b; Zhang et al., 2012; Zhang et al., 2013; Liu et al., 2014; Xie et al., 2014; Chen et al., 2018a; Weber et al., 2018; De Jonge et al., 2019; Xiao et al., 2022).

A challenging issue for the interpretation of brGDGT-based proxies arises from the mixing of brGDGTs from various sources into sedimentary archives (Peterse et al., 2009; Zell et al., 2014; De Jonge et al., 2015; Sinninghe Damsté, 2016). BrGDGTs were traditionally thought to be specific to terrestrial bacteria. However, mounting evidence suggests that brGDGTs can also be produced by marine bacteria (Zhang et al., 2012; Liu et al., 2014; Weijers et al., 2014; Zell et al., 2014; Sinninghe Damsté, 2016; Xiao et al., 2016; Xu et al., 2020). By compiling globally distributed soils and marine sediments, Xiao et al. (2016) developed a proxy, as expressed by the abundance ratio of hexamethylated to pentamethylated brGDGT (ΣIIIa/ΣIIa), to constrain the marine-derived brGDGTs with significantly higher ΣIIIa/ΣIIa values. Sinninghe Damsté (2016) proposed a threshold of $\#rings_{tetra} > 0.7$ as an indicative criterion for predominantly marine-sourced brGDGTs, primarily based on shelf sediments. The composition and environmental implication of marine-derived brGDGTs remain elusive, preventing their applications in marine environments. Additionally, microbial community producing brGDGTs can be expected to vary remarkably between terrestrial and marine settings (Bahram et al., 2018; Hoshino et al., 2020). The reported pure cultures that can biosynthesize brGDGTs, however, almost exclusively belong to terrestrial bacteria (Sinninghe Damsté et al., 2018; Halamka et al., 2021; Chen et al., 2022; Halamka et al., 2023) and little is known about the biological sources of marine-derived brGDGTs.

In addition to the commonly measured brGDGTs, the so-called overly-branched GDGTs (obGDGTs) have been detected in a semi-global range of marine surface sediments (Liu et al., 2012a; Liu et al., 2014; Xie et al., 2014; Becker, 2015). ObGDGTs differ from brGDGTs by having a higher degree of methylation (Liu et al., 2012a). ObGDGTs in marine sediments are thought to be primarily derived from anaerobic planktonic microbes (Liu et al., 2014; Xie et al., 2014). To date, very limited studies have reported the environmental distribution pattern and laboratory cultivation of obGDGTs, making it difficult to determine their biological sources and functional roles. Recently, Connock et al. (2022) presented a wide array of biomarkers in core samples from the North Atlantic Ocean, and showed the fractional abundance of obGDGTs abruptly increased during Oceanic Anoxic Event 2, implying that obGDGTs may be suitable to infer low oxygen conditions. The proxy potential of obGDGTs would benefit from detailed investigations of obGDGT distributions in marine sediments.

While it is commonly viewed that temperature and pH play a significant role in regulating the distribution of brGDGTs in natural environments (Weijers et al., 2007a; Peterse et al., 2012; Xiao et al., 2015; De Jonge et al., 2021), oxygen levels were also increasingly assumed to have an impact on brGDGTs (Weber et al., 2018; Halamka et al., 2021; Wu et al., 2021). Marine sediments are generally characterized by a redox gradient from oxic at surface to anoxic at deeper depths caused by gradual consumption of oxygen (Glud, 2008; Jørgensen et al., 2022). This gradient enables us to investigate the impact of oxygen levels on these brGDGTs and obGDGTs produced *in situ*. Additionally, bacterial communities vary significantly with sediment depth in conjunction with the redox zonation (Hiraoka et al., 2019; Hoshino et al., 2020). By

comparing bacterial community compositions and brGDGT and obGDGT distributions, and relating their variations to sediment depth, we can better understand the potential candidates contributing to these bacterial lipids and constrain their ecophysiology in marine sediments.

Here, we investigated the vertical distribution of brGDGTs and obGDGTs and of microbial 16S rRNA genes retrieved from a Mariana Trench sediment core MT03. As one of the most remote places on Earth, the Mariana Trench offers an ideal opportunity to distinguish GDGTs produced *in situ* from a terrestrial origin that usually muddles the interpretation of offshore sediments. We aimed to 1) determine the composition and distribution of brGDGTs and obGDGTs from the Mariana Trench core sediments, 2) constrain their possible sources, and 3) assess their environmental and biological implications.

2 Materials and methods

2.1 Study area and samples

The Mariana Trench is formed as the subduction of the Pacific plate beneath the eastern edge of the Philippine Sea plate. It has a total length of ca. 2500 km and a mean width of 70 km (Jamieson, 2015). Our study area is located in the southern section of the Mariana Trench covering the Challenger Deep (~11,000 m depth). The Mariana Trench is overlain by extremely oligotrophic waters. However, sediments in the Challenger Deep were found to support elevated microbial activity compared to adjacent abyssal plains (Glud et al., 2013).

During an expedition aboard RV *DongFang-Hong 2* (March 2019), a sediment core (MT03, 142.32°E, 11.12°N, water depth 8300 m, core length 320 cm) was retrieved from the Mariana Trench (Figure 1A), which was subsequently sliced into 2 cm segments at approximately 10 cm intervals. A total of 21 samples were collected at 9-287 cm depth intervals between the top and the bottom of the sediment core (320 cm depth). All sediment samples were freeze-dried at −40°C and homogenized by steel spatulas.

2.2 Lipid extraction and analysis

A portion of the freeze-dried sediment samples was ground into powder manually. Powdered sediments (3-5 g) were dispensed for lipids extraction by a modified Bligh and Dyer method (Sturt et al., 2004). Samples were extracted twice ultrasonically using a mixture of methanol (MeOH)/dichloromethane (DCM)/phosphate buffer (pH 7.4; 2:1:0.8, v/v/v) for 15 min each, and centrifuged at 3000 rpm for 5 min. Samples were then extracted with MeOH/DCM/trichloroacetic acid buffer (pH 2; 2:1:0.8, v/v/v) for two more times. All supernatants were collected; DCM and water were then added to achieve a final ratio of 1:1:0.8 for MeOH/DCM/water. The DCM phase was collected as total lipid extracts (TLEs) and dried under a N_2 stream. 50 µl synthesized C_{46}-GTGT (1.189 ng/µl) was added as an internal standard before lipid analysis.

The TLEs were re-dissolved in 200 µl methanol and centrifuged at 14,000 g for 5 min to remove large particles. GDGTs were analyzed by a Waters ACQUITY I-Class ultra-performance ion mobility liquid chromatography (UPLC) coupled with a SYNAPT G2-S*i* quadrupole time-of-flight high-resolution mass spectrometry (qTOF-HRMS) equipped with an electrospray ionization (ESI) source operated at positive mode. Separation of compounds was achieved using an ACE SuperC_{18} column (2 µm, 2.1 × 150 mm; Advanced Chromatography technologies LTD) kept at 45°C modified from Zhu et al. (2013). The injection volume was 10 µl. The solvent A was methanol (100%) and the solvent B was isopropanol (100%). Each flow phase was added with 0.04% formic acid (98%, Sigma Aldrich, Germany) and 0.1% ammonia (>25% NH_3, Sigma Aldrich, Germany). During the initial 5 min, the lipids were eluted with 100% A. Subsequently, the proportion of B was increased to 24% within the next 5 min, further increased to 60% during the 10-36 min. The proportion of solvent B was ultimately raised to 90% during the 36-45 min. Subsequently, the column was re-equilibrated with 100% A. The flow rate was maintained at 0.35 ml min^{-1} throughout the experiment.

Detection of GDGTs was achieved in Fast-DDA mode with mass ranges of *m/z* 100–2000 for MS^1 and 50–2000 for MS^2 and scan time for 0.2 s. The five most abundant ions at the scan were fragmented through collision-induced dissolution (CID) to perform data-dependent MS^2 analysis. MS setting was as follows: Capillary 2.5 kV, source temperature 120 °C, sampling cone 45, source offset 80, desolvation gas flow 800 l/hr at 350 °C, cone gas flow 50 l/hr, nebulizer gas flow 6.5 bar.

The regular brGDGTs and obGDGTs were identified by accurate molecular mass and isotope pattern as well as MS^2 mass spectra according to Liu et al. (2012b), with representative MS^2 spectra shown in Supplementary Figure S3. The peaks were integrated by extracting ion chromatograms with ± 0.05 Da mass width including adducts of $[M+H]^+$, $[M+NH_4]^+$ and $[M+Na]^+$. Concentrations of brGDGTs and obGDGTs were calculated by comparing the peak areas of target compounds and peak areas of the known amount of C_{46}-GTGT internal standard (Huguet et al., 2006). The chemical structure diagram of brGDGTs identified in this study is shown in Figure 1B.

2.3 GDGT-derived parameters

The BIT and ΣIIIa/ΣIIa indexes were adopted from Hopmans et al. (2004) and Xiao et al. (2016), respectively. The CBT and MBT indexes were calculated according to the definitions of Weijers et al. (2007a). The MI_{ob} and $MI_{ob/br}$ indexes were determined to calculate the degree of methylation of obGDGTs and obGDGTs/brGDGTs with the modifications of Liu et al. (2014).

$$BIT = \frac{Ia+IIa+IIIa}{Ia+IIa+IIIa+Crenarchaeol}$$

$$\Sigma IIIa/\Sigma IIa = \frac{IIIa}{IIa}$$

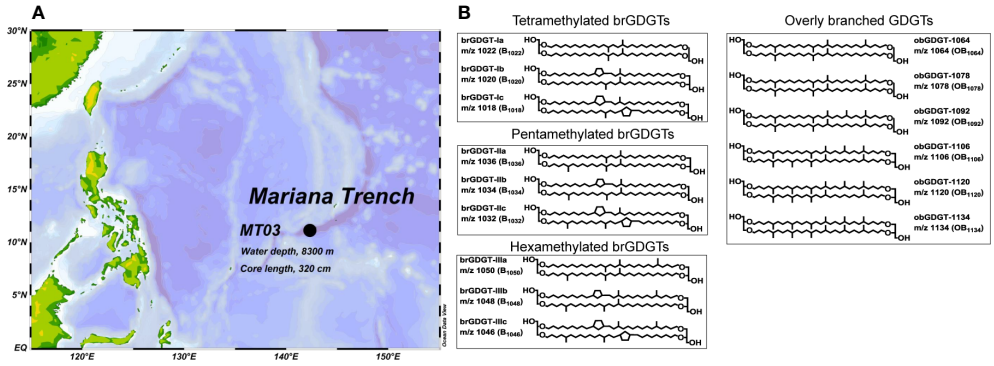

FIGURE 1
(A) Location of study site in the Mariana Trench. **(B)** Molecular structures of studied biomarkers in this work.

$$CBT = -\log\left(\frac{Ib+IIb}{Ia+IIa}\right)$$

$$MBT = \frac{Ia+Ib+Ic}{Ia+Ib+Ic+IIa+IIb+IIc+IIIa+IIIb+IIIc}$$

$$MI_{ob} = \frac{7*ob_{1064}+8*ob_{1078}+9*ob_{1092}+10*ob_{1106}+11*ob_{1120}+12*ob_{1134}}{\Sigma ob_{1064,\,1078,\,1092,\,1106,\,1120,\,1134}}$$

$$MI_{ob/br} = \frac{4*Ia+5*IIa+6*IIIa+7*ob_{1064}+8*ob_{1078}+9*ob_{1092}+10*ob_{1106}+11*ob_{1120}+12*ob_{1134}}{Ia+IIa+IIIa+\Sigma ob_{1064,\,1078,\,1092,\,1106,\,1120,\,1134}}$$

2.4 DNA extraction and 16S rRNA gene sequencing

DNA was extracted from 21 samples using the FastDNA™ SPIN Kit for Soil (MP Bio) according to manufacturer's protocols. The quantitative PCR (qPCR) was performed using a thermocycler PCR system (Quantstudio 5, ABI, United States). Bacterial 16S rRNA gene was amplified with primers Bac349F (5'–AGGCAGCAGTDRGGAAT–3') and Bac806R (5'–GGACTACYVGGGTATCTAAT–3') (Takai and Horikoshi, 2000). The real-time polymerase chain reaction was performed with the following program (PCR stage): 5 s for denaturation at 95°C, 30 s at 60°C for annealing, and 1 min at 72°C for extension. The whole process went through 35 cycles. The standard product was diluted into six gradients, with the highest concentration being 6.5×10^9 and the lowest concentration being 6.5×10^4. Triplicates analyses were performed for each sample and the standard. The R^2 values for the standard curve were > 0.98 and the efficiency was between 98–100%.

The universal primers used for archaeal and bacterial 16S rRNA gene sequencing were 515FmodF (5'-GTGYCAGCMGCCGCGGTAA-3') and 806RmodR (5'- GGACTACNVGGGTWTCTAAT-3') (Caporaso et al., 2011; Parada et al., 2016). Purified amplicons were pooled in equimolar and paired-end sequenced on an Illumina MiSeq PE300 platform/NovaSeq PE250 platform (Illumina, San Diego, USA) according to the standard protocols by Majorbio Bio-Pharm Technology Co. Ltd. (Shanghai, China).

After demultiplexing, the resulting sequences were merged by using FLASH (v1.2.11) (Magoc and Salzberg, 2011) and quality filtered by using fastp (0.19.6) (Chen et al., 2018b). Then the high-quality sequences were de-noised using DADA2 plugin in the Qiime2 (version 2020.2) pipeline with recommended parameters, which obtained single nucleotide resolution based on error profiles within samples. DADA2-denoised sequences are usually called amplicon sequence variants (ASVs). Taxonomic assignment of ASVs was performed using the Naive bayes consensus taxonomy classifier implemented in Qiime2 and the SILVA 16S rRNA database (v138). The bacterial sequences were retained to perform downstream analysis. To minimize the effects of sequencing depth, every sample was sequenced with a minimum of 100,000 clean reads. Analyses of the 16S rRNA microbiome sequencing data were performed using the free online platform of Majorbio Cloud Platform (www.majorbio.com).

Pearson correlation coefficients between bacterial orders and relative abundances of brGDGTs and obGDGTs were calculated using the R software (version 4.0.1, http://www.r-project.org). The significant positive correlations indicated that the shift of bacterial community might exert a significant impact on GDGT distribution by potentially producing brGDGTs and obGDGTs. The Positive correlations ($r > 0.65$, $p < 0.05$) were visualized as networks in Gephi (version9.0, https://gephi.org/). We further examined the presence of Tes homolog protein (e-value< $1e^{-50}$, identity >20%) in bacterial orders that showed strong positive relationship with the relative abundance of brGDGTs and obGDGTs. The bacterial genomes were not determined in our samples; instead, the Tes homolog (MA_1486) protein sequence (Zeng et al., 2022) was searched from the deposited genomes in NCBI database, which belonged to the same order of bacteria from our samples. The presence of Tes homolog indicates bacteria that are potentially capable of synthesizing brGDGTs, which may hold significant implications for identifying the biological sources of brGDGTs in the Mariana Trench in the future.

2.5 Bulk organic carbon analysis

After being freeze-dried and ground, ca. 1 g of homogenized sediment powder was digested in 5% HCl for 24 h to remove

inorganic carbon. Total organic carbon (TOC) contents were obtained using Thermo Scientific FLASH 2000 CHNS/O Elemental Analyzer. The standard error of three times determination of standard element sample was less than 0.3%.

3 Results

3.1 Bulk organic carbon content

The TOC content (expressed as weight percentage of TOC to dry weight sediment) varies in a narrow range from 0.04% to 0.18%, with an average of 0.11 ± 0.03% (avg. ± std). The highest TOC content is at 106 cm depth, and the lowest is at 136 cm depth (Figure 2A).

3.2 Composition and distribution of brGDGTs

A suite of brGDGTs and obGDGTs compounds were detected in the MT03 core. The overall variation of concentration and composition of both brGDGTs and obGDGTs along sediment depth were shown in Figure 3. The concentration and composition of brGDGTs varied significantly with sediment depth. The concentration of brGDGTs varied between 0.92 and 38.95 ng g^{-1} dry sediment (the unit " ng g^{-1}" was used in subsequent text.) in MT03 core, with an average value of 8.86 ± 8.16 ng g^{-1} (Figures 2B, 3A). The concentration of brGDGTs increased from 5.03 ± 3.10 ng g^{-1} at 9 – 164 cm depth to 15.08 ± 9.83 ng g^{-1} at 164 – 287 cm depth (Figures 2B, 3A). BrGDGT-IIIa was the dominant compound (40.06 ± 12.26% of total brGDGTs), followed by brGDGT-Ia (20.87 ± 6.90%) and brGDGT-IIa (14.46 ± 6.89%) (Table S2). The proportions of brGDGTs with one (Ib, IIb and IIIb) and two (Ic, IIc and IIIc) cyclopentyl rings were 19.64 ± 14.16% and 4.97 ± 4.79%, respectively (Figure 3C). The relative abundance of acyclic brGDGTs showed a gradual decreasing trend down core, whereas brGDGTs with one or two cyclopentyl rings exhibited a gradual increasing trend down core (Figure 3C). The classification based on the number of methyl groups showed the dominance of hexamethylated brGDGTs (IIIa, IIIb and IIIc; 47.31 ± 10.95%) over tetramethylated (Ia, Ib and Ic; 30.24 ± 8.32%) and pentamethylated (IIa, IIb and IIc; 22.45 ± 9.01%) brGDGTs.

The BIT index varied between 0.03 and 0.21 (0.07 ± 0.04), showing an overall decreasing trend with sediment depth. Whereas the ΣIIIa/ΣIIa index varied between 0.93 and 7.47 (3.39 ± 1.73), showing an overall increasing trend with large variations from the core top to the maximum sediment depth. The CBT index ranged from -0.18 to 1.22 (0.50 ± 0.49). It was high (0.87 ± 0.32) in the upper 151 cm sediment layer with fluctuations at 106 – 136 cm depth, and then gradually decreased from 0.96 to -0.03 towards the core bottom (Figure 2E). The MBT index varied between 0.15 and 0.46 (0.30 ± 0.08), and displayed dramatic variations along depth (Figure 2F).

3.3 Composition and distribution of obGDGTs

All six known obGDGTs ($obGDGT_{1064,\ 1078,\ 1092,\ 1106,\ 1120\ and\ 1134}$) were detected in the core sediments. The concentration of obGDGTs varied between 0.08 and 45.08 ng g^{-1} (9.19 ± 12.48 ng g^{-1}) (Figure 3A). The composition of obGDGTs was dominated by the $obGDGT_{1064}$ (42.77 ± 27.29% of total obGDGTs), followed by the $obGDGT_{1134}$ (26.27 ± 27.30%), $obGDGT_{1078}$ (21.05 ± 12.61%), $obGDGT_{1120}$ (7.29 ± 8.72%), $obGDGT_{1106}$ (2.44 ± 2.89%) and $obGDGT_{1092}$ (0.19 ± 0.33%) (Table S2).

The concentration and composition of obGDGTs were highly variable with sediment depth. The concentration of obGDGTs increased from less than 2 ng g^{-1} at 9 – 164 cm depth to above 8 ng g^{-1} at 164 – 287 cm depth, with the highest value occurring at 241 cm depth (45.08 ng g^{-1}) (Figure 3A). $ObGDGT_{1064\ and\ 1078}$ were the most abundant compounds above 151 cm (65.17 ± 7.92% and 30.75 ± 4.93%, respectively), but decreased sharply to 4.57% and 4.48%, respectively, at 210 cm depth, and then remained at a low level with large variability (9.47 ± 7.68% and 5.43 ± 4.34%,

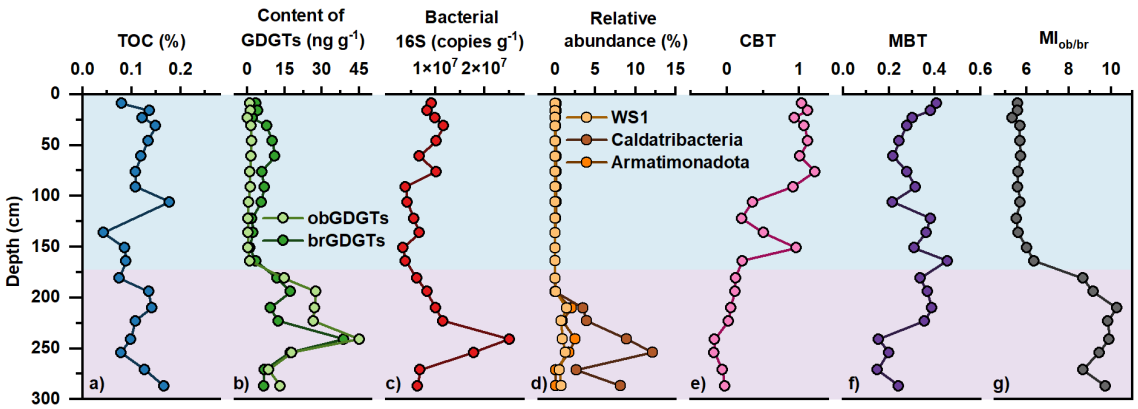

FIGURE 2
Vertical distribution of **(A)** TOC content, **(B)** absolute concentration of brGDGTs and obGDGTs, **(C)** abundance of bacterial 16S rRNA genes, **(D)** relative abundance of anaerobic bacteria, **(E)** CBT index, **(F)** MBT index, and **(G)** $MI_{ob/br}$ index in the Mariana Trench core sediments.

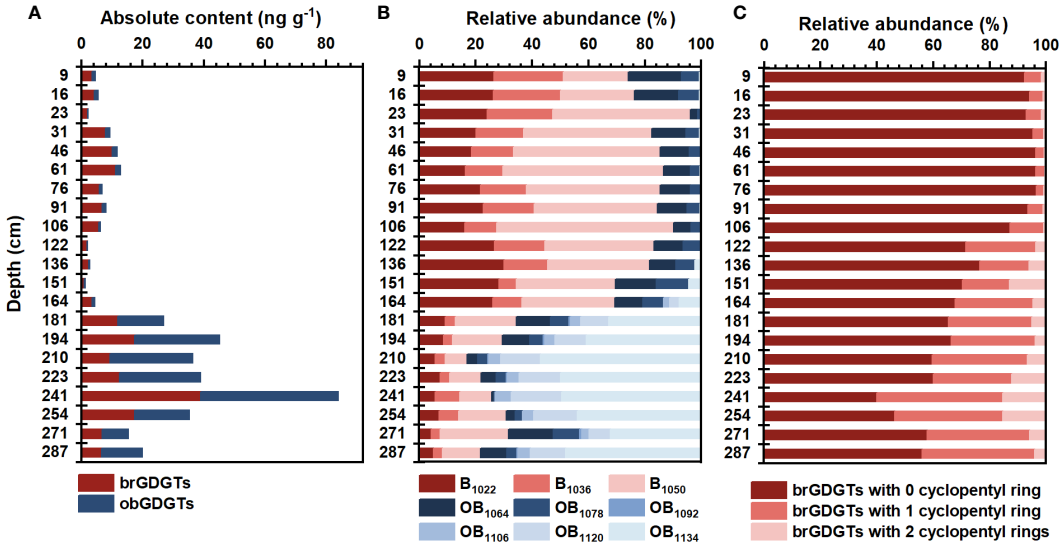

FIGURE 3
(A) Absolute concentration of brGDGTs and obGDGTs, and **(B)** relative abundance of acyclic brGDGTs and obGDGTs in the Mariana Trench core sediments; **(C)** relative abundance of brGDGTs with 0-, 1- and 2 cyclopentyl rings in the Mariana Trench core sediments. Note: The term "GDGTs" in the figure refers to the GDGTs included in the legend of the figure.

respectively) towards the core bottom. In contrast, obGDGT$_{1092, 1106, 1120 \text{ and } 1134}$ exhibited opposite downcore profiles. Specifically, they had much lower abundance above 151 cm (<0.01%, <0.01%, 0.14 ± 0.45% and 3.94 ± 4.41%, respectively), but increases strongly to 0.42%, 5.08%, 16.87 and 68.58%, respectively, at 210 cm depth, and then remained at a high level (0.43 ± 0.43%, 5.67 ± 1.14%, 18.56 ± 4.69% and 60.45 ± 6.89%, respectively) towards the core bottom (Table S2).

The MI$_{ob/br}$ index in the core MT03 varied between 5.34 and 10.27 (7.13 ± 1.87%). It was the lowest at 9 – 151 cm depth (5.34 – 6.02), and showed a rapidly increasing trend until 210 cm depth (10.27), and then remained at a high level (8.67 – 9.91) toward the bottom of the core (Figure 2G).

3.4 Composition and distribution of microbial community

The Illumina sequencing of the bacterial and archaeal 16S rRNA genes resulted in a total of 4,052,760 high-quality sequences. These sequences were clustered into 7539 ASVs with 6426 ASVs being classified to bacteria. The bacterial sequences were assigned to 382 orders, 158 classes and 57 phyla at different phylogenetic levels. Bacterial abundance varied obviously across the profile (3.4×10^6 – 2.5×10^7 copies/g) (Figure 2C). Proteobacteria (69% – 87%) was the overwhelmingly dominant bacterial phylum in the MT03 sediment core, while other major groups included Chloroflexi (4% – 13%), Actinobacteriota (2% – 4%) and Planctomycetota (1% – 4%) (Figure 4).

A depth-dependent variation of bacterial community composition was observed. In the top section of the sediment core (9 – 194 cm depth), proteobacterial orders of *Pseudomonadales*, *Rhizobiales*, and *Burkholderiales* and the Chloroflexi order of *SAR202_clade* were most abundant. The proportions of WS1 (order *WS1*) (Ferrer et al., 2011; Lee et al., 2013), Caldatribacteriota (order *JS1*) (Carr et al., 2015; Nobu et al., 2016; Liu et al., 2019; Katayama et al., 2020) and Armatimonadota (order *DG-56*) (Zhao et al., 2018; Ismail et al., 2021), which are reported as anaerobic bacteria in previous studies, remarkably increased at 194 –287 cm depth (Figure 2D).

Co-occurrence network analysis was performed to correlate relative abundance of bacterial communities to brGDGTs and obGDGTs. The results based on positive Pearson correlation ($r > 0.65$, $p < 0.05$) showed that 22 orders with the *Tes* gene were significantly related to brGDGTs and 11 orders with *Tes* were significantly related to obGDGTs (Figure 5). These orders contained the Tes homolog protein with relatively high alignment scores (e-value < $1e^{-50}$, identity > 20%), including Armatimonadota *DG-56*, Proteobacteria *Rhodospirillales*, and the Chloroflexi *SAR202_clade* (Figure 5).

4 Discussion

4.1 *In situ* production of brGDGTs and obGDGTs in the Mariana Trench sediments

The BIT index is widely used for tracking changes in the relative contribution of terrestrial and marine organic matter. Its value is typically < 0.15 for sediments from open marine settings (Schouten et al., 2013). Based on compilation of globally distributed soils and marine sediments, Xiao et al. (2016) proposed that ΣIIIa/ΣIIa index can serve as an indicator for the source of brGDGTs; it is < 0.59 in 90% of soils but increased to > 0.92 in marine sediments without significant terrestrial inputs. For the MT03 sediments, the low BIT (0.07 ± 0.04) and high ΣIIIa/ΣIIa (3.39 ± 1.73) values strongly point

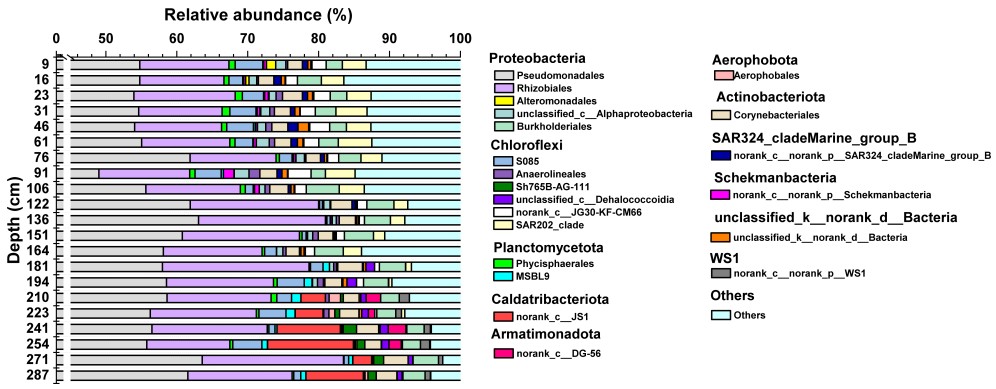

FIGURE 4
Relative abundance of bacterial communities at the order level. The legend on the right shows the phylum category belonging to different orders (e.g., Proteobacteria and Aerophobota). Groups with relative abundance < 1% were summarized as "others".

to a predominately marine source for brGDGTs. These results are in line with previous studies conducted in the Mariana Trench (Ta et al., 2019; Xiao et al., 2020), and are consistent with reported sedimentological and geochemical data (Luo et al., 2017; Lai et al., 2023).

It is noteworthy that the $\#rings_{tetra}$ index, proposed by Sinninghe Damsté (2016), has been utilized as an indicator for marine-derived brGDGTs and has found widespread application in continental shelf systems. However, emerging evidence from deep-ocean investigations, such as those conducted in the Mariana Trench, South China Sea, and Brazilian continental margin, highlights the necessity for caution when employing the $\#rings_{tetra}$ index in open-ocean deep water environments. Therefore, we only employed the BIT and ΣIIIa/ΣIIa indices to assess the *in situ* production of brGDGTs in the Mariana Trench sediments.

Marine-derived brGDGTs can come from both planktonic and benthic bacteria (Liu et al., 2014; Xiao et al., 2022). While the extent to which these sources contribute to the sedimentary brGDGT pool remains debated, growing evidence supports that marine-derived brGDGTs preserved in sediments are primarily biosynthesized by benthic bacteria, especially in deep-ocean sediments (Weijers et al., 2014; Xiao et al., 2022). The strong correlation observed between brGDGT concentrations and the abundance of bacterial 16S rRNA genes (r^2 = 0.67, p < 0.01) supports the notion that production of brGDGTs in the sediments of the Mariana Trench may be predominately endemic.

Comparing to our knowledge on brGDGTs, studies on obGDGTs are much limited. The investigation of obGDGTs was performed on suspended particulate matter from the oxygen minimum zone of the North Pacific Ocean and from the anoxic marine water columns of Black Sea and Cariaco Basin, which led to the hypothesis that their producers are marine sources, most likely anaerobic planktonic microbes (Liu et al., 2014; Xie et al., 2014). Becker (2015) investigated a variety of lipids in the Eastern Mediterranean Sea, and showed that obGDGTs were not present in the water column samples but were found in the sediments. In addition, obGDGTs in intact polar lipids were abundant in deep core sediments of the Discovery Basin (Becker, 2015). These studies show that organisms living in oxygen-depleted water column and sediments can both produce obGDGTs, while the latter possibly are the main contributors to sedimentary obGDGTs because respiration of organic matter in sediments is more likely to make the environment anaerobic. In the MT03 core, the co-occurrence of obGDGT concentrations with the abundance of bacterial 16S rRNA genes (r^2 = 0.47, p < 0.01) indicates that obGDGTs might be primarily biosynthesized within sediments, similar to the origin of brGDGTs.

4.2 Oxygen-induced changes of brGDGTs and obGDGTs

At the water-sediment interface, dissolved oxygen is gradually lost through aerobic microbial respiration and chemical species oxidation, resulting in the transition from oxic to anoxic conditions with sediment depth (Glud, 2008; Jørgensen et al., 2022). Unfortunately, due to the extreme water depth, the *in situ* oxygen profile of the MT03 core was not directly measured. Nevertheless, Liu et al. (2019) reported the pore water chemistry of the MT sediments with maximum O_2 penetration depth of 80 to 108 cm, and suggested an anaerobic condition in the deeper part of the sediments. Further, Lai et al. (2023) conducted a study on the mineralogy of the same core and reported redox changes that align with the evidence presented in this study (see below).

First, the core is characterized by prominent color variation with depth: The red-brown sediments occur in the upper layer (0 – 200 cm) and the olive-dark gray sediments in the deep layer (200 – 300 cm). According to Deaton and Balsam (1991) and Schwertmann (1993), this color change may be related to redox. Second, the strictly anaerobic bacteria Caldatribacteriota (order *JS1*) and Armatimonadota (order *DG-56*) are only prevalent in sediments deeper than 200 cm. Third, the pyrite content in the core exhibits an increase from the upper to the lower sections, accompanied by a decrease in the content of goethite, as reported by Lai et al. (2023). This observation suggests a shift towards a reducing sedimentary environment in the lower regions of the

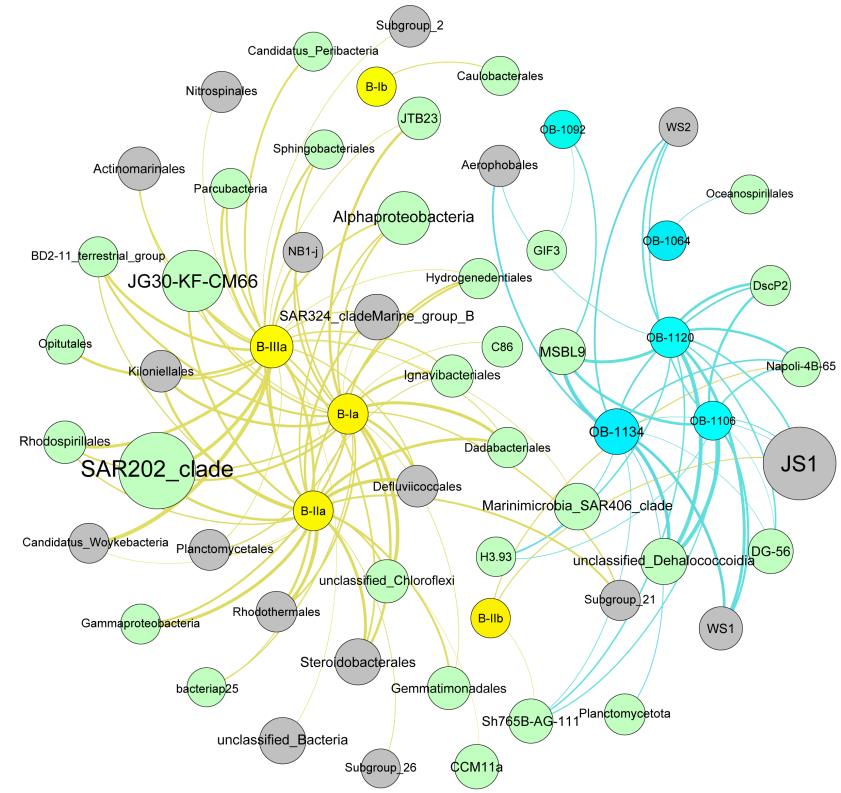

FIGURE 5
Co-occurrence network between composition of bacterial communities and relative abundance of brGDGTs and obGDGTs. The network is established based on positive Pearson correlation (R > 0.65, $p < 0.05$). The yellow, blue, green and gray nodes represent brGDGTs, obGDGTs, bacteria groups with Tes and bacteria groups without Tes, respectively. The larger the node, the higher the fractional abundance; the thicker the connection line between two nodes, the stronger the correlation. The bottom legend shows the phylum category belonging to different orders (e.g., Actinobacteria, Aerophobota). Groups marked with '√' have the *Tes* gene for the synthesis of GDGTs.

core. Taken together, these findings provide evidence supporting the presence of anoxic conditions in deeper depth of the MT03 core (Figure 4).

BrGDGT and obGDGT concentrations generally rise with increasing sediment depth, with their peak concentrations occurring at 241 cm depth, suggesting that they were likely to be produced in anoxic sediments. This is consistent with earlier studies that brGDGTs and obGDGTs are preferentially biosynthesized by anaerobic bacteria in soils, peats, lakes and marine environments (Weijers et al., 2006; Weijers et al., 2009; Wu et al., 2021; Xiao et al., 2022). The abrupt shift in brGDGT and obGDGT concentrations starting at 164 cm depth suggests that brGDGTs and obGDGTs could also be produced under low oxygen conditions, which is consistent with Halamka et al. (2021).

In addition to concentration, the composition of brGDGTs and obGDGTs is also greatly influenced by oxygen conditions. The MBT values of the upper layer sediments (0 – 164 cm depth, 0.32 ± 0.07) are slightly higher than those of the deep layer sediments (181 – 287 cm depth, 0.27 ± 0.09). However, the methylation degree of obGDGTs varies dramatically with much lower methylated $obGDGT_{1064 \text{ and } 1078}$ at 0 – 164 cm depth (92.89 ± 11.34% of total obGDGTs), and much higher methylated $obGDGT_{1092,\ 1106,\ 1120 \text{ and } 1134}$ at 181 – 287 cm depth (83.42 ± 10.85%). The deep layer sediments had significantly higher $MI_{ob/br}$ values (9.46 ± 0.55 at 181

– 287 cm depth vs. 5.69 ± 0.24 at 0 – 164 cm depth) due to the elevated methylation degree of obGDGTs and their higher increase in abundance compared to brGDGTs (Figure 2G). A similar phenomenon was observed in marine water columns in the Black Sea and Cariaco Basin (Liu et al., 2014). Previous studies have demonstrated that changing oxygen concentrations alter the brGDGT methylation number in dependent of temperature. For instance, Wu et al. (2021) discovered that the methylation degree of brGDGTs in lake sediments decreased with decreasing dissolved oxygen content of the bottom water. Our study indicates that a higher degree of methylation of brGDGTs may tend to occur toward increasing anoxic conditions.

There may be a concern regarding the potential influence of environmental changes during geological history on the distribution and composition of brGDGTs and obGDGTs in the core sediments of the Mariana Trench. The lack of suitable dating materials hinders the establishment of an accurate age framework for this study. Nevertheless, utilizing the excess Pb^{210} data from Glud et al. (2013) and Luo et al. (2017), the sedimentation rates in the southern slope (6,037 m) and the axis (10,810 m) of the Challenger Deep were estimated to be 0.02 and 0.04 cm yr^{-1}, respectively, which allowed for a rough calculation of the age of the bottom sediments in core MT03 in the range of approximately 5 – 20 kyr. Within this time span, significant alterations in the temperature and redox conditions of the bottom water in the Mariana Trench are unlikely, rendering it arduous to account for the noteworthy variations in brGDGT-based proxies and the strong correlation between brGDGT/obGDGT concentrations and bacterial 16S rRNA genes. Consequently, we propose that the observed changes in brGDGTs and obGDGTs primarily reflect the influence of oxygen levels within the sediment porewater.

4.3 Implications for paleoenvironmental reconstructions

The reliability of the empirical relationships between brGDGT-based proxies and environmental parameters is crucial for the use of brGDGTs in paleoclimatic research. It is widely recognized that the methylation and cyclization degree of terrestrial-derived brGDGTs are mainly controlled by temperature and pH, though other elements like oxygen levels, seasonality, nutrient availability, and soil chemistry may also have an impact (Weijers et al., 2007a; Xiao et al., 2015; Wu et al., 2021). However, knowledge on the primary environmental factors influencing marine-derived brGDGTs is very limited. In the MT03 core, brGDGTs are suggested to be produced within sediments by marine bacteria, hence the methylation degree of brGDGTs may be unaffected by changes in deep water temperature (2 – 4°C). The large variations, which range from -4.6°C to 14.7°C (4.3 ± 5.7°C), in the MBT/CBT-inferred estimates of temperature using the empirical correlation of Weijers et al. (2007b) do not match the bottom water temperature. The temperature may not have been the primary factor in the vertical variation of the methylation degree of brGDGTs in the MT03 core. We suggest that brGDGTs' ability to function as a temperature indicator in marine environments may be severely hampered by the impact of oxygen levels. Similarly, the CBT-inferred estimates of pH in the MT03 core using the empirical correlation of Weijers et al. (2007b) ranged from 5.5 to 9.2 (7.4 ± 1.3), also suggesting that the relationship between brGDGT cyclization and pH may be masked by oxygen levels.

Therefore, brGDGTs and obGDGTs that are primarily produced by bacteria *in situ* may serve as important tools for tracing oxygen levels in marine sediments. In the MT03 core, a significant rise in the methylation degree of brGDGTs and obGDGTs was observed under oxygen limitation. The highly methylated obGDGTs (like $obGDGT_{1120\ and\ 1134}$) are relatively more sensitive to the changes in oxygen levels. Based on the vertical variation in $MI_{ob/br}$ values, we propose 6.5 as a threshold value to identify oxic and anoxic conditions. This notion is supported by the vertical profiles of brGDGTs and obGDGTs of the suspended particulate matter in the Black Sea and Cariaco Basin (Liu et al., 2014; Xie et al., 2014). In these two regions, the $MI_{ob/br}$ values are, respectively, 6.1 ± 0.4 and 5.8 ± 0.6 for oxic water columns, and 8.0 ± 0.6 and 7.0 ± 0.6 for anoxic water columns. Further research is necessary to confirm the viability of the $MI_{ob/br}$ index in indicating oxygen levels in marine sediments.

4.4 Implications for source organisms of brGDGTs and obGDGTs

Our knowledge on biological sources of brGDGTs has been largely improved with the detection of C5 methylation brGDGTs in some strains belonging to acidobacterial subgroups 1 and 3 (Sinninghe Damsté et al., 2018; Halamka et al., 2021; Chen et al., 2022; Halamka et al., 2023). Acidobacteria are currently considered as the only confirmed sources of brGDGTs in environments where they were abundant, e.g., acidic soils and peat bogs. However, increasing evidence revealed that the potential brGDGT-producers may extend to a suite of bacteria other than Acidobacteria alone in various environmental settings (Chen et al., 2018a; De Jonge et al., 2019). On the basis that both brGDGTs and obGDGTs are probably produced *in situ* by bacteria thriving in the sediments as we discussed above, we first explored the relationship between distribution of brGDGTs (obGDGTs) and relative abundance of bacterial community in the sediment core. The results showed that the 49 bacterial groups at the order level positively related to the distribution of brGDGTs and obGDGTs (Figure 5). These bacteria included but are not limited to Caldatribacteriota (*JS1*), Proteobacteria (e.g., Alphaproteobacteria and Rhodospirillales), and Chloroflexi (e.g., G30-KF-CM66 and Napoli-4B-65). Our results show that the biological sources of these lipids could be related to diverse benthic bacterial groups in intact forms (alive or dormant) in the cold deep water marine environments, which can be significantly

different in community structure from water column plankton (Jing et al., 2022; Tian et al., 2018). The biological sources of brGDGTs and obGDGTs may also be different from those observed in soils (Chen et al., 2018a; De Jonge et al., 2019) or lacustrine water column and sediments (Weber et al., 2018; Wu et al., 2021).

To date, the brGDGTs producers that have been experimentally confirmed were all classified to phylum Acidobacteria. However, Acidobacteria only accounted for 0.60% of the total bacterial community in our samples, and they were mainly enriched in the upper layer sediments. A total of 7 subgroups of Acidobacteria have been reported, of which only 3 subgroups (2, 21, 26) are associated with brGDGTs, and all three subgroups do not contain Tes homologs. Therefore, we suggest that Acidobacteria may not be the main producers of brGDGTs in the Mariana Trench sediments. Based on co-occurrence with brGDGTs and potential indication of Tes homologs in our study, we suggest that bacteria Chloroflexi, Proteobacteria and Dadabacteria could be the potential producers of brGDGTs and Armatimonadota, Planctomycetota and Chloroflexi may probably be the producers of obGDGTs in the Mariana Trench sediments. However, it requires cultivation experiments to confirm the biosynthesis of brGDGTs and obGDGTs in these microorganisms.

5 Summary and conclusion

We examined brGDGTs and obGDGTs as well as bacterial communities in a sediment core from the Mariana Trench. The rapid increase in concentrations of brGDGTs and obGDGTs with sediment depth and their good correlation with the abundance of anaerobic bacteria suggest that brGDGTs and obGDGTs in the Mariana Trench sediments may be biosynthesized by anaerobic bacteria (either alive or dormant) in the sediments. The anaerobic sediments were characterized by significantly higher degrees of methylation and cyclization, suggesting that brGDGTs and obGDGTs may be indicative of oxygen availability. Network analysis suggests that brGDGTs in the Mariana Trench sediments may be more likely to be produced by bacterial phyla such as Chloroflexi, Proteobacteria and Dadabacteria; whereas, obGDGTs may be more likely to be produced by Armatimonadota, Planctomycetota and Chloroflexi. Our study indicates that the use of brGDGT-based proxies in paleotemperature and pH reconstructions using marine sedimentary archives may be significantly influenced by the impact of changes in bacterial community compositions and oxygen levels in the sediment.

Data availability statement

The datasets presented in this study can be found in online repositories. The names of the repository/repositories and accession number(s) can be found below BioProject, PRJNA980304.

Author contributions

ZZ, WX, FZ, YZ, and CZ conceived the study and designed the experiments. FZ and JT collected the samples. ZZ, WX, FZ, and YC performed the analyses and created the figures. ZZ and YC analyzed sequence data and provided interpretation of organic geochemical data. FZ, WX and CZ acquired funding. ZZ, WX, FZ, and CZ drafted the manuscript, and all authors contributed to writing and approved the submitted version.

Acknowledgments

We would like to thank Wei He for help drawing the figures, Yanwei Chen for help in qPCR analysis, Wenxiu Wang for analysis of dissolved organic matter (DOM) present in the pore water, and the captain and crew of R/V "Dong Fang Hong 2" for their sampling efforts during the cruise of the Mariana Trench. Financial supports for this research were provided by the National Natural Science Foundation of China (42141003, 42003063, 42206040), the Southern Marine Science and Engineering Guangdong Laboratory (Guangzhou) (No. K19313901), the Stable Support Plan Program of Shenzhen Natural Science Fund (20200925173954005), the Guangdong-Shenzhen Joint Fund (2021B1515120080), the Shenzhen Key Laboratory of Marine Archaea Geo-Omics, Southern University of Science and Technology (ZDSYS201802081843490), and the Shanghai Sheshan National Geophysical Observatory (2020Z01).

Conflict of interest

The authors declare that the research was conducted in the absence of any commercial or financial relationships that could be construed as a potential conflict of interest.

Publisher's note

All claims expressed in this article are solely those of the authors and do not necessarily represent those of their affiliated organizations, or those of the publisher, the editors and the reviewers. Any product that may be evaluated in this article, or claim that may be made by its manufacturer, is not guaranteed or endorsed by the publisher.

Supplementary material

The Supplementary Material for this article can be found online at: https://www.frontiersin.org/articles/10.3389/fmars.2023.1233560/full#supplementary-material

References

Bahram, M., Hildebrand, F., Forslund, S. K., Anderson, J. L., Soudzilovskaia, N. A., Bodegom, P. M. V., et al. (2018). Structure and function of the global topsoil microbiome. *Nature* 560, 233–237. doi: 10.1038/s41586-018-0386-6

Becker, K. W. (2015). *Biogeochemical significance and biomarker potential of novel glycerolipids and respiratory quinones in the marine environment. Doctoral Dissertation* (University of Bremen: Bremen).

Caporaso, J. G., Lauber, C. L., Walters, W. A., Berg-Lyons, D., Lozupone, C. A., Turnbaugh, P. J., et al. (2011). Global patterns of 16S rRNA diversity at a depth of millions of sequences per sample. *Proc. Natl. Acad. Sci.* 108 (supplement_1), 4516–4522. doi: 10.1073/pnas.1000080107

Carr, S. A., Orcutt, B. N., Mandernack, K. W., and Spear, J. R. (2015). Abundant Atribacteria in deep marine sediment from the Adélie Basin, Antarctica. *Front. Microbiol.* 6. doi: 10.3389/fmicb.2015.00872

Chen, Y. F., Zheng, F., Chen, S. Z., Liu, H. D., Phelps, T. J., and Zhang, C. L. (2018a). Branched GDGT production at elevated temperatures in anaerobic soil microcosm inCubations. *Org. Geochem.* 117, 12–21. doi: 10.1016/j.orggeochem.2017.11.015

Chen, Y. F., Zheng, F., Yang, H., Yang, W., Wu, R. J., Liu, X. Y., et al. (2022). The production of diverse brGDGTs by an Acidobacterium providing a physiological basis for paleoclimate proxies.. *Geochim. Cosmochim. Acta* 337, 155–165. doi: 10.1016/j.gca.2022.08.033

Chen, S. F., Zhou, Y. Q., Chen, Y. R., and Gu, J. (2018b). Fastp.: Ultra–fast All–in–one FASTQ Preprocessor. *Bioinformatics* 34, i884–i890. doi: 10.1093/bioinformatics/bty560

Connock, G. T., Owens, J. D., and Liu, X. L. (2022). Biotic induction and microbial ecological dynamics of Oceanic Anoxic Event 2. *Commun. Earth Environ.* 3, 136. doi: 10.1038/s43247-022-00466-x

Deaton, B. C., and Balsam, W. L. (1991). Visible spectroscopy; a rapid method for determining hematite and goethite concentration in geological materials. *J. Sedimentary Res.* 61, 628–632. doi: 10.1306/D4267794-2B26-11D7-8648000102C1865D

De Jonge, C., Hopmans, E. C., Stadnitskaia, A., Rijpstra, W. I. C., Hofland, R., Tegelaar, E. W., et al. (2013). Identification of novel penta- and hexamethylated branched glycerol dialkyl glycerol tetraethers in peat using HPLC-MS2, GC-MS and GC-SMB-MS. *Org. Geochem.* 54, 78–82. doi: 10.1016/j.orggeochem.2012.10.004

De Jonge, C., Kuramae, E., Radujković, D., Weedon, J. T., Janssens, I. A., and Peterse, F. (2021). The influence of soil chemistry on branched tetraether lipids in mid– and high latitude soils: Implications for brGDGT– based paleothermometry. *Geochim. Cosmochim. Acta* 310, 95–112. doi: 10.1016/j.gca.2021.06.037

De Jonge, C., Radujković, D., Sigurdsson, B. D., Sigurdsson, B. D., Weedon, J. T., Weedon, J. T., et al. (2019). Lipid biomarker temperature proxy responds to abrupt shift in the bacterial community composition in geothermally heated soils. *Org. Geochem.* 137, 103897. doi: 10.1016/j.orggeochem.2019.07.006

De Jonge, C., Stadnitskaia, A., Hopmans, E. C., Cherkashov, G., Fedotov, A., Streletskaya, I. D., et al. (2015). Drastic changes in the distribution of branched tetraether lipids in suspended matter and sediments from the Yenisei River and Kara Sea (Siberia): Implications for the use of brGDGT–based proxies in coastal marine sediments. *Geochim. Cosmochim. Acta* 165, 200–225. doi: 10.1016/j.gca.2015.05.044

Ferrer, M., Guazzaroni, M–E, Richter, M., García-Salamanca, A., Yarza, P., Suárez–Suárez, A., et al. (2011). Taxonomic and functional metagenomic profiling of the microbial community in the anoxic sediment of a sub–saline shallow lake (Laguna de Carrizo, Central SPAIN). *Microbial. Ecol.* 62, 824–837. doi: 10.1007/s00248-011-9903-y

Glud, R. N. (2008). Oxygen dynamics of marine sediments. *Mar. Biol. Res.* 4, 243–289. doi: 10.1080/17451000801888726

Glud, R. N., Wenzhöfer, F., Middelboe, M., Oguri, K., Turnewitsch, R., Canfield, D. E., et al. (2013). High rates of microbial carbon turnover in sediments in the deepest oceanic trench on Earth. *Nat. Geosci.* 6, 284–288. doi: 10.1038/ngeo1773

Günther, F., Thiele, A., Gleixner, G., Xu, B. Q., Yao, T. D., and Schouten, S. (2014). Distribution of bacterial and archaeal ether lipids in soils and surface sediments of Tibetan lakes: Implications for GDGT-based proxies in saline high mountain lakes. *Org. Geochem.* 67, 19–30. doi: 10.1016/j.orggeochem.2013.11.014

Halamka, T. A., McFarlin, J., Younkin, A. D., Depoy, J., Dildar, N., and Kopf, S. H. (2021). Oxygen limitation can trigger the production of branched GDGTs in culture. *Geochem. Perspect. Lett.* 19, 36–39. doi: 10.7185/geochemlet.2132

Halamka, T. A., Raberg, J. H., McFarlin, J. M., Younkin, A. D., Mulligan, C., Liu, X–L, et al. (2023). Production of diverse brGDGTs by Acidobacterium Solibacter usitatus in response to temperature, pH, and O_2 provides a culturing perspective on brGDGT proxies and biosynthesis. *Geobiology* 21, 102–118. doi: 10.1111/gbi.12525

Hiraoka, S., Hirai, M., Matsui, Y., Makabe, A., Minegishi, H., Tsuda, M., et al. (2019). Microbial community and geochemical analyses of trans–trench sediments for understanding the roles of hadal environments. *ISME J.* 14, 740–756. doi: 10.1038/s41396-019-0564-z

Hopmans, E. C., Weijers, J. W. H., Schefuss, E., Herfort, L., Sinninghe Damsté, J. S., and Schouten, S. (2004). A novel proxy for terrestrial organic matter in sediments based on branched and isoprenoid tetraether lipids. *Earth Planetary Sci. Lett.* 224, 107–116. doi: 10.1016/j.epsl.2004.05.012

Hoshino, T., Doi, H., Uramoto, G–I, Wörmer, L., Adhikari, R., Xiao, N., et al. (2020). Global diversity of microbial communities in marine sediment. *Proc. Natl. Acad. Sci. U.S.A.* 117, 27587–27597. doi: 10.1073/pnas.1919139117

Huguet, C., Hopmans, E. C., Febo–Ayala, W., Thompson, D. H., Sinninghe Damsté, J. S., and Schouten, S. (2006). An improved method to determine the absolute abundance of glycerol dibiphytanyl glycerol tetraether lipids. *Org. Geochem.* 37, 1036–1041. doi: 10.1016/j.orggeochem.2006.05.008

Ismail, S., Elreedy, A., Fujii, M., Ni, S–Q, Tawfik, A., and Elsamadony, M. (2021). Fatigue of anammox consortia under long–term 1,4–dioxane exposure and recovery potential: N–kinetics and microbial dynamics. *J. Hazardous Mater.* 414, 125533. doi: 10.1016/j.jhazmat.2021.125533

Jamieson, A. J. (2015). *The Hadal Zone: Life in the Deepest Oceans* (Cambridge: Cambridge University Press).

Jing, H. M., Xiao, X., Zhang, Y., Li, Z. Y., Jian, H. H., Luo, Y. F., et al. (2022). Composition and ecological roles of the core microbiome along the abyssal-hadal transition zone sediments of the mariana trench. *Microbiol. Spectr.* 10, 3. doi: 10.1128/spectrum.01988-21

Jørgensen, B., Wenzhöfer, F., Egger, M., and Glud, R. N. (2022). Sediment oxygen consumption: Role in the global marine carbon cycle. *Earth-Sci. Rev.* 228, 103987. doi: 10.1016/j.earscirev.2022.103987

Katayama, T., Nobu, M. K., Kusada, H., Meng, X–Y, Hosogi, N., Uematsu, K., et al. (2020). Isolation of a member of the candidate phylum 'Atribacteria' reveals a unique cell membrane structure. *Nat. Commun.* 11. doi: 10.1038/s41467-020-20149-5

Lai, W., Liu, X., Tian, J., Wang, H., Zhang, J., Huang, J., et al. (2023). Mineralogy of sediments in the Mariana Trench controlled by environmental conditions of the West Pacific since the Last Glacial Maximum. *J. Asian Earth Sci.* 245, 105553. doi: 10.1016/j.jseaes.2023.105553

Lee, J. W., Kwon, K., Azizi, A., Oh, H–M, Kim, W., Bahk, J–J, et al. (2013). Microbial community structures of methane hydrate–bearing sediments in the Ulleung Basin, East Sea of Korea. *Mar. Petroleum Geol.* 47, 136–146. doi: 10.1016/j.marpetgeo.2013.06.002

Liu, X. L., Lipp, J. S., Simpson, J. H., Lin, Y. S., Summons, R. E., and Hinrichs, K–U. (2012a). Mono– and dihydroxyl glycerol dibiphytanyl glycerol tetraethers in marine sediments: Identification of both core and intact polar lipid forms. *Geochim. Et Cosmochim. Acta* 89, 102–115. doi: 10.1016/j.gca.2012.04.053

Liu, Y. F., Qi, Z., Shou, L. B., Liu, J. F., Yang, S. Z., Gu, J. D., et al. (2019). Anaerobic hydrocarbon degradation in candidate phylum 'Atribacteria' (JS1) inferred from genomics. *ISME J.* 13, 2377–2390. doi: 10.1038/s41396-019-0448-2

Liu, X. L., Summons, R. E., and Hinrichs, K–U. (2012b). Extending the known range of glycerol ether lipids in the environment: structural assignments based on tandem mass spectral fragmentation patterns. *Rapid Commun. Mass Spectrometry: RCM* 26 (19), 2295–2302.doi: 10.1002/rcm.6355

Liu, X. L., Zhu, C., Wakeham, S. G., and Hinrichs, K–U. (2014). *In situ* production of branched glycerol dialkyl glycerol tetraethers in anoxic marine water columns. *Mar. Chem.* 166, 1–8. doi: 10.1016/j.marchem.2014.08.008

Luo, M., Gieskes, J., Chen, L. Y., Shi, X. F., and Chen, D. F. (2017). Provenances, distribution, and accumulation of organic matter in the southern Mariana Trench rim and slope: Implication for carbon cycle and burial in hadal trenches. *Mar. Geol.* 386, 486–498. doi: 10.1016/j.margeo.2017.02.012

Magoc, T., and Salzberg, S. L. (2011). FLASH: fast length adjustment of short reads to improve genome assemblies. *Bioinformatics* 27 (21), 2957–2963. doi: 10.1093/bioinformatics/btr507

Nobu, M. K., Dodsworth, J. A., MurugapIran, S. K., Rinke, C., Gies, E. A., Webster, G., et al. (2016). Phylogeny and physiology of candidate phylum 'Atribacteria' (OP9/JS1) inferred from cultivation–independent genomics. *ISME J.* 10, 273–286. doi: 10.1038/ismej.2015.97

Parada, A. E., Needham, D. M., and Fuhrman, J. A. (2016). Every base matters: assessing small subunit rRNA primers for marine microbiomes with mock communities, time series and global field samples. *Environ. Microbiol.* 18 (5), 1403–1414. doi: 10.1111/1462-2920.13023

Peterse, F., Kim, J–H, Schouten, S., Kristensen, D. K., Koç, N., and Sinninghe Damsté, J. S. (2009). Constraints on the application of the MBT/CBT palaeothermometer at high latitude environments (Svalbard, Norway). *Org. Geochem.* 40, 692–699. doi: 10.1016/j.orggeochem.2009.03.004

Peterse, F., van der Meer, J., Schouten, S., Weijers, J. W. H., Fierer, N., Jackson, R. B., et al. (2012). Revised calibration of the MBT–CBT paleotemperature proxy based on branched tetraether membrane lipids in surface soils. *Geochim. Et Cosmochim. Acta* 96, 215–229. doi: 10.1016/j.gca.2012.08.011

Schouten, S., Hopmans, E. C., and Sinninghe Damsté, J. S. (2013). The organic geochemistry of glycerol dialkyl glycerol tetraether lipids: A review. *Org. Geochem.* 54, 19–61. doi: 10.1016/j.orggeochem.2012.09.006

Schwertmann, U. (1993). Relations between iron oxides, soil color, and soil formation. *Soil Color* 31, 51–69. doi: 10.2136/sssaspecpub31.c4

Sinninghe Damsté, J. S. (2016). Spatial heterogeneity of sources of branched tetraethers in shelf systems: The geochemistry of tetraethers in the Berau River delta

(Kalimantan, Indonesia). *Geochim. Cosmochim. Acta* 186, 13–31. doi: 10.1016/j.gca.2016.04.033

Sinninghe Damsté, J. S., Hopmans, E. C., Pancost, R. D., Schouten, S., and Geenevasen, J. A. J. (2000). Newly discovered non–isoprenoid glycerol dialkyl glycerol tetraether lipids in sediments. *Chem. Commun.* 2000, 1683–1684. doi: 10.1039/b004517i

Sinninghe Damsté, J. S., Rijpstra, W. I. C., Foesel, B. U., Huber, K. J., Overmann, J., Nakagawa, S., et al. (2018). An overview of the occurrence of ether– and ester–linked iso–diabolic acid membrane lipids in microbial cultures of the Acidobacteria: Implications for brGDGT paleoproxies for temperature and pH. *Org. Geochem.* 124, 63–76. doi: 10.1016/j.orggeochem.2018.07.006

Sturt, H. F., Summons, R. E., Smith, K. E., Elvert, M., and Hinrichs, K–U. (2004). Intact polar membrane lipids in prokaryotes and sediments deciphered by high–performance liquid chromatography/electrospray ionization multistage mass spectrometry—-new biomarkers for biogeochemistry and microbial ecology. *Rapid Commun. Mass Spectrometry: RCM* 18 6, 617–628. doi: 10.1002/rcm.1378

Summons, R. E., Welander, P. V., and Gold, D. A. (2022). Lipid biomarkers: molecular tools for illuminating the history of microbial life. *Nat. Rev. Microbiol.* 20, 174–185. doi: 10.1038/s41579-021-00636-2

Sun, C. R., Zhang, C. L., Li, F. Y., Wang, H. Y., and Liu, W. G. (2016). Distribution of branched glycerol dialkyl glycerol tetraethers in soils on the Northeastern Qinghai-Tibetan Plateau and possible production by nitrite-reducing bacteria. *Sci. China Earth Sci.* 59, 1834–1846. doi: 10.1007/s11430-015-0230-2

Ta, K. W., Peng, X. T., Xu, H. C., Du, M. R., Chen, S., Li, J. W., et al. (2019). Distributions and sources of glycerol Dialkyl Glycerol Tetraethers in sediment cores from the mariana subduction zone. *J. Geophysical Res.: Biogeosci.* 124, 857–869. doi: 10.1029/2018JG004748

Takai, K., and Horikoshi, K. (2000). Rapid detection and quantification of members of the archaeal community by quantitative PCR using fluorogenic probes. *Appl. Environ. Microbiol.* 66, 5066–5072. doi: 10.1128/AEM.66.11.5066-5072.2000

Tian, J., Fan, L., Liu, H., Liu, J., Li, Y., Qin, Q., et al (2018). A nearly uniform distributional pattern of heterotrophic bacteria in the Mariana Trench interior. *Deep Sea Res. Part I Oceanogr. Res. Papers* 142, 116–126. doi: 10.1016/j.dsr.2018.10.002

Tierney, J. E., and Russell, J. M. (2009). Distributions of branched GDGTs in a tropical lake system: Implications for lacustrine application of the MBT/CBT paleoproxy. *Org. Geochem.* 40 (9), 1032–1036. doi: 10.1016/j.orggeochem.2009.04.014

Wang, H. Y., Dong, H. L., Zhang, C. L., Jiang, H. C., and Liu, W. G. (2016). A 12-kyr record of microbial branched and isoprenoid tetraether index in Lake Qinghai, northeastern Qinghai-Tibet Plateau : Implications for paleoclimate reconstruction. *Sci. China Earth Sci.* 59 (5), 951–960. doi: 10.1007/s11430-015-5213-4

Wang, H. Y., Liu, W. G., and Zhang, C. L. (2014). Dependence of the cyclization of branched tetraethers on soil moisture in alkaline soils from arid–subhumid China: implications for palaeorainfall reconstructions on the Chinese Loess Plateau. *Biogeosciences* 11, 6755–6768. doi: 10.5194/bg-11-6755-2014

Wang, H. Y., Liu, W. G., Zhang, C. L., Liu, Z. H., and He, Y. X. (2013). Branched and isoprenoid tetraether (BIT) index traces water content along two marsh-soil transects surrounding Lake Qinghai: Implications for paleo-humidity variation. *Org. Geochem.* 59, 75–81. doi: 10.1016/j.orggeochem.2013.03.011

Weber, Y., Sinninghe Damsté, J. S., Zopfi, J., De Jonge, C., Gilli, A., Schubert, C. J., et al. (2018). Redox–dependent niche differentiation provides evidence for multiple bacterial sources of glycerol tetraether lipids in lakes. *Proc. Natl. Acad. Sci.* 115, 10926–10931. doi: 10.1073/pnas.1805186115

Weijers, J. W. H., Panoto, E., van Bleijswijk, J. D. L., Schouten, S., Rijpstra, W. I. C., Balk, M., et al. (2009). Constraints on the biological source(s) of the orphan branched tetraether membrane lipids. *Geomicrobiol. J.* 26, 402–414. doi: 10.1080/01490450902937293

Weijers, J. W. H., Schefuß, E., Kim, J–H, Sinninghe Damsté, J. S., and Schouten, S. (2014). Constraints on the sources of branched tetraether membrane lipids in distal marine sediments. *Org. Geochem.* 72, 14–22. doi: 10.1016/j.orggeochem.2014.04.011

Weijers, J. W. H., Schefuß, E., Schouten, S., and Sinninghe Damsté, J. S. (2007b). Coupled thermal and hydrological evolution of tropical Africa over the last deglaciation. *Science* 315, 1701–1704. doi: 10.1126/science.1138131

Weijers, J. W. H., Schouten, S., Donker, J. C., Hopmans, E. C., and Sinninghe Damsté, J. S. (2007a). Environmental controls on bacterial tetraether membrane lipid distribution in soils. *Geochim. Cosmochim. Acta* 71, 703–713. doi: 10.1016/j.gca.2006.10.003

Weijers, J. W. H., Schouten, S., Hopmans, E. C., Geenevasen, J. A. J., David, O. R. P., Coleman, J. M., et al. (2006). Membrane lipids of mesophilic anaerobic bacteria thriving in peats have typical archaeal traits. *Environ. Microbiol.* 8 (4), 648–657. doi: 10.1111/j.1462-2920.2005.00941.x

Wu, J., Yang, H., Pancost, R. D., Naafs, B. D. A., Qian, S., Dang, X. Y., et al. (2021). Variations in dissolved O2 in a Chinese lake drive changes in microbial communities and impact sedimentary GDGT distributions. *Chem. Geol.* 579, 120348. doi: 10.1016/j.chemgeo.2021.120348

Xiao, W. J., Wang, Y. S., Liu, Y. S., Zhang, X., Shi, L., and Xu, Y. P. (2020). Predominance of hexamethylated 6–methyl branched glycerol dialkyl glycerol tetraethers in the Mariana Trench: source and environmental implication. *Biogeosciences* 17, 2135–2148. doi: 10.5194/bg-17-2135-2020

Xiao, W. J., Wang, Y. H., Zhou, S. Z., Hu, L. M., Yang, H., and Xu, Y. P. (2016). Ubiquitous production of branched glycerol dialkyl glycerol tetraethers(brGDGTs) in global marine environments: a new source indicator for brGDGTs. *Biogeosciences* 13, 5883–5894. doi: 10.5194/bg-13-5883-2016

Xiao, W. J., Xu, Y. P., Ding, S., Wang, Y. H., Zhang, X. Y., Yang, H., et al. (2015). Global calibration of a novel, branched GDGT–based soil pH proxy. *Org. Geochem.* 89, 56–60. doi: 10.1016/j.orggeochem.2015.10.005

Xiao, W. J., Xu, Y. P., Lin, J., Zeng, Z. Y., Liu, Y. S., Zhang, H. R., et al. (2022). Global scale production of brGDGTs by benthic marine bacteria: Implication for developing ocean bottom environmental proxies. *Global Planetary Change* 211, 103783. doi: 10.1016/j.gloplacha.2022.103783

Xie, S. T., Liu, X. L., Schubotz, F., Wakeham, S. G., and Hinrichs, K–U. (2014). Distribution of glycerol ether lipids in the oxygen minimum zone of the Eastern Tropical North Pacific Ocean. *Org. Geochem.* 71, 60–71. doi: 10.1016/j.orggeochem.2014.04.006

Xu, Y. P., Jia, Z. H., Xiao, W. J., Fang, J. S., Wang, Y. S., Luo, M., et al. (2020). Glycerol dialkyl glycerol tetraethers in surface sediments from three Pacific trenches: Distribution, source and environmental implications. *Org. Geochem.* 147, 104079. doi: 10.1016/j.orggeochem.2020.104079

Yang, H., Pancost, R. D., Dang, X. Y., Zhou, X. Y., Evershed, R. P., Xiao, G. Q., et al. (2014). Correlations between microbial tetraether lipids and environmental variables in Chinese soils: Optimizing the paleo-reconstructions in semi-arid and arid regions. *Geochim. Cosmochim. Acta* 126, 49–69. doi: 10.1016/j.gca.2013.10.041

Zell, C., Kim, J–H, Hollander, D. J., Lorenzoni, L., Baker, P. A., Silva, C. G., et al. (2014). Sources and distributions of branched and isoprenoid tetraether lipids on the Amazon shelf and fan: Implications for the use of GDGT–based proxies in marine sediments. *Geochim. Cosmochim. Acta* 139, 293–312. doi: 10.1016/j.gca.2014.04.038

Zeng, Z. R., Chen, H., Yang, H., Chen, Y. F., Yang, W., Feng, X., et al. (2022). Identification of a protein responsible for the synthesis of archaeal membrane–spanning GDGT lipids. *Nat. Commun.* 13. doi: 10.1038/s41467-022-29264-x

Zhang, C. L., Wang, J. X., Dodsworth, J. A., Willianms, A. J., Zhu, C., Hinrichs, K–U, et al. (2013). *In situ* production of branched glycerol dialkyl glycerol tetraethers in a great basin hot spring (USA). *Front. Microbiol.* 4. doi: 10.3389/fmicb.2013.00181

Zhang, C. L., Wang, J. X., Wei, Y. L., Zhu, C., Huang, L. Q., and Dong, H. L. (2012). Production of branched tetraether lipids in the lower pearl river and estuary: effects of extraction methods and impact on bGDGT proxies. *Front. Microbiol.* 2. doi: 10.3389/fmicb.2011.00274

Zhao, Y. P., Liu, S. F., Jiang, B., Feng, Y., Zhu, T., Tao, H. C., et al. (2018). Genome–centered metagenomics analysis reveals the symbiotic organisms possessing ability to cross–feed with anammox bacteria in anammox consortia. *Environ. Sci. Technol.* 52 (19), 11285–11296. doi: 10.1021/acs.est.8b02599

Zheng, F., Zhang, C. L., Chen, Y. F., Li, F. Y., Ma, C. L., Pu, Y., et al. (2016). Branched tetraether lipids in Chinese soils: Evaluating the fidelity of MBT/CBT proxies as paleoenvironmental proxies. *Sci. China Earth Sci.* 59 (7), 1353–1367. doi: 10.1007/s11430-016-5268-x

Zhu, C., Lipp, J. S., Wörmer, L., Becker, K. W., Schröder, J. M., and Hinrichs, K–U. (2013). Comprehensive glycerol ether lipid fingerprints through a novel reversed phase liquid chromatography–mass spectrometry protocol. *Org. Geochem.* 65, 46–45. doi: 10.1016/j.orggeochem.2013.10.002

frontiers | Frontiers in Marine Science

TYPE Original Research
PUBLISHED 22 December 2023
DOI 10.3389/fmars.2023.1304624

Check for updates

OPEN ACCESS

EDITED BY
Li Jianlon,
Shandong University, China

REVIEWED BY
Patrick Biber,
University of Southern Mississippi, United States
Ping Gao,
Ministry of Natural Resources, China

*CORRESPONDENCE
Karl J. Indest
karl.j.indest@usace.army.mil

RECEIVED 29 September 2023
ACCEPTED 06 December 2023
PUBLISHED 22 December 2023

CITATION
Weingarten EA, Jung CM, Crocker FH, Kneer ML, Hurst NR, Chappell MA, Berkowitz JF and Indest KJ (2023) Connecting coastal wetland microbial community characteristics with soil physicochemical properties across an estuarine salinity and vegetation gradient in Mobile Bay, AL, USA.
Front. Mar. Sci. 10:1304624.
doi: 10.3389/fmars.2023.1304624

COPYRIGHT
© 2023 Weingarten, Jung, Crocker, Kneer, Hurst, Chappell, Berkowitz and Indest. This is an open-access article distributed under the terms of the Creative Commons Attribution License (CC BY). The use, distribution or reproduction in other forums is permitted, provided the original author(s) and the copyright owner(s) are credited and that the original publication in this journal is cited, in accordance with accepted academic practice. No use, distribution or reproduction is permitted which does not comply with these terms.

Connecting coastal wetland microbial community characteristics with soil physicochemical properties across an estuarine salinity and vegetation gradient in Mobile Bay, AL, USA

Eric A. Weingarten, Carina M. Jung, Fiona H. Crocker, Marissa L. Kneer, Nia R. Hurst, Mark A. Chappell, Jacob F. Berkowitz and Karl J. Indest*

Environmental Laboratory, U.S. Army Engineer Research and Development Center, Vicksburg, MS, United States

Coastal wetlands provide a variety of ecological functions that sustain biodiverse habitats, serve as barriers to storm surge, regulate biogeochemical cycles, and yield ecosystem goods and services that benefit society. The magnitude of wetland functional delivery varies with geomorphology and landscape position, hydropattern and hydrodynamics, vegetation structure and composition, soil properties, and microbial community assemblages and activities. Here we describe soil physicochemical and microbial diversity along a vegetation and salinity gradient in the Mobile Bay estuary, AL, USA and discuss how these factors feedback on ecosystem characteristics and the delivery of ecological functions. We incorporated microbial biomass, diversity, and community composition into patterns of dominant vegetation cover type and soil properties. Stepwise model selection using permutation tests indicated that vegetation type >> soil horizon > and salinity strongly influenced microbe-soil relationships. The dominant variables governing microbial content were total sulfur concentration in surface soils and nitrate and nitrite (NO_x) for subsurface soils. All biotic and abiotic variables indicated that seasonally inundated forested wetlands represented a distinct microbial biome within the Mobile Bay estuary compared to more frequently flooded and increasingly salt-tolerant *Typha*, tidal shrub, and *Juncus* wetland types. Compared with the other wetland types examined for this study, forested wetlands contained ~80% less organic carbon content, ~75% less nitrogen,

~33% less phosphorus, and ~95% less sulfur. Our results show the benefit of incorporating microbial trait data, including metataxonomics, enzymatics, and biomass, with other ecosystem properties such as vegetation and soil characterization data.

KEYWORDS

wetlands, sea level rise, sediment microbiome, physicochemistry, estuary, plant-microbe, plant-microbe-soil

1 Introduction

Wetlands display unique characteristics due to their geomorphic position at the interface of terrestrial and aquatic ecosystems, representing one of the planet's most productive and dynamic landforms (Mitsch and Gosselink, 2015). Wetlands provide a diverse array of societally beneficial ecosystem functions, including natural infrastructure that dissipates wave energy, reduces storm surge, and provides storage for floodwaters; a biogeochemically reactive "core" that cycles nutrients, sequesters carbon, and retains and transforms elements and compounds; and habitat functions that support a wide array of fish and wildlife species (Smith et al., 1995). However, the degree to which wetlands deliver these valuable ecosystem functions varies widely based on intersections of the substrate supporting the wetland, water quality and hydropattern, and the biota utilizing the system. For example, wave attenuation mechanisms differ between dense stands of herbaceous vegetation, i.e., healthy salt marsh, and a more sparsely vegetated forested wetland characterized by large trees (Feagin et al., 2011). As a result, wetland classification schemes evolved to characterize these systems using readily observable differences in substrates, water sources and hydrodynamics, and vegetation community composition (Cowardin, 1979). For several decades, wetland classification approaches have linked wetland hydrogeomorphology with ecological functional capacity, providing opportunities to evaluate the current condition of wetlands and estimate the implications of natural or anthropogenic perturbations to wetland performance (Brinson et al., 1995).

Coastal zone impacts from both natural and anthropogenic disturbances influence the functional capacity of wetlands (Hauser et al., 2015). As the anticipated changes in coastal ecosystem forcings (e.g., intensifying storms) continue to accelerate, linking potential shifts in wetland habitat type to underlying functional outcomes becomes increasingly important (Day et al., 2008). Predicting shifts in coastal ecosystem habitats and wetland functions is of interest to various stakeholders, including agricultural and aquacultural producers, conservation groups, homeowners, businesses, and other entities (Jurjonas and Seekamp, 2018). Additionally, the United States Department of Defense maintains over 1200 military installations in the United States, disproportionately located in coastal zones (valued at up to 100 billion USD), and vulnerable to modest increases in coastal inundations (~1 m, Union of Concerned Scientists, 2016). Current efforts are underway to improve the resiliency of military infrastructure under future climate scenarios (Bassetti et al., 2022). However, a paucity of information exists regarding the underlying mechanisms associated with shifts in wetland types and functions. The research described here focused on determining the relationships among ecological components (i.e., soil characteristics, vegetation community composition, and microbial traits) that combine to deliver wetland functions.

Most critical ecosystem functions provided by wetlands are directly related to soil microorganism dynamics, including carbon mineralization, nutrient cycling, and primary production, with recent attention focused on including microbial data in ecosystem modeling (Louis et al., 2016; Blankinship et al., 2018; Sulman et al., 2018). Historically, considerations of microbial traits included a combination of laboratory and field-derived parameters such as growth rate, biomass, maintenance and growth, respiration, and soil enzyme activity (Wallenstein and Hall, 2012). More recently, high throughput sequencing approaches combined with bioinformatic analysis and computational modeling have been used to extract discreet functional traits from *in situ* soil microbial communities to elucidate the specific genera and associated biochemical pathways involved in carbon mineralization and nutrient cycling (Malik et al., 2020 and references therein). Integrating microbial trait data with more traditional wetland classification methods, leveraging historic hydrogeomorphology with more recent bioinformatics, presents new opportunities for estimating wetland spatial and functional changes.

Our study site, located at Mobile Bay, Alabama, USA, represents both the second-largest estuary and the primary depositional basin for the sixth-largest river system in the United States. Mobile Bay is a managed, working estuary where maintenance dredging of the rivers and harbor and other activities occur to support navigation for commercial and economic development (Berkowitz et al., 2019). In addition, the area provides a convenient example of a dynamic yet vulnerable ecosystem that receives significant freshwater and associated sediment inputs in the upper portion of the Bay yet is subjected to periodic saltwater pulses and coastal inundation from storms in the Gulf of Mexico in its lower and mid-bay. As a result, the ecosystem trajectory of Mobile Bay is in constant flux between processes that

either nourish or degrade the estuary, resulting in a diverse number (>40) of distinct wetland habitat types (Berkowitz at el., 2019).

To better understand wetland functional processes operating within Mobile Bay and the potential for shifts in wetland form and function as the result of climate instability or other perturbations, soil core samples were collected throughout along a salinity gradient to evaluate relationships between vegetation community composition, soil geochemical characteristics, and microbial trait data that inform our understanding of ecological function. We hypothesized that soil geochemistry and microbial community composition, diversity, and activity reflected patterns in vegetation coverage that may be altered under future climate scenarios. To test this hypothesis, we characterized the soil and microbial community characteristics of freshwater forested wetlands and three increasingly salt-tolerant wetland types.

2 Materials and methods

2.1 Sample location and collection

All soil samples were collected from the Mobile Bay estuary April 20-21, 2021. Low tide was ~0700 and high tide was ~1800. Each collection day ran ~1000-1400 to align with lowest possible water levels (<30 cm) and to keep daily tidal inundation between sites as consistent as possible. Sample locations were identified using wetland plant community maps described in Berkowitz et al. (2020), targeting the commonly encountered wetland types in the Bay while representing the wide gradient of vegetation salinity tolerances observed in the region (tolerance values derived from USDA, 2000). The elevation distribution of wetland plant communities was determined based on digital elevation mapping (Berkowitz et al., 2020). Samples were all collected within <50 km proximity of each other (Figure 1). Soil cores were collected at (i) triplicate freshwater hardwood forest wetlands (total of n=17 soil cores; salinity tolerance range for optimal growth = 0.0-1.3 ppt), (ii) triplicate *Typha domingensis* dominated emergent wetlands (n=18; 1.31-2.59 ppt), (iii) four replicate tidal shrub wetlands characterized by a mixture of herbaceous species interspersed with small pockets of sparse woody plants (n=24; 2.6-6.4 ppt), and (iv) triplicate *Juncus roemerianus* marshes (n=17; >6.4 ppt). Clear 60 cm long, 10 cm diameter core tubes were inserted into the soil, excavated, and sealed at both ends with rubber caps. Surface and subsurface horizons were identified based on the location of the organo-mineral interface. Cores were stored at 4°C prior to processing. The cores were processed as follows: The exterior tubing of each core was rinsed with 70% EtOH and cores were separated along the longitudinal axis allowing access to both surface and subsurface horizons. All soil cores were first subsampled for DNA analysis. The remaining soil material from each replicated sample location was separated by horizon, transferred to sterile bags, and manually mixed for physicochemical analysis.

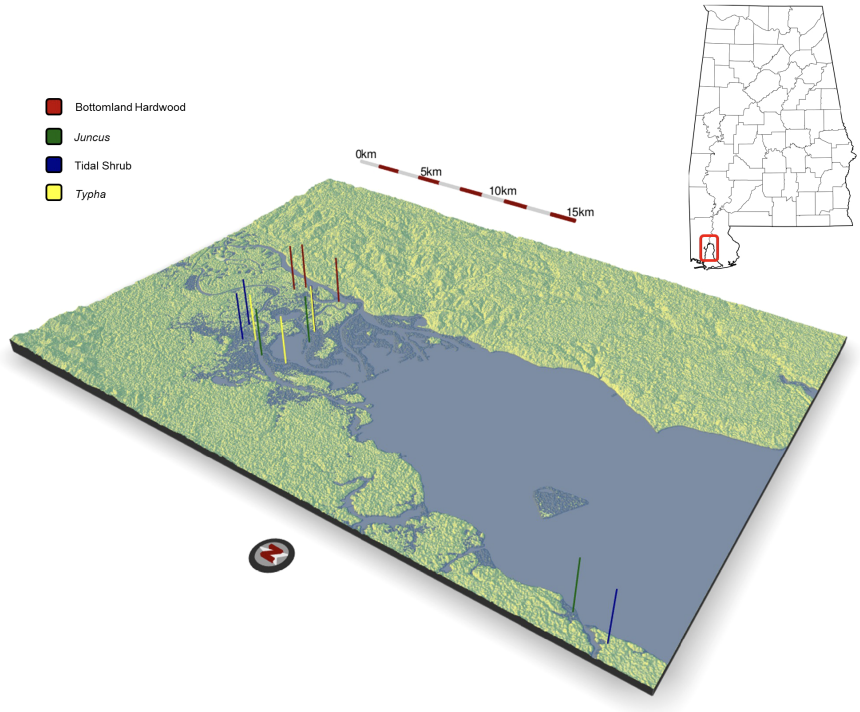

FIGURE 1
Topographic relief map of the upper Mobile Bay estuary where sediment samples were collected in April, 2021 from n=3 hardwood forest sites, n=3 *Juncus* sp. sites, n=4 tidal shrub sites, and n=3 *Typha* sp. sites. All sites were located within a distance <50 km. Map generated using the *rayshader* package in R.

2.2 Physicochemical analysis

Phospholipid fatty acid analysis (PLFA) was performed by Microbial Insights (Knoxville, TN) on 26 composited samples representing each marsh vegetation type. Viable microbial biomass was inferred from total PLFA biomarker abundance. Eukaryote abundance was inferred from polyenoic PLFA abundance. Metal reducer abundance was inferred from branched monomeric PLFA abundance. Modifications of monoenoic PLFAs which are abundant in Proteobacteria were used to infer growth rate and membrane permeability. Microbial biomass, reported as a cell count, was used to estimate microbiological abundance and activity in the sediment. Eukaryote abundance was used to estimate which wetland environment contained the most fungi relative to bacteria and archaea. Metal reducer abundance was used to infer iron and sulfur cycling as key processes in wetlands. Proteobacterial membrane proteins were used as an inference of total community stress status.

Fifty grams of wet soil from each sampling location were weighed and dried at 70°C until a constant weight was reached. Moisture content was calculated as the percentage of mass lost between wet and dry measurements. Dry bulk density was calculated as the total weight of the soil, corrected for moisture content and the volume of the soil core.

Soil extractable nutrients include nitrate and nitrite (NO_x), ammonium (NH_4^+), and orthophosphate in the soil porewater or ionically complexed with soil particles. Orthophosphate is hereafter referred to as soluble reactive phosphorus (SRP) for the inorganic form of phosphorus directly taken up by plant cells. Nutrients were released from the soil complexes with the addition of KCl salts and measured via colorimetric methods. Analysis was performed via EPA Methods 353.2 Rev. 2.0, 350.1 Rev. 2.0, and 365.1 Rev. 2.0, respectively, for NO_x, NH_4^+, and SRP (O'Dell, 1993) using a SEAL AQ2 Automated Discrete Analyzer (SEAL Analytical, Mequon, WI). Soil organic matter (SOM) content was determined via loss-on-ignition (LOI) at 550°C for 4 h. Soil porewater salinity was measured with a YSI probe from a centrifuged 1:5 slurry of field moist soil and ultrapure water (Steinmuller et al., 2020). Solid-phase organic (TOC) and inorganic (TIC) carbon were determined via a dynamic temperature ramping method with combustion temperatures of 400°C and 900°C, respectively. Analysis was performed via International Organization for Standardization, 2016 using an Elementar Soli TOC Cube (Elementar Americas, Inc., Mt Laurel, NJ). Soil carbon, nitrogen, and sulfur were determined by high-temperature combustion. Analysis was performed via International Organization for Standardization, 1996, AOAC 2012, and International Organization for Standardization, 2000 using an Elementar vario MAX cube (Elementar Americas, Inc., Mt Laurel, NJ).

Extracellular enzyme activity assays were performed using fluorescent 4-methylumbelliferone (MUF) for standardization and fluorescently labeled MUF substrates specific to each of the extracellular enzymes: β-1-4-glucosidase (β-glucosidase); β-N-acetylglucosaminidase (NAGase), and alkaline phosphatase as indicators of C, N, and P cycling, respectively. A 1:78 slurry of soil to Milli-Q water was made and shaken continuously at 25°C in the dark for 1 h to release the enzymes into solution (Kang et al., 2013). An aliquot of the soil slurry was mixed with fluorescently labeled MUF substrate. Excitation/emission wavelengths 360/460 were read on a BioTek Synergy HTX (BioTek Instruments, Inc., Winooski, VT, USA) immediately after mixing the slurry with substrate and after 24 h. Enzyme activities were calculated as converted fluorescence units to moles per gram of dry soil per hour.

2.3 DNA extraction, 16S rRNA gene amplification, and sequencing

In the lab, subsections of each sediment core were taken from the surface and the subsurface horizons using sterile utensils. DNA was extracted from each subsection using a Qiagen DNeasy PowerSoil Kit (Qiagen, Germantown, MD) following the standard protocol with the addition of a 10-minute, 70°C heating step prior to bead beating. PCR amplification of the V4 region of the 16S rRNA gene used the primers (515F/806R) and procedures recommended by the Earth Microbiome Project (Gilbert et al., 2014, https://earthmicrobiome.org/protocols-and-standards/16s/). Amplicons were cleaned using a Wizard SV Gel and PCR cleanup kit (Promega, Madison, WI) and quantified and qualified with NanoDrop. The amplicon library was normalized and prepared for sequencing following the protocol in Caporaso et al. (2011). Sequencing was performed on the Illumina MiSeq platform using a 300-cycle V2 Reagent Kit.

2.4 Sequence data processing

Illumina sequencing data was processed using *DADA2* (Callahan et al., 2016). Read lengths were not truncated to ensure forward and reverse reads could be merged (sequencing used a 300-cycle kit, allowing <50 bp of overlap for ~254 bp V4 16S gene). However, a minimum length filter of 120 bp was set. Reads were pseudo-pooled to preserve resolution of rare taxa. Chimeras as well as merged sequences longer than 256 bp or shorter than 250 bp were removed. Amplicon sequence variants (ASVs) were classified against training set 18 of the Ribosomal Database Project (RDP) database (Maidak et al., 2000). Metagenomic predictions were performed using *PICRUSt2* and the *PICRUSt2_pipeline.py* script (Douglas et al., 2020). Gene families (EC numbers) and KEGG orthologs corresponding to respiration and degradation activity were exported from the output table for analysis. Respiration pathways detected among the KEGG orthologs included aerobic respiration, nitrate reduction, sulfate reduction, methanogenesis, and fermentation. Degradation pathways detected included the breakdown of glucose, xylose, sucrose, and starch. Enzymes responsible for degradation found among the EC gene families included alpha- and beta-galactosidase, alpha- and beta-

glucosidase, alpha-N-acetylglucosiminidase, acid and alkaline phosphatase, cellulase, chitinase, xylanase, and urease.

2.5 Statistical analysis

The effect of sediment horizon and vegetation cover on each measured physicochemical parameter, enzyme assay, and PLFA analysis was first assessed with a MANOVA. As these factors were significant (p<0.001) for all variables, individual ANOVAs were performed for each, followed by a Tukey posthoc test to determine pairwise differences. Correlations between the physicochemical conditions were tested using the *cor.mtest* function in the *corrplot* package. *P*-values were adjusted for multiple comparisons using the Benjamini, Hochberg, and Yekutieli method to control for the false discovery rate. Correlations between taxonomic abundance, inferred functional groups, and physicochemistry were determined using the same significance methods.

A phylogenetic tree of the 5,000 most abundant ASVs was created using the neighbor-joining method with the *NJ* and *optim.pml* functions in the *phangorn* package. A GTR substitution model was selected by comparing AIC scores returned by the *modelTest* function. Bray-Curtis, Jaccard, and weighted UniFrac distance matrices were generated using the distance function in the *phyloseq* package. Separate PERMANOVAs were performed with the *adonis2* function in *vegan* for each distance matrix, with overlying vegetation, sediment horizon (surface v. subsurface), and porewater salinity as the independent variables. Pairwise PERMANOVAs were performed as a *post-hoc* test to determine the pairwise differences between plant species using both the *pairwise.adonis* function in the *pairwiseAdonis* package and the *pairwise.perm.manova* function in the *RVAideMemoire* package, with the model producing the higher adjusted *p*-values being selected. NMDS was performed using the *metaMDS* function in *vegan* (k=2, try=50, trymax=500) with returned 2D stress scores of 0.077-0.157.

To test the relative importance of the observed physicochemical parameters on the microbial community, the variance inflation factor (VIF) was used to reduce the effects of multicollinearity. The correlations of porewater salinity, moisture content, depth of the surface soil horizon, bulk density, soluble reactive phosphorus (SRP), nitrate + nitrite (NO_x), ammonium (NH_4^+), total inorganic carbon (TIC), total organic carbon (TOC), percent N, and percent S were initially tested for the surface and subsurface soil horizons separately. Factors were removed stepwise by highest VIF with correlations re-tested until none had VIF >10. The final surface and subsurface soil models were scaled with a zero-center (mean = 0, SD = 1). Distance-based redundancy analysis (dbRDA) was performed using the *dbrda* function (*vegan*) against the retained factor models and with the Bray-Curtis distance matrix as the dependent variable. Final stepwise, bi-directional model selection was done with the *ordistep* function and a permutation test using the *anova.cca* function (*vegan*). Variables were ranked in importance by the AIC scores returned by *ordistep* and *p*-values for each factor were recorded from the permutational ANOVA. All analyses were performed in R Studio with R version 4.2.2.

3 Results

3.1 Soil physicochemistry

Porewater salinity in both the surface and subsurface horizons was higher in herbaceous-dominated wetland soils (*Typha*, tidal shrub, *Juncus*) compared to forested wetland soils, with the difference being more pronounced in the subsurface (α=0.05, Table 1; Figure 2). Forested wetlands possessed the lowest soil moisture content and highest bulk density of the wetland communities. Herbaceous wetland soil contained significantly higher TIC, TOC, and TC concentrations relative to forested wetland soil. Like C, total N and S percentages were highest in herbaceous wetland soils. Soluble Reactive Phosphorus (SRP) was highest in tidal shrub and *Juncus* sediment. Nitrate and nitrite (NO_x) were the only nutrients observed at a significantly higher concentration in forested wetland soil than in herbaceous soil.

Porewater salinity was positively correlated with moisture content, surface horizon depth, TIC, SRP, S percent (p<0.001), TOC, TC (p=0.001), and N percent (p=0.015, Figure 3) and negatively correlated only with bulk density and NO_x (p<0.001). C, N, P, and S nutrient concentrations were higher in the wetter, less dense *sediment* found in the herbaceous wetlands as compared with forested.

3.2 Microbial richness and diversity

A total of 12,916,148 high-quality sequences were recovered from n=151 soil samples, with sequence counts rarefied to 15,425 per sample. Mean and median coverage were 93.9% and 94.0%, respectively. Species richness, measured by ASVs observed, was significantly higher in surface soil (p<0.001), as well as higher in *Typha* and tidal shrub wetlands than in the forested wetland or *Juncus* soils (p<0.03, Figure 4). Community diversity, measured by the Simpson metric, was similarly higher in the surface soil horizons than the subsurface (p=0.001) and higher in *Typha* and tidal shrub than in forested wetland soils (p<0.03). However, there was no statistically significant correlation between porewater salinity and microbial richness (p=0.065) or between porewater salinity and diversity (p=0.280).

3.3 Microbiome composition patterns

Microbial community composition differed significantly between overlying vegetation types (p<0.001), surface and subsurface soil horizon (p<0.001), and porewater salinity (p<0.001) for each beta-diversity metric. Bray-Curtis, Jaccard, and weighted UniFrac distances each showed that the categorical vegetation and horizon factors explained more variation than porewater salinity, but the interaction effects for each combination of these factors was significant as well ($p \leq 0.004$, Table 2). All pairwise comparisons between microbiota of the vegetation types also differed significantly (p adjusted ≤ 0.042, all

TABLE 1 Physicochemical parameters of wetland sediment samples collected from beneath hardwood (n=34), *Typha* sp. (n=36), tidal shrub (n=47), and *Juncus* sp. (n=34).

Depth	Vegetation	Porewater Salinity	Moisture Content	Organic Depth	Bulk Density	SRP	NOx	NH4+	TIC	TOC	TC
Surface	Hardwood	0.118±0.01^{a}	46.5±0.5^{a}	11.4±0.4^{ab}	0.648±0.02^{a}	0.290±0.01^{a}	1.21±0.04^{a}	8.86±0.21^{ab}	0.178±0.01^{a}	3.38±0.01^{a}	3.56±0.00^{a}
	Typha	1.30±0.13^{b}	79.2±1.4^{b}	13.5±0.7^{a}	0.165±0.01^{b}	0.322±0.01^{a}	0.565±0.02^{c}	7.18±0.42^{b}	0.578±0.02^{b}	12.3±1.56^{b}	12.9±1.58^{b}
	Shrub	0.860±0.10^{ab}	82.0±1.0^{b}	9.63±0.3^{b}	0.163±0.01^{b}	0.489±0.04^{bcd}	0.861±0.06^{b}	13.2±1.77^{bcd}	0.574±0.03^{b}	21.3±1.45^{d}	21.9±1.47^{d}
	Juncus	1.29±0.21^{b}	76.6±2.6^{b}	12.9±0.8^{a}	0.228±0.03^{b}	0.381±0.05^{abc}	0.675±0.02^{bc}	3.67±0.11^{a}	0.512±0.01^{bc}	10.5±0.91^{bc}	11.1±0.92^{bc}
Subsurface	Hardwood	0.155±0.01^{a}	39.9±0.8^{a}	NA	0.830±0.01^{c}	0.353±0.00^{ab}	2.55±0.15^{d}	20.2±3.13^{c}	0.131±0.00^{a}	1.62±0.01^{a}	1.75±0.01^{a}
	Typha	1.55±0.15^{b}	61.9±4.7^{c}	NA	0.492±0.07^{d}	0.419±0.03^{abc}	0.547±0.05^{c}	8.74±1.13^{abd}	0.446±0.05^{c}	5.98±0.80^{ac}	6.42±0.79^{ac}
	Shrub	1.66±0.14^{b}	76.4±1.7^{b}	NA	0.248±0.02^{b}	0.574±0.06^{d}	0.506±0.01^{c}	16.5±3.08^{cd}	0.5490.01^{b}	23.4±1.89^{d}	23.9±1.88^{d}
	Juncus	3.16±0.55^{c}	79.9±0.1^{b}	NA	0.210±0.00^{b}	0.528±0.02^{cd}	0.603±0.03^{c}	9.46±0.79^{abd}	0.580±0.01^{b}	10.1±0.24^{bc}	10.7±0.25^{bc}

Depth	Vegetation	N%	S%	β-glucosidase	NAGase	Phosphatase	Anaerobia Metal Reducers	Eukaryotes	Slowed Growth	Decreased Permeability	Cells
Surface	Hardwood	0.237±0.01^{a}	0.090±0.00^{a}	1150.9±66.9^{ab}	781.30 ±57.9^{ab}	1548.3±177^{a}	2.62±0.10^{a}	5.04±0.49^{a}	1.09±0.07^{a}	0.108±0.01^{ab}	4.82E08 ±2.14E07^{a}
	Typha	0.774±0.15^{bd}	1.32±0.02^{b}	1831.5±215^{a}	1045.6 ±220^{a}	556.48±110^{cd}	1.42±0.03^{b}	4.00±0.55^{a}	0.322±0.05^{b}	0.109±0.01^{a}	4.28E08 ±4.09E07^{ab}
	Shrub	1.16±0.08^{c}	0.973±0.08^{d}	1821.1±101^{a}	973.47 ±67.0^{a}	1179.2±37.7^{ab}	1.69±0.07^{c}	3.65±0.32^{ab}	1.08±0.05^{a}	0.152±0.01^{ab}	3.17E08 ±3.56E07^{b}
	Juncus	0.565±0.05^{ab}	1.49±0.08^{bc}	2673.3±352^{c}	708.13 ±94.2^{abc}	825.21±121^{bc}	1.39±0.05^{b}	3.68±0.22^{ab}	0.630±0.05^{bc}	0.145±0.01^{ab}	3.36E08 ±4.27E07^{b}
Subsurface	Hardwood	0.130±0.00^{a}	0.053±0.00^{a}	597.99±50.2^{b}	328.10 ±59.17^{cd}	1290.8±105^{a}	1.74±0.07^{c}	1.07±0.07^{c}	2.40±0.12^{d}	0.167±0.01^{ab}	1.75E08 ±1.66E07^{c}
	Typha	0.397±0.07^{a}	1.40±0.11^{b}	690.50±87.4^{b}	288.91 ±38.8^{d}	303.90±66.1^{d}	1.35±0.08^{b}	5.04±0.65^{a}	0.418±0.05^{bc}	0.357±0.08^{c}	1.29E08 ±1.09E07^{c}
	Shrub	1.12±0.09^{cd}	1.40±0.02^{b}	833.58±41.3^{b}	569.85 ±25.4^{bcd}	792.90±69.0^{c}	1.32±0.05^{b}	2.00±0.14^{c}	1.07±0.08^{a}	0.186±0.01^{ab}	1.21E08 ±1.29E07^{c}
	Juncus	0.537±0.02^{ab}	1.800.12^{c}	1193.4±256^{ab}	378.84 ±18.3^{bcd}	553.99±38.9^{cd}	0.974±0.04^{d}	2.24±0.15^{bc}	0.653±0.05^{c}	0.230±0.01^{b}	1.48E08 ±2.58E07^{c}

Significant differences in values across vegetation types and sediment horizons are indicated with superscripts (a,b,c,d), where values with shared letters do not differ significantly and values with unshared letters were significantly different.

10.3389/fmars.2023.1304624

10.3389/fmars.2023.1304624

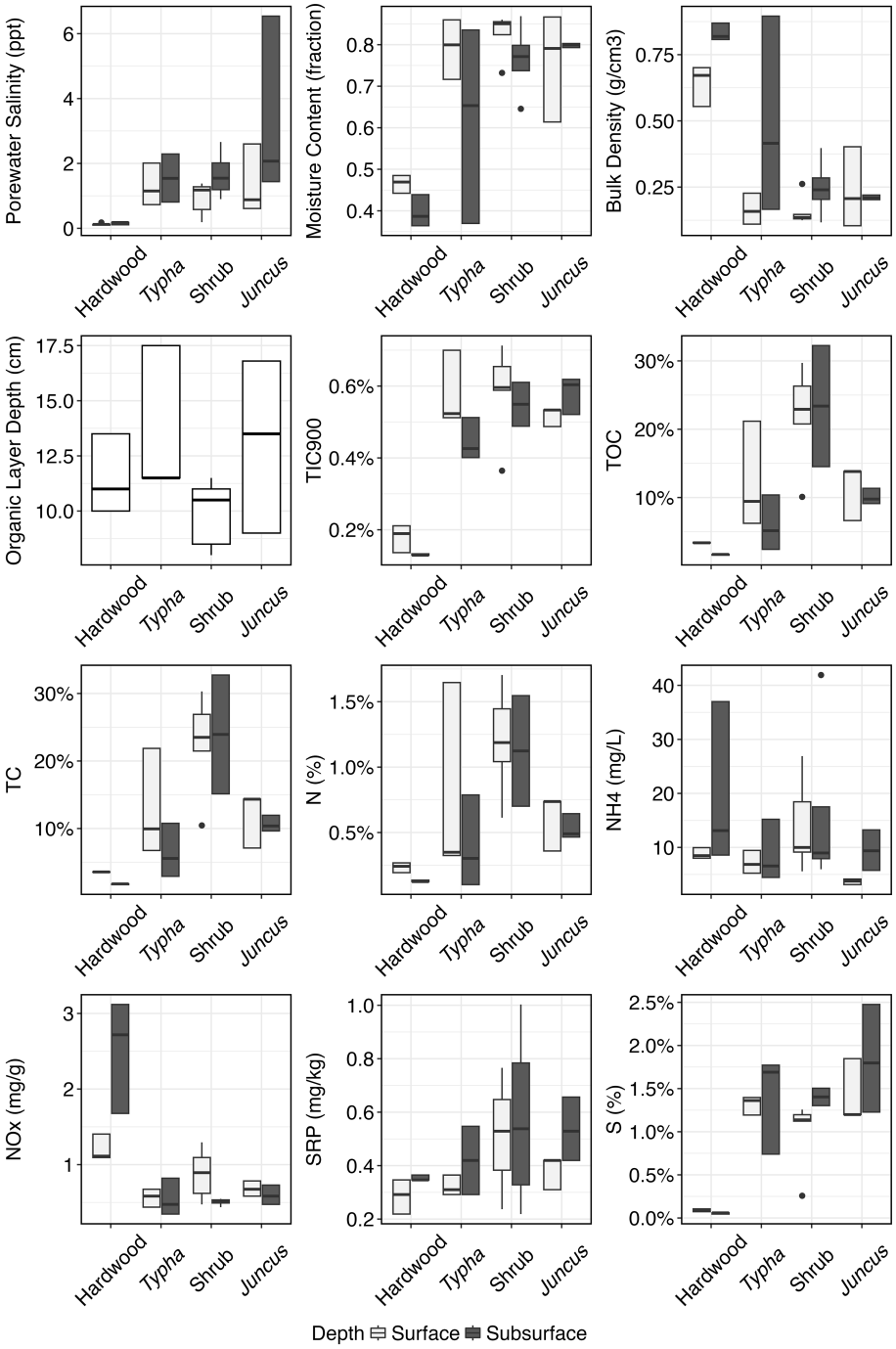

FIGURE 2
Range, lower quartile, median, and upper quartile of the measured physicochemical parameters in hardwood (n=34), *Typha* sp. (n=36), tidal shrub (n=47), and *Juncus* sp.-dominated (n=34) sediment samples. Parameters are plotted separately for the surface, organic soil horizon and the subsurface, mineralized soil horizon.

comparisons, all diversity metrics). More variation was explained for comparisons between forested wetlands and all other wetland types ($R^2 \geq 0.148$, Bray-Curtis) than between *Typha*, tidal shrub, and *Juncus* wetland types ($R^2 \leq 0.093$, Bray-Curtis). The strong differentiation of the forested wetland microbiome was readily observable using NMDS ordination of all metrics (Figure 5). There was also a visible separation of wetland habitat types by porewater salinity, particularly in the Bray-Curtis and Jaccard distance matrices.

Lacking *a priori* hypotheses for the influence of sediment physicochemistry on microbial community structure, model selection via VIF, dbRDA, and automated stepwise model

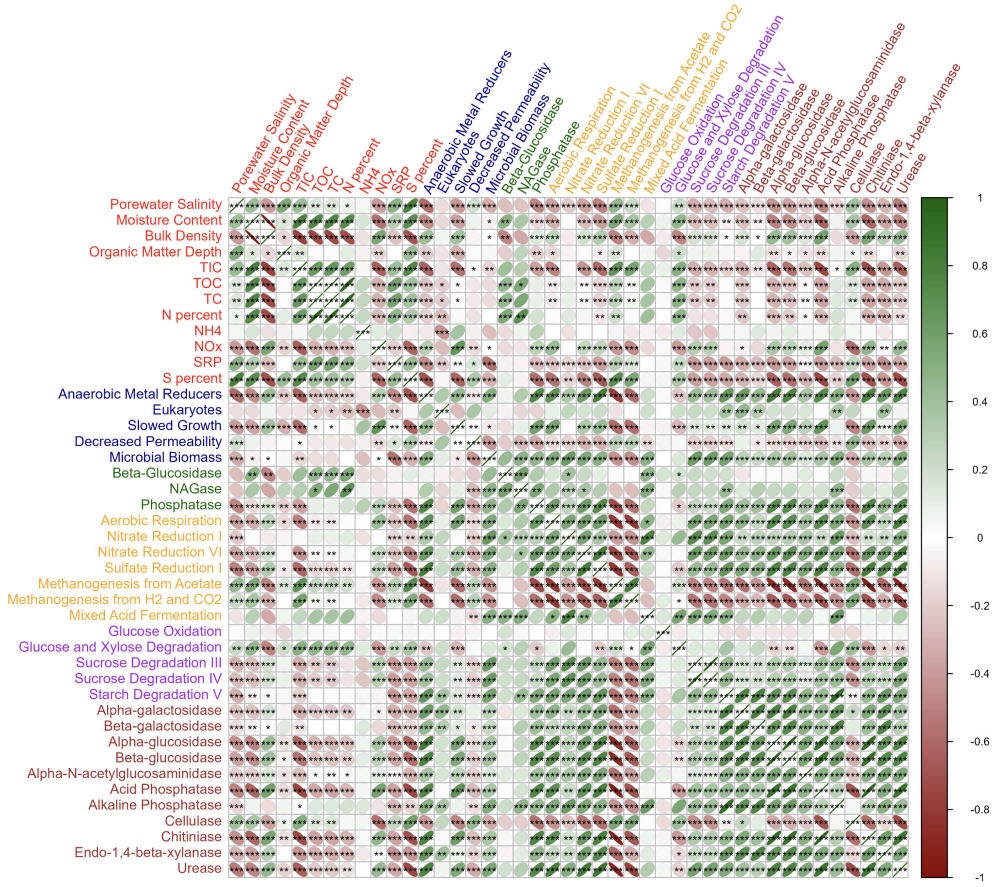

FIGURE 3
Correlation matrix between the measured physicochemical (red labels), PLFA (blue labels), extracellular enzyme activity (green labels), PICRUSt respiration pathways (yellow labels), PICRUSt degradation pathways (purple labels), and PICRUSt degradation enzymes (brown labels) data layers. Negative correlations are shown red and positive correlations shown green. Significance of correlations is denoted *p<0.05, **p<0.01, ***p<0.001. Figure generated with *corrplot* R package.

building began by including all of the measured parameters. Samples were processed separately by whether they came from the surface or subsurface horizon. Ranked by AIC scores, S content, TOC, porewater salinity, NH_4^+, surface horizon depth, and NO_x were the most influential factors explaining the community composition of the surface horizon (Table 3). In the subsurface horizon, NO_x, bulk density, porewater salinity, SRP, and NH_4^+ were the most explanatory environmental variables. Constrained ordination, like NMDS, showed separation of forested wetland soils from the other three wetland types in the first two dimensions (Figure 6). NO_x content was the only factor positively associated with forested wetland microbiota in the surface horizon. At the same time, NO_x, bulk density, and NH_4^+ were positively correlated with forested wetland microbiota in the subsurface horizon. Porewater salinity was strongly correlated with the *Typha*, tidal shrub, and *Juncus* wetland soils in both horizons. There was no visual separation by association with wetland vegetation in dbRDA dimensions 3 and 4; instead, there was a strong separation of individual sites, assumed to be based on local physicochemistry.

3.4 Microbial taxonomy and inferred activity

Of the 39.6% of sequences classified to the family level (~5,114,000), 24 families accounted for >30% of the total dataset (Figure 7). Families which varied in abundance by salinity also showed a strong correlation with bulk density and S content, wherein greater sequence abundance at high salinity also correlated with greater sequence abundance at high S content and low bulk density. This community pattern recapitulates the linkages between high salinity, high S content, and low bulk density, which dominate in the frequent tidal inundation of the mid-bay, where more herbaceous vegetation is found (Figure 8). Families which were at significantly greater abundance in more saline porewater included: Anaerolineaceae, Desulfobacteraceae, Methanomassillicoccaceae, Anaerohalosphaeraceae, Spirochaetaceae, Aggregatilineaceae, Calditrichaceae, and Prolixibacteraceae. Families which were more abundant in low salinity porewater were: Gallionellaceae, Bradyrhizobiaceae, Geobacteraceae, Nitrososphaera, Ktedonobacteraceae, and Methylococcaceae.

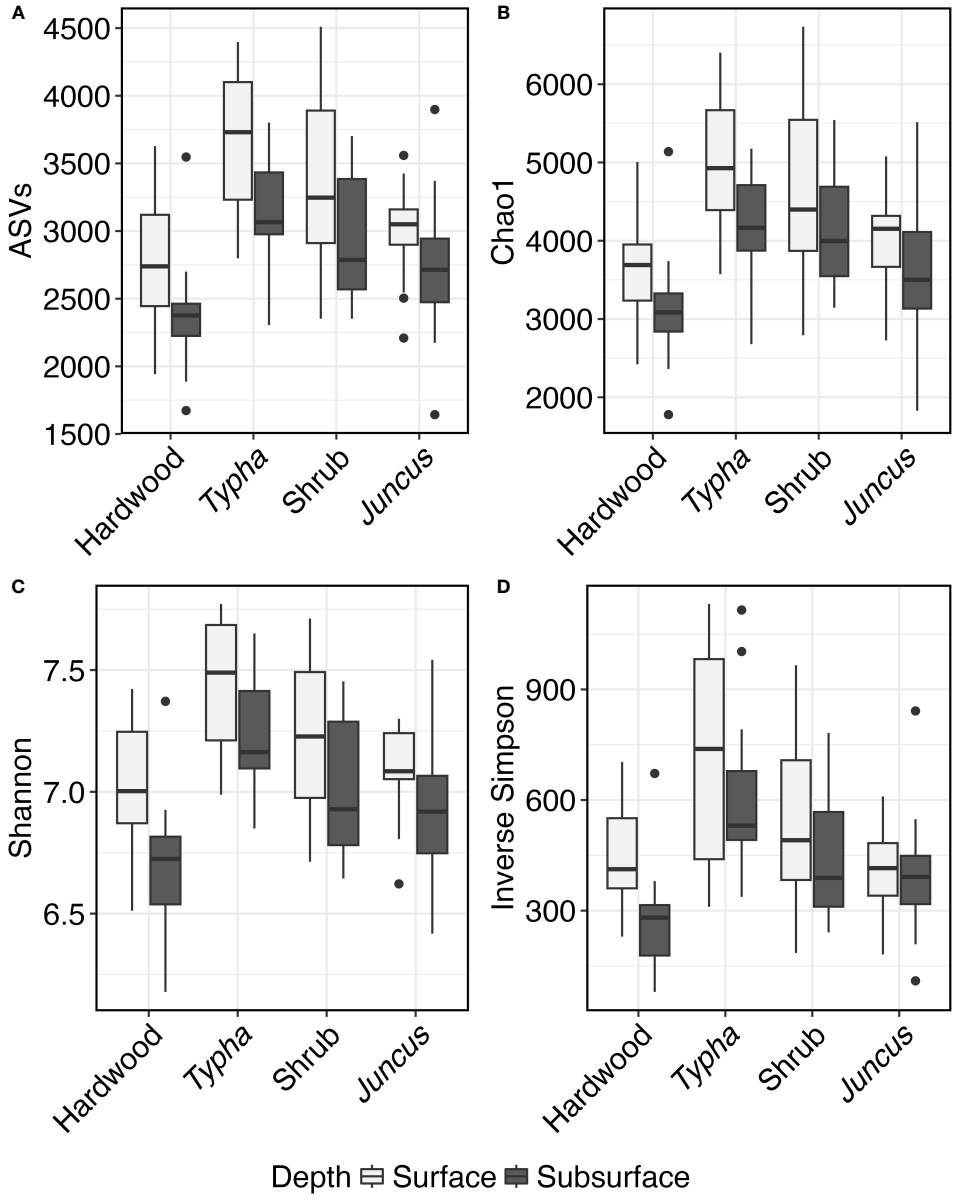

FIGURE 4
Box and whisker plot of Alpha Diversity. Range, lower quartile, median, and upper quartile of the **(A)** number of ASVs, **(B)** Chao1 metric, **(C)** Shannon metric, and **(D)** Inverse Simpson metric of high-quality V4 16S sequences collected from hardwood (n=34), *Typha* sp. (n=36), tidal shrub (n=47), and *Juncus* sp.-dominated (n=34) sediment samples. Alpha diversity scores are plotted separately for the surface, organic soil horizon and the subsurface, mineralized soil horizon.

Decomposition attributable to microbial activity was inferred through direct, fluorometric enzyme assays and PICRUSt functional prediction. Among the measured enzymes, β-glucosidase and phosphatase (p<0.001) differed between wetland types, unlike NAGase (p=0.108). β-Glucosidase activity was highest in the three herbaceous wetland soil types, while phosphatase activity was highest in the forested wetland soils (Figure 9). All of the degradation genes inferred from the 16S marker gene dataset differed significantly in abundance between vegetation types (p<0.042). Derived pathways and genes regulating soil enzymes, such as starch degradation, galactosidase, glucosidase, NAGase, phosphatase, chitinase, xylanase, and urease were all more abundant in hardwood forest soil. Inferred genes controlling metabolism, including aerobic respiration, assimilatory nitrate reduction, and sulfate reduction pathways were all highest in forested wetland soils (p<0.001). Denitrification pathway abundance was highest in herbaceous surface sediment (p=0.047), and methanogenesis pathway abundance was significantly higher in herbaceous subsurface sediment (p<0.001).

3.5 Connecting microbial activity, porewater salinity, and physicochemistry

Fluorometric phosphatase activity decreased significantly with increased porewater salinity, while β-glucosidase and NAGase

TABLE 2 Statistical results of PERMANOVA comparing microbial community composition between vegetation types (hardwood, *Typha*, tidal shrub, and *Juncus*), soil horizons (surface and subsurface), and porewater salinities across Bray-Curtis, Jaccard, and weighted UniFrac beta-diversity measurements.

Beta-Diversity Metric	Environmental Variable	R^2	F	*p*
Bray-Curtis	Vegetation	0.174	13.6	<0.001
	Soil Horizon	0.062	14.6	<0.001
	Porewater Salinity	0.041	9.52	<0.001
Jaccard	Vegetation	0.133	8.4	<0.001
	Soil Horizon	0.045	8.5	<0.001
	Porewater Salinity	0.031	5.85	<0.001
UniFrac	Vegetation	0.377	49	<0.001
	Soil Horizon	0.151	58.9	<0.001
	Porewater Salinity	0.026	10.3	<0.001

showed no relationship (Figure 3). β-glucosidase activity increased significantly with TOC, NAGase activity increased with N percent, but phosphatase activity decreased with SRP. Both aerobic and anaerobic respiration pathways were depressed by salinity, while predicted methanogenesis gene abundance increased with porewater salinity. All degradation pathways were lower in sequence count at high salinity except for cellulose, glucose, and xylose degradation. Similarly, cellulose, glucose, and xylose were the only degradation pathways that positively correlated with TIC, TOC, TC, and surface sediment horizon depth, with all other pathways having much lower abundances in high organic matter conditions. Microbial biomass (as measured by PLFA) decreased with higher salinity and was weakly negatively correlated with C content. All measures of metabolism increased significantly with high biomass, except for methanogenesis and cellulase pathway abundance. All degradation pathway abundances were positively correlated with each other, except for cellulase. Decomposition inferred from predicted gene abundance positively correlated with actual phosphatase activity but did not strongly correlate with either β-glucosidase or NAGase activity.

4 Discussion

4.1 Soil physicochemistry and microbial composition linkages

Freshwater forested wetland soils exhibited notable differences from the other wetland types examined across nearly all measured physicochemical parameters, microbial diversity characteristics, and measures of microbial activity. Porewater salinity remained near zero across all forested wetland soils, which rarely (if ever) experienced short pulses of brackish water during storm events where seawater from the Gulf of Mexico breached Mobile Bay during periods of low riverine water inputs. Conversely, the herbaceous wetland types displayed porewater salinities ranging from ~0.5 ppt to >6 ppt, where a subset of the plant communities can survive much higher salinities (up to 35 ppt in the case of the *Juncus*-dominated marshes). The difference in salinities, and associated soil physicochemical and microbial characteristics, was not unexpected, as forested wetlands occur at higher elevations and receive less tidal and more riverine influence than the other three

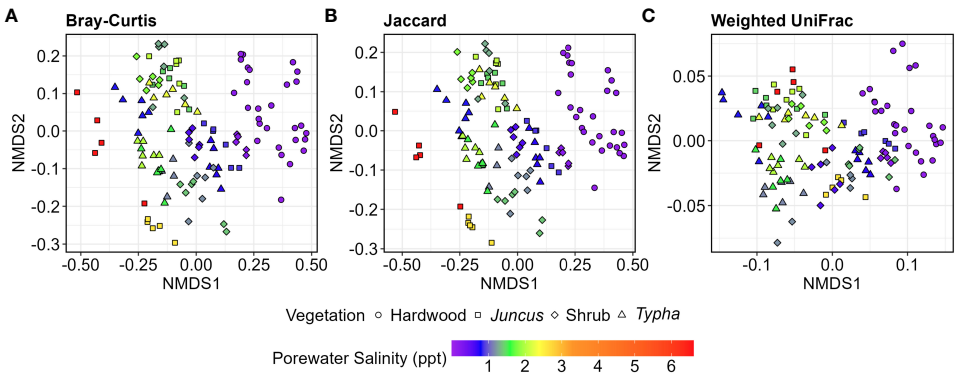

FIGURE 5
NMDS ordinations of V4 16S sequences collected from hardwood (n=34), *Juncus* sp. (n=34), tidal shrub (n=47), and *Typha* sp.-dominated (n=36) sediment samples. **(A)** Bray-Curtis distance, **(B)** Jaccard distance, **(C)** Weighted UniFrac distance of a phylogenetic tree of the 5,000 most abundant ASVs. Porewater salinity ranged 0.0-6.0 ppt and is indicated by color gradient. 2D stress ranged 0.077-0.157.

10.3389/fmars.2023.1304624

TABLE 3 Results of automated stepwise model building, retaining those physicochemical factors which best predicted microbial composition of the organic and mineralized soil horizons, separately.

Depth	Variable	AIC	F	p
Surface	Percent S	217.03	10.4	< 0.001
Surface	TOC	211.96	7.11	< 0.001
Surface	Porewater Salinity	207.93	5.94	< 0.001
Surface	NH4+	205.51	4.23	< 0.001
Surface	Organic Depth	202.62	4.63	< 0.001
Surface	NOx	200.06	4.24	< 0.001
Subsurface	NOx	171.09	9.01	< 0.001
Subsurface	Bulk Density	167.09	6	< 0.001
Subsurface	Porewater Salinity	161.83	7.2	< 0.001
Subsurface	SRP	158.43	5.17	< 0.001
Subsurface	NH4+	156.24	3.9	< 0.001

Retained variables are ranked by Akaike information criterion (AIC) scores. Returned F-scores and p-values also presented.

marsh types. Forested areas are situated at the northern end of Mobile Bay, receiving much higher mineral sediment influxes, as reflected by the much higher bulk densities and lower relative soil organic matter contents (Krauss et al., 2018). All sites co-occurred in the mid-to-upper portions of the Mobile Bay estuary along a salinity gradient with average elevations of forested wetlands (2.42 m), mixed tidal shrub (0.42 m), *Typha* (0.30 m), and *Juncus* (0.17 m). Total C, N, P, and S were each lowest in forested wetland

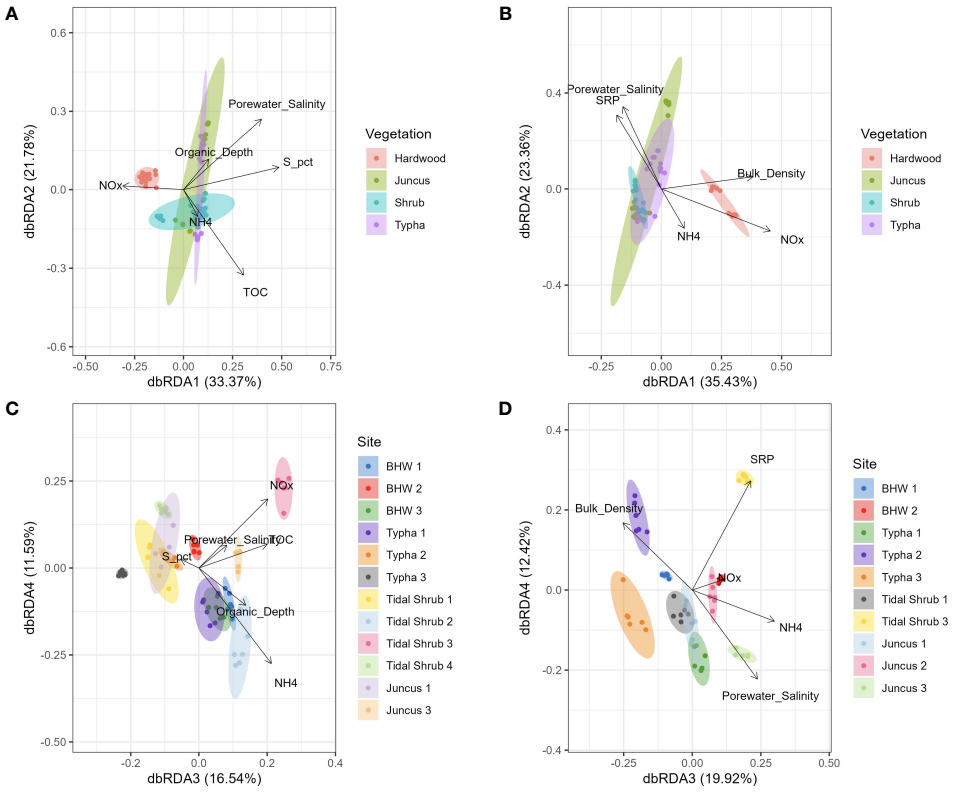

FIGURE 6
Distance-based redundancy analysis (dbRDA, Bray-Curtis distance) constrained ordination of V4 16S sequences collected from hardwood (n=34), *Juncus* sp. (n=34), tidal shrub (n=47), and *Typha* sp.-dominated (n=36) sediment samples. Samples are colored by overlying vegetation for axes 1 and 2 **(A, B)** and by sampling location in axes 3 and 4 **(C, D)**. Ordinations were performed separately for the organic soil horizon **(A, C)** and the mineralized soil horizon **(B, D)**. Arrows indicate microbiome compositional correlation with those physicochemical parameters which best explained composition as returned by the automated model selection.

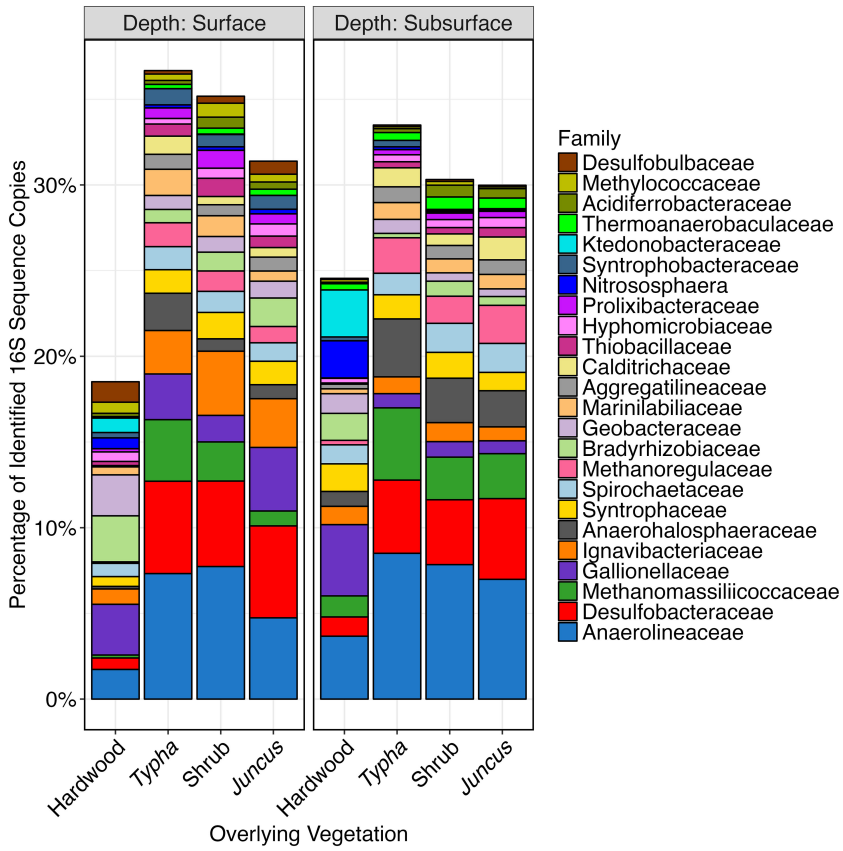

FIGURE 7
Stacked bar plot of V4 16S sequences which were identified to the family taxonomic level and which collectively comprised >30% of the total sequences generated. Samples are ordered by association with hardwood (n=34), *Typha* sp. (n=36), tidal shrub (n=47), and *Juncus* sp. (n=34) and by whether they were collected from the organic soil horizon (n=75) or the mineralized horizon (n=76).

soils where more available nutrients were likely stored in aboveground biomass (Craft, 2012; Noe et al., 2016). Porewater NH_4^+, and particularly NO_x, were the only nutrients measured at higher concentrations in forested soil, likely due to greater exposure to riverine agricultural and cattle sources of N. Higher salinity concentrations can inhibit denitrification rates (~70% decrease by increasing salinity from 1.7 ppt to 3.8 ppt, Neubauer et al., 2019) where nitrate addition dramatically stimulates decomposition (Bulseco et al., 2019), also potentially explaining the high nitrate, low OM dynamics observed in the forested wetland soils, relative to the other wetland types.

Both constrained and unconstrained ordinations of the microbial communities of the four wetland habitats consistently showed the differentiation of forested wetlands from all other wetland types as the primary factor driving dissimilarity. Dominant vegetation types showed a greater influence on microbial composition than either horizon depth or salinity, and pairwise comparisons between forested wetlands and all other wetland types were more dissimilar than comparisons between any other environmental factor. Previous studies have similarly identified vegetation-driven zonation of the wetland microbiome (Rietl et al., 2016), but salinity usually represents the dominant effect in structuring community composition (Ceccon et al., 2019; Liu et al., 2023). In our case, we propose that the salinity gradient in Mobile Bay drives vegetation zonation, representing the primary factor in partitioning microbial content.

Our data suggest that the presence of freshwater forest vegetation, seasonal hydrologic regimes, and high soil mineral content exhibited a deterministic influence on below-ground microbiota. Liu et al. (2020); Liu et al. (2023) investigated similar vegetation-salinity-microbe interactions, and reported a positive correlation between vegetation species diversity and microbial richness along with negative relationships between microbial diversity and higher salinities. Others have reported similar results. For example, Barreto et al. (2018) investigated a wetland plant-microbial community shift that displayed similar microbiome differentiation as the result of woody mangrove species encroachment into adjacent emergent salt marshes, which introduced sources of woody organic matter, root exudates, and increased oxygen delivery to the soils. This mangrove-driven aeration of the rhizosphere and subsequent increase in activity may represent a corollary for the seasonal hydrology of the forested wetland, where seasonal drying allows increased oxygenation. One contrast here was that richness and diversity did not scale well with salinity, again underscoring the primary influence of vegetation in our study.

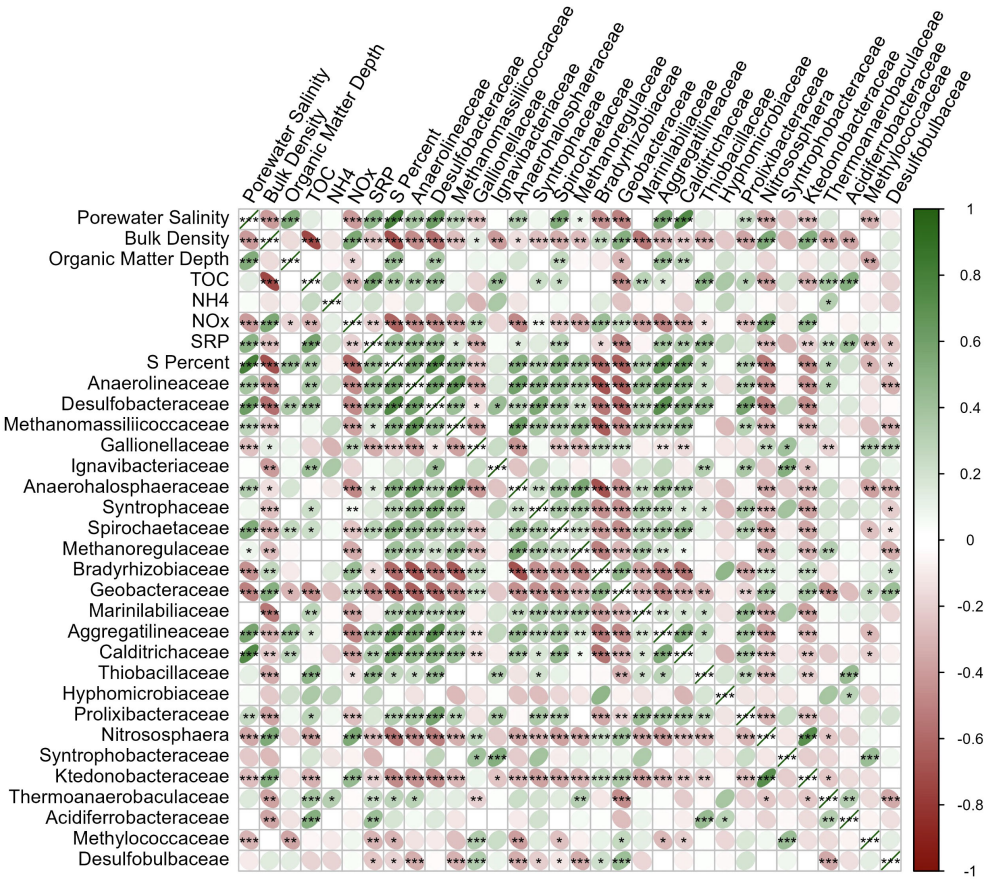

FIGURE 8
Correlation matrix of physicochemistry and those sequences identified to the family taxonomic level which collectively comprised >30% of the total sequences generated. Negative correlations are shown red and positive correlations shown green. Significance of correlations is denoted *p<0.05, **p<0.01, ***p<0.001. Figure generated with *corrplot* R package.

4.2 Comparison of surface and subsurface soil horizons

After vegetation cover, residence in either the surface or subsurface soil horizon was the second most influential factor in microbial composition. The depth of the organic layer at the marsh surface, averaging between approx. 10 and 14 cm, was deeper and contained more organic matter in *Juncus* and *Typha* soils than in tidal shrub or forested wetlands. This observation was consistent with previous descriptions of frequently inundated herbaceous wetland soil horizons (Seybold et al., 2002), suggesting a possible connection between organic horizon depth, microbial activity, and vegetation cover. Higher microbial biomass and inferred activity in the forested wetland may limit the accumulation of organic matter, especially considering that the less flooded, higher-elevation forested wetlands typically receive more allochthonous, nutrient-rich sediment deposition than the lower-elevation marshes (Hupp et al., 2019), but was observed to contain much less organic carbon. Microbial biomass was significantly higher in the surface horizon than in the subsurface layer across all vegetation types, positively correlating with PICRUSt-inferred enzyme activities and direct measurement of the constitutive β-glucosidase and NAGase enzyme activities (Moorhead et al., 2013). There was little difference in the inorganic and organic carbon ratios between the sediment horizons, in agreement with previous studies of coastal wetland soils (Unger et al., 2016).

Sampling wetland soils at arbitrary depth intervals complicates the succeeding microbiology assessment between surface and subsurface horizons. Therefore, selecting sample depth intervals based on pedogenically derived, morphologically distinct layers is often preferable (Premrov et al., 2017). Significant oxygen penetration, which leaves distinct pedomorphological markers, is limited to the top few millimeters in many tidal wetlands (Brodersen et al., 2019), while the forested wetlands experience seasonal periods of aerobic conditions during which rates of organic matter decomposition increase (limiting soil carbon accumulation) (Miao et al., 2017). Thus, differences in microbial composition and activity are likely a function of redox potential and associated organic matter decomposition dynamics, not soil horizon depth. For example, inferred aerobic respiration, nitrate reduction, and sulfate reduction KEGG pathways were more abundant at the soil surface than anaerobic metal reducer abundance (determined by PLFA). This diversity of metabolic pathways captured in the surface layer likely shows that samples collected from the surface soil layer spanned nearly the full extent of the sediment redox potential, which is reasonable within a depth of a few centimeters (Mobilian

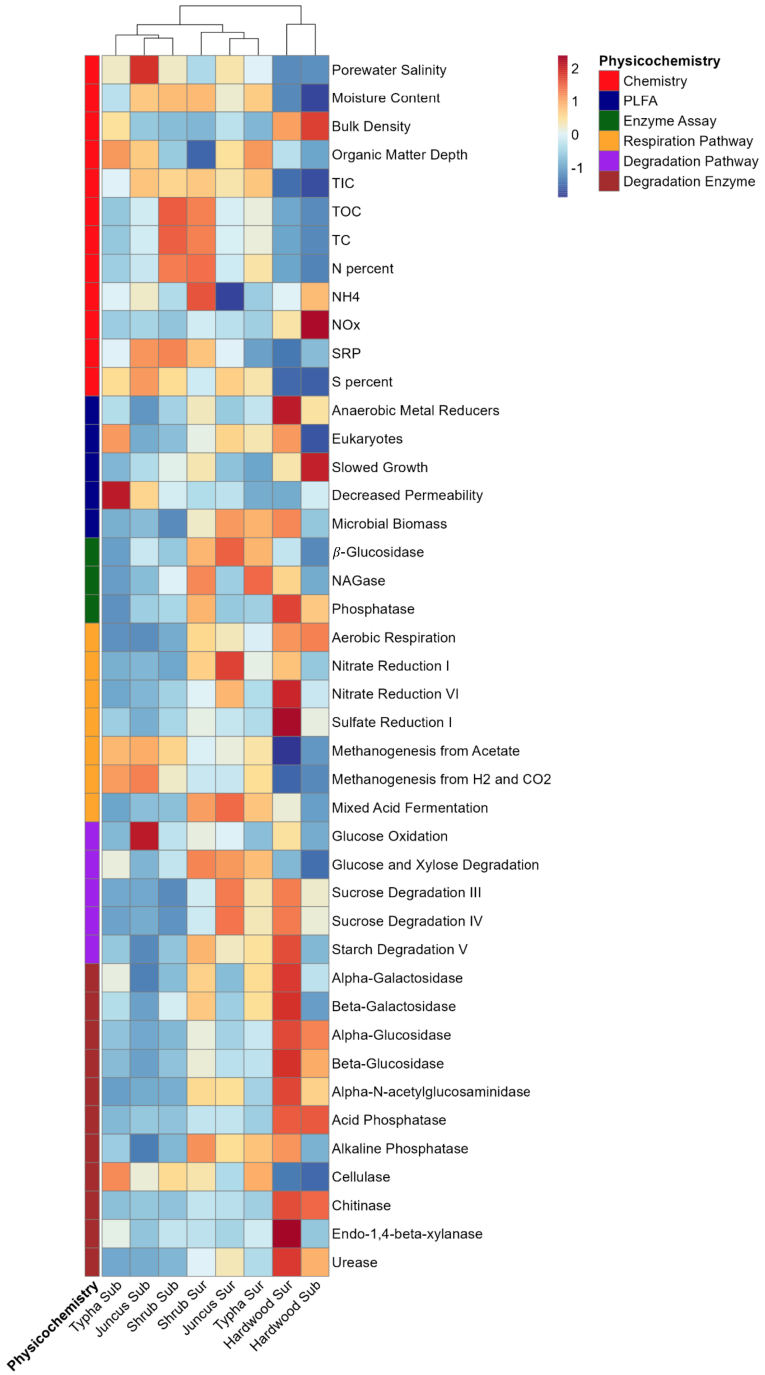

FIGURE 9
Heatmap of physicochemical (red labels), PLFA (blue labels), extracellular enzyme activity (green labels), PICRUSt respiration pathways (yellow labels), PICRUSt degradation pathways (purple labels), and PICRUSt degradation enzymes (brown labels) data layers. Scale is 0-centered and each 1-fold change represents 1 standard deviation from the mean. Columns denote vegetation-association and soil horizon (surface/organic and subsurface/mineralized). Columns are clustered by Euclidean distance. Figure generated with *pheatmap* R package.

and Craft, 2021). Methanogenic pathways were confined mainly to the subsurface horizons, where typically saturated, lower oxidation-reduction conditions prevailed (Megonigal et al., 1993). The forested wetlands represented the grand exception to this pattern, given that aerobic respiration pathways remained abundant in the subsurface and inferred methanogenesis, nitrate, and sulfate reduction pathways were minimal, likely due to the seasonal hydroperiod, and the introduction of oxygen along decomposed root channels and between mineral ped faces (Lahiri and Davidson, 2020). Large pockets of dissolved carbon and nutrients, corresponding to elevated enzyme activity and CO_2-production, were previously observed in wetland subsurface soils, highlighting their capacity for biogeochemical functions such as nutrient cycling and climate regulation (Steinmuller et al., 2019).

4.3 Estimation of salinity and its effect in comparison with vegetation

The four vegetation types were selected to assess plant-microbe abundance patterns, across a gradient of brackish to freshwater porewater salinities. The expected salinity gradient in Mobile Bay based on reported vegetation salinity tolerances was forested wetland < *Typha* < tidal shrub < *Juncus* (USDA (U.S. Department of Agriculture), 2000). As expected, salinity in the subsurface was highest in *Juncus*, followed by shrub and *Typha*, and significantly less in forested wetlands. Salinity was similar in the surface layer across all wetland types, except for *Typha* wetlands which exhibited a higher salinity than the tidal shrub. The salinity difference was sufficient to differentiate the wetland types into three salinity classes, with the forested wetlands exhibiting pure fresh conditions (<0.5 ppt) compared with the herbaceous tidal shrub, *Typha*, and *Juncus* wetlands spanning intermediate to brackish salinity (0.5-6.0 ppt, Howes et al., 2010; Poffenbarger et al., 2011). Fine-scale differentiation of microbial community structure across domains has been observed along wetland salinity gradients previously (Franklin et al., 2017; Zhang et al., 2021). We observed a similarly significant salinity effect in addition to the stronger vegetation cover and sediment horizon effects described above.

Anaerolineaceae was the most frequently observed bacterial family in our study and occurred more frequently at higher salinity. This taxon has been noted as a significant community member under similar salinity and vegetation conditions (Weingarten and Jackson, 2022) and has also been seen to be enriched when wetland salinity is elevated (Wang et al., 2019). Notably, that study also found that the sulfate-reducing order Desulfobacterales formed a close association with Anaerolinaceae in intertidal wetland sediment to promote decomposition under anaerobic and saline conditions. This relationship could be decoupled with the removal of overlying vegetation and it is potentially significant that we observe a similar dynamic along a salinity-vegetation gradient. We observed the family Desulfobacteraceae, a member of the Desulfobacterales, as the second-most-prevalent family in wetland sediment, and like Anaerolineaceae, was more abundant at higher salinity. Syntrophy between these taxa and methanogens promoted anoxic decomposition in Wang et al., and we also observed the methanogenic Methanomassillicoccaceae as the third most abundant family, again being enriched by salinity. We were surprised to observe greater predicted gene abundance for methanogenesis at higher porewater salinities and in association with more salt-tolerant vegetation, but a close relationship with Anaerolineaceae and Desulfobacteraceae abundance may explain this finding.

Microbial biomass was significantly and negatively correlated with porewater salinity. Contrary to prior research showing that microbial biomass is highest in brackish wetlands (Luo et al., 2019), we observed consistently greater microbial biomass in the forested wetland soils. Microbial biomass and C abundance in brackish marsh are potentially connected to a larger pool of plant exudates (Armstrong et al., 2000; Luo et al., 2019), making it possible that the abundance of woody plant material in the forested sites fueled the higher microbial cell abundances. Unlike mangroves, where bacterial alpha diversity is often higher than in proximate freshwater marshes (Zhang et al., 2019), forested wetlands showed lower richness and diversity than the tidal shrub or *Typha* sites. Notably, alpha-diversity metrics were similarly low in *Juncus* sp. vegetated sites, representing low diversity at the two extremes of the observed salinity gradient. This parabolic trajectory of alpha-diversity to salinity has been observed previously (Zhang et al., 2021), but it is notable that in that study, brackish marsh, occupied here by *Juncus* sp., showed the highest diversity. In Zhang et al., the highest observed diversity occurs at ~6,000 μS/cm (3.2 ppt), near the mean salinity of the gradient in that study. We did not attempt to capture the full extent of salinity in Mobile Bay, instead focusing on fresher communities that are more likely to be impacted by saltwater intrusion than those already adapted to higher salinity.

Each of the extracellular enzyme activities and most of the PICRUSt degradation pathways declined with increasing porewater salinity. The same was true for most PICRUSt-inferred metabolic pathways, implying that elevated salinity may have suppressed microbial activity which could explain the higher C content in the herbaceous sites relative to the lower salinity forested sites. A similar relationship was reported from a 28-day salt addition to wetland soil (Qu et al., 2019), with greenhouse gas production and decomposition of OM being lowest in high-salinity treatments. Cellulase was the lone enzyme (PICRUSt-inferred) enriched at higher salinity, as shown previously in response to inundation with saline water (Li et al., 2022). Methanogen abundance and associated methane production are generally negatively correlated with salinity (Sutton-Grier et al., 2011; He et al., 2022), but inferred methanogenesis was the lone metabolic pathway positively correlated with porewater salinity here. This observation was likely due to the much higher moisture content in the herbaceous sediment compared to seasonally flooded freshwater forested wetlands, with methane production strongly favored under strongly reducing conditions (Neubauer et al., 2013), in addition to potential inter-taxa cooperation described above.

4.4 Connecting microbial composition and function with physicochemistry in tidal wetlands

Several interactions observed between wetland vegetation cover, soil physicochemistry, and microbial composition and function violated broad assumptions repeatably observed in coastal wetland systems. The relationship between microbial biomass and soil C differed from a trend that favors high biomass with larger soil C content (Bastida et al., 2021). Not only was microbial biomass highest in forested wetland soil, which was the most C-limited, but the ratio of bacterial richness to biomass was also atypical, with low species richness and diversity in forested soils (high biomass) relative to the other wetland types (low biomass). Temperate and tropical forest biomes often exhibit similar very high bacterial and fungal biomass, with low diversity. In terrestrial settings, the effect has been attributed to competitive exclusion, with intense

competition reducing alpha diversity when microbial biomass is high (Delgado-Baquerizo and Eldridge, 2019). The caveat is that while microbial biomass was high and diversity low in the forested wetland soils, soil organic matter and total C were relatively low compared to the other wetland types, representing the inverse of the reported carbon-microbial community dynamics reported in terrestrial forests. High microbial biomass and activity have been linked to larger biomass plant species (Kim et al., 2022), as we saw here, but with corresponding higher prokaryotic diversity, unlike our finding. The relationship between carbon, microbial biomass, and diversity also differed from previous comparisons between mangrove wetlands and tidal marshes, where soil organic matter was positively correlated with diversity, which was higher in the mangroves relative to emergent herbaceous wetlands (Zhang et al., 2019). This difference suggests that the C – microbial biomass – prokaryotic richness/diversity dynamic in freshwater forested wetlands may be incomparable to either terrestrial forests or mangrove ecosystems.

Using automatic stepwise model building, we found percent S as the dominant factor driving microbial dissimilarity in the surface sediment layer, with disproportionate abundances of the sulfate reducer Desulfobacteraceae (Murphy et al., 2020). Interestingly, Desulfobulbaceae, a sulfate reducer commonly found in sulfate-rich wetlands (Long et al., 2021), was disproportionately abundant in the freshwater forested wetland soils, but was correlated with neither S content or salinity. Nitrate and nitrite were the strongest factors influencing the composition of the subsurface soil layer, expectedly concentrated in the NO_x-rich forested wetland soils, where the nitrate-reducer Gallionellaceae (Huang Y.M. et al., 2021) and the ammonium-oxidizer Nitrososphaera (Tourna et al., 2011) were found in greater abundance.

Further connecting physicochemistry and microbial composition to microbial metabolism using amplicon-based genomic inference tools like PICRUSt, Piphillin, or Tax4Fun is complicated by inferior representation of environmental microbiota relative to human-associated taxa in microbial databases such as SILVA and RDP. As a result, these inference tools underperform on environmental datasets (Wemheuer et al., 2020). In the results of this study, inferred sulfate-reduction genes were enriched in forested wetland soils despite higher salinity, S%, and abundance of Desulfobacteraceae in the other marsh types. Interestingly, actual measurements of β-glucosidase and NAGase did not correlate with their PICRUSt-inferred equivalents (although actual vs. inferred phosphatase did positively correlate). It is also possible that our genome-inferences are incomplete, given that we only sequenced the archaeal/bacterial 16S gene, given that much of the degradation that occurs in wetlands, particularly of lignin-rich woody material, is driven by fungal metabolism (Ma et al., 2020; Zhan et al., 2021). However, given the strong and consistent correlation between inferred respiration, degradation pathways, and salinity, total microbial activity was likely the greatest in the forested wetland soils.

Of particular interest in future studies will be how short-term changes in coastal wetland habitats, i.e., daily tidal cycles, disturbances from drought and floods, or seasonal differences intersect with long-term changes from saltwater intrusion and the expected shifts in vegetative zonation. We found, principally, that higher elevation, microtidal forested habitat was compositionally and functionally different from lower elevation, more inundated marsh habitat, but it is unknown from our study how temporally dynamic the difference may be. Wetland microbiota may be enriched with marine taxa during high tide and sediment-bound taxa during low tide (Becker et al., 2020), and it may be necessary to separate resident from transient species in estimating microbiological ecosystem function (Weingarten and Jackson, 2022). Distinct compositional patterns in wetlands have been observed with monthly tidal cycles (neap-spring, Zhao et al., 2023) and between seasons (He et al, 2020), including changes in degradation activity (Zhang et al., 2020), warranting further investigation into whether the patterns observed in Mobile Bay persist throughout the year. Extreme storm disturbance may disrupt community composition, activity, and resulting carbon cycling (Yan et al., 2020; Huang S. et al., 2021), and with more frequent disturbances expected to coincide with saltwater intrusion, Mobile Bay is an intriguing study system for investigating the strength and persistence of the plant-microbe-soil relationships we have shown.

In summary, while some of the microbial trait interactions were unexpected compared with other terrestrial and estuarine ecosystems, these results highlight the dependence of soil biogeochemical pathways on inputs from overlying vegetation, hydropatterns, and salinity, improving our understanding of the complex plant-microbe-soil feedbacks occurring in spatially- and temporally-dynamic coastal ecosystems. Results of this study can be used to inform future modeling efforts with a specific focus on linking differences in microbial community composition and activity with anticipated shifts in salinity regimes, vegetation types, and associated delivery of wetland ecosystem functions, goods, and services.

5 Conclusions

In this case study of the Mobile Bay estuary, diverse vegetation reflected the gradient of freshwater to oligohaline salinities examined as seen in other microtidal hydrologic regimes typical of the northern Gulf of Mexico and elsewhere (Coogan and Dzwonkowski, 2018; Berkowitz et al., 2020). Physicochemical and microbial community and functional parameters demonstrated that wetland vegetation type played the strongest role in differentiating soil characteristics across the freshwater forested, *Typha*, tidal shrub, and *Juncus* wetlands. Vegetation superseded the still-significant effects of soil horizon and porewater salinity. Results indicate that forested wetlands displayed several distinctive characteristics relative to the other wetlands examined, including low soil organic matter contents; low microbial diversity; low β-glucosidase activity, low methanogenesis; high microbial biomass; high phosphatase activity; high respiration, nitrate, and sulfate reduction; and more abundant PICRUSt-inferred decomposition pathways. Several of the relationships examined are atypical for either terrestrial or estuarine biogeochemistry. In particular, forested wetland soils exhibited low carbon and nutrient content and relatively low bacterial diversity, yet hosted disproportionately

high microbial biomass and high metabolic and decomposition activity, (as determined by PLFA, amplicon-seq, and PICRUSt). Some of the deviations from terrestrial or estuarine biogeochemistry may speak to the high connectivity throughout this estuary as a result of the many dynamic processes that shape this region ranging from significant riverine freshwater and sediment inputs influencing the forested wetlands to recent hurricanes and storms introducing saline waters into the herbaceous portions of the Bay. Future studies incorporating additional sampling of this region during periods of drought, riverine and coastal (i.e., storm) flooding, and following management activities that alter salinity and hydrodynamics (e.g., dredging navigation channels) may reveal clearer relationships between site geochemistry and microbial traits under a variety of scenarios. The lack of finding clear homology between these processes along the freshwater forest to oligohaline marsh wetland transition also highlights technical and computational opportunities to connect molecular microbiology and soil physicochemical properties with ecosystem functions in dynamic coastal ecosystems on the front lines of climate variability (Arneth et al., 2010; Bridgham et al., 2013).

Data availability statement

Original datasets are available in a publicly accessible repository. Sequencing data hasbeen archived in NCBI Sequence Read Archive under Accession PRJNA1051103.

Author contributions

EW: Data curation, Formal analysis, Investigation, Methodology, Visualization, Writing – original draft, Writing – review & editing. CJ: Conceptualization, Investigation, Methodology, Writing – review & editing. FC: Conceptualization, Investigation, Methodology, Writing – review & editing. MK: Data curation, Investigation, Methodology, Writing – review & editing. NH: Data curation, Investigation, Methodology, Writing – review & editing. MC: Conceptualization, Data curation, Funding acquisition, Methodology, Project administration, Resources, Supervision, Writing – review & editing. JB: Conceptualization, Data curation, Funding acquisition, Investigation, Methodology, Project administration, Resources, Supervision, Writing – review & editing. KI: Conceptualization, Data curation, Funding acquisition, Investigation, Methodology, Project administration, Resources, Supervision, Writing – review & editing.

Funding

The author(s) declare financial support was received for the research, authorship, and/or publication of this article. Project funding was provided by the Technical Director for Military Environmental Engineering and Sciences, US Army Engineer Research and Development Center.

Acknowledgments

Matthew R. Carr, Lyndsay A. Carrigee, Kayla N. Clark, Brianna M. Fernando, Cynthia L. Price, Yadav Sapkota, and Maggie A. Waites assisted with initial sample collection and processing. Banjamin D. Kocar was responsible for project administration.

Conflict of interest

The authors declare that the research was conducted in the absence of any commercial or financial relationships that could be construed as a potential conflict of interest.

Publisher's note

All claims expressed in this article are solely those of the authors and do not necessarily represent those of their affiliated organizations, or those of the publisher, the editors and the reviewers. Any product that may be evaluated in this article, or claim that may be made by its manufacturer, is not guaranteed or endorsed by the publisher.

References

AOAC (2012). *Total nitrogen, combustion. Official Methods of Analysis of AOAC INTERNATIONAL. 19th Ed* (Gaithersburg, MD, USA: AOAC INTERNATIONAL).

Armstrong, W., Cousins, D., Armstrong, J., Turner, D., and Beckett, P. (2000). Oxygen distribution in wetland plant roots and permeability barriers to gas-exchange with the rhizosphere: a microelectrode and modelling study with Phragmites australis. *Ann. Bot.* 86, 687–703. doi: 10.1006/anbo.2000.1236

Arneth, A., Harrison, S. P., Zaehle, S., Tsigaridis, K., Menon, S., Bartlein, P., et al. (2010). Terrestrial biogeochemical feedbacks in the climate system. *Nat. Geosci.* 3, 525–532. doi: 10.1038/ngeo905

Barreto, C. R., Morrissey, E., Wykoff, D., and Chapman, S. (2018). Co-occurring mangroves and salt marshes differ in microbial community composition. *Wetlands* 38, 497–508. doi: 10.1007/s13157-018-0994-9

Bassetti, L., Pontee, N., and Bird, J. (2022). *An Innovative Case Study on Coastal Resilience: Tyndall Air Force Base (TAFB), Panama City, Florida* Vol. 2022 (Ports), 23–31.

Bastida, F., Eldridge, D. J., García, C., Kenny Png, G., Bardgett, R. D., and Delgado-Baquerizo, M. (2021). Soil microbial diversity–biomass relationships are driven by soil carbon content across global biomes. *ISME J.* 15, 2081–2091. doi: 10.1038/s41396-021-00906-0

Becker, C. C., Weber, L., Suca, J. J., Llopiz, J. K., Mooney, T. A., and Apprill, A. (2020). Microbial and nutrient dynamics in mangrove, reef, and seagrass waters over tidal and diurnal time scales. *Aquat. Microbial Ecol.* 85, 101–119. doi: 10.3354/ame01944

Berkowitz, J. F., Altman, S., Reine, K. J., Wilbur, D., Kjelland, M. E., Gerald, T. K., et al. (2020). *Evaluation of the potential impacts of the proposed Mobile Harbor navigation channel expansion on the aquatic resources of Mobile Bay, Alabama.*

Berkowitz, J., Piercy, C., Welp, T., and VanZomeren, C. (2019). *Thin layer placement : technical definition for U.S. army corps of engineers applications* (Engineer Research and Development Center (U.S). doi: 10.21079/11681/32283

Blankinship, J. C., Berhe, A. A., Crow, S. E., Druhan, J. L., Heckman, K. A., Keiluweit, M., et al. (2018). Improving understanding of soil organic matter dynamics by triangulating theories, measurements, and models. *Biogeochemistry* 140 (1), 1–13. doi: 10.1007/s10533-018-0478-2

Bridgham, S. D., Cadillo-Quiroz, H., Keller, J. K., and Zhuang, Q. (2013). Methane emissions from wetlands: biogeochemical, microbial, and modeling perspectives from local to global scales. *Global Change Biol.* 19, 1325–1346. doi: 10.1111/gcb.12131

Brinson, M. M., Christian, R. R., and Blum, L. K. (1995). Multiple states in the sea-level induced transition from terrestrial forest to estuary. *Estuaries* 18, 648–659. doi: 10.2307/1352383

Brodersen, K. E., Trevathan-Tackett, S. M., Nielsen, D. A., Connolly, R. M., Lovelock, C. E., Atwood, T. B., et al. (2019). Oxygen consumption and sulfate reduction in vegetated coastal habitats: effects of physical disturbance. *Front. Mar. Sci.* 6, 14. doi: 10.3389/fmars.2019.00014

Bulseco, A. N., Giblin, A. E., Tucker, J., Murphy, A. E., Sanderman, J., Hiller-Bittrolff, K., et al. (2019). Nitrate addition stimulates microbial decomposition of organic matter in salt marsh sediments. *Global Change Biol.* 25, 3224–3241. doi: 10.1111/gcb.14726

Callahan, B. J., McMurdie, P. J., Rosen, M. J., Han, A. W., Johnson, A. J. A., and Holmes, S. P. (2016). DADA2: High-resolution sample inference from Illumina amplicon data. *Nat. Methods* 13, 581–583. doi: 10.1038/nmeth.3869

Caporaso, J. G., Lauber, C. L., Walters, W. A., Berg-Lyons, D., Lozupone, C. A., Turnbaugh, P. J., et al. (2011). Global patterns of 16S rRNA diversity at a depth of millions of sequences per sample. *Proc. Natl. Acad. Sci.* 108, 4516–4522. doi: 10.1073/pnas.1000080107

Ceccon, D. M., Faoro, H., da Cunha Lana, P., de Souza, E. M., and de Oliveira Pedrosa, F. (2019). Metataxonomic and metagenomic analysis of mangrove microbiomes reveals community patterns driven by salinity and pH gradients in Paranaguá Bay, Brazil. *Sci. Total Environ.* 694, 133609. doi: 10.1016/j.scitotenv.2019.133609

Coogan, J., and Dzwonkowski, B. (2018). Observations of wind forcing effects on estuary length and salinity flux in a river-dominated, microtidal estuary, Mobile Bay, Alabama. *J. Phys. Oceanography* 48, 1787–1802. doi: 10.1175/JPO-D-17-0249.1

Cowardin, L. M. (1979). *Classification of wetlands and deepwater habitats of the United States* (Fish and Wildlife Service, US Department of the Interior).

Craft, C. B. (2012). Tidal freshwater forest accretion does not keep pace with sea level rise. *Global Change Biol.* 18, 3615–3623. doi: 10.1111/gcb.12009

Day, J. W., Christian, R. R., Boesch, D. M., Yáñez-Arancibia, A., Morris, J., Twilley, R. R., et al. (2008). Consequences of climate change on the ecogeomorphology of coastal wetlands. *Estuaries coasts* 31, 477–491. doi: 10.1007/s12237-008-9047-6

Delgado-Baquerizo, M., and Eldridge, D. J. (2019). Cross-biome drivers of soil bacterial alpha diversity on a worldwide scale. *Ecosystems* 22, 1220–1231. doi: 10.1007/s10021-018-0333-2

Douglas, G. M., Maffei, V. J., Zaneveld, J. R., Yurgel, S. N., Brown, J. R., Taylor, C. M., et al. (2020). PICRUSt2 for prediction of metagenome functions. *Nat. Biotechnol.* 38, 685–688. doi: 10.1038/s41587-020-0548-6

Feagin, R., Irish, J., Möller, I., Williams, A., Colón-Rivera, R., and Mousavi, M. (2011). Engineering properties of wetland plants with application to wave attenuation. *Coast. Eng.* 58, 251–255. doi: 10.1016/j.coastaleng.2010.10.003

Franklin, R. B., Morrissey, E. M., and Morina, J. C. (2017). Changes in abundance and community structure of nitrate-reducing bacteria along a salinity gradient in tidal wetlands. *Pedobiologia* 60, 21–26. doi: 10.1016/j.pedobi.2016.12.002

Gilbert, J. A., Jansson, J. K., and Knight, R. (2014). The Earth Microbiome project: successes and aspirations. *BMC Biol.* 12, 1–4. doi: 10.1186/s12915-014-0069-1

Hauser, S., Meixler, M. S., and Laba, M. (2015). Quantification of impacts and ecosystem services loss in New Jersey coastal wetlands due to Hurricane Sandy storm surge. *Wetlands* 35, 1137–1148. doi: 10.7282/T3GF0WFH

He, L., She, C., Huang, J., Yang, P., Yu, H., and Tong, C. (2022). Effects of constant and fluctuating saltwater addition on CH4 fluxes and methanogens of a tidal freshwater wetland: A mesocosm study. *Estuarine Coast. Shelf Sci.* 277, 108076. doi: 10.1016/j.ecss.2022.108076

He, R., Zeng, J., Zhao, D., Huang, R., Yu, Z., and Wu, Q. L. (2020). Contrasting patterns in diversity and community assembly of phragmites australis root-associated bacterial communities from different seasons. *Appl. Environ. Microbiol.* 86, e00379–e00320. doi: 10.1128/AEM.00379-20

Howes, N. C., FitzGerald, D. M., Hughes, Z. J., Georgiou, I. Y., Kulp, M. A., Miner, M. D., et al. (2010). Hurricane-induced failure of low salinity wetlands. *Proc. Natl. Acad. Sci.* 107, 14014–14019. doi: 10.1073/pnas.0914582107

Huang, S., Sherman, A., Chen, C., and Jaffé, P. R. (2021). Tropical cyclone effects on water and sediment chemistry and the microbial community in estuarine ecosystems. *Environ. Pollut.* 286, 117228. doi: 10.1016/j.envpol.2021.117228

Huang, Y.-M., Straub, D., Blackwell, N., Kappler, A., and Kleindienst, S. (2021). Meta-omics reveal Gallionellaceae and Rhodanobacter species as interdependent key players for Fe (II) oxidation and nitrate reduction in the autotrophic enrichment culture KS. *Appl. Environ. Microbiol.* 87, e00496-21. doi: 10.1128/AEM.00496-21

Hupp, C. R., Kroes, D. E., Noe, G. B., Schenk, E. R., and Day, R. H. (2019). Sediment trapping and carbon sequestration in floodplains of the lower Atchafalaya Basin, LA: Allochthonous versus autochthonous carbon sources. *J. Geophysical Research: Biogeosciences* 124, 663–677. doi: 10.1029/2018JG004533

International Organization for Standardization (1996). *Soil quality - Determination of organic and total carbon after dry combustion*.

International Organization for Standardization (2000). *Soil quality -Determination of total sulfur by dry combustion*.

International Organization for Standardization (2016). *December 2016 - Investigation of solids temperature dependent differentiation of total carbon (TOC400, ROC, TIC900)*.

Jurjonas, M., and Seekamp, E. (2018). Rural coastal community resilience: Assessing a framework in eastern North Carolina. *Ocean Coast. Manage.* 162, 137–150. doi: 10.1016/j.ocecoaman.2017.10.010

Kang, H., Kim, S., and Freeman, C. (2013). Enzyme activities. *Methods biogeochemistry wetlands* 10, 373–384. doi: 10.2136/sssabookser10

Kim, S., Kang, H., Megonigal, J. P., and McCormick, M. (2022). Microbial activity and diversity vary with plant diversity and biomass in wetland ecosystems. *Estuaries Coasts* 45, 1434–1444. doi: 10.1007/s12237-021-01015-z

Krauss, K. W., Noe, G. B., Duberstein, J. A., Conner, W. H., Stagg, C. L., Cormier, N., et al. (2018). The role of the upper tidal estuary in wetland blue carbon storage and flux. *Global Biogeochemical Cycles* 32, 817–839. doi: 10.1029/2018GB005897

Lahiri, C., and Davidson, G. R. (2020). Heterogeneous oxygenation of wetland soils with increasing inundation: Redox potential, water depth, and preferential flow paths. *Hydrological Processes* 34, 1350–1358. doi: 10.1002/hyp.13654

Li, Y. L., Ge, Z. M., Xie, L. N., Li, S. H., and Tan, L. S. (2022). Effects of waterlogging and salinity increase on CO2 efflux in soil from coastal marshes. *Appl. Soil Ecol.* 170, 104268. doi: 10.1016/j.apsoil.2021.104268

Liu, L., Wu, Y., Yin, M., Ma, X., Yu, X., Guo, X., et al. (2023). Soil salinity, not plant genotype or geographical distance, shapes soil microbial community of a reed wetland at a fine scale in the Yellow River Delta. *Sci. Total Environ.* 856, 159136. doi: 10.1016/j.scitotenv.2022.159136

Liu, L., Zhu, K., Wurzburger, N., and Zhang, J. (2020). Relationships between plant diversity and soil microbial diversity vary across taxonomic groups and spatial scales. *Ecosphere* 11, e02999. doi: 10.1002/ecs2.2999

Long, Y., Jiang, J., Hu, X., Hu, J., Ren, C., and Zhou, S. (2021). The response of microbial community structure and sediment properties to anthropogenic activities in Caohai wetland sediments. *Ecotoxicology Environ. Saf.* 211, 111936. doi: 10.1016/j.ecoenv.2021.111936

Louis, B. P., Maron, P.-A., Viaud, V., Leterme, P., and Menasseri-Aubry, S. (2016). Soil C and N models that integrate microbial diversity. *Environ Chem Lett* 14, 331–344. doi: 10.1007/s10311-016-0571-5

Luo, M., Huang, J. F., Zhu, W. F., and Tong, C. (2019). Impacts of increasing salinity and inundation on rates and pathways of organic carbon mineralization in tidal wetlands: a review. *Hydrobiologia* 827, 31–49. doi: 10.1007/s10750-017-3416-8

Ma, Y., Huang, S., Gan, Z., Xiong, Y., Cai, R., Liu, Y., et al. (2020). The succession of bacterial and fungal communities during decomposition of two hygrophytes in a freshwater lake wetland. *Ecosphere* 11, e03242. doi: 10.1002/ecs2.3242

Maidak, B. L., Cole, J. R., Lilburn, T. G., Parker, C. T. Jr., Saxman, P. R., Stredwick, J. M., et al. (2000). The RDP (ribosomal database project) continues. *Nucleic Acids Res.* 28, 173–174. doi: 10.1093/nar/28.1.173

Malik, A. A., Martiny, J. B. H., Brodie, E. L., Martiny, A. C., Treseder, K. K., and Allison, S. D. (2020). Defining trait-based microbial strategies with consequences for soil carbon cycling under climate change. *ISME J.* 14 (1), 1–9. doi: 10.1038/s41396-019-0510-0

Megonigal, J. P., Patrick, W. Jr., and Faulkner, S. (1993). Wetland identification in seasonally flooded forest soils: soil morphology and redox dynamics. *Soil Sci. Soc. America J.* 57, 140–149. doi: 10.2136/sssaj1993.03615995005700010027x

Miao, G., Noormets, A., Domec, J.-C., Fuentes, M., Trettin, C. C., Sun, G., et al. (2017). Hydrology and microtopography control carbon dynamics in wetlands: Implications in partitioning ecosystem respiration in a coastal plain forested wetland. *Agric. For. Meteorology* 247, 343–355. doi: 10.1016/j.agrformet.2017.08.022

Mitsch, W. J., and Gosselink, J. G. (2015). *Wetlands* (Hoboken: John Wiley & Sons, Inc).

Mobilian, C., and Craft, C. B. (2021). "Wetland soils: physical and chemical properties and biogeochemical processes," in *Encyclopedia of Inland Waters (Second Edition)*, eds. T. Mehner and K. Tockner (Oxford: Elsevier), 157–168. doi: 10.1016/B978-0-12-819166-8.00049-9

Moorhead, D. L., Rinkes, Z. L., Sinsabaugh, R. L., and Weintraub, M. N. (2013). Dynamic relationships between microbial biomass, respiration, inorganic nutrients and enzyme activities: informing enzyme-based decomposition models. *Front. Microbiol.* 4, 223. doi: 10.3389/fmicb.2013.00223

Murphy, A. E., Bulseco, A. N., Ackerman, R., Vineis, J. H., and Bowen, J. L. (2020). Sulphide addition favours respiratory ammonification (DNRA) over complete denitrification and alters the active microbial community in salt marsh sediments. *Environ. Microbiol.* 22, 2124–2139. doi: 10.1111/1462-2920.14969

Neubauer, S., Franklin, R., and Berrier, D. (2013). Saltwater intrusion into tidal freshwater marshes alters the biogeochemical processing of organic carbon. *Biogeosciences* 10, 8171–8183. doi: 10.5194/bg-10-8171-2013

Neubauer, S. C., Piehler, M. F., Smyth, A. R., and Franklin, R. B. (2019). Saltwater intrusion modifies microbial community structure and decreases denitrification in tidal freshwater marshes. *Ecosystems* 22, 912–928. doi: 10.1007/s10021-018-0312-7

Noe, G. B., Hupp, C. R., Bernhardt, C. E., and Krauss, K. W. (2016). Contemporary deposition and long-term accumulation of sediment and nutrients by tidal freshwater forested wetlands impacted by sea level rise. *Estuaries Coasts* 39, 1006–1019. doi: 10.1007/s12237-016-0066-4

O'Dell, J. W. (1993). "DETERMINATION OF NITRATE-NITRITE NITROGEN BY AUTOMATED COLORIMETRY," in *Methods for the determination of metals in environmental samples* (Elsevier), 464–478. doi: 10.1016/B978-0-8155-1398-8.50026-4

Poffenbarger, H. J., Needelman, B. A., and Megonigal, J. P. (2011). Salinity influence on methane emissions from tidal marshes. *Wetlands* 31, 831–842. doi: 10.1007/s13157-011-0197-0

Premrov, A., Cummins, T., and Byrne, K. A. (2017). Assessing fixed depth carbon stocks in soils with varying horizon depths and thicknesses, sampled by horizon. *Catena* 150, 291–301. doi: 10.1016/j.catena.2016.11.030

Qu, W., Li, J., Han, G., Wu, H., Song, W., and Zhang, X. (2019). Effect of salinity on the decomposition of soil organic carbon in a tidal wetland. *J. Soils Sediments* 19, 609–617. doi: 10.1007/s11368-018-2096-y

Rietl, A. J., Overlander, M. E., Nyman, A. J., and Jackson, C. R. (2016). Microbial community composition and extracellular enzyme activities associated with Juncus roemerianus and Spartina alterniflora vegetated sediments in Louisiana saltmarshes. *Microbial Ecol.* 71, 290–303. doi: 10.1007/s00248-015-0651-2

Seybold, C. A., Mersie, W., Huang, J., and McNamee, C. (2002). Soil redox, pH, temperature, and water-table patterns of a freshwater tidal wetland. *Wetlands* 22, 149–158. doi: 10.1672/0277-5212(2002)022[0149:SRPTAW]2.0.CO;2

Smith, R. D., Ammann, A. P., Bartoldus, C. C., and Brinson, M. M. (1995). *An approach for assessing wetland functions using hydrogeomorphic classification, reference wetlands, and functional indices*.

Steinmuller, H. E., Dittmer, K. M., White, J. R., and Chambers, L. G. (2019). Understanding the fate of soil organic matter in submerging coastal wetland soils: A microcosm approach. *Geoderma* 337, 1267–1277. doi: 10.1016/j.geoderma.2018.08.020

Steinmuller, H. E., Hayes, M. P., Hurst, N. R., Sapkota, Y., Cook, R. L., White, J. R., et al. (2020). Does edge erosion alter coastal wetland soil properties? *A multi-method biogeochemical study. Catena* 187, 104373. doi: 10.1016/j.catena.2019.104373

Sulman, B. N., Moore, J. A. M., Abramoff, R., Averill, C., Kivlin, S., Georgiou, K., et al. (2018). Multiple models and experiments underscore large uncertainty in soil carbon dynamics. *Biogeochemistry* 141 (2), 109–123. doi: 10.1007/s10533-018-0509-z

Sutton-Grier, A. E., Keller, J. K., Koch, R., Gilmour, C., and Megonigal, J. P. (2011). Electron donors and acceptors influence anaerobic soil organic matter mineralization in tidal marshes. *Soil Biol. Biochem.* 43, 1576–1583. doi: 10.1016/j.soilbio.2011.04.008

Union of Concerned Scientists, (2016). The US Military on the Front Lines of Rising Seas and Union of Concerned Scientists (2016). Available at: https://www.ucsusa.org/resources/us-military-front-lines-rising-seas (Accessed December 13, 2023).

Tourna, M., Stieglmeier, M., Spang, A., Könneke, M., Schintlmeister, A., Urich, T., et al. (2011). Nitrososphaera viennensis, an ammonia oxidizing archaeon from soil. *Proc. Natl. Acad. Sci.* 108, 8420–8425. doi: 10.1073/pnas.1013488108

Unger, V., Elsey-Quirk, T., Sommerfield, C., and Velinsky, D. (2016). Stability of organic carbon accumulating in Spartina alterniflora-dominated salt marshes of the Mid-Atlantic US. *Estuarine Coast. Shelf Sci.* 182, 179–189. doi: 10.1016/j.ecss.2016.10.001

USDA (U.S. Department of Agriculture) (2000). *The PLANTS database* (Baton Rouge, LA: National Plant Data Center). Available at: http://plants.usda.gov.

Wallenstein, M. D., and Hall, E. K. (2012). A trait-based framework for predicting when and where microbial adaptation to climate change will affect ecosystem functioning. *Biogeochemistry* 109 (1), 35–47. doi: 10.1007/s10533-011-9641-8

Wang, Q., Cao, Z., Liu, Q., Zhang, J., Hu, Y., Zhang, J., et al. (2019). Enhancement of COD removal in constructed wetlands treating saline wastewater: Intertidal wetland sediment as a novel inoculation. *J. Environ. Manage.* 249, 109398. doi: 10.1016/j.jenvman.2019.109398

Weingarten, E. A., and Jackson, C. R. (2022). Microbial composition of freshwater marsh sediment responds more strongly to microcosm seawater addition than simulated nitrate or phosphate eutrophication. *Microb. Ecol.* 86, 1060–1070. doi: 10.1007/s00248-022-02111-8

Wemheuer, F., Taylor, J. A., Daniel, R., Johnston, E., Meinicke, P., Thomas, T., et al. (2020). Tax4Fun2: prediction of habitat-specific functional profiles and functional redundancy based on 16S rRNA gene sequences. *Environ. Microbiome* 15, 1–12. doi: 10.1186/s40793-020-00358-7

Yan, G., Labonté, J. M., Quigg, A., and Kaiser, K. (2020). Hurricanes accelerate dissolved organic carbon cycling in coastal ecosystems. *Front. Mar. Sci.* 7. doi: 10.3389/fmars.2020.00248

Zhan, P., Liu, Y., Wang, H., Wang, C., Xia, M., Wang, N., et al. (2021). Plant litter decomposition in wetlands is closely associated with phyllospheric fungi as revealed by microbial community dynamics and co-occurrence network. *Sci. Total Environ.* 753, 142194. doi: 10.1016/j.scitotenv.2020.142194

Zhang, C. J., Pan, J., Duan, C. H., Wang, Y. M., Liu, Y., Sun, J., et al. (2019). Prokaryotic diversity in mangrove sediments across southeastern China fundamentally differs from that in other biomes. *Msystems* 4, e00442–e00419. doi: 10.1128/mSystems.00442-19

Zhang, G., Bai, J., Tebbe, C. C., Zhao, Q., Jia, J., Wang, W., et al. (2021). Salinity controls soil microbial community structure and function in coastal estuarine wetlands. *Environ. Microbiol.* 23, 1020–1037. doi: 10.1111/1462-2920.15281

Zhang, X., Ji, Z., Shao, Y., Guo, C., Zhou, H., Liu, L., et al. (2020). Seasonal variations of soil bacterial communities in Suaeda wetland of Shuangtaizi River estuary, Northeast China. *J. Environ. Sci.* 97, 45–53. doi: 10.1016/j.jes.2020.04.012

Zhao, Z., Zhang, L., Zhang, G., Gao, H., Chen, X., Li, L., et al. (2023). Hydrodynamic and anthropogenic disturbances co-shape microbiota rhythmicity and community assembly within intertidal groundwater-surface water continuum. *Water Res.* 242, 120236. doi: 10.1016/j.watres.2023.120236

frontiers | Frontiers in Marine Science

TYPE Original Research
PUBLISHED 11 January 2024
DOI 10.3389/fmars.2023.1342750

Check for updates

OPEN ACCESS

EDITED BY
Junfu Dong,
Shandong University, China

REVIEWED BY
Haibo Jiang,
Ningbo University, China
Yufeng Yang,
Jinan University, China

*CORRESPONDENCE
Yao Sun
sunyao@ysfri.ac.cn

RECEIVED 22 November 2023
ACCEPTED 08 December 2023
PUBLISHED 11 January 2024

CITATION
Yang S, Yang Q, Song X, Zhou W, Liu J, Qi X, Chen J, Huang J, Li B and Sun Y (2024) Blue carbon in sediment from Sanggou Bay: composition, burial flux and its response to human activities.
Front. Mar. Sci. 10:1342750.
doi: 10.3389/fmars.2023.1342750

COPYRIGHT
© 2024 Yang, Yang, Song, Zhou, Liu, Qi, Chen, Huang, Li and Sun. This is an open-access article distributed under the terms of the Creative Commons Attribution License (CC BY). The use, distribution or reproduction in other forums is permitted, provided the original author(s) and the copyright owner(s) are credited and that the original publication in this journal is cited, in accordance with accepted academic practice. No use, distribution or reproduction is permitted which does not comply with these terms.

Blue carbon in sediment from Sanggou Bay: composition, burial flux and its response to human activities

Shu Yang[1,2], Qian Yang[3], Xianli Song[4], Wei Zhou[2], Jihua Liu[1], Xiandong Qi[1], Junfeng Chen[1], Jun Huang[1], Bin Li[2] and Yao Sun[3]*

[1]Institute of Marine Science and Technology, Shandong University, Qingdao, China, [2]Center Tech Tianjin Chemical Research and Design Institute, China National Offshore Oil Corporation, Tianjin, China, [3]Yellow Sea Fisheries Research Institute, Chinese Academy of Fishery Sciences, Qingdao, China, [4]Key Laboratory of Benthic Fisheries Aquaculture and Enhancement, Marine Biology Institute of Shandong Province, Qingdao, China

Marine primary production and terrestrial input are the main sources of buried carbon in sediments of marginal seas. Only marine-source carbon buried in sediments, fixed and stored by marine ecosystems, belongs to "blue carbon" and reflects marine ecosystems' carbon sink function. The pattern of buried blue carbon in sediments, its flux, and its relationship with environmental changes remain unclear. The study aimed to investigate the composition of blue carbon in the sediments of Sanggou Bay, a special type of marginal sea. The analysis of sediment carbon sources was conducted through the C/N ratio and microscopic examination. The study also examined the long-term changes in the blue carbon burial fluxes. Results showed Blue carbon, which is sea-sourced carbon, accounted for about 23% of the total carbon content and its concentration ranged from 0.17% to 0.51%, with an average of about 0.25% ± 0.10%. The content of organic blue carbon in this sea area ranges from 0.09% to 0.26%, with an average of around 0.18% ± 0.04%. It constitutes approximately 72% of the buried blue carbon in the sediment, making it the primary component of buried blue carbon. Meanwhile, the content of inorganic blue carbon ranges from 0.01% to 0.32%. Over the past 70 years, the burial fluxes of sedimentary blue carbon, organic blue carbon and inorganic blue carbon in the Sanggou Bay are about 0.54 ± 0.22 mmol/(cm^2a), 0.38 ± 0.07 mmol/(cm^2a) and 0.17 ± 0.22 mmol/(cm^2a), respectively; their long-term changes have been significantly affected by human aquaculture activities. Large-scale raft-rack aquaculture activities have caused a reduction in water flow velocity and an increase in the deposition of particulate organic matter, which in turn has led to the burial of organic blue carbon in the sediment. Additionally, the competition between aquaculture products and small calcareous organisms, such as mussels, foraminifera, may have inhibited the growth of small calcareous

organisms. We suggest this has resulted in reduced burial fluxes of inorganic blue carbon and a decrease in its proportion among total blue carbon in the sea area. Our findings imply that aquaculture activities in Sanggou Bay had a negative impact on the burial of blue carbon in the sediments.

KEYWORDS

blue carbon, sediment, burial flux, aquaculture, marginal sea, Sanggou Bay, human activity, long-term change

1 Introduction

The burial of carbon in marine sediments is an important pathway for carbon storage in the ocean. Compared to other methods of carbon storage, carbon stored in sediment is less likely to be released into the atmosphere in the short term. The IPCC has suggested that carbon buried in marine sediments is an effective way to remove CO_2 from the atmosphere (Nellemann et al., 2009). About 90% of organic carbon in global ocean sediments is concentrated in marginal seas, while for inorganic carbon the percentage is over 50% (Berner, 1982; Hedges and Keil, 1995; Falkowski et al., 2000; Tesi et al., 2007; Song, 2011). Such a large quantity of buried carbon suggests that marginal sea sediments play a crucial role in the carbon cycle of marine ecosystems. Studies have shown that, due to the proximity of the marginal sea to land, the carbon buried in its sediments includes not only the carbon fixed by marine organisms, but also the carbon imported from terrestrial sources (Pocklington and Leonard, 1979; Prahl et al., 1994; Goñi et al., 1997; Bianchi et al., 2002; Burdige, 2005; Blair and Aller, 2012; Zhang et al., 2022; Tao et al., 2023). The burial of marine-derived carbon in sediment, also known as "blue carbon" (BC), reflects the sequestration of atmospheric CO_2 by marine ecosystems through biological pumps (Honjo et al., 2008; Nellemann et al., 2009; Ma et al., 2014; Macreadie et al., 2019). Relatively, terrestrial carbon in sediment is fixed by land organisms, and its burial in marine sediments reflects the migration of terrestrial carbon pools to oceanic pools, rather than the direct carbon sink of CO_2 by marine ecosystems. We believe that these different sourced carbons indicate distinct roles in the carbon sink function. Therefore, understanding the burial patterns of BC and non-BC in sediments can provide a more accurate understanding of the carbon sink function of marginal sea sediments and marine ecosystems (Belicka and Harvey, 2009; Bianchi, 2011).

There have been many studies focusing on the carbon sink function of sediments, and the carbon burial flux and its long-term changes in marine sediments have been studied (Thunell et al., 1992; St-Onge and Hillaire-Marcel, 2001; Justić et al., 2002; Ruiz-Fernández et al., 2007; Hayes et al., 2021; Zhao et al., 2021). The sources of organic carbon have also been discussed by isotopes or C/N, etc. (Ruttenberg and Goñi, 1997; Andrews et al., 1998; Goñi et al., 1998; Huang et al., 2001; Bouchez et al., 2014; Xing et al., 2014; Sanderman et al., 2015; Geraldi et al., 2019; Zinkann et al., 2022). However, from a BC burial perspective, the burial behavior of BC, including patterns, burial flux, and its relationship with environmental changes, remains unclear.

Nearshore aquaculture sea is a unique type of marginal sea characterized by high biological activity and a significantly higher carbon sink efficiency compared to the open ocean (Boyd et al., 2010). Besides, human aquaculture significantly disturbs the carbon cycling process in this sea (Carroll et al., 2003; Kutti et al., 2008; Ren et al., 2010; Liu et al., 2014; Xu et al., 2023). Additionally, there is potential for carbon sink enhancement in aquaculture seas. Therefore, we consider this type of sea an ideal location to identify the carbon sink function of marginal sea sediments and discuss the response of this function to increasing anthropogenic pressures. In this paper, sediment core sampling is conducted in Sangou Bay, one of China's largest aquaculture bases. Based on an analysis of the sources of organic and inorganic carbon in sediments, we first identify the presence of burial BC in the sediments. We then explore how human aquaculture activities have affected the existing pattern and burial fluxes of BC over the past 70 years. This study attempts to identify the carbon sink function of marginal sea sediments more precisely.

2 Materials and methods

Sanggou Bay, located in Shandong province, China, is a significant aquaculture center. Since the late 1960s, macroalgae culture has a history of over 50 years. The predominant aquaculture species in Sanggou Bay are kelp, scallop, and oyster, and raft-rack culture is the primary mode of marine aquaculture (Guo et al., 1999). Currently, the aquaculture area has covered the whole Bay and extended beyond the bay (Li et al., 2023).

2.1 Sediment sampling

The sediment core, with a length of 1.78m, was collected by a gravity sediment core sampler at station RS-5 (Figure 1) in July 2014. Station RS-5 is situated at the junction of shellfish and kelp culture areas in the central part of Sanggou Bay. After being

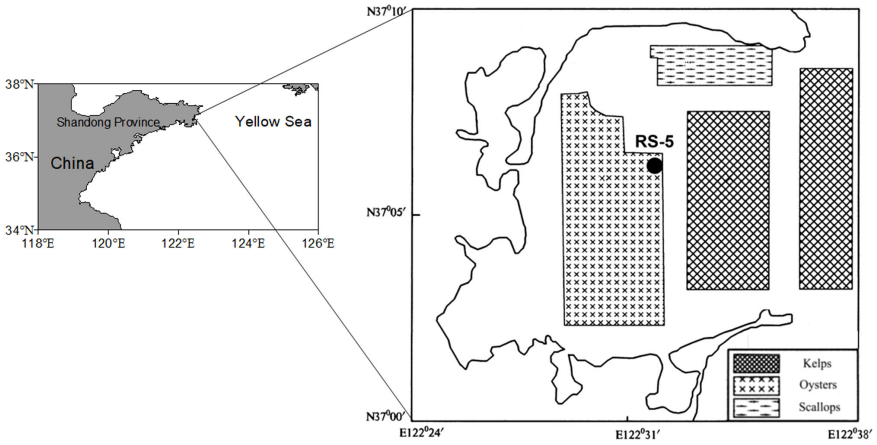

FIGURE 1
Study area and sampling station.

collected, the sample was kept refrigerated until it was divided. The sediment core was split into 1cm intervals for the upper 15cm and 2cm intervals for the remaining. The sub-samples were frozen and stored for future analysis.

2.2 Determination of sediment chronology

The chronology of sediment cores was rebuilt based on excess ^{210}Pb activities (Golberg, 1963). The age of the sediment core was determined based on sample collection date and sedimentary rate. The activities of ^{210}Pb in the sediment core were measured using a germanium detector (AMETEK Company).

2.3 Analysis of carbon and nitrogen in sediment

The sediment samples were first dried and then ground. Some ground sediments were directly detected for contents of total carbon (TC) and total nitrogen (TN) by an Elemental Analyzer Vario EL cube (Elementar Analysensysteme GmbH, German). Then, concentrated hydrochloric acid was used to fumigate ground samples for 24 hours to eliminate inorganic carbons. Subsequently, total organic carbon (TOC) was measured using the same Elemental Analyzer. The total inorganic carbon (TIC) levels were determined by subtracting TC and TOC.

2.4 Identification of organic blue carbon

The term "organic blue carbon" (OBC) in this study refers to marine-source organic carbon that is buried in sediment. And C/N ratio was used to identify the source of organic matter (Ruttenberg and Goñi, 1997; Andrews et al., 1998; Goñi et al., 1998; Kaushal and Binford, 1999; Venkatesh, 2020). The end-member values of C/N for marine and terrestrial organic matter were set at 5 and 20, respectively. The sources of TOC in Sanggou Bay sediments were analyzed using a two-end mixing model (Qian et al., 1997).

2.5 Identification of inorganic blue carbon

The term "inorganic blue carbon" (IBC) in this study refers to marine-sourced inorganic carbon that is buried in sediments, including calcareous remains of marine organisms and marine secondary carbonates. Based on current data, which indicates low levels of secondary carbonates in marine sediments globally (Sun and Turchyn, 2014), this study will only focus on inorganic carbon of marine origin. This includes calcareous remnants of various marine organisms such as shellfish, echinoderms, foraminifera, ostracoda, and coccolithophores. Secondary carbonates will not be considered in this study.

In this study, the source of inorganic carbon was distinguished by the morphological differences between terrestrial inorganic carbon minerals and marine-source inorganic carbon fractions. We first selected all calcareous remains of marine organisms in the sediments based on their morphological characteristics and then determined their total inorganic carbon. The total inorganic carbon content of these marine-source calcareous remains is the inorganic blue carbon content. For the brief operation process, we examined cleaned and sieved sediments under a microscope to identify calcareous remains of larger organisms including shellfish, echinoderms, foraminifera, ostracoda, etc. The inorganic carbon content of these remains was determined using an elemental analyzer. Carbon in the coccolithophore fossil also belongs to the marine source inorganic carbon. However, our early study found that the fossilized coccolith, examined by the polarizing microscope, was rare in Sanggou Bay sediment, so the inorganic carbon produced by coccolithophores was ignored in this study. Theoretically, the remains of freshwater mussels and other organisms may be transported into the sea by runoff, potentially interfering with the determination of marine-source inorganic carbon by the above method. However, considering the absence

of large-scale runoff injection in the surrounding area of Sanggou Bay, we suggest that the impact of inorganic carbon from terrestrial organisms on determining marine inorganic carbon can be disregarded.

2.6 Calculation of carbon burial fluxes

The burial fluxes of all types of carbon in sediments were calculated using the method introduced by Dai et al. (2007).

3 Results

The vertical distribution of ^{210}Pb in sediments in station RS-5 shows a typical attenuation trend (Figure 2), indicating that the depositional environment in this sea area is relatively stable. The sediment rate in this sea area is estimated to be 2.08 cm/a (Bai et al., 2022). The sediment core used in this study reflects the deposition of the past 70 years.

The total carbon content in RS-5 sediments was 0.87%~1.40% in the last 70 years (Bai et al., 2022) (Figure 3). It was slightly higher during the 1960s~1990s and then decreased significantly. The total organic carbon content fluctuates but has no overall trend, except for a significant increase from the 1970s to the 1980s, with an average of 0.37% ± 0.06%. The average content of total inorganic carbon was 0.77% ± 0.09%. Its time series resembled that of total carbon, being generally higher from the 1960s to 1990s and lower in the 1950s and 2000s. C/N ratios ranged from 7.1 to 9.4. The highest values occurred mainly before 1975, while the content was generally low after that.

The marine-source organic carbon content, estimated by C/N, averaged at about 0.18% ± 0.04%. The highest values were observed in 1965-1995, followed by the 2000s, and the lowest values occurred in 1950-1965. The average inorganic carbon from marine sources was approximately 0.08% ± 0.09%. The highest levels were observed prior to the 1980s, with a peak in the 1950s, after which the values decreased. BC refers to the carbon sequestered by marine organisms, which includes both organic and inorganic carbon from marine sources. Over the past 70 years, the concentration of BC in the sediments of Sanggou Bay has been found to range from 0.17% to 0.51%, with an average of 0.25% ± 0.10%. The highest levels of BC were recorded during the period of 1950-1965, after which there was a general decrease in concentration. Since the 1980s, the content of BC has remained at a consistently low level.

The burial fluxes of TC, TOC, TIC, OBC, IBC, and BC, in the aquaculture waters of Sanggou Bay, were estimated to be about

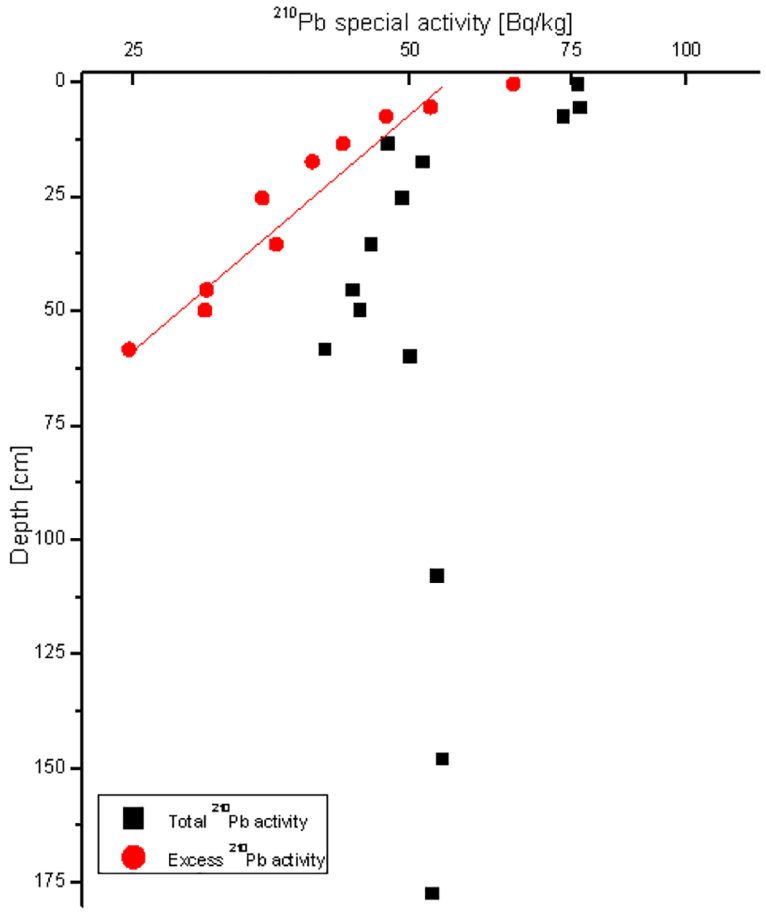

FIGURE 2
Vertical distributions of ^{210}Pb activities in stations RS-5. Quadrates indicate total ^{210}Pb activities and circles indicate excess ^{210}Pb activities.

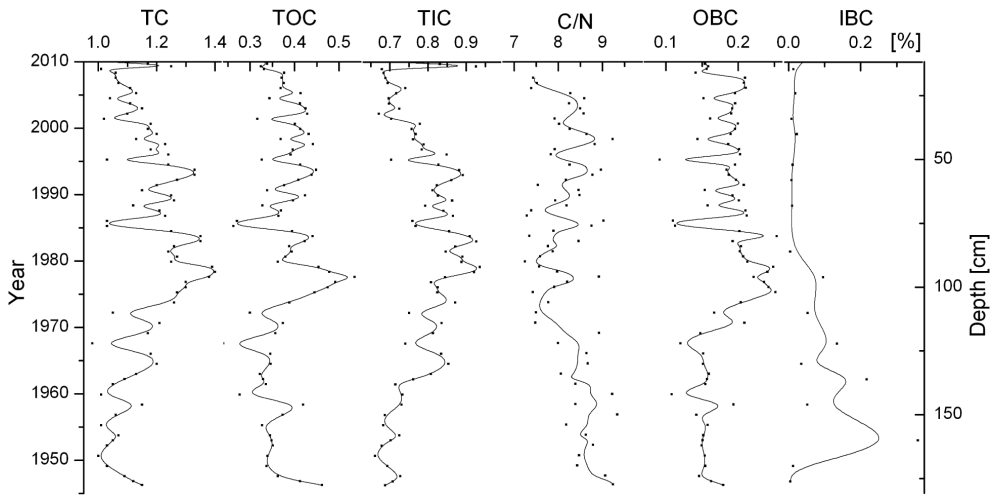

FIGURE 3
Contents and vertical distributions of TC, TOC, TIC, C/N, OBC, IBC in station RS-5.

2.42 ± 0.22 mmol/(cm^{2}a), 0.79 ± 0.09 mmol/(cm^{2}a), 1.63 ± 0.19 mmol/(cm^{2}a), 0.38 ± 0.07 mmol/(cm^{2}a), 0.17 ± 0.22 mmol/(cm^{2}a), and 0.54 ± 0.22 mmol/(cm^{2}a), respectively (Figure 4). The long-term trends of burial fluxes for the various types of carbon were generally similar to the time series of their contents in the sediments. The burial fluxes of TC, TOC and TIC in Sanggou Bay were much higher than those in the global deep sea (Hayes et al., 2021), and the buried flux of TOC in Sanggou Bay was higher than those in the most part of East China Sea and Alian Bay aquaculture area (Deng et al., 2006; Pan et al., 2021), but lower than that in Yangtze River estuary (Deng et al., 2006). However, for OBC, i.e., marine organic carbon, the buried flux in Sanggou Bay was significantly higher than that in Yangtze River estuary (Deng et al., 2006), and was similar to that in Alian Bay aquaculture area (Pan et al., 2021).

4 Discussion

4.1 Structure of the sedimentary carbon pool in Sanggou Bay

Over the past 70 years, the carbon buried in the sediments of station RS-5 is primarily inorganic carbon, with organic carbon

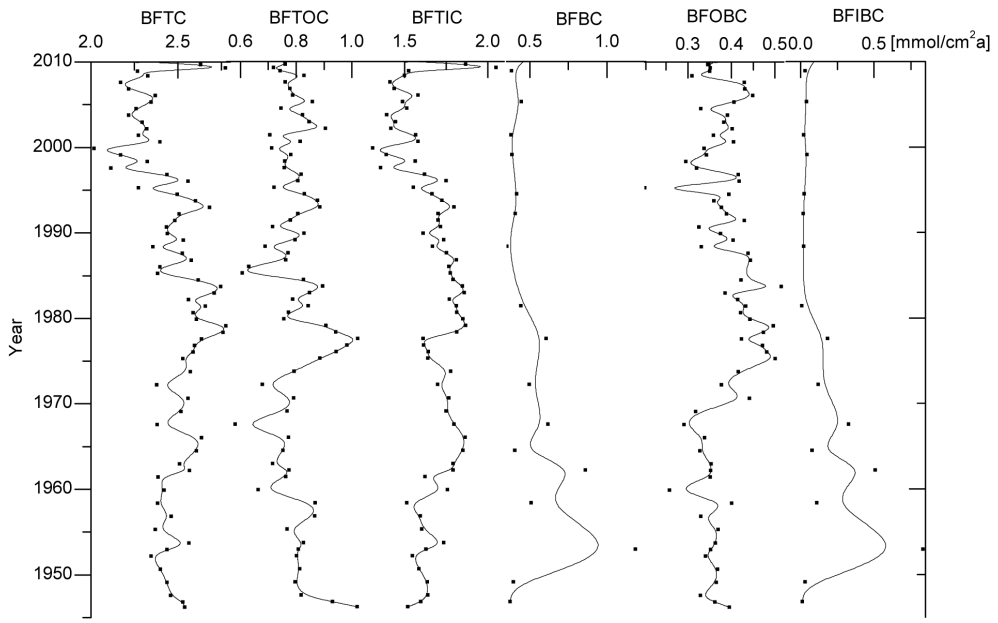

FIGURE 4
Long-term trends of burial fluxes of TC, TOC, TIC, BC, OBC, IBC in station RS-5. BFTC, BFTOC, BFTIC, BFBC, BFOBC and BFIBC indicate the burial flux of TC, TOC, TIC, BC, OBC and IBC respectively.

accounting for less than 33% on average. This pattern is similar to that found in the mouth of Sanggou Bay, indicating a high proportion of inorganic carbon burial in the sediments of the bay (Liu et al., 2014).

In the sediments located in the mouth of Sanggou Bay, the organic carbon is primarily of terrestrial origin (Liu et al., 2014). However, at station RS-5, the amount of marine organic carbon in the total organic carbon is nearly equal to that from terrestrial sources, with marine organic carbon accounting for approximately 48% on average and terrestrial sources accounting for around 52% on average. On one hand, this may suggest that central Sanggou Bay has higher primary productivity compared to the mouth of the bay (Wu et al., 2016). As a result, there is more deposition and burial of marine organic matter in the area. Otherwise, it has been observed that the speed of water flow in the mouth of the bay is higher as compared to the central bay (Zhao et al., 1996; Grant and Bacher, 2001). As a result of such high-speed water flow, the deposition of marine organic carbon, which has a smaller density and particle size, is hindered in the sediment of the mouth of Sanggou Bay. While in the central bay, where the hydrodynamics is weak, marine organic matter can deposit more effectively in the sediment environment. The sediments at station RS-5 have smaller particle sizes compared to those at the mouth of the bay, which supports this point (unpublished data).

The sediments of station RS-5 contain only about 10% ± 13% of marine inorganic carbon with the main source being terrestrial input. And this is obviously different in contrast to that in the mouth of Sanggou Bay, where inorganic carbon was mainly composed of marine inorganic carbon, and with a proportion of more than 70%. This distribution trend is noticeably different from the higher proportion of marine organic carbon in sediments at station RS5 compared to the Bay mouth. It is worth noting that the lower marine inorganic carbon proportion observed at station RS-5 is in the background that we considered both shell debris and calcareous zooplankton fossils during the marine inorganic carbon discrimination in sediments at station RS-5, whereas only shell debris carbon was examined in the mouth area of Sanggou Bay. In the sediment core from the Bay mouth, a significant amount of small shellfish remains and a visible sediment layer of small shellfish remains have been discovered, which are believed to be the primary reasons for the high proportion of marine inorganic carbon. On the other hand, there is no apparent sediment layer of small shellfish remains in the sediment from station RS-5, and small shellfish remains are sporadically found in the sediment.

Marine organic and inorganic carbon comprise BC in sediments. TC buried in the RS-5 sediments has inorganic carbon as the dominant existing form, while BC is dominant in the organic form, accounting for over 70% on average. Over the past 70 years, the pattern of BC in sediments has noticeably changed. Although OBC has been the dominant form of BC throughout the entire period, the proportion of IBC was relatively higher before the 1960s, with an average of nearly 30%. However, with the development of marine aquaculture in Sanggou Bay from the end of the 1960s, the proportion of IBC in BC decreased significantly. And the average proportion decreased to less than 10% after the 1980s.

4.2 Response of composition and burial flux of sedimental BC to human aquaculture activities in Sanggou Bay

Marine aquaculture activities in Sanggou Bay began in the late 1960s and early 1970s. Correspondingly, our data show that after that time, the burial fluxes of BC and IBC in the sediments of Sanggou Bay tended to decrease compared to the previous period, while the burial flux of OBC was significantly higher than that in the previous period, and the proportion of BC in TC and the proportion of IBC in BC also decreased compared to the previous period. We suggest this phenomenon indicates the influence of human aquaculture activity on the burial of blue carbon in sediments.

With the development of macroalgae culture since the 1960s, the sedimentation of biological detritus during the growth of macroalgae can result in a significant amount of extra organic matter being buried in the sediments (Vetter and Dayton, 1999; Carroll et al., 2003; Yang et al., 2022). Additionally, the large-scale culture of macroalgae can reduce the velocity of water flow (Zhao et al., 1996; Grant and Bacher, 2001). This can enhance the deposition and burial of suspended particulate matter into the sediments, leading to an increase in the amount of marine organic matter buried in the sediments. Correspondingly, the burial flux of OBC in RS-5 sediments significantly increased since the 1960s (Figure 5). It's worth noting that cultured macroalgae and phytoplankton in the water column have a competitive relationship. During growth, macroalgae can absorb a significant amount of nutrients from the water column. For example, kelp has excellent mechanisms for storing nutrients *in vivo* (Stewart et al., 2009). As a result, the availability of nutrients for phytoplankton growth is reduced, limiting their growth. Additionally, transport of organic matter from phytoplankton to sediments may decrease. However, the deposition of large amounts of organic matter from macroalgae culture has led to an increase in the buried flux of OBC in the sediments of this area, as well as an increase in the proportion of OBC in the total organic carbon, rather than a decreasing trend.

The trend of long-term change in the burial flux of IBC in the sediments of Sanggou Bay is significantly different from that of OBC. Before the start of mariculture activities, the abundance of phytoplankton provided a sufficient food source for small shellfish and calcareous zooplankton to grow vigorously. And the burial flux of IBC in sediments was high, as was its proportion among total inorganic carbon. After the late 1960s, the large-scale cultivation of kelp and other macroalgae began to restrict the growth of phytoplankton due to competition between different species. This limited the availability of food sources, which may restrict the growth of small calcareous organisms such as small shellfish (Xiao et al., 2022). Since the late 1970s and early 1980s, the aquaculture of large shellfish, such as scallops, has expanded and led to direct competition between farmed shellfish and small shellfish. This competition may have limited the growth of small shellfish and other small calcareous organisms (Galimany et al., 2017; Ferreira-Rodriguez et al., 2018; Xiao et al., 2022). Field survey results also support the view that the growth of zooplankton and benthic shellfish has been significantly affected by aquaculture

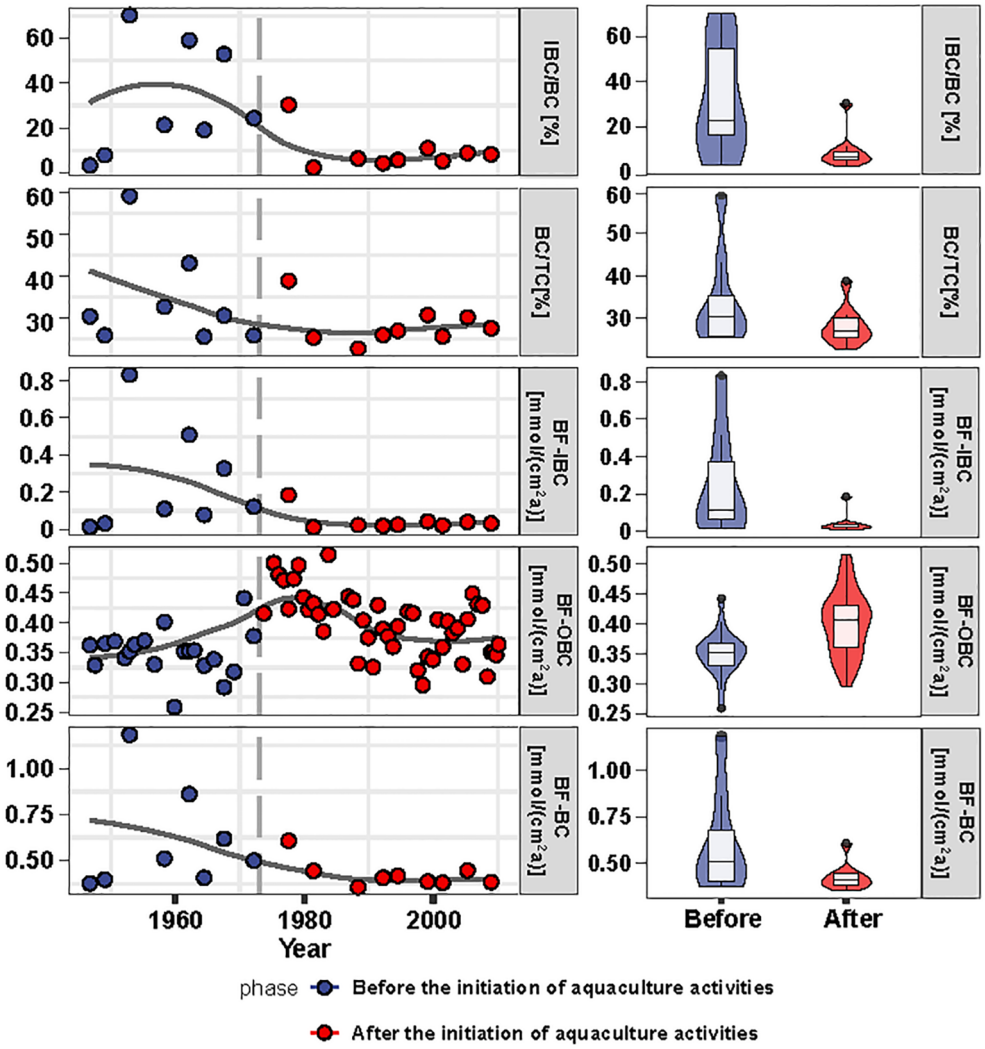

FIGURE 5
Responses of burial fluxes of BC to aquaculture activities.

activities: with the development of the aquaculture in Sanggou Bay, the zooplankton biomass decreased significantly; the abundance and diversity of benthic organisms were much lower than that before and the proportion of polychaetes increased dramatically, while the species of mollusc reduced substantially (Ji et al., 1998; Li et al., 2023). The same phenomenon was also observed in the aquaculture area in West Coast (USA) estuaries (Dumbauld et al., 2009). Large-scale farming of shellfish has made it difficult for the shells of these shellfish to be buried abundantly in sediment due to human harvesting. As a result, the decrease in the biomass of small shellfish and calcareous zooplankton may have led to a reduction in the burial rate of IBC in sediment, as well as a decrease in the proportion of IBC in the total inorganic carbon.

In Sanggou Bay, prior to aquaculture, IBC made up a significant portion of the burial flux of BC in sediments. During that period, the growth of small shellfish and calcareous zooplankton was promoted due to the abundant food provided by phytoplankton. As a result, the remains of these calcareous organisms were buried in large quantities in the sediments, leading to a relatively high flux of BC burial. After the development of aquaculture activities, the burial rate of OBC has increased. However, the burial flux of IBC decreased from about 0.28 mmol/(cm^2a) before the development of aquaculture activities to about 0.08 mmol/(cm^2a) in the 1980s and then continued to decline to about 0.03 mmol/(cm^2a). Furthermore, the proportion of IBC in BC has reduced from 26% before aquaculture to less than 4% after the 1980s. Meanwhile, the burial of BC has been declining. We believe that the decrease in burial flux of IBC and its proportion after the appearance of aquaculture were caused by the interspecific interaction of native calcareous organisms with aquaculture organisms. Therefore, the development of aquaculture activities in Sanggou Bay has reduced the burial of BC in sediments. Aquaculture activities in this study resulted in a decrease in the burial rate of BC in the sediments. However, it is important to note that a significant amount of carbon was fixed in the aquaculture products, which also falls under the category of BC (Tang and Lui, 2016). Overall, aquaculture activities have a positive impact on the carbon sink function of the surrounding waters.

4.3 The carbon sink function of marine sediment

Marginal seas are adjacent to land, and the carbon buried in their sediments includes not only the carbon fixed by marine organisms but also terrestrial-source carbon which is transported by runoff and the atmosphere. The burial of marine carbon and terrestrial carbon in the sediments are both the carbon storage of marine sediment. However, they play different roles in the carbon cycle. Marine source carbon in sediments originates from CO_2 fixed by marine organisms, which belongs to the category of BC (Nellemann et al., 2009; Mcleod et al., 2011; Macreadie et al., 2019). The burial of carbon from marine sources in sediments reflects the storage of fixed carbon in marine ecosystems. This process is an important aspect of the marine carbon sink. In contrast, terrestrial carbon originates from CO_2 absorbed by green plants on land, which is classified as green carbon and represents the carbon sink function of terrestrial ecosystems (Regnier et al., 2013). The burial of terrestrial carbon in marine sediment is a form of carbon storage. However, this carbon fixation occurs in terrestrial ecosystems and does not contribute to the carbon sink function of the oceans. Generally, the process of burying BC in marine sediments indicates the carbon sink function of marine ecosystems. On the other hand, the process of burying terrestrial carbon reflects the transfer function from the carbon pool of terrestrial ecosystems to that of marine ecosystems. Of course, the burial of terrestrial carbon into marine sediments is conducive to the long-term sequestration of this part of the carbon. In other words, the burial of BC in the sediment reflects the carbon removal function of the marine ecosystem, while the burial of terrestrial carbon in the sediment reflects the carbon sequestration assistance of the marine ecosystem. It is worth noting that the sequestration of terrestrial carbon in marine ecosystems does not significantly contribute to carbon fixation. However, it can impact the carbon cycling process in marine ecosystems by adsorption, resolution, and degradation during the transportation and burial of terrestrial carbon.

In the Sanggou Bay aquaculture sea, BC accounted for only 23% of TC burial flux in the sediment. Although the amount of carbon buried in the sediments of Sanggou Bay is 1-2 orders of magnitude higher than that in the adjacent central Yellow Sea (Yang et al., 2015), the carbon sink function of the sediments of Sanggou Bay has not increased to the same extent. This is because the carbon buried in the sediments of Sanggou Bay mostly comes from terrestrial sources. Of course, with the increasing distance away from shore, the influence of terrestrial ecosystems on the marine environment gradually decreases, and the burial flux of TC in the sediments increasingly reflects the actual carbon sink function of the marine ecosystem due to the decrease of the terrestrial carbon input.

Since the beginning of the JGOFS program, carbon burial fluxes have been estimated in sediments of many marginal seas. (Thunell et al., 1992; Sayles et al., 2001; Brunskill et al., 2002; Hayes et al., 2021; Zhao et al., 2021). However, the results of this study suggested that, due to the burial of terrestrial carbon in marginal sea sediments, the achieved results on burial fluxes of TC, total organic carbon and total inorganic carbon in marginal sea sediments include the migration process of carbon pools in terrestrial ecosystems in addition to the carbon fixation and removal function in marine ecosystems. It suggests that the carbon sink function of the marginal sea sediments might have been overestimated in previous results. Exploring the division of BC fraction in sediment and its burial behavior is necessary to accurately evaluate the carbon sink function of marginal sea sediments.

Various methods have been established to estimate organic carbon in sediments, including isotopes, C/N ratios, and biomarkers (Ruttenberg and Goñi, 1997; Andrews et al., 1998; Goñi et al., 1998; Huang et al., 2001; Bouchez et al., 2014; Xing et al., 2014; Sanderman et al., 2015; Geraldi et al., 2019; Zinkann et al., 2022); however, there are still challenges in identifying the origins of inorganic carbon in sediment samples. In this study, the source resolution of inorganic carbon was initially determined based on the morphological characteristics of inorganic carbon from various sources. We are afraid that some fragments of calcareous debris were not completely picked out due to their small size, leading to lower accuracy and precision of the experimental results. And due to the heavy workload, this method was rarely used for analyzing a large number of samples. Therefore, a fast and accurate method for analyzing the source of inorganic carbon in sediments needs to be developed. This will be a key issue in studying the function of BC sinks in sediments.

5 Conclusion

The carbon buried in the sediment of marginal seas originates from both marine production and terrestrial input. Only marine carbon, buried in the sediments, is the carbon fixed and stored by the marine ecosystem, which belongs to the category of BC and reflects the carbon sink function of the marine ecosystem. In order to deeply investigate the carbon sink function of marginal sea sediments, this study attempted to identify the buried BC in sediments in Sanggou Bay aquaculture sea area based on carbon source resolution and discussed the long-term change trend of the burial flux of BC over the past 70 years. The average BC content in the sediments of Sanggou Bay aquaculture area was 0.25% ± 0.10%, accounting for 23% of TC. OBC was the main component of BC, accounting for a proportion of about 72%. The burial flux of BC in the sediment of this sea area is about 0.54 ± 0.22 mmol/(cm^2a) for the past 70 years. The burial flux of sedimentary BC is influenced by human aquaculture. We suggest that with the development of aquaculture in Sanggou Bay, there has been a noticeable increase in the burial flux of OBC due to the sedimentation of more particulate organic matters resulting from aquaculture activities; however, due to the interspecies competition between aquaculture species and small calcareous organisms, the burial flux of IBC in sediments has significantly decreased. Overall, human aquaculture activities in Sanggou Bay

not only reduced the burial flux of BC in the sediments but also diminished the IBC proportion among BC.

Data availability statement

The raw data supporting the conclusions of this article will be made available by the authors, without undue reservation.

Author contributions

SY: Investigation, Methodology, Writing – original draft, Writing – review & editing. QY: Investigation, Writing – review & editing. XS: Writing – review & editing. WZ: Writing – review & editing. JL: Writing – review & editing. XQ: Methodology, Writing – original draft. JC: Writing – original draft. JH: Writing – original draft. BL: Writing – review & editing. YS: Writing – review & editing.

Funding

The author(s) declare financial support was received for the research, authorship, and/or publication of this article. This work was financially supported by the National Natural Science Foundation of China (NSFC) (grant numbers: U1906216, 41606130, U1406403), the Key Research and Development Program of Shandong Province (grant numbers: 2020ZLYS04) and the Key Basic Research Program of China (grant numbers: 2015CB453303).

Acknowledgments

We thank Dr. Xin Zhou, Institute of Polar Environment, University of Science and Technology of China, Hefei, for his help in analysis of ^{210}Pb activities. We also want to thank Mrs Hongxia Qiu, and Miss Sai Liu, Yellow Sea Fisheries Research Institute, Chinese Fisheries Science Academy, Qingdao, for her help with sample collection and sorting.

Conflict of interest

Authors SY, WZ, and BL were employed by the company Center Tech Tianjin Chemical Research and Design Institute Co. Ltd.

The remaining authors declare that the research was conducted in the absence of any commercial or financial relationships that could be construed as a potential conflict of interest.

Publisher's note

All claims expressed in this article are solely those of the authors and do not necessarily represent those of their affiliated organizations, or those of the publisher, the editors and the reviewers. Any product that may be evaluated in this article, or claim that may be made by its manufacturer, is not guaranteed or endorsed by the publisher.

References

Andrews, J. E., Greenaway, A. M., and Dennis, P. F. (1998). Combined carbon isotope and C/N ratios as indicators of source and fate of organic matter in a poorly flushed, tropical estuary: Hunts Bay, Kingston Harbour, Jamaica. *Estuarine Coast. Shelf Sci.* 46 (5), 743–756. doi: 10.1006/ecss.1997.0305

Bai, H. Y., Liu, S., Yang, Q., Huang, L. F., and Sun, Y. (2022). High-resolution records of the rate of carbon accumulation in the shellfish aquaculture area in Sanggou Bay and its response to human aquaculture activities. *Prog. Fishery Sci.* 43 (5), 98–105. doi: 10.19663/j.issn2095-9869.20210419002

Belicka, L. L., and Harvey, H. R. (2009). The sequestration of terrestrial organic carbon in Arctic Ocean sediments: A comparison of methods and implications for regional carbon budgets. *Geochimica Cosmochimica Acta* 73 (20), 6231–6248. doi: 10.1016/j.gca.2009.07.020

Berner, R. A. (1982). Burial of organic carbon and pyrite sulfur in the modern ocean: its geochemical and environmental significance. *Am. J. Sci.* 282 (4), 451–473. doi: 10.2475/ajs.282.4.451

Bianchi, T. S. (2011). The role of terrestrially derived organic carbon in the coastal ocean: A changing paradigm and the priming effect. *Proc. Natl. Acad. Sci.* 108 (49), 19473–19481. doi: 10.1073/pnas.1017982108

Bianchi, T. S., Mitra, S., and McKee, B. A. (2002). Sources of terrestrially-derived organic carbon in lower Mississippi River and Louisiana shelf sediments: implications for differential sedimentation and transport at the coastal margin. *Mar. Chem.* 77 (2-3), 211–223. doi: 10.1016/S0304-4203(01)00088-3

Blair, N. E., and Aller, R. C. (2012). The fate of terrestrial organic carbon in the marine environment. *Annu. Rev. Mar. Sci.* 4, 401–423. doi: 10.1146/annurev-marine-120709-142717

Bouchez, J., Galy, V., Hilton, R. G., Gaillardet, J., Moreira-Turcq, P., Pérez, M. A., et al. (2014). Source, transport and fluxes of Amazon River particulate organic carbon: Insights from river sediment depth-profiles. *Geochimica Cosmochimica Acta* 133, 280–298. doi: 10.1016/j.gca.2014.02.032

Boyd, C. E., Wood, C. W., Chaney, P. L., and Queiroz, J. F. (2010). Role of aquaculture pond sediments in sequestration of annual global carbon emissions. *Environ. pollut.* 158 (8), 2537–2540. doi: 10.1016/j.envpol.2010.04.025

Brunskill, G. J., Zagorskis, I., and Pfitzner, J. (2002). Carbon burial rates in sediments and a carbon mass balance for the Herbert River region of the Great Barrier Reef continental shelf, North Queensland, Australia. *Estuarine Coast. Shelf Sci.* 54 (4), 677–700. doi: 10.1006/ecss.2001.0852

Burdige, D. J. (2005). Burial of terrestrial organic matter in marine sediments: A re-assessment. *Global Biogeochemical Cycles* 19 (4), GB4011. doi: 10.1029/2004GB002368

Carroll, M. L., Cochrane, S., Fieler, R., Velvin, R., and White, P. (2003). Organic enrichment of sediments from salmon farming in Norway: environmental factors, management practices, and monitoring techniques. *Aquaculture* 226 (1-4), 165–180. doi: 10.1016/S0044-8486(03)00475-7

Dai, J., Song, J., Li, X., Zheng, G., Yuan, H., and Li, N. (2007). Geochemical characteristics of nitrogen and their environmental significance in Jiaozhou Bay sediment. *Quaternary Sci.* 27 (3), 347–356.

Deng, B., Zhang, J., and Wu, Y. (2006). Recent sediment accumulation and carbon burial in the East China Sea. *Global Biogeochemical Cycles* 20 (3), GB3014. doi: 10.1029/2005GB002559

Dumbauld, B. R., Ruesink, J. L., and Rumrill, S. S. (2009). The ecological role of bivalve shellfish aquaculture in the estuarine environment: a review with application to oyster and clam culture in West Coast (USA) estuaries. *Aquaculture* 290 (3-4), 196–223. doi: 10.1016/j.aquaculture.2009.02.033

Falkowski, P., Scholes, R. J., Boyle, E. E. A., Canadell, J., Canfield, D., Elser, J., et al. (2000). The global carbon cycle: a test of our knowledge of earth as a system. *Science* 290 (5490), 291–296. doi: 10.1126/science.290.5490.29

Ferreira-Rodriguez, N., Sousa, R., and Pardo, I. (2018). Negative effects of Corbicula fluminea over native freshwater mussels. *Hydrobiologia* 810, 85–95. doi: 10.1007/s10750-016-3059-1

Galimany, E., Freeman, C. J., Lunt, J., Domingos, A., Sacks, P., and Walters, L. (2017). Feeding competition between the native oyster Crassostrea virginica and the invasive mussel Mytella charruana. *Mar. Ecol. Prog. Ser.* 564, 57–66. doi: 10.3354/meps11976

Geraldi, N. R., Ortega, A., Serrano, O., Macreadie, P. I., Lovelock, C. E., Krause-Jensen, D., et al. (2019). Fingerprinting blue carbon: rationale and tools to determine

the source of organic carbon in marine depositional environments. *Front. Mar. Sci.* 263. doi: 10.3389/fmars.2019.00263

Golberg, E. (1963). Geochronology with 210Pb. *Radioactive Dating*, 121–131.

Goñi, M. A., Ruttenberg, K. C., and Eglinton, T. I. (1997). Sources and contribution of terrigenous organic carbon to surface sediments in the Gulf of Mexico. *Nature* 389 (6648), 275–278. doi: 10.1038/38477

Goñi, M. A., Ruttenberg, K. C., and Eglinton, T. I. (1998). A reassessment of the sources and importance of land-derived organic matter in surface sediments from the Gulf of Mexico. *Geochimica Cosmochimica Acta* 62 (18), 3055–3075. doi: 10.1016/S0016-7037(98)00217-8

Grant, J., and Bacher, C. (2001). A numerical model of flow modification induced by suspended aquaculture in a Chinese bay. *Can. J. Fisheries Aquat. Sci.* 58 (5), 1003–1011. doi: 10.1139/f01-027

Guo, X., Ford, S. E., and Zhang, F. (1999). Molluscan aquaculture in China. *J. Shellfish Res.* 18 (1), 19–31.

Hayes, C. T., Costa, K. M., Anderson, R. F., Calvo, E., Chase, Z., Demina, L. L., et al. (2021). Global ocean sediment composition and burial flux in the deep sea. *Global biogeochemical cycles* 35 (4), e2020GB006769. doi: 10.1029/2020GB006769

Hedges, J. I., and Keil, R. G. (1995). Sedimentary organic matter preservation: an assessment and speculative synthesis. *Mar. Chem.* 49 (2-3), 81–115. doi: 10.1016/0304-4203(95)00008-F

Honjo, S., Manganini, S. J., Krishfield, R. A., and Francois, R. (2008). Particulate organic carbon fluxes to the ocean interior and factors controlling the biological pump: A synthesis of global sediment trap programs since 1983. *Prog. Oceanography* 76 (3), 217–285. doi: 10.1016/j.pocean.2007.11.003

Huang, Y., Street-Perrott, F. A., Metcalfe, S. E., Brenner, M., Moreland, M., and Freeman, K. H. (2001). Climate change as the dominant control on glacial-interglacial variations in C3 and C4 plant abundance. *Science* 293 (5535), 1647–1651. doi: 10.1126/science.1060143

Ji, R., Mao, X., and Zhu, M. (1998). Impacts of coastal shellfish aquaculture on bay ecosystem. *J. Oceanography Huanghai Bohai Seas* 16 (1), 21–27.

Justić, D., Rabalais, N. N., and Turner, R. E. (2002). Modeling the impacts of decadal changes in riverine nutrient fluxes on coastal eutrophication near the Mississippi River Delta. *Ecol. Model.* 152 (1), 33–46. doi: 10.1016/S0304-3800(01)00472-0

Kaushal, S., and Binford, M. W. (1999). Relationship between C:N ratios of lake sediments, organic matter sources, and historical deforestation in Lake Pleasant, Massachusetts, USA. *J. Paleolimnology* 22, 439–442. doi: 10.1023/A:1008027028029

Kutti, T., Ervik, A., and Høisæter, T. (2008). Effects of organic effluents from a salmon farm on a fjord system. III. Linking deposition rates of organic matter and benthic productivity. *Aquaculture* 282 (1-4), 47–53. doi: 10.1016/j.aquaculture.2008.06.032

Li, W., Yu, X., Jiang, Z., Du, M., Jia, Y., et al. (2023). *Assessment of benthic ecological quality of Sanggou Bay through AMBI and M-AMBI approaches* (Periodical of Ocean University of China). Available at: https://link.cnki.net/urlid/37.1414.P.20231139,1341.001.

Liu, S., Yang, Q., Yang, S., Sun, Y., and Yang, G. (2014). The long-term records of carbon burial fluxes in sediment cores of culture zones from Sanggou Bay. *Acta Oceanol Sin.* 36, 30–38. doi: 10.3969/j

Ma, Z., Gray, E., Thomas, E., Murphy, B., Zachos, J., and Paytan, A. (2014). Carbon sequestration during the Palaeocene–Eocene Thermal Maximum by an efficient biological pump. *Nat. Geosci.* 7 (5), 382–388. doi: 10.1038/ngeo2139

Macreadie, P. I., Anton, A., Raven, J. A., Beaumont, N., Connolly, R. M., Friess, D. A., et al. (2019). The future of Blue Carbon science. *Nat. Commun.* 10 (1), 3998. doi: 10.1038/s41467-019-11693-w

Mcleod, E., Chmura, G. L., Bouillon, S., Salm, R., Björk, M., Duarte, C. M., et al. (2011). A blueprint for blue carbon: toward an improved understanding of the role of vegetated coastal habitats in sequestering CO_2. *Front. Ecol. Environ.* 9 (10), 552–560. doi: 10.1890/110004

Nellemann, C., Corcoran, E., Duarte, C. M., et al. (2009). *Blue carbon. A rapid response assessment* (Norway: Birkeland Trykkeri), 1–80.

Pan, Z., Tan, Y., Gao, Q., Dong, S., Fang, X., and Yan, J. (2021). A 120-year record of burial fluxes and source apportionment of sedimentary organic carbon in Alian Bay, China: Implication for the influence of mariculture activities, and regional environment changes. *Aquaculture* 535, 736421. doi: 10.1016/j.aquaculture.2021.736421

Pocklington, R., and Leonard, J. D. (1979). Terrigenous organic matter in sediments of the St. Lawrence Estuary and the Saguenay Fjord. *J. Fisheries Board Canada* 36 (10), 1250–1255. doi: 10.1139/f79-179

Prahl, F. G., Ertel, J. R., Goñi, M. A., Sparrow, M. A., and Eversmeyer, B. (1994). Terrestrial organic carbon contributions to sediments on the Washington margin. *Geochimica Cosmochimica Acta* 58 (14), 3035–3048. doi: 10.1016/0016-7037(94)90177-5

Qian, J., Wang, S., Xue, B., Chen, R., and Ke, S. (1997). A new approach to quantitatively estimate terrestrial organic carbon in lake sediments. *Chin. Sci. Bull.* 42, 1655–1658. doi: 10.1007/BF02882652

Regnier, P., Friedlingstein, P., Ciais, P., Mackenzie, F. T., Gruber, N., Janssens, I. A., et al. (2013). Anthropogenic perturbation of the carbon fluxes from land to ocean. *Nat. Geosci.* 6 (8), 597–607. doi: 10.1038/ngeo1830

Ren, Y., Dong, S., Wang, F., Gao, Q., Tian, X., and Liu, F. (2010). Sedimentation and sediment characteristics in sea cucumber Apostichopus japonicus (Selenka) culture ponds. *Aquaculture Res.* 42 (1), 14–21. doi: 10.1111/j.1365-2109.2010.02483.x

Ruiz-Fernández, A. C., Frignani, M., Tesi, T., Bojórquez-Leyva, H., Bellucci, L. G., and Páez-Osuna, F. (2007). Recent sedimentary history of organic matter and nutrient accumulation in the Ohuira Lagoon, Northwestern Mexico. *Arch. Environ. Contamination Toxicol.* 53, 159–167. doi: 10.1007/s00244-006-0122-3

Ruttenberg, K. C., and Goñi, M. A. (1997). Phosphorus distribution, C: N: P ratios, and δ^{13}Coc in arctic, temperate, and tropical coastal sediments: tools for characterizing bulk sedimentary organic matter. *Mar. Geology* 139 (1-4), 123–145. doi: 10.1016/S0025-3227(96)00107-7

Sanderman, J., Krull, E., Kuhn, T., Hancock, G., McGowan, J., Maddern, T., et al. (2015). Deciphering sedimentary organic matter sources: Insights from radiocarbon measurements and NMR spectroscopy. *Limnology Oceanography* 60 (3), 739–753. doi: 10.1002/lno.10064

Sayles, F. L., Martin, W. R., Chase, Z., and Anderson, R. F. (2001). Benthic remineralization and burial of biogenic SiO_2, $CaCO_3$, organic carbon, and detrital material in the Southern Ocean along a transect at 170 West. *Deep Sea Res. Part II: Topical Stud. Oceanography* 48 (19-20), 4323–4383. doi: 10.1016/S0967-0645(01)00091-1

Song, J. (2011). Carbon cycling processes and carbon fixed by organisms in China marginal seas. *J. Fishery Sci. China/Zhongguo Shuichan Kexue* 18 (3), 703–711. doi: 10.3724/SP.J.1118.2011.00703

Stewart, H. L., Fram, J. P., Reed, D. C., Williams, S. L., Brzezinski, M. A., MacIntyre, S., et al. (2009). Differences in growth, morphology and tissue carbon and nitrogen of Macrocystis pyrifera within and at the outer edge of a giant kelp forest in California, USA. *Mar. Ecol. Prog. Ser.* 375, 101–112. doi: 10.3354/meps07752

St-Onge, G., and Hillaire-Marcel, C. (2001). Isotopic constraints of sedimentary inputs and organic carbon burial rates in the Saguenay Fjord, Quebec. *Mar. Geology* 176 (1-4), 1–22. doi: 10.1016/S0025-3227(01)00150-5

Sun, X., and Turchyn, A. V. (2014). Significant contribution of authigenic carbonate to marine carbon burial. *Nat. Geosci.* 7 (3), 201–204. doi: 10.1038/ngeo2070

Tang, Q., and Lui, H. (2016). Strategy for carbon sink and its amplification in marine fisheries. *Strategic Study Chin. Acad. Eng.* 18 (3), 68–73.

Tao, S., Wang, A., Liu, J. T., Ye, X., Blattmann, T. M., Ran, C., et al. (2023). Characteristics of sedimentary organic carbon burial in the shallow conduit portion of source-to-sink sedimentary systems in marginal seas. *Geochimica Cosmochimica Acta* 353, 92–111. doi: 10.1016/j.gca.2023.05.006

Tesi, T., Miserocchi, S., Goñi, M. E. A., Langone, L., Boldrin, A., and Turchetto, M. (2007). Organic matter origin and distribution in suspended particulate materials and surficial sediments from the western Adriatic Sea (Italy). *Estuarine Coast. Shelf Sci.* 73 (3-4), 431–446. doi: 10.1016/j.ecss.2007.02.008

Thunell, R. C., Qingmin, M., Calvert, S. E., and Pedersen, T. F. (1992). Glacial-Holocene biogenic sedimentation patterns in the South China Sea: Productivity variations and surface water pCO_2. *Paleoceanography* 7 (2), 143–162. doi: 10.1029/92PA00278

Venkatesh, M. (2020). Appraisal of the carbon to nitrogen (C/N) ratio in the bed sediment of the Betwa River, Peninsular India. *Int. J. Sediment Res.* 35 (1), 69–78. doi: 10.1016/j.ijsrc.2019.07.003

Vetter, E. W., and Dayton, P. K. (1999). Organic enrichment by macrophyte detritus, and abundance patterns of megafaunal populations in submarine canyons. *Mar. Ecol. Prog. Ser.* 186, 137–148. doi: 10.3354/meps186137

Wu, W. G., Zhang, J. H., Wang, W., Li, J. Q., Fang, J. H., Liu, Y., et al. (2016). Distribution of chlorophyll-a concentration and its control factors in spring in Sungo Bay. *Shengtai Xuebao/Acta Ecologica Sin.* 36 (15), 4855–4863. doi: 10.5846 /stxb201501130102

Xiao, X., Liu, Y., Niu, P., Chen, X., Feng, Z., Wang, X., et al. (2022). Effects of culture of *Patinopecten yessoensis* and *Gracilaria lemaneiformis* on phytoplankton community structure based on an enclosure experiment. *Process Fishery Sci.* 43 (1), 66–76. doi: 10.19663/j.issn2095-9869.20200921003

Xing, L., Zhao, M., Gao, W., Wang, F., Zhang, H., Li, L., et al. (2014). Multiple proxy estimates of source and spatial variation in organic matter in surface sediments from the southern Yellow Sea. *Organic Geochemistry* 76, 72–81. doi: 10.1016/j.orggeochem.2014.07.005

Xu, M., Sun, C., Du, Z., and Zhu, X. (2023). Impacts of aquaculture on the area and soil carbon stocks of mangrove: A machine learning study in China. *Sci. Total Environ.* 859, 160173. doi: 10.1016/j.scitotenv.2022.160173

Yang, P., Tang, K. W., Yang, H., Tong, C., Yang, N., Lai, D. Y., et al. (2022). Insights into the farming-season carbon budget of coastal earthen aquaculture ponds in southeastern China. *Agriculture Ecosyst. Environ.* 335, 107995. doi: 10.1016/j.agee.2022.107995

Yang, S., Yang, Q., Liu, S., Cai, D., Qu, K., and Sun, Y. (2015). Burial fluxes and sources of organic carbon in sediments of the central Yellow Sea mud area over the past 200 years. *Acta Oceanologica Sin.* 34, 13–22. doi: 10.1007/s13131-015-0723-7

Zhang, Y., Galy, V., Yu, M., Zhang, H., and Zhao, M. (2022). Terrestrial organic carbon age and reactivity in the Yellow River fueling efficient preservation in marine sediments. *Earth Planetary Sci. Lett.* 585, 117515. doi: 10.1016/j.epsl.2022.117515

Zhao, B., Yao, P., Bianchi, T. S., and Yu, Z. (2021). Controls on organic carbon burial in the Eastern China marginal seas: A regional synthesis. *Global Biogeochemical Cycles* 35 (4), e2020GB006608. doi: 10.1029/2020GB006608

Zhao, J., Zhou, S. L., Sun, Y., and Fang, J. (1996). Research on Sanggou Bay aquaculture hydro-environment. *Mar. Fishery Res.* 17 (2), 68–79.

Zinkann, A. C., Wooller, M. J., Leigh, M. B., Danielson, S., Gibson, G., and Iken, K. (2022). Depth distribution of organic carbon sources in Arctic Chukchi Sea sediments. *Deep Sea Res. Part II: Topical Stud. Oceanography* 199, 105076. doi: 10.1016/j.dsr2.2022.105076

frontiers | Frontiers in Marine Science

TYPE Original Research
PUBLISHED 29 January 2024
DOI 10.3389/fmars.2023.1331680

Check for updates

OPEN ACCESS

EDITED BY
Junfu Dong,
Shandong University, China

REVIEWED BY
Zhuo-Yi Zhu,
Shanghai Jiao Tong University, China
Xiangbin Ran,
Ministry of Natural Resources, China
Hanzhi Lin,
Science Systems and Applications, Inc., United States

*CORRESPONDENCE
Hui Song
songhui2018@foxmail.com

RECEIVED 01 November 2023
ACCEPTED 28 December 2023
PUBLISHED 29 January 2024

CITATION
Zhang L, Zhou W, Wang Y, Liu Y, Chen J, Li B, Su B and Song H (2024) Overestimation of microbial community respiration caused by nitrification, and the identification of keystone groups associated with respiration. *Front. Mar. Sci.* 10:1331680. doi: 10.3389/fmars.2023.1331680

COPYRIGHT
© 2024 Zhang, Zhou, Wang, Liu, Chen, Li, Su and Song. This is an open-access article distributed under the terms of the Creative Commons Attribution License (CC BY). The use, distribution or reproduction in other forums is permitted, provided the original author(s) and the copyright owner(s) are credited and that the original publication in this journal is cited, in accordance with accepted academic practice. No use, distribution or reproduction is permitted which does not comply with these terms.

Overestimation of microbial community respiration caused by nitrification, and the identification of keystone groups associated with respiration

Lianbao Zhang[1,3,4], Wei Zhou[2], Yanwei Wang[1], Yeping Liu[1,3], Junfeng Chen[1,3], Bin Li[2], Bei Su[1] and Hui Song[1,3]*

[1]Institute of Marine Science and Technology, Shandong University, Qingdao, China, [2]Center Tech Tianjin Chemical Research and Design Institute Co., Ltd., Tianjin, China, [3]Southern Marine Science and Engineering Guangdong Laboratory, Zhuhai, China, [4]Fujian Key Laboratory of Marine Carbon Sequestration, Xiamen University, Xiamen, China

Instruction: Microbial community respiration (MCR) strongly controls the fate of organic carbon in the ocean. The balance between MCR and primary production strongly determines whether the ocean is a net sink or source of CO2 to the atmosphere. Thus, it is necessary to estimate MCR to better understand the role of oceans in the global carbon cycle. Methods based on apparent oxygen utilization (AOU) are predominant while electron transport system (ETS) assay gets increasing attention. Although methods get developed, few studies on MCR have been performed on a seasonal cycle. Because MCR is strongly associated with the temperature which changes along with the succession of seasons, it is urgent to study the MCR on a seasonal cycle.

Methods: Thus, we measured MCR using *in vivo* tetrazolium salt 2-(p-iodophenyl)-3-(p-nitrophenyl)-5-phenyltetrazolium chloride (INT) reduction rates (ETS) and oxygen-optode methods (AOU) simultaneously we measured the MCR based on AOU and ETS methods simultaneously from November 2020 to November 2021 in Aoshan Bay, China.

Results: The highest AOU appeared in autumn, followed by summer, spring, and winter, whereas the highest ETS activity appeared in summer, followed by spring, autumn and winter. The seasonal trend of MCR estimated from AOU and ETS were not consistent, and further analysis indicated that oxygen consumption induced by nitrification caused the overestimation of MCR in autumn evaluated from AOU.

Discussion: Microbial groups that were strongly correlated with MCR estimated by ETS had the ability to degrade various substrates and could get energy directly from light. It should be careful to notice the deviation of assumed organic carbon demand based on ETS caused by the alternation of day and night. Furthermore, the pattern of

bacterial groups associated with year-round MCR was distinct from season-specific MCR. This study raised a warning for caution when estimating MCR based on AOU and it was better to fully take the photoheterotrophy into account when assuming organic carbon remineralization based on ETS.

KEYWORDS

microbial community respiration, apparent oxygen utilization, electron transport system assay, photoheterotrophy, coastal ocean

1 Introduction

The metabolic activity of oceans is dominated by microorganisms; they play pivotal roles in mineralizing aquatic organic carbon, thus the overall patterns of oceanic carbon flux are largely controlled by microbes (Wang, 2018). One-half of the primary production of the biosphere occurs in the ocean (Kulk et al., 2020; Crockford et al., 2023) and a large fraction of it becomes dissolved (dissolved organic matter, DOM) (Dittmar et al., 2021). This dissolved part of the oceanic primary production is almost exclusively accessible to bacteria and archaea (Dittmar et al., 2021; Love et al., 2021). The assimilated carbon is respired or used to increase bacterial biomass, with the former accounting for 60-99% (Reinthaler and Herndl, 2005; Alonso-Sáez et al., 2007). The fate of carbon mediated by microbes strongly determines whether the ocean is net heterotrophic or autotrophic (Hansell et al., 2004; Reinthaler and Herndl, 2005). The trophic state of the ocean decides whether the ocean is a net source or net sink of CO_2 to the atmosphere, thus impacting the global climate (Holden et al., 2018; Friedlingstein et al., 2022). The primary productivity of phytoplankton and the mineralization of microorganisms affect the carbonate system. (Carla et al., 2022). It is necessary to estimate the organic carbon respiration by microbes to better understand the role of the ocean in the global carbon cycle. The amount of organic carbon respired to inorganic carbon can be quantified by microbial community respiration (MCR), thus it is a fundamental parameter in estimating the importance of bacteria in organic carbon remineralization (Guo et al., 2022).

The coastal ocean connects different carbon pools (terrestrial, atmosphere, open ocean, and sediment) and constitutes one of the most biogeochemically active zones on Earth. The general view is that the global coastal ocean is a net sink for atmospheric CO_2 (Laruelle et al., 2014; Gruber, 2015), taking up -0.45 Pg C $year^{-1}$ (Borges et al., 2005) to -0.21 Pg C $year^{-1}$ (Laruelle et al., 2010) of CO_2 from the atmosphere. This is largely induced by high primary production in these regions (Borges et al., 2005; Hernández-León et al., 2020). Although the coastal ocean covers only 7% of the global ocean, it contributes approximately 30% of the oceanic primary production (Gattuso et al., 1998). The balance between primary production and microbial respiration determines the roles of the coastal ocean in the global carbon cycle. Although MCR is reported as being strongly associated with temperature (García et al., 2023), which changes along with seasons, large fractions of previous studies on MCR have been performed within a certain time frame, with few studies being performed on a seasonal cycle. In this study, we measured MCR covering a full season cycle in Aoshan Bay to determine the seasonal dynamics of MCR and other environmental variables.

Major available approaches in MCR measurement can roughly be divided into two categories: (I) based on the measurement of the decline of a reactant (typically oxygen) or increase of a product (typically CO_2); and (II) based on the detection of the activity of enzymatic indicators (electron transport system (ETS) assay). Methods based on apparent oxygen utilization (AOU) are predominant, and 91% of the observation data of MCR are estimated with the Winkler method (Del Giorgio and Williams, 2005), which is the typical method for monitoring dynamics of oxygen concentration (Carpenter, 1965). Studies indicated that the bacterial respiration rate obtained by the Winkler method is overestimated, largely caused by the deficiencies of the method itself (Aranguren-Gassis et al., 2012; Martínez-García et al., 2013; García-Martín et al., 2019). With the development of technology, increasing methods to monitor the change of dissolved oxygen concentration have been developed, for example, the optodes sensor method (Warkentin et al., 2007). It is reported that the optodes method is better than conventional procedures (Warkentin et al., 2007). The deficiencies of the methodology are few, so does the MCR estimated based on oxygen consumption reflect the real MCR in the ocean? Thanks to accurate MCR being fundamental to estimating the carbon flow in marine food webs and the role of oceans in the global carbon cycle, we measured the MCR based on the *in vivo* INT method and optodes method continuously from November 2020 to November 2021 in Aoshan Bay, China (120°72'E, 36°36'N).

2 Methods and materials

2.1 Environmental variables determination

The temperature and salinity were recorded with Multiparameter Sonde (YSI EXO, YSI Inc.). The concentration of dissolved oxygen (DO) was measured using the Winkler method (Carpenter, 1965). The pH value of seawater was measured using a pH meter (StarA211, Thermo Fisher Scientific). For nutrient (ammonium, nitrite, nitrate,

silicate, and phosphate) analysis, seawater was prefiltered with a 0.45 μm pore-size filter (Millipore) and then stored in 15 mL tubes. Samples were measured using a Skalar SAN^{++} (AutoAnalyzer3, Seal Analytical) at Shandong University (precision: ± 0.1μmol/kg).

To measure the concentration of total organic carbon (TOC), 30 mL of seawater was transferred to 40 mL vials (CNW). All TOC samples were acidified to a pH value of 2 to 3 with 85% phosphoric acid to remove inorganic carbon and were then stored at -20 °C until analyses. The concentration of TOC was detected using an organic carbon analyzer (TOC-L CPH/CON, Shimadzu) following the high-temperature combustion method (Hansell and Carlson, 2001). Seawater used for fluorescent dissolved organic matter (FDOM) analysis was filtered through precombusted (450 °C, 6 h) 0.7 μm pore size GF/F membranes. The filtrate was stored in 40 mL precombusted (450 °C, 6 h) glass vials (CNW) at -20 °C in the dark until analysis. Absorbance and excitation-emission matrix (EEM) fluorescence spectra were recorded simultaneously using the Yvon Horiba Aqualog system (Aqualog-UV-800-C, HORIBA INSTRUMENTS INC). Excitation was scanned from 250 to 500 nm at 5 nm steps, and emission was recorded from 300 to 600 nm at 2 nm intervals. Fluorescence spectra were normalized to the area of the water Raman peak when the excitation was at 350 nm (Lawaetz and Stedmon, 2009). Three PARAFAC components (C1-C3) were identified and were compared to the OpenFluor database (Murphy et al., 2014). Two fluorescence-related parameters, biological index (BIX) and humification index (HIX), were calculated (Hansen et al., 2016). Detailed information on the calculation of HIX and BIX is provided in the Supplementary Material.

To detect the concentration of total chlorophyll a (Chl a), 1 L of seawater was filtered through 0.22 μm pore-size polycarbonate filters (47 mm diameter, Whatman). Filtered samples were stored in 15 mL tubes and subsequently transferred to -80 °C until analysis. The concentration of Chl a was determined using the 90% acetone method. First, tubes were filled with 4 mL 90% acetone and the filter was immersed in the acetone for 12 h at 4 °C. Then, the tube was centrifugated for 10 min at 4000 rpm at 18 °C. After that, the absorbance of acetone containing Chl a was measured using a spectrophotometer (UV-2700, Shimadzu) with selected wavelengths from 500-750 nm. Finally, the concentration (ug·mL^{-1}) of Chl a was calculated using the following equation: Chl a=11.47×(A664-A750)-0.40×(A630-A750), where A represents the value of absorbance at special wavelength (Jeffrey and Humphrey, 1975; Wellburn, 1994).

To measure microbial cell abundance, 2 mL triplicate seawater samples were collected and fixed by adding glutaraldehyde (final concentration of 0.5%) for 20 min in the dark at room temperature. Then the samples were fast-frozen in liquid nitrogen and stored at -80 °C until analysis. Cell abundance was measured using a flow cytometer (Accuri C6, Becton and Dickinson) following a previously established protocol (Marie et al., 1997).

2.2 Molecular analysis

To measure bacterial community structure, 1 L of seawater was prefiltered through a 20-μm-pore-size bolting cloth and then filtered through 0.22-μm-pore-size polycarbonate membranes, and the membranes were stored in 2 mL RNAase-free tube at -80 °C until DNA extraction. PowerSoil Kit (MoBio®) was used to extract DNA according to the manufacturer's protocol. The bacterial V3–V4 regions of 16S rRNA genes were amplified using primers 338F: 5'-ACTCCTACGGGAGGCAGCA-3' and 806R: 5'-GGACTACNNGGGTATCTAAT-3' (Guo et al., 2018). Amplicons were purified using an AxyPrep DNA Gel Extraction Kit (Axygen Biosciences) and then sequenced on an Illumina HiSeq 2500 platform.

Bioinformatic analysis was conducted following previous protocols (Zhang et al., 2021). Briefly, FLASH was used to merge paired-end clean reads. Then, the QIIME2 pipeline was used to denoise merged reads and remove chimera. Clean and non-chimeric sequences were further clustered into amplicon sequence variants (ASVs). To assign taxonomy, ASVs were checked against the SILVA database (v138).

2.3 Microbial community respiration rate determination

Seawater samples were collected from the surface using CTD. To elucidate how MCR varied over time at the surface of Aoshan Bay, we measured MCR using *in vivo* tetrazolium salt 2-(p-iodophenyl)-3-(p-nitrophenyl)-5-phenyltetrazolium chloride (INT) reduction rates (Martínez-García et al., 2009) and oxygen-optode methods (Jiao et al., 2021) simultaneously. Rates of MCR were estimated from the formation of INT-formazan (INT-F), the production of the reduction of the INT by electron transport system (ETS) dehydrogenase enzymes, following the protocol described by Martínez-García (Martínez-García et al., 2009) with some modifications. The optodes sensor can directly record the change in oxygen concentration and reflect the apparent oxygen consumption in the bottle. Briefly, three replicates were immediately fixed by adding formaldehyde (2% v/v final concentration) and used as dead controls.

Samples (three dead controls and three live controls, 200 mL of each) were spiked with a solution of INT (with a final concentration of 0.2 mM), meanwhile, the optodes sensors (OXSPS TROXSP5, Pyroscience, Germany) were stuck inside the incubation bottle. It should be noted that the control should be put in the dark for 20 minutes before adding INT. Then, samples were incubated in the dark for 1 h (Supplementary Figure 3) in temperature-controlled (± 0.1 °C of the *in situ* temperature) incubation chambers. After incubation, formaldehyde (2% v/v final concentration) was added to the live samples, and the samples were kept in the dark for 20 minutes. Finally, all samples were filtered through 0.22 μm pore size polycarbonate membrane filters (47 mm diameter) at pressure < 0.02 MPa, and all filters were placed into cryovials. Then, 1.6 mL propanol was added to all cryovials, and INT-F was extracted by initially sonicating the cryovials for approximately 30 min at 50 °C using an ultrasonic bath. Propanol containing the INT-F was then transferred into microfuge vials and centrifuged. Finally, the concentration of INT-F was determined by absorption spectrophotometry (UV-2700, Shimadzu spectrophotometer, Japan) at 485 nm. The optode was calibrated before every measurement and the signal was measured periodically, every 10 min. Oxygen consumption rates for each sample were obtained from the slope of the linear regressions. Detailed information on respiration rate estimation is provided in the Supplementary Material.

2.4 Statistical analyses

NMDS analysis was conducted in R using the metaMDS function in the vegan package. NMDS was performed on the relative abundance of ASVs in order to focus on relative changes in microbial community compositions.

To link MCR with physical-chemical variables and biogeochemical processes, partial least squares path modeling (PLS-PM) was performed. Latent variables, namely, nutrients and α-diversity, included more than one manifest variable, with nutrients including ammonium and nitrite, and α-diversity including Simpson, ACE, and Pielous. The model was constructed using the plspm package in R. Variables with loadings < 0.7 were removed and the remaining variables were used to perform the final PLS-PM structure equation (Gao et al., 2019). The prediction performance of models was assessed by the goodness of fit (GOF) and R^2 value.

The maximal information coefficient (MIC) can capture diverse relationships between two pairs of variables (Reshef et al., 2011). The dataset consisted of 22 microbial samples and 18 environmental variables. MIC analyses were run using B=0.6, CV=0.5, and statistically significant relationships with MIC≥0.4 (Logares et al., 2020) were considered. A precomputed p-value was used to assess MIC significance (Reshef et al., 2011).

The correlation among different species at the order level was calculated in R. Only robust (correlation coefficient ≥ 0.6 or ≤ -0.6) and statistically significant ($p < 0.05$) correlations were considered, and networks were visualized using Cytoscape v3.9.1. The fast greedy modularity optimization was used to find modules of highly correlated taxa (Clauset et al., 2004). Groups of ASVs in a module are highly connected among themselves, whereas they have fewer connections with ASVs outside the module. Positive correlations indicate the relative abundance of ASV changes along the same trend, whereas negative correlations signify the relative abundance of ASV changes in the opposite direction. We used the mantel test to calculate the correlation between different modules with *in vivo* INT reduction rate, and significant modules were chosen to do further analysis. Spearman correlation between species within the chosen module and the *in vivo* INT reduction rate were assessed in R. This was helpful in finding microbial groups that played pivotal roles in determining MCR.

3 Results

3.1 Environmental variables

The variation in season nearshore environment in Aoshan Bay causes a number of changes, including changes in temperature, DO, Chl a, nutrients, microbial community compositions, organic matter, and MCR. Sampling took place from November 2020 through November 2021.

The temperature fluctuated along with the season and the ranking of the four seasons was summer, spring, autumn, and winter (Supplementary Figure 2A). The same trend was observed in cell abundance (Supplementary Figure 2C). For DO, the situation was the opposite: DO was lower in summer than in other seasons (Supplementary Figure 2D). The value of pH ranged from 7.9 to 8.3 (Supplementary Figure 2C). The concentration of Chl a was increasing with time and peaked in summer, but decreased after summer (Supplementary Figure 2F). The coastal ocean was strongly impacted by freshwater input, thus the salinity drastically changed (Supplementary Figure 2B). Salinity was lower in autumn than in other seasons (Supplementary Figure 2B). The changes in DIN and nitrifiers are shown together in the following section to better explain the dynamics of the nitrogen cycle.

3.2 Microbial community respiration and FDOM

The MCR was estimated using *in vivo* INT reduction rates and oxygen consumption rates simultaneously. The INT reduction rate ranged from 0.022 (± 0.004) to 0.441 (± 0.045) μmol INTF L^{-1} h^{-1} and the oxygen consumption rate ranged from 0.057 (± 0.044) to 9.840 (± 0.857) μmol O_2 L^{-1} h^{-1} (Figure 1). Mean MCR was 0.124 μmol INTF L^{-1} h^{-1} and 1.544 μmol O_2 L^{-1} h^{-1}, respectively. The INT reduction rate was increasing from winter to summer and the same trend was true for the oxygen consumption rate (Figure 1). When it shifted from summer to autumn, the INT reduction rate decreased while the oxygen consumption rate still increased (Figure 1). Thus, the MCR was the highest in summer based on ETS but the highest in autumn based on oxygen consumption rate (Figure 1). According to the season, four different periods of respiration rates were defined: spring, summer, autumn, and winter. The INT reduction rate was summer (0.251 μmol INTF L^{-1} h^{-1}) > spring (0.104 μmol INTF L^{-1} h^{-1}) > autumn (0.077 μmol INTF L^{-1} h^{-1}) > winter (0.050 μmol INTF L^{-1} h^{-1}), whereas the oxygen consumption rate was autumn (3.262 μmol O_2 L^{-1} h^{-1}) > winter (1.405 μmol O_2 L^{-1} h^{-1}) > summer (1.150 μmol O_2 L^{-1} h^{-1}) > spring (0.724 μmol O_2 L^{-1} h^{-1}). These results reflected the divergence of MCR estimated with different methods.

The PARAFAC model decomposed three components (C1, C2, and C3), which were statistically validated using the split-half validation (Supplementary Figure 4). These components were confirmed with the OpenFluor database (Murphy et al., 2014). C1 (Maxex/em=250(310)/398 nm) and C2 (Maxex/em=250(360)/480 nm) were characterized as humic-like components, and C3 (Maxex/em=275/323 nm) exhibited protein-like component properties. C1 and C2 had similar variations in that fluorescence intensity increased over time and peaked in autumn (Figure 1B). In contrast, the fluctuation of C3 was more slight and a peak appeared in winter (Figure 1B). Besides, HIX increased with time and peaked in autumn. These results indicated that refractory humic-like components accumulated in autumn. The differences in BIX in winter, spring, and autumn were slight, and BIX in summer was higher than in other seasons (Figure 1B).

3.3 Microbial community dynamics

At the phylum level, communities were dominated by Proteobacteria (58.3%), Bacteroidota (20.1%), and Actinobacteriota

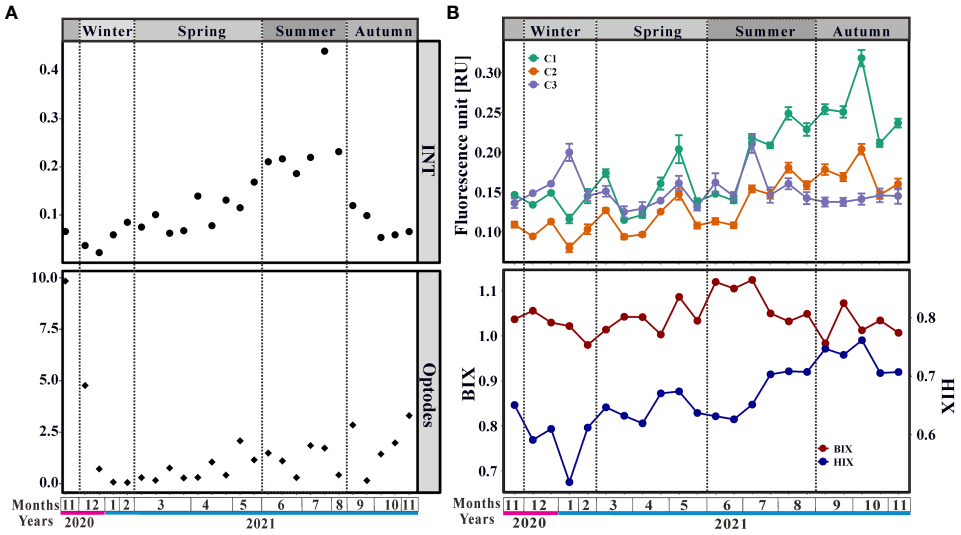

FIGURE 1
Changes of **(A)** INT reduction rates (μmol INTF L^{-1} h^{-1}) and oxygen consumption rates (μmol O_2 L^{-1} h^{-1}), and **(B)** components of Fluorescent Dissolved Organic Matter (FDOM).

(8.6%) (Figure 2A), while at the order level, communities were dominated by Rhodobacterales (32.8%), Flavobacteriales (17.6%), Actinomarinales (6.3%), Alteromonadales (4.0%), Burkholderiales (3.4%), and Oceanospirillales (3.3%) (Figure 2B). The relative abundance of Proteobacteria reached a peak in late January, lasted until March, and then decreased (Figure 2A). Actinobacteriota was higher in autumn than in other seasons (Figure 2A). It should be noted that the relative abundance of Cyanobacteria peaked in August and then decreased with time (Figure 2A). Differences among seasons were little for Bacteroidota (Figure 2A). Although no hypoxia occurred in Aoshan Bay (Supplementary Figure 2D), the sulfate-reducing bacteria Desulfobacterota was abundant in groups throughout the year (Figure 2A), being highest in spring and lowest in winter (Figure 2A).

Rhodobacterales (33%), Flavobacteriales (18%), Actinomarinales (6%), and Alteromonadales (4%) were predominant throughout the year at the order level (Figure 2B). Oceanospirillales were significantly higher in summer than in other seasons and the same was true for Chitinophagales and Vibrionales (Figure 2B). Actinomarinales accounted for a larger proportion in autumn than in other seasons (Figure 2B). Alteromonadales were higher in winter and summer than in spring and autumn (Figure 2B). As for Burkholderiales, the relative abundance was higher in the first (winter and spring) half of the year than in the second (summer and autumn) half (Figure 2B). SAR11_clade was clearly higher in later spring than in other periods (Figure 2B). Similar to Cyanobacteria, the bloom of synechococcales appeared in late summer and decreased with time (Figure 2B).

Dissolved inorganic nitrogen (DIN) concentration changed along with the seasons (Figure 3A). Ammonium, nitrite, and nitrate were highest in autumn as compared to the rest of the year (Figure 3A). The concentration of ammonium changed little, being low before August

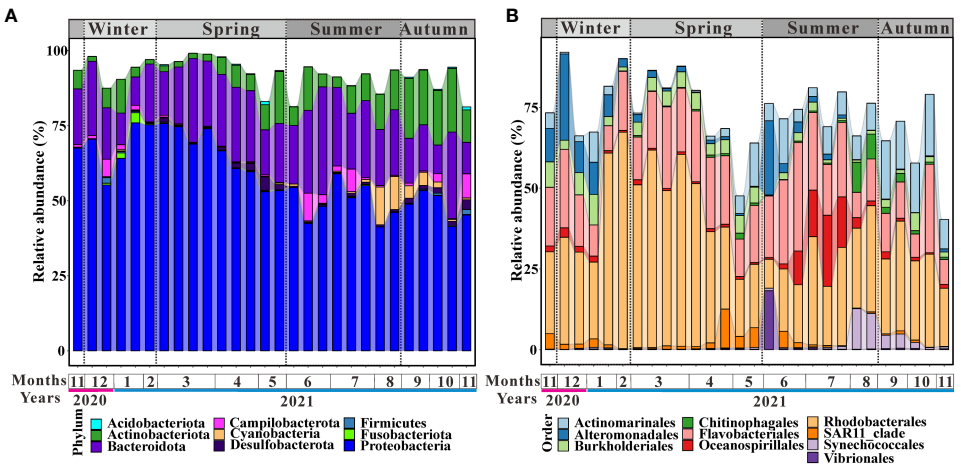

FIGURE 2
Microbial community compositions at **(A)** phylum and **(B)** order level.

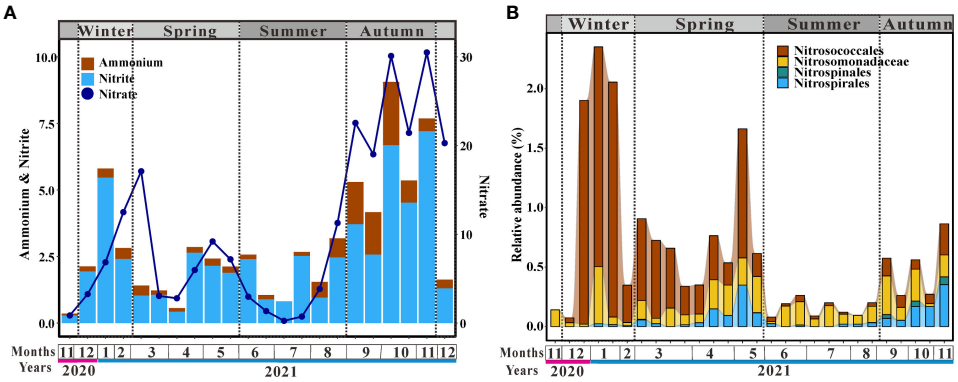

FIGURE 3
Changes of **(A)** dissolved inorganic nitrogen and **(B)** relative abundance of major nitrifiers.

and then increasing, causing ammonium accumulation in autumn (Figure 3A). Although the concentration of nitrite fluctuated with each month, it was higher in autumn than in other seasons (Figure 3A). Nitrate concentration increased in winter and early spring, but then dropped, with the lowest value appearing in summer (Figure 3A). The concentration of nitrate increased from July onward, peaking in autumn (Figure 3A). Nitrifiers were widespread in the coastal ocean and four species were found in Aoshan Bay (Figure 3B). In winter and spring, ammonium-oxidizing bacteria (AOB) belonging to Nitrosococcales were clearly dominant (Figure 3B). Nitrosomonadaceae, another group affiliated to AOB, dominated the nitrifying bacteria in summer (Figure 3B). Nitrite-oxidizing bacteria (NOB), Nitrospinales and Nitrospirales, were higher in autumn than in other seasons (Figure 3B). Bloom of Nitrospirales was also observed in the second half of spring (Figure 3B). In summary, AOB was the dominant nitrifier in Aoshan Bay except in autumn, during which the relative abundance of AOB was not clearly higher than that of NOB (Figure 3B).

3.4 Links between physical-chemical parameters and microbial activities

MCR was well explained by our block variables (R^2 = 0.86) and provided a good fit to our data (GOF of 0.62; Figure 4A). Temperature showed the largest effect on MCR via direct (path coefficient = 0.38) and indirect (path coefficient = 0.37) effects. There were strong positive correlations between TOC and MCR, and a similar trend was observed between cell abundance and MCR (Figure 4A). It was meaningful to notice the negative effect of nutrients on DO (Figure 4A).

To investigate how individual species responded to physical-chemical parameters, MIC was used to determine the correlation of single species with multiple abiotic environmental variables (Figure 4B). Nitrite was the variable with the highest number of associated species (3.7%), followed by HIX (3.6%), salinity (3.5%), silicate (3.4%), C1 (3.4%) and C2 (3.0%) components of FDOM, DO (2.7%), ETS (2.5%), and DIN (2.2%) (Figure 4B). The

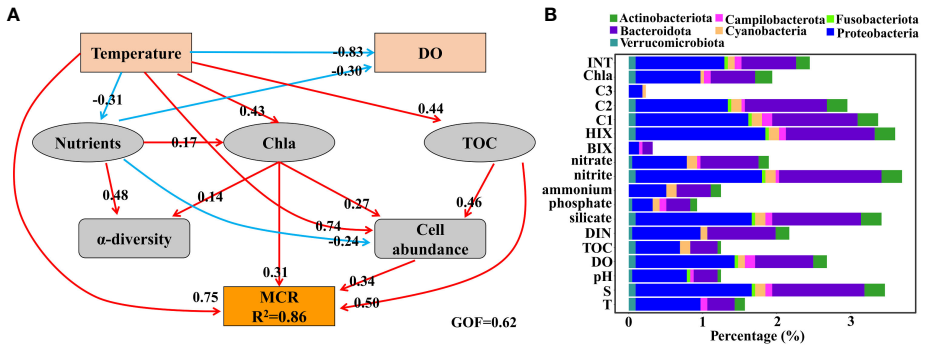

FIGURE 4
(A) Partial least squares path analysis for microbial community respiration (MCR), showing the relationships between selected physical-chemical parameters, characteristics of microbes, and MCR. GOF, goodness of fit; DO, dissolved oxygen; TOC, total organic carbon; Chl a, chlorophyll (a) Red and blue lines represent positive and negative correlations, respectively. For simplicity, only effects that were not less than 0.1 are shown in the plot. Meanwhile, the effects of oxygen on other parameters are also not shown in the plot as a result of no hypoxia in the sampling field. **(B)** The percentage of ASVs significantly correlated with various environmental parameters (based on maximal information coefficient). Information on the taxonomy of ASVs is shown in different colors.

remaining variables displayed associations with individual species that were of less than 2% (Figure 4B). Proteobacteria featured a greater proportion of individual species associations with almost all physical-chemical parameters than other groups (Figure 4B). Except for Proteobacteria, species affiliated with Bacteroidota were associated dominantly with almost all environmental variables (Figure 4B). Species significantly related to INT belonged to Actinobacteriota (0.18%), Proteobacteria (1.20%), Fusobacteriota (0.05%), Cyanobacteria (0.09%), Campilobacterota (0.09%), Bacteroidota (0.74%), and Verrucomicrobiota (0.09%) (Figure 4B).

3.5 Keystone microbial groups linking MCR

The NMDS plot calculated from the bacterial communities on the basis of the Bray-Curtis index displayed that samples collected during the same season preferred to cluster together and microbial dynamics were significantly related to seasons (Supplementary Figure 4). Furthermore, MIC displayed that 2.5% of ASVs significantly associated with INT that represented the intensity of MCR (Figure 4B). Because much information is lost at lower taxonomic levels, network and mantel tests were conducted to detect microorganisms strongly determining MCR at the order level. Five major modules based on the co-occurrence of groups (hereafter referred to as Modules 1-5) were identified (Figure 5A). Among them, Module 1 significantly positively correlated with the *in vivo* INT reduction rate (Mantel test, $p<0.05$). Within Module 1, by correlating the Spearman correlation coefficient between module membership with MCR assessed by the *in vivo* INT reduction rate method, we identified orders that were significantly correlated with MCR. Results showed that 14 orders were significantly correlated to MCR throughout the year (Figure 5B). Three orders were strongly associated with MCR in spring, while there were six in summer, zero in autumn, and one in winter (Figure 5B).

4 Discussion

4.1 The divergence of MCR estimated based on *in vivo* INT reduction rate and oxygen consumption rate

It is worth noting that the peak of MCR appeared in summer based on the *in vivo* INT reduction rate, and in autumn based on the optodes method, (Figure 1A). Studies prove that MCR is strongly impacted by characteristics and concentration of organic matter (Cleveland et al., 2007; Alonso-Sáez et al., 2008; Chin et al., 2023). In Aoshan Bay, changes in FDOM indicated that the humic-like components accumulated in autumn (Figure 1B). In general, humic-like components are recalcitrant to microbial degradation and accumulate in field and incubation experiments (Tanaka et al., 2014; Zheng et al., 2019). The relationship between MCR and the concentration of organic carbon is generally significantly positive (Alonso-Sáez et al., 2008), and the results of PLS-PM supported this (Figure 4A). It can be inferred that MCR should be lower in autumn than in summer because the organic matter is more refractory, meanwhile, the concentration of it is lower in autumn than in summer. Furthermore, temperature is another important environmental factor determining MCR, which has been supported in our study (Figure 4A), and generally MCR is positively correlated with temperature and peaks in summer (Lucea et al., 2005; Apple et al., 2006; Smith et al., 2021). Changes of organic carbon pool and temperature supported that MCR should be highest in summer than in other seasons. The change of the *in vivo* INT reduction rate was in accordance with this view, however, this was not true to the oxygen consumption rate (Figure 1A). This implied that MCR constituted less proportion of total oxygen consumption in autumn and there were other processes causing oxygen depletion.

Nitrifiers are universal in oceans (Karner et al., 2001; Wuchter et al., 2006; Bayer et al., 2022) and nitrification is an important

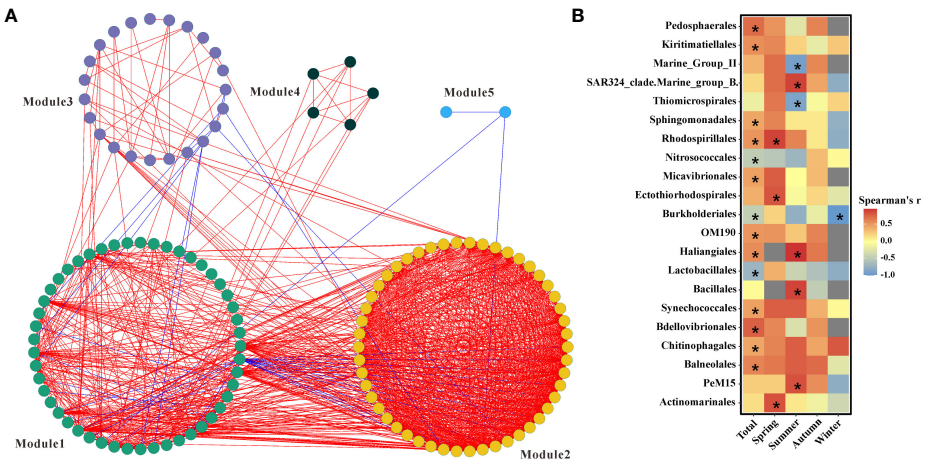

FIGURE 5
(A) Network interactions between microbial groups. Red and blue lines indicate positive and negative interactions between microbial groups, respectively. **(B)** significant correlations between microbial groups involved in module 1 and the *in vivo* INT reduction rate.

oxygen sink. There are many studies exploring the role of nitrification in oxygen consumption. A study in the Changjiang River plume indicated that oxygen demands of nitrification accounted for 0.32 to 318% of the community respiration rate (Hsiao et al., 2014). Studies based on other estuaries or fjords found that nitrification can constitute 20-30% and even up to 64% of the total oxygen consumption (Lipschultz et al., 1986; Berounsky and Nixon, 1993; Pakulski et al., 1995; Dai et al., 2008; Grundle and Juniper, 2011). A recent study supported that nitrification was universal in the ocean and was largely determined by its substrates (Tang et al., 2023). The negative effect of nutrients on DO in Aoshan Bay was in accordance with previous studies (Figure 4A). All these studies prove that nitrification plays a crucial role in oxygen depletion in coastal oceans, and the estimation of MCR based on AOU in the eutrophic coastal ocean was uncertain.

The change of DIN showed that substrates of nitrification, ammonium, and nitrite, were significantly higher in autumn than in other seasons (Figure 3A). A previous study indicated that the nitrification rate was positively correlated with ammonium concentration (Hsiao et al., 2014). This suggested that the nitrification rate would be higher in autumn than in other seasons. Results of MIC displayed that the proportion of ASVs associated with nitrite was the largest (Figure 4B), which further supported that nitrification played a pivotal role in Aoshan Bay. The relative abundance of nitrifiers, including Nitrospinales and Nitrospirales, was clearly higher in autumn than in other seasons (Figure 3B). There were little differences in Nitrosomonadaceae levels in the different seasons (Figure 3B). However, Nitrosococcales were higher in winter than in other seasons (Figure 3B). Nitrosococcales and Nitrosomonadaceae are AOB (Prosser et al., 2014; Ward et al., 2021), while Nitrospinales and Nitrospirales are NOB (Jing et al., 2022). Considering that the concentration of nitrite was higher than ammonium in winter (Figure 3B), although the relative abundance of AOB was highest in winter (Figure 3A), the nitrification rate was low. The same situation was true in spring. Nitrification is not as important as MCR in oxygen depletion in summer, since nitrifiers are less competitive than phytoplankton for ammonium and nitrite in this season (Hampel et al., 2018; Zakem et al., 2018). Nitrification was a more important oxygen sink in autumn than in other seasons in Aoshan Bay. This explains the difference between the *in vivo* INT reduction rate and oxygen consumption rate estimated by the optodes method in autumn. The oxygen consumption rate could not accurately reflect MCR because nitrification constituted a large proportion of total oxygen consumption in autumn.

As discussed above, nitrification contributes to biological oxygen demand and causes discrepancies in estimating MCR based on the apparent oxygen consumption rate in Aoshan Bay. Besides, reduced substrates, such as HS^-, Fe^{2+}, and methane, also contribute to oxygen demand (Friedrich et al., 2014; Fennel and Testa, 2019). It had been reported that the difference of MCR evaluated by AOU and *in vivo* INT could be used to estimate the activities of aerobic chemoautotrophy, which played an important role in maintaining the aphotic ocean system with carbon and energy scarcity (Li X et al., 2023). One of the potential ways to solve this problem is to estimate MCR and the concentration of key reduced elements (e.g., ammonium, nitrite, and sulfide) simultaneously. The dynamics of nutrients might be used to calibrate the MCR rate.

Whether the ocean is a net sink or a source of CO_2 to the atmosphere is essential for understanding the role of the ocean in mitigating climate change. The balance between MCR and primary production strongly determines the air-sea CO_2 flux, thus numerous researchers focus on MCR. The change of AOU was widely used to estimate MCR in coastal oceans that receive excessive nutrients from the land (Carol et al., 2023). Both aerobic respiration and chemoautotrophy are sensitive to substrate concentration (Kache et al., 2021). The results of this study support the idea that MCR based on AOU was overestimated, especially in eutrophic coastal oceans. These areas are predominant for primary production and microbial respiration, accompanied by active chemoautotrophic processes. It has been reported that intense nitrification plays a vital role in oxygen consumption in estuarine areas (Lu et al., 2020). In other regions with particularly high nutrient concentrations, the rate of aerobic chemoautotrophic processes even exceeds that of respiration (Hsiao et al., 2014). Therefore, relying solely on AOU for estimating MCR may not be accurate enough. It could be inferred that the amount of atmospheric carbon absorbed by the ocean was underestimated in previous studies. It is better to measure MCR based on AOU and *in vivo* INT simultaneously to obtain more accurate values of MCR in eutrophic ocean zones. It is necessary to update the database of MCR, especially those measured based on AOU in coastal areas and continental shelf sea.

4.2 Keystone groups significantly associated with MCR

As discussed above, the MCR assessed by AOU was not always accurate, thus values estimated by INT were chosen for performing further analysis. Microbial community compositions changed with the change in seasons (Gilbert et al., 2012; Hu et al., 2023) and the results of NMDS were consistent with this view (Supplementary Figure5). It can be inferred that the species significantly associated with MCR were different according to the seasons. MIC showed that large proportions of ASVs (Figure 4B) were significantly correlated with INT and were used to estimate MCR. Considering the complex interactions among different species, they were first separated into modules. The result of the mantel test indicated that only module 1 had a significant correlation with the *in vivo* INT reduction rate. The relative abundance of module 1 was less than 20% from January to April, whereas it was more than 25% in other months. The pattern of bacterial groups associated with year-round MCR is distinct from season-specific MCR (Figure 5B). These keystone groups could roughly be divided into four categories.

The first clade was associated with products of photoautotrophs. Pedosphaerales have been reported to be the rhizosphere microbiota of many plants (Walters et al., 2018; Yurgel et al., 2018), and their relative abundance was higher from May to September than in any other months. In the study field, green tide caused by the macroalgae

Ulva prolifera has occurred yearly since 2007 and started in May (Cao et al., 2019). Pedosphaerales, tightly associated with eukaryotic hosts, rapidly responded to the green tide and played an important role in transforming the large amount of organic matter produced by the green tide. Thus, it was a key group in determining MCR. It has been reported that OM190 was tightly associated with macroalgae (Bengtsson and Øvreås, 2010; Bondoso et al., 2017) and the relative abundance of Thiomicrospirales strongly correlated with the diatom abundance (Liu et al., 2019). A study in the estuary found that Bacillales was a major β-glucosidase producer and this enzyme was fundamental in mediating the degradation of carbohydrates (Eswaran and Khandeparker, 2019). A further study indicated that Bacillales accounted for the highest proportions of microbial communities in the seagrass meadows (Jiang et al., 2015).

The advantage or characteristic of the second clade was that they contained genes involved in degrading complex compounds that were recalcitrant to other microorganisms. A study indicated that species involved in Kiritimatiellales are enriched in sulfatases and play an important role in degrading highly sulfate polysaccharides (Van Vliet et al., 2019). It was reported that groups involved in the bacterial order Sphingomonadales have the ability to degrade various hydrocarbons, including a wide range of aromatic compounds (Kertesz et al., 2019). In general, aromatic compounds are not optimal substrates and accumulate in the field (Medeiros et al., 2015) and incubation experiments (Zheng et al., 2019). The capacity to utilize aromatic compounds provides Sphingomonadales more chances to survive. Species in the order Chitinophagales can degrade complex carbohydrates including chitin (Hou et al., 2021). Although many bacteria accumulate intracellular glycogen as an energy source, only a few bacteria are able to utilize exogenous glycogen. It has been reported that members involved in the order Balneolales encoded the genes for pullulanase, which facilitated the depolymerization and exogenous utilization of glycogen (Ataeian et al., 2022).

The third clade included groups that were able to get energy, all or part of it, from light. Synechococcales are an important primary producer (Singh and Bhadury, 2018). The common characteristic of Rhodospirillales is that they contain photosynthetic pigments and fill a phototrophic niche (King et al., 2010; Pfennig and Trüper, 2019). Recent studies found that groups affiliated with Ectothiorhodospirales are purple sulfur bacteria (Oren, 2014) that are capable of photosynthesis. The high activity and *in situ* cell numbers of Actinomarinales in coastal sands suggested it was a keystone heterotroph for carbon mineralization (Miksch et al., 2021). Another study further suggested that Actinomarinales might be photoheterotrophs with rhodopsin and heliorhodopsin (López-Pérez et al., 2020). A previous study indicated that the SAR324 clade displayed plasticity energy-related metabolic pathways and was presumed to be photoheterotrophy (Boeuf et al., 2021). Proteorhodopsin-based phototrophy might constitute an important source of energy and cause deviation of measured MCR following assumed organic carbon remineralization between day and night (Munson-McGee et al., 2022). Microbial community composition should be fully taken into account and this might be an effective way to assess variations caused by variables among lineages.

Groups affiliated to the fourth clade were dominated by predators and organisms at higher trophic levels. The order Micavibrionales, assigned to the Bdellovibrio and like organisms (BALOs), is obligate predatory bacteria (Davidov et al., 2006). A recent study demonstrated that the abundance of Micavibrionales was likely linked to phytoplankton dynamics (Ezzedine et al., 2020). Similarly, Bdellovibrionales is also an important predatory bacteria (Beck et al., 2005), and a study about BALOs indicated that the rates of assimilating carbon of predatory bacteria were 211% higher than that of non-predatory bacteria (Hungate et al., 2021). Little is known about the bacterial order Haliangiales. It is involved in Myxococcota that feed on the other microbes they encounter (Whitworth et al., 2021).

All species discussed above were positively associated with MCR, while there were three species, namely, Nitrosococcales, Burkholderiales, and Lactobacillales, that demonstrated a negative correlation with MCR throughout the year (Figure 5B), partly because they were strongly negatively associated with MCR in special seasons. Nitrosococcales are an important ammonia-oxidizing bacteria (Ward et al., 2021) and were positively associated with MCR in autumn (Figure 5B). This further supports that nitrifiers play a vital role in the cycle of elements in autumn. However, this group showed a negative correlation with MCR especially in summer, when photoautotrophs dominated the ecosystem. Burkholderiales and Lactobacillales showing the highest negative correlations to MCR in winter might be caused by the low temperature (De Vrieze et al., 2015; Levy-Booth et al., 2021). It had been reported that blooms of Marine_group_II coincided with decreases in Chl a in the Santa Barbara Channel (Murray et al., 1999). This partly explained the significant negative correlation between Marine_group_II and MCR in summer. Thiomicrospirales are important sulfur-oxidizing bacteria (Lecoeuvre et al., 2021) and significantly negatively correlated to MCR in summer when photoautotrophic microorganisms dominated the food web.

Although some keystone groups were rare, previous studies documented that rare microorganisms played a pivotal role in many biogeochemical processes (Banerjee et al., 2018). Overall, the common characteristic of these crucial groups that strongly impacted MCR is the capacity to effectively get energy and utilize various substrates. The total amount of energy is conserved according to the first law of thermodynamics. Under this situation, the stronger capability of getting more energy is beneficial to their survival.

5 Conclusion

Although it is a common view that MCR plays a fundamental role in shaping the oceanic carbon cycle, few studies have been performed on a seasonal cycle. Activities of microorganisms are strongly associated with the season, however, a single study on MCR cannot reflect the impacts of environmental parameters along with seasons on MCR. To better understand the roles of the ocean in the global carbon cycle, we measured MCR throughout the whole year based on AOU and ETS in Aoshan Bay. The seasonal trends of MCR based on AOU and ETS were not consistent (Figure 6). The

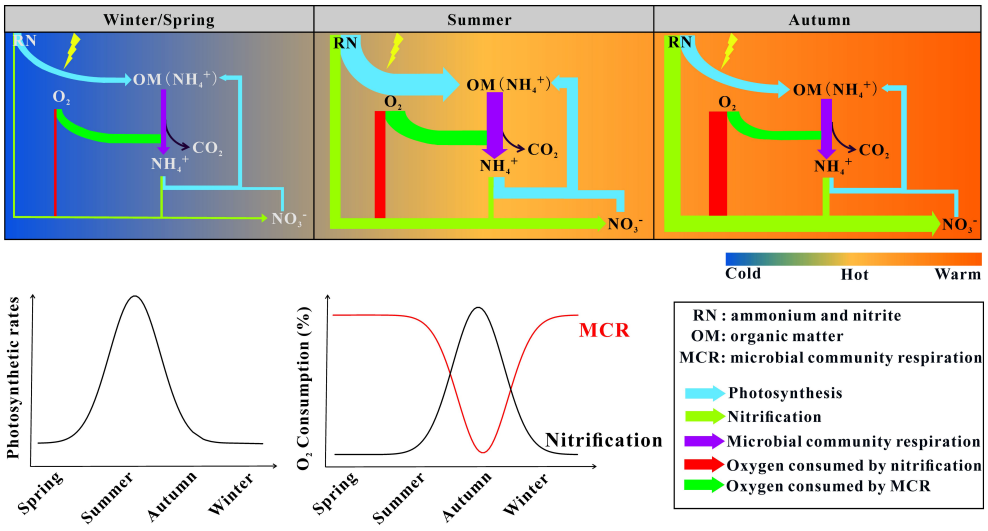

FIGURE 6
| Major biogeochemical processes involved in oxygen consumption. The width of the arrows represents the flux of nitrogen and oxygen.

MCR peaked in summer based on ETS, while it peaked in autumn based on AOU. Further analysis proved that nitrification caused the overestimation of MCR based on AOU. Although previous studies supported that nitrification was an important oxygen sink, they did not explicitly illustrate the effects of nitrification on MCR estimation based on AOU. This study proved that the overestimation of MCR was caused by nitrification based on AOU, which might affect the estimation of the flow of carbon through marine plankton food webs. To calibrate MCR, it is better to monitor the dynamics of reduced nutrients when using AOU. Based on the results of the *in vivo* INT reduction rate, groups strongly associated with MCR were identified. These keystone groups were capable of utilizing various substrates or getting energy directly from light. Caution is necessary when assuming organic carbon remineralization based on MCR inferred from ETS, and, in future research, attention should be paid to the deviation caused by photoheterotrophy.

Data availability statement

The raw data supporting the conclusions of this article will be made available by the authors, without undue reservation.

Author contributions

LZ: Formal Analysis, Writing – original draft. WZ: Writing – review & editing. YW: Writing – review & editing. YL: Writing – review & editing. JC: Writing – review & editing. BL: Writing – review & editing. BS: Writing – review & editing. HS: Methodology, Writing – review & editing.

Funding

The author(s) declare financial support was received for the research, authorship, and/or publication of this article. This work was funded by Southern Marine Science and Engineering Guangdong Laboratory (Zhuhai) (SML2020SP004), the Key Research and Development Program of Shandong Province (2020ZLYS04), the National Key Research and Development Program of China (2018YFA0605800), the National Natural Science Foundation of China (42188102), and the Opening Foundation of Fujian Key Laboratory of Marine Carbon Sequestration Research Fund, Xiamen University (FKLMCS2023002).

Acknowledgments

We sincerely thank TingYat Lee for his assistance in editing the original manuscript. We also thank Xiao Chen, Hongwei Ren, and Xianrui Song for their support during this experiment.

Conflict of interest

Authors WZ and BL were employed by the company Center Tech Tianjin Chemical Research and Design Institute Co., Ltd.

The remaining authors declare that the research was conducted in the absence of any commercial or financial relationships that could be construed as a potential conflict of interest.

Publisher's note

All claims expressed in this article are solely those of the authors and do not necessarily represent those of their affiliated organizations, or those of the publisher, the editors and the reviewers. Any product that may be evaluated in this article, or claim that may be made by its manufacturer, is not guaranteed or endorsed by the publisher.

Supplementary material

The Supplementary Material for this article can be found online at: https://www.frontiersin.org/articles/10.3389/fmars.2023.1331680/full#supplementary-material.

References

Alonso-Sáez, L., Gasol, J. M., Arístegui, J., Vilas, J. C., Vaqué, D., Duarte, C. M., et al. (2007). Large-scale variability in surface bacterial carbon demand and growth efficiency in the subtropical northeast Atlantic Ocean. *Limnol. Oceanogr.* 52 (2), 533–546. doi: 10.4319/lo.2007.52.2.0533

Alonso-Sáez, L., Vázquez-Domínguez, E., Cardelus, C., Pinhassi, J., Sala, M. M., Lekunberri, I., et al. (2008). Factors controlling the year-round variability in carbon flux through bacteria in a coastal marine system. *Ecosystems* 11 (3), 397–409. doi: 10.1007/s10021-008-9129-0

Apple, J. K., Del Giorgio, P., and Michael Kemp, W. (2006). Temperature regulation of bacterial production, respiration, and growth efficiency in a temperate salt-marsh estuary. *Aquat. microbial ecologyaquat Microb. Ecol.* . 43 (3), 243–254. doi: 10.3354/AME043243

Aranguren-Gassis, M., Teira, E., Serret, P., Martínez-García, S., and Fernández, E. (2012). Potential overestimation of bacterial respiration rates in oligotrophic plankton communities. *Mar. Ecol. Prog. Ser.* 453, 1–10. doi: 10.3354/meps09707

Ataeian, M., Liu, Y., Kouris, A., Hawley, A. K., and Strous, M. (2022). Ecological interactions of cyanobacteria and heterotrophs enhances the robustness of cyanobacterial consortium for carbon sequestration. *Front. Microbiol.* 13. doi: 10.3389/fmicb.2022.780346

Banerjee, S., Schlaeppi, K., and van der Heijden, M. (2018). Keystone taxa as drivers of microbiome structure and functioning. *Nat. Rev. Microbiol.* 16 (9), 567–576. doi: 10.1038/s41579-018-0024-1

Bayer, B., McBeain, K., Carlson, C., and Santoro, A. (2022). Carbon content, carbon fixation yield and dissolved organic carbon release from diverse marine nitrifiers. *Limnology Oceanography.* 68, 84-96. doi: 10.1002/lno.12252

Beck, S., Schwudke, D., Appel, B., Linscheid, M., and Strauch, E. (2005). Characterization of outer membrane protein fractions of Bdellovibrionales. *FEMS Microbiol. Letters.* 243 (1), 211–217. doi: 10.1016/j.femsle.2004.12.006

Bengtsson, M. M., and Øvreås, L. (2010). Planctomycetes dominate biofilms on surfaces of the kelp Laminaria hyperborea. *BMC Microbiol.* 10 (1), 1–12. doi: 10.1186/1471-2180-10-261

Berounsky, V. M., and Nixon, S. W. (1993). Rates of nitrification along an estuarine gradient in Narragansett Bay. *Estuaries Coasts.* 16 (4), 718–730. doi: 10.2307/1352430

Boeuf, D., Eppley, J. M., Mende, D. R., Malmstrom, R. R., Woyke, T., and DeLong, E. F. (2021). Metapangenomics reveals depth-dependent shifts in metabolic potential for the ubiquitous marine bacterial SAR324 lineage. *Microbiome.* 9 (1), 1–18. doi: 10.1186/s40168-021-01119-5

Bondoso, J., Godoy-Vitorino, F., Balague, V., Gasol, J. M., Harder, J., and Lage, O. M. (2017). Epiphytic Planctomycetes communities associated with three main groups of macroalgae. *FEMS Microbiol. Ecology.* 93 (3), fiw255. doi: 10.1093/femsec/fiw255

Borges, A. V., Delille, B., and Frankignoulle, M. (2005). Budgeting sinks and sources of CO_2 in the coastal ocean: Diversity of ecosystems counts. *Geophysical Res. Letters.* 32 (14). doi: 10.1029/2005GL023053

Cao, Y., Wu, Y., Fang, Z., Cui, X., Liang, J., and Song, X. (2019). Spatiotemporal patterns and morphological characteristics of Ulva prolifera distribution in the Yellow Sea, China in 2016–2018. *Remote Sensing.* 11 (4), 445. doi: 10.3390/rs11040445

Carla, F. B., Denis, P., Lucía,, Ricardo, I., Valeria, S., Rubén, M., et al. (2022). Physical and biological effects on the carbonate system during summer in the Northern Argentine Continental Shelf (Southwestern Atlantic). *J. Mar. Syst.* 237, 103828. doi: 10.1016/j.jmarsys.2022.103828

Carol, E., Galliari, M. J., Santucci, L., Nuñez, F., and Faleschini, M. (2023). Assessment of groundwater-driven dissolved nutrient inputs to coastal wetlands associated with marsh-coastal lagoons systems of the littoral of the outer Río de la Plata estuary. *Sci. Total Environ.* 885, 163942. doi: 10.1016/j.scitotenv.2023.163942

Carpenter, J. H. (1965). The Chesapeake Bay Institute technique for the Winkler dissolved oxygen method. *Limnology Oceanography.* 10 (1), 141–143. doi: 10.4319/lo.1965.10.1.0141

Chin, M., Lau, S., Midot, F., Jee, M., Lo, M., Sangok, F., et al. (2023). Root exclusion method for separating soil respiration components: Review and methodological considerations. *Pedosphere.* 33, 683–699. doi: 10.1016/j.pedsph.2023.01.015

Clauset, A., Newman, M. E., and Moore, C. J. (2004). Finding community structure in very large networks. *Phys. Rev. E* .70 (6), 66111. doi: 10.1103/PhysRevE.70.066111

Cleveland, C. C., Nemergut, D. R., Schmidt, S. K., and Townsend, A. R. (2007). Increases in soil respiration following labile carbon additions linked to rapid shifts in soil microbial community composition. *Biogeochemistry.* 82 (3), 229–240. doi: 10.1007/s10533-006-9065-z

Crockford, P., Halevy, I., Milo, R., Bar On, Y., and Ward, L. M. (2023). The geologic history of primary productivity. *Curr. Biol.* 33, 4741-4750. doi: 10.1016/j.cub.2023.09.040

Dai, M., Wang, L., Guo, X., Zhai, W., Li, Q., He, B., et al. (2008). Nitrification and inorganic nitrogen distribution in a large perturbed river/estuarine system: the Pearl River Estuary, China. *Biogeosciences* .5 (5), 1227–1244. doi: 10.5194/bg-5-1227-2008

Davidov, Y., Huchon, D., Koval, S. F., and Jurkevitch, E. (2006). A new α-proteobacterial clade of Bdellovibrio-like predators: implications for the mitochondrial endosymbiotic theory. *Environ. Microbiol.* 8 (12), 2179–2188. doi: 10.1111/j.1462-2920.2006.01101.x

De Vrieze, J., Saunders, A. M., He, Y., Fang, J., Nielsen, P. H., Verstraete, W., et al. (2015). Ammonia and temperature determine potential clustering in the anaerobic digestion microbiome. *Water Res.* 75, 312–323. doi: 10.1016/j.watres.2015.02.025

Del Giorgio, P., and Williams, P. (2005). Respiration in aquatic ecosystems. *OUP Oxford.* 1, 1–17. doi: 10.1093/acprof:oso/9780198527084.003.0001

Dittmar, T., Lennartz, S. T., Buck-Wiese, H., Hansell, D., Santinelli, C., Vanniet, C., et al. (2021). Enigmatic persistence of dissolved organic matter in the ocean. *Nat. Rev. Earth Environ.* 2, 570–583. doi: 10.1038/s43017-021-00183-7

Eswaran, R., and Khandeparker, L. (2019). Seasonal variation in β-glucosidase-producing culturable bacterial diversity in a monsoon-influenced tropical estuary. *Environ. Monit. Assessment.* 191 (11), 1–11. doi: 10.1007/s10661-019-7818-0

Ezzedine, J. A., Jacas, L., Desdevises, Y., and Jacquet, S. (2020). Bdellovibrio and like organisms in Lake Geneva: an unseen elephant in the room? *Front. Microbiol.* 11. doi: 10.3389/fmicb.2020.00098

Fennel, K., and Testa, J. M. (2019). Biogeochemical controls on coastal hypoxia. *Annu. Rev. Mar. Sci.* 11 (1), 105–130. doi: 10.1146/annurev-marine-010318-095138

Friedlingstein, P., Jones, M. W., O'Sullivan, M., Andrew, R. M., Bakker, D. C., Hauck, J., et al. (2022). Global carbon budget 2021. *Earth System Sci. Data.* 14 (4), 1917–2005. doi: 10.5194/essd-14-1917-2022

Friedrich, J., Janssen, F., Aleynik, D., Bange, H. W., Boltacheva, N., Çagatay, M., et al. (2014). Investigating hypoxia in aquatic environments: diverse approaches to addressing a complex phenomenon. *Biogeosciences.* 11 (4), 1215–1259. doi: 10.5194/bg-11-1215-2014

Gao, X., Chen, H., Govaert, L., Wang, W., and Yang, J. (2019). Responses of zooplankton body size and community trophic structure to temperature change in a subtropical reservoir. *Ecol. Evolution.* 9 (22), 12544–12555. doi: 10.1002/ece3.5718

García, F. C., Clegg, T., O'Neill, D. B., Warfield, R., Pawar, S., and Yvon-Durocher, G. (2023). The temperature dependence of microbial community respiration is amplified by changes in species interactions. *Nat. Microbiol.* 8 (2), 272–283. doi: 10.1038/s41564-022-01283-w

García-Martín, E. E., Daniels, C. J., Davidson, K., Lozano, J., Mayers, K. M., McNeill, S., et al. (2019). Plankton community respiration and bacterial metabolism in a North Atlantic Shelf Sea during spring bloom development (April 2015). *Prog. In Oceanography.* 177, 101873. doi: 10.1016/j.pocean.2017.11.002

Gattuso, J.-P., Frankignoulle, M., and Wollast, R. (1998). Carbon and carbonate metabolism in coastal aquatic ecosystems. *Annu. Rev. Ecol. Systematics.* 29, 405–434. doi: 10.1146/annurev.ecolsys.29.1.405

Gilbert, J. A., Steele, J. A., Caporaso, J. G., Steinbrück, L., Reeder, J., Temperton, B., et al. (2012). Defining seasonal marine microbial community dynamics. *ISME J.* 6 (2), 298–308. doi: 10.1038/ismej.2011.107

Gruber, N. J. N. (2015). Carbon at the coastal interface. 517(7533). *Nature.* 517, 148–149. doi: 10.1038/nature14082

Grundle, D. S., and Juniper, S. K. (2011). Nitrification from the lower euphotic zone to the sub-oxic waters of a highly productive British Columbia fjord. *Mar. Chem.* 126 (1-4), 173–181. doi: 10.1016/j.marchem.2011.06.001

Guo, C., Ke, Y., Chen, B., Zhang, S., and Liu, H. (2022). Making comparable measurements of bacterial respiration and production in the subtropical coastal waters. *Mar. Life Sci. Technology.* 4 (3), 414–427. doi: 10.1007/s42995-022-00133-2

Guo, Y., Zhao, Y., Zhu, T., Li, J., Feng, Y., Zhao, H., et al. (2018). A metabolomic view of how low nitrogen strength favors anammox biomass yield and nitrogen removal capability. *Water Res.* 143, 387–398. doi: 10.1016/j.watres.2018.06.052

Hampel, J. J., McCarthy, M. J., Gardner, W. S., Zhang, L., Xu, H., Zhu, G., et al. (2018). Nitrification and ammonium dynamics in Taihu Lake, China: seasonal competition for ammonium between nitrifiers and cyanobacteria. *Biogeosciences.* 15 (3), 733–748. doi: 10.5194/bg-15-733-2018

Hansell, D. A., and Carlson, C. A. (2001). Biogeochemistry of total organic carbon and nitrogen in the Sargasso Sea: control by convective overturn. *Deep Sea Res. Part II Topical Stud. Oceanography.* 48 (8-9), 1649–1667. doi: 10.1016/S0967-0645(00)00153-3

Hansell, D. A., Ducklow, H. W., Macdonald, A. M., and O-Neil Baringer, M. (2004). Metabolic poise in the North Atlantic Ocean diagnosed from organic matter transports. *Limnology Oceanography.* 49 (4), 1084–1094. doi: 10.4319/lo.2004.49.4.1084

Hansen, A. M., Kraus, T. E., Pellerin, B. A., Fleck, J. A., Downing, B. D., and Bergamaschi, B. A. (2016). Optical properties of dissolved organic matter (DOM): Effects of biological and photolytic degradation. *Limnology Oceanography.* 61 (3), 1015–1032. doi: 10.1002/lno.10270

Hernández-León, S., Koppelmann, R., Fraile-Nuez, E., et al. (2020). Large deep-sea zooplankton biomass mirrors primary production in the global ocean. *Nat. Communication.* 11, 6048. doi: 10.1038/s41467-020-19875-7

Holden, P. B., Edwards, N. R., Ridgwell, A., Wilkinson, R., Fraedrich, K., Lunkeit, F., et al. (2018). Climate–carbon cycle uncertainties and the Paris Agreement. *Nat. Climate Change.* 8 (7), 609–613. doi: 10.1038/s41558-018-0197-7

Hou, Y., Li, B., Feng, G., Zhang, C., He, J., Li, H., et al. (2021). Responses of bacterial communities and organic matter degradation in surface sediment to Macrobrachium nipponense bioturbation. *Sci. Total Environment.* 759, 143534. doi: 10.1016/j.scitotenv.2020.143534

Hsiao, S.-Y., Hsu, T.-C., Liu, J.-w., Xie, X., Zhang, Y., Lin, J., et al. (2014). Nitrification and its oxygen consumption along the turbid Chang Jiang River plume. *Biogeosciences* .11 (7), 2083–2098. doi: 10.5194/bg-11-2083-2014

Hu, W., Zheng, N., Zhang, Y., Bartlam, M., and Wang, Y. (2023). Spatiotemporal dynamics of high and low nucleic acid-content bacterial communities in Chinese coastal seawater: assembly process, co-occurrence relationship and the ecological functions. *Front. Microbiol.* 14. doi: 10.3389/fmicb.2023.1219655

Hungate, B. A., Marks, J. C., Power, M. E., Schwartz, E., van Groenigen, K. J., Blazewicz, S. J., et al. (2021). The functional significance of bacterial predators. *mBio.* 12 (2), e00466–e00421. doi: 10.1128/mBio.00466-21

Jeffrey, S., and Humphrey, G. (1975). New spectrophotometric equations for determining chlorophylls a, b, c1 and c2 in higher plants, algae and natural phytoplankton. *Biochem. Physiol. Pflanz* 167, 191–194. doi: 10.1016/S0015-3796(17)30778-3

Jiang, Y. F., Ling, J., Wang, Y. S., Chen, B., Zhang, Y. Y., and Dong, J. D. (2015). Cultivation-dependent analysis of the microbial diversity associated with the seagrass meadows in Xincun Bay, South China Sea. *Ecotoxicology.* 24 (7), 1540–1547. doi: 10.1007/s10646-015-1519-4

Jiao, N., Liu, J., Edwards, B., Lv, Z., Cai, R., Liu, Y., et al. (2021). Correcting a major error in assessing organic carbon pollution in natural waters. *Sci. Advances.* 7 (16), eabc7318. doi: 10.1126/sciadv.abc7318

Jing, H., Xiao, X., Zhang, Y., Li, Z., Jian, H., Luo, Y., et al. (2022). Composition and ecological roles of the core microbiome along the abyssal-hadal transition zone sediments of the mariana trench. *Microbiol. Spectrum.* 10 (3). doi: 10.1128/spectrum.01988-21

Kache, S., Bartl, I., Wäge-Recchioni, J., and Voss, M. (2021). Influence of organic particle addition on nitrification rates and ammonium oxidiser abundances in Baltic seawater. *Mar. Ecol. Prog. Ser.* 674, 59–72. doi: 10.3354/meps13797

Karner, M. B., DeLong, E. F., and Karl, D. M. (2001). Archaeal dominance in the mesopelagic zone of the Pacific Ocean. *Nature.* 409 (6819), 507. doi: 10.1038/35054051

Kertesz, M. A., Kawasaki, A., and Stolz, A. (2019). Aerobic hydrocarbon-degrading alphaproteobacteria: Sphingomonadales. *Taxonomy Genomics Ecophysiology Hydrocarbon-Degrading Microbe.* chapter 4, 105–124. doi: 10.1007/978-3-030-14796-9_9

King, A. J., Freeman, K. R., McCormick, K. F., Lynch, R. C., Lozupone, C., Knight, R., et al. (2010). Biogeography and habitat modelling of high-alpine bacteria. *Nat. Commun.* 1 (1), 1–6. doi: 10.1038/ncomms1055

Kulk, G., Platt, T., Dingle, J., Jackson, T., Jönsson, B. F., Bouman, H. A., et al. (2020). Primary production, an index of climate change in the ocean: satellite-based estimates over two decades. *Remote Sens. 12* 5, 826. doi: 10.3390/rs12050826

Laruelle, G. G., Dürr, H. H., Slomp, C. P., and Borges, A. (2010). Evaluation of sinks and sources of CO_2 in the global coastal ocean using a spatially-explicit typology of estuaries and continental shelves. *Geophysical Res. Letters.* 37 (15), L0567. doi: 10.1029/2010GL043691

Laruelle, G. G., Lauerwald, R., Pfeil, B., and Regnier, P. (2014). Regionalized global budget of the CO_2 exchange at the air-water interface in continental shelf seas. *Global Biogeochemical Cycles.* 28 (11), 1199–1214. doi: 10.1002/2014GB004832

Lawaetz, A. J., and Stedmon, C. A. (2009). Fluorescence intensity calibration using the Raman scatter peak of water. *Appl. Spectroscopy.* 63 (8), 936–940. doi: 10.1366/000370209788964548

Lecoeuvre, A., Ménez, B., Cannat, M., Chavagnac, V., and Gérard, E. J. (2021). Microbial ecology of the newly discovered serpentinite-hosted Old City hydrothermal field (southwest Indian ridge). *ISME J.* 15 (3), 818–832. doi: 10.1038/s41396-020-00816-7

Levy-Booth, D. J., Hashimi, A., Roccor, R., Liu, L.-Y., Renneckar, S., Eltis, L. D., et al. (2021). Genomics and metatranscriptomics of biogeochemical cycling and degradation of lignin-derived aromatic compounds in thermal swamp sediment. *ISME J.* 15 (3), 879–893. doi: 10.1038/s41396-020-00820-x

Li, X., Zhao, X., Dang, H., Zhang, C., Fernández-Urruzola, I., Liu, Z., et al. (2023). High variability in organic carbon sources and microbial activities in the hadopelagic waters. *Limnology Oceanography* 68, 1704–1718. doi: 10.1002/lno.12379

Lipschultz, F., Wofsy, S. C., and Fox, L. E. (1986). Nitrogen metabolism of the eutrophic Delaware River ecosystem. *Limnology Oceanography.* 31 (4), 701–716. doi: 10.4319/lo.1986.31.4.0701

Liu, Y., Debeljak, P., Rembauville, M., Blain, S., and Obernosterer, I. (2019). Diatoms shape the biogeography of heterotrophic prokaryotes in early spring in the Southern Ocean. *Environ. Microbiol.* 21 (4), 1452–1465. doi: 10.1111/1462-2920.14579

Logares, R., Deutschmann, I. M., Junger, P. C., Giner, C. R., Krabberød, A. K., Schmidt, T. S., et al. (2020). Disentangling the mechanisms shaping the surface ocean microbiota. *Microbiome.* 8 (1), 1–17. doi: 10.1186/s40168-020-00827-8

López-Pérez, M., Haro-Moreno, J. M., Iranzo, J., and Rodriguez-Valera, F. (2020). Genomes of the "Candidatus Actinomarinales" order: highly streamlined marine epipelagic actinobacteria. *mSystems.* 5 (6), e01041–e01020. doi: 10.1128/mSystems.01041-20

Love, C., Arrington, E., Gosselin, K., Reddy, C., Mooy, B., Nelson, R., et al. (2021). Microbial production and consumption of hydrocarbons in the global ocean. *Nat. Microbiol.* 6, 489–498. doi: 10.1038/s41564-020-00859-8

Lu, Y., Cheung, S., Chen, L., Kao, S.-J., Xia, X., Gan, J., et al. (2020). New insight to niche partitioning and ecological function of ammonia oxidizing archaea in subtropical estuarine ecosystem. *Biogeosciences* 17, 6017–6032. doi: 10.5194/bg-17-6017-2020,2020

Lucea, A., Duarte, C. M., Agustí, S., and Kennedy, H. (2005). Nutrient dynamics and ecosystem metabolism in the Bay of Blanes (NW Mediterranean). *Biogeochemistry.* 73 (2), 303–323. doi: 10.1007/s10533-004-0059-4

Marie, D., Partensky, F., Jacquet, S., and Vaulot, D. (1997). Enumeration and cell cycle analysis of natural populations of marine picoplankton by flow cytometry using the nucleic acid stain SYBR Green I. *Appl. Environ. Microbiol.* 63 (1), 186–193. doi: 10.1128/AEM.63.1.186-193.1997

Martínez-García, S., Fernández, E., Aranguren-Gassis, M., and Teira, E. (2009). *In vivo* electron transport system activity: a method to estimate respiration in natural marine microbial planktonic communities. *Limnology Oceanography Methods* 7 (6), 459–469. doi: 10.4319/lom.2009.7.459

Martínez-García, S., Fernández, E., del Valle, D. A., Karl, D. M., and Teira, E. (2013). Experimental assessment of marine bacterial respiration. *Aquat. Microbial Ecology.* 70 (3), 189–205. doi: 10.3354/ame01644

Medeiros, P. M., Seidel, M., Powers, L. C., Dittmar, T., Hansell, D. A., and Miller, W. L. (2015). Dissolved organic matter composition and photochemical transformations in the northern North Pacific Ocean. *Geophysical Res. Letters.* 42 (3), 863–870. doi: 10.1002/2014GL062663

Miksch, S., Meiners, M., Meyerdierks, A., Probandt, D., Wegener, G., Titschack, J., et al. (2021). Bacterial communities in temperate and polar coastal sands are seasonally stable. *ISME Commun.* 1 (1), 1–11. doi: 10.1038/s43705-021-00028-w

Munson-McGee, J. H., Lindsay, M. R., Sintes, E., Brown, J. M., D'Angelo, T., Brown, J., et al. (2022). Decoupling of respiration rates and abundance in marine prokaryoplankton. *Nature.* 612, 1–7. doi: 10.1038/s41586-022-05505-3

Murphy, K. R., Stedmon, C. A., Wenig, P., and Bro, R. (2014). OpenFluor–an online spectral library of auto-fluorescence by organic compounds in the environment. *Analytical Methods* 6 (3), 658–661. doi: 10.1039/c3ay41935e

Murray, A., Blakis, A., Massana, R., Strawzewski, S., Passow, U., Alldredge, A., et al. (1999). A time series assessment of planktonic archaeal variability in the Santa Barbara Channel. *Aquat. Microbial Ecology.* 20 (2), 129–145. doi: 10.3354/ame020129

Oren, A. J. T. P. (2014). The family ectothiorhodospiraceae. *Prokaryotes.* chapter 9, 199–222. doi: 10.1007/978-3-642-38922-1_248

Pakulski, J. D., Benner, R., Amon, R., Eadie, B., and Whitledge, T. (1995). Community metabolism and nutrient cycling in the Mississippi River plume: evidence for intense nitrification at intermediate salinities. *Mar. Ecol. Prog. Ser.* 117, 207–218. doi: 10.3354/meps117207

Pfennig, N., and Trüper, H. G. (2019). The rhodospirillales (Phototrophic or photosynthetic bacteria). *Handb. Microbiol.* chapter 3, 14-24. doi: 10.1201/9781351072939

Prosser, J. I., Head, I. M., and Stein, L. Y. (2014).). The family nitrosomonadaceae in The Prokaryotes: Alphaproteobacteria and Betaproteobacteria. *Springer Berlin/ Heidelberg*. chapter 8, 901–918. doi: 10.1007/978-3-642-30197-1_372

Reinthaler, T., and Herndl, G. (2005). Seasonal dynamics of bacterial growth efficiencies in relation to phytoplankton in the southern North Sea. *Environ. Sci.* .39 (1), 7–16. doi: 10.3354/AME039007

Reshef, D. N., Reshef, Y. A., Finucane, H. K., Grossman, S. R., McVean, G., Turnbaugh, P. J., et al. (2011). Detecting novel associations in large data sets. *Science.* 334 (6062), 1518–1524. doi: 10.1126/science.120543

Singh, T., and Bhadury, P. (2018). Distribution patterns of marine planktonic cyanobacterial assemblages in transitional marine habitats using 16S rRNA phylogeny. *Phycological Res.* 66 (3), 189–198. doi: 10.1111/pre.12224

Smith, T., Clegg, T., Bell, T., and Pawar, S. (2021). Systematic variation in the temperature dependence of bacterial carbon use efficiency. *Ecol. Letters.* 24. 2123-2133. doi: 10.1111/ele.13840

Tanaka, K., Kuma, K., Hamasaki, K., and Yamashita, Y. (2014). Accumulation of humic-like fluorescent dissolved organic matter in the Japan Sea. *Sci. Rep.* 4 (1), 1–7. doi: 10.1038/srep05292

Tang, W., Ward, B., Beman, M., Bristow, L., Clark, D., and Fawcett, S. (2023). Database of nitrification and nitrifiers in the global ocean. *Earth System Sci. Data Discussions.* 2023, 1–66. doi: 10.5194/essd-2023-194

Van Vliet, D. M., Palakawong Na Ayudthaya, S., Diop, S., Villanueva, L., Stams, A. J., and Sánchez-Andrea, I. (2019). Anaerobic degradation of sulfated polysaccharides by two novel Kiritimatiellales strains isolated from Black Sea sediment. *Front. Microbiol.* 10. doi: 10.3389/fmicb.2019.00253

Walters, W. A., Jin, Z., Youngblut, N., Wallace, J. G., Sutter, J., Zhang, W., et al. (2018). Large-scale replicated field study of maize rhizosphere identifies heritable microbes. *Proc. Natl. Acad. Sci.* 115 (28), 7368–7373. doi: 10.1073/pnas.1800918115

Wang, L. (2018). Corrigendum to Microbial control of carbon cycle in the ocean. *Natl. Sci. Review.* 5, 442. doi: 10.1093/nsr/nwy047

Ward, L., Johnston, D., and Shih, P. (2021). Phanerozoic radiation of ammonia oxidizing bacteria. *Sci. Rep.* 11 (1), 1–9. doi: 10.1038/s41598-021-81718-2

Warkentin, M., Freese, H. M., Karsten, U., and Schumann, R. (2007). New and fast method to quantify respiration rates of bacterial and plankton communities in freshwater ecosystems by using optical oxygen sensor spots. *Appl. Environ. Microbiol.* 73 (21), 6722–6729. doi: 10.1128/AEM.00405-07

Wellburn, A. R. (1994). The spectral determination of chlorophylls a and b, as well as total carotenoids, using various solvents with spectropho-tometers of different resolution. *J. Plant Physiol.* 144, 307–313. doi: 10.1016/S0176-1617(11)81192-2

Whitworth, D. E., Sydney, N., and Radford, E. (2021). Myxobacterial genomics and post-genomics: A review of genome biology, genome sequences and related 'Omics studies. *Microorganisms* . 9 (10), 2143. doi: 10.3390/microorganisms9102143

Wuchter, C., Abbas, B., Coolen, M. J., Herfort, L., van Bleijswijk, J., Timmers, P., et al. (2006). Archaeal nitrification in the ocean. *Proc. Natl. Acad. Sci.* 103 (33), 12317–12322. doi: 10.1073/pnas.0600756103

Yurgel, S. N., Douglas, G. M., Dusault, A., Percival, D., and Langille, M. (2018). Dissecting community structure in wild blueberry root and soil microbiome. *Front. Microbiol.* 9. doi: 10.3389/fmicb.2018.01187

Zakem, E. J., Al-Haj, A., Church, M. J., van Dijken, G. L., Dutkiewicz, S., Foster, S. Q., et al. (2018). Ecological control of nitrite in the upper ocean. *Nat. Commun.* 9 (1), 1–13. doi: 10.1038/s41467-018-03553-w

Zhang, L., Chen, M., Chen, X., Wang, J., Zhang, Y., Xiao, X., et al. (2021). Nitrifiers drive successions of particulate organic matter and microbial community composition in a starved macrocosm. *Environ. Int.* 157, 106776. doi: 10.1016/ j.envint.2021.106776

Zheng, Q., Chen, Q., Cai, R., He, C., Guo, W., Wang, Y., et al. (2019). Molecular characteristics of microbially mediated transformations of Synechococcus-derived dissolved organic matter as revealed by incubation experiments. *Environ. Microbiol.* 21 (7), 2533–2543. doi: 10.1111/1462-2920.14646

frontiers | Frontiers in Marine Science

TYPE Original Research
PUBLISHED 14 March 2024
DOI 10.3389/fmars.2024.1373643

Check for updates

OPEN ACCESS

EDITED BY
Junfu Dong,
Shandong University, China

REVIEWED BY
Jie Lian,
Shenzhen Technology University, China
Ehui Tan,
Hainan University, China

*CORRESPONDENCE
Kenneth Mopper
kmopper@odu.edu
Jihua Liu
liujihua1982@foxmail.com

RECEIVED 20 January 2024
ACCEPTED 21 February 2024
PUBLISHED 14 March 2024

CITATION
Wang R, Liu J, Xu Y, Liu L and Mopper K (2024) Unraveling sources of cyanate in the marine environment: insights from cyanate distributions and production during the photochemical degradation of dissolved organic matter.
Front. Mar. Sci. 11:1373643.
doi: 10.3389/fmars.2024.1373643

COPYRIGHT
© 2024 Wang, Liu, Xu, Liu and Mopper. This is an open-access article distributed under the terms of the Creative Commons Attribution License (CC BY). The use, distribution or reproduction in other forums is permitted, provided the original author(s) and the copyright owner(s) are credited and that the original publication in this journal is cited, in accordance with accepted academic practice. No use, distribution or reproduction is permitted which does not comply with these terms.

Unraveling sources of cyanate in the marine environment: insights from cyanate distributions and production during the photochemical degradation of dissolved organic matter

Rui Wang[1,2], Jihua Liu[1,2]*, Yongle Xu[1,2], Li Liu[1,2] and Kenneth Mopper[3]*

[1]Institute of Marine Science and Technology, Shandong University, Qingdao, China, [2]Qingdao Key Laboratory of Ocean Carbon Sequestration and Negative Emission Technology, Shandong University, Qingdao, China, [3]Department of Chemistry and Biochemistry, Old Dominion University, Norfolk, VA, United States

Cyanate is a nitrogen and energy source for diverse marine microorganisms, playing important roles in the nitrogen cycle. Despite the extensive research on cyanate utilization, the sources of this nitrogen compound remain largely enigmatic. To unravel the sources of cyanate, distributions and production of cyanate during photochemical degradation of natural dissolved organic matter (DOM) were investigated across various environments, including freshwater, estuarine, coastal areas in Florida, and the continental and slope regions of the North American mid-Atlantic Ocean (NATL). Cyanate production was also examined during the photochemical degradation of exudates from a typical strain of *Synechococcus*, an important phytoplankton component. To deepen our understanding of the sources and production mechanisms of cyanate, its production was assessed during the photochemical degradation of a natural seawater DOM supplemented with five nitrogen–containing compounds with distinguishing structures and functional groups. Generally, cyanate exhibited higher concentrations in the Florida coastal, estuarine, and freshwater environments than the NATL. However, cyanate distribution did not consistently align with its production rates. Despite significantly low concentrations in the NATL, DOM from this region exhibited cyanate production rates comparable to estuarine and Florida coastal environments. Although relatively high cyanate concentrations were observed in the freshwaters, DOM in this environment exhibited very low cyanate production rates. A highly significant correlation was observed between cyanate and chlorophyll *a* (Chl *a*) concentrations in these areas. Moreover, in most estuarine and NATL stations, cyanate concentration and production rate in the Chl *a* maximum layer were significantly higher than in other layers. Cyanate was produced during the photochemical degradation of the *Synechococcus* exudates. The cyanate production was significantly enhanced when the natural seawater DOM was supplemented with GlycylGlycine, 4-(methylamino) benzoic

acid, 4-[ethyl(methyl)amino] benzaldehyde or methyl 2-aminobenzoate. Our study implies that photochemical degradation of marine DOM, especially phytoplankton-derived DOM, is a substantial source of cyanate in the ocean. Additionally, cyanate may form during the degradation of peptides and small aromatic compounds in DOM, providing novel insights into the nitrogen cycle.

KEYWORDS

cyanate, photochemical degradation of dissolved organic matter, *Synechococcus* sp. CB0110 exudates, nitrogen-containing compound, DOM, marine nitrogen cycle

1 Introduction

Nitrogen is an essential element for microorganisms, playing vital roles in marine biogeochemical cycles. Marine microbes utilize both inorganic and organic nitrogen compounds. The inorganic nitrogen compounds, such as nitrate and ammonium, serve as essential nutrients for primary producers (Bristow et al., 2017; Hutchins and Capone, 2022). Additionally, the organic nitrogen compounds, such as amino acids and urea, represent crucial alternative nitrogen sources for non-diazotrophic phytoplankton (Berman and Bronk, 2003; Zubkov et al., 2003; Bronk et al., 2007; Scanlan et al., 2009; Berthelot et al., 2019). However, most bioavailable organic nitrogen compounds in the ocean have not been fully characterized (Sipler and Bronk, 2015). Therefore, investigating the sources of new bioavailable nitrogen compounds is imperative for further understanding of the nitrogen cycle in the ocean.

Cyanate, a simple organic nitrogen compound, can be taken up by microbes through a substrate-specific ABC-type transporter (*cynABD*) and subsequently be decomposed into NH_4^+ and CO_2 by cyanase (Kamennaya et al., 2008; Kamennaya and Post, 2011, 2013). Initially considered toxic to living organisms at high concentrations, cyanate can undergo detoxification within cells. For instance, cyanate in the cells of cyanobacteria, bacteria, fungi, and plants can be decomposed to NH_4^+ and CO_2 by cyanase (Carepo et al., 2004; Elleuche and Pöggeler, 2008; Kebeish and Al-Zoubi, 2017). Cyanate also serves as an organic nitrogen source in both terrestrial and marine environments. It is recently found that cyanate serves as an active nitrogen or energy source for soil microbes (Mooshammer et al., 2021). The discovery of the cyanase gene in various marine microbes, particularly in the picocyanobacterial strains, such as *Synechococcus* sp. WH7803, WH7804, WH8102, *Prochlorococcus* sp. MED4, NATL1A, underscores the growing importance of cyanate in marine biogeochemistry and microbial ecology (Palenik et al., 2003; Rocap et al., 2003; Kamennaya et al., 2008; Kamennaya and Post, 2011). It has been revealed that many of the *Synechococcus* and *Prochlorococcus* strains can utilize cyanate as sole nitrogen source for growth (Palenik et al., 2003; Rocap et al., 2003; Kamennaya et al., 2008). A recent study reveals that *Synechococcus* dominates cyanase transcripts in the surface water of non-polar oceans (Mao et al., 2021). In nitrogen-limiting surface waters, *Prochlorococcus* and *Synechococcus* can utilize cyanate as an alternative nitrogen source (Ustick et al., 2021). Therefore, utilization of cyanate may significantly affect primary productivity in the ocean.

Adding to its emerging biogeochemical significance, cyanate also plays a substantial role in nitrification, where ammonia is oxidized to nitrate via nitrite in the ocean (Stein, 2015). *Nitrososphaera gargensis*, an ammonia-oxidizing Thaumarchaeota isolate, utilizes cyanate as the sole nitrogen source and reductant by converting it to ammonium and CO_2 via cyanase. In the Gulf of Mexico, Thaumarchaeota utilizes cyanate as an energy and nitrogen source, even though no cyanase gene was identified in the genomic data of Thaumarchaeota in this environment (Kitzinger et al., 2019). Additionally, genes encoding cyanate cyanase/lyase have been identified in the genomes of several marine Nitrospinae and Nitrospirae, two important nitrite-oxidizing bacteria (Pachiadaki et al., 2017; Koch et al., 2019). A recent study reveals that cyanate is a significant nitrogen source for Nitrospinae in the Gulf of Mexico, fulfilling more than half of their nitrogen demand (Kitzinger et al., 2020). *Nitrospira moscoviensis*, a nitrite-oxidizing bacterium that encodes cyanase, can directly convert cyanate to ammonium and CO_2, supplying cyanase-lacking ammonia bacterium, *Nitrosomonas nitrosa*, with ammonium as a source of energy and reductant (Palatinszky et al., 2015). Furthermore, cyanate supports anaerobic ammonium oxidation (anammox) in the oxygen-deficient zone (Babbin et al., 2017; Ganesh et al., 2018; Widner et al., 2018). Observations of cyanate uptake by microbial communities in the North Atlantic coastal waters (Widner et al., 2016a; Widner and Mulholland, 2017) and the Eastern Tropical South and North Pacific oxygen-deficient zone (Widner et al., 2018a, b) further highlight its ecological significance.

The quantitative significance of cyanate utilization in the marine environment depends on the flux and availability of cyanate. However, previous studies rarely examine the source of cyanate in the ocean, leaving it largely enigmatic. Although cyanate is identified as an intermediate product in carbamyl phosphate and urea degradation within cells, this pathway does not constitute the primary source of cyanate in the ocean (Qian et al., 1997; Purcarea et al., 2003). The recent development of a nanomolar cyanate detection method by Widner et al. has facilitated the

measurement of cyanate concentrations in seawater (Widner et al., 2013). Cyanate concentrations range from a few to tens of nanomoles in the Chesapeake Bay Mouth (Widner et al., 2013), the coastal North Atlantic Ocean (Widner et al., 2016; Widner and Mulholland, 2017), and oxygen-deficient zone in the Eastern Tropical South and North Pacific Ocean (Widner et al., 2018a, b). Typically, it exhibits lower concentrations in the surface layer, with peak values occurring below the chlorophyll *a* (Chl *a*) maximum layer in the euphotic zone, displaying similar vertical distribution profiles to other reactive nitrogen compounds, such as urea, ammonium, and nitrite (Widner et al., 2016). Interestingly, areas with high Chl *a* concentration tend to exhibit higher cyanate concentrations (Widner and Mulholland, 2017). The distribution profiles of cyanate in the ocean strongly suggest that the origin of cyanate is highly correlated to the activity of phytoplankton, providing insights into a potential source.

In a recent study, cyanate production is observed during the decay of the natural microbial community assemblages collected during a dinoflagellate bloom (Zhu et al., 2023), which further indicates that cyanate is produced by phytoplankton or through the degradation of phytoplankton-derived organic matter. Furthermore, it has been found that cyanate concentrations increase linearly in the cultures of two marine diatoms during their late stationary phase (Widner et al., 2016). However, cyanate production became slow or stopped when the cultures were moved to darkness in the late stationary phase (Widner, 2016). The cessation of cyanate production in the diatom cultures under dark conditions suggests that light is an essential factor in cyanate production with cyanate possibly being produced through the photochemical degradation of diatom-derived organic matter in the cultures. Photosynthesis of phytoplankton is one of the primary sources of dissolved organic matter (DOM) in the euphotic zone of marine environment (Azam and Malfatti, 2007). Therefore, we hypothesize that the photochemical degradation process of marine DOM, especially phytoplankton-derived DOM, might be an important source of cyanate in the ocean. Due to the variations in composition and sources of DOM, the potential production of cyanate during the photochemical degradation of DOM may differ in different environments. This study examined the distribution of cyanate in the freshwaters, estuarine, coastal areas along Florida coastline and continental and slope regions of the North American mid-Atlantic Ocean (NATL), as well as the production of cyanate during the photochemical degradation of DOM collected from multiple depths in the euphotic zone of these environments.

In addition to eukaryotic algae, picocyanobacteria are also important primary producers in the ocean (Li, 1995; Scanlan, 2012; Flombaum et al., 2013). Whether cyanate can be produced from the DOM released by picocyanobacteria remains unknown. Therefore, to further explore the source of cyanate, the photochemical production of cyanate was also examined during photochemical degradation of DOM secreted by *Synechococcus* sp. CB0101 (*Syn*CB0101–DOM), a typical picocyanobacterial strain widely distributed in estuarine and coastal environments (Marsan et al., 2014; Fucich et al., 2019). Photochemical experiments were also conducted with a natural seawater DOM that was supplemented with five nitrogen–containing compounds with different structures and functional groups to gain insights into possible photochemical precursors of cyanate. The overall goal of this study is to enhance our understanding of the role of cyanate in marine environments by investigating its distribution, sources, and production mechanisms in various environments.

2 Materials and methods

2.1 Cyanate and DOM sampling

Natural water samples of cyanate and DOM were collected from 13 stations across various environments (Figure 1), including freshwater, estuarine, coastal areas along the Florida coastline, and the continental and slope regions of the NATL. Pine Glades Lake and Nine Mile Pond were two freshwater stations in the Everglades National Park, Florida. Bay Mouth was an estuarine station situated in the Chesapeake Bay mouth. Naples Pier and Edward B. Knight Pier were coastal stations in the Gulf of Mexico and Key West, Florida, respectively. Light Tower, Station 14, Station 24, Station 36, Station 37, Station 11, Station 33, and Station 39 extended along the continental and slope regions of the NATL (34–37°N).

Only surface water samples were collected from the two freshwater stations and the two coastal stations in Florida. Water samples were taken using a polypropylene bucket in September 2018 at these sampling stations. The polypropylene bucket had been pre-cleaned and rinsed multiple times with sample water before collection. In addition to the surface layer samples, samples from beneath the surface layers were also collected in the Estuarine and the NATL stations. Water samples at Bay Mouth and Light Tower were collected aboard an R/V *Slover* cruise operated by Old Dominion University in May, 2016. Furthermore, samples from the continental and slope regions of the NATL were collected during the *R/V Hugh R. Sharp* cruise in August 2016. These samples were collected from Niskin bottles attached to a rosette equipped with a SeaBird Electronics 911plus Conductivity, Temperature and Depth sensor package. *In-situ* Chl *a* fluorescence in multiple layers of the stations in the continental and slope regions of the NATL was measured by a fluorometer (ECO-AFL/FL, WET Labs) mounted to the water sampler and converted to µg/L (Selden et al., 2021). Detailed information on the sampling stations and depths for cyanate and DOM is provided in Supplementary Table S1.

Upon collection, water samples were filtered through a 0.2 µm Supor Pall capsule filter using a peristaltic pump. Triplicate subsamples (~1.5 to 2 mL) were transferred from the filtrate and placed into polypropylene tubes to determine cyanate. The cyanate samples were stored at -80°C freezer until derivatization and subsequent analysis using high-performance liquid chromatography (HPLC). Additionally, around 4 L filtrate was transferred to pre-combusted (450 °C for 5 h) amber glass bottles as the DOM for the follow-up photochemical experiment described below. The DOM samples were stored in a 4 °C fridge before conducting the photochemical experiment within one week.

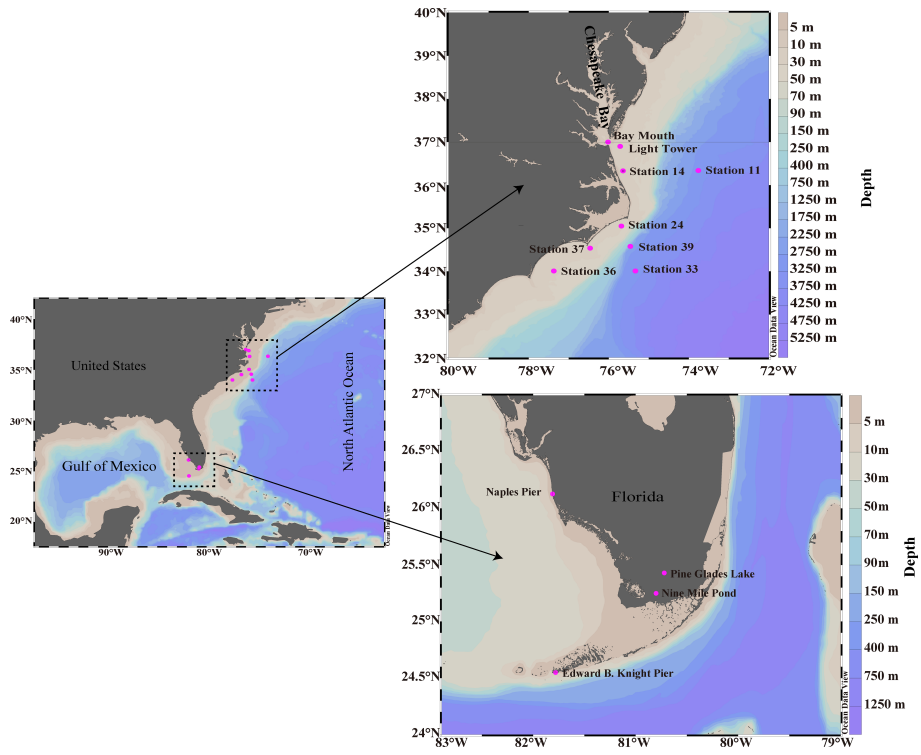

FIGURE 1
Cyanate and DOM sampling stations in the freshwater (Pine Glades Lake and Nine Mile Pond), Estuarine (Bay Mouth), coastal areas along the Florida coastline (Edward B. Knight Pier and Naples Pier), and the continental and slope areas of the NATL (Light Tower, Station 11, Station 14, Station 24, Station 33, Station 36, Station 37 and Station 39). See Supplementary material for additional information about the sampling in Table S1.

2.2 Photochemical degradation experiments on euphotic zone DOM in various environments

To investigate whether cyanate is produced during the photochemical degradation of DOM, photochemical experiments were conducted on the DOM samples collected from euphotic zones across various environments in a UV solar simulator, as described elsewhere (Minot et al., 2006; Helms et al., 2008; Widner et al., 2016). The solar simulator employs 12 Q-Panel UV340 bulbs as the light source, mimicking the spectral shape of natural sunlight within the 295–365 nm range (Minot et al., 2006; Helms et al., 2008). The reason for choosing UVA lamps as the light source is that the dominance of the solar spectrum within this range constitutes the primary wavelengths where photochemical degradation of DOM occurs.

Each DOM sample was divided into six round-bottom quartz flasks (500-mL each). Three flasks were wrapped in aluminum foil to serve as the dark control group, while the remaining three were designated as the light group. All flasks in the dark control and light groups were placed simultaneously in the simulator and irradiated for 8 hours at 20 ± 2 °C. The 8-hour irradiation period in this solar simulator corresponds to approximately 10.2 hours of mid-day inter-sunlight at 37°N (Minot et al., 2006; Helms et al., 2008; Widner et al., 2016).

Approximately 2 mL of samples were collected from each flask in the dark control and light group before and after irradiation and filled into polypropylene tubes to determine cyanate concentration. The production of cyanate in both the light and dark groups was calculated after the 8-hour photochemical experiment, respectively. The cyanate production rate was determined as the difference between the production rate in the light and dark control groups. To accommodate variations in concentration and composition of DOM across different environment, the cyanate production rates were normalized to the initial absorption coefficient of DOM at 300 nm. The absolute (non-normalized) cyanate production rates were also listed in Table S1.

2.3 Photochemical degradation experiments on DOM secreted by *Synechococcus* sp. CB0101

To further investigate the potential production of cyanate during the photochemical degradation of phytoplankton-derived DOM, cyanate concentrations were monitored during photochemical degradation of DOM secreted by a typical picocyanobacterial strain, *Synechococcus* sp. CB0101. The strain, belonging to *Synechococcus* sub-cluster 5.2, was isolated from the Baltimore Inner Harbor in Chesapeake Bay (Marsan et al., 2014; Fucich et al., 2019).

Synechococcus sp. CB0101 was cultured in SN medium with 15‰ salinity (SN15 medium) at 22°C under constant cool white light with an intensity of 20–30 µm E m^{-2} s^{-1} (Waterbury et al., 1986). To minimize the background DOM in the SN15 medium, aged seawater and Milli-Q water were mixed at a ratio of 1:1 (v/v) and used as the medium base. In addition, no EDTA and vitamin

B12 were added to the SN15 medium. Initially, *Synechococcus* sp. CB0101 was pre-cultured in SN15 medium to mid-logarithmic growth phase in a small volume. Subsequently, the cells were collected by centrifugation at 6000 × *g* for 5 minutes and resuspended in SN15 medium. About 5% of the resuspended cells (v/v) were inoculated into SN15 medium for expanded culture of *Synechococcus* sp. CB0101. Samples for determining the cell abundance of *Synechococcus* sp. CB0101 were taken in triplicates daily. Briefly, 1.98 mL of the culture medium was transferred to a 2 mL tube, and 20 µL of 50% glutaraldehyde was added and thoroughly mixed. The sample was then fixed in the dark for 15 minutes, rapidly frozen in liquid nitrogen for approximately 15 minutes, and stored at -80°C freezer for subsequent analysis. The samples were measured immediately after sampling using a BD Accuri C6 Flow Cytometer (BD Bioscience, Franklin Lakes, NJ, USA). The growth curve of *Synechococcus* sp. CB0101 was plotted based on its cell abundance over the incubation period.

Upon reaching the mid-logarithmic growth phase, the culture medium of *Synechococcus* sp. CB0101 was filtered through a 0.22 µm polycarbonate membrane. The resulting filtrate was collected and stored in an amber glass bottle as *Syn*CB0101–DOM. The DOM in the culture medium (Medium–DOM) was also collected immediately after inoculation using the same procedure as *Syn*CB0101–DOM and served as control in the subsequent photochemical experiment. Both *Syn*CB0101–DOM and Medium–DOM were stored in a refrigerator at 4°C before conducting the photochemical degradation experiment. All the glassware used in the experiment had been pre-combusted at 450°C for 4 hours in a muffle furnace to prevent potential organic matter contamination.

To conduct the photochemical experiment, both *Syn*CB0101–DOM and Medium–DOM were brought from the refrigerator, warmed to room temperature, and gently inverted to mix. Subsequently, 50 mL of *Syn*CB0101–DOM was transferred to each of 6 quartz tubes, with three designated as the light group and the remaining three wrapped in aluminum foil to serve as the dark group. The light and dark groups for Medium–DOM were prepared using the same procedure as for *Syn*CB0101–DOM, serving as control. The 12 quartz tubes containing Medium–DOM and *Syn*CB0101–DOM were placed simultaneously in the UV solar, as described in section 2.2. The photochemical degradation experiment was conducted for 8 hours at 20 ± 2 °C. Approximately 1.5 mL of sample was transferred from each quartz tube at 0 h, 2 h, 4 h, 6 h and 8 h to determine cyanate concentration.

2.4 Photochemical experiment on natural seawater DOM supplemented with different nitrogen–containing compounds

To further elucidate the source and mechanism underlying cyanate production, a photochemical experiment was conducted on a coastal seawater DOM sample supplemented with five different nitrogen–containing compounds. The coastal seawater DOM sample was collected from the surface seawater in a coastal area (75.085°W, 38.328°N) near Ocean City, Delaware, USA. Approximately 3.5 L *in-situ* seawater was collected using a polypropylene bucket, filled into an amber glass bottle, and kept in a cooler filled with several ice packs. The water sample was transported to the laboratory within 4 hours, and immediately filtered through a 0.22 µm polycarbonate membrane. The resulting filtrate was transferred to another amber glass bottle as the coastal seawater DOM sample. The amber glass bottles were combusted at 450°C for 5 h in a muffle furnace before use. Five nitrogen–containing compounds, namely *N*-Acetyl-D-glucosamine (Sigma A8625), GlycylGlycine (Sigma 1042330100), 4-(methylamino) benzoic acid (Sigma 119695), 4-[ethyl(methyl)amino] benzaldehyde (Sigma CDS023138), and methyl 2-aminobenzoate (Sigma 236454), each with distinct structures or functional groups, were selected as model compounds. Stock solutions of these compounds, each at a concentration of 100 mM, were prepared using Milli-Q water and stored at 4°C before use. The stock solutions were diluted to 100 µM as working solutions.

To conduct the photochemical degradation experiment, five nitrogen-containing compounds were supplemented to a coastal seawater sample, respectively, resulting in five amended groups. The coastal seawater sample was divided into 30 pre-combusted (450 °C for 5 h) quartz tubes, each receiving 40 mL. These tubes were further divided into five groups, each consisting of six tubes. Subsequently, each working solution of the five nitrogen–containing compounds was separately added to the six tubes in each group, with each tube receiving 10 mL, resulting in a final nitrogen-containing compound concentration of 20 µM. Additionally, another six quartz tubes were filtered with 50 mL of the coastal seawater sample, each without adding any nitrogen–containing compounds, serving as a control group. To account for the effects of darkness, three tubes in each amended and control group was wrapped in aluminum foil, serving as dark control. All quartz tubes in the amended and control groups were placed in the solar simulator, as mentioned in section 2.2. The samples were irradiated at 20 ± 2 °C for 8 hours. At 0 and 8 hours, subsamples were transferred from each tube in the amended and control groups into 2 mL tubes and stored at -80 °C for subsequent cyanate concentration analysis. Before the photochemical experiment, UV-visible absorption spectra (200–700 nm, at 1 nm intervals) of the DOM in the control and nitrogen–containing compound amended groups were measured using an Agilent 8543 diode array spectrophotometer with a 1 cm quartz cuvette. Milli-Q water was used as the blank. Absorbance values were converted to Napierian absorption coefficients using the following formula:

$$a = \frac{2.303A}{l}$$

where "*a*" is Napierian absorption coefficient (m^{-1}), "A" is absorbance, and "L" is path length (m) (Green and Blough, 1994; Helms et al., 2013).

2.5 Measurement of cyanate concentration

Cyanate concentration was measured by pre-column fluorescence derivatization using 2-aminobenzoic acid (ABA) (Sigma-Aldrich, ≥ 99.5% purity) as the derivatization reagent on a modular Shimadzu high-performance liquid chromatography (HPLC) system, with modifications according to Widner et al. (Widner et al., 2013;

Widner and Mulholland, 2017). Potassium cyanate (KOCN, Sigma-Aldrich, 96%) was utilized to prepare standards at various concentrations. Both standards and samples were derivatized simultaneously using the same procedure. Briefly, 1.0 mL of either a water sample or a standard solution was initially reacted with 0.4 mL of 30 mM ABA to form the 2, 4-quinazolinedione derivative in a pre-combusted (450°C for 5 h) 4 mL amber borosilicate glass vial (Fisher Scientific) with a polypropylene cap (Sigma-Aldrich, PTFE/silicone septum). The derivatization reaction occurred in a 35°C water bath for 30 min. Immediately upon removal of the vials from the water bath, 1.4 mL of 12 N HCl (reagent grade) was added to each sample, resulting in a final concentration of 6 N HCl. Due to the strong acidity of the derived samples, there was potential for corrosion to HPLC metal components, adversely affecting column efficiency and longevity. Therefore, the pH of the derivatized standards and samples was adjusted to ~7 before injection. Usually, an equal number of 4 mL amber borosilicate glass vials were employed based on the number of standards and samples. Then, 900 µL of the derived samples and standards were added to each vial and mixed with 1 mL of 0.5 M boric acid buffer (pH = 9.5) and 540 µL of 10 N NaOH. About 1.5 mL of these mixtures were transferred to 2 mL HPLC autosampler vials after cooling to room temperature. Cyanate was then quantified on the HPLC equipped with a fluorescence detector (RF-10AXL), configured with excitation and emission wavelengths of 312 and 370 nm. The mobile phase comprised 60:40 5% trifluoroacetic acid (TFA)/100% methanol, and the flow rate was 0.1 mL/min. Both of the TFA and methanol were of HPLC grade and were purchased from Fisher Scientific. A poly (styrene-divinylbenzene) column with broad pH stability (Hamilton, PRP-1, 2.1 × 150 mm, 5 µm) was used. The sample injection volume was 100 µL, and the run time was 15 min. The method detection limit was 0.4 nmol L^{-1} (Widner et al., 2013). An independent sample t-test was used to analyze the differences in cyanate concentration and production rate between the Chl *a* maximum layers and other water depths at the same sampling station and the differences in cyanate production between the nitrogen-containing amended and control group using SPSS Statistics Software (IBM, Armonk, NY, USA).

3 Results

3.1 Distributions of cyanate in different environments

Cyanate concentrations in the surface water were measured in various aquatic environments. Stations located in the freshwater, estuarine, and coastal areas of Florida demonstrated higher cyanate concentrations compared to those in the continental and slope regions of the NATL (Figure 2). The cyanate concentrations in these stations ranged from 4.17–18.7 nmol L^{-1} (Figure 2). On average, the two coastal stations in Florida exhibited the highest concentrations, with 15.4 nmol L^{-1} at Naples Pier in the Gulf of Mexico and 18.7 nmol L^{-1} at Edward. Knight Pier in the Key West, Florida (Figure 2). Additionally, the Bay Mouth station in the Chesapeake Bay also exhibited a relatively high concentration of 12.5 nmol L^{-1} (Figure 2). In contrast to the higher concentrations observed in the stations in the estuarine and coastal areas in Florida, the two freshwater stations within the Everglades National Park displayed lower cyanate concentrations (Figure 2). Specifically, Pine Glades Lake displayed a concentration of 4.17 nmol L^{-1}, while Nine Mile Pond exhibited a concentration of 9.36 nmol L^{-1} (Figure 2). Stations in the NATL generally exhibited lower cyanate concentrations, with most values remaining below 5 nmol L^{-1} (Figure 2).

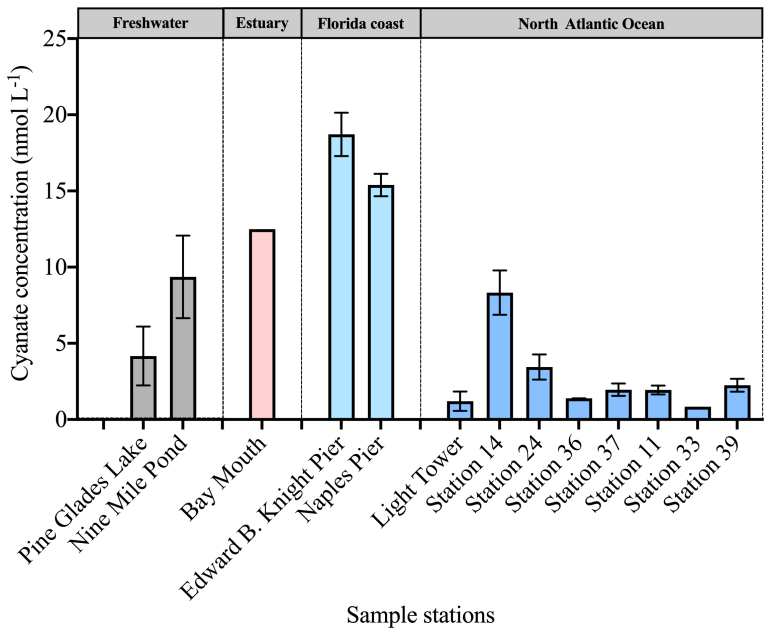

FIGURE 2
Cyanate concentrations in surface layers of sampling stations across diverse environments.

Cyanate concentrations were also measured in multiple water layers at stations in Chesapeake Bay and the continental and slope regions of the NATL. Across these stations and their associated water layers, cyanate concentrations ranged from 0.84–16.9 nmol L^{-1} (Figure 3). In most water layers, cyanate concentrations were below 5 nmol L^{-1} (Figure 3). Furthermore, a consistent pattern emerged across most stations, with lower cyanate concentrations in the surface layer than in other water layers within the same stations. These stations encompassed Bay Mouth, Light Tower, Station 36, Station 37, and Station 11 (Figure 3). Notably, within the five stations, cyanate concentrations in the Chl *a* maximum layer surpassed those in other water layers at the same stations. For instance, at Bay Mouth, cyanate concentration in the surface layer was 12.5 nmol L^{-1}, was 16.9 nmol L^{-1} in the Chl *a* maximum layer of this station (Figure 3). Likewise, at the Light Tower station, cyanate concentration in the Chl *a* maximum layer (5.6 nmol L^{-1}) was significantly ($P< 0.05$) higher than that in the surface layer (1.2 nmol L^{-1}) (Figure 3). Although the surface layer cyanate concentration at station 11 was 1.94 nmol L^{-1}, a significantly higher cyanate concentration was observed in the Chl *a* maximum layer (12.0 nmol L^{-1}, $P< 0.01$) (Figure 3). Additionally, at depths of 244 m and 272 m in station 11, cyanate concentrations were 3.3 nmol L^{-1} and 6.0 nmol L^{-1}, respectively (Figure 3). These concentrations were also significantly ($P< 0.05$) lower than that in the Chl *a* maximum layer but higher than that in the surface layer (Figure 3).

3.2 Photochemical production of cyanate from DOM in the euphotic zone across various environments

Photochemical experiments were conducted with DOM collected from various depths within the euphotic zone across diverse environments to investigate the production of cyanate during the photochemical degradation process of marine DOM, particularly the phytoplankton-derived DOM. Cyanate concentrations showed distinct distribution patterns between cyanate production rate and concentrations.

Cyanate production rates from DOM in surface waters across various environments ranged from 0.054–1.3 nM m h^{-1} (Figure 4). Among the DOM samples examined, a relatively high cyanate production rate (1.2 nM m h^{-1}) was observed from DOM collected at the Bay Mouth station in Chesapeake Bay (Figure 4). Additionally, DOM collected from stations in the coastal areas in Florida and the continental and slope regions of the NATL exhibited average cyanate production rates of 0.56 nM m h^{-1} and 0.46 nM m h^{-1}, respectively (Figure 4). Notably, despite the deficient cyanate concentration (0.84 nmol L^{-1}) in the surface layer of station 33, a high cyanate production rate of 1.3 nM m h^{-1} from the collected DOM in this station was observed, suggesting efficient cyanate utilization in this area (Figures 3, 4). In contrast, DOM from the two freshwater stations in the Everglades National Park exhibited the lowest cyanate production rates, with Pine Glades Lake and Nine Mile Pond with rates of 0.054 nM m h^{-1} and 0.22 nM m h^{-1}, respectively (Figure 4).

Across different water layers within the euphotic zone, the cyanate production rate of DOM ranged from 0.15–2.7 nM m h^{-1} (Figure 5). Except for the 8.1 m water layer of station 14, the cyanate production rate of DOM in the surface water of all other stations was lower than that in the subsurface layers within the same station (Figure 5). Moreover, the 8 m layer in Bay Mouth and Light Tower, and the 18.8 m layer in station 14, were three Chl *a* maximum layers. Interestingly, DOM in these layers exhibited a higher cyanate production rate than other water layers within the same station. For

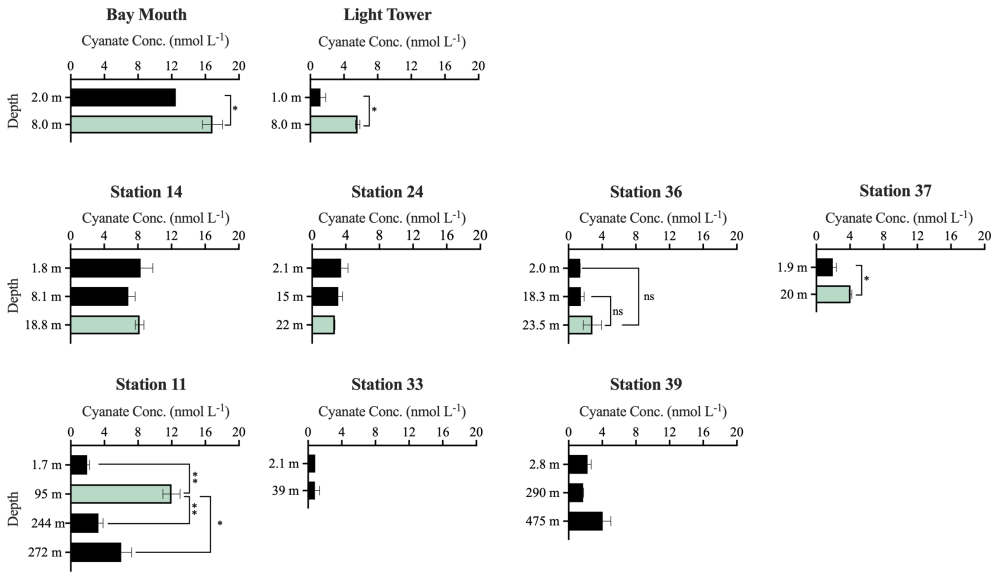

FIGURE 3
Cyanate concentrations at different water layers of stations in the Chesapeake Bay Mouth and the continental and slope regions of the NATL. The green columns specifically represent cyanate concentration in the Chl *a* maximum layer. No significant ("ns"), significant (*, $P< 0.05$), or highly significant (**, $P< 0.01$) differences in cyanate concentrations between the Chl *a* maximum layer and other layers at Bay Mouth, Light Tower, Station 36, Station 37, and Station 11 were indicated.

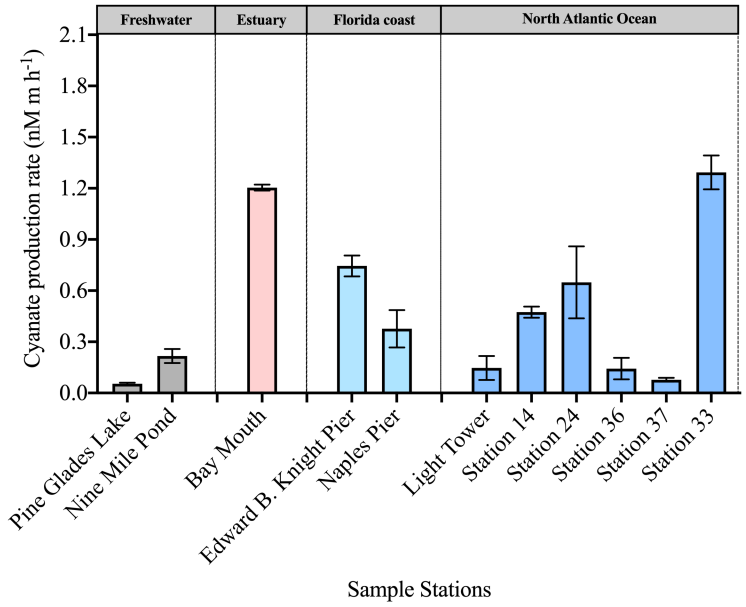

FIGURE 4
Photochemical production rate of cyanate from DOM collected in the surface layers of stations across diverse environments.

example, in the Chl *a* maximum layer of Light Tower, DOM had a cyanate production rate of 2.7 nM m h^{-1}, which was significantly ($P< 0.01$) higher than the rate observed in the surface layer (0.15 nM m h^{-1}) at this station (Figure 5). Likewise, in the Chl *a* maximum layer of station 14, the cyanate production rate of DOM (2.3 nM m h^{-1}) was also significantly higher than that in the surface layer (0.47 nM m h^{-1}) ($P< 0.05$) and in the 8.1 m water layer (0.25 nM m h^{-1}) ($P< 0.01$) of the same station (Figure 5). These results highly indicate that the photochemical degradation process of marine DOM, especially the phytoplankton-derived DOM, is an important source of cyanate in the marine environment.

3.3 Photochemical production of cyanate from DOM secreted by *Synechococcus* sp. CB0101

The production of cyanate was examined during photochemical degradation of *Syn*CB0101–DOM, in order to further investigate the potential production of cyanate from phytoplankton-derived DOM. *Synechococcus* sp. CB0101 underwent a slow growth phase for approximately 10 days, followed by a logarithmic growth phase from day 10 to day 22 (Figure 6A). By day 22, cell abundance reached 1.5 × 10^9 cells mL^{-1} (Figure 6A). Concurrently, a substantial amount of DOM was secreted by *Synechococcus* sp. CB0101 during its growth, causing the DOM concentration in the culture medium to increase from 43 µmol C L^{-1} on day 0 to 602 µmol C L^{-1} on day 22 (Figure 6A). In this study, *Syn*CB0101–DOM was collected on day 22, which was the mid-logarithmic growth phase of *Synechococcus* sp. CB0101.

The cyanate concentrations at each time point, as shown in Figure 6B, were subtracted from the initial cyanate concentrations in Medium–DOM or *Syn*CB0101–DOM, indicating the net production of cyanate during photochemical degradation of these two DOM samples. Cyanate was produced during photochemical degradation of Medium–DOM and *Syn*CB0101–DOM (Figure 6B), with cyanate concentrations increasing at the same trend within the first 2 hours of irradiation. Remarkably, the production of cyanate began to rise rapidly during the photochemical degradation of *Syn*CB0101–DOM after 2 hours of light exposure, resulting in approximately 125 nM of cyanate produced after 8 hours of irradiation. However, only 24 nM cyanate was produced during photochemical degradation of Medium–DOM (Figure 6B). No cyanate was produced in the dark group of either Medium–DOM or *Syn*CB0101–DOM.

3.4 Photochemical production of cyanate from natural seawater DOM supplemented with various nitrogen–containing compounds

Five nitrogen-containing compounds each with distinct structures and functional groups, were supplemented to the coastal seawater DOM sample collected near the Ocean City as mentioned in section 2.4. *N*-Acetyl-*D*-glucosamine is the main component of bacterial peptidoglycan and lipopolysaccharides in the ocean (Riemann and Azam, 2002). The remaining four nitrogen–containing compounds comprise peptides and aromatic compounds, which are common constituents in aquatic DOM (He et al., 2023). The photoproduction of cyanate was examined during the irradiation of the nitrogen–containing compound amended and unamended seawater DOM sample to explore the potential sources of cyanate production in seawater.

The five nitrogen–containing compounds exhibited unique light absorption features. The absorption spectra of DOM supplemented with *N*-Acetyl-*D*-glucosamine or GlycylGlycine resembled that of the

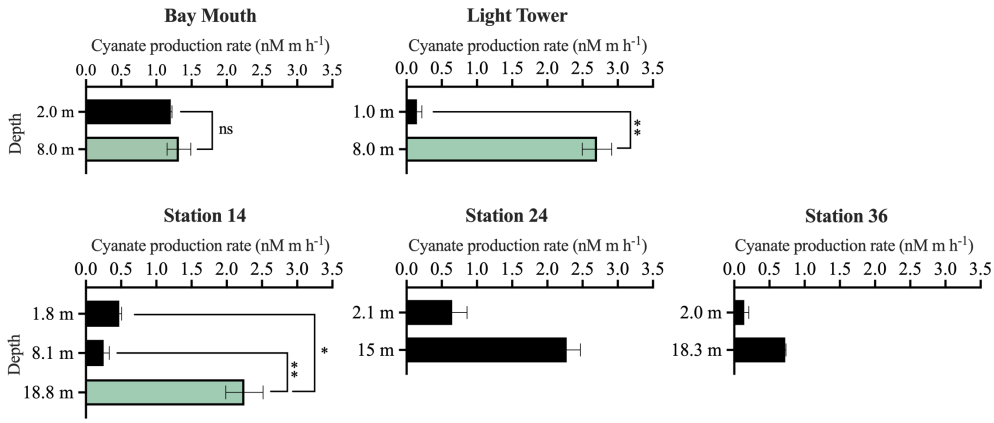

FIGURE 5
Photochemical production of cyanate from DOM collected at different water layers within the euphotic zone of the stations in the Chesapeake Bay Mouth and the continental shelf and slope regions of the NATL. The green columns specifically represent the cyanate production rate in the Chl *a* maximum layer. No significant ("ns"), significant (*, P< 0.05), or highly significant (**, P< 0.01) differences in cyanate production rate between the Chl *a* maximum layer and other layers at Bay Mouth, Light Tower, and Station 14 were indicated.

DOM in the control group, exhibiting an exponential decrease in absorption coefficient as wavelength increased. Conversely, the DOM supplemented with 4-(methylamino) benzoic acid, methyl 2-aminobenzoate, or 4-[ethyl(methyl)amino]benzaldehyde displayed distinct absorption spectra, featuring prominent light absorption peaks at 279 nm (59.6 m^{-1}), 326 nm (24.0 m^{-1}) and 356 nm (103.7 m^{-1}), respectively (Figure 7).

As no cyanate production occurred in any of the dark groups, cyanate production in control and each nitrogen–containing compound amended group was determined by measuring the change in cyanate concentration before and after 8 hours of irradiation. With the exception of DOM amended with *N*-Acetyl-*D*-glucosamine, the DOM amended with the other four nitrogen–containing compounds exhibited significantly higher cyanate production than the DOM in the control group (18.8 nM) (Figure 8). The most substantial cyanate production was observed in the DOM amended with GlycylGlycine, yielding 29.3 nM cyanate after 8 hours of irradiation (Figure 8). Cyanate production from the DOM amended with 4-(methylamino) benzoic acid (29.005 nM) closely resembled that of GlycylGlycine (Figure 8). Interestingly, despite being isomers, cyanate production in the DOM amended with 4-(methylamino) benzoic acid (29.0 nM) significantly exceeded that of the DOM amended with methyl 2-aminobenzoate (21.7 nM) (Figure 8), indicating that the relative positions of the functional groups around the ring affect the photoreactivity.

4 Discussion

4.1 Potential sources of cyanate in different environments

In this study, distributions of cyanate across various environments were investigated. Cyanate concentrations in the

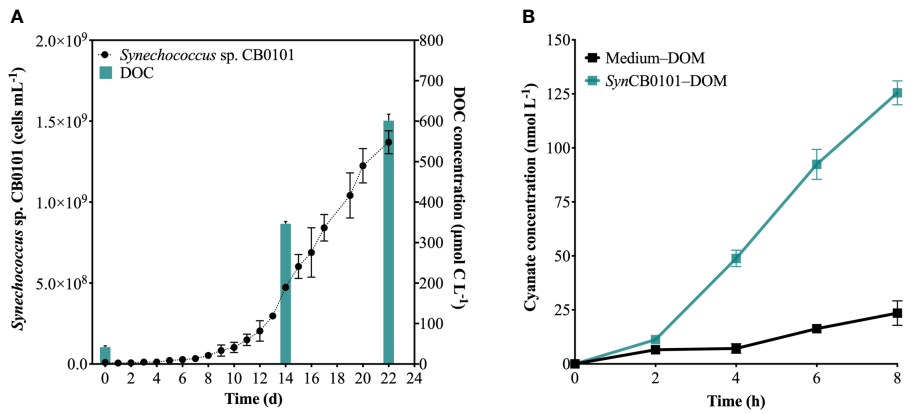

FIGURE 6
Photochemical production of cyanate from *Syn*CB0101–DOM. **(A)** Changes in cell abundance and DOC concentration in the culture medium during the growth of *Synechococcus* sp. CB0101; **(B)** Changes in cyanate concentration during the photochemical degradation processes of *Syn*CB0101–DOM and Medium–DOM.

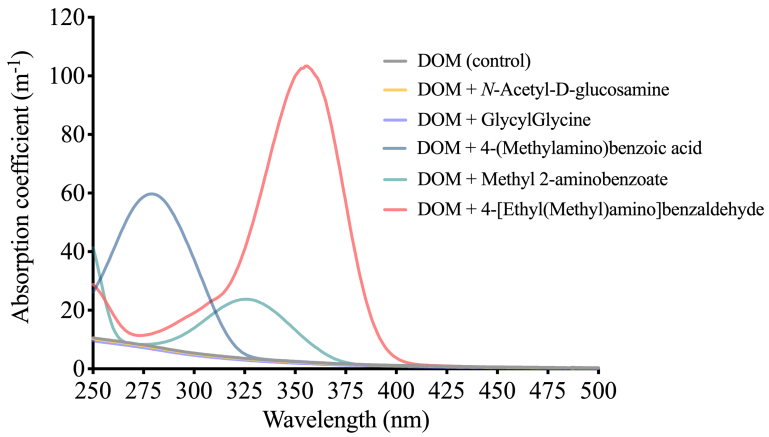

FIGURE 7
Absorption coefficients of a natural DOM supplemented with five different nitrogen–containing compounds.

Chesapeake Bay estuary and the continental and slope regions of the NATL generally agree with the findings of Widner et al. in nearby areas (Widner et al., 2013; Widner et al., 2016; Widner and Mulholland, 2017). Cyanate concentration was initially assessed in a freshwater environment (Pine Glades Lake and Nine Mile Pond) in this study, where a decoupling between its concentration and production rate was observed (Figures 2, 4). The elevated cyanate levels in this region may be attributed to a lower utilization rate. However, there is no documented utilization of cyanate by freshwater microorganisms. Additionally, this phenomenon may suggest the existence of alternative sources contributing to cyanate accumulation. The extensive use of urea as a nitrogen fertilizer in agriculture, with global usage increasing over 100-fold in the past 40 years, comprises over 50% of global urea consumption. Given urea's conversion propensity to cyanate (Dirnhuber and Schutz, 1948), elevated cyanate concentrations in the freshwater environment may result from urea degradation in soil. Furthermore, the urea retained in the soil can be transported to estuarine and coastal environments, becoming a substantial component of total dissolved organic nitrogen (Glibert et al., 2006). A previous study monitored urea concentrations in a Chesapeake Bay tributary for five years, revealing that urea concentration could reach up to 10 µM, surpassing urea concentrations in surface waters of the Chesapeake Bay estuary by over 50-fold (Glibert et al., 2005). Therefore, the relatively higher cyanate concentrations in the Chesapeake Bay estuary and Florida coastal environments may result from urea degradation from terrestrial and riverine sources. Additionally, urea constitutes a significant portion of domestic sewage (Glibert et al., 2006). Edward. Knight Pier and Naples Pier located along Florida's coastline are near urban areas with sewage discharges. Therefore, the high cyanate concentrations at these two stations may stem from urea degradation from nearby domestic sewage.

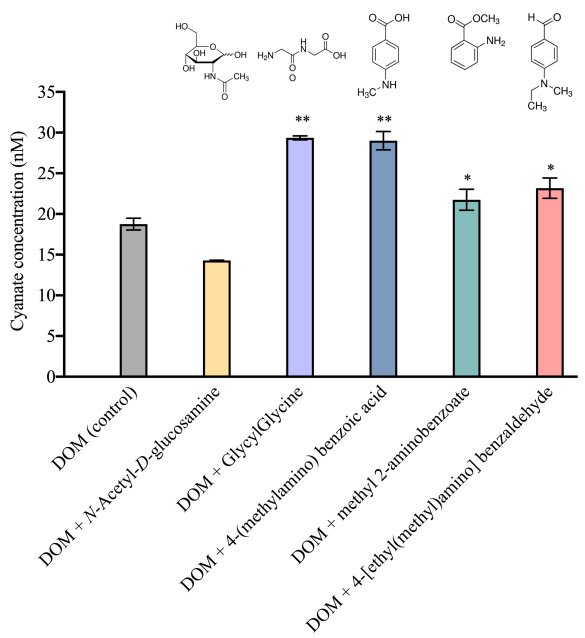

FIGURE 8
Photochemical production of cyanate from natural DOM supplemented with five different nitrogen–containing compounds after 8 hours of irradiation. Significant (*, P<0.05) or highly significant (**, P<0.01) differences in cyanate production between the nitrogen–containing compound amended and control groups were indicated.

Generally, the impact of terrestrial organic matter input on the NATL appears relatively insignificant when compared to estuarine and coastal regions. Consequently, cyanate in this environment is likely primarily generated through *in-situ* biological or abiotic processes. Additionally, it's intriguing to observe a discrepancy between the relatively low cyanate concentration and its high production rate in the NATL (Figures 2–5). Previous studies have demonstrated the capability of microbial communities in the coastal area of the NATL to utilize cyanate, with uptake rates comparable to the photoproduction rates from DOM collected at the NATL stations in this study (Widner et al., 2016). Therefore, it's conceivable that the cyanate produced undergoes rapid consumption in the NATL, resulting in its low concentrations.

4.2 Disparities in sources and composition of DOM in various environments accounting for variations in cyanate production during their photochemical degradation processes

Previous studies primarily addressed cyanate utilization, leaving the sources of cyanate largely unknown (Kitzinger et al., 2019; Linder, 2019; Sáez et al., 2019; Mooshammer et al., 2021). The results of this study reveal that cyanate can be produced by photochemical degradation of DOM in diverse environments. However, the cyanate production rate varies among the DOM samples, probably reflecting differences in their sources and composition. The DOM samples collected in different environment contexts in this study exhibit variations in the sources and composition. For instance, the two freshwater stations, Nine Mile Pond and Pine Glades Lake, located in a subtropical freshwater wetland within Everglades National Park, Florida, USA, primarily consist of humic-like substances from marsh soil. Additionally, due to the proximity of the Everglades Agricultural Area to the northern part of the sampling sites, the DOM in this area is partly characterized by high molecular weight, peat-soil, and highly oxidized agricultural soil-derived DOM (Yamashita et al., 2010). In contrast, Naples Pier and Edward B. Knight Pier, located in southwestern Florida along the Gulf of Mexico and at the southernmost Key West, are minimally influenced by freshwater inputs from the Everglades. Therefore, the DOM in these areas predominantly originates from autochthonous sources (Jaffé et al., 2004). The Chesapeake Bay estuary, impacted by freshwater influx from nearby rivers and the mixing with coastal waters from the NATL, exhibits a DOM comprising both terrestrial and marine origins. In comparison, the DOM in the NATL is comparatively dominated by marine-derived DOM (Loh et al., 2006). Despite elevated cyanate concentrations in freshwater environments, the photochemical production rates of cyanate from DOM in such environments are markedly lower than those in the Chesapeake Bay estuary, coastal areas in Florida, and the continental and slope regions of the NATL (Figures 2, 4). This suggests that, unlike terrestrial DOM, photochemical degradation of marine DOM constitutes a substantial source of cyanate. Consequently, the differences in the sources and composition of DOM in freshwater, Chesapeake Bay estuary, coastal areas in Florida, and the NATL may be potentially crucial factors accounting for the observed variations in cyanate production rates within these diverse environments.

4.3 Photochemical degradation of phytoplankton-derived DOM: a substantial source of cyanate in the marine environment

It is noteworthy that the cyanate production rates from DOM in the Chl *a* maximum layer at Light Tower and Station 14 are significantly higher than those from other depths within the same station (Figure 5). Similarly, in the Chesapeake Bay estuary and the continental and slope regions of the NATL, cyanate concentrations in Chl *a* maximum layers of most stations in these areas surpassed those in other water layers within the same station (Figure 3). Additionally, a strong positive correlation between Chl *a* and cyanate concentrations in different water layers was identified using the Mantel test (Figure 9). This aligns with previous findings indicating higher cyanate concentrations in areas with elevated Chl *a* concentrations in the coastal areas of the NATL (Widner and Mulholland, 2017). Moreover, Widner et al. reported cyanate accumulation in the cultures of two prevalent diatom species in coastal and oceanic environments (Widner et al., 2016). Recent research also reveals cyanate production from the decomposition of organic matter in a station located near the mouth of the Lafayette River Virginia, during a *Margalefidinium polykrikoides* bloom (Zhu et al., 2023). In the marine environment, Chl *a* maximum layer is typically characterized by high biomass and productivity, hosting abundant microorganisms engaged in various biogeochemical processes (Xie et al., 2020; Mao et al., 2021). Consequently, this layer contains substantial organic matter produced by primary producers and other microorganisms. Therefore, the high cyanate production rates in the Chl *a* maximum layers highly suggested that DOM from the Chl *a* maximum layer is very photoreactive and the photochemical degradation of phytoplankton-derived DOM is a substantial source of cyanate in the marine environment.

Furthermore, *Synechococcus*, a key primary producer widely distributed in marine environments, contributes nearly half of ocean productivity (Scanlan, 2012; Flombaum et al., 2013). The DOM secreted by *Synechococcus* constitutes a substantial part of the marine DOM pool (Zhao et al., 2017). This study observed cyanate production during the photochemical degradation of DOM secreted by *Synechococcus* sp. CB0101 (Figure 6), further supporting that the photochemical degradation of phytoplankton-derived DOM is an important source of cyanate in the ocean.

The light intensity of the photochemical experiment in this study resembled the light conditions in the surface seawater at noon at 37°N latitude. However, there is a large difference in light intensity and spectrum between the Chl *a* maximum layer and

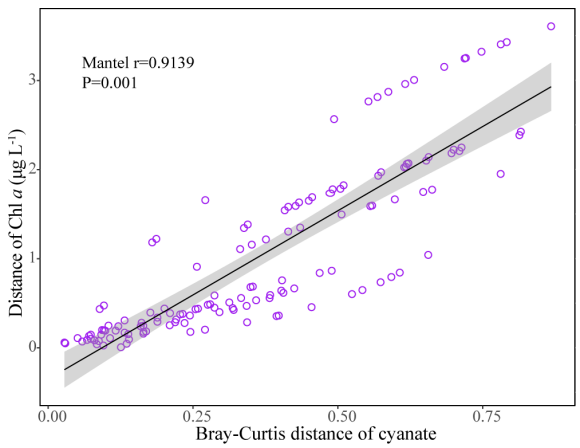

FIGURE 9
Correlation between cyanate and Chl *a* concentrations in different water layers of sampling stations in the Chesapeake Bay estuary and the continental and slope regions of the NATL.

the surface layer. Therefore, it is necessary to systematically investigate cyanate production during photochemical degradation of DOM produced by different microorganisms during different growth stages, such as eukaryotic, prokaryotic primary producers, and heterotrophic bacteria, by simulating the light intensity under various environmental conditions. It has been found that cyanase transcripts are prevalent in marine microorganisms, particularly in *Synechococcus*, *Prochlorococcus* and nitrifying bacteria, spanning from the ocean surface to the chlorophyll maximum layer (Mao et al., 2021). Consequently, utilization of cyanate catalyzed by cyanase potentially plays an important role in the marine nitrogen cycle within the chlorophyll maximum layer. If cyanate is photochemically produced from the degradation of DOM under the light condition in the Chl *a* maximum layer, it will become available for utilization by surrounding microorganisms, serving as an important nitrogen source. Additionally, in the marine environment, microorganisms and organic matter in the Chl *a* maximum layer are typically transported into surface water through vertical mixing (Huisman et al., 2006). If this DOM is further degraded after being brought into the surface layer, the cyanate produced will provide potentially available nitrogen sources for the surface microorganisms. Numerous marine microorganisms have been found to utilize cyanate as a nitrogen source (Kitzinger et al., 2019; Sato et al., 2022). Therefore, the revelation that cyanate can be generated during the photochemical degradation of DOM in this study provides important insight into the marine nitrogen cycle.

4.4 Processes and mechanisms underlying cyanate production in the marine environment

The composition and structure of marine DOM are complex, with nitrogen-containing compounds being a significant component. DOM constituents include sugars, proteins, and some aromatic and aliphatic compounds (Kujawinski and Behn, 2006; Sleighter and Hatcher, 2008; Seidel et al., 2022). In this study, the photochemical production of cyanate from the natural DOM, supplemented with GlycylGlycine, methyl 2-aminobenzoate, 4-(methylamino) benzoic acid, or 4-[ethyl(methyl)amino] benzaldehyde, exhibited marked enhancement compared to the DOM in the control group (Figure 8). Chromophoric dissolved organic matter (CDOM) is the primary component responsible for light absorption in the ocean. High-energy UV light absorbed by CDOM is sufficient to break down its chemical bonds, leading to alterations of its composition or the generation of new compounds, such as small nitrogen–containing molecules (Santos et al., 2014; Mopper et al., 2015). The photochemical degradation of CDOM can also induce the production of a series of free radicals, leading to further oxidation or degradation of other DOM, including colorless DOM and CDOM. GlycylGlycine does not exhibit significant light absorption characteristics in the ultraviolet-visible light region and belongs to colorless DOM. Therefore, the increase in cyanate production in the GlycylGlycine–amended group may be attributed to bond photolysis and the production of free radicals during photochemical degradation of the natural DOM, which in turn promoted GlycylGlycine degradation/oxidation followed by cyanate production. Methyl 2-aminobenzoate, 4-(methylamino) benzoic acid, or 4-[ethyl(methyl)amino] exhibited strong light absorption characteristics at wavelengths of 272 nm, 325 nm, and 350 nm, respectively, and belong to CDOM. Therefore, cyanate produced in amended groups with these three nitrogen–containing compounds may have originated from photochemical degradation of these compounds or from enhanced degradation of the natural DOM induced by free radicals generated during photochemical degradation of these nitrogen–containing compounds. Furthermore, these results support the significance of the photochemical degradation of polypeptides and aromatic compounds in the ocean as a potential source of cyanate. Notably, despite 4-(methylamino) benzoic acid and methyl 2-aminobenzoate being isomers, the cyanate produced during photochemical degradation of the coastal DOM differed when supplemented with these two compounds. This discrepancy may be attributed to the positions of functional groups on their respective benzene ring. Specifically, 4-(methylamino) benzoic acid features a benzene ring with a carboxylic acid group and a methylamino group at the 4-position. In contrast, the benzene ring of methyl 2-aminobenzoate incorporates a carboxylic ester group and an amino group at the 2-position. It has been previously shown that the relative position of functional groups around the rings affects the compound's photoreactivity and consequently its quantum yields (Sun et al., 2015). A systematic study of the effects of positional isomers on the photoproduction of cyanate would likely yield new insights into the photoreactivity of marine DOM.

5 Conclusions

Cyanate is an important organic nitrogen and energy source for various microbial organisms. This study investigated the distribution and production of cyanate during the photochemical degradation of DOM from various environments to understand its sources. Cyanate concentrations varied markedly with depth in freshwater, Chesapeake Bay estuary, coastal areas in Florida, and the continental and slope regions of the NATL, and are highly correlated with Chl *a* concentrations. Additionally, our findings also provide strong evidence that photochemical degradation of marine DOM, especially phytoplankton-derived DOM, is a major source of cyanate in the ocean. Furthermore, it was found that cyanate is likely produced from peptides and aromatic compounds present in DOM. The findings of this study provide new insights into the roles of cyanate in the marine nitrogen cycle. It appears that cyanate's photochemical production may be useful for studying photodegradation pathways of DOM and nitrogen-containing DOM precursors.

Data availability statement

The original contributions presented in the study are included in the article/Supplementary Material. Further inquiries can be directed to the corresponding authors.

Author contributions

RW: Conceptualization, Formal analysis, Funding acquisition, Methodology, Writing – review & editing. JL: Funding acquisition, Writing – review & editing. YX: Writing – review & editing. LL: Formal analysis, Writing – review & editing. KM: Writing – review & editing, Methodology, Supervision.

Funding

The author(s) declare that financial support was received for the research, authorship, and/or publication of this article. This work was supported by awards from the Key Research and Development Program of Shandong Province (2020ZLYS04), the China Postdoctoral Science Foundation (2022M711897), the Natural Science Foundation of Shandong province (ZR2022QD116), the U.S. National Science Foundation (OCE-1155666, OCE-1459698 and OCE-1543784) and the Fujian Key Laboratoryof Marine Carbon Sequestration (FKLMCS2023001).

Acknowledgments

We would like to thank the captain and all the crew of the R/V Hugh R. Sharp cruise for their dedication and support. In particular, we thank Brittany Winder for her help in the cruise planning and preparation. We thank Dr. Margaret R. Mulholland and Peter W. Bernhardt for providing all the lab facilities and their assistance in handling the HPLC for measurement of cyanate samples.

Conflict of interest

The authors declare that the research was conducted in the absence of any commercial or financial relationships that could be construed as a potential conflict of interest.

Publisher's note

All claims expressed in this article are solely those of the authors and do not necessarily represent those of their affiliated organizations, or those of the publisher, the editors and the reviewers. Any product that may be evaluated in this article, or claim that may be made by its manufacturer, is not guaranteed or endorsed by the publisher.

Supplementary material

The Supplementary Material for this article can be found online at: https://www.frontiersin.org/articles/10.3389/fmars.2024.1373643/full#supplementary-material

References

Azam, F., and Malfatti, F. (2007). Microbial structuring of marine ecosystems. *Nat. Rev. Microbiol.* 5, 782–791. doi: 10.1038/nrmicro1747

Babbin, A. R., Peters, B. D., Mordy, C. W., Widner, B., Casciotti, K. L., and Ward, B. B. (2017). Multiple metabolisms constrain the anaerobic nitrite budget in the Eastern Tropical South Pacific. *Global Biogeochem. Cy.* 31, 258–271. doi: 10.1002/2016gb005407

Berman, T., and Bronk, D. A. (2003). Dissolved organic nitrogen: a dynamic participant in aquatic ecosystems. *Aquat. Microb. Ecol.* 31, 279–305. doi: 10.3354/ame031279

Berthelot, H., Duhamel, S., L'Helguen, S., Maguer, J. F., Wang, S., Cetinić, I., et al. (2019). NanoSIMS single cell analyses reveal the contrasting nitrogen sources for small phytoplankton. *ISME J.* 13, 651–662. doi: 10.1038/s41396-018-0285-8

Bristow, L. A., Mohr, W., Ahmerkamp, S., and Kuypers, M. M. M. (2017). Nutrients that limit growth in the ocean. *Curr. Biol.* 27, R474–R478. doi: 10.1016/j.cub.2017.03.030

Bronk, D. A., See, J. H., Bradley, P., and Killberg, L. (2007). DON as a source of bioavailable nitrogen for phytoplankton. *Biogeosciences* 4, 283–296. doi: 10.5194/bg-4-283-2007

Carepo, M. S. P., Nina de Azevedo, J. S., Porto, J. I. R., Bentes-Sousa, A. R., Batista, J. D. S., Da Silva, A. L. C., et al. (2004). Identification of Chromobacterium violaceum genes with potential biotechnological application in environmental detoxification. *Genet. Mol. Res.* 3, 181–194.

Dirnhuber, P., and Schutz, F. (1948). The isomeric transformation of urea into ammonium cyanate in aqueous solutions. *Biochem. J.* 42, 628–632.

Elleuche, S., and Pöggeler, S. (2008). A cyanase is transcriptionally regulated by arginine and involved in cyanate decomposition in Sordaria macrospora. *Fungal Genet. Biol.* 45, 1458–1469. doi: 10.1016/j.fgb.2008.08.005

Flombaum, P., Gallegos, J. L., Gordillo, R. A., Rincón, J., Zabala, L. L., Jiao, N., et al. (2013). Present and future global distributions of the marine Cyanobacteria *Prochlorococcus* and Synechococcus. *Proc. Natl. Acad. Sci. U.S.A.* 110, 9824–9829. doi: 10.1073/pnas.1307701110

Fucich, D., Marsan, D., Sosa, A., and Chen, F. (2019). Complete genome sequence of subcluster 5.2 Synechococcus sp. strain CB0101, isolated from the Chesapeake Bay. *Microbiol. Resour. Announc.* 8, e00484–e00419. doi: 10.1128/MRA.00484-19

Ganesh, S., Bertagnolli, A. D., Bristow, L. A., Padilla, C. C., Blackwood, N., Aldunate, M., et al. (2018). Single cell genomic and transcriptomic evidence for the use of alternative nitrogen substrates by anammox bacteria. *ISME J.* 12, 2706–2722. doi: 10.1038/s41396-018-0223-9

Glibert, P. M., Harrison, J., Heil, C., and Seitzinger, S. (2006). Escalating worldwide use of Urea – a global change contributing to coastal eutrophication. *Biogeochemistry* 77, 441–463. doi: 10.1007/s10533-005-3070-5

Glibert, P. M., Trice, T. M., Michael, B., and Lane, L. (2005). Urea in the tributaries of the chesapeak and coastal bays of Maryland. *Water Air Soil Poll.* 160, 229–243. doi: 10.1007/s11270-005-2546-1

Green, S. A., and Blough, N. V. (1994). Optical absorption and fluorescence properties of chromophoric dissolved organic matter in natural waters. *Limnol. Oceanogr.* 39, 1903–1916. doi: 10.4319/lo.1994.39.8.1903

He, C., Yi, Y., He, D., Cai, R., Chen, C., and Shi, Q. (2023). Molecular composition of dissolved organic matter across diverse ecosystems: Preliminary implications for biogeochemical cycling. *J. Environ. Manage.* 344, 118559. doi: 10.1016/j.jenvman.2023.118559

Helms, J. R., Stubbins, A., Perdue, E. M., Green, N. W., Chen, H., and Mopper, K. (2013). Photochemical bleaching of oceanic dissolved organic matter and its effect on absorption spectral slope and fluorescence. *Mar. Chem.* 155, 81–91. doi: 10.1016/j.marchem.2013.05.015

Helms, J. R., Stubbins, A., Ritchie, J. D., Minor, E. C., and Kieber, D. J. (2008). Absorption spectral slopes and slope ratios as indicators of molecular weight, source and photobleaching of chromophoric dissolved organic matter. *Limnol. Oceanogr.* 53, 955–969. doi: 10.4319/lo.2008.53.3.0955

Huisman, J., Pham Thi, N. N., Karl, D. M., and Sommeijer, B. (2006). Reduced mixing generates oscillations and chaos in the oceanic deep chlorophyll maximum. *Nature* 439, 322–325. doi: 10.1038/nature04245

Hutchins, D. A., and Capone, D. G. (2022). The marine nitrogen cycle: new developments and global change. *Nat. Rev. Microbiol.* 20, 401–414. doi: 10.1038/s41579-022-00687-z

Jaffé, R., Boyer, J. N., Lu, X., Maie, N., Yang, C., Scully, N. M., et al. (2004). Source characterization of dissolved organic matter in a subtropical mangrove-dominated

estuary by fluorescence analysis. *Mar. Chem.* 84, 195–210. doi: 10.1016/j.marchem.2003.08.001

Kamennaya, N. A., Chernihovsky, M., and Post, A. F. (2008). The cyanate utilization capacity of marine unicellular cyanobacteria. *Limnol. Oceanogr.* 53, 2485–2494. doi: 10.4319/lo.2008.53.6.2485

Kamennaya, N. A., and Post, A. F. (2011). Characterization of cyanate metabolism in marine *synechococcus* and prochlorococcus spp. *Appl. Environ. Microb.* 77, 291–301. doi: 10.1128/aem.01272-10

Kamennaya, N. A., and Post, A. F. (2013). Distribution and expression of the cyanate acquisition potential among cyanobacterial populations in oligotrophic marine waters. *Limnol. Oceanogr.* 58, 1959–1971. doi: 10.4319/lo.2013.58.6.1959

Kebeish, R., and Al-Zoubi, O. (2017). Expression of the cyanobacterial enzyme cyanase increases cyanate metabolism and cyanate tolerance in Arabidopsis. *Environ. Sci. pollut. Res. Int.* 24, 11825–11835. doi: 10.1007/s11356-017-8866-z

Kitzinger, K., Marchant, H. K., Bristow, L. A., Herbold, C. W., Padilla, C. C., Kidane, A. T., et al. (2020). Single cell analyses reveal contrasting life strategies of the two main nitrifiers in the ocean. *Nat. Commun.* 11, 767. doi: 10.1038/s41467-020-14542-3

Kitzinger, K., Padilla, C. C., Marchant, H. K., Hach, P. F., Herbold, C. W., Kidane, A. T., et al. (2019). Cyanate and urea are substrates for nitrification by Thaumarchaeota in the marine environment. *Nat. Microbiol.* 4, 243–234. doi: 10.1038/s41564-018-0316-2

Koch, H., van Kessel, M. A. H. J., and Lucker, S. (2019). Complete nitrification: insights into the ecophysiology of comammox Nitrospira. *Appl. Microbiol. Biot.* 103, 177–189. doi: 10.1007/s00253-018-9486-3

Kujawinski, E. B., and Behn, M. D. (2006). Automated analysis of electrospray ionization fourier transform ion cyclotron resonance mass spectra of natural organic matter. *Anal. Chem.* 78, 4363–4373. doi: 10.1021/ac0600306

Li, W. K. W. (1995). Composition of ultraphytoplankton in the central North Atlantic. *Mar. Ecol. Prog. Ser.* 122, 1–8. doi: 10.3354/meps122001

Linder, T. (2019). Cyanase-independent utilization of cyanate as a nitrogen source in ascomycete yeasts. *World J. Microb. Biot.* 35, 3. doi: 10.1007/s11274-018-2579-4

Loh, A. N., Bauer, J. E., and Canuel, E. A. (2006). Dissolved and particulate organic matter source-age characterization in the upper and lower Chesapeake Bay: A combined isotope and biochemical approach. *Limnol. Oceanogr.* 51, 1421–1431. doi: 10.4319/lo.2006.51.3.1421

Mao, X., Chen, J., van Oosterhout, C., Zhang, H., Liu, G., Zhuang, Y., et al. (2021). Diversity, prevalence, and expression of cyanase genes (*cynS*) in planktonic marine microorganisms. *ISME J.* 16, 602–605. doi: 10.1038/s41396-021-01081-y

Marsan, D., Wommack, K. E., Ravel, J., and Chen, F. (2014). Draft genome sequence of synechococcus sp. Strain CB0101, isolated from the Chesapeake bay estuary. *Genome Announc.* 2, e01111–e01113. doi: 10.1128/genomeA.01111-13

Minot, E. C., Pothen, J., Dalzell, B. J., Abdulla, H., and Mopper, K. (2006). Effects of salinity changes on the photodegradation and ultraviolet-visible absorbance of terrestrial dissolved organic matter. *Limnol. Oceanogr.* 51, 2181–2186. doi: 10.4319/lo.2006.51.5.2181

Mooshammer, M., Wanek, W., Jones, S. H., Richter, A., and Wagner, M. (2021). Cyanate - a low abundance but actively cycled nitrogen compound in soil. *Commun. Earth Environ.* 2, 161. doi: 10.1101/2020.07.12.199737

Mopper, K., Kieber, D. J., and Stubbins, A. (2015). "Marine photochemistry of organic matter," in *Biogeochemistry of Marine Dissolved Organic Matter*. Eds. D. A. Hansel and C. A. Carlson (The Netherlands: Elsevier), 389–450.

Pachiadaki, M. G., Sintes, E., Bergauer, K., Brown, J. M., Record, N. R., Swan, B. K., et al. (2017). Major role of nitrite-oxidizing bacteria in dark ocean carbon fixation. *Science* 358, 1046–1051. doi: 10.1126/science.aan8260

Palatinszky, M., Herbold, C., Jehmlich, N., Pogoda, M., Han, P., von Bergen, M., et al. (2015). Cyanate as an energy source for nitrifiers. *Nature* 524, 105–108. doi: 10.1038/nature14856

Palenik, B., Brahamsha, B., Larimer, F. W., Land, M., Hauser, L., Chain, P., et al. (2003). The genome of a motile marine Synechococcus. *Nature* 424, 1037–1042. doi: 10.1038/nature01943

Purcarea, C., Ahuja, A., Lu, T., Kovari, L., Guy, H. I., and Evans, D. R. (2003). Aquifex aeolicus aspartate Transcarbamoylase, an enzyme specialized for the efficient utilization of unstable carbamoyl phosphate at elevated temperature. *J. Biol. Chem.* 278, 52924–52934. doi: 10.1074/jbc.M309383200

Qian, M., Eaton, J. W., and Wolff, S. P. (1997). Cyanate-mediated inhibition of neutrophil myeloperoxidase activity. *Biochem. J.* 326, 159–166. doi: 10.1042/bj3260159

Riemann, L., and Azam, F. (2002). Widespread *N*-Acetyl-*D*-Glucosamine uptake among pelagic marine bacteria and tts ecological implications. *Appl. Environ. Microb.* 68, 5554–5562. doi: 10.1128/AEM.68.11.5554-5562.2002

Rocap, G., Larimer, F. W., Malfatti, J., Malfatti, S., Chain, P., Ahlgren, N. A., et al. (2003). Genome divergence in two P*rochlorococcus* ecotypes reflects oceanic niche differentiation. *Nature* 424, 1042–1047. doi: 10.1038/nature01947

Sáez, L. P., Cabello, P., Ibáñez, M. I., Luque-Almagro, V. M., Roldán, M. D., and Moreno-Vivián, C. (2019). Cyanate assimilation by the alkaliphilic cyanide-degrading bacterium *Pseudomonas pseudoalcaligenes* CECT5344: Mutational Analysis of the cyn Gene Cluster. *Int. J. Mol. Sci.* 20, 3008. doi: 10.3390/ijms20123008

Santos, L., Santos, E. B. H., Dias, J. M., Cunha, A., and Almeida, A. (2014). Photochemical and microbial alterations of DOM spectroscopic properties in the estuarine system Ria de Aveiro. *Photoch. Photobio. Sci.* 13, 1146–1159. doi: 10.1039/c4pp00005f

Sato, M., Hashihama, F., and Takeda, S. (2022). Effects of cyanate enrichment on growth of natural phytoplankton populations in the subtropical Pacific. *J. Oceanogr.* 79, 1–12. doi: 10.1007/s10872-022-00658-1

Scanlan, D. J. (2012). "Marine picocyanobacteria," in *Ecology of cyanobacteria II: Their diversity in space and time*. Ed. B. A. Whittom (Berlin, Germany: Springer Science + Business media B.V), 503–533.

Scanlan, D. J., Ostrowski, M., Mazard, S., Dufresne, A., Garczarek, L., Hess, W. R., et al. (2009). Ecological genomics of marine picocyanobacteria. *Microbiol. Mol. Biol. Rev.* 73, 249–299. doi: 10.1128/MMBR.00035-08

Seidel, M., Vemulapalli, S. P. B., Mathieu, D., and Dittmar, T. (2022). Marine dissolved organic matter shares thousands of molecular formulae yet differs structurally across major water masses. *Environ. Sci. Technol.* 56, 3758–3769. doi: 10.1021/acs.est.1c04566

Selden, C. R., Chappell, P. D., Clayton, S., Macías-Tapia, A., Bernhardt, P. W., and Mulholland, M. R. (2021). A coastal N_2 fixation hotspot at the Cape Hatteras front: Elucidating spatial heterogeneity in diazotroph activity via supervised machine learning. *Limnol. Oceanogr.* 66, 1832–1849. doi: 10.1002/lno.11727

Sipler, R. E., and Bronk, D. A. (2015). "Dynamics of dissolved organic nitrogen," in *Biogeochemistry of marine dissolved organic matter*, Eds. D. A. Hansel and C. A. Carlson (Amsterdam, The Netherlands: Elsevier B.V.) 127–232.

Sleighter, R. L., and Hatcher, P. G. (2008). Molecular characterization of dissolved organic matter (DOM) along a river to ocean transect of the lower Chesapeake Bay by ultrahigh resolution electrospray ionization Fourier transform ion cyclotron resonance mass spectrometry. *Mar. Chem.* 110, 140–152. doi: 10.1016/j.marchem.2008.04.008

Stein, L. A. (2015). Microbiology: Cyanate fuels the nitrogen cycle. *Nature* 524, 43–44. doi: 10.1038/nature14639

Sun, L., Qian, J., Blough, N. V., and Mopper, K. (2015). Insights into the photoproduction sites of hydroxyl radicals by dissolved organic matter in natural waters. *Environ. Sci. Technol. Lett.* 2 (12), 352–356. doi: 10.1021/acs.estlett.5b00294

Ustick, L. J., Larkin, A. A., Garcia, C. A., Garcia, N. S., Brock, M. L., Lee, J. A., et al. (2021). Metagenomic analysis reveals global-scale patterns of ocean nutrient limitation. *Science* 372, 287–291. doi: 10.1126/science.abe6301

Waterbury, J. B., Watson, S. W., Valois, F. W., and Franks, D. G. (1986). Biological and ecological characterization of the marine unicellular cyanobacterium *Synechococcus*. *Can. Bull. Fish Aquat. Sci.* 214, 71–120.

Widner, B., Fuchsman, C. A., Chang, B. X., Rocap, G., and Mulholland, M. R. (2018a). Utilization of urea and cyanate in waters overlying and within the eastern tropical north Pacific oxygen deficient zone. *FEMS Microbiol. Ecol.* 94, fiy138. doi: 10.1093/femsec/fiy138

Widner, B., Mordy, C. W., and Mulholland, M. R. (2018b). Cyanate distribution and uptake above and within the Eastern Tropical South Pacific oxygen deficient zone. *Limnol. Oceanogr.* 63, 177–192. doi: 10.1002/lno.10730

Widner, B., and Mulholland, M. R. (2017). Cyanate distribution and uptake in North Atlantic coastal waters. *Limnol. Ooceanogr.* 62, 2538–2594. doi: 10.1002/lno.10588

Widner, B., Mulholland, M. R., and Mopper, K. (2016). Distribution, sources, and sinks of cyanate in the coastal North Atlantic Ocean. *Environ. Sci. Technol. Lett.* 3, 297–302. doi: 10.1021/acs.estlett.6b00165

Widner, B. (2016). *The marine cyanate cycle [doctoral dissertation]* (Norfolk (VA): Old Dominion University).

Widner, B., Mulholland, M. R., and Mopper, K. (2013). Chromatograhic determination of nanomolar cyanate concentrations in Estuaine and Sea Waters by precolumn fluorescence derivatization. *Anal. Chem.* 85, 6661–6666. doi: 10.1021/ac400351c

Xie, Z., He, Y., Wang, M., Zhang, S., Kong, L., Lin, L., et al. (2020). Dissecting microbial community structure and metabolic activities at an oceanic deep chlorophyll maximum layer by size-fractionated metaproteomics. *Prog. Oceanogr.* 188, 102439. doi: 10.1016/j.pocean.2020.102439

Yamashita, Y., Scinto, L. J., Maie, N., and Jaffé, R. (2010). Dissolved organic matter characteristics across a subtropical wetland's landscape: application of optical properties in the assessment of environmental dynamics. *Ecosystems* 13, 1006–1019. doi: 10.1007/s10021-010-9370-1

Zhao, Z., Gonsior, M., Luek, J., Timko, S., Ianiri, H., Hertkorn, N., et al. (2017). Picocyanobacteria and deep-ocean fluorescent dissolved organic matter share similar optical properties. *Nat. Commun.* 8, 15284. doi: 10.1038/ncomms15284

Zhu, Y., Mulholland, M. R., Macías, T. A., Echevarría, M. A., Pérez, V. E., and Bernhardt, P. (2023). Cyanate dynamics under algal blooms and sediment resuspension events in a shallow micro-tidal estuary in the lower Chesapeake Bay. *Estuar. Coast. Shelf S.* 281, 108188. doi: 10.1016/j.ecss.2022.108188

Zubkov, M. V., Fuchs, B. M., Tatran, G. A., Burkill, P. H., and Amann, R. (2003). High rate of uptake of organic nitrogen compounds by Prochlorococcus cyanobacteria as a key to their dominance in oligotrophic oceanic waters. *Appl. Environ. Microb.* 69, 1299–1304. doi: 10.1128/AEM.69.2.1299-1304.2003

frontiers | Frontiers in Marine Science

TYPE Original Research
PUBLISHED 17 May 2024
DOI 10.3389/fmars.2024.1408958

Check for updates

OPEN ACCESS

EDITED BY
Junfu Dong,
Shandong University, China

REVIEWED BY
Muhamad Syaifudin,
Hokkaido University, Japan
Zhu Liu,
Hainan University, China

*CORRESPONDENCE
Hong Du
hdu@stu.edu.cn

RECEIVED 29 March 2024
ACCEPTED 30 April 2024
PUBLISHED 17 May 2024

CITATION
Pei P, Aslam M, Yang C, Ye P, Ke X, Liang Z, Li T, Chen W and Du H (2024) Temporal variations of biological nitrogen fixation and diazotrophic communities associated with artificial seaweed farms.
Front. Mar. Sci. 11:1408958.
doi: 10.3389/fmars.2024.1408958

COPYRIGHT
© 2024 Pei, Aslam, Yang, Ye, Ke, Liang, Li, Chen and Du. This is an open-access article distributed under the terms of the Creative Commons Attribution License (CC BY). The use, distribution or reproduction in other forums is permitted, provided the original author(s) and the copyright owner(s) are credited and that the original publication in this journal is cited, in accordance with accepted academic practice. No use, distribution or reproduction is permitted which does not comply with these terms.

Temporal variations of biological nitrogen fixation and diazotrophic communities associated with artificial seaweed farms

Pengbing Pei[1], Muhammad Aslam[1,2], Chunyou Yang[1], Peilin Ye[1], Xiao Ke[1], Zhanhua Liang[1], Tangcheng Li[3], Weizhou Chen[1] and Hong Du[1,4]*

[1]Guangdong Provincial Key Laboratory of Marine Biotechnology, College of Science, Shantou University, Shantou, China, [2]Faculty of Marine Sciences, Lasbela University of Agriculture, Water and Marine Sciences (LUAWMS), Lasbela, Pakistan, [3]Guangdong Provincial Key Laboratory of Marine Disaster Prediction and Prevention, College of Science, Shantou University, Shantou, China, [4]Shantou University-Università Politecnica delle Marche (STU-UNIVPM) Joint Algal Research Center, College of Science, Shantou University, Shantou, China

Diazotrophic communities contribute inorganic nitrogen for the primary productivity of the marine environment by biological nitrogen fixation (BNF). They play a vital role in the biogeochemical cycle of nitrogen in the marine ecological environment. However, there is still an incomplete understanding of BNF and diazotrophs in artificial seaweed farms. Therefore, this study comprehensively investigated the temporal variations of BNF associated with *Gracilariopsis lemaneiformis*, as well as the diazotrophic communities associated with macroalgae and its surrounding seawater. Our results revealed that a total of 13 strains belonging to Proteobacteria and Bacteroidetes were identified as N_2-fixing bacteria using azotobacter selective solid medium and *nifH* gene cloning. Subsequently, BNF and diazotrophic communities were characterized using the acetylene reduction method and high-throughput sequencing of the *nifH* gene, respectively. The results showed that nitrogenase activity and *nifH* gene abundance of epiphytic bacteria on *G. lemaneiformis* varied significantly among four different cultivation periods, i.e., Cultivation Jan. (CJ), Cultivation Feb. (CF), Cultivation Mar. (CM), Cultivation Apr. (CA). Among them, the nitrogenase activity and *nifH* gene abundance of epiphytic bacteria on *G. lemaneiformis* in CM were significantly higher than those in CJ, CF, and CA, indicating that the BNF of eiphytic bacteria on *G. lemaneiformis* was markedly enhanced. Combined with the data on environmental factors, it was found that the low concentration of nitrogen and phosphorus in CM might considerably boost the BNF of epiphytic bacteria in *G. lemaneiformis*. The sequencing results of the *nifH* gene showed that the α-diversity of diazotrophic communities associated with *G. lemaneiformis* and seawater in CM was higher than that in other cultivation periods. In addition, the diazotrophic communities on *G. lemaneiformis* were significantly different in CJ, CF, CM, and CA, and they were significantly diverse from diazotrophic communities in seawater. LEfSe analysis indicated that Rhodobacterales, Hyphomonadaceae, *Robiginitomaculum*, and *Robiginitomaculum antarcticum* within α-proteobacteria played a remarkable role in BNF in response to nitrogen

nutrient deficiency. Taken together, these results provide a unique insight into the interaction between macroalgae and its epiphytic bacteria and lay a foundation for further research on the mechanism of action of nitrogen-cycling microorganisms associated with macroalgae.

KEYWORDS

nifH* gene, biological nitrogen fixation (BNF), diazotrophic communities, cultivation periods, *Gracilariopsis lemaneiformis

1 Introduction

Seaweed farms are important ecosystems along subtropical coastlines, playing a vital role in improving the quality of coastal waters and maintaining the ecological balance of subtropical regions (Kim et al., 2017; Zhang et al., 2017a). The carbon fixed by cultivated seaweed may either be buried in sediments or exported to the deep sea, thus establishing seaweed farms ecosystem as a major contributor of marine carbon sink (Duarte et al., 2017; Zhang et al., 2017b; Hasselström et al., 2018). To a certain extent, seaweed cultivation can mitigate wave energy, protect shorelines, enhance pH, and supply oxygen to the waters. This contribution aids in climate change adaptation by locally reducing the effects of ocean acidification and de-oxygenation (Duarte et al., 2017). In subtropical marine environments, seaweeds are considered crucial primary producers of organic matter (Neori, 2008). However, despite the richness of organic matter in seaweed farm ecosystems, they tend to become oligotrophic environments due to the significant consumption of inorganic nitrogen nutrients in the water caused by large-scale seaweed cultivation (Yang et al., 2015).

Microorganisms are a crucial component of seaweed farm ecosystems, and there is mounting evidence highlighting their importance in biogeochemical cycling and the overall health of these ecosystems (Azam and Malfatti, 2007; Rousk and Bengtson, 2014; Egan and Gardiner, 2016). These microorganisms primarily include epiphytic microbes in seaweed and seawater, which significantly regulate the circulation of marine nutrient elements (Dang and Lovell, 2016). Functional microbes have garnered substantial attention among these microorganisms due to their pivotal roles. Nitrogen-fixing microorganisms, also known as diazotrophs, are important functional microorganisms in marine environments (Cardini et al., 2017). Although diazotrophs may differ significantly in taxonomy, they harbor similar functional genes that enable them to perform the same ecological functions. BNF performed by diazotrophs, involves the reduction of atmospheric N_2 to bioavailable ammonium (Caffin et al., 2018). This process constitutes a significant source of bioavailable nitrogen in numerous marine and freshwater environments (Bonnet et al., 2016; Geisler et al., 2019). In addition, BNF by marine diazotrophs compensates for the loss of nitrogen through sinking and denitrification, thereby sustaining the primary productivity of marine ecosystems (Yang et al., 2019). Diazotrophic communities are affected by many key factors, such as energy to sustain nitrogenase activity, availability of vitamins and micronutrients, oxidized environments, and concentrations of dissolved inorganic nitrogen (Geisler et al., 2019). For instance, adequate inorganic nitrogen to meet the nitrogen requirements of diazaotrophs means that consequential rates of marine BNF process do not occur (Knapp, 2012).

Many coral reefs still hold relatively high biological productivity despite low dissolved inorganic nitrogen (DIN) concentrations in marine environments (Messer et al., 2017). This seemingly paradoxical phenomenon can be attributed to the crucial role played by associated BNF in providing bioavailable nitrogen to coral reef habitats (Zhang et al., 2016; Lesser et al., 2018). Additionally, diazotrophs have been identified as a significant component of coral symbionts (Olson and Lesser, 2013; Zhang et al., 2016). In our previous observations, we find that the growth status of *G. lemaneiformis* maintains normal in the marine environment with low concentration of inorganic nitrogen (data not shown). This discrepancy between the availability of inorganic nutrients and the growth of *G. lemaneiformis* can be understood to mean that there are new bioavailable nitrogen sources besides the inorganic nutrients to sustain the growth of macroalgae. New nitrogen sources may be derived from the BNF drove by associated diazotrophs in many marine and freshwater environments (Sohm et al., 2011; Geisler et al., 2019). Although this inconsistent phenomenon has been demonstrated in coral reef habitats, the role of associated diazotrophs and BNF in the cultivation environment of *G. lemaneiformis* farms remains unclear.

Diazotrophic communities form specific species associations with their hosts (Lema et al., 2012), and differences in diazotrophic communities are observed under different environmental conditions (Lema et al., 2014). The significant effects of environmental conditions on diazotrophs' diversity and community structure may alter their ability to perform BNF (Feng et al., 2018). It is worth noting that the environmental conditions for the growth of *G. lemaneiformis* may vary during the entire cultivation period. Therefore, it is imperative to study the nitrogenase activity, *nifH* gene abundance of epiphytic bacteria on *G. lemaneiformis*, and the variations of diazotrophic community associated with *G. lemaneiformis* and seawater.

In recent years, high-throughput sequencing has provided a more comprehensive view of microbial communities in different environments and has been employed to investigate the diversity and composition of bacterial communities associated with seaweed farms (Xie et al., 2017; Liang et al., 2019; Selvarajan et al., 2019; Wang et al., 2020, 2021; Pei et al., 2021). The functional *nifH* gene encodes a conserved subunit of nitrogenase ferritin and is present in all known diazotrophs (Zehr et al., 2003). The *nifH* gene is consistent with 16S rRNA gene phylogeny and serves as an ideal molecular target (Gaby and Buckley, 2012). It is widely used to study the diversity and community composition of diazotrophs (Yang et al., 2019). However, the *nifH* gene has seldom been studied in high-throughput sequencing of diazotrophic communities associated with *G. lemaneiformis* and seawater, and comprehensive knowledge about the role of environmental variables in shaping the diazotrophic communities of *G. lemaneiformis* and seawater is limited. Thus, it is necessary to investigate the nitrogenase activity, *nifH* gene abundance of epiphytic bacteria on *G. lemaneiformis*, and the diversity and composition of diazotrophic communities associated with *G. lemaneiformis* and seawater to enhance our understanding of seaweed farms ecosystem functioning.

In this study, we aim to achieve the following objectives: (i) isolate and identify culturable N_2-fixing bacteria by plate streaking and PCR identification; (ii) measure nitrogenase activity and *nifH* gene abundance in epiphytic bacteria on *G. lemaneiformis* using acetylene reduction and qPCR; and (iii) explore the diversity and composition of diazotrophic communities associated with *G. lemaneiformis* and seawater through high-throughput sequencing of the *nifH* gene. This study provides a scientific foundation for further understanding of the BNF function of diazotrophs associated with the macroalgae *G. lemaneiformis*.

2 Materials and methods

2.1 Collection location and sampling

Samples of *G. lemaneiformis* and seawater were collected seasonally (Cultivation in January, CJ; Cultivation in February, CF; Cultivation in March, CM; Cultivation in April, CA) from artificial seaweed farms located in Zoumapu Village, Nan'ao Island of Guangdong Province (117°2′39″E, 23°28′32″N). At each month, three replicate *G. lemaneiformis* were collected for composition of diazotrophic communities and BNF analyses, respectively. In addition, three replicate seawater at each month were collected for composition of diazotrophic communities analyses. Three replicate surface (0.5 m depth) seawater were collected at each month (0.5 L) for physicochemical analyses. Full details of the sampling information can be found in Supplementary Tables S1 and S2. The cultivation of *G. lemaneiformis* has been shown to affect various dissolved and particulate forms of nitrogen and phosphorus in seaweed farms (Huang et al., 2017; Zhang et al., 2018). Therefore, differences in nutrient loads during various cultivation periods may influence the diversity of diazotrophic communities associated with seaweed and seawater. The latitude and longitude were measured by GPS (Garmin GPS72H) from the sampling site. The algal samples were stored in sterile polyethylene bags with surrounding seawater, while the seawater samples were stored in sterile polyethylene bottles. Algal and seawater samples were stored at 4°C and transported to the laboratory within two hours.

2.2 Isolation and identification of culturable N_2-fixing bacteria

2.2.1 Isolation of N_2-fixing bacteria

In the laboratory, *G. lemaneiformis* samples were washed three times with autoclaved seawater to eliminate loosely attached epiphytes, sand particles and other attached settlements (Stabili et al., 2017; Karthick and Mohanraju, 2018). After rinsing, sterile cotton buds were used to swab repeatedly firmly attached epiphytic bacteria from algae. They were spread on azotobacter selective solid medium (ASSM), or algae was spread directly on the ASSM. The ASSM consists of 0.1 g K_2HPO_4, 0.005 g $Na_2MoO_4{\cdot}2H_2O$, 0.05 g $CaSO_4{\cdot}2H_2O$, 0.2 g $MgSO_4{\cdot}7H_2O$, 0.03 g $FeCl_3{\cdot}6H_2O$, 5.0 g sucrose, 0.5 g yeast extract, 15.0 g agar, and 1.0 L filtered seawater (Head and Carpenter, 1975). Additionally, 0.1 mL seawater sample was dropped onto the ASSM, and the bacteria solution was evenly spread using a sterile spreader. The plates were then incubated at 25°C for 4 days. Morphological i.e. (size, shape, color etc) different bacterial colonies were picked with inoculating loop to make streak on plates for getting purified colonies. This step was repeated twice in order to obtain pure individual colonies (22 colonies from *G. lemaneiformis*, 6 colonies from seawater), which were then preserved at -80°C in marine broth supplemented with 25% sterile glycerol.

2.2.2 DNA extraction and 16S rRNA gene sequencing

The DNA of pure bacterial colonies was extracted following the procedures described in the DNA extraction kit (TIANGEN Biotech, Beijing). The 16S rRNA gene was amplified using the universal primers 27F (5'-AGAGTTTGATCMTGGCTCAG-3') and 1492R (5'-TACGGYTACCTTGTTACGACTT-3') (Pei et al., 2024). PCR was carried out in 30 μL reaction mixture containing 1.0 μL genomic DNA, 15.0 μL Super Mix (Sigma), 1.0 μL of each primer, and 12.0 μL H_2O under thermal cycle of 96°C for 5 min, 35 cycles of 20 s at 96°C, 30 s at 62°C and 10 min at 72°C, followed by 72°C for 10 min in a Bio-rad T100™ Thermal Cycler (Bio-Rad, USA). The quality of PCR products was verified by 1% agarose electrophoresis gel. The 3730XL DNA Analyzer (ABI, USA) was used for sequencing of pure isolates. The sequencing primers used for the 16S rRNA gene were V4-515F (5'-GTGCCAGCAGCCGCGGTAA-3') and V4-806R (5'-GGACTACCAGGGTATCTAA-3'). The genetic relationship between different samples and known bacterial species were determined according to blast results. The most closely related bacterial species was selected as the species identification information of the sample. Different strains with identical description of matched species and accession number were considered to be the same species. The sequence data reported in this study has been deposited in the NCBI GenBank database under

the accession number SUB11205054. All data are available at: https://submit.ncbi.nlm.nih.gov/subs/?search=SUB11205054.

2.2.3 Identification of N_2-fixing bacteria and phylogenetic diversity analysis

The *nifH* gene of potential N_2-fixing bacteria was amplified using the universal primers PolF (5'-TGCGAYCCSAARGCBGACTC-3') and PolR (5'-ATSGCCATCATYTCRCCGGA-3') (Poly et al., 2001). PCR was carried out in 20 μL reaction mixture containing 2.0 μL genomic DNA, 1.0 μL of each primer, 10.0 μL 2×Master Mix, and 6.0 μL H_2O under thermal cycle of 98°C for 30 s, 35 cycles of 10 s at 98°C, 30 s at 68°C and 30 s at 72°C, followed by 72°C for 2 min in a Bio-rad T100^{TM} Thermal Cycler (Bio-Rad, USA). PCR products were verified by running them on a 2% agarose electrophoresis gel and subsequently subjected to sequencing by using a 3730XL DNA Analyzer (ABI, USA). The primers used for sequencing of the *nifH* gene were the same as those used for amplification of the *nifH* gene.

The *nifH* gene sequence was translated to protein sequence (https://web.expasy.org/translate/). The *nifH* gene sequences of various N_2-fixing bacteria were blasted to check their sequence homology against other sequences from NCBI GenBank (https://blast.ncbi.nlm.nih.gov/Blast.cgi). The protein sequences of *nifH* gene of 23 known N_2-fixing bacteria with the highest homology were selected. The aligned protein sequences were used to construct the phylogenetic trees with the neighbor joining method using the MEGA 11.0.13 software. The sequences were compiled and aligned using ClustalW embedded in MEGA 11.0.13. For reliability, the bootstrap test was performed with 1000 replications in the phylogenetic trees (Aslam et al., 2023).

2.3 Determination of nitrogenase activity of epiphytic bacteria on *G. lemaneiformis*

We employed the standard method, the reduction of C_2H_2 to C_2H_4 (Cardini et al., 2017), to assess the nitrogenase activity of epiphytic bacteria on *G. lemaneiformis* during a full dark-light cycle (D: L=12 h: 12 h) incubation. Nitrogenase catalyzes not only the reduction of N_2 to NH_3, but also the reduction of C_2H_2 to C_2H_4. C_2H_2 and N_2 have similar affinity for nitrogenase, and their reduction processes are parallel related. Since C_2H_2 and C_2H_4 but not N_2 and NH_3 can be separated using gas chromatography, the reduction of C_2H_2 to C_2H_4 can be used to indirectly estimate N_2 fixation by organisms. The reaction formulas of $N_2 + 6H^+ + 6e^- \rightarrow 2NH_3$ and $3C_2H_2 + 6H^+ + 6e^- \rightarrow 3C_2H_4$ show that the reduction of 3 grams C_2H_2 is equivalent to the reduction of 1 gram N_2, so the amount of N_2 fixation can be calculated. First, 1.0 g (fresh weight, FW) of the *G. lemaneiformis* sample was accurately weighed and placed in a 20 mL headspace vial. Then, 7 mL artificial seawater filtered by 0.22 μm filter was injected into the vial. The artificial seawater composition included 26.518 g NaCl, 2.447 g $MgCl_2$, 3.305 g $MgSO_4$, 1.141 g $CaCl_2$, 0.725 g KCl, 0.202 g $NaHCO_3$, 0.083 g NaBr, 1.0 L dH_2O, pH=7.0-7.2. Following the addition of 1.5 mL C_2H_2 and sealing the vial with pliers, the vials were incubated in a constant temperature illumination incubator for 48 h (temperature: 20 ± 0.5°C, light intensity: 100 ± 5 $\mu mol \cdot m^{-2} \cdot s^{-1}$, light cycle: L: D=12 h: 12h). The content of ethylene (C_2H_4) in gas sample was detected by gas chromatograph (Agilent 7890B GC-FID, Agilent USA). Nitrogenase activity was expressed as nmol C_2H_4 produced per sample per hour.

$$[C_2H_4 nmol/(g \cdot h)] = \frac{Volume(C_2H_4, \mu l) * Concentration(\mu mol/mL)}{Sample(g) * Time(h) * 22.4}$$

2.4 Quantification of the *nifH* gene copy number

The total DNA from *G. lemaneiformis* and its epiphytic bacteria was extracted using the procedures described by Pei et al. (2021). The primers PolF and PolR were used to quantify the number of *nifH* gene copies. Appropriate *nifH* gene sequences were obtained from the NCBI database and synthesized by BGI. Bacteria containing the *nifH* gene were inoculated in the liquid medium with ampicillin resistance, and the *nifH* gene plasmid was extracted using TIANprep Mini Plasmid Kit (DP103-03, TIANGEN). Standard curves of *nifH* gene copy numbers were established by serially diluting plasmids containing the *nifH* gene, resulting in final concentrations ranging from 10^2 to 10^8 copies/μL. The qPCR was carried out in 20 μL reaction mixture containing 2.0 μL plasmid DNA, 0.6 μL of each primer, 10.0 μL 2×Talent qPCR Premix, and 6.8 μL RNase-free ddH_2O under thermal cycle of 95°C for 3 min, 40 cycles of 5 s at 95°C, 15 s at 60°C and 15 s at 60°C in a Real-time Fluorescence Quantitative PCR System (qTOWER^{3}G, Jena). The specificity of amplification products was verified by melting-curve analysis, and the amplified fragments were verified by electrophoresis on a 2% agarose gel to confirm the expected sizes of the amplicon. The qPCR efficiency (E) was 86.17%, and the R^2 of standards was 0.9996. The total DNA from *G. lemaneiformis* and its epiphytic bacteria was substituted for plasmid DNA for the qPCR experiment. All samples and standard reactions were performed in triplicate, and average values were calculated. The number of *nifH* copies was ultimately expressed as per gram of algal fresh weight.

2.5 Determination of physicochemical factors

The seawater temperature (Temp.), salinity (Sal.), pH, and dissolved oxygen (DO), were measured using an *In-Situ* SMARTPOLL MP (U.S.A). Briefly, seawater samples were filtered with a 0.45 μm mixed cellulose ester microporous filter membrane (MF-Millipore HAWP04700, USA) within 2 hours. The filtered seawater samples were added with chloroform (2‰, v/v=chloroform: seawater) and stored at low temperatures for subsequent detection. Ammonia (NH_4-N), nitrate (NO_3-N), nitrite (NO_2-N), total nitrogen (TN), reactive phosphorus (PO_4-P), and total phosphorus (TP) levels in the seawater samples were analyzed according to standard methods described by AQSIQ (2007). The content of chlorophyll *a* (Chl-*a*) was determined by acetone extraction and spectrophotometry as described in the national standard method (GB17378.7-2007).

2.6 Amplicon sequencing of the *nifH* gene

2.6.1 DNA extraction

Total DNA from *G. lemaneiformis* and its epiphytic bacteria was extracted using a DNA extraction kit (JL-50, Guangzhou Jianlun Biological Technology Co., LTD.). Total DNA from seawater was extracted using CTAB method (Pei et al., 2021). The concentration and purity were measured using the NanoDrop One (Thermo Fisher Scientific, MA, USA).

2.6.2 DNA sample amplification, PCR product purification, library construction and sequencing

The diazotrophic communities were characterized by the *nifH* gene, which was amplified using the universal primers containing 12 bp barcode PolF and PolR (Poly et al., 2001). The PCR was carried out in 50 μL reaction mixture, containing 25.0 μL 2×Premix Taq (Takara Biotechnology, Dalian Co. Ltd., China), 1.0 μL each primer, 3.0 μL DNA template, and 20 μL RNase-free ddH_2O under thermal cycle of 94°C for 5 min, 30 cycles of 30 s at 94°C, 30 s at 52° C and 30 s at 72°C, followed by 72°C for 10 min in a BioRad S1000 Thermal Cycler (Bio-Rad Laboratory, CA, USA). The length and concentration of the PCR products were detected by 1% agarose gel electrophoresis. PCR products were mixed in equidensity ratios according to the GeneTools Analysis Software (Version4.03.05.0, SynGene). The mixture of PCR products was purified with E.Z.N.A. Gel Extraction Kit (Omega, USA). Sequencing libraries were generated using NEBNext® Ultra™ II DNA Library Prep Kit for Illumina® (New England Biolabs, MA, USA). The library quality was assessed on the Qubit@ 2.0 Fluorometer (Thermo Fisher Scientific, MA, USA). At last, the library was sequenced on an Illumina Nova6000 platform and 250 bp paired-end reads were generated (Guangdong Magigene Biotechnology Co. Ltd., Guangzhou, China). The sequence data reported in this study have been deposited in the NCBI GenBank database under the accession number SRP368355. All data are available at: https://www.ncbi.nlm.nih.gov/sra/?term=PRJNA824550.

2.7 Data analysis

2.7.1 Sequencing data processing

The primers were removed by using cutadapt software (https://github.com.marcelm/cutadapt/) according to the primer information at the beginning and end of sequence to obtain the paired-end clean reads. Paired-end clean reads were merged using usearch -fastq_mergepairs (V10, http://www.drive5.com/usearch/) according to the relationship of the overlap between the paired-end reads. Fastp (version 0.14.1, https://github.com/OpenGene/fastp) was used to control the quality of the raw data by sliding window (-W 4 -M 20) to obtain the paired-end clean tags.

2.7.2 OTU cluster and species annotation

OTUs were clustered based on the UPARSE method by removing the chimera sequence, singleton OTU, and the OTU annotated as chloroplasts or mitochondria (16S amplicons). For each representative sequence, the silva (https://www.arb-silva.de/) database was used to annotate taxonomic information by usearch -sintax (set the confidence threshold to default to ≥ 0.8). The taxonomy of the species annotation was divided into seven levels: kingdom, phylum, class, order, family, genus, and species. R software was used to analyze the common and endemic species, community composition, and richness of species. In order to study phylogenetic relationship of different OTUs, the KRONA software (http://sourceforge.net/projects/krona/) was used to visualize the results of individual sample annotations.

2.7.3 Alpha diversity

The Richness and Shannon indices were calculated using usearch-alpha_div (V10, http://www.drive5.com/usearch/) and plotted using OriginPro 9.0 software. The differences in the alpha diversity index between groups (GL and SW) were analyzed using R software.

2.7.4 Comparison analysis between samples

Linear Discriminant Analysis Effect Size (LEfSe) was used to find the biomarker of each group based on homogeneous OTU_table. Initially, a non-parametric factorial Kruskal Wallis (kw) sum-rank test was used to detect species with significant difference in abundance among different groups. Secondly, Wilcoxon rank sum test was used to judge the difference between the two groups. Finally, a linear discriminant analysis (LDA) was used to evaluate the impact of significant species (LDA score) by setting LDA score ≥ 2 and obtained the biomarkers in different groups.

2.8 Statistical analysis

The nitrogenase activity and *nifH* gene abundance of epiphytic bacteria on *G. lemaneiformis*, the physicochemical factors of seawater, and the alpha diversity of diazotrophic communities associated with *G. lemaneiformis* and seawater were analyzed using one-way ANOVA (Pei et al., 2021). The analysis of significant difference of data was carried out using SPSS 19.0 software, with the significant threshold set to 0.05. The differences among the diazotrophic communities associated with *G. lemaneiformis* and seawater in different cultivation periods were performed by the Permutational Multivariate Analysis of Variance (PERMANOVA) with Adonis function from the vegan package in R software (Xie et al., 2017).

3 Results

3.1 Diversity of culturable N_2-fixing bacteria

A total of 28 single colonies were screened from *G. lemaneiformis* and seawater, out of which 16 bacterial species were identified based on 16S rRNA gene. As shown in Table 1, at

10.3389/fmars.2024.1408958

TABLE 1 16S rRNA gene sequence identity of twenty-eight bacterial isolates obtained from *G. lemaneiformis* and seawater.

Sample source	Isolate	Description of matched species	Accession number	Percentage identification/%	Phylum
G. lemaneiformis (22 isolates)	Gl4-1	*Cobetia* sp. *5-11-6-3*	LC549335.1	100.00	Proteobacteria
	Gl6	*Cobetia* sp. *5-11-6-3*	LC549335.1	100.00	Proteobacteria
	Gl4-2	*Cobetia amphilecti*	MK967021.1	100.00	Proteobacteria
	Gl-co-b	*Labrenzia aggregata*	MK493546.1	100.00	Proteobacteria
	Gl-co-l1	*Phaeobacter* sp.	MK801658.1	100.00	Proteobacteria
	Gl-co-l5	*Phaeobacter* sp.	MK801658.1	100.00	Proteobacteria
	GN1	*Alteromonas australica*	MY234253.1	99.53	Proteobacteria
	GN7	*Dokdonia* sp. *NBRC 100807*	AB681248.1	100.00	Bacteroidetes
	GN15	*Dokdonia* sp. *NBRC 100807*	AB681248.1	100.00	Bacteroidetes
	GN24	*Dokdonia* sp. *NBRC 100807*	AB681248.1	100.00	Bacteroidetes
	GN10	*Loktanella ponticola*	NR_134070.1	99.44	Proteobacteria
	GN17	*Loktanella ponticola*	NR_134070.1	99.40	Proteobacteria
	GN21	*Loktanella ponticola*	NR_134070.1	99.44	Proteobacteria
	GN13	*Ruegeria* sp.	MT484146.1	100.00	Proteobacteria
	GN14	*Cellulophaga lytica*	MG456766.1	100.00	Bacteroidetes
	GN16	*Dokdonia genika*	AB681247.1	100.00	Bacteroidetes
	GN22	*Ruegeria atlantica*	HQ908706.1	100.00	Proteobacteria
	GPN8	*Dokdonia* sp. *NBRC 100805*	AB681246.1	99.66	Bacteroidetes
	GPN10	*Loktanella ponticola*	NR_134070.1	99.46	Proteobacteria
	GPN12	*Loktanella ponticola*	NR_134070.1	99.34	Proteobacteria
	GPN13	*Loktanella ponticola*	NR_134070.1	99.32	Proteobacteria
	GPN15	*Loktanella ponticola*	NR_134070.1	99.31	Proteobacteria
Seawater (6 isolates)	SW6	*Vibrio alginolyticus*	AP022865.1	100.00	Proteobacteria
	SN6	*Vibrio harveyi*	MN847615.1	99.41	Proteobacteria
	SN7	*Vibrio cyclitrophicus*	MN945296.1	98.96	Proteobacteria
	SN8	*Vibrio* sp.	MG099501.1	100.00	Proteobacteria
	SN9	*Vibrio* sp.	MG099501.1	99.92	Proteobacteria
	SN12	*Vibrio* sp.	MG099501.1	100.00	Proteobacteria

The strains named beginning with "G" and "S" were isolated from *G. lemaneiformis* and seawater, respectively. Isolate labeled with same color belongs to the same species.

the phylum level, these isolates were classified into Proteobacteria (75%) and Bacteroidetes (25%).

The target gene *nifH* was analyzed to identify N_2-fixing bacteria in various environment. The *nifH* gene target band of 23 strains was amplified by PCR and was about 360 bp in size (Supplementary Figure S1), consistent with the expected result. These strains with targeted bands were preliminarily believed to contain the *nifH* gene. To further verify the presence of *nifH* gene in these strains, 20 μL PCR product was sequenced using the PolF forward primer. Sequencing results showed that 23 strains were successfully sequenced.

Combined with the results of 16S species identification, 13 N_2-fixing bacteria were formally obtained from *G. lemaneiformis* and its seawater and classified into *Cobetia* (2 species, Gl4-1, Gl6, Gl4-2), *Labrenzia* (1 species, Gl-co-b), *Phaeobacter* (1 species, Gl-co-l1, Gl-co-l5), *Loktanella* (1 species, GN10, GN17, GN21, GPN10, GPN12, GPN13, GPN15), *Dokdonia* (3 species, GN16, GN24, GPN8), *Ruegeria* (1 species, GN22), *Vibrio* (4 species, SW6, SN6, SN7, SN8, SN9, SN12) at the genus level. The nitrogenase gene (*nifH*) sequence details of all N_2-fixing bacteria are shown in Supplementary Table S3. The amino acid sequence details of the *nifH* gene of 13 N_2-fixing bacteria are shown in Supplementary Table S4.

The phylogenetic tree constructed for the N_2-fixing bacteria represents their closest relatives as obtained from the GeneBank (Figure 1). The *nifH* gene sequences of most N_2-fixing bacteria were

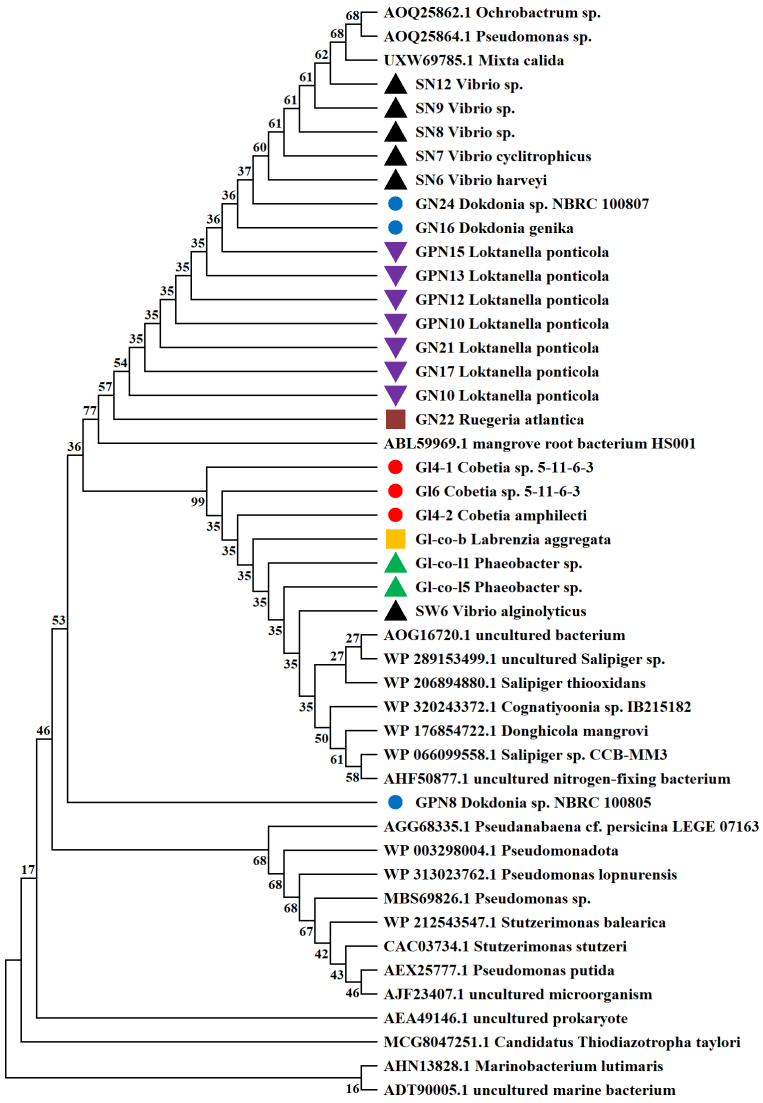

FIGURE 1
Phylogenetic tree of 13 various N_2-fixing bacteria created with MEGA 11.0.13 using the Neighbor-Joining method. Strains harboring the same color belong to the same genus.

closely related to those of mangrove root bacterium HS001 species, but were estranged from GPN8.

3.2 Main physicochemical factors of seawater

The physicochemical factors of seawater from different cultivation periods of study areas including Temp., pH, Sal., DO, NH_4-N, NO_3-N, NO_2-N, dissolved inorganic nitrogen (DIN), PO_4-P, Chl-*a*, TN, and TP levels are shown in Figure 2. The Temp. and pH of CJ were significantly ($p < 0.05$) lower than those of CF, CM, and CA (Figure 2A), whereas the Sal. and DO of CJ were significantly ($p < 0.05$) higher than those of CF, CM, and CA (Figure 2B). The concentrations of NH_4-N, NO_3-N, NO_2-N, DIN, PO_4-P, and TP in CJ were significantly ($p < 0.05$) higher than those in CF, CM, and CA (Figures 2C–F). There were no significant differences ($p > 0.05$) in TN between different cultivation periods (Figure 2F).

3.3 BNF associated with *G. lemaneiformis*

Considerable variations in nitrogenase activity and *nifH* gene abundance of epiphytic bacteria on *G. lemaneiformis* were observed during different cultivation periods, as shown in Figure 3. The nitrogenase activity of epiphytic bacteria in CM was the highest, reaching 1.96 ± 0.20 nmol C_2H_4 g^{-1} frond h^{-1}, which was significantly ($p < 0.05$) higher than that in CJ, CF, and CA (Figure 3A). Similarly, the *nifH* gene abundance of epiphytic bacteria in CM was the highest, reaching 2.22×10^5 copies·(g·frond)$^{-1}$, which was significantly ($p < 0.05$) higher than

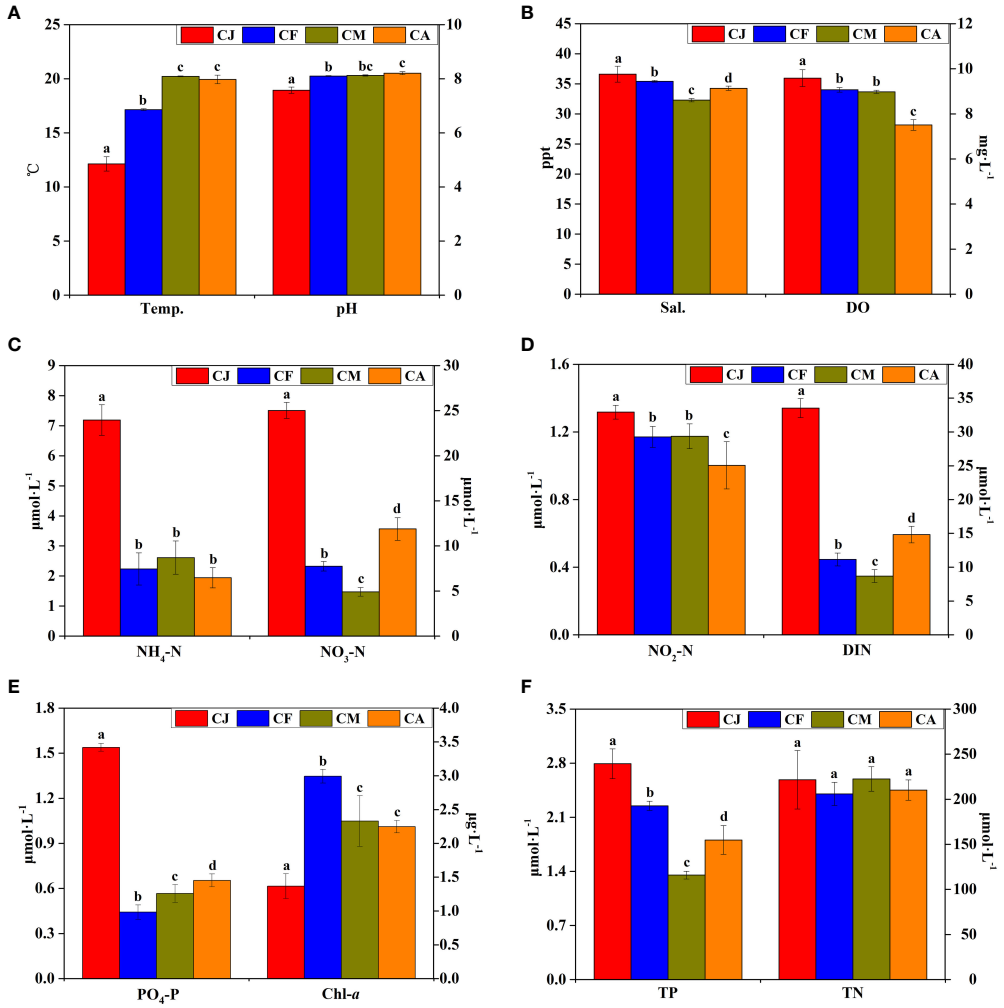

FIGURE 2
Main physicochemical factors of seawater during different cultivation periods. CJ, Cultivation Jan.; CF, Cultivation Feb.; CM, Cultivation Mar.; CA, Cultivation Apr.; Temp., temperature; Sal., salinity; DO, dissolved oxygen; NH_4-N, ammonia; NO_3-N, nitrate; NO_2-N, nitrite; DIN, dissolved inorganic nitrogen; PO_4-P, reactive phosphorous; Chl-*a*, chlorophyll *a*; TN, total nitrogen; TP, total phosphorous. Different letters (a, b, c, d) denote significant ($p < 0.05$) differences in physicochemical factors of seawater between different cultivation periods. Conventional physicochemical factors **(A, B)**, inorganic nitrogen concentration **(C, D)**, phosphate and chlorophyll **(E)**, total nitrogen and phosphorus concentration **(F)** of seawater.

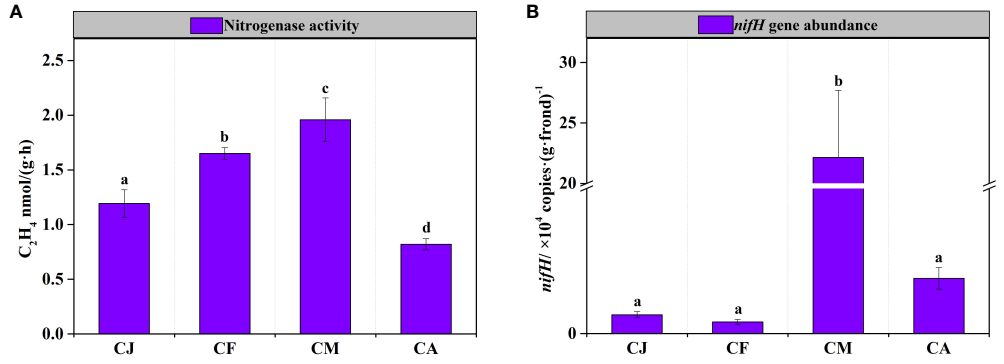

FIGURE 3
BNF of epiphytic bacteria on *G. lemaneiformis* during different cultivation periods. CJ, Cultivation Jan.; CF, Cultivation Feb.; CM, Cultivation Mar.; CA, Cultivation Apr. Different letters (a, b, c, d) denote significant ($p < 0.05$) differences in nitrogenase activity **(A)** and *nifH* gene abundance **(B)** of epiphytic bacteria on *G. lemaneiformis* between different cultivation periods.

that in CJ, CF, and CA (Figure 3B). Seawater physicochemical factors affected nitrogenase activity and *nifH* gene abundance differently. Notably, Temp., pH, and Chl-*a* positively influenced nitrogenase activity, while Sal., NH_4-N, NO_3-N, DIN, PO_4-P, and TP had a negative effect (Table 2). In addition, Sal. and TP had a negative effect on *nifH* gene abundance (Table 2).

3.4 Diversity of diazotrophic communities associated with *G. lemaneiformis* and seawater

Twelve *G. lemaneiformis* samples (i.e., 3 GL.CJ, 3 GL.CF, 3 GL.CM, 3 GL.CA) and twelve seawater samples (i.e., 3 SW.CJ, 3 SW.CF, 3 SW.CM, 3 SW.CA) were analyzed using Novaseq sequencing of *nifH* gene. A total 2,143,939 effective sequences were obtained with an average of 89,331 tags per sample (n=24). Sequences were clustered into operational taxonomic units (OTUs) at the 97% similarity level to generate 10,021 OTUs from the 32 samples. The OTUs were classified into 25 phyla, 46 classes, 82 orders, 128 families, and 150 genera. The Richness of GL.CM was 141.50 ± 2.12 per sample, which was significantly ($p < 0.05$) higher than that of GL.CJ (45.00 ± 12.73), GL.CF (59.00 ± 9.54), and GL.CA (75.00 ± 5.66) (Figure 4). Similarly, the Richness of SW.CM was significantly ($p < 0.05$) higher than that of SW.CJ, SW.CF, and GL.CA (Figure 4). Besides, the Shannon was the highest in GL.CM compared with SW.CJ, SW.CF, and GL.CA (Figure 4). Likewise, SW.CM had the highest Shannon compared with SW.CJ, SW.CF, and GL.CA (Figure 4). Notably, the diversity of diazotrophic communities associated with seawater was much higher than that of *G. lemaneiformis*.

TABLE 2 Linear regression analysis (presented as R^2 values) of the influence of seawater physicochemical factors on nitrogenase activity and *nifH* gene abundance.

Variable	Nitrogenase activity	*nifH* gene abundance
Temp.	**0.478****	0.285^{ns}
pH	**0.450****	0.092^{ns}
Sal.	***0.483*****	***0.568*****
DO	0.000^{ns}	0.004^{ns}
NH_4-N	***0.468*****	*0.075*^{ns}
NO_3-N	***0.816*****	*0.313*^{ns}
NO_2-N	*0.047*^{ns}	0.000^{ns}
DIN	***0.754*****	*0.253*^{ns}
PO_4-P	***0.648*****	*0.112*^{ns}
Chl-*a*	**0.485****	0.014^{ns}
TN	*0.002*^{ns}	0.087^{ns}
TP	***0.529*****	***0.539*****

Temp., temperature; Sal., salinity; DO, dissolved oxygen; NH_4-N, ammonia; NO_3-N, nitrate; NO_2-N, nitrite; DIN, dissolved inorganic nitrogen; PO_4-P, reactive phosphorous; Chl-a, chlorophyll *a*; TN, total nitrogen; TP, total phosphorous. Bold values indicate a significant positive linear relationship and bold italicized values indicate a significant negative linear relationship. **$p < 0.01$, ***$p < 0.001$, ns, not significant.

3.5 Temporal comparison of diazotrophic communities

Based on the analysis of OTUs, an nMDS (non-metric multidimensional scaling) ordination biplot indicated clear clustering of diazotrophic communities (Figure 5A). The stress value was 0.102. The diazotrophic communities of *G. lemaneiformis* samples generally clustered together, while with a strong clustering was observed at seawater samples. Notably, the diazotrophic communities of *G. lemaneiformis* were obviously distinct with that of seawater.

The community composition of diazotrophs associated with *G. lemaneiformis* differed considerably in various cultivation periods (Figure 5B and Supplementary Figure S2). In contrast, the community composition of diazotrophs associated with seawater was similar in diverse cultivation periods (Figure 5C and Supplementary Figure S2). Proteobacteria was the most predominant phylum in GL.CM, with a relative abundance of 51.259%, followed by Crenarchaeota (19.049%) and Cyanobacteria (3.349%). Proteobacteria was also the most predominant phylum in SW.CJ, SW.CF, SW.CM, and SW.CA, but there were no significant differences among them. *G. lemaneiformis* collected from GL.CM exhibited significantly ($p < 0.05$) disparate diazotrophic communities compared to GL.CJ, GL.CF, and GL.CA. For instance, Crenarchaeota was the most predominant phylum in GL.CF, with a relative abundance of 35.959%, was significantly ($p < 0.05$) higher than that in GL.CM. The second dominant phylum was Cyanobacteria, with relative abundances of 9.188% in GL.CJ, 19.597% in GL.CF, and 11.239% in GL.CA, were significantly ($p < 0.05$) higher than that in GL.CM. On the other hand, there is a relative abundance of Proteobacteria and Actinobacteria in GL.CM was significantly ($p < 0.05$) higher than that in GL.CJ, GL.CF, and GL.CA.

3.6 Linear discriminant analysis effect size

LEfSe was used to find biomarkers with marked differences in abundance between two or more groups. In different cultivation periods, there were significant changes in the biomarkers associated with *G. lemaneiformis* and seawater (Figures 6 and 7). In SW.CJ, SW.CF, and SW.CA, the top 3 biomarkers significantly influencing the difference between groups (GL versus SW) were identical (Supplementary Figure S3). Likewise, the top 3 biomarkers significantly influencing the difference between groups (GL versus SW) were similar in GL.CJ, GL.CF, and GL.CA (Supplementary Figure S3). In CM, 31 biomarkers were significantly enriched in diazotrophic communities associated with seawater, among which γ-proteobacteria, δ-proteobacteria and Nitrosomonadales had a more significant influence on the difference between groups (GL.CM vs SW.CM) (Figure 6). However, there were 11 significantly enriched biomarkers in diazotrophic communities associated with *G. lemaneiformis*, and 5 (α-proteobacteria, *Robiginitomaculum antarcticum*, *Robiginitomaculum*, Hyphomonadaceae, and Rhodobacterales) of 11 had greater influence on difference between groups (GL.CM vs SW.CM) (Figure 6). Interestingly, 4 biomarkers that significantly enriched in diazotrophic communities associated

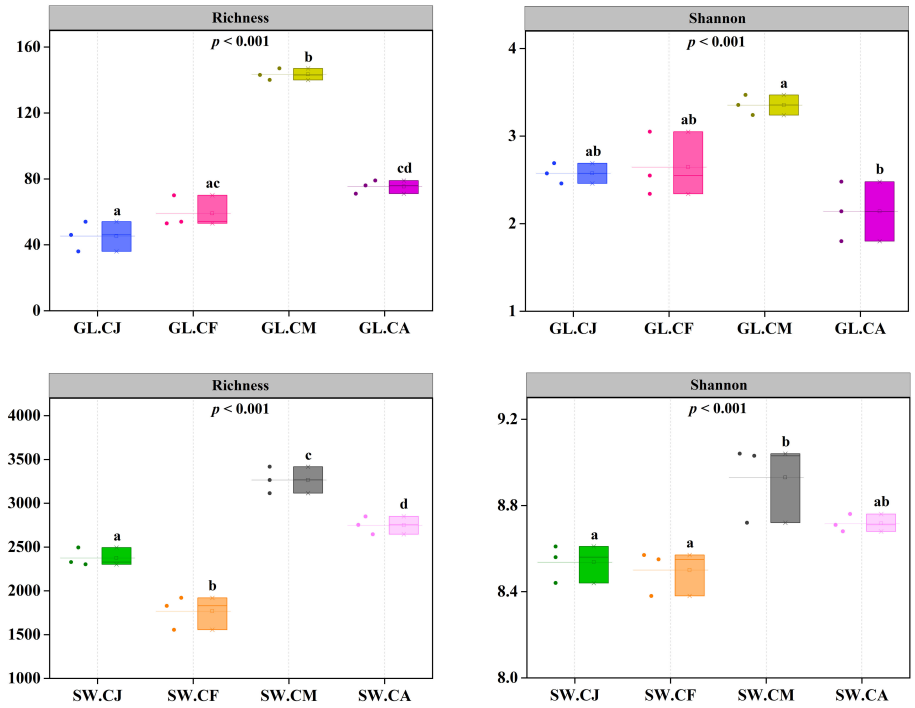

FIGURE 4
The diversity of diazotrophic communities in different cultivation periods. CJ, Cultivation Jan.; CF, Cultivation Feb.; CM, Cultivation Mar.; CA, Cultivation Apr.; GL, *G. lemaneiformis*; SW, seawater. Different letters (a, b, c, d) denote significant ($p < 0.05$) differences in diversity of diazotrophic communities associated with *G. lemaneiformis* and seawater between different cultivation periods.

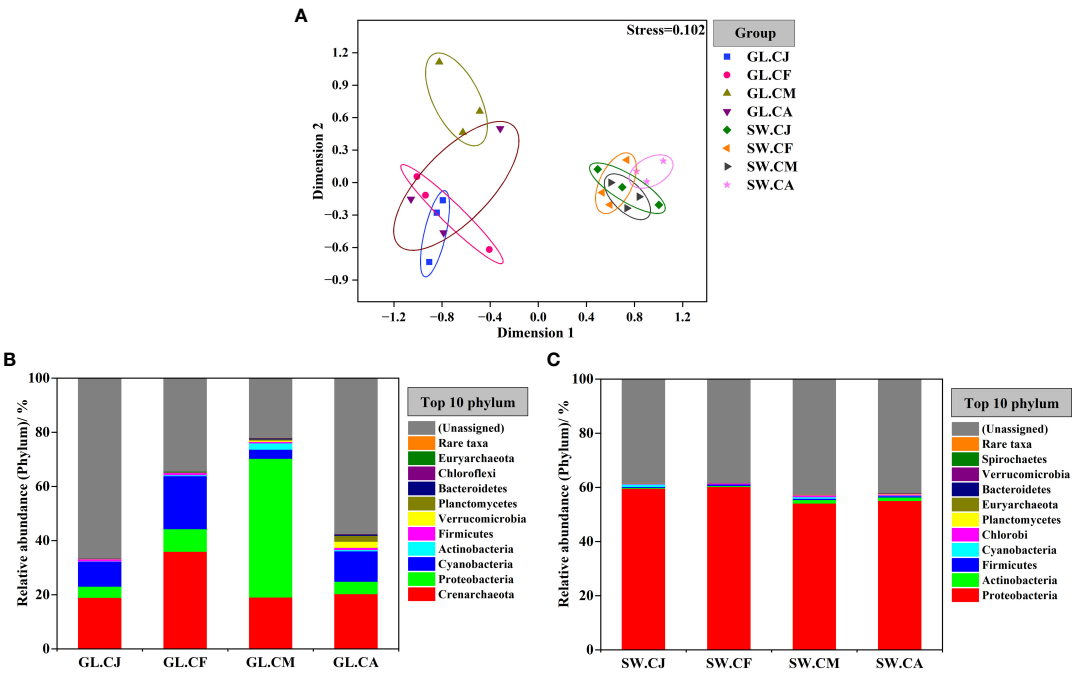

FIGURE 5
Difference comparison and temporal variations of the diazotrophs communities composition. Non-metric multidimensional scaling (nMDS) based on Bray-Curtis measure **(A)**. The communities composition of diazotrophs associated with *G. lemaneiformis* **(B)** and seawater **(C)** at phylum level in different cultivation periods. CJ, Cultivation Jan.; CF, Cultivation Feb.; CM, Cultivation Mar.; CA, Cultivation Apr.; GL, *G. lemaneiformis*; SW, seawater.

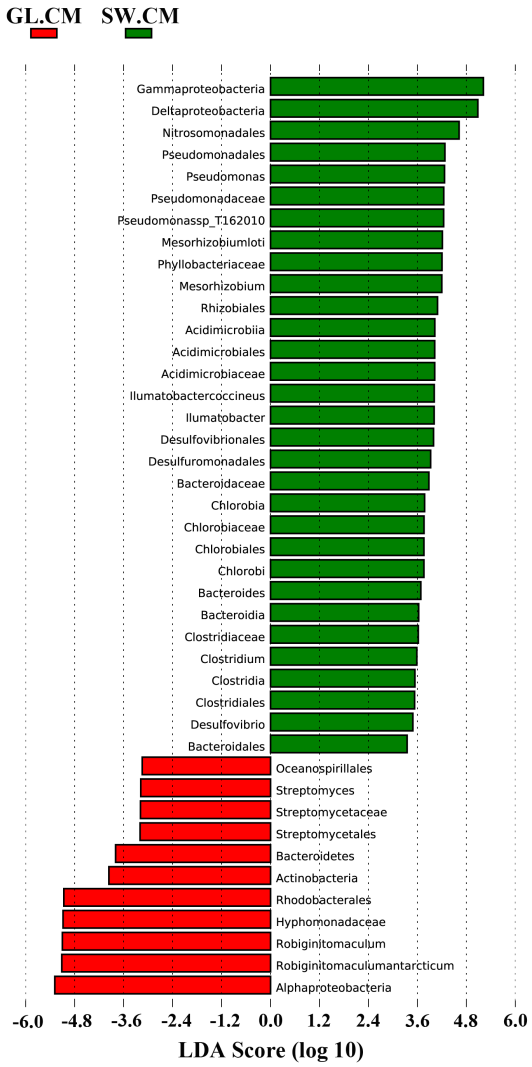

FIGURE 6
The LDA score histogram of significantly different biomarkers associated with *G. lemaneiformis* and seawater in CM. CM, Cultivation Mar.; GL, *G. lemaneiformis*; SW, seawater.

with *G. lemaneiformis* in four cultivation periods (CJ, CF, CM, CA) were Rhodobacterales, Hyphomonadaceae, *Robiginitomaculum*, *Robiginitomaculum antarcticum* and had a more significant influence on difference between groups (GL) (Figure 7).

4 Discussions

With the large-scale cultivation of seaweed, the coastal marine environment rich in N resources will become a N-limited environment. The concentration of N_2 in the atmosphere is much higher than that of other inorganic N in the ocean (Bernhard, 2010). Thus this N source becomes potential nutrient source for marine primary productivity. The conversion of N_2 into ammonium relies heavily on the diazotrophic communities (Bernhard, 2010). In recent times, an increasing number of studies have emphasized diazotrophs in seawater (Gradoville et al., 2017; Delmont et al., 2018; Chen et al., 2019), but there are few reports on the epiphytic diazotrophs in marine plants. Furthermore, the relationships between diazotrophs in marine plants and those in seawater remain largely unexplored. This study employed isolation and identification techniques, acetylene reduction, qPCR, and high-throughput *nifH* gene sequencing technology to analyze nitrogenase activity, *nifH* gene abundance in epiphytic bacteria on *G. lemaneiformis*, as well as variations in the diversity and composition of diazotrophic communities associated with *G. lemaneiformis* and seawater during different cultivation periods.

4.1 The diversity of culturable N_2-fixing bacteria

The current study observed a higher diversity of N_2-fixing bacteria derived from the surface of macroalgae (*G. lemaneiformis*) compared to the surrounding seawater. Our previous findings have reported that the number of functional bacteria isolated from seaweed capable of growth on marine agar was higher than those isolated from the surrounding seawater (Pei et al., 2024). We assume that bacteria attached to the surface of algae are more likely to grow on marine agar media than planktonic bacteria. This hypothesis is supported by Jensen and Fenical (1994), who believed that the adaptations evolved by bacteria on algae may enhance their ability to form colonies on artificial media. Moreover, the harvested seaweed can be used as raw material for agar production (Yang et al., 2015), which makes it easier for these bacteria on algae to grow on agar media. Previous studies point out that the survival strategies evolved by seawater bacteria, including responses to starvation, may dramatically reduce their ability to

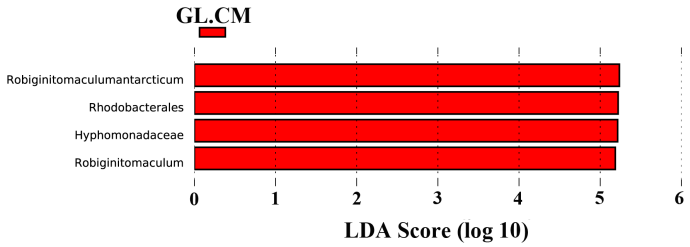

FIGURE 7
The LDA score histogram of significantly different biomarkers associated with *G. lemaneiformis* in different cultivation periods. CM, Cultivation Mar.; GL, *G. lemaneiformis*.

form colonies on nutrient-rich agar media (Roszak and Colwell, 1987). Large portions of bacterial populations are dormant due to the reduced size and activity of bacteria led by starvation.

Most of the N_2-fixing bacteria genera identified in our study have not been reported in previous studies, which may be closely related to the type of sample and the environment (Shieh et al., 1989; Bentzon-Tilia et al., 2014; Castellano-Hinojosa et al., 2016). Bentzon-Tilia et al. (2014) isolated 16 strains of N_2-fixing bacteria from low-oxygen waters in the Baltic Sea, identified as *Pseudomonas stutzeri* 2A38. Castellano-Hinojosa and co-workers isolated 21 strains of N_2-fixing bacteria from the rhizosphere of *Lolium perenne*, belonging to *Bacillus*, *Paenibacillus*, *Pseudoxanthomonas*, *Burkholderia*, *Staphylococcus* (Castellano-Hinojosa et al., 2016). In another study by Shieh, 7 distinct groups of N_2-fixing bacteria were isolated from *Zostera marina*, primarily falling into the *Vibrio* and *Photobacterium* genera (Shieh et al., 1989). Genus *Vibrio*, belonging to the γ-proteobacteria class, has consistently been identified as a core member of diazotrophic communities associated with various coral species, as evidenced by *nifH* gene sequencing in previous studies (Olson et al., 2009; Zhang et al., 2016). Our current study isolated 4 *Vibrio* (*Vibiro alginolyticus*, *Vibrio harveyi*, *Vibrio cyclitrophicus*, *Vibrio* sp.) from the seawater surrounding *G. lemaneiformis* macroalgae. These findings suggest that these *Vibrio* bacteria likely represent diazotrophic communities associated with the seawater, as supported by molecular identification of the *nifH* gene. As heterotrophs, *Vibrio* can readily use labile sugars derived from macroalgae as a carbon source to sustain their growth (Cárdenas et al., 2018), which may partly explain high abundance of culturable *Vibrio* in the seawater microbiome. In addition, ecology of *Vibrio* has also been reported in other coastal ecosystems (Haas et al., 2016; Kelly et al., 2022). For instance, in the ecosystem of coral reefs, Vibrionaceae with support of DOC released by algae, which ultimately dominate in bacterial communities (Haas et al., 2016). The molecular structure of these compounds released by algae is one of the main factors affecting the microbial community that metabolize them (Kelly et al., 2022).

4.2 The N_2 fixation of epiphytic bacteria associated with *G. lemaneiformis*

The findings mentioned above unequivocally establish the presence of diazotrophic microorganisms in *G. lemaneiformis*. To gain insights into how these diazotrophic communities associated with *G. lemaneiformis* react to environmental variations across distinct cultivation periods, we employed acetylene reduction and qPCR techniques to assess both nitrogenase activity and *nifH* gene abundance in association with *G. lemaneiformis*. The results indicate that the highest nitrogenase activity of epiphytic bacteria associated with *G. lemaneiformis* was observed in the CM cultivation period (Figure 8), reaching 1.958 nmol C_2H_2 g^{-1}·algae·h^{-1}. Based on the established correlation, where the reduction of 3 grams of C_2H_2 is equivalent to the reduction of 1 gram of N_2 (Cardini et al., 2017), it can be estimated that epiphytic bacteria carried by 1 ton of *G. lemaneiformis* can fix approximately 0.531×10^{10} nmol of N_2 annually. Notably, it has been reported that the annual yield of *Gracilaria* reached 610,824 tons in 2022, as per data from the 2023 China Fishery Statistical Yearbook. Since *G. lemaneiformis* significantly contributes to this yield, it is estimated to fix around 0.185×10^{7} moles of N_2 annually. This observation suggests that the diazotrophs associated with *G. lemaneiformis* convert atmospheric N_2 into a new nitrogen source for the marine environment through BNF. This newly introduced N source serves a dual purpose. On the one hand, it can be used as an additional N source for marine organisms. On the other hand, it serves as a supplementary

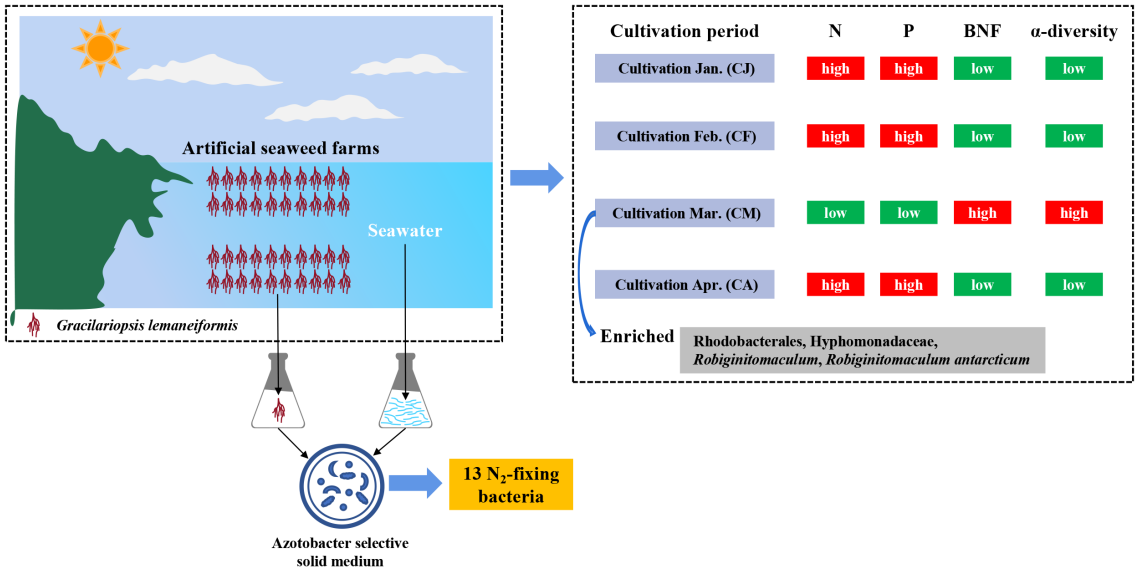

FIGURE 8
A conceptual image summarizing the major results in this study.

N source for marine organisms, particularly in conditions of N deficiency.

Our study found that the N and P levels in the CM seawater were significantly lower compared to CJ, CF, and CA (Figure 8). According to the preliminary data of *G. lemaneiformis* harvested by local farmers every month, it can be seen that the yield of *G. lemaneiformis* reaches the maximum in the CM period. Yang et al. (2006) have pointed out that the cultivated *G. lemaneiformis* harbors a high productivity and can absorb a large amount of N and P. Therefore, this significant reduction regarding the N and P levels in CM seawater can be attributed to the substantial consumption of N and P by *G. lemaneiformis*. Furthermore, the growth environment of *G. lemaneiformis* is characterized as oligotrophic (DIN < 9 μmol·L^{-1}, PO_4-P < 0.6 μmol·L^{-1}), which potentially prompts diazotrophs associated with *G. lemaneiformis* to fix more N_2 to meet the N demands of the entire marine environment. Cardini et al. (2017) demonstrated that epiphytic N_2 fixation, such as in seagrass like *Halophila stipulacea*, is crucial in supplying N to marine plants in oligotrophic environments. Similarly, N_2 fixation associated with *Posidonia oceanica* significantly contributes to N requirements for primary productivity (Agawin et al., 2017). These findings highlight that nutrient deficiency in the marine environment may enhance the N_2-fixing capabilities of diazotrophs in preparation for nutrient stress. Moreover, during the CM period, the seawater temperature reached its maximum of 20.23°C, which is also optimal for indoor *G. lemaneiformis* cultivation (Liu et al., 2019b, 2019a). Indeed, previous research by Wahbeh and Mahasneh (1984) revealed that heterotrophic bacteria, which also include heterotrophic diazotrophs, predominantly dominated the epiphytic bacteria on the roots, stems, and leaves of halophile plants at higher temperatures. Building on this, subsequent work by Cardini et al. (2017) demonstrated that under elevated temperature, the heterotrophic bacteria residing on the roots, stems, and seagrass leaves exhibited higher rates of N_2 fixation. Furthermore, it's worth noting that long-term warming has been shown to significantly increase the abundance of diazotrophs by 86.3%, as reported by Feng et al. (2019). This information leads us to speculate that the elevated nitrogenase activity observed with *G. lemaneiformis* in the CM period may be attributed to accumulating a higher number of heterotrophic diazotrophs on the surface of *G. lemaneiformis*.

4.3 The *nifH* gene abundance of epiphytic bacteria associated with *G. lemaneiformis*

We measured quantitative *nifH* gene abundance associated with *G. lemaneiformis* in various cultivation periods to test this hypothesis. Our findings demonstrated that during the CM period, the *nifH* gene abundance in epiphytic bacteria on *G. lemaneiformis* reached 22.15×10^4 copies/g, a significantly higher level than CJ, CF, and CA. These results strongly suggest that microorganisms containing the *nifH* gene became notably enriched on the surface of *G. lemaneiformis* during the CM period (Figure 8), and they played a significant role in BNF under conditions of nutrient deficiency and elevated temperature, as depicted in Figure 3. Prior studies have indicated that temperature, light, and nutrient availability can affect nitrogenase activity, *nifH* gene transcription, and N_2 fixation rate in N_2-fixing cyanobacteria (Church et al., 2005). Nitrogenase activity and *nifH* gene abundance associated with *G. lemaneiformis* were low in CJ. This could be attributed to a few factors. Firstly, it's possible that planktonic microorganisms, including diazotrophs, had not firmly adhered to the surface of *G. lemaneiformis* during CJ, and the catalytic activity of nitrogenase decreased significantly due to the lower temperature (12.13°C). Secondly, the high concentration of inorganic nutrients in the seawater (DIN: 33.53 μmol·L^{-1}; NH_4-N: 7.19 μmol·L^{-1}; PO_4-P: 1.54 μmol·L^{-1}) could have contributed to the weakening of BNF associated with *G. lemaneiformis*. Hence, we propose that the nutrients needed by *G. lemaneiformis* and its epiphytic bacteria to complete their life activities can be provided by sufficient inorganic nutrients in seawater, and little depends on BNF associated with *G. lemaneiformis*. This hypothesis is supported by numerous previous studies which supposed that BNF of Cyanobacteria and Proteobacteria decreases significantly with the increase of DIN concentration (Knapp, 2012; Bentzon-tilia et al., 2015), indicating that DIN can maintain their growth (Masuda et al., 2013; Bentzon-tilia et al., 2015). Furthermore, DIN was significantly negatively correlated with N_2 fixation in tropical estuarine eutrophication regions and was independent of season (Jabir et al., 2020). NH_4-N, the main component of DIN in some estuary regions (Jabir et al., 2020), controls the N_2 fixation rate by inhibiting the synthesis of new nitrogenase (Rees et al., 2006). In the present study, NH_4-N concentration in seawater reached 7.19 μmol·L^{-1} in CJ, significantly higher than in CF, CM, and CA. Hence, it can be seen that the nitrogenase activity and *nifH* gene abundance associated with *G. lemaneiformis* in CJ may also be inhibited by higher ammonium concentration. Although the relationship between DIN availability and N_2 fixation in marine environments is very complicated, DIN plays an essential role in the construction of diazotrophic communities (Messer et al., 2017), which in turn may influence BNF associated with *G. lemaneiformis*.

4.4 Comparison of diazotrophic communities between algae and seawater

Although high-throughput sequencing technology is widely used to study the microbial community associated with macroalgae such as *G. lemaneiformis* (Xie et al., 2017; Pei et al., 2021), it has not been broadly applied to the *nifH* gene to explore the diazotrophic communities associated with *G. lemaneiformis*. Our previous research only obtained a tiny amount of information about diazotrophs (Pei et al., 2021), and we could not fundamentally understand the diazotrophs associated with *G. lemaneiformis* and its surrounding seawater, and the role of functional microorganisms in the cultivation of ecological environment remained to be studied. The current study showed that the diazotrophic communities associated with *G. lemaneiformis* significantly differed in various cultivation periods, especially in

CM. In contrast, the diazotrophic communities associated with seawater have little change in distinct cultivation periods. To the best of our knowledge, only some reports on diazotrophs are associated with macroalgae. However, more attention has been paid to diazotrophs associated with coral (Zhang et al., 2016), mangrove rhizosphere (Zhang et al., 2017a), and seawater (Messer et al., 2017). Therefore, this is the first study that used *nifH* gene high-throughput sequencing to explore the diazotrophs associated with red macroalgae *G. lemaneiformis*. Studies have shown that α-Proteobacteria, δ-Proteobacteria and γ-Proteobacteria are the main diazotroph groups associated with most corals (Lema et al., 2012; Zhang et al., 2016). Moreover, δ-proteobacteria and γ-proteobacteria are the most predominant diazotrophic communities associated with mangrove rhizosphere (Alzubaidy et al., 2016; Zhang et al., 2017a). In the present study, α-proteobacteria and Thermoprotei, the main diazotrophic groups associated with *G. lemaneiformis* differed significantly in various cultivation periods (Supplementary Figure S1A). However, α-proteobacteria, δ-proteobacteria and γ-proteobacteria were the main diazotrophic groups associated with seawater, similar in different cultivation periods (Supplementary Figure S1B). The above results indicate that these diazotrophic groups may play a vital role of BNF in the cultivation environment of *G. lemaneiformis*. Findings show that diazotrophic communities associated with marine organisms (e.g. corals) are species-specific and environment-specific due to the differences of species and environment conditions (Lema et al., 2012). Notably, the relative abundance of α-proteobacteria associated with *G. lemaneiformis* in CM reached 47.972%, much higher than that in CJ, CF, and CA. We speculate that the higher abundance of α-proteobacteria could contribute to the significant increase in nitrogenase activity and *nifH* gene abundance associated with *G. lemaneiformis*. LEfSe analysis results showed that the biomarkers with more significant influence on difference between groups (GL vs SW) remained the same in CJ, CF, and CA (Supplementary Figures S2A, B, D). However, the biomarkers with more significant influence on difference between groups (GL vs SW) had noticeable changes in CM, reflected primarily in α-proteobacteria, *Robiginitomaculum*, and *Robiginitomaculum antarcticum* (Figure 6). Consequently, α-proteobacteria plays a significant role of BNF in response to oligotrophic conditions, reflected in the remarkable increase of nitrogenase activity and *nifH* gene abundance in CM.

To further explore the diazotrophic communities composition under the class α-proteobacteria, a comprehensive analysis was conducted at the order, family, and genus level. The current study observed significant differences in the dominant diazotrophic communities associated with *G. lemaneiformis* at the order, family, and genus levels in different cultivation periods (Supplementary Figures S1C, E, G), while the dominant diazotrophic communities associated with seawater were similar (Supplementary Figures S1D, F, H). Microbial groups with higher relative abundance found in α-proteobacteria, including Rhodobacterales (36.915%), Hyphomonadaceae (36.743%), and *Robiginitomaculum* (36.722%), were dominant diazotrophic groups associated with *G. lemaneiformis* in CM. Predictive functional results from Lesser and coworkers uncovered that genera within the Rhodobacterales with putative N_2-fixing capabilities (Lesser et al., 2018). These findings are confirmed by a previous study indicating that the *nifHDK* genes were detected in the Rhodobacterales genome (Tsoy et al., 2016). The existence of significant BNF associated with *G. lemaneiformis* in CM was further supported by the above studies. These bacteria exhibit extreme metabolic flexibility under environmental conditions related to variability in pO_2, light availability, and carbon source (Lesser et al., 2018). The family Hyphomonadaceae encompasses several members (Lee et al., 2005, 2007) that are widely distributed in diverse environments, including surface water (Deng et al., 2013), freshwater (Driscoll et al., 2017), deep-sea (Zhang et al., 2013), and marine sediment (Zhao et al., 2019). The family Hyphomonadaceae is currently composed of eleven well-defined genera: *Hyphomonas*, *Maricaulis*, *Hirschia*, *Oceanicaulis*, *Robiginitomaculum*, *Woodsholea*, *Hellea*, *Henriciella*, *Ponticaulis*, *Litorimonas*, and *Algimonas* (Lee et al., 2007; Deng et al., 2013). LefSe analysis results displayed that the biomarkers with more significant influence on difference between groups (GL.CJ vs GL.CF vs GL.CM vs GL.CA) were Rhodobacterales, Hyphomonadaceae, *Robiginitomaculum*, *Robiginitomaculum antarcticum* (Figure 7). As a result, Rhodobacterales, Hyphomonadaceae, *Robiginitomaculum*, and *Robiginitomaculum antarcticum* within the α-proteobacteria play a significant role in BNF in response to oligotrophic conditions (Figure 8).

A study on symbiotic diazotrophic bacterial communities has indicated that Rhizobiales belonging to the class α-proteobacteria are stable and dominant diazotrophic groups associated with *Acropora* coral species (Lema et al., 2012). In our study, there were no variations in the relative abundance of Rhizobiales (SW.CJ: 2.382%; SW.CF: 2.931%; SW.CM: 1.821%: SW.CA: 1.953%) within different cultivation periods, indicating that Rhizobiales are also stable and dominant diazotrophic groups associated with seawater. Besides, we also found two dominant diazotrophic groups from δ-proteobacteria associated with seawater, such as Desulfuromonadale and Desulfovibrionales, belonging to the sulfate-reducing bacteria (Zhang et al., 2017a). It has been reported that the order Desulfovibrionales has strong adaptability to marine environmental stresses, such as anthropogenic heavy metal contamination and oil pollution (Varon-Lopez et al., 2014), which suggests that Desulfovibrionales may contribute substantially to BNF in coastal seawater. *Pseudomonas* within the γ-proteobacteria is not only a diazotrophic genus (Zhang et al., 2016), but also the dominant bacterial genus associated with seawater in this study.

5 Conclusions

Thirteen N_2-fixing bacteria carrying the *nifH* gene were isolated, screened, and identified from *G. lemaneiformis* and its surrounding seawater. Notably, *G. lemaneiformis* exhibited the highest nitrogenase activity and *nifH* gene abundance in the CM period, underlining the substantial contribution of epiphytic bacteria to BNF. Linear regression assessments revealed strong negative correlations between nitrogenase activity and several variables, including Sal., NH_4-N, NO_3-N, DIN, PO_4-P, and TP, while positive correlations were evident with Temp., pH, and Chl-*a*.

Furthermore, *nifH* gene abundance exhibited negative associations with Sal. and TP. These results emphasize the intricate interplay between diazotrophic activity and environmental conditions. Our results also showed the highest alpha-diversity of diazotrophic communities associated with *G. lemaneiformis* and seawater during the CM period. The diazotrophic communities linked to *G. lemaneiformis* displayed pronounced differences among cultivation periods, distinguishing them from seawater-associated ones. Conversely, the diazotrophic communities in seawater appeared relatively stable across different cultivation phases. Of particular significance, our findings highlighted specific taxa, such as the order Rhodobacterales, the family Hyphomonadaceae, and the genus *Robiginitomaculum* and the species *Robiginitomaculum antarcticum* within the α-proteobacteria class, as significant contributors to BNF, particularly in response to oligotrophic environmental conditions. These results significantly advance our understanding of diazotrophs associated with *G. lemaneiformis*, providing a foundation for future investigations into the underlying mechanisms and ecological implications of their activities in the marine environment.

Data availability statement

The datasets presented in this study can be found online repositories, the names of the repository/repositories and accession number(s) can be found in the article/Supplementary Material.

Author contributions

PP: Conceptualization, Data curation, Formal analysis, Investigation, Methodology, Software, Validation, Visualization, Writing – original draft, Writing – review & editing. MA: Methodology, Software, Validation, Writing – review & editing. CY: Investigation, Methodology, Validation, Writing – review & editing. PY: Investigation, Methodology, Validation, Writing – review & editing. XK: Investigation, Methodology, Validation, Writing – review & editing. ZL: Investigation, Methodology, Validation, Writing – review & editing. TL: Validation, Writing – review & editing. WC: Methodology, Validation, Writing – review & editing. HD: Funding acquisition, Project administration, Resources, Supervision, Validation, Writing – review & editing.

Funding

The author(s) declare financial support was received for the research, authorship, and/or publication of this article. This research was supported by several sources, including Project supported by Southern Marine Science and Engineering Guangdong Laboratory(Zhuhai) (SML2023SP204), the Program for University Innovation Team of Guangdong Province (2022KCXTD008), the Science and Technology Plan Projects of Guangdong Province (2021B1212050025), and the China Agriculture Research System of MOF and MARA (CARS-50).

Acknowledgments

We thank Guangdong Magigene Biotechnology Co. Ltd. for providing sequencing services, and the Shaowu Zhu villager of artificial seaweed farms located in Zoumapu Village, Nan'ao Island of Guangdong Province for his help with sampling.

Conflict of interest

The authors declare that the research was conducted in the absence of any commercial or financial relationships that could be construed as a potential conflict of interest.

Publisher's note

All claims expressed in this article are solely those of the authors and do not necessarily represent those of their affiliated organizations, or those of the publisher, the editors and the reviewers. Any product that may be evaluated in this article, or claim that may be made by its manufacturer, is not guaranteed or endorsed by the publisher.

Supplementary material

The Supplementary Material for this article can be found online at: https://www.frontiersin.org/articles/10.3389/fmars.2024.1408958/full#supplementary-material

References

Agawin, N. S. R., Ferriol, P., Sintes, E., and Moyà, G. (2017). Temporal and spatial variability of *in situ* nitrogen fixation activities associated with the Mediterranean seagrass *Posidonia oceanica* meadows. *Limnol. Oceanogr.* 62, 2575–2592. doi: 10.1002/lno.10591

Alzubaidy, H., Essack, M., Malas, T. B., Bokhari, A., Motwalli, O., Kamanu, F. K., et al. (2016). Rhizosphere microbiome metagenomics of gray mangroves (*Avicennia marina*) in the Red Sea. *Gene* 576, 626–636. doi: 10.1016/j.gene.2015.10.032

AQSIQ (2007). *Specifications for Oceanographic Survey. Part 4: Survey of Chemical Parameters in Sea Water* (Beijing: Stand. Press China), 16–26.

Aslam, M., Pei, P., Ye, P., Li, T., Liang, H., Zhang, Z., et al. (2023). Unraveling the Diverse Profile of N-Acyl Homoserine Lactone Signals and Their Role in the Regulation of Biofilm Formation in *Porphyra haitanensis*-Associated *Pseudoalteromonas galatheae*. *Microorganisms* 11, 2228. doi: 10.3390/microorganisms11092228

Azam, F., and Malfatti, F. (2007). Microbial structuring of marine ecosystems. *Nat. Rev. Microbiol.* 5, 782–791. doi: 10.1038/nrmicro1747

Bentzon-Tilia, M., Farnelid, H., Jürgens, K., and Riemann, L. (2014). Cultivation and isolation of N_2-fixing bacteria from suboxic waters in the Baltic Sea. *FEMS Microbiol. Ecol.* 88, 358–371. doi: 10.1111/fem.2014.88.issue-2

Bentzon-tilia, M., Severin, I., Hansen, L. H., and Riemann, L. (2015). Genomics and ecophysiology of heterotrophic nitrogen-fixing bacteria isolated from estuarine surface water. *MBio* 6, 1–11. doi: 10.1128/mBio.00929-15

Bernhard, A. (2010). The nitrogen cycle: processes, players, and human impact. *Nat. Educ. Knowl.* 2, 1–8.

Bonnet, S., Berthelot, H., Turk-Kubo, K., Cornet-Barthaux, V., Fawcett, S., Berman-Frank, I., et al. (2016). Diazotroph derived nitrogen supports diatom growth in the South West Pacific: A quantitative study using nanoSIMS. *Limnol. Oceanogr.* 61, 1549–1562. doi: 10.1002/lno.10300

Caffin, M., Moutin, T., Ann Foster, R., Bouruet-Aubertot, P., Michelangelo Doglioli, A., Berthelot, H., et al. (2018). N_2 fixation as a dominant new N source in the western tropical South Pacific Ocean (OUTPACE cruise). *Biogeosciences* 15, 2565–2585. doi: 10.5194/bg-15-2565-2018

Cárdenas, A., Neave, M. J., Haroon, M. F., Pogoreutz, C., Rädecker, N., Wild, C., et al. (2018). Excess labile carbon promotes the expression of virulence factors in coral reef bacterioplankton. *ISME J.* 12, 59–76. doi: 10.1038/ismej.2017.142

Cardini, U., van Hoytema, N., Bednarz, V. N., Al-Rshaidat, M. M. D., and Wild, C. (2017). N_2 fixation and primary productivity in a red sea *Halophila stipulacea* meadow exposed to seasonality. *Limnol. Oceanogr.* 63, 786–798. doi: 10.1002/lno.10669

Castellano-Hinojosa, A., Correa-Galeote, D., Palau, J., and Bedmar, E. J. (2016). Isolation of N_2-fixing rhizobacteria from *Lolium perenne* and evaluating their plant growth promoting traits. *J. Basic Microbiol.* 56, 85–91. doi: 10.1002/jobm.201500247

Chen, T., Chen, Y. L., Sheu, D., Chen, H., and Lin, Y. (2019). Community and abundance of heterotrophic diazotrophs in the northern South China Sea : Revealing the potential importance of a new alphaproteobacterium in N_2 fixation. *Deep. Res. Part I* 143, 104–114. doi: 10.1016/j.dsr.2018.11.006

Church, M. J., Short, C. M., Jenkins, B. D., Karl, D. M., and Zehr, J. P. (2005). Temporal patterns of nitrogenase gene (*nifH*) expression in the oligotrophic North Pacific Ocean. *Appl. Environ. Microbiol.* 71, 5362–5370. doi: 10.1128/AEM.71.9.5362-5370.2005

Dang, H., and Lovell, C. R. (2016). Microbial surface colonization and biofilm development in marine environments. *Microbiol. Mol. Biol. Rev.* 80, 91–138. doi: 10.1128/MMBR.00037-15

Delmont, T. O., Quince, C., Shaiber, A., Esen, Ö.C., Lee, S. T., Rappé, M. S., et al. (2018). Nitrogen-fixing populations of Planctomycetes and Proteobacteria are abundant in surface ocean metagenomes. *Nat. Microbiol.* 3, 804–813. doi: 10.1038/s41564-018-0176-9

Deng, W., Zhang, Y., Xie, X., Zhao, Z., and Fu, Y. (2013). *Euryhalocaulis caribicus* gen. nov., sp. nov., a new members of the family *Hyphomonadaceae* isolated from the Caribbean Sea. *Curr. Microbiol.* 66, 606–612. doi: 10.1007/s00284-013-0314-9

Driscoll, C. B., Otten, T. G., Brown, N. M., and Dreher, T. W. (2017). Towards long-read metagenomics: Complete assembly of three novel genomes from bacteria dependent on a diazotrophic cyanobacterium in a freshwater lake co-culture. *Stand. Genomic Sci.* 12, 1–16. doi: 10.1186/s40793-017-0224-8

Duarte, C. M., Wu, J., Xiao, X., Bruhn, A., and Krause-Jensen, D. (2017). Can seaweed farming play a role in climate change mitigation and adaptation? *Front. Mar. Sci.* 4. doi: 10.3389/fmars.2017.00100

Egan, S., and Gardiner, M. (2016). Microbial dysbiosis: Rethinking disease in marine ecosystems. *Front. Microbiol.* 7. doi: 10.3389/fmicb.2016.00991

Feng, J., Penton, C. R., He, Z., Nostrand, J. D., Yuan, M. M., and Wu, L. (2019). Long-term warming in Alaska enlarges the diazotrophic community in deep soils. *MBio* 10, 1–12. doi: 10.1128/mBio.02521-18

Feng, G., Sun, W., Zhang, F., Orlić, S., and Li, Z. (2018). Functional transcripts indicate phylogenetically diverse active ammonia-scavenging microbiota in sympatric sponges. *Mar. Biotechnol.* 20, 131–143. doi: 10.1007/s10126-018-9797-5

Gaby, J. C., and Buckley, D. H. (2012). A comprehensive evaluation of PCR primers to amplify the *nifH* gene of nitrogenase. *PLoS One* 7, e42149. doi: 10.1371/journal.pone.0042149

Geisler, E., Bogler, A., Rahav, E., and Bar-Zeev, E. (2019). Direct detection of heterotrophic diazotrophs associated with planktonic aggregates. *Sci. Rep.* 9, 1–9. doi: 10.1038/s41598-019-45505-4

Gradoville, M. R., Bombar, D., Crump, B. C., Letelier, R. M., Zehr, J. P., and White, A. E. (2017). Diversity and activity of nitrogen-fixing communities across ocean basins. *Limnol. Oceanogr.* 62, 1895–1909. doi: 10.1002/lno.10542

Haas, A. F., Fairoz, M. F. M., Kelly, L. W., Nelson, C. E., Dinsdale, E. A., Edwards, R. A., et al. (2016). Global microbialization of coral reefs. *Nat. Microbiol.* 1, 1–7. doi: 10.1038/nmicrobiol.2016.42

Hasselström, L., Visch, W., Gröndahl, F., Nylund, G. M., and Pavia, H. (2018). The impact of seaweed cultivation on ecosystem services-a case study from the west coast of Sweden. *Mar. pollut. Bull.* 133, 53–64. doi: 10.1016/j.marpolbul.2018.05.005

Head, W. D., and Carpenter, E. J. (1975). Nitrogen fixation associated with the marine macroalga *Codium fragile*. *Limnol. Oceanogr.* 20, 815–823. doi: 10.4319/lo.1975.20.5.0815

Huang, Y. S., Ou, L. J., and Yang, Y. F. (2017). Nutrient competition between macroalgae *Gracilaria lemaneiformis* and phytoplankton in coastal waters of Nan'ao island, Guangdong. *Oceanol. Limnol. Sin.* 48, 806–813. doi: 10.11693/hyhz20170200031

Jabir, T., Vipindas, P. V., Jesmi, Y., Valliyodan, S., Parambath, P. M., Singh, A., et al. (2020). Nutrient stoichiometry (N:P) controls nitrogen fixation and distribution of diazotrophs in a tropical eutrophic estuary. *Mar. pollut. Bull.* 151, 110799. doi: 10.1016/j.marpolbul.2019.110799

Jensen, P. R., and Fenical, W. (1994). Strategies for the discovery of secondary metabolites from marine bacteria: Ecological perspectives. *Annu. Rev. Microbiol.* 48, 559–584. doi: 10.1146/annurev.mi.48.100194.003015

Karthick, P., and Mohanraju, R. (2018). Antimicrobial potential of epiphytic bacteria associated with seaweeds of little Andaman, India. *Front. Microbiol.* 9. doi: 10.3389/fmicb.2018.00611

Kelly, L. W., Nelson, C. E., Petras, D., Koester, I., Quinlan, Z. A., Arts, M. G. I., et al. (2022). Distinguishing the molecular diversity, nutrient content, and energetic potential of exometabolomes produced by macroalgae and reef-building corals. *Proc. Natl. Acad. Sci. U. S. A.* 119, e2110283119. doi: 10.1073/PNAS.2110283119

Kim, J. K., Yarish, C., Hwang, E. K., Park, M., and Kim, Y. (2017). Seaweed aquaculture: Cultivation technologies, challenges and its ecosystem services. *Algae* 32, 1–13. doi: 10.4490/algae.2017.32.3.3

Knapp, A. N. (2012). The sensitivity of marine N_2 fixation to dissolved inorganic nitrogen. *Front. Microbiol.* 3. doi: 10.3389/fmicb.2012.00374

Lee, K., Lee, H. K., Choi, T. H., and Cho, J. C. (2007). *Robiginitomaculum antarcticum* gen. nov., sp. nov., a member of the family *Hyphomonadaceae*, from Antarctic seawater. *Int. J. Syst. Evol. Microbiol.* 57, 2595–2599. doi: 10.1099/ijs.0.65274-0

Lee, K. B., Liu, C., Anzai, Y., Kim, H., Aono, T., and Oyaizu, H. (2005). The hierarchical system of the "*Alphaproteobacteria*": Description of *Hyphomonadaceae* fam. nov., *Xanthobacteraceae* fam. nov. and *Erythrobacteraceae* fam. nov. *Int. J. Syst. Evol. Microbiol.* 55, 1907–1919. doi: 10.1099/ijs.0.63663-0

Lema, K. A., Willis, B. L., and Bourne, D. G. (2014). Amplicon pyrosequencing reveals spatial and temporal consistency in diazotroph assemblages of the *Acropora millepora* microbiome. *Environ. Microbiol.* 16, 3345–3359. doi: 10.1111/1462-2920.12366

Lema, K. A., Willis, B. L., and Bourneb, D. G. (2012). Corals form characteristic associations with symbiotic nitrogen-fixing bacteria. *Appl. Environ. Microbiol.* 78, 3136–3144. doi: 10.1128/AEM.07800-11

Lesser, M. P., Morrow, K. M., Pankey, S. M., and Noonan, S. H. C. (2018). Diazotroph diversity and nitrogen fixation in the coral *Stylophora pistillata* from the Great Barrier Reef. *ISME J.* 12, 813–824. doi: 10.1038/s41396-017-0008-6

Liang, Z., Liu, F., Wang, W., Zhang, P., Sun, X., Wang, F., et al. (2019). High-throughput sequencing revealed differences of microbial community structure and diversity between healthy and diseased *Caulerpa lentillifera*. *BMC Microbiol.* 19, 1–15. doi: 10.1186/s12866-019-1605-5

Liu, X., Wen, J., Chen, W., and Du, H. (2019a). Physiological effects of nitrogen deficiency and recovery on the macroalga *Gracilariopsis lemaneiformis* (Rhodophyta). *J. Phycol.* 55, 830–839. doi: 10.1111/jpy.12862

Liu, X., Wen, J., Zheng, C., Jia, H., Chen, W., and Du, H. (2019b). The impact of nitrogen deficiency and subsequent recovery on the photosynthetic performance of the red macroalga *Gracilariopsis lemaneiformis*. *J. Appl. Phycol.* 31, 2699–2707. doi: 10.1007/s10811-019-1745-x

Masuda, T., Furuya, K., Kodama, T., Takeda, S., and Harrison, P. J. (2013). Ammonium uptake and dinitrogen fixation by the unicellular nanocyanobacterium *Crocosphaera watsonii* in nitrogen-limited continuous cultures. *Limnol. Oceanogr.* 58, 2029–2036. doi: 10.4319/lo.2013.58.6.2029

Messer, L. F., Brown, M. V., Furnas, M. J., Carney, R. L., McKinnon, A. D., and Seymour, J. R. (2017). Diversity and activity of diazotrophs in great barrier reef surface waters. *Front. Microbiol.* 8. doi: 10.3389/fmicb.2017.00967

Neori, A. (2008). Essential role of seaweed cultivation in integrated multi-trophic aquaculture farms for global expansion of mariculture: An analysis. *J. Appl. Phycol.* 20, 567–570. doi: 10.1007/s10811-007-9206-3

Olson, N. D., Ainsworth, T. D., Gates, R. D., and Takabayashi, M. (2009). Diazotrophic bacteria associated with Hawaiian *Montipora* corals : Diversity and abundance in correlation with symbiotic dinoflagellates. *J. Exp. Mar. Bio. Ecol.* 371, 140–146. doi: 10.1016/j.jembe.2009.01.012

Olson, N. D., and Lesser, M. P. (2013). Diazotrophic diversity in the Caribbean coral, *Montastraea cavernosa*. *Arch. Microbiol.* 195, 853–859. doi: 10.1007/s00203-013-0937-z

Pei, P., Aslam, M., Du, H., Liang, H., Wang, H., Liu, X., et al. (2021). Environmental factors shape the epiphytic bacterial communities of *Gracilariopsis lemaneiformis*. *Sci. Rep.* 11, 1–15. doi: 10.1038/s41598-021-87977-3

Pei, P., Aslam, M., Wang, H., Ye, P., Li, T., Liang, H., et al. (2024). Diversity and ecological function of urease-producing bacteria in the cultivation environment of *Gracilariopsis lemaneiformis*. *Microb. Ecol.* 87, 35. doi: 10.1007/s00248-023-02339-y

Poly, F., Monrozier, L. J., and Bally, R. (2001). Improvement in the RFLP procedure for studying the diversity of *nifH* genes in communities of nitrogen fixers in soil. *Res. Microbiol.* 152, 95–103. doi: 10.1016/S0923-2508(00)01172-4

Rees, A. P., Law, C. S., and Woodward, E. M. S. (2006). High rates of nitrogen fixation during an *in-situ* phosphate release experiment in the Eastern Mediterranean Sea. *Geophys. Res. Lett.* 33, 2–5. doi: 10.1029/2006GL025791

Roszak, D. B., and Colwell, R. R. (1987). Survival strategies of bacteria in the natural environment. *Microbiol. Rev.* 51, 365–379. doi: 10.1128/mr.51.3.365-379.1987

Rousk, J., and Bengtson, P. (2014). Microbial regulation of global biogeochemical cycles. *Front. Microbiol.* 5, 1–3. doi: 10.3389/fmicb.2014.00103

Selvarajan, R., Sibanda, T., Venkatachalam, S., Ogola, H. J. O., Christopher Obieze, C., and Msagati, T. A. (2019). Distribution, interaction and functional profiles of

epiphytic bacterial communities from the rocky intertidal seaweeds, South Africa. *Sci. Rep.* 9, 1–13. doi: 10.1038/s41598-019-56269-2

Shieh, W. Y., Simidu, U., and Maruyama, Y. (1989). Enumeration and characterization of nitrogen-fixing bacteria in an eelgrass (*Zostera marina*) bed. *Microb. Ecol.* 18, 249–259. doi: 10.1007/BF02075812

Sohm, J. A., Webb, E. A., and Capone, D. G. (2011). Emerging patterns of marine nitrogen fixation. *Nat. Rev. Microbiol.* 9, 499–508. doi: 10.1038/nrmicro2594

Stabili, L., Rizzo, L., Pizzolante, G., and Alifano, P. (2017). Spatial distribution of the culturable bacterial community associated with the invasive alga *Caulerpa cylindracea* in the Mediterranean Sea. *Mar. Environ. Res.* 125, 90–98. doi: 10.1016/j.marenvres.2017.02.001

Tsoy, O. V., Ravcheev, D. A., Čuklina, J., and Gelfand, M. S. (2016). Nitrogen fixation and molecular oxygen: Comparative genomic reconstruction of transcription regulation in Alphaproteobacteria. *Front. Microbiol.* 7. doi: 10.3389/fmicb.2016.01343

Varon-Lopez, M., Dias, A. C. F., Fasanella, C. C., Durrer, A., Melo, I. S., Kuramae, E. E., et al. (2014). Sulphur-oxidizing and sulphate-reducing communities in Brazilian mangrove sediments. *Environ. Microbiol.* 16, 845–855. doi: 10.1111/1462-2920.12237

Wahbeh, M. I., and Mahasneh, A. M. (1984). Heterotrophic bacteria attached to leaves, rhizomes and roots of three seagrass species from Aqaba (Jordan). *Aquat. Bot.* 20, 87–96. doi: 10.1016/0304-3770(84)90029-9

Wang, J., Mao, Y., Du, G., Li, X., and Tang, X. (2021). On microbial community of *Pyropia haitanensis* by metagenomic analysis. *J. Oceanol. Limnol.* 39, 1091–1102. doi: 10.1007/s00343-020-0189-0

Wang, W., Wu, L., Xu, K., Xu, Y., Ji, D., Chen, C., et al. (2020). The cultivation of *Pyropia haitanensis* has important impacts on the seawater microbial community. *J. Appl. Phycol.* 32, 2561–2573. doi: 10.1007/s10811-020-02068-6

Xie, X., He, Z., Hu, X., Yin, H., Liu, X., and Yang, Y. (2017). Large-scale seaweed cultivation diverges water and sediment microbial communities in the coast of Nan'ao Island, South China Sea. *Sci. Total Environ.* 598, 97–108. doi: 10.1016/j.scitotenv.2017.03.233

Yang, Y., Chai, Z., Wang, Q., Chen, W., He, Z., and Jiang, S. (2015). Cultivation of seaweed *Gracilaria* in Chinese coastal waters and its contribution to environmental improvements. *Algal Res.* 9, 236–244. doi: 10.1016/j.algal.2015.03.017

Yang, Q. S., Dong, J., Ahmad, M., Ling, J., Zhou, W. G., Tan, Y. H., et al. (2019). Analysis of *nifH* DNA and RNA reveals a disproportionate contribution to nitrogenase activities by rare plankton-associated diazotrophs. *BMC Microbiol.* 19, 1–12. doi: 10.1186/s12866-019-1565-9

Yang, Y. F., Fei, X. G., Song, J. M., Hu, H. Y., Wang, G. C., and Chung, I. K. (2006). Growth of *Gracilaria lemaneiformis* under different cultivation conditions and its effects on nutrient removal in Chinese coastal waters. *Aquaculture* 254, 248–255. doi: 10.1016/j.aquaculture.2005.08.029

Zehr, J. P., Jenkins, B. D., Short, S. M., and Steward, G. F. (2003). Nitrogenase gene diversity and microbial community structure: A cross-system comparison. *Environ. Microbiol.* 5, 539–554. doi: 10.1046/j.1462-2920.2003.00451.x

Zhang, X. Y., Li, G. W., Wang, C. S., Zhang, Y. J., Xu, X. W., Li, H., et al. (2013). *Marinicauda pacifica* gen. nov., sp. nov., a prosthecate alphaproteobacterium of the family *Hyphomonadaceae* isolated from deep seawater. *Int. J. Syst. Evol. Microbiol.* 63, 2248–2253. doi: 10.1099/ijs.0.046656-0

Zhang, A., Wen, X., Yan, H., He, X., Su, H., Tang, H., et al. (2018). Response of microalgae to large-seaweed cultivation as revealed by particulate organic matter from an integrated aquaculture off Nan'ao Island, South China. *Mar. pollut. Bull.* 133, 137–143. doi: 10.1016/j.marpolbul.2018.05.026

Zhang, Y., Yang, Q., Ling, J., Van Nostrand, J. D., Shi, Z., Zhou, J., et al. (2016). The shifts of diazotrophic communities in spring and summer associated with coral *Galaxea astreata*, *Pavona decussata*, and *Porites lutea*. *Front. Microbiol.* 7. doi: 10.3389/fmicb.2016.01870

Zhang, Y., Yang, Q., Ling, J., Van Nostrand, J. D., Shi, Z., Zhou, J., et al. (2017a). Diversity and structure of diazotrophic communities in mangrove rhizosphere, revealed by high-throughput sequencing. *Front. Microbiol.* 8. doi: 10.3389/fmicb.2017.02032

Zhang, Y., Zhang, J., Liang, Y., Li, H., Li, G., Chen, X., et al. (2017b). Carbon sequestration processes and mechanisms in coastal mariculture environments in China. *Sci. China Earth Sci.* 60, 2097–2107. doi: 10.1007/s11430-017-9148-7

Zhao, H., Zhang, C., Wu, Y., Zhang, X., Rong, Q., Xu, Z., et al. (2019). *Thalassorhabdomicrobium marinisediminis* gen. Nov., sp. nov., a member of the family *Hyphomonadaceae* isolated from the bohai sea. *Int. J. Syst. Evol. Microbiol.* 69, 1794–1799. doi: 10.1099/ijsem.0.003394

frontiers | Frontiers in Marine Science

TYPE Original Research
PUBLISHED 03 June 2024
DOI 10.3389/fmars.2024.1373716

Check for updates

OPEN ACCESS

EDITED BY
Li Jianlon,
Shandong University, China

REVIEWED BY
Xianbiao Lin,
Ocean University of China, China
Xin Ming,
Ministry of Natural Resources, China

*CORRESPONDENCE
Junxiao Zhang
zhangjunxiao2021@163.com
Jibiao Zhang
zhangjb@gdou.edu.cn

RECEIVED 20 January 2024
ACCEPTED 20 May 2024
PUBLISHED 03 June 2024

CITATION
Liang H, Zhang J, Zhang J, Zhang P, Deng X, Chen J, Wang Z, Long C, Lu C, Wang D and Liang Y (2024) Unveiling the eutrophication crisis: 20 years of nutrient development in Zhanjiang Bay, China. *Front. Mar. Sci.* 11:1373716. doi: 10.3389/fmars.2024.1373716

COPYRIGHT
© 2024 Liang, Zhang, Zhang, Zhang, Deng, Chen, Wang, Long, Lu, Wang and Liang. This is an open-access article distributed under the terms of the Creative Commons Attribution License (CC BY). The use, distribution or reproduction in other forums is permitted, provided the original author(s) and the copyright owner(s) are credited and that the original publication in this journal is cited, in accordance with accepted academic practice. No use, distribution or reproduction is permitted which does not comply with these terms.

Unveiling the eutrophication crisis: 20 years of nutrient development in Zhanjiang Bay, China

Haorui Liang[1,2], Junxiao Zhang[1,2]*, Jibiao Zhang[3]*, Peng Zhang[3], Xue Deng[4], Jiyu Chen[1,2], Zhiliang Wang[1,2], Chao Long[5], Chuqian Lu[6,7], Di Wang[1,2] and Yuzhao Liang[1,2]

[1]South China Sea Marine Survey Center, Ministry of Natural Resources, Guangzhou, China, [2]Key Laboratory of Marine Environmental Survey Technology and Application, Ministry of Natural Resources, Guangzhou, China, [3]College of Chemistry and Environmental Science, Guangdong Ocean University, Zhanjiang, China, [4]State Environmental Protection Key Laboratory of Coastal Ecosystem, National Marine Environmental Monitoring Center, Dalian, China, [5]Marine Environmental Engineering Center, South China Sea Institute of Oceanology, Chinese Academy of Sciences, Guangzhou, China, [6]South China Sea Environmental Monitoring Center, State Oceanic Administration, Guangzhou, China, [7]Nansha Islands Coral Reef Ecosystem National Observation and Research Station, Hainan, China

Coastal eutrophication is a major issue of marine pollution. The main factors controlling eutrophication must be identified to ensure effective marine environmental management according to the respective local conditions. Zhanjiang Bay (ZJB), located northwest of the South China Sea, is a semi-closed bay influenced by complex water flows and the development of surrounding cities. In this study, we investigated the development of nutrient concentrations and compositions in ZJB seawater over the past 20 years and the factors influencing eutrophication based on several field investigations from 2006 to 2022 and historical data. High concentrations of dissolved inorganic phosphorus (DIP) and dissolved inorganic nitrogen (DIN) were the main contributors to the severe long-term eutrophication in ZJB; however, light eutrophication was observed in the outer bay, primarily caused by chemical oxygen demand (COD) and DIP. The primary sources of COD and nutrients were riverine freshwater, sewage outfalls, mariculture and domestic effluents carried by rivers. Tidal effects diluted the nutrient concentrations in the bay with seawater from the outer bay, thereby playing a key role in nutrient redistribution. The DIN: DIP ratio of ZJB showed long-term nitrogen restriction and excess phosphorus, primarily owing to mariculture activities. Marine undertakings can exert various impacts on water quality. Eliminating illegal aquaculture and launching aquaculture tailwater treatment can improve water quality, whereas practices such as channel dredging may worsen it. This study demonstrates the intricate dynamics of the ZJB ecosystem and offers valuable insights for effective environmental management and conservation efforts.

KEYWORDS

eutrophication, nutrient dynamics, annual variation, coastal, Zhanjiang Bay

1 Introduction

Nutrients such as nitrogen (N), phosphorus (P), and silicon (Si) are crucial components of marine environments that help sustain the health and ecological balance of marine ecosystems. Appropriate concentrations of nutrients in seawater promote the growth, development, and reproduction of organisms while also sustaining primary productivity in the ocean; however, an imbalance in nutrient concentrations and composition may lead to marked changes in marine ecosystems. For example, dissolved inorganic P (DIP) and dissolved inorganic N (DIN) are the most effective forms for phytoplankton uptake (Cotner and Biddanda, 2002). An excess or deficiency of either element can result in N or P depletion, thereby impeding the development of phytoplankton and influencing primary productivity. Moreover, excessive nutrient levels may cause significant phytoplankton blooms and high primary productivity, resulting in eutrophication, red tides, algal blooms, water hypoxia, and acidification (Wang et al., 2021a; Zhang et al., 2023a, 2023b). These factors can degrade the affected environments, directly threaten biodiversity and habitats, and cause massive mortality of marine organisms, ultimately harming marine ecosystems and human society (Deegan et al., 2012; Maúre et al., 2021; He et al., 2023).

In recent decades, increasing terrestrial anthropogenic inputs have substantially altered the nutrient structures of coastal waters (Howarth and Marino, 2006; Caffrey et al., 2007; Lin et al., 2021; Wang et al., 2021c; Lin and Lin, 2022). Excess nutrients lead to eutrophication in freshwater (Conley et al., 2009; Jiang et al., 2023; Qin et al., 2023) and marine systems (Howarth and Marino, 2006; Deegan et al., 2012, 2012; Ke et al., 2022), which is particularly evident in coastal waters near areas experiencing rapid urbanization and population growth (Wang et al., 2021c). Nutrients accumulate because of urban development, including sewage from agriculture, industry, farming. Increased N loading is a key driver of eutrophication in most coastal waters (Sinha et al., 2017; Ke et al., 2022). From 1900 to 2000, N discharge from rivers to global nearshore marine ecosystems increased by up to 18 Tg N/year (Beusen et al., 2016). Furthermore, it is worth noting that global P loading increased by 40%–50% between 1980 and 2015 (Beusen et al., 2022). Although the increasing trend has slowed owing to the implementation of P emission control policies (Howarth and Marino, 2006), coastal phosphate concentrations have markedly increased in recent decades because of human activities (Zhang et al., 2009; He et al., 2023). This increase is expected to have a profound impact on N and P cycling in marine ecosystems, thus threatening biogeochemical cycles and exacerbating eutrophication in coastal ecosystems.

For decades, Zhanjiang Bay (ZJB), China, has been severely affected by rapid urban development, resulting in ecological degradation and increased eutrophication (Li et al., 2014, 2020; Zhang et al., 2021; Lao et al., 2022). The nutrient levels in ZJB have increased because of direct discharge from sewage outfalls along the coast, including agricultural, industrial and domestic effluents. Human activities reduce river discharge, increasing the intrusion of external seawater from the outer bay towards the north (Lao et al., 2022). ZJB is mainly connected to the external sea through a narrow channel in the southeastern region, resulting in low hydrodynamics and poor exchange of water masses and nutrients between the inside and outside of the bay, which has led to the deterioration of water quality in the bay (Zhang et al., 2021; Lao et al., 2022). Numerous studies have focused on the sources, distribution, and eutrophication levels of various nutrients in ZJB; however, comprehensive long-term studies on the drivers of eutrophication in ZJB are limited.

This study investigated the interannual variation in nutrients and eutrophication levels in ZJB based on 18 cruise surveys conducted from 2006 to 2022 and combined with historical data. Furthermore, this study examined the main contributors to eutrophication in different regions of ZJB. Additionally, the effects of tidal action, biochemical processes, and urban development in the ZJB over the past 20 years on nutrient structure and water quality were analyzed. This study presents long-term basic survey data and addresses critical issues related to the marine environment in ZJB, including (1) changes in nutrient structure and composition over an extended period; (2) differences between the various regions, such as the freshwater end-member and the seawater end-member, on nutrient composition in a typical semi-closed bay; and (3) identifications of the main factors contributing to seawater eutrophication in the various regions. Elucidating these aspects will provide theoretical and empirical support for ecological preservation and environmental management of ZJB as well as critical information for assessing and managing coastal ecosystems worldwide.

2 Materials and methods

2.1 Study area

ZJB is a semi-closed bay in the northwest South China Sea, covering an area of approximately 300 km^2, and is surrounded by Zhanjiang City, Nanshan Island, and Donghai Island on its west, east, and south boundaries, respectively. As an important mariculture area in the South China Sea, over 25% of the sea area of ZJB are covered by open mariculture (such as oysters and fish) to enclose the sea and cultivate (seafood species such as shrimp). The bay experiences a subtropical oceanic monsoon climate (Zhou et al., 2020) with a water retention time of approximately 10 days (Shi et al., 2020). ZJB is fed by several rivers; the northern Suixi River is the primary source of freshwater with a runoff of 7.9×10^9 m^3/yr, accounting for over 90% of the total river inflow in the bay (Li et al., 2021). Additionally, the discharge of land sewage is approximately 1.5×10^8 m^3/yr (Li et al., 2021), accounting for less than 2% of river runoff. The injection of sewage, mariculture, and river water introduces considerable amounts of nutrients and pollutants, leading to a substantial terrestrial pollution burden (Fu et al., 2020).

Based on geographical features, there have been three mouths around the bay historically (Figure 1). The first location is to the north, between Nansan Island and the Potou Zone, leading to the mouth of the Jian River. The narrowest part of the path on the side of the ZJB is approximately 500 m wide. The waters of the upper

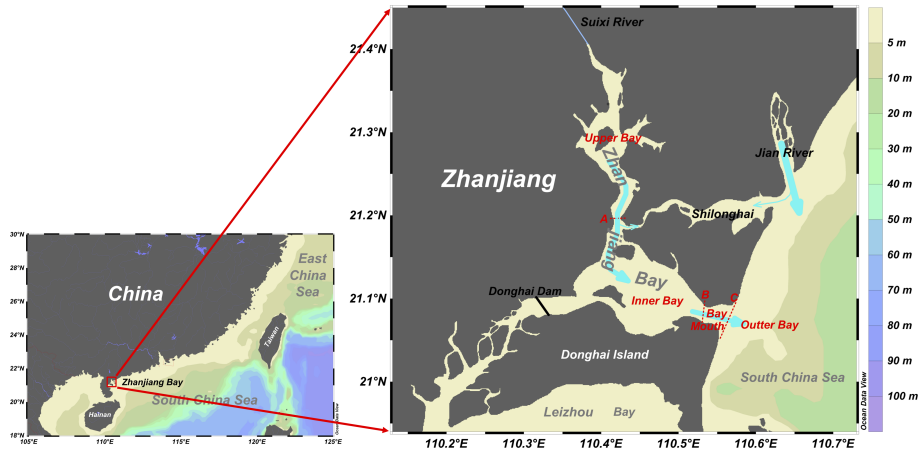

FIGURE 1
Map of ZJB and its geographical features. The red dashed lines with the red letters A, B, and C are the borders of the various sections in ZJB.

ZJB and the Jian River meet in this narrow and shallow waterway, named Shilonghai, resulting in minimal water exchange through this narrow bay mouth. The second location is situated to the southwest, between Zhanjiang City and Donghai Island, and connects to Leizhou Bay to the south; however, the construction of the Donghai Dam in the late 1960s halted the water exchange between the ZJB and Leizhou Bay. The third location is to the east, between the Nansan and Donghai Islands, and is directly connected to the South China Sea, which is the most critical water exchange channel between ZJB and the outer seawater.

In ZJB, tides and tidal currents are primarily irregular semi-diurnal tides after the Pacific tidal waves enter the South China Sea (Zu et al., 2008). These tides are influenced by the ZJB terrain, resulting in complex variations in tidal rise and fall around the bay. Based on the mixing effect of upstream freshwater and outer seawater, as well as the nutrient distribution characteristics, ZJB is divided into four parts: the upper bay, inner bay, bay mouth, and the outer bay (Figure 1). The upper bay can be described as the "neck" of the ZJB, as the channels narrow upstream from south to north, concentrating the energy following tidal influx and increasing the upstream tidal range, hence increasing the tidal capacity (Wang et al., 2021b). Freshwater from Suixi River flows into the inner bay mostly through this narrow channel. The inner bay is markedly impacted by surrounding ports, fisheries, and aquaculture, resulting in complex physical and biochemical processes. The average water depth is approximately 10 m, except in the Zhanjiang Port Channel area, which has been dredged to over 20 m depth. During neap tide, some areas may be exposed to the lowest tidal level of approximately 4 cm. The bay mouth exhibits a narrow tube effect, resulting in exceptionally high flow velocity and flow rate during both ebb and flood tides, showing reciprocal motion (Zhang et al., 2017); however, the small width (only approximately 2 km) complicates the export of nutrients and pollutants from within ZJB through the bay mouth. The outer bay is a section of the South China Sea that interacts with the interior of the ZJB, primarily through tidal movement. During flood tide, external seawater intrudes into the bay, and mixed water flows out of the bay during ebb tide.

2.2 Field survey and data collection

The average yearly hydrological, nutrient, and other parameter data for ZJB were obtained from Lu et al. (2002) for 1998 to 2001 and from Zhang et al. (2009) for 2002 to 2006. The data for August 2007 and quarterly survey data for 2019 were obtained from Cheng et al. (2009) and (Zhang et al., 2020b; Zhang et al., 2021), respectively. In addition, 18 field surveys were conducted in ZJB from 2006 to 2022, as shown in Table 1, and detailed sampling stations are shown in Supplementary Figure S1. Surveys were conducted during high tide (spring tide) and low tide (neap tide) in March 2008, August and November 2010, April 2013, January, March, and June 2014, and March 2021, to explore the influence of tides on nutrients and other substances. The year is divided into four seasons based on temperature variations: spring (March-May), summer (June–August), autumn (September–November), and winter (December–February) (Zhou et al., 2020).

Water samples were collected by using a 10 L plexiglass sampler, from the surface layer (0.5–1.0 m below the surface) and the bottom layer (2.0 m above the bottom if water depth exceeded 10 m). Seawater samples were analyzed according to "The specification for marine monitoring - Part 4: Seawater analysis" (GB 17378.4–2007), which was promulgated by the China National Standardization Management Committee. Immediately after the sample was boarded, the temperature was measured using a thermometer at an accuracy of 0.1 °C. Subsequently, dissolved oxygen (DO) samples were collected, preserved using manganese chloride and alkaline potassium iodide solutions, and titrated within 24 h using the Winkler method. Samples for measuring nutrients, such as phosphate, nitrate, nitrite, and ammonia, were filtered through acid-cleaned 0.45 μm acetate cellulose filters and stored at -20°C until laboratory analysis through spectrophotometry. Salinity and

TABLE 1 Data sources.

Year	Month	Number of stations	Tidal Investigation	Resources
1998–2001	–	Average value		(Lu et al., 2002)
2002–2006	–	Average value		(Zhang et al., 2009)
2006	May	8		This study
2007	August	15		(Cheng et al., 2009)
2008	March	20	√	This study
2010	August November	20 20	√	This study
2013	April November	20 20	√	This study
2014	January March June	23 32 23	√ √ √	This study
2016	March	20		This study
2017	April	23		This study
2019	January April June November	23 32 24 24		(Zhang et al., 2020b, 2021)
2020	August November	24 24		This study
2021	January March July November	21 21 21 21	√	This study
2022	January	21		This study

chemical oxygen demand (COD) samples were collected in 250 mL plastic bottles and stored at room temperature. Salinity was measured using a conductance salinity meter, and the COD concentration was titrated using alkaline potassium permanganate.

2.3 Eutrophication level

The eutrophication level in ZJB was determined based on the concentrations of COD, DIN, and DIP in the water. The commonly used eutrophication index (EI) was employed (Andersen et al., 2017; Ke et al., 2022; He et al., 2023), as shown in Equation 1.

$$EI = \frac{COD \times DIN \times DIP}{4500} \times 10^6 \quad (1)$$

where the units of COD, DIN, and DIP are expressed in $mg{\cdot}L^{-1}$. Generally, when EI<1, the water is not eutrophic; the water is eutrophic when EI>1: ① 1≤EI<2: light eutrophication; ② 2≤EI<5: moderate eutrophication; ③ 5≤EI<15: high eutrophication; ④ EI≥15: severe eutrophication.

To improve water quality, it is essential to clarify the main factors controlling water eutrophication; however, when considering the three primary parameters that affect water eutrophication, COD typically has a magnitude of 1, whereas DIN and DIP typically have magnitudes of 0.1 and 0.01, respectively. Therefore, it is difficult to accurately calculate the contribution of different parameters to the eutrophication level, owing to the large order of magnitude in differences. In Equation 1, 10^6 is a constant introduced to balance the order of magnitude difference of different parameters, and 4,500 is an empirical constant to judge the state of eutrophication. Therefore, a scientific counting method was used to express each parameter in Equation 1, ensuring that the significant numbers were of the same order of magnitude. The orders of magnitude of COD, DIN, and DIP were unified, as described by Equation 2:

$$EI = \frac{COD \times DIN' \times 10^{-1} \times DIP' \times 10^{-2}}{4500} \times 10^6 \quad (2)$$

This was then simplified into Equation 3:

$$EI = \frac{COD \times DIN' \times DIP'}{4.5} \quad (3)$$

In this formula, COD, DIN', and DIP' have the same order of magnitude and are all 1. The change in each parameter directly determines the change in the final EI, which directly reflects their contribution to the level of eutrophication.

2.4 Term definitions

Apparent oxygen utilization (AOU) represents the discrepancy between the actual measured DO concentration and air-equilibrated concentration under the same physical and chemical conditions (Benson and Krause, 1984). The AOU was calculated according to the modified expression (Equations 4–6) by Garcia and Gordon (1992):

$$AOU = DO_{saturated} - DO_{observed} \quad (4)$$

$$\ln DO_{saturated} = A_0 + A_1T_s + A_2T_s^2 + A_3T_s^3 + A_4T_s^4 + A_5T_5^2 + S(B_0 + B_1T_s^2 + B_2T_s^2 + B_3T_s^3) + B_1T_s^2 + C_0S^2 \quad (5)$$

$$T_s = \ln[(298.15 - t)/(273.15 + t)] \quad (6)$$

where A_i, B_i, and C_0 are constants that can be found in Garcia and Gordon (1992); T_s is scaled temperature, and t is temperature in °C; S is seawater salinity. When AOU values exceed zero, the aquatic ecosystem experiences a net loss of oxygen owing to community respiration. Conversely, negative AOU values suggest a net gain in oxygen, indicative of community production processes.

To minimize the effect of salinity on nutrient distribution in the seawater of ZJB, salinity-normalized nutrients (N-nutrients) were calculated using Equation 7:

$$N - nutrient = Nutrient \times AverageSalinity/Salinity_{observed} \quad (7)$$

where the nutrient could be any type of nutrient, such as nitrate and phosphate; the average salinity was 27.4 during all surveys.

2.5 Static analyses

The field survey data were first cleaned and formatted to remove erroneous or incomplete records and ensure that the data were consistent in terms of units. Linear regression analysis was used to analyze the relationships between nutrient concentrations and environmental variables. One-way analysis of variance with Tukey's test was used to examine significant differences. Correlation analyses were performed using a significance level of $p < 0.05$.

A map of the study area with the spatial distribution of all parameters was generated using Ocean Data View 4.7.8, using the weighted-average gridding interpolation method (Reiner, 2021). Curves and plots of the historical changes and relationships between nutrients were produced using Data Graph 5.0 (Visual Data Tools, Inc.).

3 Results

3.1 Hydrological characteristics

Over the past two decades, substantial seasonal changes have been observed in the temporal distribution of seawater temperature and salinity in ZJB. Seawater temperatures varied from 17.9–32.1°C (n = 486) in the spring to 25.9–34.3°C (n = 202) in the summer. In fall, the temperatures dropped to approximately 20.4–31.8°C (n = 277) and reached their annual minimum in winter, approximately 15.7–24.8°C (n = 195). Salinity varied from 8.6–33.1 (mean 27.5 ± 0.2) in spring to 8.4–33.4 (mean 27.9 ± 0.3) in summer, 13.5–30.1 (mean 26.0 ± 0.1) in autumn, and 16.8–31.4 (mean 28.8 ± 0.2) in winter.

Regarding spatial distribution, sea temperature in various regions of ZJB exhibited minimal variation across the four seasons, primarily influenced by seasonal and climate changes. In contrast, seawater salinity displayed distinct spatial distribution characteristics in different regions during the same season (Figure 2A). In the upper bay, the main freshwater end-member of the ZJB, seawater salinity decreased during spring and summer but increased during autumn and winter. The difference in seawater salinity in spring and summer exceeded 20 but dropped to approximately 10 in autumn and winter (Figure 2B); however, in other areas of ZJB, the salinity difference between the maximum and minimum values was minimal. Overall, salinity in the inner bay was lower than that at the bay mouth, whereas the outer bay exhibited the highest salinity. Seasonally, salinity was highest in winter, followed by spring, and was lowest in autumn. In addition, the surface and bottom water exhibited similar characteristics in terms of temperature and salinity distributions.

3.2 Interannual variations of main water quality parameters

3.2.1 Nutrient variations

Over the past 20 years, the nutrient concentrations in ZJB have undergone pronounced temporal and spatial changes. The temporal distributions of DIN and DIP in ZJB showed similar characteristics (Figures 3A, B). From 1998 to 2001, the mean concentrations of DIN and DIP remained stable, at 0.287 ± 0.033 mg·L^{-1} and 0.025 ± 0.008 mg·L^{-1}, respectively (Lu et al., 2002). Subsequently, the DIN and DIP changed periodically over time. Since 2001, DIN and DIP concentrations have increased. DIN reached 0.823 mg·L^{-1} in 2005, and DIP reached its maximum of approximately 0.077 mg·L^{-1} in 2007. Then, DIN and DIP began to decrease, with an average of 0.252 mg·L^{-1} and 0.030 mg·L^{-1} in 2008, respectively. The concentration of both compounds continued to increase until 2010, when DIN and DIP were 0.500 mg·L^{-1} and 0.089 mg·L^{-1}, respectively. After that, DIN and DIP decreased to their lowest values in 2013–2014, with an average of 0.125 mg·L^{-1} and 0.012 mg·L^{-1}, respectively. Both concentrations increased again, reaching a peak in 2017, and remained relatively stable with little change until 2020. In 2021, DIN and DIP decreased to 0.435 mg·L^{-1} and 0.027 mg·L^{-1} but increased again to 0.768 mg·L^{-1} and 0.055 mg·L^{-1} in 2022, respectively.

The spatial distribution of nutrient concentrations in ZJB was mapped horizontally for 16 years, from 2006 to 2022, using available historical and survey data (Supplementary Figures S2, S3). The concentrations of nutrients in ZJB exhibited interannual variation, with the highest values observed in the northern upper bay, followed

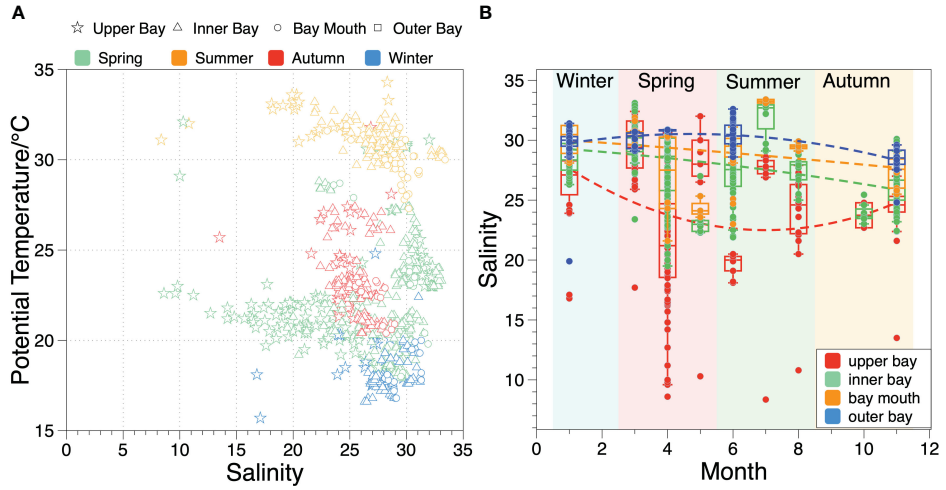

FIGURE 2
Potential temperature and salinity variations in ZJB in the last two decades. **(A)** relationship between potential temperature and salinity of ZJB in different seasons, the symbols indicate different regions, and the colors indicate different seasons; **(B)** the variation of salinity in each section of ZJB during different seasons, and different colors represent different regions of the bay.

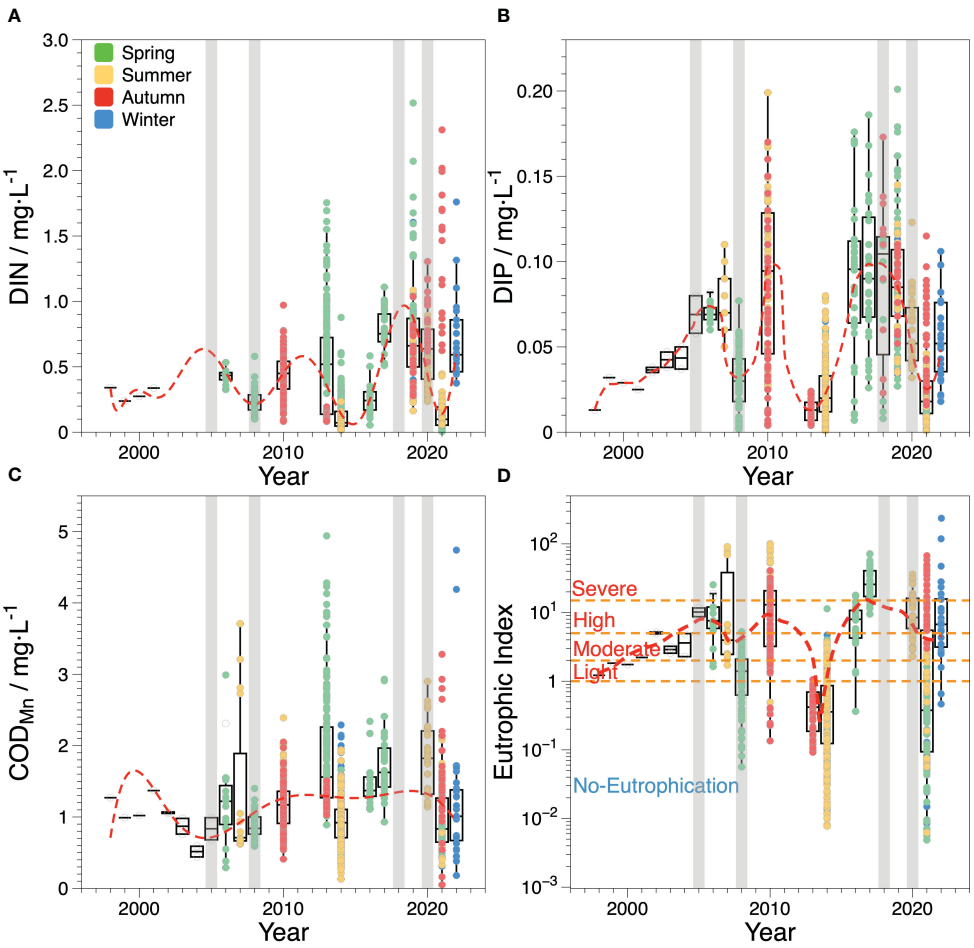

FIGURE 3
Box-and-whiskers plot (with IQR) showing the median and IQR measurements of annual variation of main water quality parameters in ZJB during the last two decades. The different colors of the points in **(A–C)** indicate the investigation seasons and the red dashed lines indicate the approximate trend of each parameter. The orange dash lines in **(D)** represent the critical values for each eutrophication level. The gray areas indicate the period of major marine engineering activities in ZJB.

by the inner bay, and the lowest values in the outer bay. In a narrow waterway where the upper bay water meets the inner bay water, a large amount of water with a high nutrient concentration from the upper bay immerses into the inner bay. Furthermore, the seawater exchange between the inner and outer bays caused outward output or inward invasion during different periods, particularly in the horizontal distribution of DIP in 2014 and 2017.

3.2.2 Composition changes of inorganic nitrogen

Over the past two decades, there have been changes in the composition and structure of inorganic nitrogen in the seawater of ZJB (Figure 4). From 2006 to 2013, the concentration of ammonia, similar to that of nitrate, was relatively high. In 2013, the average concentration of ammonia in seawater was as high as 0.217 mg·L^{-1}, which was higher than that of nitrate in the same period (0.142 mg·L^{-1}). Additionally, the ammonia concentration in the upper bay was higher than that in the other bay areas. Since 2013, nitrate concentrations have increased significantly, whereas ammonia and nitrite concentrations have remained stable. Nitrate was consistently the most abundant compound in ZJB, followed by ammonia, with nitrite being the least abundant. The nitrate concentration increased in the upper and inner bays, except for a significant decrease in 2021. In contrast, the nitrate concentration in the bay mouth and outer bay increased significantly to over 0.6 mg·L^{-1} in 2017, following low levels between 2013 and 2016. Subsequently, the concentration steadily decreased.

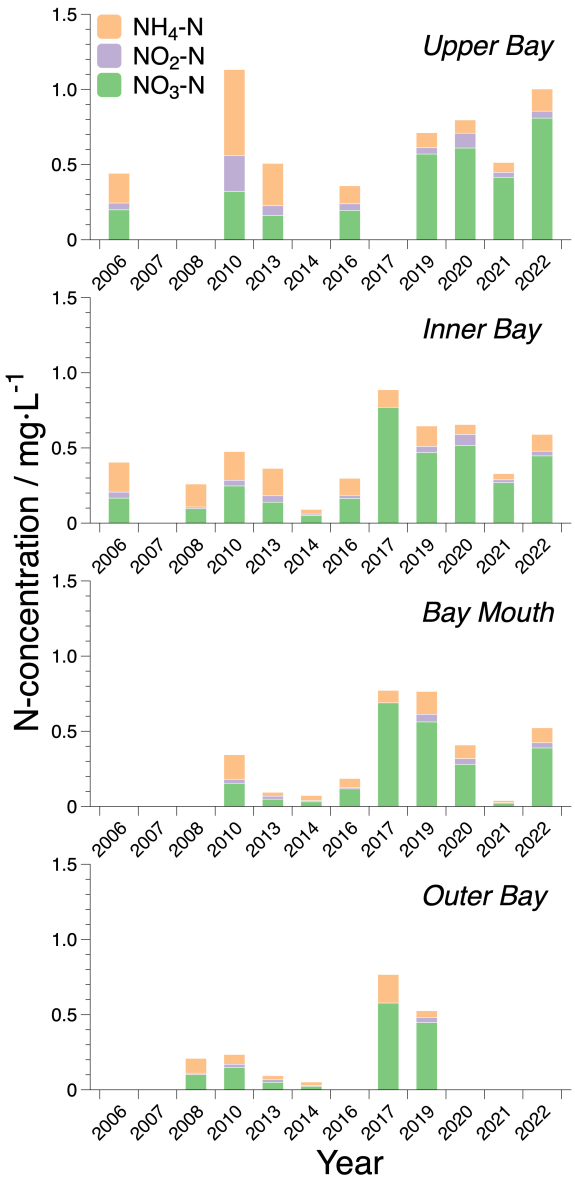

FIGURE 4
Interannual variation composition variations of different nitrogen components in different regions of ZJB.

3.2.3 COD

From 1998 to 2005, the average concentration of COD in ZJB varied from 0.87 to 1.37 mg·L^{-1} (Lu et al., 2002; Zhang et al., 2009). Except for 2003, when the COD concentration was the lowest, the COD concentration changed little and fluctuated around 1 mg·L^{-1} in other periods. After that, the average concentration of COD ranged from 0.79 ± 0.21 mg·L^{-1} to 1.87 ± 0.81 mg·L^{-1} between 2006 and 2022 (Figure 3C). Although the average COD concentration in ZJB has not changed substantially in the past 20 years, there were some seasonal differences. During the same period, the COD was highest in spring, followed by summer, and was lowest in autumn and winter. Especially in the spring of 2013, COD was as high as 4.94 mg·L^{-1} in some areas and exceeded 3 mg·L^{-1} in most areas. In addition, COD decreased significantly in 2021, with an average of 0.79 ± 0.21 mg·L^{-1}, which is approximately only half of the average concentrations of 1.62 ± 0.49 mg·L^{-1} and 1.78 ± 0.56 mg·L^{-1} in 2017 and 2020, respectively.

3.2.4 Eutrophication level

From 1998 to 2004, eutrophication levels in ZJB ranged from light (1≤E<2) to moderate (2≤E<5) (Figure 3D). The eutrophication level increased between 2005 and 2007, intensifying from south to north. Some regions even experienced severe eutrophication during this time. In 2007, waters in the upper and inner bay areas exhibited severe eutrophication. As eutrophication was gradually reduced from the inner bay to the outer bay, the bay mouth area was essentially at a mild eutrophication level (Supplementary Figure S4). Eutrophication began to improve in 2008; however, in 2010, eutrophication rapidly deteriorated, with most areas experiencing high or severe eutrophication, similar to 2007. Water quality improved once more between 2013 and 2014, and most areas were no longer affected by eutrophication, except for some areas in the upper bay that experienced light eutrophication. From 2016 to 2022, ZJB experienced prolonged periods of high or severe eutrophication, with the exception of 2021, when water quality improved and became non-eutrophic in most locations. Severe eutrophication was mainly observed in the northern upper bay during each period, whereas moderate eutrophication was observed in the inner bay.

Overall, the water quality of ZJB showed a horizontal distribution of steady improvement from north to south, with similar surface and bottom distributions. Eutrophication was the most serious in the upper bay area, followed by the inner bay area, and the water quality outside the bay was generally acceptable.

4 Discussion

4.1 Eutrophication contributors

Seawater eutrophication in ZJB has been severe for a long time owing to diverse reasons in different regions (Figure 5). In the upper bay, the northernmost Suixi River carries large amounts of inorganic (including nutrients such as N and P) and organic (such as organophosphorus compounds, organic acids, and aldehydes) matters into ZJB, together with nutrients discharged from mariculture activities, leading to high concentrations of COD, N, and P (Lao et al., 2022) and long-term eutrophication, with the contribution of DIN being the largest, followed by DIP, and COD contributing the least (typically<30%; Figure 5A). Typically, phosphate and ammonia are strongly associated with urban catchments, whereas nitrate in rivers is correlated with the quantity of cultivated land in the surrounding areas (Ferrier et al., 2001). Thus, the increased use of N fertilizer in land-based farming and aquaculture contributes more than 70% of the DIN in the watershed of ZJB (Zhou et al., 2021). Eutrophication increased significantly when multiple sources and high concentrations of DIN contributed more than 40% in the upper bay. The acceleration of DIN further worsened the eutrophication. Nevertheless, as the DIP contribution increased and exceeded 60%, a decrease in DIN over the same period (Figure 3) led to an increase in the DIP contribution, resulting in a general decrease in eutrophication to moderate or mild levels. Furthermore, the increased and seasonal variations in activities, such as agricultural production and mariculture in ZJB (Zhang et al., 2022), had a significant impact on land-based inputs of DIP and DIN, resulting in the highest contribution of DIP in spring, followed by summer, and the lowest in autumn, with the opposite pattern for DIN. It should be mentioned that even with 20%–40% COD contributions, the water was typically not eutrophic during spring and summer when DIN contributions were comparatively low. This phenomenon reflects the high contribution of COD, which corresponds to a decrease in the DIN levels. Eutrophication levels increased as COD contributions decreased and DIN contributions increased. Thus, DIN is the primary factor contributing to elevated eutrophication levels in the upper bay region and is the most significant contributor to marine eutrophication (Balasuriya et al., 2022).

In the inner bay, the water quality was predominantly non-eutrophic when the COD contributions exceeded 20%, similar to that in the upper bay; however, the pattern was different when the COD contribution decreased to below 20%. The contributions of

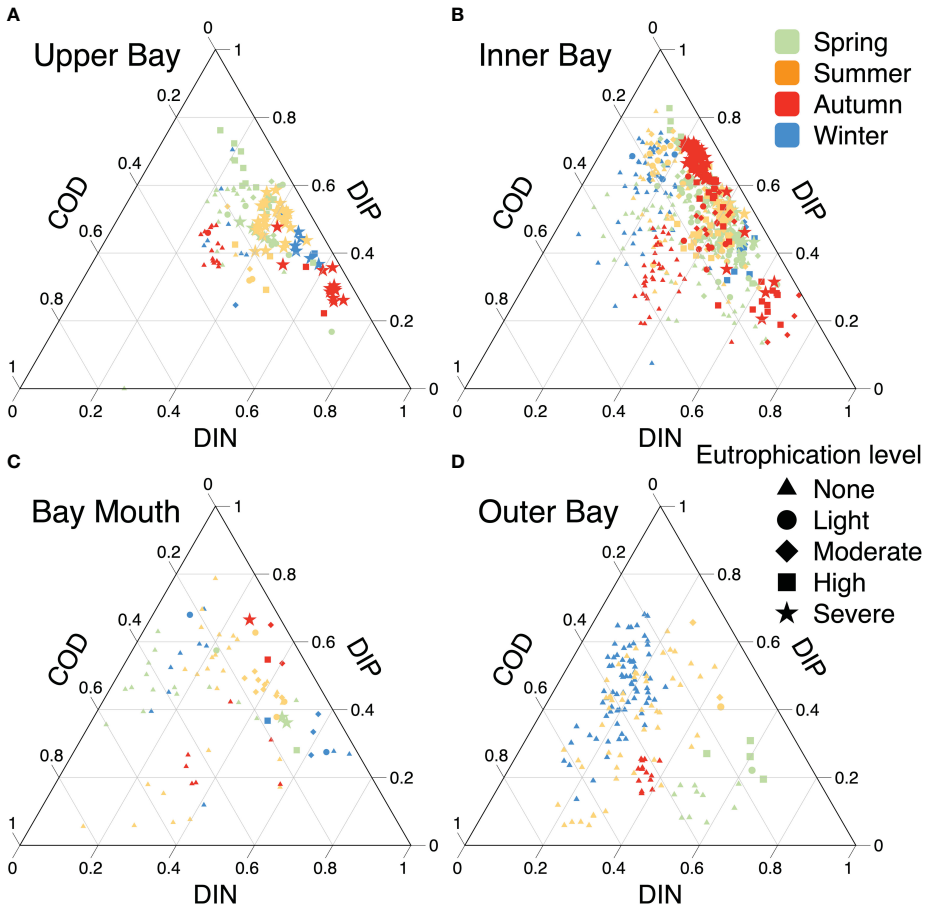

FIGURE 5
The contribution of water quality parameters to the variation of eutrophication level in different regions of ZJB. **(A–D)** represent the upper bay, inner bay, bay mouth and outer bay, respectively. Seasons are indicated by different colors. The symbols represent the different eutrophication levels in the ZJB, and the triangle with "none" indicates that seawater is not eutrophic.

DIN and DIP to the inner bay did not exhibit significant seasonal trends. The level of eutrophication in the inner bay was directly proportional to the concentrations of DIN or DIP, and an increase in either nutrient worsened eutrophication. This was because in addition to the waters from the upper bay, industry, aquaculture, harbor inputs, and seawater from outside the ZJB also affect the inner bay area, as do other minute inlets. This is similar to Lake Mendota and Lake Monona in Wisconsin, USA, where high concentrations of P driven by runoff from farmland and urban areas lead to eutrophication (Carpenter, 2008). Therefore, the inner bay area is less susceptible to seasonal changes in runoff than the upper bay. Consequently, the inner bay area experienced more severe and prolonged eutrophication. Moreover, when the DIN and DIP contributions are comparable, the eutrophication level is relatively mild owing to the lower levels of additional nutrients from anthropogenic discharges combined with a stable water quality environment that maintains N and P in a steady state; however, excessive terrestrial N or P discharge can lead to severe eutrophication. Therefore, DIN and DIP in the inner bay are crucial factors that lead to eutrophication.

There was no significant difference in the eutrophication level at the bay mouth because it mainly served as a water exchange channel between the inner and outer bays; however, the outer bay was significantly different from the upper and inner bays because the contribution of DIN was relatively low (<40%) and the water was not eutrophic. COD and DIP dominated the eutrophication level in the outer bay, which was consistent with the water adjacent to Hainan Island (Zhang et al., 2020a). Eutrophication increased as the contribution rate of DIN increased, indicating that DIN may be the main contributor to eutrophication.

Overall, DIN and DIP were the main controlling factors leading to eutrophication in ZJB, but the key contributors varied by area and time period. Water quality management also needs to adapt to local conditions.

4.2 Impact of hydrodynamics on annual nutrient variation

Tidal currents drive the movement of water masses, facilitating the mixing of nutrient-rich freshwater with external high-salinity seawater (Lao et al., 2022). This mixing helps redistribute nutrients throughout the bay. The analysis of nutrient variations over different seasons during high and low tides across multiple years depicted unique patterns across diverse regions of ZJB.

The results indicated that in the upper bay, DIN and DIP levels were higher during low tide in the wet season (such as summer), but higher during high tide in the dry season (such as spring) (Figure 6). This may be attributed to the complex topography of ZJB, which has a significant impact on tidal flows. During high tide, the upper bay channel narrows, causing tidal energy to accumulate (Wang et al., 2021b) and resulting in high-salinity seawater entering the upper reaches and mixing with nutrient-rich freshwater (Lao et al., 2022). During low tide, high-nutrient water is reenergized through narrow channels and enters the inner bay, where it is thoroughly mixed. This tidal movement increases the nutrient content, resulting in the upper bay having a lower nutrient content at high tide than at low tide. The inner bay is a vital mixing zone, receiving low-salinity and high-nutrient water from the upper bay and high-salinity and low-nutrient water from the outer bay. In addition, the discharge of domestic and industrial effluents and port activities introduce a considerable amount of nutrients, thus the tidal influence on the inner bay is minimal compared to that on the upper bay. Moreover, the inner bay plays an important role in water exchange, with little variation in nutrient concentrations throughout the tidal cycle because of the rapid flow, short water residence time, and high turbulent diffusion; however, the outer bay experiences pronounced nutrient peaks throughout the year at low tide, particularly in autumn, because of the concentration of tidal energy in the narrow structure at the bay mouth, which promotes continuous water exchange between the inner and outer bays. Owing to continuous tidal action, a large amount of nutrient-rich water is transported out of the bay at low tide, resulting in long-term higher nutrient concentrations in the outer bay at low tide than at high tide.

4.3 Terrigenous input contributes to eutrophication

The water quality in ZJB is primarily influenced by two sources: freshwater from the Suixi River in the northern upper bay and high-salinity seawater in the southeastern outer bay. This can be observed from the spatial and temporal variations of salinity in ZJB (Figure 2), which gradually increases from the upper bay to the outer bay. The variations in DO and salinity in ZJB showed similar characteristics, but COD showed the opposite trend, with low-salinity zones typically corresponding to low DO and high COD (Figure 7). The COD levels in the ZJB waters show interannual variations similar to those of domestic sewage, mariculture, and industrial wastewater discharges (Zhang et al., 2022). Elevated COD levels in seawater indicate the presence of organic matter inputs that consume oxygen during decomposition, resulting in low DO levels. This situation is expected to improve gradually with the injection of external seawater.

Owing to the escalating annual intrusion of high-salinity seawater from the outer bay, seawater from outside the bay continuously infiltrates the upper bay (Lao et al., 2022). Consequently, diluted freshwater from the Suixi River only accounted for approximately 7% in summer, whereas high-salinity seawater from the outer bay continued to dominate, accounting for approximately 89%. In addition, reduced runoff resulted in diminished input from upstream rivers in autumn and winter, with river water accounting for only approximately 1%, and the intrusion of high-salinity seawater from outside the bay increasing to approximately 94% (Li et al., 2020), resulting in high salinity of approximately 25–30 throughout the interior of ZJB, with no apparent low-salinity zones in the upper bay. Although hypersaline water intrusion from the outer bay has long dominated ZJB, the contribution of nutrients from freshwater (ranging from 54% to 90%) remains significantly higher than that from the outer bay (ranging from 18% to 45%) (Lao et al., 2022). This discrepancy

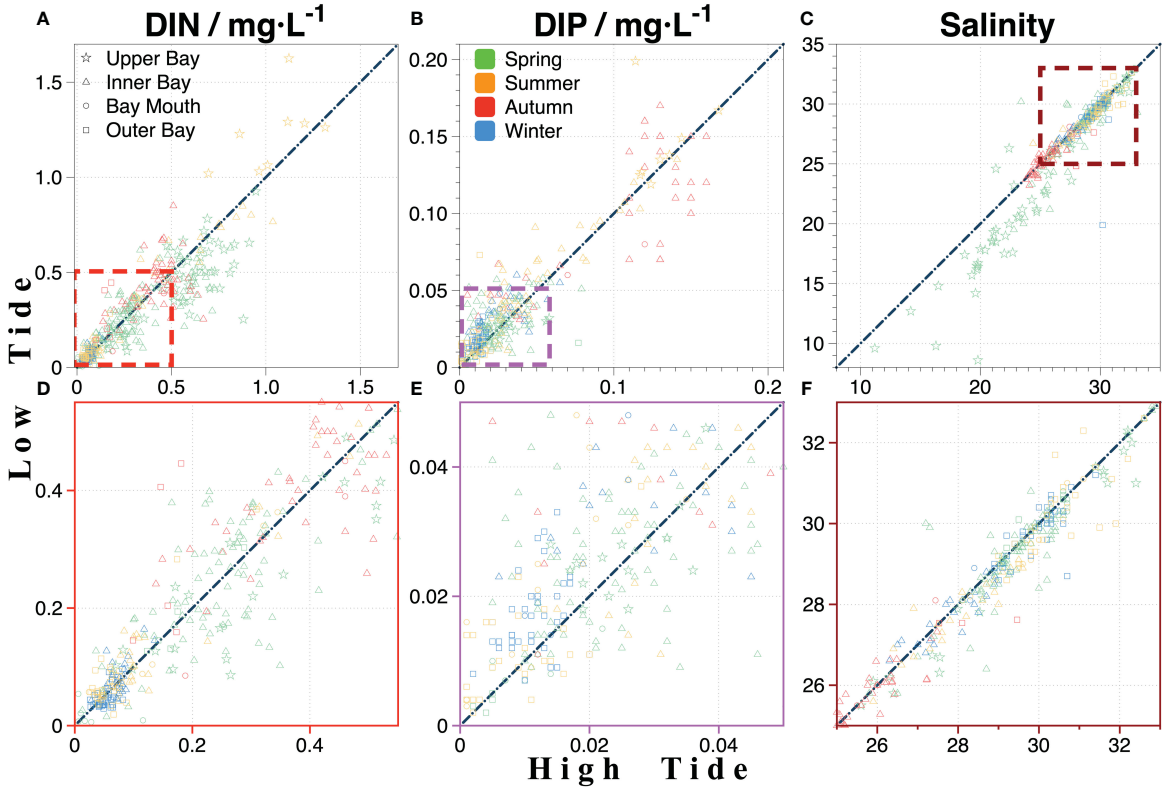

FIGURE 6
Tidal influence on the nutrient variation in ZJB; **(A–C)** are the variation of DIN, DIP, and salinity during high tide and low tide, respectively; **(D, E)** are the magnification diagram of DIN and DIP in **(A, B)** at concentrations below 0.5 and 0.05, respectively; **(F)** is the magnification diagram of salinity variation between 25 and 33.

is primarily attributed to the Suixi River, which carries pollutants such as agricultural runoff, domestic sewage, and industrial effluent into the bay (Zhang et al., 2021; He et al., 2023), thus influencing the nutrient composition and water quality of ZJB.

In recent decades, DIN and DIP concentrations in ZJB have been negatively correlated with salinity (Figure 7), comparable to those in Tokyo Bay (Aoki et al., 2022). The primary sources of nutrients in ZJB are inputs from upstream rivers, discharge of industrial and domestic wastewater (Zhang et al., 2021), and mariculture activities in the bay (Li et al., 2020). Consequently, the nutrient levels in the bay were markedly higher than those in the seawater outside the bay. Changes in DIP levels in ZJB over the past two decades (Figure 3B) are generally consistent with changes in P fertilizer use (He et al., 2023), suggesting that upstream agricultural production is a major source of DIP in the bay; however, P discharge from agricultural production is decreasing because of the implementation of P restriction policies and the promotion of P-free products (Li et al., 2019). In 2010, the DIP levels were significantly higher in the inner bay than in the upper bay because of the transport of large amounts of phosphate from various factories and sewage discharge points (Zhang et al., 2021). In addition, DIN levels in ZJB are mainly caused by the discharge of urban agricultural fertilizers and industrial and domestic wastewater (Li et al., 2020; He et al., 2023; Zhang et al., 2023a), which is consistent with other offshore waters such as the Black Sea (Alkan et al., 2022), the Chinese coast (Wang et al., 2020) and the Elbe estuary in Germany (Dähnke et al., 2008). Freshwater runoff is the primary source of terrestrial DIN in the upper bay, with N fertilizer and soil N contributing approximately 70%, and sewage and feces contributing the remaining 30% (Li et al., 2020). Studies have identified the use of N fertilizers as a leading cause of biodiversity loss (Guignard et al., 2017). When these fertilizers are translocated into nearby creeks, they can trigger eutrophication in the affected water bodies, which can further exacerbate eutrophication in the inner bay region after mixing with inner bay waters. Therefore, when water with high concentrations of DIN and DIP in the upper bay mixes with the water in the inner bay, these nutrients can worsen the eutrophication problem in the inner bay, resulting in a decline in water quality and harm to the ecosystem.

4.4 Biological processes

N and P are essential biogenic elements in seawater. With carbon, they constitute the marine carbon and nitrogen cycles. During photosynthesis, phytoplankton absorb inorganic N and P at a constant ratio of 16:1, which is known as the Redfield ratio (Gruber and Deutsch, 2014). The Redfield ratio is commonly used to identify the limiting nutrient elements of marine productivity

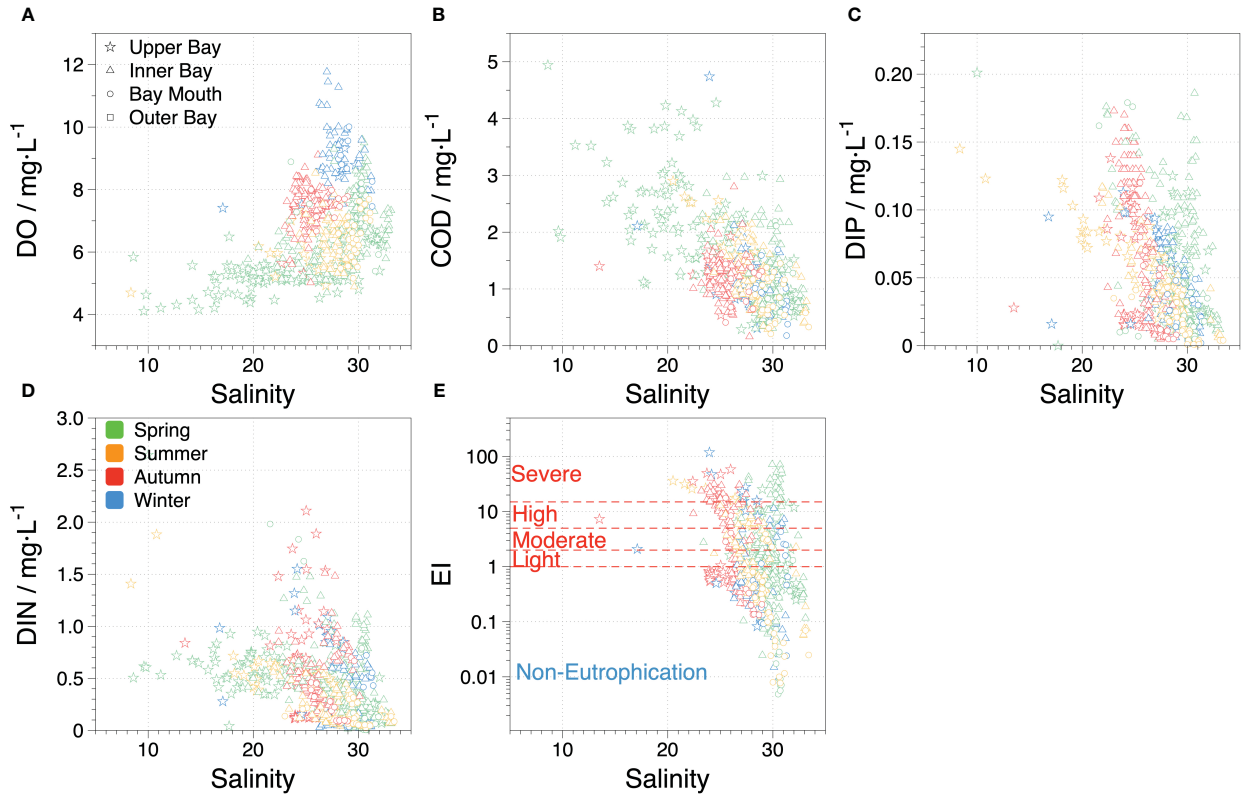

FIGURE 7
Effects of terrestrial inputs and physical mixing on nutrient variations; **(A, B)** indicate the relationships between DO, COD, and salinity in ZJB, respectively. **(C, D)** indicate the relationships between nutrients and salinity in ZJB, respectively. **(E)** indicates the relationship between eutrophication and salinity in ZJB. The colors indicate different seasons, and the symbols indicate the different areas in the ZJB.

(Peñuelas et al., 2013); however, the 'Redfield Sea' is unlikely to be in a steady state, with N-fixing organisms in seawater having lower maximum growth rates owing to the greater energetic cost of breaking the N_2 triple bond by N fixation. This results in the formation of nitrate-limited waters, and hence, seawater N limitation must be more severe than P limitation (Tyrrell, 1999); this difference can also be seen in the characteristics of long-term changes in DIN: DIP in the open ocean such as the Pacific and Indian Oceans (Olsen et al., 2016) (Figure 8). Over the last 20 years, ZJB has mostly experienced DIN: DIP ratios below 16, indicating severe nitrogen limitation, which is consistent with China's coastal mariculture zones (DIN: DIP of approximately 7–11) (Feng et al., 2024). However, this contrasts with the long-term P-limited state in nearshore areas (Figure 8), such as the South Yellow Sea (Chen et al., 2023), Pearl River Estuary (Yao et al., 2022), Chinese rivers (Feng et al., 2024), and offshore central Japan (Katazakai and Zhang, 2021). These coastal waters receive a substantial amount of nutrients from land inputs. N is significantly more abundant than P and frequently exceeds the aquatic carrying capacity, leading to a shift from weak oceanic N limitation to stronger coastal P limitation. Nevertheless, in contrast to other coastal regions, nearshore mariculture areas have developed distinct nutrient structures owing to anthropogenic interventions in mariculture activities and associated effluent discharge, despite also being influenced by land inputs. In mariculture, farmed organisms typically require more P than N, resulting in the amount of phosphorus fertilizer being typically higher than that of N fertilizer; however, excess fertilizer remaining in the water may have a negative impact on the nutrient structure of the mariculture area, leading to long-term N limitation. Therefore, P is continuously in excess during photosynthesis in ZJB, which indirectly explains why the correlation between DIP and AOU is not as significant as that between DIN and AOU (Figure 9).

In addition to photosynthesis, biologically active processes involving N and P (such as nitrification, denitrification, and heterotrophic and anaerobic oxidation of ammonia) are significantly influenced by various factors, with DO being one of the most significant. The seawater in ZJB was oversaturated with DO for a prolonged period according to the decadal negative concentration of AOU. AOU was lowest during winter (-5.26 ± 0.98 mg·L^{-1}) and highest in spring (-2.63 ± 1.18 mg·L^{-1}). The biological activities of ZJB are predominantly nitrification and photosynthesis because adequate DO in water prevents denitrification. For the AOU, the DO deviated from saturation for two reasons. First, the effect of land-based inputs. Low-oxygen, nutrient-rich freshwater from upstream rivers was physically mixed with high-salinity, oxygen-rich seawater from the inner bay (Figure 7A), as previously discussed. The second factor was the biological activity of nutrients in seawater at different DO concentrations. To mitigate the effects of salinity changes, we

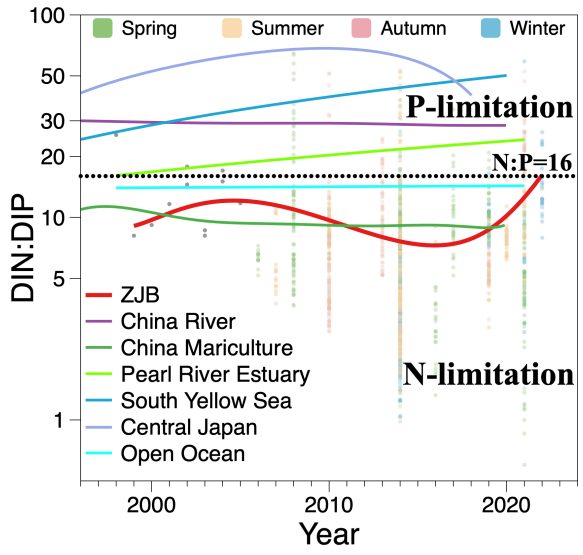

FIGURE 8
The variations in DIN: DIP in different aquatic environments across decades. The colored dots are the seasonal investigation data, and the gray dots during 1998–2005 are yearly averaged values from references shown in Table 1. The colored lines represent DIN: DIP variations in different worldwide aquatic environments, where the red line indicates the main variation trend in ZJB; the Chinese river and coastal mariculture data are from Feng et al. (2024), the Pearl River Estuary close to Hongkong coastal area data are from Yao et al. (2022), the South Yellow Sea data are from Chen et al. (2023), the data of Central Japan are from Katazakai and Zhang (2021), and the data of the open ocean including the Pacific Ocean and India Ocean are from Olsen et al. (2016).

analyzed the relationship between salinity-normalized nutrients and the AOU, as shown in Figure 9. High concentrations of both N-DIP and N-DIN corresponded to high AOU levels.

The region with high N-DIN values was primarily located in the upper bay during the spring (Figure 9B). And the ammonia was the highest in the upper bay compare to the whole ZJB, especially in 2010 (Figure 4). Phytoplankton preferentially assimilates high concentrations of ammonia because it requires less energy and does not undergo redox reactions (Zehr and Ward, 2002). Although nitrifying microorganisms (converting NH_4^+ to NO_3^- under aerobic conditions) are partially inhibited by intense light owing to shallow water depths (Gruber, 2008), elevated levels of suspended particulate matter from riverine sources may serve dual roles, providing not only the substrate but also a protective environment for nitrifying organisms when combined with high levels of ammonia and sufficient nighttime hours. Nitrification is a key pathway for ammonia depletion, as demonstrated by the variation in nitrite content in ZJB. Nitrite, an important intermediate product of nitrate assimilation, nitrification, and denitrification (Gruber, 2008), has a short turnover time of only 3–7 days in seawater (Lipschultz et al., 1996), produced and immediately consumed during biological activity. Significant correlations between nitrite, normalized nitrate, and nitrite versus normalized ammonia were observed in the upper bay during spring (Figures 9F, G), indicating that large amounts of nitrite intermediates were produced by phytoplankton photosynthesis and nitrification by ammonia-oxidizing microorganisms. After offsetting the oxygen production (photosynthesis) and consumption (nitrification) processes, the DO in the seawater remained oversaturated, indicating that ammonia was also an important N source for photosynthesis. In other areas of ZJB, nitrate was significantly higher than ammonia, and the correlation between nitrate and nitrite (r^2 = 0.96) was stronger than that in the upper bay area (r^2 = 0.74); nitrite was mainly generated by nitrate through photosynthesis. Furthermore, the decrease in ammonia resulted in a lower oxygen consumption level by nitrification, causing the AOU to be significantly lower than that of the upper bay area and the DO to increase significantly.

During the other seasons, ammonia was considerably lower than nitrate, and nitrite was reduced. Higher concentrations of nitrate were still used for photosynthesis, and weaker nitrification due to less ammonia resulted in lower AOU levels than in spring. Additionally, although the inner bay simultaneously exhibited high levels of nitrate and ammonia, there was no correlation between ammonia and nitrite levels. In addition, although ammonium inhibits the uptake of nitrate by phytoplankton, the chronically lower levels of ammonia in ZJB were not sufficient to inhibit nitrate uptake or have toxic effects on phytoplankton growth (Domingues et al., 2011). Therefore, nitrification occurred mainly in the upper bay area, whereas in the rest of the bay, nitrate was the primary nitrogen source for photosynthesis. Moreover, phytoplankton growth and biomass may be limited by low temperatures during winter (Cullen, 1991); however, seawater temperature during winter ranged between 15–20°C owing to geographical characteristics of ZJB (Figure 2), which allowed phytoplankton to efficiently uptake nitrate (Figure 9F; nitrate vs nitrite, r^2 = 0.96). Furthermore, photosynthetic oxygen production exceeded nitrification oxygen consumption owing to the inhibition of ammonia-oxidizing microorganisms at lower temperatures, resulting in the lowest AOU and the highest degree of water DO supersaturation.

4.5 Impact of marine engineering

Over the past 20 years, ZJB has experienced a series of marine engineering activities that have remarkably impacted the marine ecological environment. Large-scale clean-ups and demolitions of marine aquaculture pile foundations, illegal fishing facilities, and navigation obstructions occurred in ZJB in 2005 and 2011–2012, thereby improving the unstable and complex aquaculture environment of ZJB. By reducing excessive external nutrient loading as a primary measure of adaptive management (Cooke et al., 2016), N and P concentrations in the water column of ZJB decreased significantly in the following years (Figures 3A, B). This suggests that the reduction in unregulated aquaculture activities led to an improvement in the excess discharge of nitrogen and phosphorus fertilizers during the aquaculture process, further verifying the effect of mariculture on the nutrient concentration and structure of seawater in ZJB; however, the COD concentration increased slightly (Figure 3C), indicating that the source of COD in the water was less related to agricultural activities and was still dominated by land-based pollution discharge.

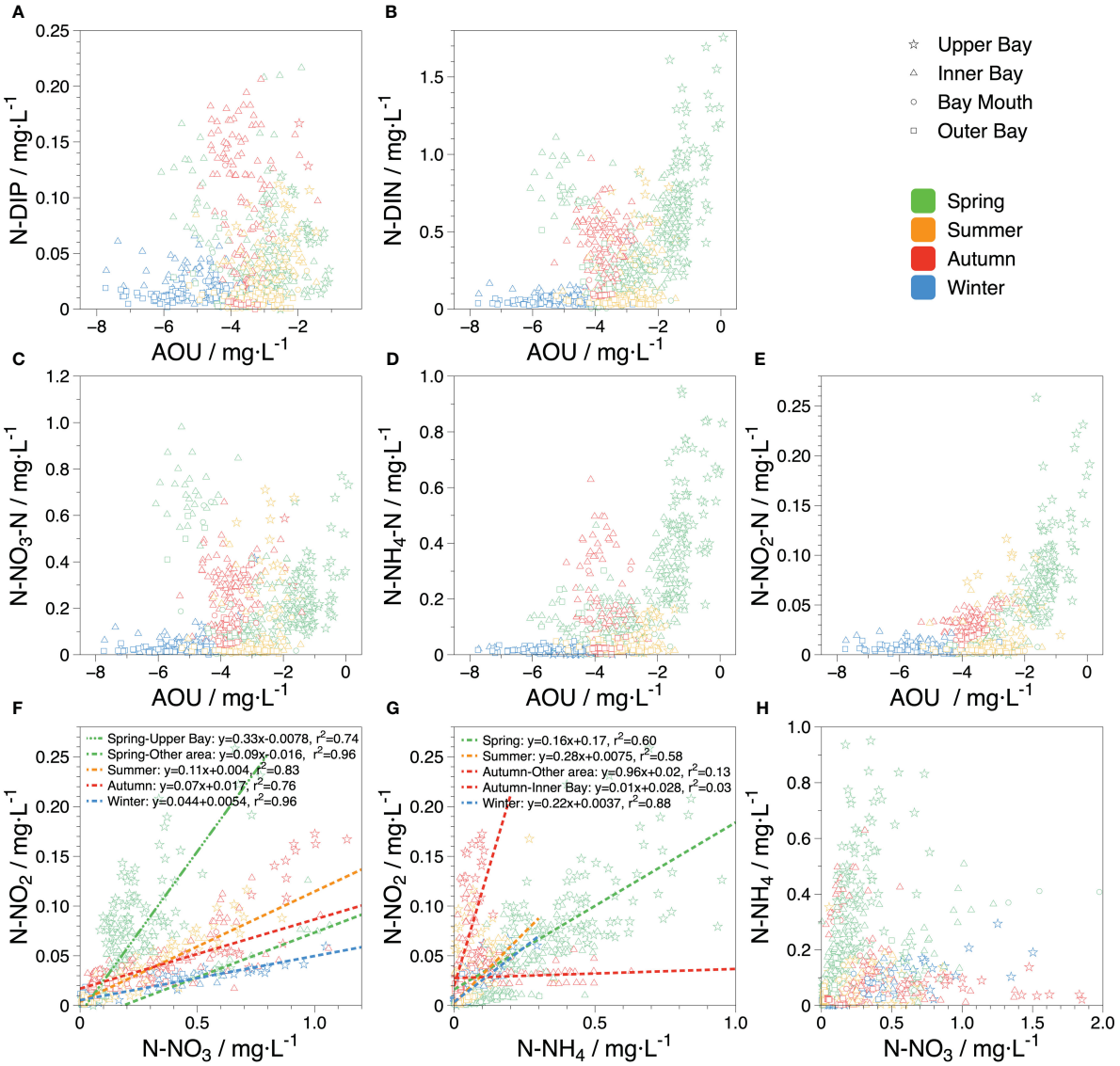

FIGURE 9
Relationship between different salinity-normalized nutrients and AOU in the seawater of ZJB. **(A)** indicates the relationship between N-DIP and AOU; **(B)** indicates the relationship between N-DIN and AOU; **(C–E)** indicate the relationship between different forms of salinity-normalized nitrogen and AOU; **(F, G)** indicate the relations of salinity-normalized nitrate vs nitrite and ammonia vs nitrite; **(H)** indicates the relations between nitrate and ammonia.

In addition to marine environment improvement works, such as clean-up and demolition, a series of sea-related projects exacerbated marine environment problems. Around 2008, the Zhanjiang municipal government implemented the "One Bay, Two Banks" plan and started implementing the ZJB long-distance navigation channel expansion dredging project. In addition, 300,000 tons and 400,000 tons worth of navigation channel dredging and expansion activities were conducted in the ZJB during 2018–2021. These dredging and reclamation activities resulted in the resuspension of deep-seabed sediments in the water column. Although sandy sediments can quickly return to the seabed, fine-grained sediments (e.g., silt and mud) remain suspended longer. Nutrient concentrations are higher in surface sediments (the upper 15 cm) than in bottom sediments because deeper sediments are in a hypoxic environment that favors denitrification processes (Galloway et al., 2004). Consequently, sediments that return to the water column under anoxic conditions may undergo nitrate reduction, particularly in areas with high turbidity (Jickells, 2005); however, DO in ZJB remained supersaturated, and no instances of hypoxia or anoxia were observed during the monitoring period. Consequently, denitrification is inhibited when anoxic sediments are resuspended in the water column in an oxygen-rich environment, and the release of nutrients from the sediment is accelerated by drastic dredging works (Chen et al., 2021). The long duration of dredging projects will result in the dissolution of large quantities of soluble regenerative nutrients into seawater, leading to an increase in N and P concentrations in the water column (Lohrer and Wetz,

2003). In addition, the inner bay area was already subjected to high nutrient concentrations from multiple sources, which led to a marked increase in nutrients during the corresponding period. This was consistent with the findings of a dredging project in Lake Yuehu (Zhang et al., 2010). Furthermore, the increased density of harbor vessel traffic following channel expansion dredging also contributes to nutrient input (Raudsepp et al., 2019), thus having long-term effects on water quality. Consequently, N, P, and COD levels in ZJB increased substantially between 2008–2010 and 2018–2021 (Figure 3), indicating high or even severe eutrophication. Moreover, the Zhanjiang government conducted a large-scale interception and remediation project in 2020 that resulted in significant reductions in seaward flows from several sewage outfalls. Therefore, the N and P concentrations were significantly reduced in summer when the runoff was high; however, when the runoff was reduced in autumn and winter, the effects of the dredging projects in the bay and other impacts were reflected again, with the N and P concentrations and eutrophication levels in ZJB increasing. Therefore, marine projects seriously affect the nutrient concentration and structural composition of ZJB and aggravate eutrophication.

5 Conclusion

Nutrients in ZJB seawater have significantly increased during the previous 20 years, leading to long-term eutrophication. As a typical semi-closed bay, the upper and inner bays are under high or severe eutrophication, mainly caused by DIN and DIP; however, the eutrophication level in the outer bay is typically low, and the main contributors are COD and DIP. In addition, tidal action, biological activity, land inputs, and marine engineering strongly influence nutrient structure and concentration. Driven by tidal action, freshwater in the northern part of the upper bay transports large amounts of terrestrial nutrients into the bay. It mixes with high-salinity seawater from the outer bay, promoting nutrient redistribution in the inner bay. Furthermore, the DO in ZJB remained supersaturated for a long period because of the vigorous photosynthesis produced by the abundance of nutrients. Moreover, because of mariculture and related wastewater discharge, ZJB has been in a state of excess P and N limitation for a long time, affecting primary productivity. In addition, marine projects in ZJB have substantially impacted the aquatic environment. Eliminating illegal aquaculture and launching aquaculture tailwater treatment can significantly improve water quality, whereas dredging waterways and other projects can exacerbate the deterioration of water quality. Unfortunately, some analyses were limited by missing or inconsistent historical data and a lack of direct evidence of nutrient use through biological data, which needs to be further investigated in future studies.

Data availability statement

The raw data supporting the conclusions of this article will be made available by the authors, without undue reservation.

Author contributions

HL: Methodology, Writing – original draft, Conceptualization. JXZ: Supervision, Writing – review & editing, Data curation, Funding acquisition. JBZ: Supervision, Writing – review & editing, Methodology. PZ: Data curation, Investigation, Writing – review & editing. XD: Writing – review & editing. ZW: Data curation, Writing – review & editing. CL: Writing – review & editing, Data curation, Investigation. CQL: Writing – review & editing, Data curation, Investigation. DW: Investigation, Writing – review & editing. YL: Investigation, Writing – review & editing. JC: Investigation, Writing – review & editing.

Funding

The author(s) declare financial support was received for the research, authorship, and/or publication of this article. This work was supported by Research and Development Projects in Key Areas of Guangdong Province (2020B1111020004), Science and Technology Projects in Guangzhou (202201011334), Guangdong Basic and Applied Basic Research Foundation (2023A1515012769).

Acknowledgments

We are grateful for the reviewers' careful review and valuable suggestions to improve the manuscript. We thank all members of the research team and others who participated in this study.

Conflict of interest

The authors declare that the research was conducted in the absence of any commercial or financial relationships that could be construed as a potential conflict of interest.

Publisher's note

All claims expressed in this article are solely those of the authors and do not necessarily represent those of their affiliated organizations, or those of the publisher, the editors and the reviewers. Any product that may be evaluated in this article, or claim that may be made by its manufacturer, is not guaranteed or endorsed by the publisher.

Supplementary material

The Supplementary Material for this article can be found online at: https://www.frontiersin.org/articles/10.3389/fmars.2024.1373716/full#supplementary-material

References

Alkan, A., Serdar, S., Fİdan, D., Akbaş, U., ZengİN, B., and Kiliç, M. B. (2022). Spatial, temporal, and vertical variability of nutrients in the Southeastern Black Sea. *Chemosphere* 302, 134809. doi: 10.1016/j.chemosphere.2022.134809

Andersen, J. H., Carstensen, J., Conley, D. J., Dromph, K., Fleming-Lehtinen, V., Gustafsson, B. G., et al. (2017). Long-term temporal and spatial trends in eutrophication status of the Baltic Sea: Eutrophication in the Baltic Sea. *Biol. Rev.* 92, 135–149. doi: 10.1111/brv.12221

Aoki, K., Shimizu, Y., Yamamoto, T., Yokouchi, K., Kishi, K., Akada, H., et al. (2022). Estimation of inward nutrient flux from offshore into semi-enclosed sea (Tokyo Bay, Japan) based on *in-situ* data. *Estuar. Coast. Shelf Sci.* 274, 107930. doi: 10.1016/j.ecss.2022.107930

Balasuriya, B. T. G., Ghose, A., Gheewala, S. H., and Prapaspongsa, T. (2022). Assessment of eutrophication potential from fertiliser application in agricultural systems in Thailand. *Sci. Total Environ.* 833, 154993. doi: 10.1016/j.scitotenv.2022.154993

Benson, B. B., and Krause, D. (1984). The concentration and isotopic fractionation of oxygen dissolved in freshwater and seawater in equilibrium with the atmosphere1: Oxygen solubility in seawater. *Limnol. Oceanogr.* 29, 620–632. doi: 10.4319/lo.1984.29.3.0620

Beusen, A. H. W., Bouwman, A. F., Van Beek, L. P. H., Mogollón, J. M., and Middelburg, J. J. (2016). Global riverine N and P transport to ocean increased during the 20th century despite increased retention along the aquatic continuum. *Biogeosciences* 13, 2441–2451. doi: 10.5194/bg-13-2441-2016

Beusen, A. H. W., Doelman, J. C., Beek, L. P. H. V., Puijenbroek, P. J. T. M. V., Mogollón, J. M., Grinsven, H. J. M. V., et al. (2022). Exploring river nitrogen and phosphorus loading and export to global coastal waters in the Shared Socio-economic pathways. *Glob. Environ. Change* 72, 102426–. doi: 10.1016/j.gloenvcha.2021.102426

Caffrey, J. M., Chapin, T. P., Jannasch, H. W., and Haskins, J. C. (2007). High nutrient pulses, tidal mixing and biological response in a small California estuary: Variability in nutrient concentrations from decadal to hourly time scales. *Estuar. Coast. Shelf Sci.* 71, 368–380. doi: 10.1016/j.ecss.2006.08.015

Carpenter, S. R. (2008). Phosphorus control is critical to mitigating eutrophication. *Proc. Natl. Acad. Sci.* 105, 11039–11040. doi: 10.1073/pnas.0806112105

Chen, X., Wang, Y., Sun, T., Huang, Y., Chen, Y., Zhang, M., et al. (2021). Effects of sediment dredging on nutrient release and eutrophication in the gate-controlled estuary of northern taihu lake. *J. Chem.* 2021, 7451832. doi: 10.1155/2021/7451832

Chen, X., Wei, Q., Jian, H., Li, D., Yu, Z., and Yao, Q. (2023). Long-term variation in nutrients in the South Yellow Sea in response to anthropogenic inputs. *Mar. pollut. Bull.* 192, 115039. doi: 10.1016/j.marpolbul.2023.115039

Cheng, H., Ma, Q., and Yang, F. (2009). Level of eutrophication and phytoplankton diversity in Zhanjiang Bay. *Trans. Oceanol. Limnol.* 3, 121–126. doi: 10.3969/j.issn.1003-6482.2009.03.018

Conley, D. J., Paerl, H. W., Howarth, R. W., Boesch, D. F., Seitzinger, S. P., Havens, K. E., et al. (2009). Controlling eutrophication: nitrogen and phosphorus. *Science* 323, 1014–1015. doi: 10.1126/science.1167755

Cooke, G. D., Welch, E. B., Peterson, S., and Nichols, S. A. (2016). *Restoration and management of lakes and reservoirs. 3rd edition* (Boca Raton: CRC Press). doi: 10.1201/9781420032109

Cotner, J. B., and Biddanda, B. A. (2002). Small players, large role: microbial influence on biogeochemical processes in pelagic aquatic ecosystems. *Ecosystems* 5, 105–121. doi: 10.1007/s10021-001-0059-3

Cullen, J. J. (1991). Hypotheses to explain high-nutrient conditions in the open sea. *Limnol. Oceanogr.* 36, 1578–1599. doi: 10.4319/lo.1991.36.8.1578

Dähnke, K., Bahlmann, E., and Emeis, K. (2008). A nitrate sink in estuaries? An assessment by means of stable nitrate isotopes in the Elbe estuary. *Limnol. Oceanogr.* 53, 1504–1511. doi: 10.4319/lo.2008.53.4.1504

Deegan, L. A., Johnson, D. S., Warren, R. S., Peterson, B. J., Fleeger, J. W., Fagherazzi, S., et al. (2012). Coastal eutrophication as a driver of salt marsh loss. *Nature* 490, 388–392. doi: 10.1038/nature11533

Domingues, R. B., Barbosa, A. B., Sommer, U., and Galvão, H. M. (2011). Ammonium, nitrate and phytoplankton interactions in a freshwater tidal estuarine zone: potential effects of cultural eutrophication. *Aquat. Sci.* 73, 331–343. doi: 10.1007/s00027-011-0180-0

Feng, Y., Xiong, Y., Hall-Spencer, J. M., Liu, K., Beardall, J., Gao, K., et al. (2024). Shift in algal blooms from micro- to macroalgae around China with increasing eutrophication and climate change. *Glob. Change Biol.* 30, e17018. doi: 10.1111/gcb.17018

Ferrier, R.o. C., Edwards, A.n. C., Hirst, D.a., Littlewood, I.@an G., Watts, C.a. D., and Morris, R. (2001). Water quality of Scottish rivers: spatial and temporal trends. *Sci. Total Environ.* 265, 327–342. doi: 10.1016/S0048-9697(00)00674-4

Fu, D., Zhong, Y., Chen, F., Yu, G., and Zhang, X. (2020). Analysis of dissolved oxygen and nutrients in zhanjiang bay and the adjacent sea area in spring. *Sustainability* 12, 889. doi: 10.3390/su12030889

Galloway, J. N., Dentener, F. J., Capone, D. G., Boyer, E. W., Howarth, R. W., Seitzinger, S. P., et al. (2004). Nitrogen cycles: past, present, and future. *Biogeochemistry* 70, 153–226. doi: 10.1007/s10533-004-0370-0

Garcia, H. E., and Gordon, L. I. (1992). Oxygen solubility in seawater: Better fitting equations. *Limnol. Oceanogr.* 37, 1307–1312. doi: 10.4319/lo.1992.37.6.1307

Gruber, N. (2008). "The marine nitrogen cycle," in *Nitrogen in the marine environment, 2nd edition* (Burlington: Elsevier), 1–50. doi: 10.1016/B978–0-12–372522–6.00001–3

Gruber, N., and Deutsch, C. A. (2014). Redfield's evolving legacy. *Nat. Geosci.* 7, 853–855. doi: 10.1038/ngeo2308

Guignard, M. S., Leitch, A. R., Acquisti, C., Eizaguirre, C., Elser, J. J., Hessen, D. O., et al. (2017). Impacts of nitrogen and phosphorus: from genomes to natural ecosystems and agriculture. *Front. Ecol. Evol.* 5. doi: 10.3389/fevo.2017.00070

He, G., Lao, Q., Jin, G., Zhu, Q., and Chen, F. (2023). Increasing eutrophication driven by the increase of phosphate discharge in a subtropical bay in the past 30 years. *Front. Mar. Sci.* 10. doi: 10.3389/fmars.2023.1184421

Howarth, R. W., and Marino, R. (2006). Nitrogen as the limiting nutrient for eutrophication in coastal marine ecosystems: Evolving views over three decades. *Limnol. Oceanogr.* 51, 364–376. doi: 10.4319/lo.2006.51.1_part_2.0364

Jiang, X., Liu, C., Cai, J., Hu, Y., Shao, K., Tang, X., et al. (2023). Relationships between environmental factors and N-cycling microbes reveal the indirect effect of further eutrophication on denitrification and DNRA in shallow lakes. *Water Res.* 245, 120572. doi: 10.1016/j.watres.2023.120572

Jickells, T. (2005). External inputs as a contributor to eutrophication problems. *J. Sea Res.* 54, 58–69. doi: 10.1016/j.seares.2005.02.006

Katazakai, S., and Zhang, J. (2021). A quarter-century of nutrient load reduction leads to halving river nutrient fluxes and increasing nutrient limitation in coastal waters of central Japan. *Environ. Monit. Assess.* 193, 573. doi: 10.1007/s10661-021-09279-5

Ke, S., Zhang, P., Ou, S., Zhang, J., Chen, J., and Zhang, J. (2022). Spatiotemporal nutrient patterns, composition, and implications for eutrophication mitigation in the Pearl River Estuary, China. *Estuar. Coast. Shelf Sci.* 266, 107749. doi: 10.1016/j.ecss.2022.107749

Lao, Q., Wu, J., Chen, F., Zhou, X., Li, Z., Chen, C., et al. (2022). Increasing intrusion of high salinity water alters the mariculture activities in Zhanjiang Bay during the past two decades identified by dual water isotopes. *J. Environ. Manage.* 320, 115815. doi: 10.1016/j.jenvman.2022.115815

Li, B., Bicknell, K., and Renwick, A. (2019). Peak phosphorus, demand trends and implications for the sustainable management of phosphorus in China. *Resour. Conserv. Recycl.* 146, 316–328. doi: 10.1016/j.resconrec.2019.03.033

Li, J., Cao, R., Lao, Q., Chen, F., Chen, C., Zhou, X., et al. (2020). Assessing seasonal nitrate contamination by nitrate dual isotopes in a monsoon-controlled bay with intensive human activities in south China. *Int. J. Environ. Res. Public. Health* 17, 1921. doi: 10.3390/ijerph17061921

Li, J., Chen, F., Zhang, S., Huang, C., Chen, C., Zhou, F., et al. (2021). Origin of the particulate organic matter in a monsoon-controlled bay in southern China. *J. Mar. Sci. Eng.* 9, 541. doi: 10.3390/jmse9050541

Li, X.-Y., Li, B., and Sun, X.-L. (2014). Effects of a coastal power plant thermal discharge on phytoplankton community structure in Zhanjiang Bay, China. *Mar. pollut. Bull.* 81, 210–217. doi: 10.1016/j.marpolbul.2013.08.006

Lin, G., and Lin, X. (2022). Bait input altered microbial community structure and increased greenhouse gases production in coastal wetland sediment. *Water Res.* 218, 118520. doi: 10.1016/j.watres.2022.118520

Lin, X., Lu, K., Hardison, A. K., Liu, Z., Xu, X., Gao, D., et al. (2021). Membrane inlet mass spectrometry method (REOX/MIMS) to measure 15N-nitrate in isotope-enrichment experiments. *Ecol. Indic.* 126, 107639. doi: 10.1016/j.ecolind.2021.107639

Lipschultz, F., Zafiriou, O. C., and Ball, L. A. (1996). Seasonal fluctuations of nitrite concentrations in the deep oligotrophic ocean. *Deep Sea Res. Part II Top. Stud. Oceanogr.* 43, 403–419. doi: 10.1016/0967-0645(96)00003-3

Lohrer, A. M., and Wetz, J. J. (2003). Dredging-induced nutrient release from sediments to the water column in a southeastern saltmarsh tidal creek. *Mar. pollut. Bull.* 46, 1156–1163. doi: 10.1016/S0025-326X(03)00167-X

Lu, J., Fang, H., Li, K., Zhang, L., and Li, Q. (2002). Water quality investigation and assessment on seawater in zhanjiang port-bay. *Environ. Prot. Transp.* 23, 16–18.

Maúre, E. D. R., Terauchi, G., Ishizaka, J., Clinton, N., and DeWitt, M. (2021). Globally consistent assessment of coastal eutrophication. *Nat. Commun.* 12, 6142. doi: 10.1038/s41467-021-26391-9

Olsen, A., Key, R. M., Van Heuven, S., Lauvset, S. K., Velo, A., Lin, X., et al. (2016). The Global Ocean Data Analysis Project version 2 (GLODAPv2) – an internallyconsistent data product for the world ocean. *Earth Syst. Sci. Data* 8, 297–323. doi: 10.5194/essd-8-297-2016

Peñuelas, J., Poulter, B., Sardans, J., Ciais, P., van der Velde, M., Bopp, L., et al. (2013). Human-induced nitrogen–phosphorus imbalances alter natural and managed ecosystems across the globe. *Nat. Commun.* 4, 2934. doi: 10.1038/ncomms3934

Qin, B., Zhang, Y., Zhu, G., and Gao, G. (2023). Eutrophication control of large shallow lakes in China. *Sci. Total Environ.* 881, 163494. doi: 10.1016/j.scitotenv.2023.163494

Raudsepp, U., Maljutenko, I., Kõuts, M., Granhag, L., Wilewska-Bien, M., Hassellöv, I.-M., et al. (2019). Shipborne nutrient dynamics and impact on the eutrophication in the Baltic Sea. *Sci. Total Environ.* 671, 189–207. doi: 10.1016/j.scitotenv.2019.03.264

Reiner, S. (2021) Ocean data view. Available at: https://odv.awi.de.

Shi, Y., Jia, L., and Zhang, H. (2020). Analysis of the water residence time and influencing factors in zhanjiang bay. *Environ. Sci. Technol. China* 43, 17–24. doi: 10.19672/j.cnki.1003–6504.2020.11.003

Sinha, E., Michalak, A. M., and Balaji, V. (2017). Eutrophication will increase during the 21st century as a result of precipitation changes. *Science* 357, 405–408. doi: 10.1126/science.aan2409

Tyrrell, T. (1999). The relative influences of nitrogen and phosphorus on oceanic primary production. *Nature* 400, 525–531. doi: 10.1038/22941

Wang, J., Beusen, A. H. W., Liu, X., Van Dingenen, R., Dentener, F., Yao, Q., et al. (2020). Spatially explicit inventory of sources of nitrogen inputs to the yellow sea, east China sea, and south China sea for the period 1970–2010. *Earths Future* 8, 1–14. doi: 10.1029/2020EF001516

Wang, J., Bouwman, A. F., Liu, X., Beusen, A. H. W., Van Dingenen, R., Dentener, F., et al. (2021a). Harmful algal blooms in chinese coastal waters will persist due to perturbed nutrient ratios. *Environ. Sci. Technol. Lett.* 8, 276–284. doi: 10.1021/acs.estlett.1c00012

Wang, Y., Liu, D., Xiao, W., Zhou, P., Tian, C., Zhang, C., et al. (2021c). Coastal eutrophication in China: Trend, sources, and ecological effects. *Harmful Algae* 107, 102058. doi: 10.1016/j.hal.2021.102058

Wang, S., Zhou, F., Chen, F., Meng, Y., and Zhu, Q. (2021b). Spatiotemporal distribution characteristics of nutrients in the drowned tidal inlet under the influence of tides: A case study of zhanjiang bay, China. *Int. J. Environ. Res. Public. Health* 18, 2089. doi: 10.3390/ijerph18042089

Yao, H., Wang, J., Han, Y., Jiang, X., and Chen, J. (2022). Decadal acidification in a subtropical coastal area under chronic eutrophication. *Environ. pollut.* 293, 118487. doi: 10.1016/j.envpol.2021.118487

Zehr, J. P., and Ward, B. B. (2002). Nitrogen cycling in the ocean: new perspectives on processes and paradigms. *Appl. Environ. Microbiol.* 68, 1015–1024. doi: 10.1128/AEM.68.3.1015-1024.2002

Zhang, P., Chen, Y., Peng, C., Dai, P., Lai, J., Zhao, L., et al. (2020a). Spatiotemporal variation, composition of DIN and its contribution to eutrophication in coastal waters adjacent to Hainan Island, China. *Reg. Stud. Mar. Sci.* 37, 101332. doi: 10.1016/j.rsma.2020.101332

Zhang, H., Cheng, W., Qiu, X., Feng, X., and Gong, W. (2017). Tide-surge interaction along the east coast of the Leizhou Peninsula, South China Sea. *Cont. Shelf Res.* 142, 32–49. doi: 10.1016/j.csr.2017.05.015

Zhang, J., Fu, M., Zhang, P., Sun, D., and Peng, D. (2023a). Unravelling nutrients and carbon interactions in an urban coastal water during algal bloom period in zhanjiang bay, China. *Water* 15, 900. doi: 10.3390/w15050900

Zhang, P., Peng, C., Zhang, J., Zhang, J., Chen, J., and Zhao, H. (2022). Long-term harmful algal blooms and nutrients patterns affected by climate change and anthropogenic pressures in the zhanjiang bay, China. *Front. Mar. Sci.* 9. doi: 10.3389/fmars.2022.849819

Zhang, P., Peng, C.-H., Zhang, J.-B., Zou, Z.-B., Shi, Y.-Z., Zhao, L.-R., et al. (2020b). Spatiotemporal urea distribution, sources, and indication of DON bioavailability in zhanjiang bay, China. *Water* 12, 633. doi: 10.3390/w12030633

Zhang, X., Yao, C., Zhang, B., Tan, W., Gong, J., Wang, G., et al. (2023b). Dynamics of benthic nitrate reduction pathways and associated microbial communities responding to the development of seasonal deoxygenation in a coastal mariculture zone. *Environ. Sci. Technol.* 57, 15014–15025. doi: 10.1021/acs.est.3c03994

Zhang, L., Yu, L., and Tang, M. (2009). Eutrophication and red tide in coastal waters of Zhanjiang port. *Water Resour. Prot.* 25, 50–54.

Zhang, J., Zhang, Y., Zhang, P., Li, Y., Li, J., Luo, X., et al. (2021). Seasonal phosphorus variation in coastal water affected by the land-based sources input in the eutrophic Zhanjiang Bay, China. *Estuar. Coast. Shelf Sci.* 252, 107277. doi: 10.1016/j.ecss.2021.107277

Zhang, S., Zhou, Q., Xu, D., Lin, J., Cheng, S., and Wu, Z. (2010). Effects of sediment dredging on water quality and zooplankton community structure in a shallow of eutrophic lake. *J. Environ. Sci.* 22, 218–224. doi: 10.1016/S1001-0742(09)60096-6

Zhou, X., Chen, C., Chen, F., and Song, Z. (2021). Changes in net anthropogenic nitrogen input in the watershed region of Zhanjiang Bay in south China from 1978 to 2018. *Environ. Dev. Sustain.* 23, 17201–17219. doi: 10.1007/s10668-021-01335-x

Zhou, F., Lu, X., Chen, F., Zhu, Q., Meng, Y., Chen, C., et al. (2020). Spatial-monthly variations and influencing factors of dissolved oxygen in surface water of zhanjiang bay, China. *J. Mar. Sci. Eng.* 8, 403. doi: 10.3390/jmse8060403

Zu, T., Gan, J., and Erofeeva, S. Y. (2008). Numerical study of the tide and tidal dynamics in the South China Sea. *Deep Sea Res. Part Oceanogr. Res. Pap.* 55, 137–154. doi: 10.1016/j.dsr.2007.10.007

frontiers | Frontiers in Marine Science

TYPE Original Research
PUBLISHED 12 June 2024
DOI 10.3389/fmars.2024.1394502

Check for updates

OPEN ACCESS

EDITED BY
Li Jianlon,
Shandong University, China

REVIEWED BY
Nur Ili Hamizah Mustaffa,
Universiti Putra Malaysia, Malaysia
Guisheng Song,
Tianjin University, China

*CORRESPONDENCE
Qun Sun
sunqun@tust.edu.cn

RECEIVED 01 March 2024
ACCEPTED 25 April 2024
PUBLISHED 12 June 2024

CITATION
Guo W-N, Sun Q, Wang S-Q and Zhang Z-H (2024) Characterizing spatio-temporal variations of dimethyl sulfide in the Yellow and East China Sea based on BP neural network.
Front. Mar. Sci. 11:1394502.
doi: 10.3389/fmars.2024.1394502

COPYRIGHT
© 2024 Guo, Sun, Wang and Zhang. This is an open-access article distributed under the terms of the Creative Commons Attribution License (CC BY). The use, distribution or reproduction in other forums is permitted, provided the original author(s) and the copyright owner(s) are credited and that the original publication in this journal is cited, in accordance with accepted academic practice. No use, distribution or reproduction is permitted which does not comply with these terms.

Characterizing spatio-temporal variations of dimethyl sulfide in the Yellow and East China Sea based on BP neural network

Wen-Ning Guo, Qun Sun*, Shuai-Qi Wang and Zhi-Hao Zhang

College of Ocean and Environment, Tianjin University of Science and Technology, Tianjin, China

Dimethyl sulfide (DMS), an organic volatile sulfide produced from Dimethylsulfoniopropionate (DMSP), exerts a significant impact on the global climate change. Utilizing published literature data spanning from 2005 to 2020, a BP neural network (BPNN) model of the surface seawater DMS in the Yellow and East China Sea (YECS) was developed to elucidate the influence of various marine factors on the DMS cycle. Results indicated that the six parameters inputted BPNN model, that include the time (month), latitude and longitude, sea-surface chlorophyll a (Chl-a), sea-surface temperature (SST), and sea-surface salinity (SSS), yielded the optimized simulation results (R^2 = 0.71). The optimized estimation of surface seawater DMS in the YECS were proved to be closely aligned with the observed data across all seasons, which demonstrated the model's robust applicability. DMS concentration in surface seawater were found to be affected by multiple factors such as Chl-a and SST. Comparative analysis of the three environmental parameters revealed that Chl-a exhibited the most significant correlation with surface seawater DMS concentration in the YECS (R^2 = 0.20). This underscores the pivotal role of chlorophyll in phytoplankton photosynthesis and DMS production, emphasizing its importance as a non-negligible factor in the study of DMS and its sulfur derivatives. Furthermore, surface seawater DMS concentration in the YECS exhibited positive correlations with Chl-a and SST, while displaying a negative correlation with SSS. The DMS concentration in the YECS show substantial seasonal variations, with the maximum value (5.69 nmol/L) in summer followed in decreasing order by spring (3.96 nmol/L), autumn (3.18 nmol/L), and winter (1.60 nmol/L). In the YECS, there was a gradual decrease of DMS concentration from the nearshore to the offshore, especially with the highest DMS concentration concentrated in the Yangtze River Estuary Basin and the south-central coastal part off the Zhejiang Province. Apart from being largely composed by the release of large amounts of nutrients from anthropogenic activities and changes in ocean temperature, the spatial and temporal variability of DMS may be driven by additional physicochemical parameters.

KEYWORDS

dimethyl sulfide, BP neural network, the Yellow and East China Sea, spatial and temporal variations, Yangtze river estuary

1 Introduction

Dimethyl sulfide (DMS) generated by marine phytoplankton, serves as a crucial contributor to the volatile gases with the marine biochemical cycle. The amount of DMS emitted from the ocean to the atmosphere, exceeding more than 90% of the total sulfide emissions (Liss et al., 1997), which is an important participant in the global sulfur cycle (Andreae, 1990). Fung et al. (2022) highlighted that the prominence of pre-industrial DMS as a source of sulfate, with 57% derived from DMS, exerting a more pronounced effect on suppressing aerosol indirect radiative forcing than pristine present-day (−2.2 W m^{-2} in standard versus −1.7 W m^{-2}). Upon entering the atmosphere via sea-air exchange, DMS undergoes photochemical oxidation to yield products such as methanesulfonic acid (MSA) and SO_2. The subsequent oxidation and conversion of DMS to SO_2 in the troposphere are crucial processes in generating and expanding sulfur-containing aerosols with the marine boundary layer (Sciare et al., 2000). These aerosols can also undergo long-range transport and affect background aerosol sulfate levels in continental regions (Sarwar et al., 2023). Further oxidation of SO_2 in the atmosphere results in the formation of non-marine sulfate aerosol (nss-SO_4^{2-}) (Vogt and Liss, 2009). Most of the oxidation products of DMS in the atmosphere exhibit high acidity, influencing the natural acidity of precipitation in the coastal areas (Ayers et al., 1991; Archer et al., 2013). Additionally, nss-SO_4^{2-} is a key participant in the global sulfur cycle, which is involved in the formation of cloud condensation nuclei (CCN). This process elevates the concentration of CCN, thereby augmenting the reflection and scattering rate of solar radiation from clouds. Consequently, these phenomena exert profound affects on the balance of surface solar radiation, thus influencing the global climate (Charlson et al., 1987; Kloster et al., 2007; Quinn and Bates, 2011).

Surface seawater DMS is produced from its precursor Dimethylsulfoniopropionate (DMSP) by algal enzymes or microbial enzymes, and DMSP is synthesized and released by algae through a series of reactions utilizing sulfate from seawater (Challenger and Simpson, 1948). Coral and macroalgae are the main sources of dissolved acrylate and DMSP to the reef ecosystem (Xue et al., 2022). DMS is generated and eliminated by three pathways, namely, bacterial consumption, photochemical oxidation, and sea-air exchange (Kettle and Andreae, 2000; Toole et al., 2004; Kloster et al., 2005). Throughout the cycle of DMS generation and removal, the final production of DMS is a joint contribution of biogenic conditions and many environmental factors (Shen et al., 2021). For the high-productivity YECS, there is a big difference in the contribution of DMSP-producing ability of different algal species to DMS. Chrysophyceae and Pyrrophyceae are the major producer of high DMS, and Bacillariophyceae is minor DMS producer (Keller et al., 1989), which result in a signifcant spatiotemporal variations of DMS in the YECS. A large number of studies have showed Chl-a is the main environmental factor in the study of DMS, and concluded that the surface DMS and Chl-a concentration show a significant positive correlation (Zhang et al., 2008; Yang et al., 2014; Li et al., 2015). SST can change the solubility of DMS in seawater and indirectly affect the DMS concentration by influencing biological activities (biotic enzyme activities) (Yu et al., 2015). These studies revealed the considerable complexity of the oceanic DMS cycle. Given the ecological role of DMS and its potential impact on global climate, a large number of studies have focused on characterizing the dynamics of this compound in seawater. The scarcity of missing DMS data in the Chinese coastal ocean limits the development of simple prediction algorithms to characterize its spatial and temporal variability, and the estimation of DMS concentrations in the YECS is of particular importance. Estimating the surface DMS concentration can enhance comprehension of the spatial and temporal distribution of DMS, as well as the correlation with marine environmental factors in the East China Shelf. This can lead to a better understanding of the sulfur cycle, which is significant for mitigating global warming and maintaining marine ecosystem stability.

Several methods and models have been proposed for the prediction and hindcasting of DMS, mainly including multiple linear regression method, coupled sea-air model, coupled ecological model of DMS, generalized mixed additive statistical model (GAMM), etc. Shen et al. (2019) established a multivariate statistical model to discuss the relationship between Chl-a and DMS concentration in the surface layer of YECS. Grandey and Wang (2015) used a coupled air-sea model to investigate the global DMS changes under the RCP4.5 scenario. Li et al. (2022) simulated the near-future (mid-21st century) surface DMS concentration in the Yellow Sea using a coupled DMS modular ecological model for the eastern Chinese shelf area. Li et al. (2023b) used the GAMM model to simulate the DMS concentration in the East China Sea from 1998 to 2020. To some extent, these models can improve the regional characterization of YECS at small scales. However, the accuracy of the output DMS, particularly with the simple linear regression method, still has limitations to meet the needs of constructing a complete and accurate DMS level distribution model. Compared with the models mentioned above, artificial neural networks (ANNs), as an important branch of artificial intelligence, can learn complex and nonlinear functions from a large amount of data, and achieve the best simulation effect through self-adjustment and optimization of the learning data.

Traditionally, the collection of ocean dimethyl sulfide (DMS) data has relied on discrete samples obtained from in situ observations, resulting in significant gaps and sparsity in global ocean DMS observations. In recent years, recent advancements in artificial intelligence methods, particularly neural networks, have emerged as promising tools to address this data deficiency. The ANNs are commonly used for predictive reconstruction of oceanic dimethyl sulfide (DMS). McNabb and Tortell (2022) presented improves upon existing statistical DMS models by capturing 62% of the observed DMS variability in the northeast subarctic Pacific and showing significant regional patterns associated with mesoscale oceanic variability. Wang et al. (2020) obtained a global oceanic DMS distribution based on ANN at a spatial resolution of 1°×1°. The predictions made by the ANN model were reasonable when compared to the raw data in the global database (R^2 = 0.66). Bell et al. (2021) found that the ANN models were able to predict seasonally averaged seawater DMS trends in the North Atlantic when compared with the global DMS climatology. The models' accuracy surpasses that of traditional multiple linear regression

10.3389/fmars.2024.1394502

algorithms, indicating that the neural network's DMS model results can well simulate most of the real-world values, and that the individual predictors extracted by the model effectively explain their respective explanatory variance of DMS concentration. However, a common challenge identified across these studies pertains to the inability of neural networks to directly discern the potential relationships between DMS concentrations and relevant marine environmental factors. Consequently, these models exhibit limitations in elucidating the underlying mechanisms driving the DMS cycle. Despite these limitations, the findings from these tests facilitate inductive inference regarding the significance of the factors influencing the DMS cycle. Furthermore, there has been no research on the application of neural networks to DMS in the Chinese sea area.

Thus, this paper presents a DMS estimation model for the YECS based on neural networks. Improved long-term seawater DMS concentration data from 2005-2020 are expected to positively impact the estimated DMS fluxes into the YECS atmosphere and may contribute to the parameterization of atmospheric biogenic sulfur aerosol concentrations. The model was trained and tested using oceanic factors that have a significant correlation with DMS as input variables. The validated results were then compared with previous empirical algorithms or biochemical coupling model to assess whether the application of the ANNs improves the estimate capacity of DMS in YECS. We evaluated the contribution of each variable to the DMS variance using the optimal DMS estimation model. The test results allow for an inductive inference of the importance of the factors involved in the DMS cycle. Our new modeling approach significantly improved upon previous methods and estimated regional DMS distributions consistent with potential patterns of oceanographic change. Notably, regional patterns in nutrient supply and ocean physical mixing dynamics largely explain modeled DMS concentrations. The significance of YECS as a global source of atmospheric sulfur is further emphasized.

2 Data and methods

2.1 Data

This study is based on the *in situ* observation data in the published literature compiled by Shen et al. (2019) and then collected the observation data of surface DMS concentration and related impact factors in YECS from 2005 to 2020 by reviewing the literature, of which a total of 19 cruises were conducted in the spring, 18 cruises in the summer, 14 cruises in the autumn, and 12 cruises in the winter. The observation stations of the total of 63 cruises are as shown in Figure 1. The study area of this paper is (24°-34°N, 118°-130°E), and 2780 sets of sea surface chlorophyll (Chl-a), sea surface temperature (SST), and sea surface salinity (SSS) data were collected.

2.2 Model building methodology

The Back Propagation neural network (BPNN) is a kind of multi-layer feed-forward neural network trained according to the error backpropagation algorithm, which belongs to one of the

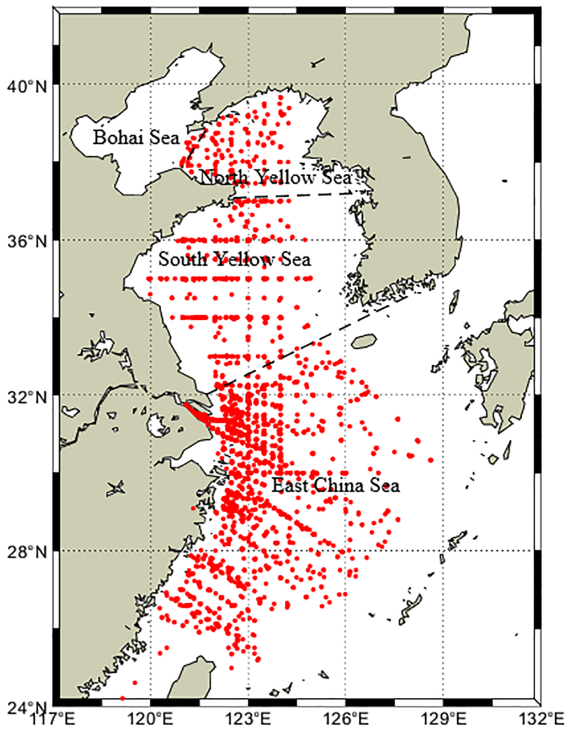

FIGURE 1
Distributions of *in-situ* stations in the YECS. The black dashed line is the dividing line between the Bohai Sea, the North Yellow Sea, the South Yellow Sea and the East China Sea.

ANNs models. The backpropagation algorithm contains two processes, the forward propagation of the signal and the back propagation of the error (Figure 2). Forward propagation refers to the input signal (feature) applied to the output node through the hidden layer and is transformed to the output node through the nonlinear transformation that generates an output signal. When the actual output does not match the desired value, the output error

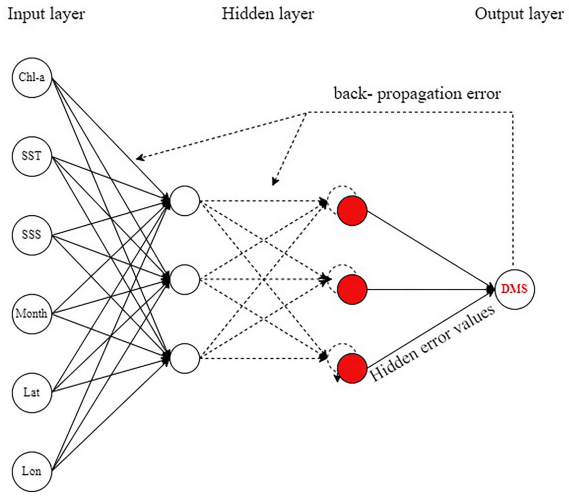

FIGURE 2
Structure of BP neural network.

is back propagated to the input layer and distributed to the neurons in each layer to obtain the error signal obtained from each layer. The error signal obtained from each layer is used as the basis for adjusting the weights of each unit. After repeated learning and training, the connection strength of each node is continuously adjusted so that the error is in the direction of the gradient direction. After repeated learning and training, the connection strength of each node is continuously adjusted so that the error decreases in the direction of the gradient, and the weights and thresholds corresponding to the minimum error are determined, to achieve the effect that the output results are close to the actual value, and the training is finished at this time (Fu et al., 2021a).

Generally, increasing the number of neurons and the depth of the network during training can improve the learning ability of the network to extract useful information from the training set. However, the modeling dataset is only 2780 sets of data, which is a small dataset compared to the ocean database, and a neural network with too much depth and complexity will learn the features of a large amount of noisy data because of the insufficient data in the training set when it performs inversion operation, resulting in the poor generalization ability of the model and overfitting phenomenon easily. To avoid this phenomenon, one BPNN model was proposed after repeated debugging with the appropriate network depth, size, number of hidden layers, learning rate, and other parameters (Table 1). Meanwhile, a dropout layer was added in each hidden layer to ensure that some neurons can be randomly deleted during the training process, reducing the complexity and parameters of the neural network, effectively avoiding the problem of overfitting and improving the accuracy of the estimation results of the BPNN. The result accuracy is improved.

This study presents the BPNN of YECS constructed with the parameter combinations of time month, latitude and longitude, Chl-a, SST, and SSS, and the estimated fitting results of the DMS concentration of the surface seawater are obtained. In the construction process, the total amount of 2780 data sets was firstly divided into 2224 data training sets and 556 data test sets according to the 8:2 division ratio, and the different modeling parameters and combinations screened out were used as neurons in the input layer for the modeling algorithm, and after repeated adjustments of the algorithmic model to obtain the optimal estimation parameter scheme. The 2015 DMS-related data (300 data points) are singled out to serve as an external validation dataset for the modeling, which is to facilitate the comparison with the accuracy of related DMS forecast hindcasting methods. The remaining 2480 data sets are divided into 1984 training sets and 496 test sets according to the same partition ratio to participate in the final BPNN model weight, and the test set responses are used as the validation results of this experiment. The BPNN structure consists of one input layer, three hidden layers, and one output layer, and the input parameters are transformed by the built-in nonlinear function of the hidden layer, and the output error of the hidden layer is used as the weight adjustment to it continuously approximates to the real value of DMS concentration observation and finally outputs the DMS fitted value.

TABLE 1 Selected parameters of BPNN model

Parameters	Value
Input Layer, Output Layer	1
Hidden layer	3
Number of nodes in hidden layer	256
Epoch	1500
Learning rate	0.001
Dropout rate	0.2

To obtain the results of BPNN estimation with optimal DMS concentration, experimental protocols EXP1-6 (Table 2) were set up and three groups of control experiments were conducted, in which the control groups EXP1 and EXP2 could explore the effect of salinity change on DMS concentration, EXP3 and EXP4 to observe the percentage of variance in DMS interpretation due to differences in temporal and spatial variations, and EXP5 and EXP6 to facilitate the comparison between the DMS cycling process of other marine factors not considered to be involved in modeling the moderating role of the three elements of chlorophyll, SST, and sea surface salinity.

To evaluate the accuracy and credibility of the final reconstruction results, we used the following parameters as evaluation indicators. The coefficient of determination, R^2, is a statistical indicator used to assess the goodness of fit of a regression model. It indicates the proportion of variability in the dependent variable that can be explained by the model, i.e. how well the model fits the data, and could be defined as,

$$R^2 = \frac{SSR}{SST} = 1 - \frac{SSE}{SST}$$

in which the sum of squares regression (SSR) is the sum of the difference between the predicted value and the mean of variable to quantify its variability explained by regressions model. The sum of squares of residuals (SSE) is the error between the estimate and the true value, and the sum of squares of total deviations (SST) is the error between the mean and the true value.

Both the Root Mean Squared Error (RMSE) and Mean Absolute Error (MAE) are commonly used as a measure of the difference between the predicted and measured values of a model to assess the degree of fit of the model on the given data. Theoretically, the higher the R^2, the smaller the MAE and RMSE, the better the model fits a dataset.

3 Results

3.1 Validation of BPNN model and its applicability analysis

Table 3 presents the evaluation parameters of the BPNN model for each experimental scheme. The algorithm was used to model the data, resulting in R^2 values of 0.71 for the test set. The RMSE values was 2.55 nmol/L, and the MAE values was 1.63 nmol/ L. The results of the BPNN test set constructed from the combination of EXP1 parameters demonstrate the greatest R^2 with MAE and RMSE values slightly higher than those of EXP2 by 10.9% and 17.0%,

TABLE 2 Experimental setup of parameter combinations in BPNN model.

Experimental name	Parameter combinations
EXP1	Month+Lat+Lon+Chl-a+SST+SSS
EXP2	Month+Lat+Lon+Chl-a+SST
EXP3	Lat+Lon+Chl-a+SST+SSS
EXP4	Month+Chl-a+SST+SSS
EXP5	Month+Lat+Lon
EXP6	Chl-a+SST+SSS

TABLE 3 Evaluation parameters of the DMS estimation model based on BP neural network.

Experiment	R^2	MAE	RMSE	r
EXP1	0.71	1.63	2.55	0.84
EXP2	0.70	1.47	2.18	0.81
EXP3	0.62	1.68	2.81	0.76
EXP4	0.61	1.69	2.66	0.73
EXP5	0.37	2.05	3.26	0.69
EXP6	0.31	2.14	3.68	0.47

respectively. This discrepancy may be attributed to the discrete-valued deviation errors that affect the model's accuracy (Bell et al. 2021). These results suggest that EXP1 is the optimal parameter training combination for this study. Moreover, comparison of the R^2, RMSE, and MAE of all parameter experiments (Figure 3) revealed that alterations in input parameters had a positive or negative impact on model accuracy. This suggests that, in addition to temporal position, the involvement of chlorophyll, SST, and salinity in the modeling of DMS is of significance.

To further validate the best BPNN model, the data were divided into four groups of data according to season, namely, spring (March-May), summer (June-August), autumn (September-November), and winter (December-February), to assess the seasonal applicability of the surface seawater DMS concentration in YECS. From the fit (correlation coefficient r) between the predicted values and the observations of surface seawater DMS in different seasons (Figure 4), the estimation results of the optimal BPNN model, EXP1, were better in all four seasons.

The MAE and RMSE of the best BPNN model were smaller in the winter, 0.37 and 0.51 nmol/L, and 1.9 and 2.86 nmol/L in the summer (Table 4), which indicated that the best BP neural network had the best applicability in the winter and the worst applicability in the summer. The MAE and RMSE of the optimal BPNN model in the four seasons did not differ much, and the explained variance of the DMS concentration in YECS exceeded 60%, which indicated that the applicability of the optimal BP neural network was still good.

3.2 Evaluation of DMS estimations in the YECS

Figure 5 shows the monthly DMS concentration in the YECS estimated based on the optimal BPNN model. The surface seawater DMS in the YECS exhibits pronounced seasonal variation, peaking during spring and summer and declining in autumn and winter. Particularly notable are elevated DMS concentrations in the coastal area of Changshan Islands in the North Yellow Sea and the southward sea area of the Yangtze River estuary in the East China Sea, as well as the area near Zhoushan Islands. The maximum DMS concentration typically occurs in April along the coastal area of Zhejiang and Fujian Provinces, with the fitted maximum value slightly underestimating the observed concentration by approximately 7 nmol/L (Figure 6). This discrepancy diminishes towards offshore regions. Notably, the area around Hupi Reef manifests as a hotspot for DMS concentration, reaching approximately 23 nmol/L. Similarly, elevated DMS concentrations

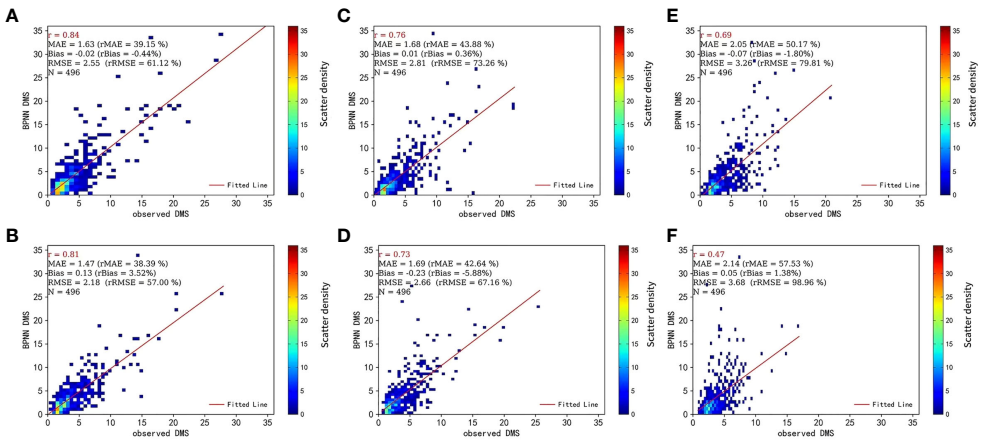

FIGURE 3
Validations of BPNN in the YECS. **(A)** EXP1, **(B)** EXP2, **(C)** EXP3, **(D)** EXP4, **(E)** EXP5, **(F)** EXP6. Note that r is the correlation coefficient; rMAE,rBias,rRMSE represent the relative mean error, relative bias, and relative root-mean-square error; respectively. N is the number of test samples. The color indicates the density of scattered data.

10.3389/fmars.2024.1394502

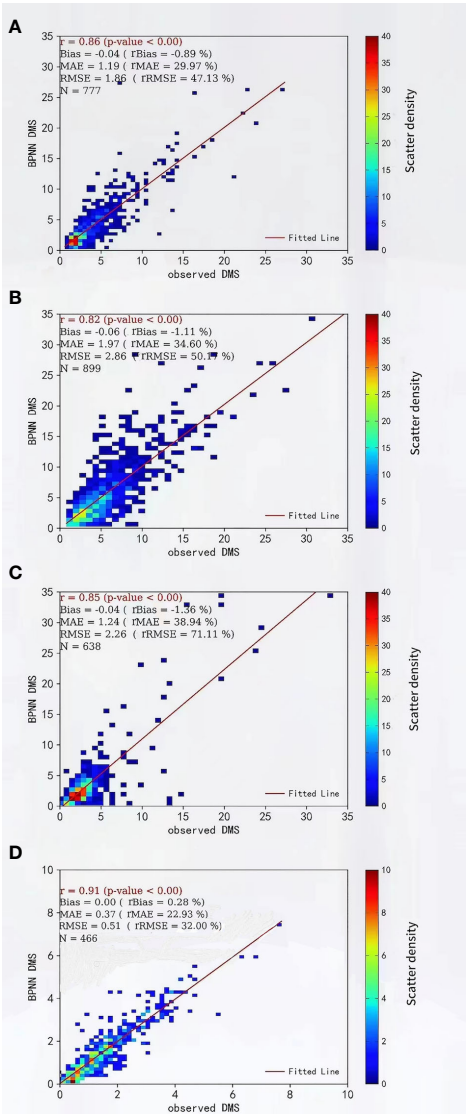

FIGURE 4
Seasonal applicability of DMS estimated based on the optimal BPNN in the YECS **(A)** Spring, **(B)** Summer, **(C)** Autumn, **(D)** Winter.

are observed in the eastern East China Sea, aligning closely with areas of high DMS observation, particularly in proximity to Jeju Island and the Korean Peninsula, which is highly coincident with the area of high value of DMS observation (Figure 5). From the analysis of significant discrepancy in the location of Hupi Reef in April, it is suggested that in addition to the abundance of Chl-a in the spring phytoplankton population, the substantial influx of nutrients supplied to the surface by upwelling may be one of the reasons for the outbreak of DMS. In early summer, elevated DMS values were recorded in June in the North Yellow Sea near Korea Bay and Zhoushan Islands, with a broad range of high values (about 7-11 nmol/L) extending from the Yellow Sea to the western part of the East China Sea. In July, the high DMS concentrations were mainly concentrated along the coasts of Chengshanjiao and Hangzhou Bay. Compared with the observations, the fitted concentrations of DMS were relatively high in the Yangtze River estuary basin and the north-south Yellow Sea demarcation line (the coastal area of Shandong Peninsula). There were sporadic anomalously high DMS concentrations along the Yangtze River estuary in October, although the difference from the observed concentrations was large (7-10 nmol/L), the overall phenomenon in the estimated area was in perfect agreement with the conclusion of the previous studies related to DMS in autumn (anomalously high DMS in October). The DMS concentrations in the South Yellow Sea were marginally higher than the observed values (about 2-3 nmol/L) in August and November, and the model performed best in winter, with the disparity between the actual and estimated values being nearly identical to the observed values. The minimal difference between the real and estimated values is almost maintained at 0-1.50 nmol/L, suggesting that the decrease in SST coupled with a sharp decrease in Chl-a is the main reason for the low DMS in winter. These findings closely mirror the spatial and temporal distribution characteristics of the surface DMS concentration in YECS from 2005 to 2020 collected in the literature (Figure 7), which further demonstrates that the BPNN model based on the parameter combinations of EXP1 is feasible to be used for estimating the surface DMS concentration in YECS.

Analysis of the discrepancy between observed and estimated monthly averages (Figure 6) reveals that the majority of errors fall within the range of -2 to 1 nmol/L. Areas exhibiting minimal discrepancies are primarily situated in the Yellow Sea and the eastern East China Sea offshore waters. However, certain estimated values exhibit significant deviations, with some data points deviating by 10 nmol/L lower (in April) or 8 nmol/L higher (in June) compared to the true values. These deviations are particularly prominent in the Changjiang River mouth basin (Figure 6), with the original data points representing the extreme values. This indicates that the discrete anomalous signals of the high-concentration DMS exert a substantial impact on the accuracy and applicability of the BPNN model, which leads to a large difference in the spatial applicability of the best BPNN model in the Yellow Sea and the East China Sea. Consequently, there is a notable divergence in the spatial applicability of the optimal BPNN model in the Yellow Sea and East China Sea: the applicability is good in the offshore areas of the Yellow Sea and East China Sea, while the applicability in the extreme regions along the Yangtze River estuary and the Jeju Peninsula is relatively poor. These findings underscore the importance of considering localized environmental factors and anomalous signals when assessing the predictive performance of modeling approaches in marine ecosystems.

In general, compared with the DMS observation data, the optimal BPNN model developed in this paper has better applicability in the spatial and temporal distribution characteristics of DMS in the YECS,

TABLE 4 Seasonal applicability of the best BP model.

Season	R^2	MAE	RMSE	r
Spring	0.64	1.19	1.86	0.86
Summer	0.62	1.97	2.86	0.82
Autumn	0.66	1.24	2.26	0.85
Winter	0.66	0.37	0.51	0.91

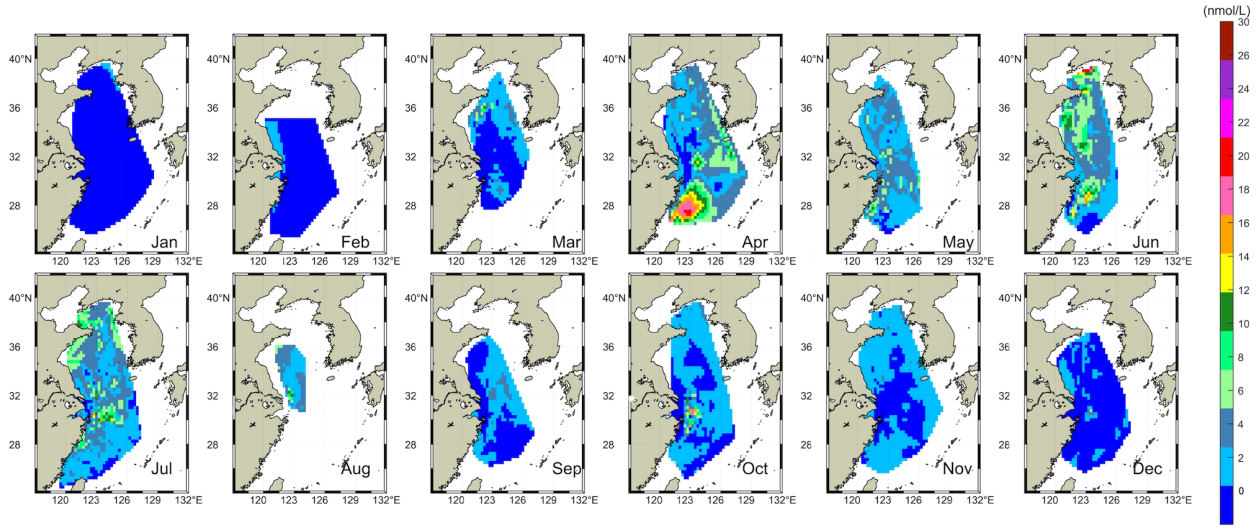

FIGURE 5
Monthly DMS in the YECS estimated based on BPNN.

which may be related to the spatial and temporal information of month and latitude/longitude as the predictor variables. Although the parameters considered in this paper are not comprehensively compared with the models based on various ocean physicochemical properties such as MLD, photosynthetically active radiation (PAR) (Galí et al., 2018), upwelling, and phytoplankton abundance, the parameters required by this model are easy to obtain, and the methodology is relatively simple, and it is also able to accurately analyze the seasonal characteristics of the DMS in the surface layer of YECS and the overall trend of changes.

In addition to the comparing the BPNN model's performance with the original observation data, to better evaluate the estimation ability of the BP model, this study compares the hindcast results with other statistical models commonly used in similar studies. Like the generalized mixed additive statistical model (GAMM) and multivariate statistical methods based on the same DMS dataset and parameter combinations. Li et al. (2023a) employed the GAMM model to obtain the hindcast DMS dataset of the East China Sea, in which the GAMM model DMS concentration was set as the response variable, and other parameters (longitude, latitude, month, SST, and Chl-a) were set as the explanatory variables. Validation of the GAMM model against the 2015 East China Sea DMS measured data yielded a correlation coefficient of 0.65 and RMSE= 0.59 nmol/L. Shen et al. (2019) established a suitable multivariate statistical model for surface DMS concentration in the Chinese offshore based on the same combination of parameters and obtained R^2 = 0.55 and

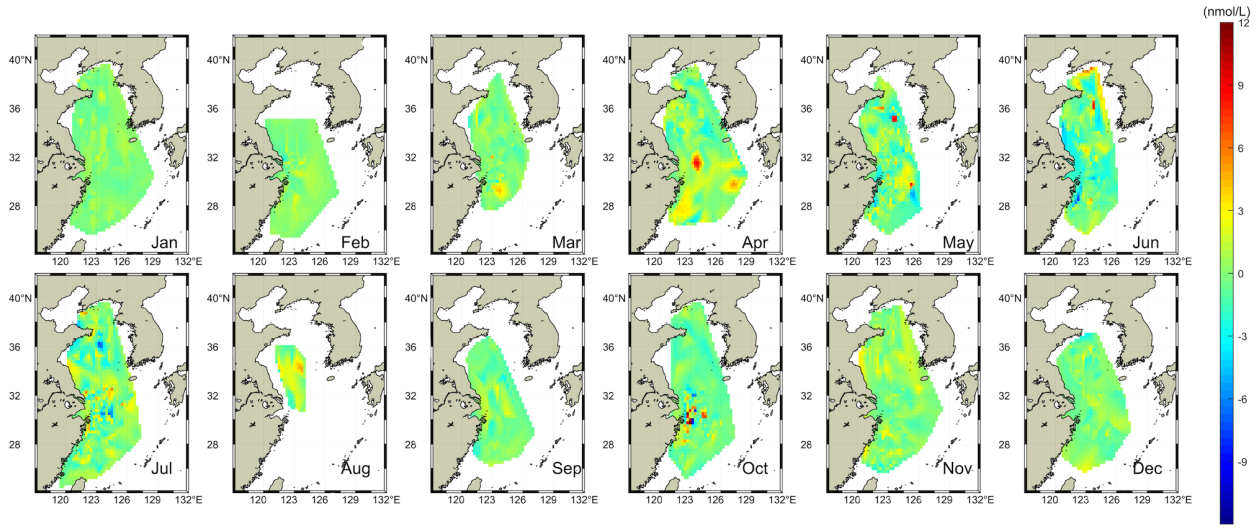

FIGURE 6
Difference between observed data and BPNN results from 2005 to 2020 in YECS. (Difference = Observed value - BPNN value).

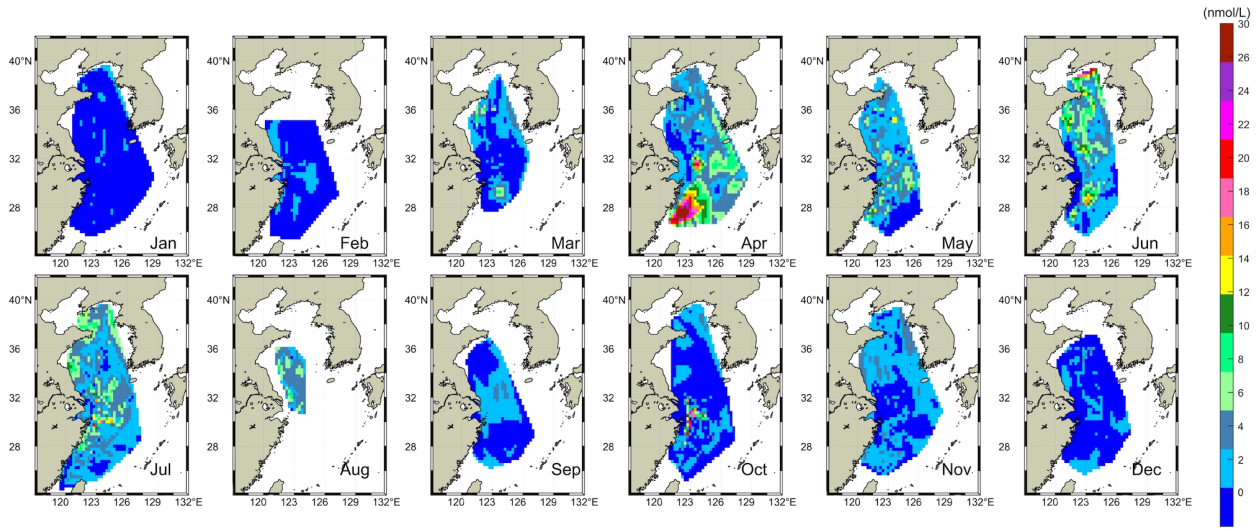

FIGURE 7
Seasonal distributions of monthly mean observed DMS in YECS from 2005 to 2020.

RMSE=2.24nmol/L. Despite the significant differences in accuracy reported by various models when applied to DMS dataset in YECS, the correlation coefficient of the present experiment after external validation was obtained as r=0.95, RMSE=1.64 nmol/L, and the estimation results of the optimal BPNN, R^2 = 0.71 and RMSE=2.55nmol/L in our study. It indicates superior accuracy compared to the aforementioned evaluation metrics. This reaffirms the BPNN model's efficacy in estimating DMS concentration in YECS.

4 Discussion

4.1 Spatial and temporal variations of DMS

Seasonal variations of sea surface temperature (SST), salinity (SSS), chlorophyll (Chl-a) concentration, and DMS concentration obtained based on *in situ* observations from 2005 to 2020 are given in Figure 8. Without considering the inter-annual and intra-

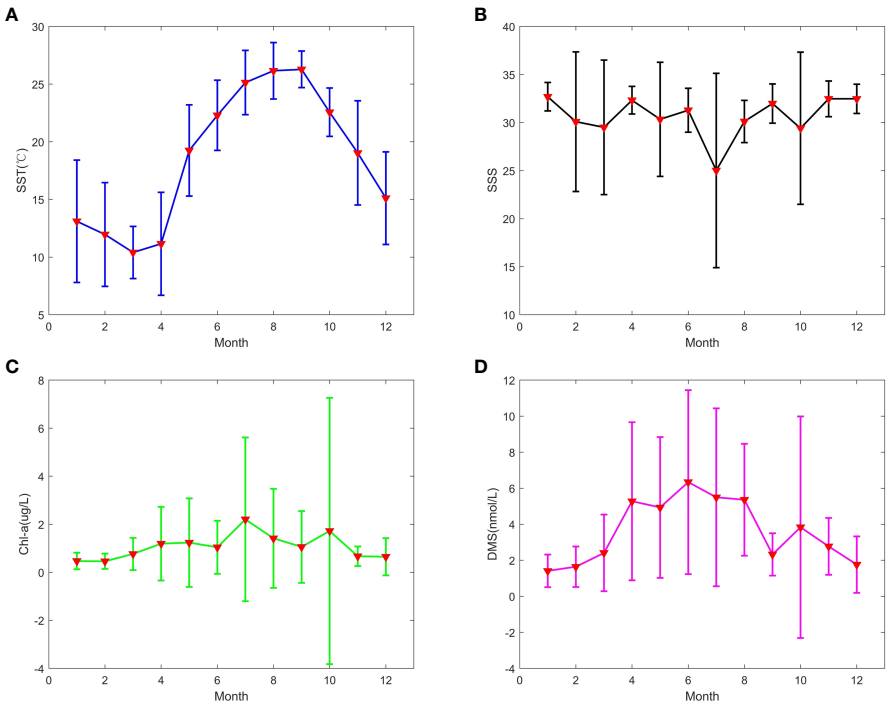

FIGURE 8
Seasonal variations of SST **(A)**,salinity **(B)**,chlorophyll **(C)** and DMS **(D)** in YECS.

seasonal variations of biogenic substances, the surface DMS concentration in YECS showed obvious seasonal variations, which started to increase in March, peaked in April and June, and gradually decreased to a low peak in autumn and winter. The highest value of DMS concentration, 41.21 nmol/L, appeared in April 2017, and its concentration was 41.19 nmol/L in mid-July 2011. It is interesting to note that there were many high values of DMS in the summer and autumn seasons, which led to the fact that the June, July, and October standard deviation of DMS concentration was slightly larger than other months, and the minimum DMS concentration of 0.03 nmol/L existed in December 2009.

The seasonal variation of DMS concentration in the YECS were similar to those of Chl-a concentration and SST (Figure 8), with positive correlations (correlation coefficients r = 0.31, 0.23) and some negative correlations (correlation coefficients r = -0.12) with salinity. Seasonal variations of DMS were characterized by a maximum in summer, followed by a minimum in winter (summer > spring > autumn > winter), with average concentrations of 5.69, 3.96, 3.18, and 1.60 nmol/L, respectively, in all seasons. The lower concentrations of DMS in winter compared to spring and summer are due to reduced solar radiation, resulting in lower sea surface temperatures and decreased phytoplankton activity and productivity. This, in the aggregate, leads to lower SSTs and lower phytoplankton activity and productivity, with a corresponding decrease in zooplankton predation (Yu et al., 2015). It also diminished the rate of DMS secretion from DMSP, resulting in a correspondingly lower peak DMS concentration.

Since DMS and DMSP originate from seaweeds, phytoplankton species and biomass are considered to be important factors in controlling seawater DMS and DMSP concentrations (Liu et al., 2022). The size of phytoplankton biomass can directly influence the concentration of DMS in marine areas. So the main reason for the high DMS in summer and autumn is the rapid reproduction and efficient production of phytoplankton, but the algal species that cause the change of DMS during the high production period in summer and autumn are different in different sea areas. Previous authors have extensively studied the contribution of different algal species in releasing DMSP and DMS content. Their findings suggest that dinoflagellates, golden algae, and methanogens are high producers of DMS (Ma and Yang, 2023), while diatoms and cryptophytes are low producers of DMS (Yang et al., 2012). According to the research, the highest intracellular DMSP content was found in Hirschsprungia (golden algae) at 689 ± 81 mmol L^{-1}, followed by Anterior Gourami (dinoflagellates) at 666 ± 0 mmol L^{-1}, and Streptophyta (diatoms) at only 9 ± 1 mmol L^{-1} (Liss et al., 1994). Additionally, Nudibranchs, which are unicellular organisms distinct from algae, have a much higher DMS production capacity than diatoms due to their higher cellular DMSP content and DMSP lyase activity (Guo et al., 2022).

Consequently, the higher DMS production capacity of phytoplankton in the East China Sea in summer than in autumn is mainly related to the dominance of methanotrophs in phytoplankton abundance (Yang et al., 2008). On the one hand, the proportion of DMS-producing methanotrophs increased with the temperature rise (Zhang et al., 2014). The upwelling along the Zhejiang coast transported a large amount of nutrients to the estuary of the Yangtze River, which promoted the release of chlorophyll from phytoplankton. Suitable temperature intervals and abundant nutrients are optimal for the growth of methanotrophs in environments with high Chl-a concentrations. On the other hand, the cell abundance of dominant algal species was higher in summer compared to autumn, which was dominated by diatoms (Yang et al., 2011). Instead, the phytoplankton population was dominated by diatoms (97.8%), and the production of DMS in the autumn decreased significantly (Yang et al., 2014; Fu et al., 2021b). Although diatoms are low producers of DMS, when they have absolute dominance in phytoplankton species, they can significantly contribute to the production of these compounds. Zheng et al. (2014) report the phytoplankton community in Jiaozhou Bay is primarily composed of diatoms and flagellates, with two peaks of phytoplankton cell counts in February and October(1.108×10^7 cell/m^3 and 4.587×10^6 cell/m^3). Similarly, the abundance of phytoplankton cells detected on the northeast side of Zhoushan Islands was 1.9×10^4 cells/L (Jia et al., 2017). It proves that the amount of DMS produced by large numbers of diatoms is still significant. In contrast to the East China Sea, the flagellates were the predominant algal species responsible for DMS production in the Yellow Sea. Browman et al. (2013) report a 3-fold increase in the growth rate of flagellates from 0.23 to 0.61 d^{-1} between 15 and 20°C, along with almost no growth below 10°C. During the summer, the Yellow Sea experiences high temperatures (22.7 ± 3.8°C) which promote the growth and reproduction of flagellates. These organisms account for 59.6% of the total phytoplankton abundance, leading to a high production of DMS in the northern Yellow Sea. However, the decrease in seawater temperature in the autumn(16.7 ± 3.6°C)weakened its effect on DMS production. Toward spring, the temperature gradually rose and harmful algal blooms occurred frequently in the East China Sea (Yang et al., 2012). At this time, large diatoms and active flagellates dominated the high production of DMS near Hangzhou Bay in early spring and April (Figure 5).

Figure 7 illustrates the monthly average distribution patterns of DMS aboard observation data from 2005 to 2020. In the horizontal distribution, a discernible spatial trend emerges, depicting a gradual decline in DMS concentration along the Zhejiang Province coastline extending towards the open sea. This pattern is intricately linked to the substantial discharge of anthropogenic nutrient salts in the vicinity of the Yangtze River estuary. The average concentration of DMS in YECS was 3.67 nmol/L in March or early spring. Subsequently, there was a progressive rise noted in mid-spring (April), and gradually extended to the far sea, with high concentrations in the coastal area of Liaodong Peninsula and the boundary of the Bohai and Yellow Seas. Notably, a focal point of elevated DMS values emerged in the area of Hangzhou Bay located to the south of the Yangtze River mouth from 26°N-30°N, with 28° N as the center line (the range of concentrations was 26.24-35.09 nmol/L). This distribution bears resemblance to the spatial patterns of Chl-a, likely attributable to both anthropogenic nutrient inputs and phytoplankton blooms in the central Yellow Sea during spring. The zenith of DMS concentration was attained in June, reaching a

peak value of 36.83 nmol/L in the northern Yellow Sea, proximate to the Changshan Islands. Additionally, heightened DMS levels were observed near the area of the mouth of the Yangtze River in the southern Yellow Sea (about 23.60 nmol/L). In September, DMS levels surpassed those in the central Yellow Sea near the Changshan Islands. Subsequently, a decline in DMS concentration commenced in September, punctuated by minor peaks in mid-autumn (October), primarily concentrated in the Yangtze River mouth and Hangzhou Bay areas, where the highest concentration recorded was approximately 37.83 nmol/L. The occurrence of these peaks is ostensibly linked to the proliferation of diatom blooms within this maritime region during autumn. In YECS, Chl-a, DMS, and SST all reached a low peak in winter, and the DMS concentration was lower than 3.65 nmol/L, with the lowest concentration of only 0.03 nmol/L. The peaks of Chl-a, DMS, and SST in YECS were all in the winter.

During the period spanning from early spring to late autumn, persistent high concentrations of dimethyl sulfide (DMS) have been consistently observed in the Yangtze River estuary basin and downstream areas of Hangzhou Bay, Zhejiang Province (Figures 5, 7). This phenomenon is primarily attributed to the discharge of nutrient salts from agricultural and industrial sources, coupled with favorable sea surface temperatures (SST), which create optimal nutrient conditions for phytoplankton proliferation. Consequently, there is a notable proliferation of phytoplankton populations, particularly dominated by diatoms and golden algae, in the vicinity of the Yangtze River mouth. This proliferation ultimately results in abnormally high DMS concentrations around the Zhoushan Islands during autumn.

Unlike environmental parameters such as Chl-a and SST, we do not believe that the level of salinity variability significantly affects the spatial distribution of DMS in YECS. The distribution characteristics of DMS in spring and summer suggest that the enrichment of DMS in the Yangtze River estuary is related to the large amount of nutrients brought by the Changjiang (Yangtze River) Diluted Water (CDW) (Yang et al., 2012) and the favorable SST (Figure 8) that accelerates phytoplankton production efficiency. Speeckaert et al. (2019) observed that the high salinity environment was not conducive to DMS release, and we also revealed no significant correlation between salinity and DMS here. First of all, the abundant nutrients provide conducive nutritional conditions for the growth of microorganisms along the Yangtze River estuary. However, with the burgeoning growth of population and heightened anthropogenic activities (agricultural and industrial runoff), a large number of organic nutrients, such as phosphate and nitrate, have been escalated into China's estuarine and riverine systems. This influx has notably exacerbated the impact on the phytoplankton in the Yangtze River estuary in the East China Sea and other coastal seas (Walling, 2006). In spring and summer, substantial quantities of nutrients are transported by CDW into the East China Sea, leading to elevated DMS concentrations in the estuary and its proximal waters.

At the same time, the offshore of the East China Sea is affected by the oligotrophic Kuroshio and the Taiwan Warm Current (TWC), resulting in low Chl-a concentration, and correspondingly reduced DMS concentration. Secondly, suitable SST is favorable to foster heightened activity of biological enzymes (DMSP lyase in phytoplankton cells) and accelerate the rate of DMSP cleavage to DMS, while too-low or too-high seawater temperature will limit the activity of heterotrophic organisms. It is noteworthy that the anomalous deviations of high Chl-a and DMS concentrations in October were significantly larger than those in other months (Figures 7, 8), which may be attributed to the increase of Chl-a concentration due to the large amount of nutrients brought in by the upwelling along the Fujian coast and the lower SST in the autumn, which led to the occurrence of the high-value zone of DMS concentration along the Fujian coast (Hao et al., 2019). In summary, the distribution of nutrients and SST in the eastern shelf and the influence of the phytoplankton population resulted in the spatial distribution of high DMS in the Changjiang estuary and juxtaposed with a gradual decrease of DMS offshore.

4.2 Analysis of influencing factors of DMS

Light intensity, chlorophyll, SST, nutrients, mixed layer depth, and other factors are pivotal parameters of the marine ecosystems. Variations in these parameters directly affects the living environment of plankton. DMS is produced by the phytoplankton growth and demise cycle, forming the ecological cycle of DMS. The entire cycle, encompassing the release of dimethylsulfoniopropionate (DMSP) to the production and removal of DMS, is subject to modulation by diverse oceanographic factors.

Chl-a is a key pigment that serves as a marker for important phytoplankton groups, such as diatoms and seaweeds, providing a visual measure of phytoplankton biomass within specific marine regions (Fu et al., 2021b). Numerous studies, both domestically and internationally, have consistently underscored a critical relationship between Chl-a concentration, DMSP production rate, and the concentration of DMS. The rate of DMS production was found to be higher in the microlayer and closely associated with the level of chlorophyll a (Zhang et al., 2008) (correlation coefficient r = 0.8828). During the modeling process outlined in this paper, we meticulously analyzed the distinct contribution of each environmental factor. Our findings emphasized that Chl-a had the highest explained variance at 20% (R^2 = 0.20), followed by SST at 8% (R^2 = 0.08), and salinity at only 3% (R^2 = 0.03). This suggests that chlorophyll content has substantial impact on the surface layer of YECS DMS compared to SST and salinity. In April, the coasts of Zhejiang and Fujian witnessed a notable outbreak of DMS (Figure 7) attributable to the spring bloom and high density of Chl-a. This fostered the production of the dominant algal species of DMS, along with the large amount of nutrients carried by the upwelling, which nourished the phytoplankton abundance. The epicenter of the high value of DMS was concentrated along the coast of Zhejiang and Fujian. During the spring and summer seasons in the Yellow Sea, when the Chl-a concentration is low, the dominance of diatoms in the phytoplankton community is relatively waned. Meanwhile, the proportion of methanogens and other algae in the phytoplankton community is instead high. The correlation between the surface DMS concentration and the Chl-a concentration in the two seasons is 0.46 and 0.48, respectively (Shen et al., 2021).

Yang et al. (2014) comprehensively explores the impact of temperature, nutrients, and other factors on the distribution of DMS, as well as its production and consumption rates in the highly productive waters of YECS. Favorable temperatures play a pivotal role in facilitating the growth of phytoplankton, with zooplankton abundance peaks occurring under moderate temperatures alongside ample food availability. Daphnia magna emerges as a significant species in YECS ecosystem. The intensified predation of Daphnia magna increases significantly within the temperature range of 15~25°C, and the concentration of DMS is elevated (Yu et al., 2015). At higher concentrations of CO_2 and temperatures, bacterial production of DMS may decrease, leading to a decrease in DMS concentration (Yan et al., 2023). The decrease in the spatial extent of high DMS concentration, alongside their migration towards the eastern shelf coast during the transition from June to July, may indeed be linked to the increase in SST.

The relationship between salinity and DMS production is somewhat controversial. Gao et al. (2017) reported a significant positive correlation between DMS and Chl-a, temperature, and salinity in the Yangtze River estuary during winter (Correlation coefficient between salinity and DMS is r=0.414). However, during summer, the correlation between salinity and DMS was not as pronounced (r=0.060) in this research. Conversely, Guo et al. (2022) calculated a statistically significant negative correlation (r= -0.236) between DMS and salinity in the Bohai and North Yellow Seas in summer. Li et al. (2015) concluded that the surface salinity of the North Yellow Sea during winter did not significantly influence the productivity and consumption rate of DMS. It is noteworthy that DMS production tends to be lower during winter, as evidenced by the overall DMS concentration in YECS, which typically ranges from 0.07-3.65 nmol/L (Figure 7). Furthermore, the salinity remains stable within the range of (33-34) during this season. The observed strong correlation between DMS and salinity in the Yangtze River estuary during winter can be attributed to the reduction of biological activity on the sea surface caused by low SST and high salinity, which due to current systems such as the CDW and TWC. Yet, it is crucial to acknowledge that this correlation does not take into account the internal interaction of environmental elements. Our study found no significant correlation between the overall surface salinity and DMS concentration in YECS. This conclusion was drawn based on the negative correlation between the monthly mean salinity and DMS concentration from 2005 to 2020, the minimal difference between the indicators of EXP1 and EXP2 in the BP model (Table 3), and the results of the sensitivity tests of the individual environmental factors.

Moreover, it is crucial to note that while most disparities between BPNN estimates and observations fell within minimal margins (0-2 nmol/L) (Figure 6), the occurrence of extreme DMS values during specific months (April, May, June, and October) underscores the necessity of considering a broader range of environmental factors beyond those examined in this study. This discrepancy likely stems from the intricate interplay of physical, chemical, and biological processes within near-shore regions. The concentration of DMS is influenced not only by variables such as Chl-a, SST, and SSS (which were incorporated into the modeling) but also by factors like nutrient concentration, upwelling dynamics (Mansour et al., 2023), ENSO phenomena and the depth of the mixed layer (MLD), among others.

For instance, the Zhoushan fishery, situated in a well-developed upwelling zone along Zhejiang Province's coast, experiences nutrient-rich seawater upwelling from the deep sea's lower layers to the ocean's upper layer. This continuous nutrient influx sustains phytoplankton growth, leading to enhanced DMS production in the vicinity of Zhoushan. The slightly lower estimated DMS concentration along the Zhejiang and Fujian coasts in March and April, compared to the original observed concentrations, may be associated with this phenomenon (Figure 6). The variability of DMS emission fluxes associated with ENSO primarily arises from heightened wind speeds during La Niña events. High-frequency ENSO impacts positively the sea-air exchange fluxes of DMS (Xu et al., 2016), potentially eliciting a favorable response of DMS concentrations in the East China Sea to ENSO occurrences in the Pacific Ocean. The oceanic mixing layer serves as a reservoir for a considerable amount of heat generated by diverse dynamical processes. When the mixing layer depth is relatively shallow, a positive correlation is observed between mixing depth and nutrient concentrations. As the mixing layer deepens, the nutrient layer replenishes the upper ocean with increased nutrients, thereby augmenting chlorophyll responses. The elevated DMS concentration in the low/mid-latitude region is propelled by the combination of shallow MLD and intense irradiance (Wang et al., 2020). Situated in the subtropical low-latitude zone, the Yangtze River estuary basin experiences low cloud cover and high light intensity during summer. The MLD in this region is influenced by the CDW and the Kuroshio, both of which contribute to MLD deepening. Variations in these factors may trigger DMS outbreaks along the Yangtze River estuary coast during the summer months (Figure 5).

5 Conclusions

Based on the BPNN algorithm, a new method for estimating surface seawater DMS of the YECS is proposed by utilizing the physicochemical parameters. The spatiotemporal variations of the DMS were analyzed and the environmental factors influencing on DMS was discussed, leading to the following key conclusions:

(1) The surface DMS in YECS can be optimally estimated utilizing the seawater BPNN model, exhibiting the highest explainable variance (71%) and superior simulation accuracy. The model incorporates six crucial parameters: month, latitude, longitude, Chl-a, SST, and SSS.

(2) Sensitivity tests underscored the predominant role of Chl-a in influencing DMS levels in YECS surpassing the impact of SST and salinity. As the foremost parameter shaping DMS response, the mechanistic underpinnings of Chl-a should be prioritized in DMS forecasting and hindcasting studies. A comparative evaluation of BPNN model performance across different parameter combinations of reveals that the

effect of salinity on DMS concentration in YECS is negligible.

(3) The concentration of DMS in the YECS was influenced by a confluence of environmental factors and precursor biomass. It was positively correlated with Chl-a and SST, while displaying a negative correlation with SSS. Leveraging the optimal model, we scrutinized the spatial and temporal distribution of DMS concentrations in YECS. The results delineated higher DMS concentrations during spring and summer compared to autumn and winter. Specifically, elevated concentrations of DMS were higher in the coastal waters(121°-123°E, 27°-28°N) and (124°-127°E, 29°-32°N) during spring, with coastal regions exhibiting higher concentrations relative to that of the open sea. Moreover, a discernible gradient of decreasing DMS concentrations was noted from the Yangtze River estuary towards offshore regions.

(4) The model developed in this paper aligns with existing literature regarding seasonal variations and spatial distributions. However, the estimation error is exacerbated by the intricate interplay of physical, chemical, and biological processes impacting the surface DMS concentration in near-shore waters. In addition to incorporating Chl-a, SST, SSS, time, and location information, this study recommends further exploration of physicochemical parameters such as photosynthetically active radiation(PAR), nutrient concentration, MLD, ENSO, and other relevant factors in the modeling framework.

Data availability statement

The dataset in this study are observational data and are not available to the public. Requests to access the datasets should be directed to Guo Wenning, 358120152@qq.com.

Author contributions

GW: Conceptualization, Data curation, Formal analysis, Funding acquisition, Investigation, Methodology, Project administration, Resources, Software, Supervision, Validation, Visualization, Writing – original draft, Writing – review & editing. SQ: Formal analysis, Funding acquisition, Project administration, Resources, Supervision, Validation, Writing – review & editing. WS: Validation, Writing – review & editing. ZZ: Validation, Writing – review & editing.

Funding

The author(s) declare financial support was received for the research, authorship, and/or publication of this article. This project was supported by National Key Research and Development Program of China (2023YFC3108203) and Laoshan Laboratory Science and Technology Innovation Program (LSKJ202202104).

Acknowledgments

We would like to thank Prof. Liang Zhao and his team at the Physical Oceanography Laboratory for their support and help. We would like to thank Jia-Wei Shen for organizing and providing the observation data.

Conflict of interest

The authors declare that the research was conducted in the absence of any commercial or financial relationships that could be construed as a potential conflict of interest.

Publisher's note

All claims expressed in this article are solely those of the authors and do not necessarily represent those of their affiliated organizations, or those of the publisher, the editors and the reviewers. Any product that may be evaluated in this article, or claim that may be made by its manufacturer, is not guaranteed or endorsed by the publisher.

References

Andreae, M. O. (1990). Ocean-atmosphere interactions in the global biogeochemical sulfur cycle. *Mar. Chem.* 30, 1–29. doi: 10.1016/0304-4203(90)90059-L

Archer, S. D., Kimmance, S. A., Stephens, J. A., Hopkins, F. E., Bellerby, R. G. J., Schulz, K. G., et al. (2013). Contrasting responses of DMS and DMSP to ocean acidification in Arctic waters. *Biogeosciences* 10, 1893–1908. doi: 10.5194/bg-10-1893-2013

Ayers, G. P., Ivey, J. P., and Gillett, R. W. (1991). Coherence between seasonal cycles of dimethyl sulphide, methanesulphonate and sulphate in marine air. *Nature* 349, 404–406. doi: 10.1038/349404a0

Bell, T. G., Porter, J. G., Wang, W.-L., Lawler, M. J., Boss, E., Behrenfeld, M. J., et al. (2021). Predictability of seawater DMS during the North Atlantic aerosol and marine ecosystem study (NAAMES). *Front. Mar. Sci.* 7. doi: 10.3389/fmars.2020.596763

Browman, H., Boyd, P. W., Rynearson, T. A., Armstrong, E. A., Fu, F., Hayashi, K., et al. (2013). Marine phytoplankton temperature versus growth responses from polar to tropical waters – outcome of a scientific community-wide study. *PloS One* 8, 63091–63108. doi: 10.1371/journal.pone.0063091

Challenger, F., and Simpson, M. I. (1948). Studies on biological methylation; a precursor of the dimethyl sulphide evolved by Polysiphonia fastigiata; dimethyl-2-carboxyethylsulphonium hydroxide and its salts. *Biochem. J.* 3, 1591–1597. doi: 10.1039/jr9480001591

Charlson, R. J., Lovelock, J. E., Andreae, M. O., and Warren, S. G. (1987). Oceanic phytoplankton, atmospheric sulphur, cloud albedo and climate. *Nature* 326, 655–661. doi: 10.1038/326655a0

Fu, X., Liu, W., and Hu, H. (2021a). Remote sensing inversion modeling of chlorophyll-a concentration in Wuliangsuhai Lake based on BP neural network. *JPCS* 1955, 012103–012109. doi: 10.1088/1742-6596/1955/1/012103

Fu, X., Sun, J., Wei, Y., Liu, Z., Xin, Y., Guo, Y., et al. (2021b). Seasonal shift of a phytoplankton (>5 μm) community in Bohai Sea and the adjacent Yellow Sea. *Diversity* 13, 65–84. doi: 10.3390/d13020065

Fung, K. M., Heald, C. L., Kroll, J. H., Wang, S., Jo, D. S., Gettelman, A., et al. (2022). Exploring dimethyl sulfide (DMS) oxidation and implications for global aerosol radiative forcing. *Atmos. Chem. Phys.* 22, 1549–1573. doi: 10.5194/acp-22-1549-2022

Galí, M., Levasseur, M., Devred, E., Simó, R., and Babin, M. (2018). Sea-surface dimethylsulfide (DMS) concentration from satellite data at global and regional scales. *Biogeosciences* 15, 3497–3519. doi: 10.5194/bg-15-3497-2018

Gao, N., Yang, G.-P., Zhang, H.-H., and Liu, L. (2017). Temporal and spatial variations of three dimethylated sulfur compounds in the Changjiang Estuary and its adjacent area during summer and winter. *Environ. Chem.* 14, 160–177. doi: 10.1071/EN16158

Grandey, B. S., and Wang, C. (2015). Enhanced marine sulphur emissions offset global warming and impact rainautumn. *Sci. Rep.* 5, 13055–13061. doi: 10.1038/srep13055

Guo, Y., Peng, L., Liu, Z., Fu, X., Zhang, G., Gu, T., et al. (2022). Study on the seasonal variations of dimethyl sulfide, its precursors and their impact factors in the Bohai Sea and North Yellow Sea. *Front. Mar. Sci.* 9. doi: 10.3389/fmars.2022.999350

Hao, Q., Chai, F., Xiu, P., Bai, Y., Chen, J., Liu, C.-G., et al. (2019). Spatial and temporal variation in chlorophyll a concentration in the Eastern China Seas based on a locally modified satellite dataset. Estuar. *Coast. Shelf Sci.* 220, 220–231. doi: 10.1016/j.ecss.2019.01.004

Jia, T., Zhang, H.-H., and Zhang, S.-H. (2017). Concentration distribution and influencing factors of dimethyl organic sulfide in the East China Sea in fall. *Mar. Environ. Sci. (in Chinese)* 36, 21–28. doi: 10.13634/j.cnki.mes.2017.01.004

Keller, M. D., Bellows, W. K., and Guillard, R. R. L. (1989). Dimethyl sulfide production in marine phytoplankton. *J. Am. Chem. Soc.*, 167–182. doi: 10.1021/bk-1989-0393.ch011

Kettle, A. J., and Andreae, M. O. (2000). Flux of dimethylsulfide from the oceans: A comparison of updated data sets and flux models. *J. Geophys. Res. Atmos.* 105, 26793–26808. doi: 10.1029/2000JD900252

Kloster, S., Feichter, J., Maier-Reimer, E., Six, K. D., Stier, P., and Wetzel, P. J. B. (2005). DMS cycle in the marine ocean-atmosphere system – a global model study. *Biogeosciences* 3, 29–51. doi: 10.5194/bgd-2-1067-2005

Kloster, S., Six, K. D., Feichter, J., Maier-Reimer, E., Roeckner, E., Wetzel, P., et al. (2007). Response of dimethylsulfide (DMS) in the ocean and atmosphere to global warming. *J. Geophys. Res-biogeo.* 112, 3005–1-3005-13. doi: 10.1029/2006JG000224

Li, S. Y., Sun, Q., and Guo, W. (2023a). Variability of DMS in the East China Sea and its response to different ENSO categories. *Ecol. Indic.* 147, 109963–109972. doi: 10.1016/j.ecolind.2023.109963

Li, S. Y., Sun, Q., Yao, J., and Zhao, L. (2023b). Characterization of spatial and temporal variations of dimethyl sulfide in the East China Sea and analysis of influencing factors. *Chin. Environ. Sci. (in Chinese)* 43, 2470–2479. doi: 10.19674/j.cnki.issn1000-6923.20230104.015

Li, C.-X., Yang, G.-P., and Wang, B.-D. (2015). Biological production and spatial variation of dimethylated sulfur compounds and their relation with plankton in the North Yellow Sea. *Cont. Shelf Res.* 102, 19–32. doi: 10.1016/j.csr.2015.04.013

Li, F., Zhao, L., Shen, J. W., Yao, J., and Wang, S. (2022). Modeling and analysis of DMS concentration changes in the Yellow Sea under the future RCP4.5 scenario. *Chin. Environ. Sci. (in Chinese)* 42, 4304–4314. doi: 10.19674/j.cnki.issn1000-6923.20220507.005

Liss, P. S., Hatton, A. D., Malin, G., Nightingale, P. D., and Turner, S. M. (1997). Marine sulphur emissions. *Philos. Trans. R. Soc B* 352, 159–169. doi: 10.1098/rstb.1997.0011

Liss, P. S., Malin, G., Turner, S. M., and Holligan, P. M. (1994). Dimethyl sulphide and *Phaeocystis*: A review. *J. Mar. Syst.* 5, 41–53. doi: 10.1016/0924-7963(94)90015-9

Liu, C.-Y., Han, L., Wang, L.-L., Li, P.-F., and Yang, G.-P. (2022). Dimethylsulfoniopropionate, dimethylsulfide, and acrylic acid of a typical semi-enclosed bay in the western Yellow Sea: Spatiotemporal variations and influencing factors. *Mar. Chem.* 245, 104159–104171. doi: 10.1016/j.marchem.2022.104159

Ma, Q.-Y., and Yang, G.-P. (2023). Roles of phytoplankton, microzooplankton, and bacteria in DMSP and DMS transformation processes in the East China Continental Sea. *Prog. Oceanogr.* 213, 103003–103016. doi: 10.1016/j.pocean.2023.103003

Mansour, K., Decesari, S., Ceburnis, D., Ovadnevaite, J., and Rinaldi, M. (2023). Machine learning for prediction of daily sea surface dimethylsulfide concentration and emission flux over the North Atlantic Ocean, (1998–2021). *Sci. Total Environ.* 871, 162123–162136. doi: 10.1016/j.scitotenv.2023.162123

McNabb, B. J., and Tortell, P. D. (2022). Improved prediction of dimethyl sulfide (DMS) distributions in the northeast subarctic Pacific using machine-learning algorithms. *Biogeosciences* 19, 1705–1721. doi: 10.5194/bg-19-1705-2022

Quinn, P. K., and Bates, T. S. (2011). The case against climate regulation via oceanic phytoplankton sulphur emissions. *Nature* 480, 51–56. doi: 10.1038/nature10580

Sarwar, G., Kang, D., Henderson, B. H., Hogrefe, C., Appel, W., and Mathur, R. (2023). Examining the impact of dimethyl sulfide emissions on atmospheric sulfate over the continental U.S. *Atmos* 14, 11–19. doi: 10.3390/atmos14040660

Sciare, J., Mihalopoulos, N., and Dentener, F. J. (2000). Interannual variability of atmospheric dimethylsulfide in the southern Indian Ocean. *J. Geophys. Res. Atmos.* 105, 26369–26377. doi: 10.1029/2000JD900236

Shen, J.-W. (2019). Research and Application of Dimethyl Sulfur Cycle Modeling in YECS. No. 29, 13th Street, Binhai New Area, Tianjin, China: Tianjin University of Science and Technology. Master's Degree Dissertation. doi: 10.27359/d.cnki.gtqgu.2019.000272

Shen, J.-W., Zhao, L., Wang, S.-J., and Li, Y.-X. (2019). Multivariate analysis and modeling of dimethyl sulfide and environmental factors in the Yellow and East China Seas. *Chin. Environ. Sci.(in Chinese)* 39, 2514–2522. doi: 10.19674/j.cnki.issn1000-6923.2019.0300

Shen, J.-W., Zhao, L., Zhang, H.-H., Wei, H., and Guo, X. (2021). Controlling factors of annual cycle of dimethylsulfide in the Yellow and East China seas. *Mar. pollut. Bull.* 169, 112517–112525. doi: 10.1016/j.marpolbul.2021.112517

Speeckaert, G., Borges, A. V., and Gypens, N. (2019). Salinity and growth effects on dimethylsulfoniopropionate (DMSP) and dimethylsulfoxide (DMSO) cell quotas of Skeletonema costatum, Phaeocystis globosa and Heterocapsa triquetra. *Estuar. Coast. Shelf Sci.* 226, 106275–106285. doi: 10.1016/j.ecss.2019.106275

Toole, D. A., Kieber, D. J., Kiene, R. P., White, E. M., Bisgrove, J., Del Valle, D. A., et al. (2004). High dimethylsulfide photolysis rates in nitrate-rich Antarctic waters. *Geophys. Res. Lett.* 31, 1019863–1019866. doi: 10.1029/2004GL019863

Vogt, M., and Liss, P. (2009). Dimethylsulfide and climate. Surface ocean-lower atmosphere processes. *Geophys. Res.* 187, 197–232. doi: 10.1029/2008GM000790

Walling, D. E. (2006). Human impact on land–ocean sediment transfer by the world's rivers. *Geomo* 79, 192–216. doi: 10.1016/j.geomorph.2006.06.019

Wang, W.-L., Song, G., Primeau, F., Saltzman, E. S., Bell, T. G., and Moore, J. K. (2020). Global ocean dimethyl sulfide climatology estimated from observations and an artificial neural network. *Biogeosciences* 17, 5335–5354. doi: 10.5194/bg-17-5335-2020

Xu, L., Cameron-Smith, P., Russell, L. M., Ghan, S. J., Liu, Y., Elliott, S., et al. (2016). DMS role in ENSO cycle in the tropics. *J. Geophys. Res. Atmos.* 121, 1–22. doi: 10.1002/2016JD025333

Xue, L., Kieber, D. J., Masdeu-Navarro, M., Cabrera-Brufau, M., Rodríguez-Ros, P., Gardner, S. G., et al. (2022). Concentrations, sources, and biological consumption of acrylate and DMSP in the tropical Pacific and coral reef ecosystem in Mo'orea, French Polynesia. *Front. Mar. Sci.* 9. doi: 10.3389/fmars.2022.911522

Yan, S.-B., Li, X.-J., Xu, F., Zhang, H.-H., Wang, J., Zhang, Y., et al. (2023). High-resolution distribution and emission of dimethyl sulfide and its relationship with pCO2 in the Northwest Pacific Ocean. *Front. Mar. Sci.* 10. doi: 10.3389/fmars.2023.1074474

Yang, G.-P., Jing, W.-W., Kang, Z.-Q., Zhang, H.-H., and Song, G.-S. (2008). Spatial variations of dimethylsulfide and dimethylsulfoniopropionate in the surface microlayer and in the subsurface waters of the South China Sea during springtime. *Mar. Environ. Res.* 65, 85–97. doi: 10.1016/j.marenvres.2007.09.002

Yang, G. P., Song, Y. Z., Zhang, H. H., Li, C. X., and Wu, G. W. (2014). Seasonal variation and biogeochemical cycling of dimethylsulfide (DMS) and dimethylsulfoniopropionate (DMSP) in the Yellow Sea and Bohai Sea. *J. Geophys. Res-oceans.* 119, 8897–8915. doi: 10.1002/2014JC010373

Yang, G.-P., Zhang, H.-H., Zhou, L.-M., and Yang, J. (2011). Temporal and spatial variations of dimethylsulfide (DMS) and dimethylsulfoniopropionate (DMSP) in the East China Sea and the Yellow Sea. *Cont. Shelf Res.* 31, 1325–1335. doi: 10.1016/j.csr.2011.05.001

Yang, G.-P., Zhuang, G.-C., Zhang, H.-H., Dong, Y., and Yang, J. (2012). Distribution of dimethylsulfide and dimethylsulfoniopropionate in the Yellow Sea and the East China Sea during spring: Spatio-temporal variability and controlling factors. *Mar. Chem.* 138-139, 21–31. doi: 10.1016/j.marchem.2012.05.003

Yu, J., Tian, J.-Y., and Yang, G.-P. (2015). Effects of Harpacticus sp. (Harpacticoida, copepod) grazing on dimethylsulfoniopropionate and dimethylsulfide concentrations in seawater. *J. Sea Res.* 99, 17–25. doi: 10.1016/j.seares.2015.01.004

Zhang, S.-H., Yang, G.-P., Zhang, H.-H., and Yang, J. (2014). Spatial variation of biogenic sulfur in the south Yellow Sea and the East China Sea during summer and its contribution to atmospheric sulfate aerosol. *Sci. Total Environ.* 488-489, 157–167. doi: 10.1016/j.scitotenv.2014.04.074

Zhang, H.-H., Yang, G.-P., and Zhu, T. (2008). Distribution and cycling of dimethylsulfide (DMS) and dimethylsulfoniopropionate (DMSP) in the sea-surface microlayer of the Yellow Sea, China, in spring. *Cont. Shelf Res.* 28, 2417–2427. doi: 10.1016/j.csr.2008.06.003

Zheng, S., Sun, X.-X., Zhao, Y.-F., and Sun, S. (2014). Annual variation of species composition and abundance distribution of phytoplankton in 2010 in the Jiaozhou Bay. *Mar. Sci. (in Chinese)* 38, 1–6. doi: 10.11759/hykx20130222002

frontiers | Frontiers in Marine Science

TYPE Original Research
PUBLISHED 08 July 2024
DOI 10.3389/fmars.2024.1433305

Check for updates

OPEN ACCESS

EDITED BY
Junfu Dong,
Shandong University, China

REVIEWED BY
Sai Wang,
Hainan University, China
Hu He,
Chinese Academy of Sciences (CAS), China
Naicheng Wu,
Ningbo University, China

*CORRESPONDENCE
Liangliang Huang
llhuang@glut.edu.cn

RECEIVED 15 May 2024
ACCEPTED 24 June 2024
PUBLISHED 08 July 2024

CITATION
Wang C, Huang L, Kang B, Zhu L, Liu H, Zhao S, Cheng Y, Shahab A and Yan Y (2024) Interspecific differences in ecological stoichiometric characteristics of invertebrates and their influencing factors from the Beibu Gulf, China.
Front. Mar. Sci. 11:1433305.
doi: 10.3389/fmars.2024.1433305

COPYRIGHT
© 2024 Wang, Huang, Kang, Zhu, Liu, Zhao, Cheng, Shahab and Yan. This is an open-access article distributed under the terms of the Creative Commons Attribution License (CC BY). The use, distribution or reproduction in other forums is permitted, provided the original author(s) and the copyright owner(s) are credited and that the original publication in this journal is cited, in accordance with accepted academic practice. No use, distribution or reproduction is permitted which does not comply with these terms.

Interspecific differences in ecological stoichiometric characteristics of invertebrates and their influencing factors from the Beibu Gulf, China

Caiguang Wang[1,2], Liangliang Huang[1,3]*, Bin Kang[4], Liang Zhu[1,2], Hao Liu[1,3], Shuwen Zhao[1], Yanan Cheng[1], Asfandyar Shahab[1] and Yunrong Yan[5]

[1]College of Environmental Science and Engineering, Guilin University of Technology, Guilin, China, [2]Guangxi Key Laboratory of Environmental Pollution Control Theory and Technology, Guilin, China, [3]Guangxi Collaborative Innovation Center for Water Pollution Control and Water Safety in Karst Areas, Guilin, China, [4]College of Fisheries, Ocean University of China, Qingdao, China, [5]College of Fisheries, Guangdong Ocean University, Zhanjiang, China

Invertebrates can store carbon (C), nitrogen (N), phosphorus (P), and other elements in their body tissues at theoretically homeostatic rates, thus playing an important role in the biogeochemical cycle of aquatic ecosystems. To sustain homeostasis, consumers must either balance their resource supply or adjust their stoichiometric features in response to environmental changes. However, there is limited understanding regarding potential differences in the ecological stoichiometric characteristics of marine invertebrates. To explore the ecological stoichiometric characteristics of marine invertebrates, the C, N, P, calcium (Ca), $\delta^{13}C$, and $\delta^{15}N$ contents of 18 invertebrate species were analyzed from the Beibu Gulf. The results revealed that the ranges of elemental variations (C, N, and P) in invertebrates were 25.17%-47.34%, 6.14%-14.13%, and 0.26%-1.31%, respectively. The content of P in invertebrates exhibited the most significant variation, leading to alterations in C:P and N:P ratios. A significant negative correlation was observed between P content and body weight in invertebrates ($p < 0.01$). Furthermore, the C and N content of invertebrates were significantly negatively correlated with $\delta^{13}C$ ($p < 0.01$), suggesting that the variations in C content and N content in invertebrates are influenced by different food sources, while P content varies according to body size. Our results also indicated significant interspecific differences in the ecological stoichiometry of invertebrates from the Beibu Gulf ($p < 0.05$). Invertebrate growth may be inhibited by P, and they do not maintain strict homeostasis, with stable homeostasis observed in higher trophic levels.

KEYWORDS

ecological stoichiometry, stable isotope, homeostatic, marine invertebrates, Beibu Gulf

Introduction

Ecological stoichiometry offers a unifying conceptual framework that integrates various facets of aquatic biology, encompassing fish physiology, population ecology, community dynamics, ecosystem functions, and evolutionary processes (Bogotá-Gregory et al., 2020). This theory explores the balance of energy and diverse elements within ecological processes, proposing that the elemental composition of organisms reflects their chemical element requirements and the extent of elemental homeostasis (Sterner and Elser, 2002; Fernández-Martínez, 2022). All living organisms are composed of a series of fundamental chemical elements, especially carbon (C), nitrogen (N), phosphorus (P), among others (Sterner and Elser, 2002), and their ecological stoichiometric characteristics serve as crucial indicators for growth and development, life history changes, and biological characteristics of organisms (Peñuelas et al., 2019). However, the proportions of these elements in organisms exhibit significant variation, both across taxa and trophic groups (Elser et al., 2000; Peñuelas et al., 2019; May and El-Sabaawi, 2022).

The primary focus of current ecological stoichiometry research is on nutrient dynamics (Laspoumaderes et al., 2022), microbial nutrition (Wang Z. et al., 2022), host-pathogen relationships (Price et al., 2021), consumer-driven nutrient cycles (Leroux et al., 2020), biogeography of organic matter stoichiometry (Martiny et al., 2013), population dynamics and elementome diversity (Williamson and Ozersky, 2019; Fernández-Martínez, 2022), forest succession and recession (Bin et al., 2022), nutrient limitation (Hessen et al., 2004), food webs (Pacioglu et al., 2021), biological evolution (Jeyasingh et al., 2014), biological invasions (González et al., 2010; Williamson and Ozersky, 2019), and biogeochemical niches (Sardans et al., 2021). However, the ecological stoichiometry of marine invertebrates remains largely unexplored. Invertebrates, as the main consumers within marine ecosystems, play a pivotal role in the material cycle of ecosystems. The C:N:P contents of these consumers serve as an indicator of their respective elemental demand ratios. Any imbalance in these nutritional ratios between consumers and their prey can significantly affect the growth, reproduction, metabolism, and ultimately the ecological processes of the entire population (Sterner et al., 1992; Regnier et al., 2013).

Inter- and intraspecific differences in organismal stoichiometry have been confirmed across various animal taxa, offering significant insights into evolutionary patterns within this domain (Vanni et al., 2002). The ecological stoichiometry of fishery catches exhibits both intra- and interspecific variations, primarily influenced by ontogeny and environmental conditions such as food quality, nutritional status, resources, and habitat (Benstead et al., 2014; Sullam et al., 2015). Some organisms undergo substantial shifts in their elemental composition during development, specifically vertebrates. For instance, the formation of phosphorus-rich bones results in a significant increase in whole-body P content in species like fish, amphibians, and reptiles (Sterrett et al., 2015; Tiegs et al., 2016). Furthermore, the distribution and proportion of carbon-rich lipids, nitrogen-rich muscles, and carbon-rich invertebrate chitin shell materials also significantly affect the ecological stoichiometric characteristics of organisms during development (Pilati and Vanni, 2007; Boros et al., 2015). These changes are also affected by biological genetic characteristics, with different organisms exhibiting unique morphological structures. Additionally, interspecific differences in ecological stoichiometry may arise from variations in food sources (Naddafi et al., 2009; Sun et al., 2014). Food stoichiometry can affect nutrient acquisition and growth rates in consumers, as well as the rate and proportion of the release of nutrient waste into the environment (Elser and Urabe, 1999). For example, daphniids consuming phosphorus-deficient food will experience alterations in their growth rate and body P content (DeMott et al., 2004). Changes in the stoichiometric characteristics of C, N, and P are inherently linked to material circulation and energy flow, which regulate the relationship between the trophic levels within the food web by affecting the biodiversity and species abundance of the community, exerting a decisive influence on the structure and function of ecosystems (Sardans et al., 2012; Wang et al., 2018a). Conversely, the structure of food webs and nutrient cycling can also influence the stoichiometry of C, N, and P.

The Beibu Gulf (105°40′~110°10′ E, 17°00′~21°45′ N) is a semi-enclosed bay in the northern South China Sea, characterized by its tropical and subtropical climate. This unique geographical environment contributes to its high productivity and abundant fishery resources (Qiao and Li, 2007). However, significant declines have been observed in the primary high-quality fishery resources and their communities in the Beibu Gulf due to factors such as overfishing, environmental pollution, and global climate change (Lao et al., 2021; Xu et al., 2022). Current studies on fishery catches in the Beibu Gulf mainly focus on the biological characteristics of economic fish species (Li et al., 2009; Wang J. et al., 2022), biotoxicology (Koongolla et al., 2022; Lu and Wang, 2023), as well as fishery resources investigations and dynamic analysis (Hou et al., 2021). However, systematic research data on the ecological stoichiometry of species within marine ecosystems are conspicuously lacking.

The examination of the ecological stoichiometry of invertebrates is essential for understanding the cycling of C, N, and P nutrients within the increasingly impacted coastal marine ecosystem. This study aimed to explore the ecological stoichiometric characteristics of invertebrates and their influencing factors by analyzing the contents of C, N, P, calcium (Ca), $\delta^{13}C$, and $\delta^{15}N$ in invertebrates from the Beibu Gulf. We hypothesized that variations in elemental stoichiometry among invertebrates could be attributed to changes in body size, genetic relationships, and available food sources. We further explored interspecific variations in the C:N:P contents of invertebrates and the drivers responsible for its homeostasis changes. The results will provide evidence to reveal the balance of C, N, and P elements among consumers, thereby guiding for biogeochemical cycle, conservation, and management of fishery resources in the Beibu Gulf.

Materials and methods

Sampling

In April and August 2022, a fishing vessel equipped with a 441-kilowatt main engine was deployed in the Beibu Gulf to collect marine invertebrates via bottom trawling (Figure 1). The trawl net was 20 meters in length, 8 meters in width, and 3 meters in height,

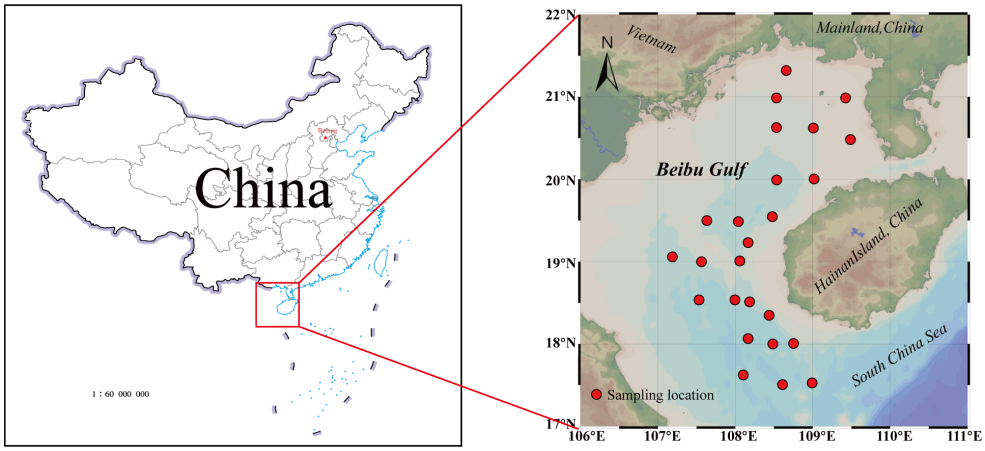

FIGURE 1
Distribution of sampling sites in the Beibu Gulf.

with mesh sizes ranging between 1 and 5 centimeters. All samples were stored at -20 °C before being transported to the laboratory for further analysis.

Sample preparation and element determination

All invertebrates were thawed and weighed to the nearest ± 0.1 g, with total length measured using vernier calipers to an accuracy of ± 1 mm. The invertebrates underwent gutting and freeze-drying processes, followed by grinding into fine powder using a grinding mill and sieving through a 60-mesh sieve to ensure homogeneity. Smaller individuals from both shellfish and shrimp samples were combined into a single sample. A 2.5-4.0 mg dry sample was embedded in tin capsules and analyzed for C and N using an elemental analyzer (EA2400II). For the determination of $\delta^{13}C$ and $\delta^{15}N$, 0.40-0.45 mg of each sample was weighed and embedded in tin capsules and burned at high temperature in an EA Isolink Elemental Analyzer (Thermo Fisher Scientific, Waltham, MA, USA) to produce CO_2 and N_2. The gas was analyzed by a 253 Plus Isotope Mass Spectrometer (Thermo Fisher Scientific, Waltham, MA, USA) for stable isotope analysis. P and Ca contents were determined by ICP-OES (Optima 7000DV). Prior to analysis, approximately 0.2 g of dried sample was digested in 7 mL of mixed acid (HNO_3:H_2O_2 = 5:2) using microwave digestion. The mixture was then heated on a hot plate at 100 °C for 30 minutes to evaporate excess acid, diluted to 50 mL with ultrapure water, and subsequently analyzed by ICP-OES. The recovery rates of Ca and P were 91.67 ± 6.76% and 92.86 ± 6.37%, respectively. The results of C, N, P, and Ca contents are expressed as dry mass percentages (%), while the C:N, C:P, and N:P ratios are molar ratios of elements.

Statistical analyses

The basic statistical analysis of the C, N, and P contents and their ratios was initially carried out for all invertebrate samples. The normal distribution was tested by Kolmogorov-Smirnov test. Differences in the ecological stoichiometric characteristics among invertebrate taxa were analyzed by principal coordinate analysis (PCoA) and analysis of similarities (ANOSIM). One-way analysis of variance (ANOVA) was utilized to compare the C, N, and P contents and $\delta^{13}C$ and $\delta^{15}N$ values across different taxa. Pearson correlation analysis was conducted to determine the relationship between elemental contents and ratios, body weight, $\delta^{13}C$ and $\delta^{15}N$. All statistical analyses were performed using SPSS 23.0, Excel 2016, and graphing was done with R (Version 4.0.3) and OriginPro 2021.

Results

Elemental composition of invertebrates

A total of 18 species of invertebrates (n = 130) were collected in this study, revealing significant variations in their elemental contents (Table 1). Specifically, the ranges for C, N, and P contents were 25.17%-47.34%, 6.14%-14.13%, and 0.26%-1.31%, respectively. The ratios of C:N, C:P, and N:P varied between 3.67-6.87, 55.72-348.08, and 4.67-42.72, respectively. Among these elements, the coefficient of variation (CV) was highest for P, followed by N and C. Notably, larger variations in P content corresponded to more significant changes in both C:P and N:P ratios, whereas the C:N ratio demonstrated relatively minor variations.

Relationship of ecological stoichiometry characteristics of invertebrates

Correlation analysis revealed that the C:N and N content, C:P and P content, and N:P and P content of invertebrates in the Beibu Gulf were all significantly negatively correlated. Conversely, there was a significant positive correlation between C:P and C content, N:

10.3389/fmars.2024.1433305

TABLE 1 C, N and P contents and their ratios in invertebrate taxa from the Beibu Gulf.

Items	Statistics	Shrimps (*n*=34)	Crabs (*n*=18)	Shellfish (*n*=57)	Cephalopods (*n*=19)	Sea cucumber (*n*=2)
C%	Mean ± SD	43.67 ± 2.51	31.33 ± 2.96	42.73 ± 1.89	45.22 ± 1.25	35.53 ± 0.45
	range	39.42-47.12	25.17-35.58	39.61-46.14	43.46-47.34	35.21-35.85
	CV	5.74	9.44	4.43	2.77	1.27
N%	Mean ± SD	12.83 ± 0.92	7.88 ± 0.98	10.48 ± 1.58	12.53 ± 0.74	8.80 ± 0.14
	range	11.38-14.13	6.14-9.04	7.84-13.31	10.99-13.62	8.70-8.90
	CV	7.14	12.42	15.09	5.90	1.61
P%	Mean ± SD	0.82 ± 0.12	0.95 ± 0.20	0.55 ± 0.11	0.90 ± 0.22	0.27 ± 0.01
	range	0.62-1.01	0.64-1.31	0.34-0.80	0.38-1.15	0.26-0.27
	CV	14.79	21.33	20.39	24.87	0.45
C:N	Mean ± SD	3.99 ± 0.39	4.66 ± 0.29	4.88 ± 0.90	4.22 ± 0.25	4.71 ± 0.02
	range	3.67-4.76	4.21-5.34	3.88-6.87	3.94-4.65	4.70-4.72
	CV/%	9.87	6.13	18.47	5.83	0.33
C:P	Mean ± SD	140.45 ± 22.53	88.58 ± 18.49	210.27 ± 50.23	143.82 ± 59.37	346.06 ± 2.85
	range	116.04-186.93	55.72-118.42	135.43-332.95	100.60-310.92	344.05-348.08
	CV/%	16.04	20.88	23.89	41.28	0.82
N:P	Mean ± SD	35.58 ± 6.99	19.00 ± 3.75	43.82 ± 9.90	39.42 ± 15.17	73.47 ± 0.85
	range	25.03-49.00	11.65-23.99	30.13-58.87	23.22-75.59	72.87-74.07
	CV/%	19.66	19.71	22.59	44.07	1.16

P and C content, N:P and N content, N content and C content ($p < 0.01$) (Figure 2). Notably, the correlation between the C:P and P content, as well as the N:P and P content of invertebrates, was the strongest ($r > 0.8$) (Figure 2), indicating that the C:P and N:P ratios were mainly influenced by the change in P content. Furthermore, the correlation analysis indicated no significant correlation between the P content of the invertebrates and the Ca content ($p > 0.05$) (Figure 2).

Variations in the ecological stoichiometric characteristics of invertebrates

A total of 18 invertebrate species were categorized into 5 groups: cephalopods, crabs, sea cucumber, shellfish, and shrimps. The results from the ANOSIM showed that the ecological stoichiometric characteristics varied significantly among these different categories of invertebrates. Furthermore, it was observed

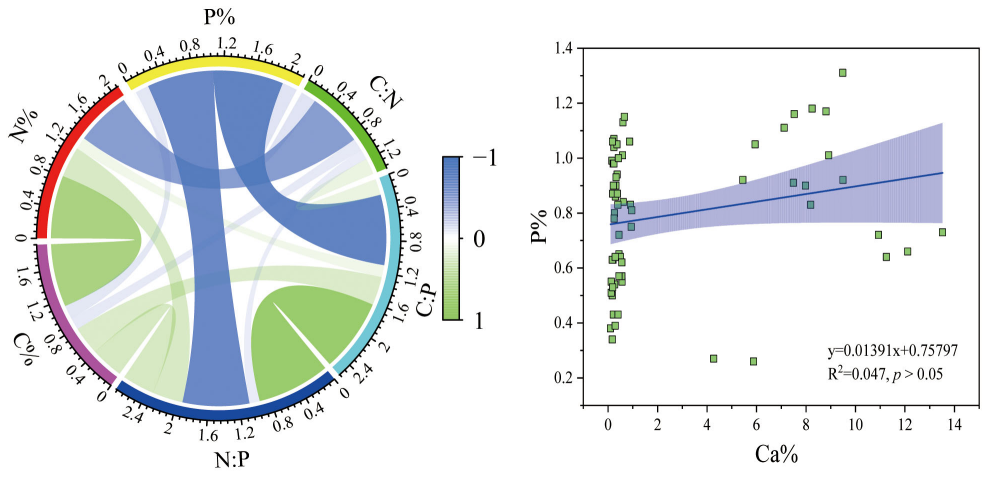

FIGURE 2
Analysis of the correlation relationships between elements in invertebrates from the Beibu Gulf.

that invertebrates from different taxa consisted of different elements (R = 0.535, p = 0.001) (Figure 3).

The one-way ANOVA results indicated significant difference in the C, N, and P content, as well as the C:N, C:P, and N:P ratios among different invertebrates ($p < 0.05$) (Figure 4). Cephalopods, shellfish, and shrimps exhibited significantly higher C content than sea cucumber and crabs, with crabs having the lowest C content. Shrimps had the highest N content, followed by cephalopods, shellfish, sea cucumber, and crabs, respectively. Cephalopods, crabs, and shrimps had significantly higher P content compared to shellfish and sea cucumber, with the least in sea cucumber. The C:N ratios of crabs, sea cucumber, and shellfish were significantly greater than those of shrimps. The C:P and N:P ratios were the highest in sea cucumber, followed by shellfish, cephalopods, shrimps, and crabs, respectively.

The relationship between ecological stoichiometry characteristics of invertebrates and δ^{15}N, δ^{13}C and body weight

The δ^{15}N values in the studied invertebrates ranged from 7.99‰ to 13.81‰, while the δ^{13}C values ranged from -13.01‰ to -22.73‰. Significant differences were observed in the δ^{15}N and δ^{13}C values across different invertebrate taxa ($p < 0.05$) (Figure 5). Specifically, the δ^{15}N values of cephalopods and shrimps were significantly higher than those of other invertebrates. Furthermore, the δ^{13}C values of shellfish, shrimps, and cephalopods were significantly higher than those of crabs and sea cucumber.

The correlation analysis revealed significant negative correlations between the C and N content and δ^{13}C of these invertebrates in the Beibu Gulf. Additionally, a significant negative correlation was observed between the P content of these invertebrates and their body weight. Conversely, the ratios of C:P and N:P demonstrated a significant positive correlation with body weight ($p < 0.01$) (Table 2).

Discussion

Element composition and differences of different invertebrates

The results show P content of invertebrates in the Beibu Gulf changes the most, with coefficients of variation in the order of P > N > C, which is consistent with other species (Vanni et al., 2002; Sun et al., 2014). The growth rate hypothesis presumes that P is a primary determinant of population dynamics, and the variations in P content within organisms influence changes in the C:N:P ratios (Elser et al., 2003). In this study, the most notable change was observed in P content, resulting in substantial alternations in both C:P and N:P ratios. Hendrixson et al. (2007) proposed a strong correlation between P content and phylogeny, along with a broad spectrum of interspecific variation in P content. Phylogenetic imprinting is evident in the ecological stoichiometry of invertebrates, and patterns of nutrient composition across species introduce additional, potentially phylogenetically-based variations to these patterns (González et al., 2018; Allgeier et al., 2020). The concentrations of elements such as C, N, and P in the tissues of

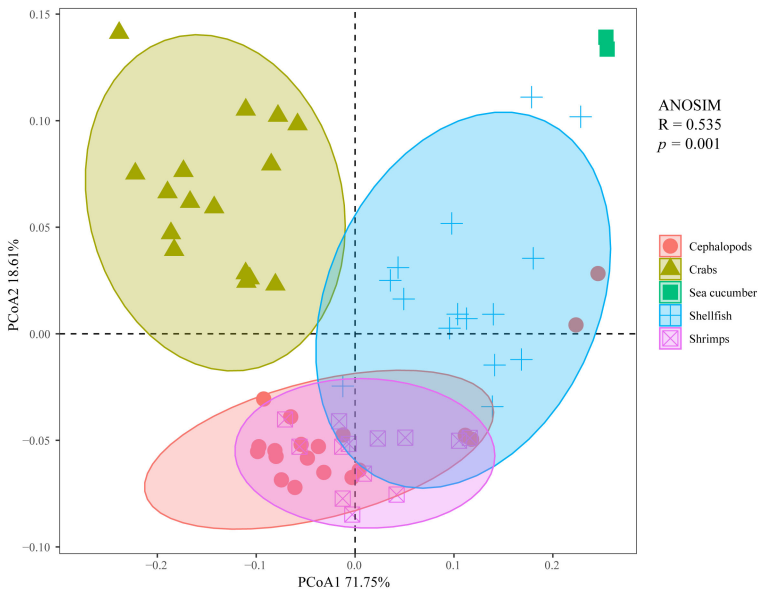

FIGURE 3
Principal coordinate analysis (PCoA)+analysis of similarities (ANOSIM) diagram of the contents and ratios of C, N, and P among different categories of invertebrates from the Beibu Gulf.

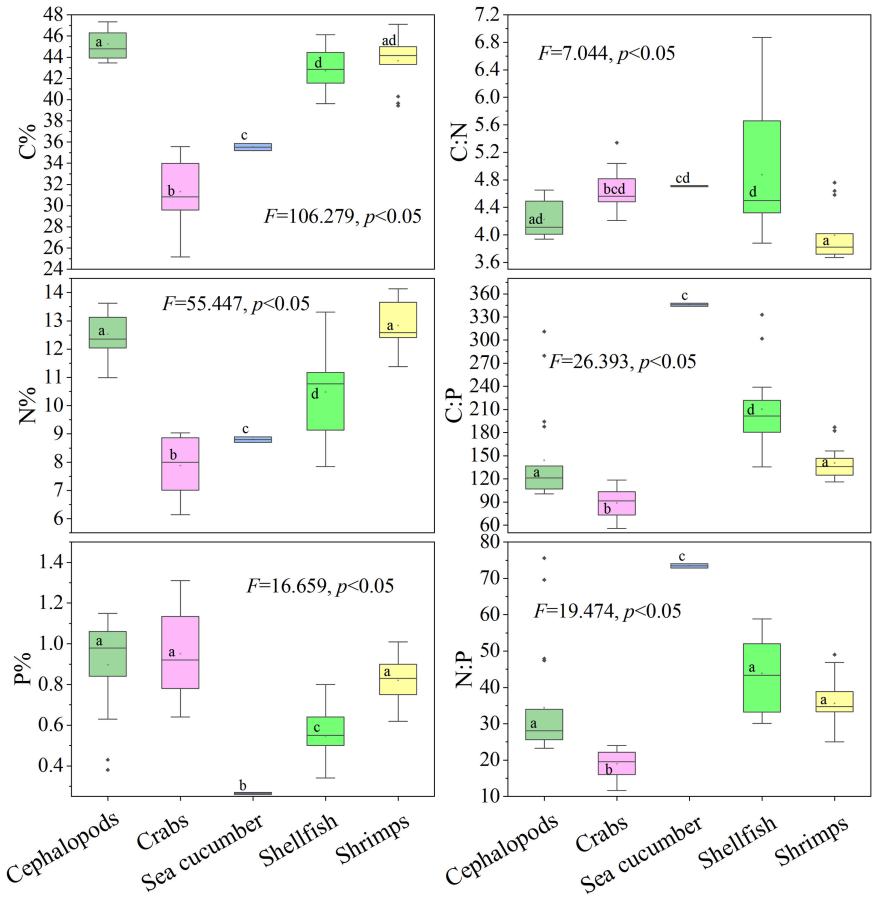

FIGURE 4
Box diagram of the contents and ratios of C, N, and P in different categories of invertebrates from the Beibu Gulf Significant differences are designated by different lower-case letters ($p < 0.05$).

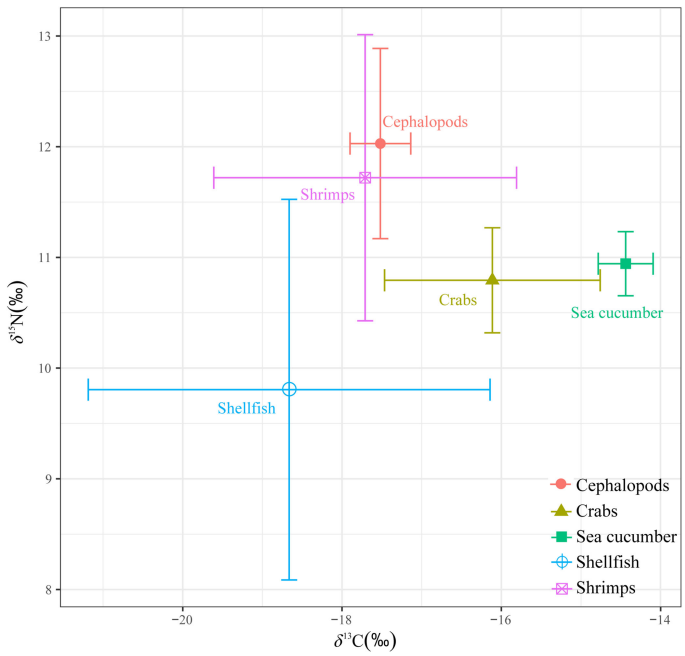

FIGURE 5
Biplots of $\delta^{13}C$ and $\delta^{15}N$ of invertebrates from the Beibu Gulf.

TABLE 2 Analysis of the correlation between C, N, and P contents and their ratios with $\delta^{15}N$, $\delta^{13}C$, and body weight of invertebrates from the Beibu Gulf.

Species	Variable	C%	N%	P%	C:N	C:P	N:P
Invertebrates	$\delta^{15}N$	-0.034	0.092	0.166	-0.228	-0.119	-0.055
	$\delta^{13}C$	-0.480**	-0.321**	0.172	-0.061	-0.249	-0.232
	body weight	-0.128	-0.070	-0.423**	-0.068	0.431**	0.458**

Values given are correlation coefficients (r), **Statistical significance ($p < 0.01$).

aquatic organisms were influenced by their environmental abundance and bioavailability, as well as the type, developmental stage, and physiological condition of the organism (Pinto et al., 2022). Analyzing elemental correlations can elucidate the interconnectedness of these elements. For example, negative correlations between elements may highlight elemental mass balance, where an increase in one element leads to a decrease in another (Allgeier et al., 2020). A significant positive correlation was observed between the N and C contents of invertebrates in this study. The muscles and shells of invertebrates are abundant in C and N elements, which suggests that C and N contents concurrently increase with the individual development of invertebrates, indicating a synergistic effect between these elements that promote growth and metabolism (Small and Pringle, 2010). However, there was no significant correlation between P content and Ca content in this study, indicating that the development of invertebrates' bones did not influence P content. Invertebrates' bones contain minimal amounts of P, and many invertebrates have a high proportion of chitin, a polysaccharide rich in nitrogen and carbon (Small and Pringle, 2010), which is primarily associated with their exoskeletons. Therefore, it is speculated that changes in P content of invertebrates are mainly related to the growth rate hypothesis trend and that P synthesis transporters are necessary to support organismal growth during development.

The availability of nutrients plays a pivotal role in determining organism growth, population structure, species interaction, and ecosystem stability (Allgeier et al., 2020). Therefore, identifying the type of nutrient that is insufficiently supplied becomes essential for maintaining system stability. Ecological stoichiometry defines the element with the least supply relative to demand as the "limiting" element (Sterner and Elser, 2002). The C:P and N:P ratios in invertebrates were high in this study, while the C:N ratio was low. Specifically, among the elements required by invertebrates, P content was relatively the smallest. Furthermore, a significant negative correlation was observed between the P content of invertebrates and body weight, indicating that P may constrain invertebrate growth. This is attributed to the insufficient P available to produce the RNA necessary for protein synthesis, resulting in developmental growth retardation (González et al., 2018).

The ecological stoichiometric characteristics of different invertebrates exhibited significant differences (Figure 3). Many invertebrates have a high proportion of chitin, which is a nitrogen- and carbon-rich polysaccharide that is mainly found in their exoskeletons (Small and Pringle, 2010). Therefore, organisms with larger surface area/volume ratios due to chitinous structures should have higher C and N contents (Allgeier et al., 2020). This is consistent with the findings of Allgeier et al. (2020) that shrimp had higher C and N contents. However, crabs have a larger surface area-to-volume ratio and a chitinous shell but had the lowest C and N contents in this study. Crabs have larger and thicker hard shells. Although they contain nitrogen- and carbon-rich chitin-which also contributes to their lower P content, the proportion of more carbon- and nitrogen-rich muscle is less, accounting for approximately half of their wet weight, resulting in a lower overall body C and N contents. In addition, the P content of sea cucumber was found to be lower than that in other species, with both C and N contents also relatively low, reflecting the findings of Allgeier et al. (2020). This may be attributed to the feeding habits of sea cucumbers, which are detritivores that feed on ocean sediments (Sales et al., 2023). Since the C, N, and P contents of the sediments are all low (Chen et al., 2021), sea cucumber absorbs fewer C, N and P contents.

Factors affecting ecological stoichiometry of invertebrates

Carbon and nitrogen stable isotopes ($\delta^{13}C$ and $\delta^{15}N$) serve as effective tools for studying the nutrient cycle and energy flow within ecosystems (Wang et al., 2018b, 2020). In aquatic organisms, the $\delta^{13}C$ value reflects the primary food sources of the consumer, with different $\delta^{13}C$ values indicating different food sources, while the $\delta^{15}N$ values can determine the trophic level of organisms (Liu et al., 2018; Wang et al., 2019, 2020). The C and N contents in invertebrates were found to be correlated with $\delta^{13}C$ in this study, indicating that feeding habit significantly influences variations in C and N contents within these organisms. Given the highly variable availability of food resources in nature and the diverse range of foods consumed by marine organisms, their food stoichiometry also varies widely. Interspecific variations in ecological stoichiometry among invertebrates may be associated with variations in food sources (Cross et al., 2003; Lemoine et al., 2014). The water quality characteristics of the Beibu Gulf are complex and diverse, with an abundance of bait sources (Lao et al., 2021). Changes in the nutrient level of the water body can alter the composition of basic resources and bait, thereby directly or indirectly affecting the element content of consumers. Studies have shown that changes in the quality of basic resources limit the elemental content within higher trophic levels, with implications for not only primary consumers but across multiple trophic levels (Small and Pringle, 2010; Wang et al., 2021). For instance, the eutrophication of aquatic ecosystems can affect the stoichiometric properties of omnivorous fish (Mäkelin and Villnäs,

2022). The stoichiometry of omnivorous fish is influenced by the quantity and quality of phytoplankton, which are regulated by nutrients and light (Dickman et al., 2008). Therefore, changes in bioecological stoichiometry are more likely to reflect changes in environmental conditions that affect the availability of elements in consumer food or basic resources than modifications in biological traits (McIntyre and Flecker, 2010). The elemental composition of animals is, in fact, more flexible and less homeostatic than previously assumed. While certain species may exhibit homeostatic mechanisms for self-regulating stoichiometry, it is important to note that not all fishery catches exhibit identical elemental compositions. Instead, the contents of various elements can greatly differ among species.

The key life history and ecological traits of an organism, including its nutrient uptake, storage, and transfer mechanisms, are significantly affected by body size (Amundrud and Srivastava, 2016). A meta-analysis of all individual species based on body weight revealed a negative correlation between P content and body weight, which finding is consistent with the results of the study by González et al. (2018). The decrease in P content with increasing body size is due to the lower growth rate of large organisms compared to small organisms (Sterner and Elser, 2002; Wang et al., 2023). Both growth rate and RNA content decrease with age. The growth rate hypothesis presumes that organisms with higher growth rates have higher phosphorus contents due to the increased synthesis of phosphorus-rich rRNA required for their rapid protein synthesis (Elser et al., 2003). Furthermore, genetic relationships also play an important role in shaping the ecological stoichiometric characteristics of C, N, and P in invertebrates. Our analysis identified distinct clusters of closely related invertebrate taxa and clear separations between distantly related taxa (Figure 3), suggesting significant differences among different invertebrate groups. Variations in elemental composition and proportions among consumers are mainly associated with phylogenetic differences that influence factors such as body size, growth rate, and resource allocation to structural components within the body. Cross et al. (2005) suggested that phylogeny may be more important than local environmental conditions or species composition within higher taxonomic groups in determining the elemental composition of consumers at least at the class or higher level.

Homeostasis in organisms

A key challenge in ecological stoichiometry is to explore the capacity of living organisms to sustain homeostasis in elemental composition. The demand for chemical elements by organisms is largely determined by individual investments in structural resources, such as vertebrates' investment in phosphorus-rich bones, arthropods' investment in carbon- and nitrogen-rich chitin and muscles, and plants' investment in carbon-rich cellulose and lignin (Leal et al., 2017). Additionally, physiological processes such as growth and reproduction also influence the elemental requirements of organisms (Leal et al., 2017). Variations in the steady-state levels of elements between different organisms, such as between plants and animals, can lead to significant differences in the organism's stoichiometry (Sterner and Elser, 2002; Persson et al., 2010). Therefore, each species should maintain an optimal balance of biological elemental composition, with different taxa exhibiting different elements and increasing differences as taxonomic distance and evolutionary time increase (Peñuelas et al., 2019). Furthermore, species demonstrate a degree of flexibility and adaptability, altering their elemental stoichiometry in response to changes in the composition and/or environmental conditions of neighboring species (Sardans and Peñuelas, 2014). In light of this, the size of the area of the principal coordinate analysis (PCoA) confidence interval (i.e., the size of the variation in element composition) were applied to represent the degrees of homeostasis of species or taxa (Figure 3). A smaller PCoA area indicates a smaller change in the content and ratio of C, N, and P, indicating species with stricter homeostasis. On the contrary, a larger area on PCoA indicates a greater change in the content and ratio of C, N, and P, indicating species with less strict homeostasis. In addition, species or taxa with relatively larger PCoA areas had lower δ^{15}N values, while those with smaller PCoA areas had higher δ^{15}N values. A correlation between homeostasis and trophic level was observed in this study, with species or taxa occupying higher trophic levels maintaining stricter homeostasis. This finding aligns with the research results of Feng et al. (2023), which indicated that the stoichiometric stability of aquatic organisms increased with their trophic level.

Conclusion

Our research has indicated significant interspecific differences in the ecological stoichiometric traits of invertebrates within the Beibu Gulf. The growth of these invertebrates appears to be constrained by P, and they do not exhibit strict homeostasis, with higher trophic levels displaying greater stability. In future studies, we plan to integrate our results with recent data on marine biological resources in the Beibu Gulf, including total biomass, fishing amount, and natural mortality rates. We also plan to explore the total content and ratios of C, N, and P across various marine ecosystem sizes, as well as their origins and contributions. Furthermore, we intend to assess its impact on the succession of fishery catch communities, thereby enhancing the application of ecological stoichiometry in marine ecology research.

Data availability statement

The raw data supporting the conclusions of this article will be made available by the authors, without undue reservation.

Ethics statement

The animal study was approved by Guilin University of Technology, Guilin China. The study was conducted in accordance with the local legislation and institutional requirements.

Author contributions

CW: Conceptualization, Data curation, Formal Analysis, Investigation, Software, Visualization, Writing – original draft, Writing – review & editing. LH: Conceptualization, Data curation, Investigation, Methodology, Writing – original draft, Writing – review & editing. BK: Methodology, Writing – review & editing, Supervision. LZ: Investigation, Visualization, Writing – review & editing. HL: Investigation, Visualization, Writing – review & editing. SZ: Data curation, Visualization, Writing – review & editing. YC: Data curation, Visualization, Writing – review & editing. AS: Writing – review & editing, Validation. YY: Writing – review & editing, Investigation, Supervision.

Funding

The author(s) declare financial support was received for the research, authorship, and/or publication of this article. This study was financially supported by the National Natural Science Foundation of China (U20A2087), the Key Research and Development Program of Guangxi (Guike AB22035050).

Acknowledgments

We thank all the staff of Guibei Fishing Boat No. 98388 for their sampling assistance, and the reviewers for the revision of the manuscript.

Conflict of interest

The authors declare that the research was conducted in the absence of any commercial or financial relationships that could be construed as a potential conflict of interest.

Publisher's note

All claims expressed in this article are solely those of the authors and do not necessarily represent those of their affiliated organizations, or those of the publisher, the editors and the reviewers. Any product that may be evaluated in this article, or claim that may be made by its manufacturer, is not guaranteed or endorsed by the publisher.

References

Allgeier, J. E., Wenger, S., and Layman, C. A. (2020). Taxonomic identity best explains variation in body nutrient stoichiometry in a diverse marine animal community. *Sci. Rep.* 10, 13718. doi: 10.1038/s41598-020-67881-y

Amundrud, S. L., and Srivastava, D. S. (2016). Trophic interactions determine the effects of drought on an aquatic ecosystem. *Ecology* 97, 1475–1483. doi: 10.1890/15-1638.1

Benstead, J. P., Hood, J. M., Whelan, N. V., Kendrick, M. R., Nelson, D., Hanninen, A. F., et al. (2014). Coupling of dietary phosphorus and growth across diverse fish taxa: a meta-analysis of experimental aquaculture studies. *Ecology* 95, 2768–2777. doi: 10.1890/13-1859.1

Bin, H., Li, Q., Zhang, P., Li, W., Xue, X., Zou, S., et al. (2022). Effects of Elevation on Ecological Stoichiometry of Plant Leaves, Litter, and Soils in Pseudotsuga sinensis Forest in the Karst Mountain region, Southwest China. *J. Soil Sci. Plant Nutr.* 22, 3582–3597. doi: 10.1007/s42729-022-00911-y

Bogotá-Gregory, J. D., Lima, F. C. T., Correa, S. B., Silva-Oliveira, C., Jenkins, D. J., Ribeiro, F. R., et al. (2020). Biogeochemical water type influences community composition, species richness, and biomass in megadiverse Amazonian fish assemblages. *Sci. Rep.* 10, 15349. doi: 10.1038/s41598-020-72349-0

Boros, G., Sály, P., and Vanni, M. J. (2015). Ontogenetic variation in the body stoichiometry of two fish species. *Oecologia* 179, 329–341. doi: 10.1007/s00442-015-3349-8

Chen, D., Ke, Z., and Tan, Y. (2021). Distribution of C/N/P stoichiometry in suspended particulate matter and surface sediment in a bay under serious anthropogenic influence: Daya Bay, China. *Environ. Sci. pollut. Res.* 28, 29177–29187. doi: 10.1007/s11356-021-12812-1

Cross, W. F., Benstead, J. P., Frost, P. C., and Thomas, S. A. (2005). Ecological stoichiometry in freshwater benthic systems: recent progress and perspectives. *Freshw. Biol.* 50, 1895–1912. doi: 10.1046/j.1461-0248.2003.00481.x

Cross, W. F., Benstead, J. P., Rosemond, A. D., and Wallace, J. B. (2003). Consumer-resource stoichiometry in detritus-based streams. *Ecol. Lett.* 6, 721–732. doi: 10.1046/j.1461-0248.2003.00481.x

DeMott, W. R., Pape, B. J., and Tessier, A. J. (2004). Patterns and sources of variation in Daphnia phosphorus content in nature. *Aquat. Ecol.* 38, 433–440. doi: 10.1023/B:Aeco.0000035183.53389.66

Dickman, E., Newell, M. J. M., González, M. J., and Vanni, M. J. (2008). Light, nutrients, and food-chain length constrain planktonic energy transfer efficiency across multiple trophic levels. *Proc. Natl. Acad. Sci. United. States America* 105, 18408–18412. doi: 10.1073/pnas.0805566105

Elser, J. J., Acharya, K., Kyle, M., Cotner, J., Makino, W., Markow, T., et al. (2003). Growth rate-stoichiometry couplings in diverse biota. *Ecol. Lett.* 6, 936–943. doi: 10.1046/j.1461-0248.2003.00518.x

Elser, J. J., Fagan, W. F., Denno, R. F., Dobberfuhl, D. R., Folarin, A., Huberty, A., et al. (2000). Nutritional constraints in terrestrial and freshwater food webs. *Nature* 408, 578–580. doi: 10.1038/35046058

Elser, J. J., and Urabe, J. (1999). The stoichiometry of consumer-driven nutrient recycling: Theory, observations, and consequences. *Ecology.* 80, 735–751. doi: 10.1890/0012-9658(1999)080[0735:TSOCDN]2.0.CO;2

Feng, M. J., Cheng, H. W., Zhang, P. Y., Wang, K., Wang, T., Zhang, H., et al. (2023). Stoichiometric stability of aquatic organisms increases with trophic level under warming and eutrophication. *Sci. Total. Environ.* 856, 160106. doi: 10.1016/j.scitotenv.2022.160106

Fernández-Martínez, M. (2022). From atoms to ecosystems: elementome diversity meets ecosystem functioning. *New Phytol.* 234, 35–42. doi: 10.1111/nph.17864

González, A. L., Céréghino, R., Dézerald, O., Farjalla, V. F., Leroy, C., Richardson, B. A., et al. (2018). Ecological mechanisms and phylogeny shape invertebrate stoichiometry: A test using detritus-based communities across Central and South America. *Dryad. Digital. Repository.* 32, 2448–2463. doi: 10.1111/1365-2435.13197

González, A. L., Kominoski, J. S., Danger, M., Ishida, S., Iwai, N., and Rubach, A. (2010). Can ecological stoichiometry help explain patterns of biological invasions? *Oikos* 119, 779–790. doi: 10.1111/j.1600-0706.2009.18549.x

Hendrixson, H. A., Sterner, R. W., and Kay, A. D. (2007). Elemental stoichiometry of freshwater fishes in relation to phylogeny, allometry and ecology. *J. Fish. Biol.* 70, 121–140. doi: 10.1111/j.1095-8649.2006.01280.x

Hessen, D. O., Ågren, G. I., Anderson, T. R., Elser, J. J., and de Ruiter, P. C. (2004). Carbon sequestration in ecosystems: The role of stoichiometry. *Ecology* 85, 1179–1192. doi: 10.1890/02-0251

Hou, G., Zhang, H., Wang, J., Chen, Y., and Lin, J. (2021). Stock assessment of 19 perciformes in the beibu gulf, China, using a length-based bayesian biomass method. *Front. Mar. Sci.* 8. doi: 10.3389/fmars.2021.731837

Jeyasingh, P. D., Cothran, R. D., and Tobler, M. (2014). Testing the ecological consequences of evolutionary change using elements. *Ecol. Evol.* 4, 528–538. doi: 10.1002/ece3.950

Koongolla, J. B., Lin, L., Yang, C. P., Pan, Y. F., Li, H. X., Liu, S., et al. (2022). Microplastic prevalence in marine fish from onshore Beibu Gulf, South China Sea. *Front. Mar. Sci.* 9. doi: 10.3389/fmars.2022.964461

Lao, Q., Liu, G., Shen, Y., Su, Q., and Lei, X. (2021). Biogeochemical processes and eutrophication status of nutrients in the northern Beibu Gulf, South China. *J. Earth Syst. Sci.* 130, 199. doi: 10.1007/s12040-021-01706-y

Laspoumaderes, C., Meunier, C. L., Magnin, A., Berlinghof, J., Elser, J. J., Balseiro, E., et al. (2022). A common temperature dependence of nutritional demands in ectotherms. *Ecol. Lett.* 25, 2189–2202. doi: 10.1111/ele.14093

Leal, M. C., Seehausen, O., and Matthews, B. (2017). The ecology and evolution of stoichiometric phenotypes. *Trends Ecol. Evol.* 32, 108–117. doi: 10.1016/j.tree.2016.11.006

Lemoine, N. P., Giery, S. T., and Burkepile, D. E. (2014). Differing nutritional constraints of consumers across ecosystems. *Oecologia* 174, 1367–1376. doi: 10.1007/s00442-013-2860-z

Leroux, S. J., Wiersma, Y. F., and Vander, E. W. (2020). Herbivore impacts on carbon cycling in boreal forests. *Trends Ecol. Evol.* 35, 1001–1010. doi: 10.1016/j.tree.2020.07.009

Li, Z., Lu, H., Gan, X., and Jin, X. (2009). Growth and mortality of bottom threadfin bream nemipterus bathybius in the mouth of beibu gulf,South China sea. *Fisheries. Sci.* 28, 556–562. doi: 10.16378/j.cnki.1003-1111.2009.10.004

Liu, Y., Liu, G., Yuan, Z., Liu, H., and Lam, P. K. S. (2018). Heavy metals (As, Hg and V) and stable isotope ratios (δ^{13}C and δ^{15}N) in fish from Yellow River Estuary, China. *Sci. Total. Environ.* 613-614, 462–471. doi: 10.1016/j.scitotenv.2017.09.088

Lu, G. Y., and Wang, W. X. (2023). Tissue-based trace element pollution of clam Ruditapes philippinarum in China: Hotspot identification and multiple nonlinear analysis. *Sci. Total. Environ.* 868, 161598. doi: 10.1016/j.scitotenv.2023.161598

Mäkelin, S., and Villnäs, A. (2022). Food sources drive temporal variation in elemental stoichiometry of benthic consumers. *Limnol. Oceanogr.* 67, 784–799. doi: 10.1002/lno.12034

Martiny, A. C., Pham, C. T. A., Primeau, F. W., Vrugt, J. A., Moore, J. K., Levin, S. A., et al. (2013). Strong latitudinal patterns in the elemental ratios of marine plankton and organic matter. *Nat. Geosci.* 6, 279–283. doi: 10.1038/ngeo1757

May, E. M., and El-Sabaawi, R. W. (2022). Life stage and taxonomy the most important factors determining vertebrate stoichiometry: A meta-analysis. *Ecol. Evol.* 12, e9354. doi: 10.1002/ece3.9354

McIntyre, P. B., and Flecker, A. S. (2010). Ecological stoichiometry as an integrative framework in stream fish ecology. *Am. Fisheries. Soc. Symposium.* 73, 539–558.

Naddafi, R., Eklov, P., and Pettersson, K. (2009). Stoichiometric constraints do not limit successful invaders: zebra mussels in swedish lakes. *PloS One* 4, e5345. doi: 10.1371/journal.pone.0005345

Pacioglu, O., Amărioarei, A., Duțu, L. T., Plăvan, G., Iţcuş, C., Plăvan, O., et al. (2021). The structure and functionality of communities and food webs in streams along the epigean–hypogean continuum: unifying ecological stoichiometry and metabolic theory of ecology. *Aquat. Sci.* 83, 63. doi: 10.1007/s00027-021-00815-6

Peñuelas, J., Fernández-Martínez, M., Ciais, P., Jou, D., Piao, S., and Obersteiner, M. (2019). The bioelements, the elementome, and the biogeochemical niche. *Ecology* 100, e02652. doi: 10.1002/ecy.2652

Persson, J., Fink, P., Goto, A., Hood, J. M., Jonas, J., and Kato, S. (2010). To be or not to be what you eat: regulation of stoichiometric homeostasis among autotrophs and heterotrophs. *Oikos* 119, 741–751. doi: 10.1111/j.1600-0706.2010.18545.x

Pilati, A., and Vanni, M. J. (2007). Ontogeny, diet shifts, and nutrient stoichiometry in fish. *Oikos* 116, 1663–1674. doi: 10.1111/j.2007.0030-1299.15970.x

Pinto, F. R., Duarte, A. M., Silva, F., Barroso, S., Mendes, S., Pinto, E., et al. (2022). Annual, variations in the mineral element content of five fish species from the Portuguese coast. *Food Res. Int.* 158, 111482. doi: 10.1016/j.foodres.2022.111482

Price, T. L., Harper, J., Francoeur, S. N., Halvorson, H. M., and Kuehn, K. A. (2021). Brown meets green: light and nutrients alter detritivore assimilation of microbial nutrients from leaf litter. *Ecology* 102, e03358. doi: 10.1002/ecy.3358

Qiao, Y., and Li, Z. (2007). The relationship between the main features of land form, the distritubton of bottom sediment and fishery distribution. *Trans. Oceanol. Limnol.* S1), 232–238. doi: 10.13984/j.cnki.cn37-1141.2007.s1.030

Regnier, P., Friedlingstein, P., Ciais, P., Mackenzie, F. T., Gruber, N., Janssens, I. A., et al. (2013). Anthropogenic perturbation of the carbon fluxes from land to ocean. *Nat. Geosci.* 6, 597–607. doi: 10.1038/ngeo1830

Sales, S. S., Lourenço, H. M., Bandarra, N. M., Cardoso, C., Brito, P., Botelho, M. J., et al. (2023). Elemental composition and in *vitro* bioaccessibility assessment of holothuroids. *J. Food Composition. Anal.* 115, 104986. doi: 10.1016/j.jfca.2022.104986

Sardans, J., Janssens, I. A., Ciais, P., Obersteiner, M., and Peñuelas, J. (2021). Recent advances and future research in ecological stoichiometry. *Perspect. Plant Ecol. Evol. Syst.* 50, 125611. doi: 10.1016/j.ppees.2021.125611

Sardans, J., and Peñuelas, J. (2014). Climate and taxonomy underlie different elemental concentrations and stoichiometries of forest species: the optimum "biogeochemical niche. *Plant Ecol.* 215, 441–455. doi: 10.1007/s11258-014-0314-2

Sardans, J., Rivas-Ubach, A., and Peñuelas, J. (2012). The elemental stoichiometry of aquatic and terrestrial ecosystems and its relationships with organismic lifestyle and ecosystem structure and function: a review and perspectives. *Biogeochemistry* 111, 1–39. doi: 10.1007/s10533-011-9640-9

Small, G. E., and Pringle, C. M. (2010). Deviation from strict homeostasis across multiple trophic levels in an invertebrate consumer assemblage exposed to high chronic phosphorus enrichment in a Neotropical stream. *Oecologia* 162, 581–590. doi: 10.1007/s00442-009-1489-4

Sterner, R. W., and Elser, J. J. (2002). *Ecological stoichiometry: the biology of elements from molecules to the biosphere* (Press, Princeton, NJ: Princeton Univ).

Sterner, R. W., Elser, J. J., and Hessen, D. O. (1992). Stoichiometric relationships among producers, consumers and nutrient cycling in pelagic ecosystems. *Biogeochemistry* 17, 49–67. doi: 10.1007/BF00002759

Sterrett, S. C., Maerz, J. C., and Katz, R. A. (2015). What can turtles teach us about the theory of ecological stoichiometry? *Freshw. Biol.* 60, 443–455. doi: 10.1111/fwb.12516

Sullam, K. E., Dalton, C. M., Russell, J. A., Kilham, S. S., El-Sabaawi, R., German, D. P., et al. (2015). Changes in digestive traits and body nutritional composition accommodate a trophic niche shift in Trinidadian guppies. *Oecologia* 177, 245–257. doi: 10.1007/s00442-014-3158-5

Sun, P., Li, X., Gong, X., Liu, Y., Zhang, X., and Wang, L. (2014). Carbon, nitrogen and phosphorus ecological stoichiometry of Lateolabrax macultus and Acanthogobius ommaturus in the Estuary of Yangtze River, China. *Acta Ecol. Sin.* 34, 196–203. doi: 10.1016/j.chnaes.2013.06.009

Tiegs, S. D., Berven, K. A., Carmack, D. J., and Capps, K. A. (2016). Stoichiometric implications of a biphasic life cycle. *Oecologia* 180, 853–863. doi: 10.1007/s00442-015-3504-2

Vanni, M. J., Flecker, A. S., Hood, J. M., and Headworth, J. L. (2002). Stoichiometry of nutrient recycling by vertebrates in a tropical stream: linking species identity and ecosystem processes. *Ecol. Lett.* 5, 285–293. doi: 10.1046/j.1461-0248.2002.00314.x

Wang, Z., Cébron, A., Baillard, V., and Danger, M. (2022). Nitrogen to phosphorus ratio shapes the bacterial communities involved in cellulose decomposition and copper contamination alters their stoichiometric demands. *FEMS Microbiol. Ecol.* 98, fiac107. doi: 10.1093/femsec/fiac107

Wang, J., Luo, K., Fan, Y., Deng, Y., He, X., and Yan, Y. (2022). Feeding ecology of Nemipterus japonicus in Beibu Gulf. *Prog. Fishery. Sci.* 44 (1), 47–57. doi: 10.19663/j.issn2095-9869.20210606001

Wang, S., Luo, B. K., Qin, Y. J., Su, L. H., Stewart, S. D., Wang, T. T., et al. (2020b). Consumer-diet discrimination of δ^{13}C and δ^{15}N: Source- and feeding-oriented patterns based on gut content analysis in a large subtropical river of China. *River. Res. Appl.* 36, 1124–1136. doi: 10.1002/rra.3644

Wang, S., Luo, B. K., Qin, Y. J., Zhao, J. G., Wang, T. T., Stewart, S. D., et al. (2020a). Fish isotopic niches associated with environmental indicators and human disturbance along a disturbed large subtropical river in China. *Sci. Total. Environ.* 750, 141667. doi: 10.1016/j.scitotenv.2020.141667

Wang, S., Tang, J. P., Su, L. H., Fan, J. J., Chang, H. Y., Wang, T. T., et al. (2019). Fish feeding groups, food selectivity, and diet shifts associated with environmental factors and prey availability along a large subtropical river, China. *Aquat. Sci.* 81, 31. doi: 10.1007/s00027-019-0628-1

Wang, S., Wang, L., Chang, H. Y., Li, F., Tang, J. P., Zhou, X. A., et al. (2018b). Longitudinal variation in energy flow networks along a large subtropical river, China. *Ecol. Model.* 387, 83–95. doi: 10.1016/j.ecolmodel.2018.08.019

Wang, S., Wang, T. T., Tang, J. P., Wang, L., Yang, Y., Lin, H. J., et al. (2018a). Longitudinal variation in fish prey utilization, trophic guilds, and indicator species along a large subtropical river, China. *Ecol. Evol.* 8, 11467–11483. doi: 10.1002/ece3.4577

Wang, S., Wang, T. T., Xia, W. T., Chen, Z. B., Stewart, S. D., Yang, F. J., et al. (2021). Longitudinal pattern of resource utilization by aquatic consumers along a disturbed subtropical urban river: Estimating the relative contribution of resources with stable isotope analysis. *Ecol. Evol.* 11, 16763–16775. doi: 10.1002/ece3.8304

Wang, C. G., Zhu, L., Huang, L. L., Xu, H., Xu, P., He, X. B., et al. (2023). Ecological stoichiometric characteristics of three dominant fish species from the Beibu Gulf: inter- and intraspecific variations. *Front. Ecol. Evol.* 11. doi: 10.3389/fevo.2023.1176052

Williamson, F., and Ozersky, T. (2019). Lake characteristics, population properties and invasion history determine impact of invasive bivalves on lake nutrient dynamics. *Ecosystems* 22, 1721–1735. doi: 10.1007/s10021-019-00371-z

Xu, Q., Huang, M., Yang, S., Li, X., Zhao, H., Tang, J., et al. (2022). Ecological stoichiometry influences phytoplankton alpha and beta diversity rather than the community stability in subtropical bay. *Ecol. Evol.* 12, e9301. doi: 10.1002/ece3.9301

frontiers | Frontiers in Marine Science

TYPE Original Research
PUBLISHED 16 July 2024
DOI 10.3389/fmars.2024.1386686

Check for updates

OPEN ACCESS

EDITED BY
Li Jianlon,
Shandong University, China

REVIEWED BY
Karen L. Casciotti,
Stanford University, United States
Xin Sun,
Carnegie Institution for Science (CIS),
United States

*CORRESPONDENCE
Clara A. Fuchsman
cfuchsman@umces.edu

RECEIVED 15 February 2024
ACCEPTED 18 June 2024
PUBLISHED 16 July 2024

CITATION
Huanca-Valenzuela P, Cram JA and Fuchsman CA (2024) Niche differentiation in microorganisms capable of using alternative reduced nitrogen sources studied across depth and between oxic and anoxic ocean regions.
Front. Mar. Sci. 11:1386686.
doi: 10.3389/fmars.2024.1386686

COPYRIGHT
© 2024 Huanca-Valenzuela, Cram and Fuchsman. This is an open-access article distributed under the terms of the Creative Commons Attribution License (CC BY). The use, distribution or reproduction in other forums is permitted, provided the original author(s) and the copyright owner(s) are credited and that the original publication in this journal is cited, in accordance with accepted academic practice. No use, distribution or reproduction is permitted which does not comply with these terms.

Niche differentiation in microorganisms capable of using alternative reduced nitrogen sources studied across depth and between oxic and anoxic ocean regions

Paulina Huanca-Valenzuela, Jacob A. Cram and Clara A. Fuchsman*

Horn Point Laboratory, University of Maryland Center for Environmental Science, Cambridge, MD, United States

Introduction: Assimilation of reduced nitrogen is less energetically costly than assimilation of oxidized forms. In the open ocean, ammonium is generally absent from the water column, including in oxygen-deficient zones (ODZs). Some microorganisms can use alternative organic reduced nitrogen forms like urea and cyanate, as indicated by the presence of cyanase (*cynS*) and urease (*ureC*) genes.

Methods: Here we examine the Hawaii Ocean Time series, two stations in the Eastern Tropical South Pacific ODZ and one in the Eastern Tropical North Pacific ODZ, using phylogenetic read placement of metagenomic reads to define the proportion of each taxon capable of using cyanate and/or urea in oxic and anoxic environments.

Results: An improved phylogenetic tree found that Thioglobaceae and Verrucomicrobia had the capability to use urea. Our detailed examination of all the microbial groups able to use cyanate and urea illuminated that niche differentiation, an adaptation to minimize competition, determines chosen nitrogen sources, partitioning by depth and oxygen. Urease genes were found in Picocyanobacteria and SAR11 in surface waters, Thaumarchaeota and *Nitrospina* in deep waters, Thioglobaceae and *Cand*. Scalindua in ODZs, and Verrucomicrobia in the deep oxycline. In the ODZs, the percentage of Anammox bacteria that contained *cynS* was double that of those containing *ureC*, and their *cynS* transcripts were abundant, indicating a preference for cyanate over urea.

Discussion: While *Prochlorococcus* could utilize cyanate in the deep chlorophyll maximum, in the ODZs, *Prochlorococcus* uses nitrite rather than compete with *Cand*. Scalindua for cyanate, even though cyanate is present. SAR11 and *Prochlorococcus* may compete for urea in surface waters, but for SAR11, the presence of *ureC* was negatively correlated with nitrate concentration ($p = 10^{-17}$), with ~ 40% of SAR11 genomes containing the *ureC* gene in oxic surface waters

but none at depth, indicating that SAR11 bacteria switched to using nitrate when available. In the oxycline above the ODZ, where Thaumarchaeota and *Nitrospina* both could use urea, 50% of *Nitrospina* were also able to use cyanate, and their cyanase transcripts were present. This use of dissolved organic N should allow a higher biomass of N-cycling microbes and higher N-transformation rates than in a system competing for ammonia only.

KEYWORDS

oxygen deficient zones, urea, cyanate, urease, cyanase, Hawaii Ocean Time Series

Introduction

Oxygen-deficient zones (ODZs) are regions of the ocean that naturally have < 10 nM oxygen (Revsbech et al., 2009; Tiano et al., 2014). However, the oxygen content of the Pacific Ocean has been decreasing since the 1980s, and ODZs are expanding (Stramma et al., 2008; Horak et al., 2016; Ito et al., 2017). Ocean ODZs host 30%–50% of marine fixed-N loss (DeVries et al., 2013). In ODZs, bacteria and archaea utilize nitrate and nitrite as electron donors instead of oxygen (Lam et al., 2009), leading to N_2 production by heterotrophic denitrification (Org. C + $2NO_3^- \rightarrow N_2 + CO_2$) and Anammox ($NO_2 + NH_4^+ \rightarrow N_2$) (Dalsgaard et al., 2012; Babbin et al., 2014). Anammox is considered linked to denitrification in a 30% to 70% ratio because Anammox needs the ammonia produced by denitrification (Devol, 2003). However, measured rates do not always follow these proportions (Babbin et al., 2020). Ammonium concentrations are extremely low in both ODZs and the oxic oligotrophic ocean (< 10 nM), probably because of consumption by phytoplankton in surface waters, efficient scavenging by ammonia-oxidizing Thaumarchaeota in oxic deeper waters, and Anammox bacteria in ODZs (Priddle et al., 1997; Martens-Habbena et al., 2009; Widner et al., 2018a). It has been modeled that competition for ammonia between Anammox and nitrite-oxidizing bacteria causes oscillations in the volume of anoxic water and the amount of N loss in ODZs (Penn et al., 2019). Utilization of organic nitrogen provides an adaptive capacity for accessing reduced nitrogen pools other than ammonium. Urea and cyanate are two examples of small, reduced organic N sources.

Urea (CH_4N_2O) is a reduced nitrogen compound that is produced both as an excretion product by crustacean and gastropod zooplankton (Miller and Glibert, 1998; Pitt et al., 2009; Thibodeau et al., 2020) and as a part of organic matter degradation (Cho et al., 1996; Berman et al., 1999). Microorganisms can metabolize urea by using the enzyme urease, encoded by the gene *ureC*, which catalyzes urea hydrolysis (Hausinger, 2004). In the Atlantic, urea averaged 25%–30% of total N uptake and was generally maximal in the euphotic zone (Painter et al., 2008). In the oxic waters above the Eastern Tropical North Pacific (ETNP) ODZ, uptake experiments using dual ^{13}C and ^{15}N isotopically labeled urea demonstrated that the N in urea was preferentially assimilated over the carbon, indicating that organisms were using urea as a N source (Widner et al., 2018a).

Urea concentrations are typically in the nanomolar range (50–350 nM) (Painter et al., 2008; Kitzinger et al., 2019; Takeda et al., 2020). Urea in the subtropical North Pacific (HOT) ranged from 50 to 150 nM in the top 200 m, with a maximum at the chlorophyll maximum (Takeda et al., 2020). In the ETNP, urea concentrations as high as 1.5 μM were found at coastal stations, but concentrations were much lower offshore (generally 0–150 nM) (Widner et al., 2018a). At the station examined further here, measurements of urea showed that urea was generally absent from the water column, with concentrations below the detection limit (b.d.l.; 70 nM) until 958 m in the oxycline below the ODZ, where urea concentration reached 0.71 μM, possibly due to zooplankton migrating to that depth (Widner et al., 2018a).

Cyanate is a small organic form of reduced nitrogen (OCN^-) that can be produced abiotically from photoproduction, biotic organic matter degradation, and senescent algal cultures (Widner et al., 2016). Cyanase (*cynS*) is an enzyme that catalyzes the conversion of cyanate to CO_2 and ammonia (Johnson and Anderson, 1987). In the marine environment, cyanate is measured in the nanomolar concentration range using a recently developed chromatographic method (Widner et al., 2013). Therefore, cyanate concentrations have only been measured in a few places in the ocean, such as the coastal North Atlantic (0.4 nM to 11 nM; Widner and Mulholland, 2017), the Gulf of Mexico (median 11.5 nM; Kitzinger et al., 2019), and the ETNP and ETSP ODZs. In the oxic ocean, the cyanate vertical distribution resembles the vertical distribution of ammonium and nitrite, with a primary maximum right below the chlorophyll maximum (Widner et al., 2016). In the ETSP and ETNP, cyanate uptake was observed in the euphotic zone, although it accounted for less than 2% of total N uptake (Widner et al., 2018b, 2018a). Cyanate uptake was also detected in the upper ETNP ODZ but was lower than 0.4 nM/h (Widner et al., 2018a). In the ETSP, cyanate concentrations along a transect at 17°S ranged from below detection (0.4 nM) to 45 nM in oxic waters, but concentrations in the ODZ only reached 7 nM (Widner et al., 2018b). In the ETNP ODZ, cyanate concentrations

were much higher, ranging from below detection to 50 nM in the upper ODZ (Widner et al., 2018a).

Most microorganisms prefer ammonia over nitrate for assimilation because reducing oxidized N compounds, like nitrate, for use in proteins or DNA has an extra energy cost (Glibert et al., 2016). As primary producers, picocyanobacteria *Prochlorococcus* and *Synechococcus* need to obtain N from inorganic sources but can also use the small organic compounds cyanate and urea (Rocap et al., 2003; Kamennaya and Post, 2011). In oligotrophic regions, Picocyanobacteria contribute greatly to primary production (Rii et al., 2016). *Prochlorococcus* ecotypes and abundances change dramatically in depth profiles, with highlighted ecotypes in the surface, Low Light I in the middle of the euphotic zone and Low Light II and Low Light IV at the bottom (Ahlgren et al., 2006; Johnson et al., 2006; Zinser et al., 2007). Specific ecotypes (Low Light V, AMZ3) of *Prochlorococcus* live at the top of ODZs when > 1% blue light overlaps with anoxic water (Cepeda-Morales et al., 2009; Ulloa et al., 2021). In the ETNP ODZ, all of the *Prochlorococcus* contained the gene for urease but not cyanase; only an extremely small proportion of Low Light I *Prochlorococcus* contained the gene for cyanase above the ODZ (Widner et al., 2018a). However, the proportion of *Prochlorococcus* that can use urea and cyanate in the environment, outside the ETNP, has not been quantified.

In the ocean, many microbial groups that contain the urease or cyanase gene have been shown to have key roles in the nitrogen cycle. Three key N-cycling microbes can use both urea and cyanate. First, some cultured isolates of Thaumarchaeota were found to have urease and can use urea as a sole N source (Qin et al., 2014). In the environment, Thaumarchaeota can use urea degradation to fuel the dissimilatory process of ammonia oxidation to obtain energy along with carbon assimilation (Tolar et al., 2017; Shiozaki et al., 2021). The presence of *ureC* is widespread in Thaumarchaeota genomes, with 60%–100% of Thaumarchaeota in the coastal time series SPOT and in the ETNP (Ahlgren et al., 2017; Widner et al., 2018a). However, in the Gulf of Mexico, only between 10% and 15% of Thaumarchaeota cells contain the *ureC* gene, indicating that not all Thaumarchaeota have urease (Kitzinger et al., 2019). Thaumarchaeota can also grow on cyanate as the only energy and nitrogen source but do not have the cyanase gene (Palatinszky et al., 2015), so we cannot presently trace this ability in the population. Secondly, some *Nitrospina* single-cell genomes were found to contain genes for urea and cyanate degradation (Pachiadaki et al., 2017). The marine nitrite-oxidizing bacteria *Nitrospina* are aerobic and obligate chemolithotrophs that oxidize nitrite to nitrate and use CO_2 as the sole C-source (Spieck et al., 2014). In the ETNP ODZ, *Nitrospina* had one copy per genome of urease at the top of the ODZ, but only ~ 50% of *Nitrospina* had cyanase (*cynS*) (Widner et al., 2018a). Thirdly, cyanase was found in the first *Cand.* Scalindua genome (van de Vossenberg et al., 2013). *Cand.* Scalindua are free-living bacteria (Fuchsman et al., 2017, 2012) that undergo the Anammox process, producing N_2 gas. Later, single-cell genomes of *Cand.* Scalindua were found to also have genes for urea transport and urease (Ganesh et al., 2018). *Cand.* Scalindua possessed one copy of the cyanase gene per genome in the ETNP and were the only bacteria able to use cyanate in the ODZ (Widner et al., 2018a). When dual ^{13}C and ^{15}N isotopically labeled cyanate was used by Anammox bacteria in the ETNP ODZ, the C in cyanate was assimilated but the N was not, indicating dissimilatory use of the N (Widner et al., 2018a). Experimental data in the ETSP ODZ showed that Anammox N_2 production rates could be supported by the N in cyanate (Babbin et al., 2017). Urea could only stimulate Anammox N_2 production rates after a 1.5-day lag time, indicating that the Anammox bacteria were not utilizing the urea *in situ* at the time of sampling (Babbin et al., 2017). Thus, urea and cyanate have the potential to be important reactants for microbes mediating the marine N cycle.

Stable isotope probing has indicated that some SAR11 can utilize urea in Arctic surface waters (Connelly et al., 2014), and isolates of estuarine ecotypes of SAR11 also can assimilate urea (Lanclos et al., 2023). SAR11 is an abundant growing group of free-living marine heterotrophic Alphaproteobacteria with small cells and streamlined genomes (Morris et al., 2002; Rappe et al., 2002; Giovannoni et al., 2005). The fact that SAR11 can utilize urea is particularly interesting, as most of the microbes that use urea and cyanate as N sources are autotrophic (Widner et al., 2018a). Although SAR11 in oxic waters utilizes oxygen, SAR11 bacteria in ODZs encode genes for nitrate reductase of the *narG* variety, and different SAR11 ecotypes live in ODZs compared to oxic waters (Tsementzi et al., 2016). In the ETNP ODZ, ~ 10% of SAR11 contained the urease gene (*ureC*) (Widner et al., 2018a). However, the use of urea by SAR11 has not otherwise been investigated in the oligotrophic ocean.

Some eukaryotic algae also have the ability to use cyanate. Analysis of marine planktonic metatranscriptomes from TARA oceans (global ocean sampling at three depths) has shown that *cynS* transcripts were as prevalent as those for *ureC* (Mao et al., 2022). In the large size fraction (> 0.8 µm), various eukaryotic algae produced *cynS* transcripts, including Pelagophytes, Dinophytes, Bacillariophyta, and fungi. In the smaller size fraction (< 0.8 µm), *Synechococcus cynS* transcripts dominated surface waters, whereas *Prochlorococcus* and unclassified microbes contributed to the *cynS* transcripts at the deep chlorophyll maximum (DCM) (Mao et al., 2022). The abundance of *cynS* transcripts negatively correlated with dissolved inorganic N concentrations (Mao et al., 2022). Although total *cynS* transcripts were reduced in the mesopelagic region compared to the euphotic zone, *Nitrospina cynS* transcripts were found in the mesopelagic region (Mao et al., 2022).

In this paper, we use phylogenetic read placement of metagenomic reads to examine the spatial distribution of microbes that utilize urea and cyanate at 3 ODZ stations and three sampling dates from the oxic Hawaii Ocean Time Series (HOT) station in the subtropical North Pacific. The study of the proportions and abundance of cyanase *cynS* and urease *ureC* has been previously reported in and above the ETNP ODZ (Widner et al., 2018a). However, since 2017, sequences of *ureC* previously classified as "unknown" have been assigned to new taxonomic groups. The phylogenetic tree for urease was significantly improved here to include genes from *Cand.* Scalindua (Anammox) single-cell genomes (Ganesh et al., 2018), S-oxidizing Thioglobus isolates (Marshall and Morris, 2015; Shah and Morris, 2015), and Verrucomicrobia and Alphaproteobacteria MAGs (Sun

and Ward, 2021; Zhang et al., 2023), increasing the number of microbes with known biogeochemical functions examined. Additionally, we complete the ETNP metagenomic profile, first published in 2017, by adding new metagenomes covering the bottom of the ODZ and the deep oxycline. Our detailed examination of all the microbial groups with the ability to use cyanate and urea illuminates that niche differentiation rather than direct competition determines gene depth profiles.

Methods

The metagenomic reads from the genes *ureC* and *cynS* were extracted from the metagenomic databases of interest (ETSP, ETNP, and HOT), and subsequently placed and aligned by using phylogenetic read placement methods onto phylogenetic trees containing aligned amino acid sequences of urease or cyanase enzymes of known taxonomic groups (Supplementary Figures S1, S2). Once the reads were placed in the tree, we classified the reads according to the taxonomy of the sequence of known taxonomic groups. We then estimated the ratio of *ureC* and/or *cynS* to the housekeeping gene RNA polymerase (*rpoB*). The ratio *ureC/rpoB* and *cynS/rpoB* were expressed as % of the total prokaryotic community (Archaea + Bacteria) or as the total of specific microbial taxa across depth profiles at each station.

Compilation of metagenomic data

Metagenomes from microbial communities were obtained from publicly available datasets across four station locations in the Pacific (Figure 1). Detailed depth profiles of cellular metagenomes from St ALOHA were obtained as part of the Hawaii Ocean Time-series (HOT) (22°45°N and 158°W) for May (HOT 272), August (HOT 275), and November 2015 (HOT 278) and were downloaded from Bioproject PRJNA352737 (Luo et al., 2020). Nutrient and CTD measurements for these cruises can be downloaded with the Hawaii Ocean Time Series Data Organization and Graphical System (HOT-DOGS) application at the University of Hawai'i at Mānoa (https://hahana.soest.hawaii.edu/hot/hot-dogs/) and in the supplement to the original paper (Luo et al., 2020). For Eastern Tropical South Pacific (ETSP) Station 9 (13°S and 82.2°W) and Station 17 (16.7°S and 79°W) sampled in July 2013, metagenomes were obtained from Bioproject PRJNA704804 (Fuchsman et al., 2022). Hydrographic and nutrient data from this ETSP cruise have previously been published (Peters et al., 2018; Fuchsman et al., 2022). Cyanate data from this ETSP cruise were published, but urea was not measured (Widner et al., 2018b) (Supplementary Figure S3). Metagenomes from ETNP Station 136 (17.04°N, 106.54°W) in April 2012 can be found in Bioproject PRJNA350692 (Fuchsman et al., 2017), and nutrient data for ETNP ST136 can be seen in Fuchsman et al. (2017). Cyanate and urea concentration data from this ETNP cruise are published (Widner et al., 2018a), and data for ST136 is included here (Supplementary Figure S4). Temperature, salinity, and nutrient metadata for all samples can be found in Supplementary Table S1.

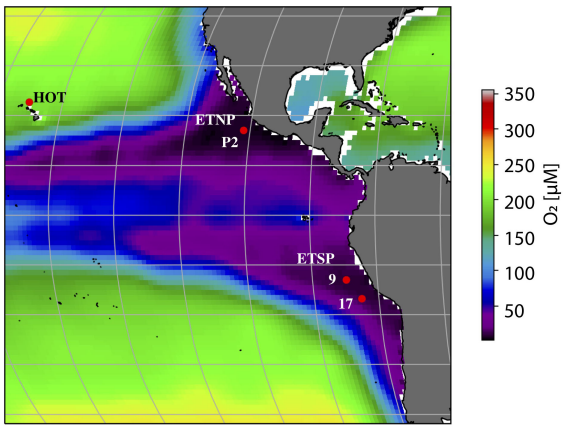

FIGURE 1
Location of the stations. Map of World Ocean Atlas 2018 oxygen concentration at 250 m (Garcia et al., 2019). The color scale indicates oxygen concentration (in µM), and the red dots indicate station locations for the Hawaii Time Series (HOT; oxic), and ODZ stations are from the ETNP (P2) and ETSP (ST9 and ST17).

In this paper, we add five metagenomes to existing ETNP ST136 (600 m [deep ODZ], 800 m [ODZ boundary], 1,000 m [hypoxic]) and ETSP ST17 (80 m [oxic], 125 m [hypoxic]) depth profiles. As described in Fuchsman et al. (2017, 2022), 4 L of water from the CTD was filtered through 0.2 µm SUPOR filters on board the ship and immediately frozen at -80°C. These filters were extracted in June 2023, following the protocol in Fuchsman et al. (2017); DNA was extracted from filters using freeze–thaw followed by incubation with lysozyme and proteinase K and phenol/chloroform extraction. Libraries were created and run on a NovaSeq 6000 at the Northwest Genomics Center (Seattle, WA). The two new ETSP metagenomes can be found with the rest of the 2013 ETSP metagenomes at Bioproject PRJNA704804, but the three new 2012 ETNP metagenomes are in Bioproject PRJNA1083228.

All ETSP samples, new and old, were assembled separately, and assemblies are available at Bioproject PRJNA704804. Samples were quality-screened using Trimmomatic v0.39 (Bolger et al., 2014) and assembled using Megahit v1.2.8 (Li et al., 2015). To find the genes of interest in the assembled contigs, genes were called and annotated with Prokka 1.14.6 (Seemann, 2014). Sequence information about the new metagenomes can be found in Supplementary Table S2.

Transcripts of sequences corresponding to station P2 (16°55 N, 107°09 W) in the ETNP in May 2018 were obtained from the oxycline and top of the ODZ (76–150 m) (Mattes et al., 2022), downloaded from BioProject PRJNA727903, and processed following the same methodology described below. These transcript samples were sampled over multiple days at the station, and thus, due to variations such as internal waves, oxygen concentrations from the samples do not change linearly with depth (Mattes et al., 2022). STP2 is geographically close to ETNP ST136, examined for metagenomes.

Phylogenetic read placement technique

Phylogenetic trees for urease (*ureC*) (Supplementary Figure S1) and cyanase (*cynS*) (Supplementary Figure S2) from Widner et al.

(2018a) and nitrite oxidoreductase (*nxrB*) from Fuchsman et al. (2017) were updated using assembled sequences from the ETSP, marine single-cell genomes (Berube et al., 2018), and eukaryotic assemblies from the MMETSP (Keeling et al., 2014). Hydrazine oxidoreductase (*hzo*) data have already been published (Fuchsman et al., 2022). Nitrate reductase gene (*narG*) data for Thioglobaceae was obtained using a phylogenetic tree modified by Fuchsman et al. (2017).

The RNA polymerase (*rpoB*) phylogenetic tree has already been published (Fuchsman and Hays, 2023). A set of reference amino acid sequences (encoding for the genes *nxrB*, *ureC*, and *cynS* separately) were used as a query to be blasted against custom databases for the assembled protein ETSP 2013 dataset and for single-celled genomes and eukaryotic assemblies using blastp (Altschul et al., 1997). References and assembled sequences were aligned using MUSCLE v3.8.1551 (Edgar, 2004). The alignment was used to build a phylogenetic tree with bootstrapping using RAxML-ng (Kozlov et al., 2019) and later visualized using FigTree v1.4.4 (https://github.com/rambaut/figtree/releases). The tree constructed using RAxML-ng was used as the reference frame to place the metagenomic reads from the ETSP, ETNP, and HOT datasets.

As described previously (Fuchsman et al., 2023), read placement was done by recruiting short metagenomic reads via a tblastn search of the metagenomes (using an *e*-value of ≤ 5). The reads were trimmed to remove Ns and converted to amino acid sequences. After the quality trimming, only sequences longer than 100 bp (33 amino acids) were kept. The amino acid-translated reads were then aligned against the reference sequences using PaPaRa 2.0 (Berger and Stamatakis, 2011). The nonoverlapping paired read ends were then combined into one sequence in the same alignment using a Python script, and they were later placed in the tree using EPA-ng v0.3.6 with filter-max as 1 (Barbera et al., 2019). Placed reads have a pendant length, indicating the similarity between a query read and the location it places on the tree. Reads that were placed with a pendant length greater than 2 were removed; 1% or less of reads were removed at this step. To sort the reads into taxonomic groups, the reads in each group were enumerated using the assigned subcommand of Gappa v0.6.1 and a taxonomy file listing the taxonomy of the tree reference sequences (Czech et al., 2020). Taxonomic read counts were normalized using the method previously described by Fuchsman et al. (2019) where normalization factors for each sample were determined by dividing 48,556,135 (the number of reads in the 100-m ETNP sample) by the number of good-quality reads in the sample. The read counts were multiplied by the sample normalization factor, divided by the gene length (1,704 base pairs (bp) for *ureC*, 468 bp for *cynS*, 3847 bp for *rpoB*, and 1,275 bp for *nxrB*), and then multiplied by 100 to make visualization easier. We refer to these numbers as normalized reads. We then calculated the percentage of the total microbial community containing *cynS* and *ureC* by dividing the normalized reads for *cynS* or *ureC* by the combined Bacteria- and Archaea-normalized reads for single-copy core gene RNA polymerase (*rpoB*). Similarly, we calculated the proportions of individual taxa containing *cynS* or *ureC* by dividing by *rpoB* normalized reads for that taxa. The numerical results from these analyses can be found in Supplementary Table 3.

The errors in these analyses can be broken into three types of error. For HOT 272 (May 2015), 700 m and 1,000 m samples were sequenced twice. Our analysis of these duplicate samples produced almost identical results; the average standard deviation between *ureC* groups was 0.05 normalized reads for 700 m and 0.15 normalized reads for 1,000 m. These data indicated that we have good reproducibility. However, there are two systemic caveats to this analysis: (1) some organisms may be missing from the phylogenetic trees, and (2) gene lengths vary between organisms. In the case of incomplete phylogenetic trees, it is less accurate to place sequences when there are no near relatives to that sequence. We have minimized this source of error by building trees both with known genomes and with environmentally assembled contigs. In terms of length variability, any differences between organisms' genes and our estimates of gene length will result in misestimated gene ratios. However, the magnitude of such an error is small: the average length of reference genes composing the trees here were *cynS* = 460 bp ± 40 bp, *ureC* = 1,706 bp ± 23 bp, and *rpoB* = 3,815 bp ± 333 bp. RNA polymerase (*rpoB*) was the longest gene with the most variability. This variability in *rpoB* would change a proportion of *ureC/rpoB* of 100% by ± 10%.

Results

In this paper, we describe the proportion of the community harboring *ureC* or *cynS* from functional gene/single-copy core gene ratios, with the understanding that this value is complicated by functional gene copies per cell. For HOT, the *ureC/rpoB* ratios were > 100% of the microbial prokaryotic community (Bacteria and Archaea) in surface waters (top 100 m depth), indicating that many organisms harbored more than one *ureC* gene per cell. This value decreased to ~ 30% in the mesopelagic, indicating that 30% or fewer organisms harbored this gene. In the ODZs, ~ 30% of the community had *ureC*, but below the ETNP ODZ and at 80 m in the ETSP ST17, ~ 60% of the community had the *ureC* gene. Some microbial groups containing *ureC* were present in both the ODZs and oxic sampling dates, like *Nitrospina*, Thaumarchaeota, and Picocyanobacteria. However, at the ODZ stations, we observed more diverse groups containing *ureC* than at HOT, including Anammox bacteria (*Cand.* Scalindua), Verrucomicrobia, and members of the Gammaproteobacteria, including *Thioglobus* (Figure 2A).

At HOT, up to 25% of the total bacterial and archaeal communities had *cynS* genes at the DCM, but 8%–10% of the community had *cynS* in most of the upper euphotic zone, decreasing to < 2% from 150 to 250 m and to < 0.5% in the mesopelagic. The majority of *cynS* reads correspond to *Prochlorococcus*; for example, at HOT 275 (August 2015), *Prochlorococcus cynS* reached 24.1% of the total community at 100 m. *Nitrospina cynS* was present at depth, reaching 1.4% at 150 m. In the mesopelagic zone at HOT, < 1% of the community contained the *cynS* gene. In the ODZs, less than 12% of the total bacterial and archaeal communities had *cynS* genes (Figure 2B). Among the ODZ microbial communities, the highest abundance of

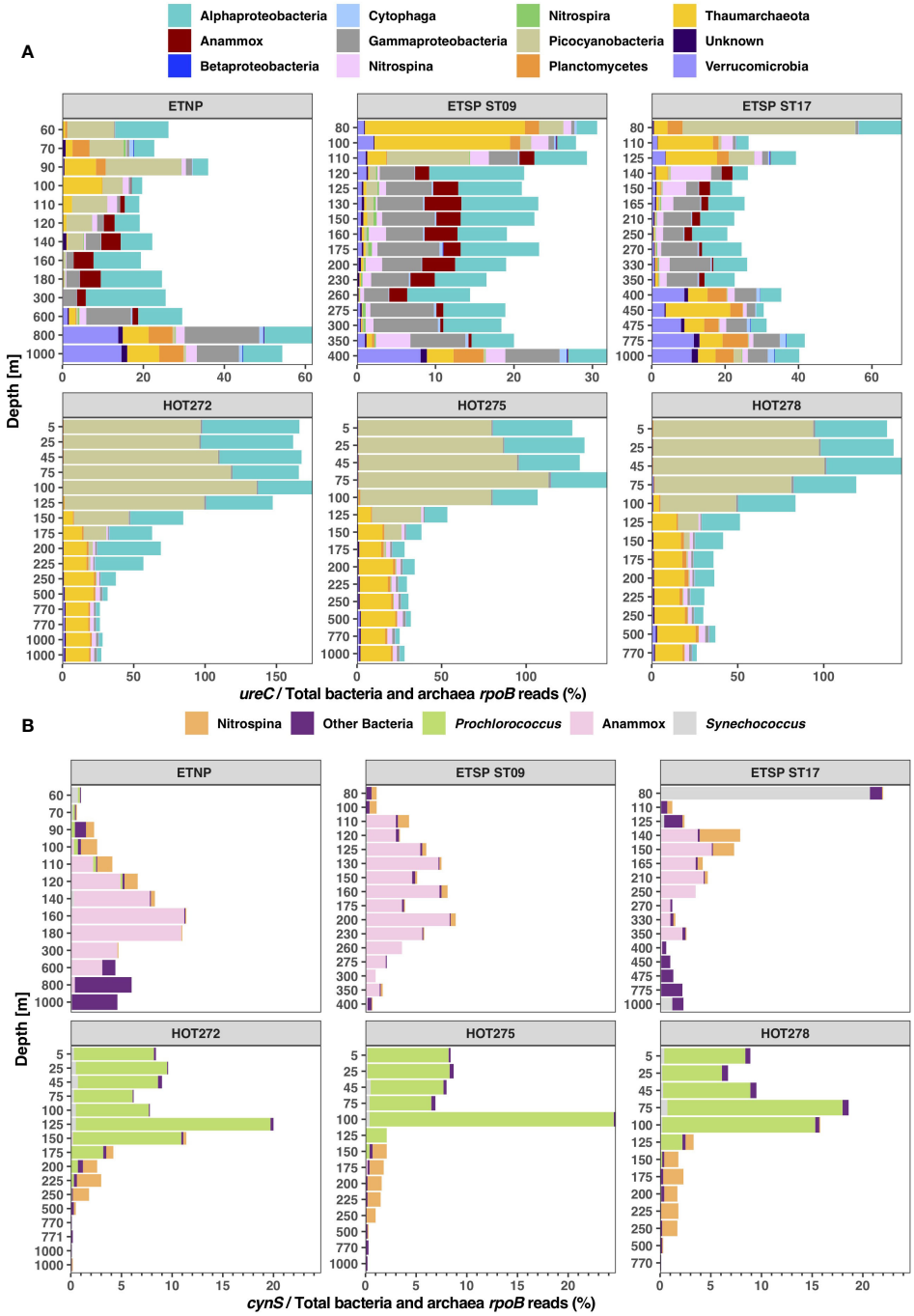

FIGURE 2
Abundance of urease and cyanase in the total microbial community. Stacked bar charts showing **(A)** the ratio of total *ureC* reads/total bacterial and archaeal *rpoB* reads in percentage, and **(B)** the ratio of total *cynS* reads/total bacterial and archaeal *rpoB* reads in percentage, classified by taxonomic groups according to depth at ODZ stations (ETNP, ETSP ST09, ETSP ST17) and HOT 272 (May), 275 (Aug), and 278 (Nov). The depth is not to scale.

cynS corresponded to *Cand*. Scalindua (Anammox), with up to 11.1% of the community in the ETNP at 160 m (Figure 2B). The second highest abundant *cynS* gene was "other bacteria", a group of unclear taxonomy including many proteobacteria but also single representatives from other phyla such as *Nitrospira* and Verrucomicrobia (Supplementary Figure S2). The other bacteria *cynS* group was mostly found in the oxyclines above and below the ODZs. When examined on an individual reference level, the majority of the other bacteria reads placed on environmental assembled contigs with a minority placed on *Alteromonas*. The highest abundance of *Nitrospina cynS* was 4% of the total microbial community at 140 m at ETSP station 17, the top of the ODZ at that station (Figure 2B). *Synechococcus cynS* was dominant at ETSP ST17 80 m, a fully oxic depth, reaching 20% of the community. We

also checked the presence of *cynS* in eukaryotic groups like algae. Eukaryotic algae could not be normalized to a percent of the bacterial and archaeal communities and are thus are examined separately. At the ODZ stations, we only found algae *cynS* above the ODZs: 11 normalized reads at 70 m depth at ETNP station 136, four normalized reads from ETSP station 9 at 80 m, and seven reads at 80 m from ETSP ST17 (Supplementary Figure S5). At HOT, algae *cynS* reads were found at the DCM, with three algae *cynS* normalized reads in the 125–150-m range for HOT 272, six to nine algae *cynS* normalized reads at 100–125 m depth for HOT 275, and four algae *cynS* normalized reads in the 75–100-m range for HOT 278 (Supplementary Figure S5). The algae *cynS* normalized reads at HOT, ETSP ST9, and the ETNP were from Pelagomonales, but at ETSP ST17, five reads were Pelagomonales, but two were Phaeocystis. Though present, algae *cynS* were never abundant.

Proportion of taxa harboring functional genes

In this section, we will describe the ratios of taxon-specific functional genes *ureC* and *cynS* to taxon-specific *rpoB* reads for a variety of groups important to biogeochemical cycling. We also explore the proportions of the taxon-specific functional genes nitrite oxidoreductase (*nxrB*; *Nitrospina*), nitrate reductase (*narG; Thioglobaceae*) and hydrazine oxidoreductase (*hzo*; Anammox) to support our taxon-specific *rpoB* data.

Anammox *cynS*, *ureC*, and *hzo*

Anammox bacteria were found only in the ODZ core. The abundance of Anammox, measured by *rpoB* gene copy number, was highest in the ETNP station, comprising up to ~ 10% of the prokaryotic community at 300 m, but decreased at the bottom of the ODZ. In contrast, its total abundance peaked at 6% for both ETSP stations (Figure 3A). Anammox bacteria have both *ureC* and *cynS* genes. Anammox *cynS* games are usually almost twice as abundant as Anammox *ureC* genes within each depth (Figure 3B). In the ETNP ODZ, the highest Anammox *cynS* to *rpoB* ratio was 116.4% at 180 m, while the *ureC* to *rpoB* ratio was 56.1%. At the ETSP ODZ station 17, the *cynS* abundance was 157% of Anammox bacteria, versus 80.5% of *ureC* reads at 210 m. The highest abundance of *cynS* reads was found in the ETSP ST9, with 177.6% *cynS* reads and 80.5% *ureC* reads at 275 m. The gene for hydrazine oxidoreductase (*hzo*, a key gene in the Anammox process) showed similar patterns and abundance to the *cynS* gene in the ETSP stations (Figure 3B); however, in the ETNP and the ETSP ST17, the abundance of *hzo* was lower than that of *cynS* at some depths in the ODZ core.

Nitrospina cynS, *ureC*, and *nxrB*

The abundance of *Nitrospina* (Figure 4A) estimated using the *rpoB* gene was highest in the ODZ ETSP station 17, reaching 11.4% of the prokaryotic community at 140 m, which was the oxic/anoxic transition. The abundance of *Nitrospina* was below 6% of the prokaryotic community in the other two ODZ stations and was below 3% at HOT. The *Nitrospina* community has both genes *cynS* and *ureC*, but a higher proportion of *Nitrospina* had *ureC* than *cynS* in the ODZ and at HOT (Figure 4B). Within the sampling dates at HOT, the proportion of *Nitrospina* with *ureC* varied between 77.1% and 161.3%, and for *cynS*, varied between 37.4% to 118.8% in the top 250 m, but there was a marked decrease in the proportion of *Nitrospina* with *cynS* at depth, with values of 2%–3% at 750 m and below (Figure 4B; Supplementary Figure S6). In the ETNP station, the abundance of *ureC* was also higher than *cynS*; the *cynS* reads were between 25.9% and 63.4% and *ureC* was ~ 100% of *Nitrospina* (Figure 4B). In the ETSP ODZ ST9, *ureC* reads were between 46% and 107.8% and *cynS* reads were between 2.6% and 45.8%. The proportion of both *cynS* and *ureC* genes was lower than the proportion of the gene nitrite oxidoreductase (*nxrB*) (Figure 4B), a key gene in the nitrite oxidation pathway in *Nitrospina*, which is often found at two copies per genome (Lücker et al., 2013; Fuchsman et al., 2017).

Thioglobaceae *ureC*

The abundance of Thioglobaceae estimated using the *rpoB* was higher in the mesopelagic (Figure 5A). At the ETSP stations, Thioglobaceae reached ~ 11% of the prokaryotic community in the ODZ, but only reached 5.6% in the ETNP ODZ. At HOT, Thioglobaceae reached 7% of the prokaryotic community with a maximum at 500 m (Figure 5A). Using the *rpoB* gene, the Thioglobaceae group was composed of subclades SUP05, Arctic-96BD19, and a new ODZ clade (phylogenetic tree; Supplementary Figure S7). The ODZ clade had the highest abundance, reaching 10.7% of the community at ETSP ST9 at 350 m and 10.5% at 350 m at ETSP ST17 (Figure 6). Similarly, in the ETNP, the ODZ clade was the most abundant, increasing from 1.6% at 110 m to a maximum of 5% of the community at 300 m depth, but then decreasing at the bottom of the ODZ (Figure 6). Additionally, we observe that the Thioglobaceae in the ODZ contained nitrate reductase (*narG*). In the ETNP, *narG* was approximately one copy per genome, but in the ETSP, it was approximately two copies per genome (Figure 5B). Given the ecotype abundances, we can conclude that the ODZ Thioglobaceae clade can reduce nitrate. At all three ODZ stations, the Arctic-96BD19 clade was abundant in the hypoxic oxyclines above and below the ODZs but was generally < 1% of the community in the ODZ. For example, at ETSP ST17, the abundance of the Arctic-96BD19 was 5.6% at 110 m in hypoxic oxycline above the ODZ and 7.7% at 450 m in hypoxic oxycline below the ODZ, but < 1% of the community in the ODZ. The sulfide-oxidizing SUP05 clade had a low abundance (< 1.4%) in all the ODZ stations. At HOT, only the Arctic-96BD19 clade was present, with abundances that increased with depth from 0.4% of the community at 150 m to a maximum of 8% at 500 m and then decreased to 2% at 1000 m (Figure 6).

We observed that Thioglobaceae had urease but no cyanase genes. At HOT, the proportion of Thioglobaceae with *ureC* reads was below 7.5% in the top 250 m for the majority of the sampling dates, with the exception of one point: 18.8% of Thioglobaceae at 150 m at HOT 278 (November) had the *ureC* gene, and 10%–20% of Thioglobaceae contained *ureC* at 1000 m (Figure 5B).

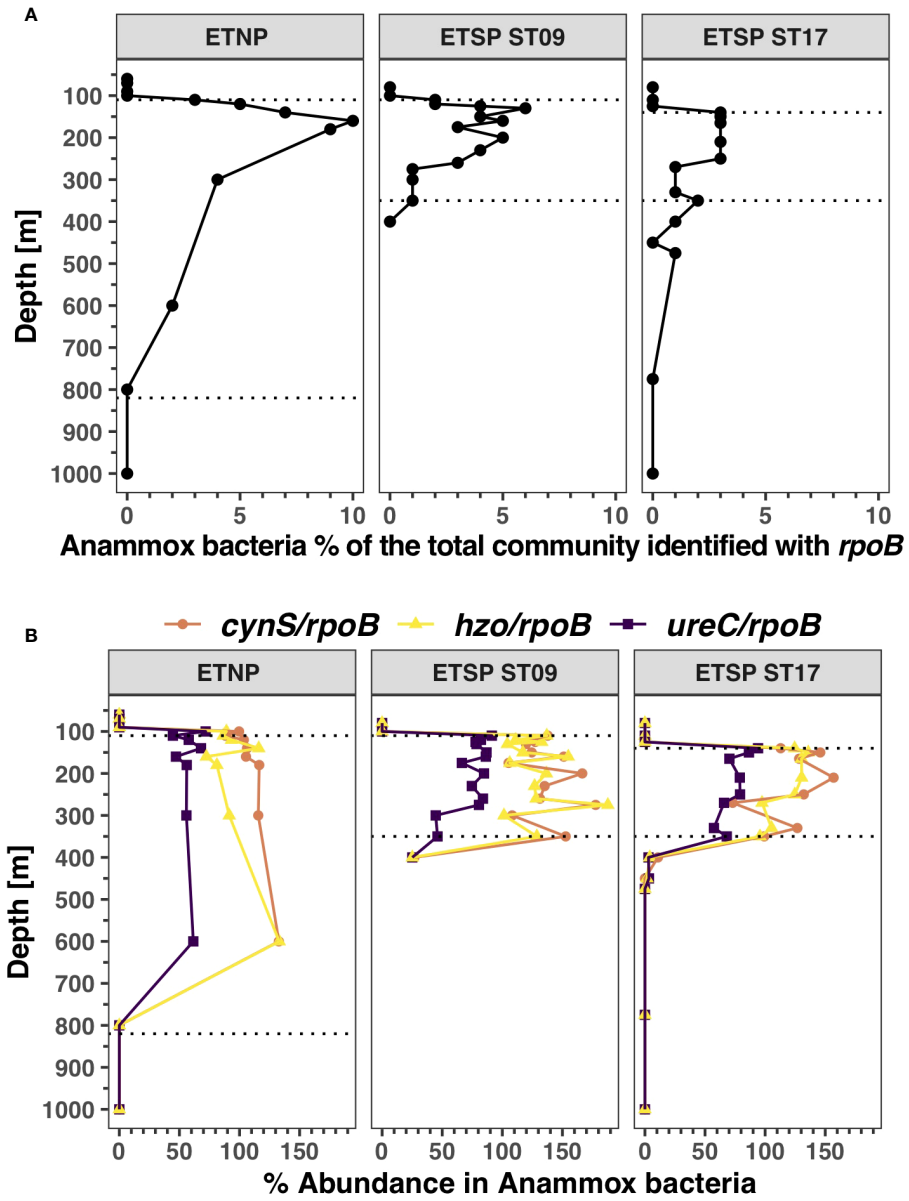

FIGURE 3
Distribution of Anammox bacteria and its functional genes in ODZs. **(A)** Percentage of the bacterial and archaeal community identified as Anammox bacteria (*Cand*. Scalindua) using RNA polymerase (*rpoB*). **(B)** Functional gene abundance in Anammox bacteria for cyanase (*cynS*), urease (*ureC*), and hydrazine oxidoreductase (*hzo*) as Anammox-specific *cynS*/*rpoB* ratios (orange), *hzo*/*rpoB* ratios (yellow), and *ureC*/*rpoB* ratios (purple). Each panel corresponds to a different ocean region. The area between the dotted lines corresponds to the ODZ core.

Contrastingly, at the ODZ stations, the proportion of Thioglobaceae with *ureC* increased inside the ODZ core. In the ETNP, the proportion of Thioglobaceae with *ureC* was 27.5% at 90 m in the hypoxic oxycline but varied between 60.3% and 109.3% in the ODZ core and decreased to 20% at the bottom of the ODZ (Figure 5B). Similarly, in the ETSP ODZ ST9, the proportion of Thioglobaceae with *ureC* in the oxic region reached 22.1% at 100 m in hypoxic waters above the ODZ but varied between 71.6% and 109.8% in the ODZ core; in the ETSP ST17, the proportion of Thioglobaceae with *ureC* varied from 9.7% at 110 m depth in oxic waters to 87.3%–111.8% in the ODZ but then decreased to 21.7% at 475 m in the hypoxic oxycline below the ODZ (Figure 5B). Thus, Thioglobaceae particularly contained the *ureC* gene in the ODZ.

SAR11 *ureC*

The abundance of SAR11 at HOT, according to *rpoB*, ranged between 24.9% and 39.4% (Figure 7A). SAR11 made up to 60% of the microbial community identified with the *rpoB* gene in the ETNP in the ODZ core (Fuchsman et al., 2017) but decreased to 5% at the bottom of the ODZ (Figure 7A). Contrastingly, the abundance of SAR11 in the ETSP stations was 6% to 32% of the microbial community. The SAR11 genomes had urease but no cyanase

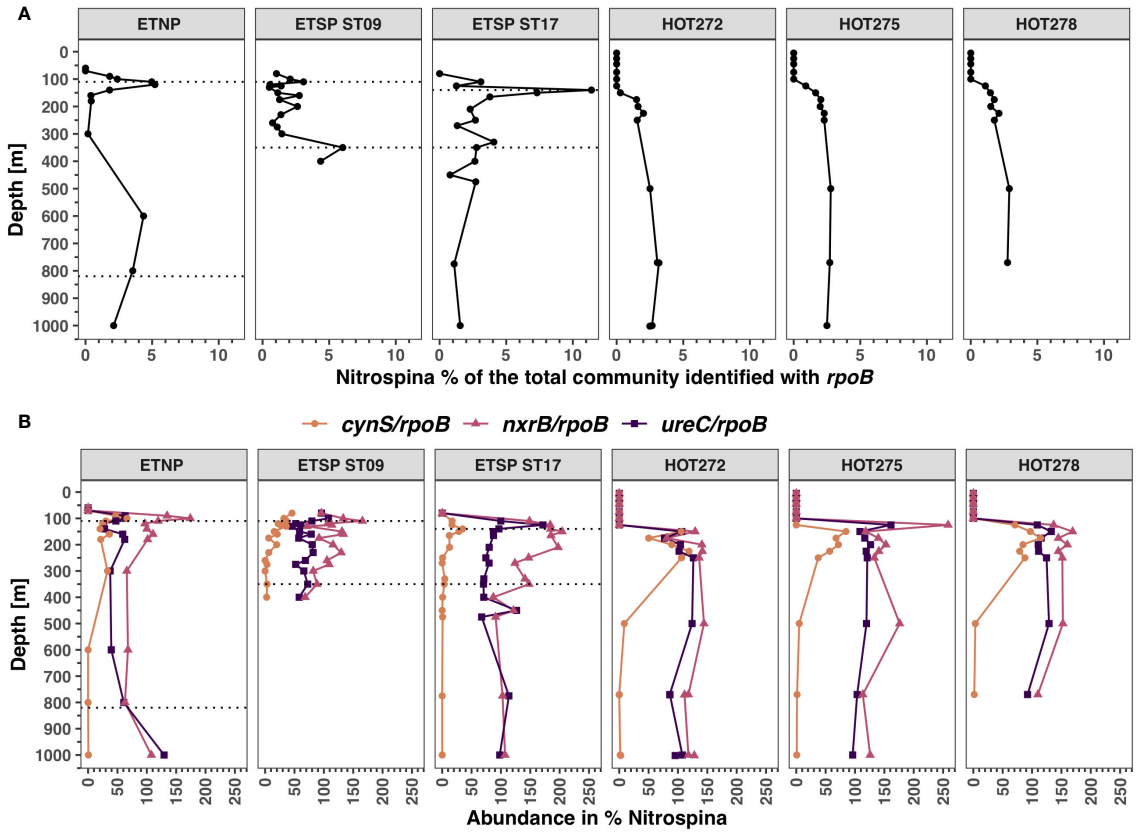

FIGURE 4
Distribution of *Nitrospina* and its functional genes in ODZs and HOT. **(A)** Percentage of the bacterial and archaeal community identified as *Nitrospina* using RNA polymerase (*rpoB*). **(B)** Abundance of cyanase, nitrite oxidoreductase, and urease in % of *Nitrospina* for *cynS/rpoB* ratios (orange), *nxrB/rpoB* ratios (pink), and *ureC/rpoB* ratios (purple). Each panel corresponds to a different ocean region. The area between the dotted lines corresponds to the ODZ core.

genes. The proportion of the *ureC* gene was higher at HOT, specifically on the surface (30%–42.6%), and decreased with depth, reaching < 1% of SAR11 at 500 m and below (Figure 7B; Supplementary Figure S8). In the ODZs, the proportions of the *ureC* reads were low but had a slight increase compared to the hypoxic waters above and below the ODZ, reaching 6.2% of SAR11 at 260 m at the ETSP ST9, 5.5% of SAR11 at 250 m in the ETSP ST17, and 10% of SAR11 at 300 m in the ETNP. Below the ODZ core, the proportion of SAR11 with *ureC* decreased to below 1% (Figure 7B).

We observed that *ureC* reads could be assigned to different SAR11 subgroups: subgroup 1a.3, subgroup ODZ, subgroup IV, subgroup V, and two unidentified subgroups (I, II). The proportion of each subgroup varied according to the presence of oxygen. Inside the ODZs, 100% of the SAR11 *ureC* reads corresponded to the ODZ subgroup (Figure 7C). In the ETSP ST17, subgroup 1a.3 *ureC* was found only in the oxic waters on top of the ODZ (27.8% of SAR11 *ureC* at 110 m) but was below 1.2% at 350 m, increasing to 25% in the hypoxic oxycline below the ODZ at 475 m. All the sampling dates for HOT had similar profiles; for example, in HOT 272 (May 2015), two subgroups contributed to most of the SAR11 *ureC* abundance: subgroup V and subgroup 1a.3, whereas the other subgroups had *ureC* abundances below 13.5% of SAR11 *ureC*. Subgroup 1a.3 *ureC* abundance varied between 31.4% and 57.7% of total SAR11 *ureC*, decreasing with depth. Subgroup V *ureC* abundance, on the other hand, increased with depth, peaking at 250 m depth. While the ODZ subgroup had the most abundant SAR11 *ureC* in the deep water at HOT, the total SAR11 *ureC* at these depths was negligible (Figures 7B, C).

Verrucomicrobia *ureC*

The abundance of Verrucomicrobia, calculated using the *rpoB* gene, was extremely low in the top 250 m at HOT, at < 1% of the prokaryotic community, but increased in the meso and bathypelagic, reaching 2% of the community at 4,000 m (Figure 8A; Supplementary Figure S9). Verrucomicrobia abundance estimated using the *rpoB* gene was consistently 1%–2% of the community in the ODZ core in the ETSP ODZ ST9 and ST17. However, the abundance of Verrucomicrobia increased in hypoxic waters both above and below the ODZ, reaching 7.9% of the community in station 17 at 400 m, 6.9% at 400 m in ST9, and 4.5% at 1,000 m in the ETNP. We only identified urease in Verrucomicrobia, not cyanase. In the ETNP, the abundance of *ureC* reads in the oxic waters above the ODZ and in the ODZ varied between 2.3% and 10% of Verrucomicrobia (Figure 8B). However, at the bottom of the ETNP ODZ, 100% of Verrucomicrobia had

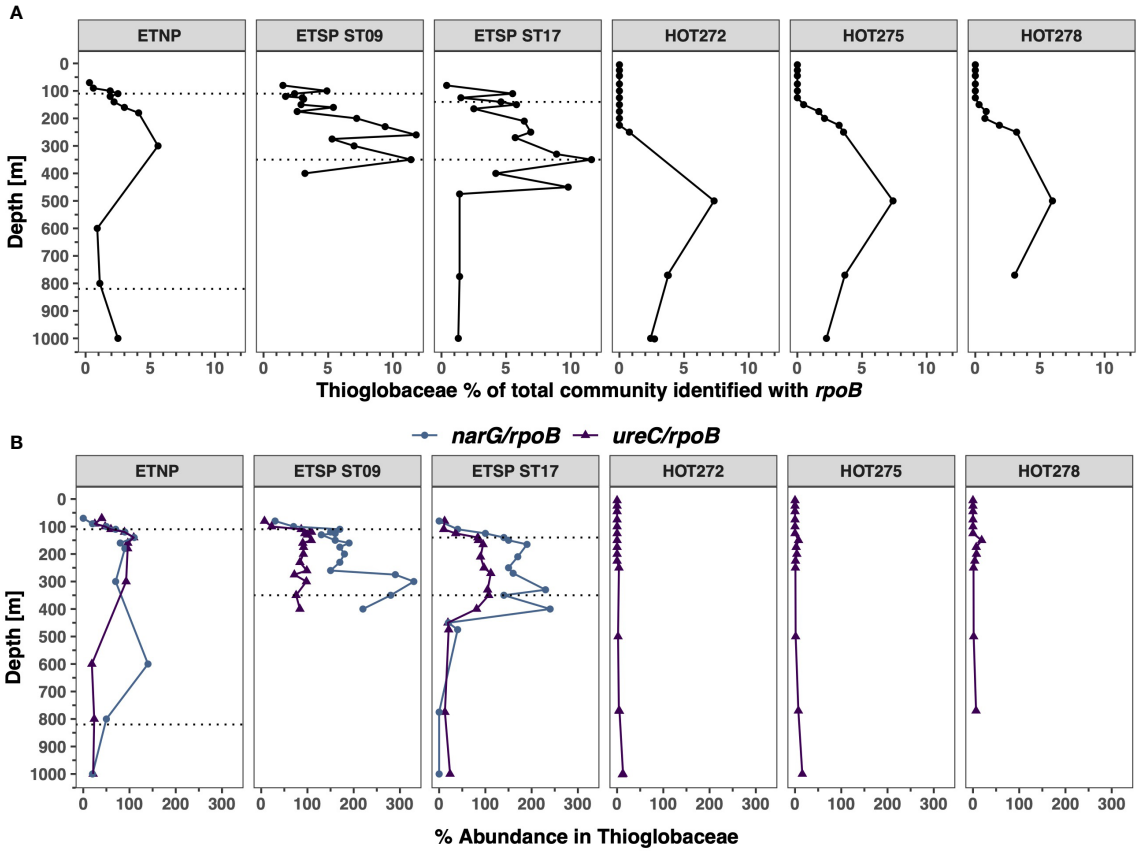

FIGURE 5
Distribution of Thioglobaceae and its functional genes in ODZs and HOT. **(A)** Abundance of the Thioglobaceae in % of the total bacterial and archaeal community identified with *rpoB*. **(B)** Abundance of urease and nitrate reductase in % of Thioglobaceae for *ureC/rpoB* ratios (purple) and *narG/rpoB* ratios (blue). Each panel corresponds to a different ocean region. The area between the dotted lines corresponds to the ODZ core.

ureC (Figure 8B). At ETSP ST17, the proportion of Verrucomicrobia with *ureC* was higher in the hypoxic waters above the ODZ at 63.9% of Verrucomicrobia at 110 m, decreasing in ODZ waters to 14.2%–27.7%, but increasing again below the ODZ to 112.5% at 400 m (Figure 8B). Similarly, at ETSP ST9, the proportion of Verrucomicrobia with *ureC* was higher in the hypoxic waters above the ODZ (66% at 100 m) and below (117.4% at 400 m depth) than in the ODZ core (6.7%–25.8%) (Figure 8B). For all ODZ stations, the proportions of Verrucomicrobia with *ureC* were higher in the hypoxic regions above and below the ODZ than in the ODZ.

Thaumarchaeota *ureC*

Thaumarchaeota abundance, estimated with the *rpoB* gene, was higher at HOT and increased with depth, reaching 30%–40% of the prokaryotic community at 500 m at all sampling dates and then decreasing to 20%–30% at 750–4,000 m (Figure 9A; Supplementary Figure S10). In contrast, at the ODZ stations, the abundance of Thaumarchaeota was higher in areas above and below the ODZ core. In the oxic waters above the ETNP ODZ, Thaumarchaeota *rpoB* reads reached a maximum of 11.5% of the community at 100 m, decreasing to < 1% in the ODZ, but below the ODZ, Thaumarchaeota *rpoB* reads once again reached 11% of the community (Figure 9A). At ETSP ST9 and ST17, the *rpoB* abundance was also < 1% of the community in the ODZ core. However, in hypoxic waters below the ODZ core, Thaumarchaeota were 6.2% of the community at 400 m depth in ST9 and 28.1% of the community at ST17 at 450 m (Figure 9A).

The proportion of Thaumarchaeota with *ureC* had similar trends with depth at each station (Figure 9B). For HOT, > 100% of Thaumarchaeota contained *ureC* at 100 m, but this proportion steadily declined until 250 m; 60%–70% of Thaumarchaeota had *ureC* from 250 to 1,000 m (Figure 9B). However, at 4,000 m, 100% of Thaumarchaeota again had the *ureC* gene (Supplementary Figure S10). Similarly, in the ODZ stations, in the oxic waters above the ODZ, > 100% of Thaumarchaeota contained *ureC*, and below the ODZs, the proportion of Thaumarchaeota with *ureC* was in the 60%–70% range (Figure 9B). The proportion of Thaumarchaeota with *ureC* decreased in the ODZs, but the abundance of Thaumarchaeota was also quite low in these regions (Figure 9).

Cyanobacteria *cynS* and *ureC*

Picocyanobacteria abundance identified with the *rpoB* gene was highest at HOT (Figure 10A), particularly at the surface. The sampling dates 272 (May), 275 (August), and 278 (November) had similar *rpoB* profiles, so only one profile is described here. At

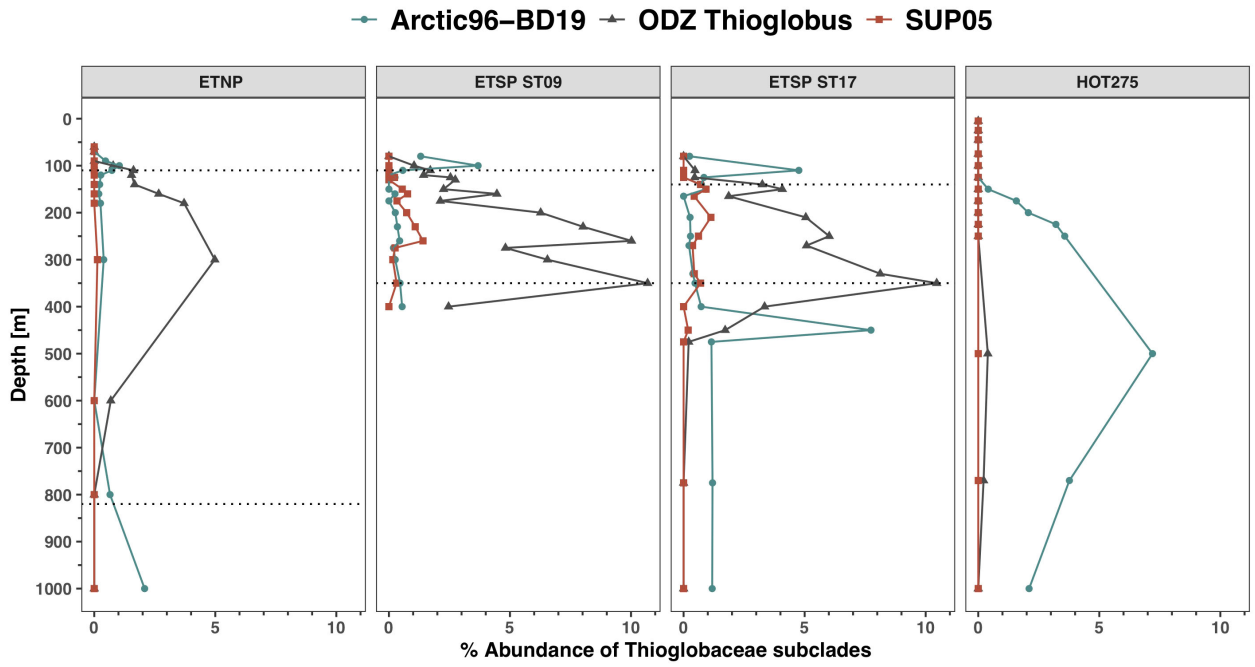

FIGURE 6
Thioglobaceae *rpoB* subclades distribution in ODZs and HOT. Depth profile of normalized metagenomic reads encoding for enzyme RNA polymerase (*rpoB*) of the Thioglobaceae subclades, expressed as % of the total bacterial and archaeal community, in the ODZ stations (ETNP, ETSP ST09, ETSP ST17) and at a representative HOT sampling date (HOT 275; August 2015). The area between the dotted lines corresponds to the ODZ core.

sampling date 272 (May 2015), the abundance of Picocyanobacteria estimated with the *rpoB* gene increased steadily with depth from 32.4% at 5 m, reaching the highest abundance of 53.9% at 100 m; below 100 m, the abundance decreased, reaching 0.6% of the microbial community at 225 m. The abundance of picocyanobacteria in the ETNP (Figure 10A) was highest at 60 m, comprising 15.4% of the prokaryotic community, but then it decreased with depth, with a small maximum in the upper ODZ (Figure 10A). Picocyanobacteria in the ETSP were generally low since profiles skipped surface waters: at ST9, it was below 2%, and ST17 only had Picocyanobacteria at 80 m (~ 20% of the community) (Figure 10A).

We calculated the total number of Picocyanobacteria that contained the *ureC* gene (Figure 10B). Picocyanobacteria *ureC* abundances at HOT were higher on the surface (~ 150%) and decreased with depth to 50%, close to 100 m depth (Figure 10B). In the ODZs, however, the ETNP and ETSP ST9 had an increase in the *ureC* with depth from < 10% in oxic waters to 100% to 130% in the ODZ (Figure 10B). Among the Picocyanobacteria that had *ureC*, we found four phylotypes: *Synechococcus*, High Light *Prochlorococcus* (HL), Low Light I *Prochlorococcus* (LLI), Low Light IV *Prochlorococcus* (LLIV), and uncharacterized *Prochlorococcus* (Figure 10C). The Picocyanobacteria *ureC* groups had similar profiles at the three sampling dates examined at the oxic station (HOT). For example, at HOT 272, the HL *Prochlorococcus* was ~ 100% of the total Picocyanobacteria *ureC* from 5 to 100 m, but below 125 m depth, the abundance of HL *Prochlorococcus* decreased to 10.4% at 225 m depth (Figure 10C). The LLI *Prochlorococcus* *ureC* increased from 28% of the total Picocyanobacteria *ureC* at 125 m to 59.7% at 225 m (Figure 10C).

In the ETSP ST9, the High Light *Prochlorococcus ureC* group was not detected in the water column, and LLI *Prochlorococcus ureC* was only present at 2.1% at 80 m depth, probably because much of the euphotic zone was not sampled. Uncharacterized *Prochlorococcus ureC* was 21.9% of the total Picocyanobacteria *ureC* at 80 m. However, the LLIV *Prochlorococcus ureC* group had the highest *ureC* abundance out of the total Picocyanobacteria *ureC*, changing from 49% of Picocyanobacteria at 80 m to a maximum of 87.1% at 110 m and 66.7% at 150 m (Figure 10C). In addition, the *Synechococcus ureC* group ranged from 12 to 33.3% of the total Picocyanobacteria *ureC* in the ODZ (Figure 10C). In the ETNP, HL *Prochlorococcus ureC* had a low abundance, generally below 3.4% of total Picocyanobacteria *ureC*, and LLI *Prochlorococcus ureC* abundance decreased with depth, from 86.5% at 60 m depth to 0.7% at 120 m depth. The uncharacterized *Prochlorococcus ureC* increased with depth, reaching a maximum of 25.1% of total Picocyanobacteria *ureC* at 110 m (Figure 10C). The LLIV *Prochlorococcus* group had the highest *ureC* abundance; within the ODZ, the LLIV *Prochlorococcus ureC* varied between 63.1% and 75% of total Picocyanobacteria *ureC*.

In the ODZ stations, the abundance of total Picocyanobacteria containing *cynS* was up to 31.2% at ETSP ST9. In ETSP ST17, the percentage of total Picocyanobacteria containing *cynS* was 116.2% at 80 m but was negligible in the ETNP (Figure 10D). At HOT, the abundance was 10% to 30% in the top 50 m but increased, reaching

10.3389/fmars.2024.1386686

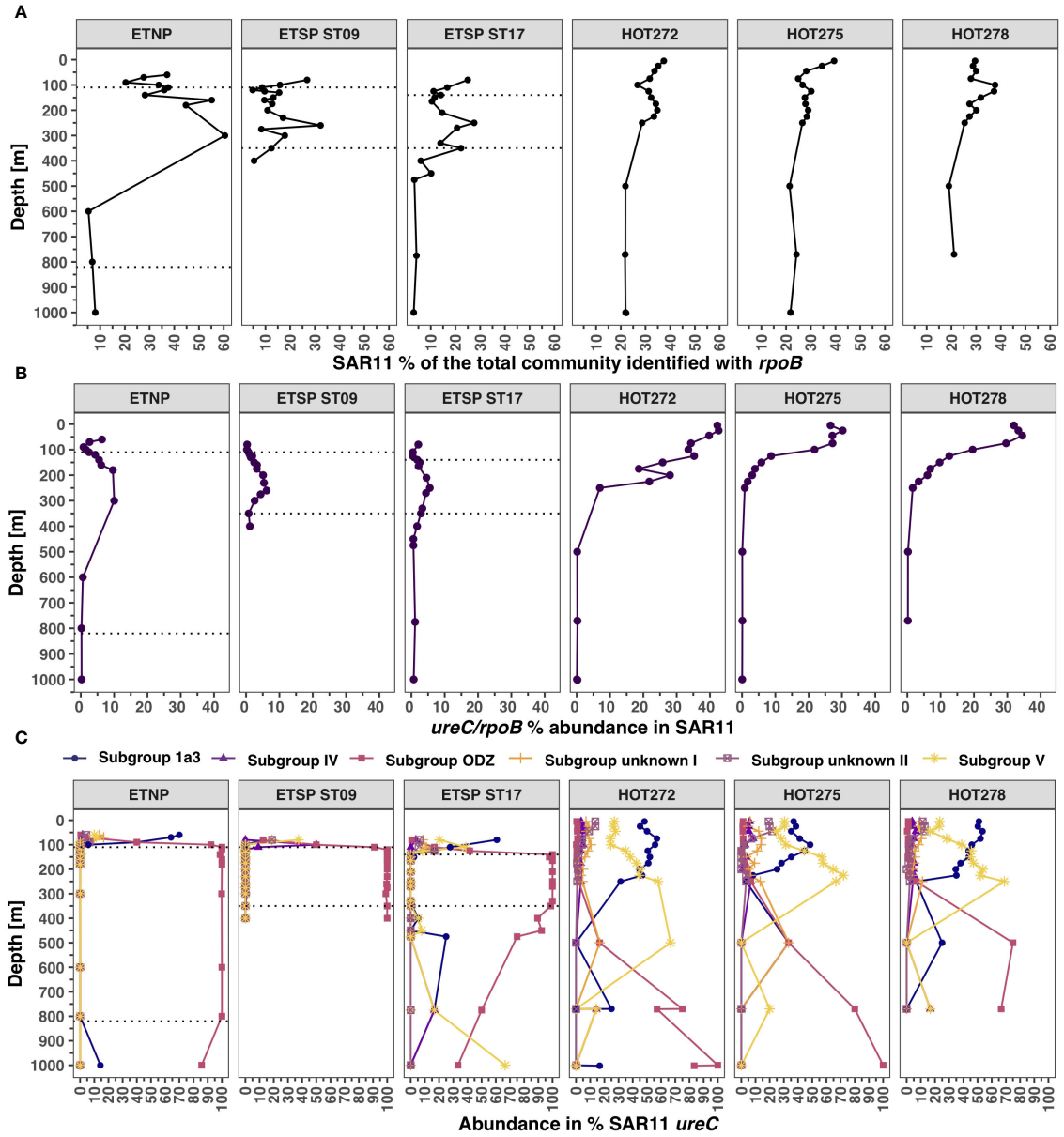

FIGURE 7
Distribution of SAR11 and its urease genes in ODZs and HOT. **(A)** Abundance of SAR11 in the total bacterial and archaeal community identified with *rpoB*. **(B)** Abundance of urease in % of the SAR11 from *ureC/rpoB* ratios. **(C)** Abundance of each SAR subgroup (*ureC*) calculated from the total SAR11 *ureC*. Each panel corresponds to a different ocean region. The area between the dotted lines corresponds to the ODZ core.

70% at 100 m at HOT 275 and 278 (Figure 10D). At HOT 272, Picocyanobacteria *cynS* had two peaks: one of ~ 50% between 100 and 150 m depth and a secondary peak of ~ 70% at around 200 m depth (Figure 10D). Picocyanobacteria *cynS* can be separated into *Prochlorococcus* and *Synechococcus* (Figure 10E). At HOT, *Prochlorococcus cynS* abundance varied between 80% and 100% of the total Picocyanobacteria *cynS*, whereas at ETSP ST9 and ST17, *Synechochocus cynS* was ~ 90%–100% of the total Picocyanobacteria *cynS* (Figure 10E). In the ETNP, *Synechococcus cynS* abundance peaked in the oxic region, composing 78.3% of Picocyanobacteria *cynS* at 60 m depth, the primary chlorophyll maximum, but was negligible in the ODZ (Figure 10E).

ureC and *cynS* expression in transcriptional data

Although the transcript data and the metagenomic reads data from the ETNP shown here do not correspond to the same sample collection date (April 2018 versus April 2012, respectively), we observed similar trends between datasets. When *ureC* transcripts from STP2 in the ETNP were also analyzed, we observed several groups: Picocyanobacteria had the highest abundance of *ureC* transcripts, with 16.4 normalized *ureC* transcripts at depths of 106 m and 150 m, and the general alphaproteobacteria and gammaproteobacteria groups also had significant numbers of

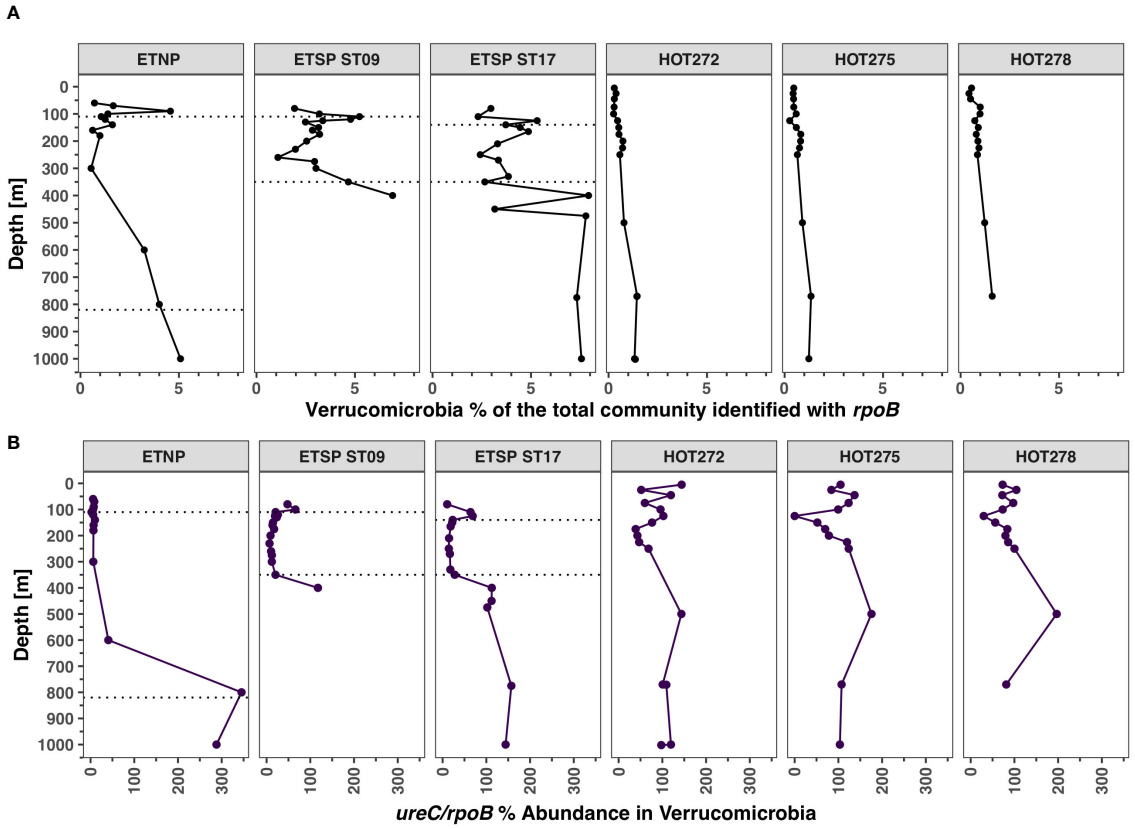

FIGURE 8
Distribution of Verrucomicrobia and its urease genes in ODZs and HOT. **(A)** Abundance of Verrucomicrobia in the total bacterial and archaeal community identified with *rpoB*. **(B)** Abundance of urease in % of Verrucomicrobia from *ureC/rpoB* ratios. Each panel corresponds to a different ocean region. The area between the dotted lines corresponds to the ODZ core.

transcripts. Key N cycling microbes had low abundances of *ureC* transcripts: Thaumarchaeota had 1 to 2.5 normalized *ureC* transcripts at oxic depths; Anammox bacteria (*Cand.* Scalindua) had 2.4 normalized *ureC* transcripts at 112 m depth and 2.7 at 150 m depth; and *Nitrospina ureC* transcript abundances were low but present at all the sampled depths, with abundances between 0.2 and 1.8 normalized *ureC* transcripts (Figure 11A). Verrucomicrobia had low numbers of transcripts throughout, with three normalized reads at 150 m. The *cynS* transcripts in station P2 were dominated by transcripts of Anammox bacteria (*Cand.* Scalindua) (Figure 11B), with 104.4 normalized transcripts at 112 m and 83.2 normalized transcripts at 150 m depth. After Anammox bacteria (*Cand.* Scalindua), the second-highest number of *cynS* transcripts belonged to "other bacteria". *Nitrospina cynS* transcripts were found at 106 m and 112 m with a maximum of 2.9 normalized *cynS* transcripts at 112 m depth (Figure 11B).

Discussion

Many microorganisms prefer reduced nitrogen forms for assimilation (Glibert et al., 2016). However, ammonium concentrations are extremely low in both ODZs and the oxic oligotrophic ocean (Martens-Habbena et al., 2009; Widner et al., 2018a). One adaptation to ammonium limitation is for microbes to use small organic reduced N sources, such as urea and cyanate. Urea and cyanate concentrations are also generally in the nanomolar range (Painter et al., 2008; Widner et al., 2018a; Kitzinger et al., 2019; Takeda et al., 2020, 2018b). However, the ability to use urea or cyanate in addition to ammonium increases microbes' chances of obtaining reduced N. Some microbes may have the ability to utilize multiple N sources, but preferentially choose one over the others; however, this preference may be overridden by environmental concentrations of these sources (Aldunate et al 2020; Qin et al 2024).

The ETNP ST136 was the only station examined here with both measured urea and cyanate concentrations (Supplementary Figure S1). Urea was undetectable in the water column until 900 m. In contrast, cyanate was measured at high concentrations (40 nM) at several depths in the surface and upper ODZ (Supplementary Figure S3; Widner et al., 2018a). However, the detection limit for urea (70 nM) was much higher than the detection limit for cyanate (0.4 nM), so it is difficult to compare (Widner et al., 2018a). At our ETSP stations, cyanate concentrations were low but measurable in the ODZ (Supplementary Figure S4; Widner et al., 2018b). Though urea was below detection in the ETNP ODZ, sources of urea were likely available. Crustacean and gastropod zooplankton excrete urea (Miller and Glibert, 1998; Thibodeau et al., 2020). Despite the anoxia, crustacean and gastropod zooplankton migrate into ODZs

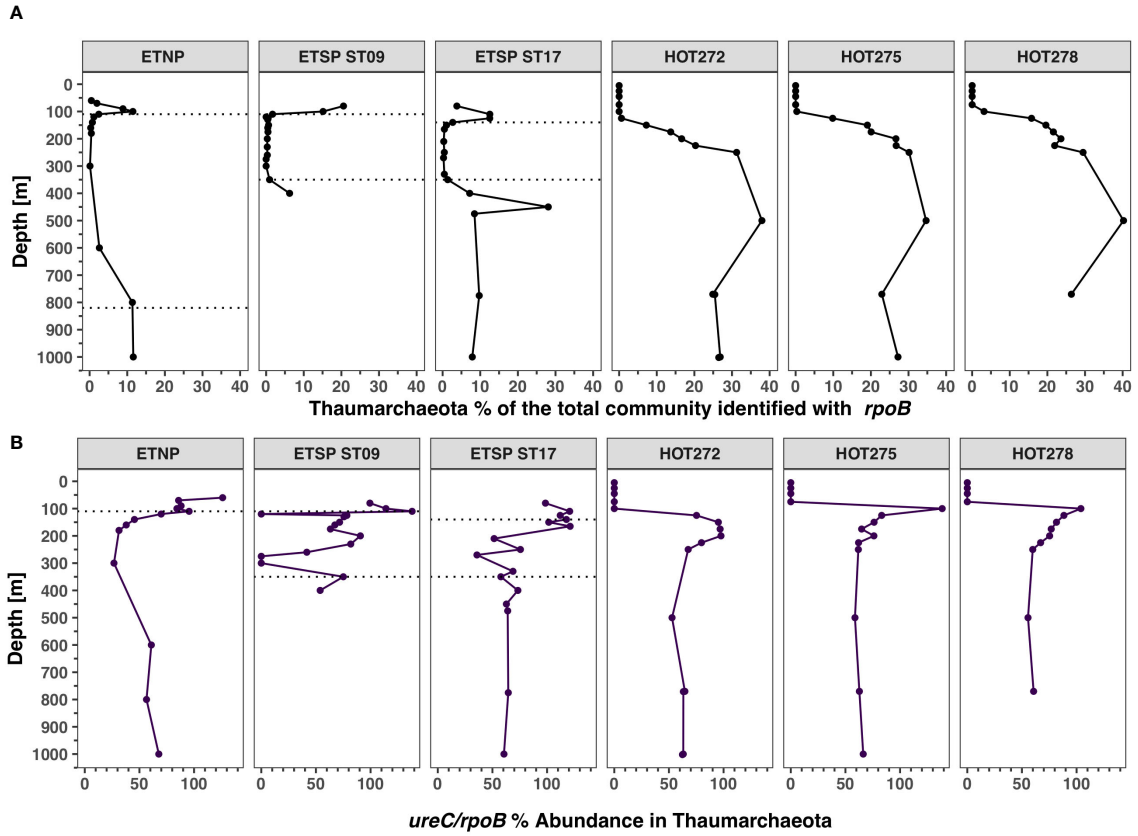

FIGURE 9
Distribution of Thaumarchaeota and its urease genes in ODZs and HOT. Depth profile of metagenomic reads encoding for enzyme beta subunit of RNA polymerase (*rpoB*) and urease subunit alpha (*ureC*). **(A)** Abundance of Thaumarchaeota in the total bacterial and archaeal community identified with *rpoB*. **(B)** Abundance of urease in % of the Thaumarchaeota from *ureC/rpoB* ratios. Each panel corresponds to a different ocean region. The area between the dotted lines corresponds to the ODZ core.

(Bianchi et al., 2014; Maas et al., 2014; Wishner et al., 2020) and likely excrete urea there. Additionally, urea is produced as a part of organic matter degradation (Cho et al., 1996; Berman et al., 1999). While, in the ocean, the majority of organic matter degradation occurs in the upper water column, degradation does occur throughout (Brown et al., 2022).

By analyzing the abundance of normalized reads of the genes in metagenomes for cyanase (*cynS*) and urease (*ureC*), we found that the proportion of each taxonomic group with the ability to utilize urea or cyanate varied among the individual groups with depth and between oxic waters and ODZs. This variation implies niche differentiation in cyanate and urea utilization in the ocean.

Niche partitioning of cyanase and urease

Unlike Mao et al. (2022), who found that *cynS* in larger-size fractionated samples (>0.8 µm) was dominated by eukaryotic phytoplankton, we only observed small numbers of algae-derived *cynS* at all stations. The highest normalized reads were found at the DCM for each station and corresponded to Pelagomonales. The lack of algae-derived *cynS* in the ODZs was not surprising, as eukaryotic algae do not thrive in the ODZs (Fuchsman et al., 2022; Wong et al., 2023), but algae *cynS* reads were also not particularly abundant at HOT (Supplementary Figure S5). This finding could be because HOT is dominated by Picocyanobacteria rather than eukaryotic algae, though eukaryotic algae are definitely present (Rii et al., 2016). Part of the difference between our results and those of Mao et al. (2022) could also be because our data were obtained from bulk water samples dominated by bacteria, while Mao et al. examined > 0.8 µm fractions enriched in eukaryotic algae. In either case, our results imply that eukaryotic algae are present but not dominant consumers of cyanate in the systems studied here.

Both *Nitrospina* and *Cand.* Scalindua Anammox bacteria have representatives with cyanase and urease, but the two bacterial groups appear to have different preferences for urea and cyanase (Figures 3, 4). The Anammox (*Cand.* Scalindua) bacterial community, which can use these compounds for dissimilatory energy production, had a higher proportion of Anammox bacteria containing the *cynS* gene compared to *ureC*, indicating a preference for cyanate over urea (Figure 3). These results are consistent with rate data from our 2013 ETSP cruise, which showed that Anammox N_2 production rates could be supported by the N in cyanate while urea could only stimulate Anammox N_2 production rates after a 1.5-day lag time (Babbin et al., 2017), indicating that the Anammox bacteria were not utilizing the urea *in situ* at the time of sampling.

10.3389/fmars.2024.1386686

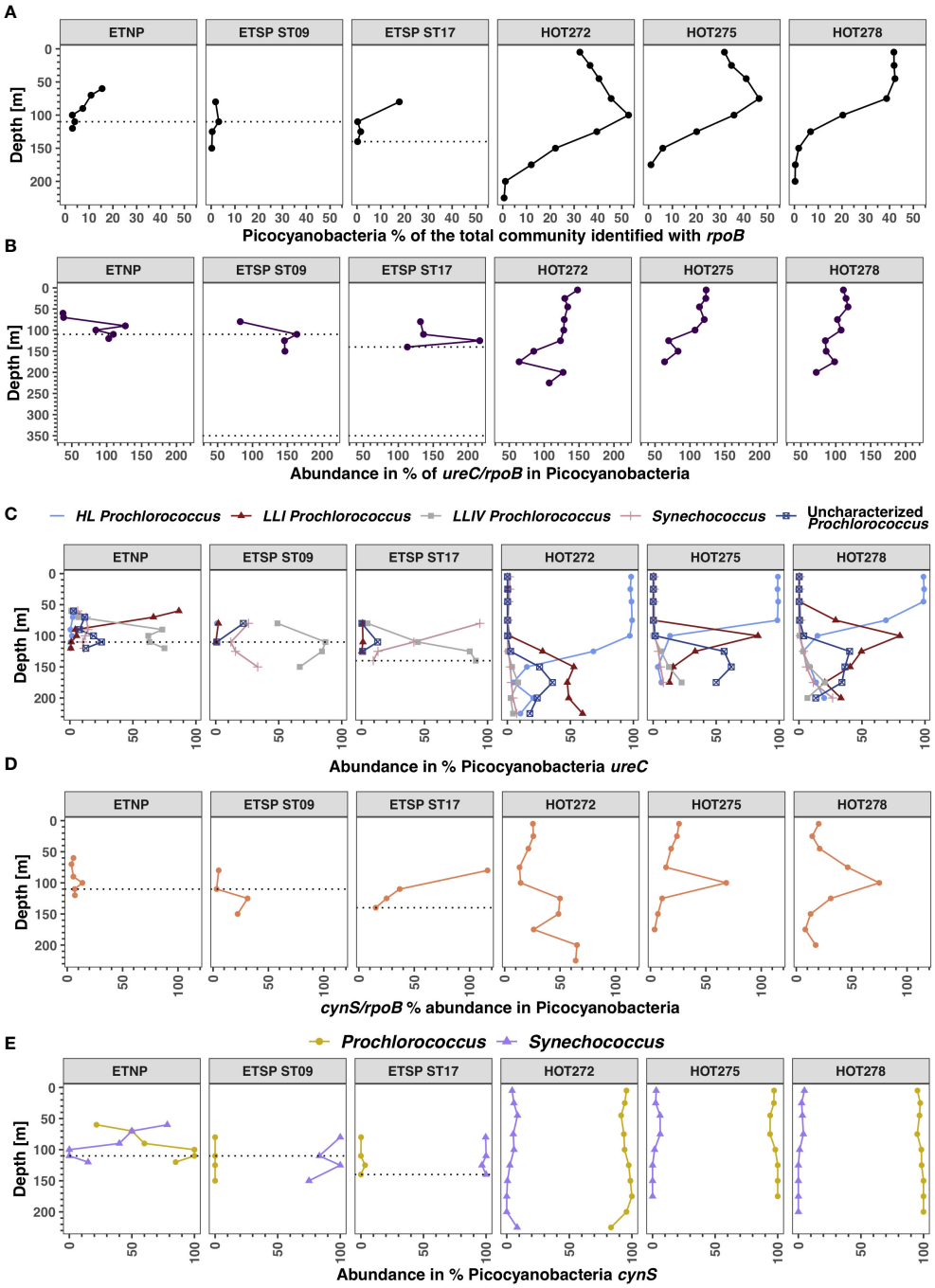

FIGURE 10
Distribution of Picocyanobacteria and its functional genes in ODZs and HOT. **(A)** Abundance of Picocyanobacteria in the total bacterial and archaeal community identified with *rpoB*. **(B)** Abundance of urease in % of the total Picocyanobacteria from *ureC/rpoB* ratios. **(C)** Abundance in % of each of the Picocyanobacteria ecotypes containing *ureC* out of the total Picocyanobacteria *ureC*. **(D)** Abundance of cyanase in % of the total Picocyanobacteria from *cynS/rpoB* ratios. **(E)** *Prochlorococcus* and *Synechococcus cynS* abundance calculated as % of the total Picocyanobacteria *cynS*. Each panel corresponds to a different ocean region. The area between the dotted lines corresponds to the ODZ core; the ODZs extend beyond the region shown in the figure.

Similar results were observed with the ETNP transcripts (Figure 11), where the highest abundance of the *cynS* transcript in the ODZ core corresponded to *Cand.* Scalindua and the abundance of *ureC* in the transcript data was low in numbers compared to *cynS*. These transcripts imply that Anammox bacteria (*Cand.* Scalindua) were actively transcribing the *cynS* gene to metabolize cyanate in the ETNP, and assimilation rate data from the ETNP ODZ indicate that cyanate was used both for C assimilation and N dissimilation (Widner et al., 2018a). Contrastingly, the proportion of *Nitrospina* with *ureC* was higher than for *cynS* both at HOT and

in ODZ waters, indicating a metabolic preference for urea as a reduced nitrogen form over cyanate. Additionally, expression of *Nitrospina ureC* transcripts was similar in numbers and present at all depths, but *Nitrospina cynS* transcripts showed lower expression (< 1 *cynS* transcript) in oxic water but increased to 2.2 and 2.9 at 106 and 112 m depth in the ODZ (Figure 11). These observations suggest that *Nitrospina* could be actively transcribing both genes to possibly metabolize both cyanate and urea in the upper ETNP ODZ. The transcript numbers were low, but they contrasted with the distribution of *ureC* and *cynS* metagenomic reads (Figure 4). A possible explanation for the presence of *cynS* transcripts from *Nitrospina* in the upper ODZ could be due to the high cyanate concentrations (40 nM) at the top of the ETNP ODZ (Supplementary Figure S3; Widner et al., 2018a). The differences in the organic N preferences of Anammox and *Nitrospina* bacteria may prevent them from competing where their depth ranges overlap, except when an abundantly reduced N resource is available.

Although Thaumarchaeota does not possess the *cynS* gene, members of the group can use cyanate and urea both for nitrification (dissimilatory) and for assimilation (Kitzinger et al., 2019). Here we only examine urease in Thaumarchaeota since the cyanase gene in these archaea is unknown. At HOT,

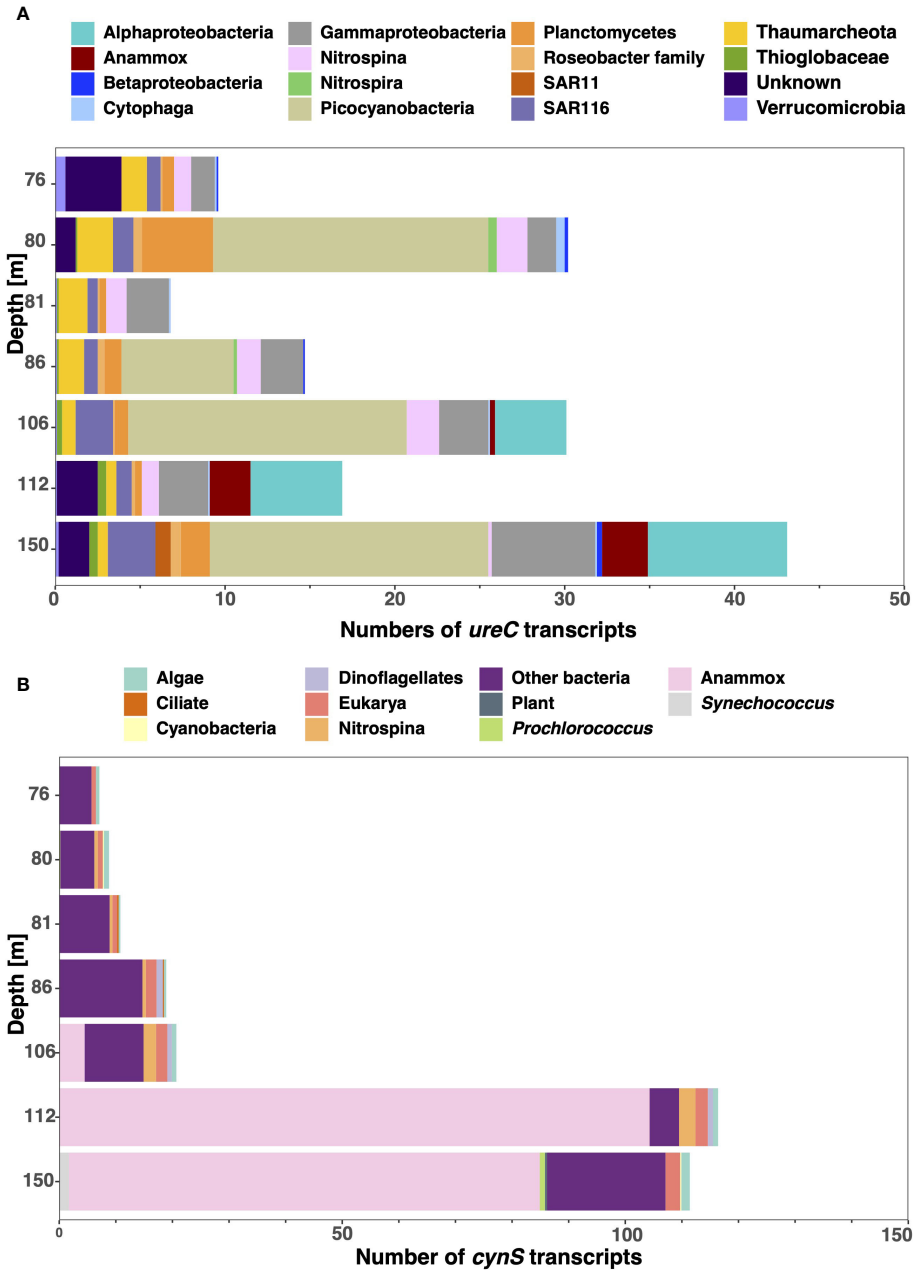

FIGURE 11
Urease and cyanase gene expression in the ETNP. Stacked bar chart showing the normalized urease and cyanase transcripts of station P2 in the ETNP sampled in May 2018. **(A)** The *ureC* transcripts are classified by taxonomic groups. **(B)** The *cynS* transcripts are classified by taxonomic groups. The graphs include the oxycline and top of the ODZ (76–150 m) with 106–150 m sampled from the ODZ. The depth is not to scale.

Thaumarchaeota abundance increased from depths of 100 to 500 m but then decreased again in deeper waters (Figure 9A). The proportion of Thaumarchaeota with *ureC* reached 100% at ~ 175 m but then decreased to 60%–70% at 500 to 1000 m (Figure 9B). However, at 4,000 m, 100% of Thaumarchaeota again had the *ureC* gene (Supplementary Figure S10). In the ODZ stations, the abundances of Thaumarchaeota and its *ureC* gene were high in hypoxic areas above the ODZ (Figure 9). *ureC* transcripts from the ETNP mirrored these findings, with abundant *ureC* transcripts for Thaumarchaeota in the upper oxycline but fewer in the ODZ (Figure 11). However, similar to at HOT, in the 500- to 1,000-m range below the ODZs, 60%–70% of Thaumarchaeota had *ureC*. There is little previous data about Thaumarchaeota *ureC* in deep waters. Thaumarchaeota subpopulations (ecotypes) vary with depth and with coastal to offshore regions (Luo et al., 2014; Santoro et al., 2017, 2015). In the Arctic Ocean, the abundance of Thaumarchaeota *ureC* increased with depth from the surface to 100 m, but there was no data for deep waters (Shiozaki et al., 2021). In the more coastal Gulf of Mexico, only between 10% and 15% of Thaumarchaeota cells contain an *ureC* gene (Kitzinger et al., 2019), while 60%–100% of Thaumarchaeota contain *ureC* at SPOT (Ahlgren et al., 2017). It seems likely that only some ecotypes of Thaumarchaeota have *ureC*. In the open ocean datasets examined here, Thaumarchaeota is the dominant microbe with *ureC* at depth, but a smaller proportion of the population contains *ureC* in the mesopelagic.

Contrastingly, SAR11 bacteria were abundant (estimated by *rpoB*) throughout the water column, but the abundance of *ureC* from SAR11 was highest in surface waters and decreased with depth (Figure 7). Urea is likely used for assimilation in SAR11. The abundance of the *ureC* reads gives an insight into the potential this microbial group has to use urea in oxic waters with low concentrations of other N-containing nutrients. At HOT, nitrate, an oxidized form of N, was not detected in surface waters (Supplementary Figure S11; Supplementary Table S1). In fact, the proportion of SAR11 containing *ureC* negatively correlated with nitrate concentrations (log (nitrate) = − 0.053 * proportion of SAR11 with urease + 1.1487; R^2 = 0.89, p-value = $1E^{-17}$) (Supplementary Figure S12). In contrast, in the ETNP and ETSP, the SAR11 *ureC* read abundances were low but tended to increase slightly (5%–10%) in the ODZ regions. The phylotypes of SAR11 *ureC* were completely different in oxic waters and in the ODZ, with an ODZ-specific *ureC* phylotype. SAR11 *ureC* was identified in ETNP *ureC* transcripts, but only at 150 m, the deepest depth sampled for transcripts. Ammonium is often undetectable (< 10 nM) in ODZ regions, but nitrate concentrations are high (~ 20 µM), so oxidized sources of N are present (Fuchsman et al., 2018; Widner et al., 2018b, 2018a). Urease appears to be less advantageous to SAR11 when oxidized sources of inorganic N are present, even though energy is needed to convert oxidized N to reduced N.

In Picocyanobacteria, we observed different proportions of *cynS* and *ureC* from different Picocyanobacteria groups occurring at different depths. For example, at HOT 275 (August 2015), on the surface, the majority of *ureC* reads corresponded to HL *Prochlorococcus* (Figure 10C), followed by a peak of the LLI *Prochlorococcus* at 100 m depth; the uncharacterized *Prochlorococcus* peaked at 150 m depth, whereas in the ODZs, LLIV *Prochlorococcus ureC* had the highest abundance. We hypothesize that uncharacterized *Prochlorococcus* corresponds to the uncultured NC1/LLVII ecotype of *Prochlorococcus* found in ITS data from these stations (Fuchsman et al., 2023). Our *ureC* data corresponds to the typical cascade of *Prochlorococcus* ecotypes with depth (Fuchsman et al., 2023).

The distribution of Picocyanobacteria *cynS* varied between stations and between depths (Figure 10D). At HOT, the abundances of picocyanobacteria *cynS* were lower in the top 50 m (10%–30%) but increased, reaching 70% at 150 m at HOT 272 and 100 m at HOT 275 and 278 (Figure 10D). The majority of these reads correspond to members of the *Prochlorococcus* group, but it is not possible to assign *cynS* to specific ecotypes (Supplementary Figure S2). Some *Prochlorococcus* can utilize nitrate under N-limited conditions (Martiny et al., 2009; Berube et al., 2016). However, the distribution of cyanase in *Prochlorococcus* is not consistent with a negative correlation with nitrate. Rather, cyanase becomes the most abundant at the depth where nitrate first becomes measurable (Supplementary Figure S11; Supplementary Table S1), which is also in the region of the DCM (Supplementary Figure S5), where LLI *Prochlorococcus* is dominant (Fuchsman et al., 2023). While we do not have cyanate concentrations from HOT, in the North Atlantic, there are often cyanate maxima at the primary nitrite maxima, right below the DCM (Widner et al., 2016). Thus, more *Prochlorococcus* may be able to use cyanate at depths where it is available. The DCM region is also where eukaryotic algae have the cyanase gene (Supplementary Figure S5). For the ODZ stations, a larger proportion of picocyanobacteria had *cynS* in the ETSP compared to the ETNP; *Synechococcus* was the main picocyanobacteria containing *cynS* in the ETSP (Figure 10E). This is consistent with published ITS data, which indicated that *Synechococcus* was more abundant in our ETSP dataset than in the ETNP (Fuchsman et al., 2023). Indeed, transcripts from the ETNP indicated that *Prochlorococcus* was using urea, but not cyanate, in and above the ODZ (Figure 11). Thus, the ODZ *Prochlorococcus* are not competing with Anammox for cyanate in the ODZs. Stable isotopes of ODZ *Prochlorococcus* cells indicate that they primarily utilize nitrite, a partially oxidized form of inorganic N, which reaches 2–3 µM in ODZs (Aldunate et al., 2020). Thus, Picocyanobacteria and SAR11, which use urea or cyanate for assimilation rather than dissimilation, can use oxidized forms of nitrogen instead of urea and cyanate and appear to prefer these more abundant oxidized N compounds.

Identification of new urease-containing taxa

We identified two new groups of bacteria that use urea in low oxygen conditions: the Gammaproteobacteria Thioglobaceae and

an unknown Verrucomicrobia. The Thioglobaceae clade has two distinct published subclades. A cultured strain EF1 of the SUP05 subgroup is capable of respiration with either oxygen or nitrate to oxidize sulfide to fuel carbon fixation (Shah et al., 2017). The EF1 culture can perform nitrate reduction and some steps of the denitrification pathway but cannot produce nitrogen gas (Shah et al., 2017). A cultured strain of the Arctic96BD-19 subgroup oxidized reduced sulfur, particularly thiosulfate, with oxygen but was a mixotroph, increasing growth in the presence of glucose (Marshall and Morris, 2013). In the ocean, the Arctic96BD-19 subgroup primarily lives where oxygen is present, and SUP05 primarily lives where sulfide is available (Walsh et al., 2009). Due to its ability to store elemental S, SUP05 can metabolize for some time after being taken out of more coastal sulfidic regions (Callbeck et al., 2018; Shah et al., 2019). In offshore ODZs, sulfide is not present. Instead of two clades of Thioglobacaea, by looking at the *rpoB* phylogenetic tree (Supplementary Figure S7), we observed three subclades: Arctic96-BD19, SUP05, and a new ODZ clade of Thioglobaceae. The ODZ clade of Thioglobaceae dominated in ODZs (Figure 6). While we have defined this clade using *rpoB* data, not genomic data, we can see that all the Thioglobaceae in the ODZ have a *narG*-type of nitrate reductase (Figure 5). Additionally, based on the fact that the cultured Thioglobaceae clades are both autotrophic (Marshall and Morris, 2013; Shah et al., 2017), we assume that the ODZ clade is also autotrophic.

The members of the ODZ-specific subclade of Thioglobaceae appear to all be capable of using urea in the ODZ (100%), while the Arctic96BD-19 subclade only had 10%–20% of its members having *ureC* in oxic waters (Figures 5, 6). Thioglobaceae abundance (from *rpoB*) was only high in deep water (> 250 m) at HOT (Figure 5A). In contrast, at the ODZ stations, the abundance of Thioglobaceae was higher in the hypoxic and anoxic water columns (Figure 5). The ODZ clade was the clade with the highest abundances in the ODZ core, so this clade likely contributed to the high number of *ureC* reads there. Thus, the ODZ Thioglobaceae may have a greater preference for using urea in the ODZ than does the oxic Thioglobaceae Arctic96-BD19 at HOT. We did not see many *ureC* transcripts for Thioglobaceae in the ETNP ODZ (Figure 11), but the depth range of the transcripts only reached 150 m, and the maximal proportions of Thioglobaceae with *ureC* in the metagenomes were deeper than that (300 m) in the ODZ (Figure 6).

Verrucomicrobia has the potential to use urea. At HOT, the abundance of Verrucomicrobia was low (< 2%) (Figure 8A), but the proportion of Verrucomicrobia with *ureC* was high (29.8%–150%) (Figure 8B). Contrastingly in the ODZ, the abundance of Verrucomicrobia examined with the *rpoB* gene is slightly higher (2%–4%), but the proportion of *ureC* is low (2%–25%) in the ODZ core (Figure 8). In the hypoxic waters below the ODZs, Verrucomicrobia abundance increased to 5%–7% of the community, and all of the Verrucomicrobia contained the *ureC* gene (Figure 8). Verrucomicrobia had low numbers of transcripts throughout the ETNP oxycline and upper ODZ, with three normalized reads at 150 m. However, activity below the ODZ, where *ureC* in Verrucomicrobia was the most abundant, is still unknown (Figure 11). Verrucomicrobia is a phylum of bacteria whose members have many biogeochemical functionalities. Some Verrucomicrobia are heterotrophs that degrade polysaccharides and cellulose compounds and are often nitrogen fixers (Nixon et al., 2019; Delmont et al., 2022). Other members of the Verrucomicrobia phylum are methanotrophs (Schmitz et al., 2021; Howe et al., 2023). MAGs from the ETNP ODZ indicate that Verrucomicrobia had the *napA* type of nitrate reductase but did not have the rest of the denitrification pathway (Zhang et al., 2023). Verrucomicrobia MAGs from the ETNP were related to methane-oxidizing Verrucomicrobia of the Pedosphaerales group (Howe et al., 2023; Zhang et al., 2023), but methane monooxygenase is not present in these incomplete MAGs. Methane oxidizers are heterotrophs, and their carbon source is methane, so they need an external source of N (Sieburth et al., 1987). We cannot be sure of the metabolism of the Verrucomicrobia in our systems, but we can see that under low but not zero oxygen conditions, Verrucomicrobia were present and could utilize urea.

Though the majority of the unknown contigs on the urease (*ureC*) tree have now been identified (Supplementary Figure S1), and we have a good understanding of which microbes are using urea in ODZs, the cyanase tree (*cynS*) still has an Other Bacteria group with unclear taxonomy (Supplementary Figure S2). This group had significant numbers of metagenomic reads in the oxyclines above and below the ODZs and was fairly abundant in the ETNP transcripts (Figures 2, 11). Thus, there appears to be another key player still to be identified using cyanase in the oxyclines around ODZs.

Conclusions

An interesting common feature of the microbial taxa we analyzed was that the majority correspond to cells that are either photo or chemoautotrophs, including picocyanobacteria, *Nitrospina*, Thaumarcheota, Anammox, and Thioglobaceae (Table 1). This is probably because most heterotrophs can assimilate N from organic matter. Methane oxidizers, potentially such as the Verrucomicrobia discussed above, are heterotrophs but use methane, a C1 compound that contains no N, as a C source and thus need to assimilate N from the environment. SAR11 may seem like an exception to this trend. However, SAR11 is a small free-living heterotroph that has one carbon (C1) metabolism; it consumes methyl groups in dissolved organic matter (Sun et al., 2011; Tripp, 2013). For example, SAR11 can consume methylated arsenate, which contains no N (Giovannoni et al., 2019). Thus, in such cases, SAR11 must need additional sources of N, such as nitrate or urea.

Microbial access to alternative reduced nitrogen forms such as urea and cyanate might provide them with a selective advantage in offshore oceanic regions, contributing to the observed patterns of taxonomic distributions. The differences in cyanase and urease depth profiles between microbes imply niche differentiation. Different microbes have higher proportions of genes for urease in different parts of the water column: SAR11 and *Prochlorococcus* in surface waters, Verrucomicrobia in hypoxic waters, Thioglobacaea in ODZ waters, and Thaumarchaeota in the lower euphotic zone/mesopelagic. Additionally, *Prochlorococcus* could utilize cyanate in

TABLE 1 Summary of microbial urea and cyanate preference in different ocean regions for the bacteria/archaea examined and whether each bacteria/archaea is autotrophic.

	Anammox bacteria	Nitrospina	Picocyanobacteria	SAR11	Thaumarchaeota	Thioglobaceae	Verrucomicrobia
Surface oxic	X	X	Urea + cyanate	Urea	X	X	X
Deep euphotic zone	X	Urea + Cyanate	X	X	Urea	X	Urea
Deep oxic	X	Urea	X	X	Urea	X	Urea
ODZ	Cyanate	Urea	X	A little urea	X	Urea	X
Autotrophic	Yes	Yes	Yes	No	Yes	Yes	?

X, the organism does not use urea or cyanate in that region; ODZ, oxygen-deficient zone.

the euphotic zone, and *Nitrospina* could utilize cyanate at 150–250 m under oxic conditions, and Anammox bacteria (*Cand.* Scalindua) could utilize cyanate in the ODZs (Table 1). Described differently, the organisms differentiated their N sources rather than compete with each other: *Cand.* Scalindua uses cyanate in the ODZ, while Thioglobacaea uses urea in the core. In the edges of the ODZ, *Nitrospina* utilizes urea, but in the oxycline above the ODZ, where Thaumarchaeota and *Nitrospina* both could use urea, 50% of *Nitrospina* are also able to use cyanate, and cyanase transcripts are present, and in the oxycline below the ODZ, all Verrucomicrobia could utilize urea. While *Prochlorococcus* could utilize cyanate in the DCM, in the ODZ, *Prochlorococcus* use nitrite rather than compete with *Cand.* Scalindua for cyanate, even though cyanate is present. SAR11 and *Prochlorococcus* may compete for urea in surface waters, but we show that SAR11 bacteria switch to nitrate as soon as it is available. This niche differentiation could be attributed to adaptation to avoid microbial competition over nitrogen sources.

Cyanate and urea are only two small, reduced organic N compounds of many. Amino acids and nucleosides, for example, are also small reduced organic N compounds that are measurable at nanomolar concentrations in the ocean (Yamashita and Tanoue, 2003), excreted by zooplankton (Webb and Johannes, 1967; Clifford et al., 2017; Maas et al., 2020), produced by organic matter degradation (e.g., Lehmann et al., 2020), and assimilated by microbes (Zubkov et al., 2008; Clifford et al., 2019; Maas et al., 2020). Experiments indicate that Thaumarcheota and *Nitrospina* can also assimilate N from amino acids (Bayer et al., 2021; Parada et al., 2022). Our work highlights that other chemoautotrophs, such as S oxidizers, and heterotrophs that use C1 metabolisms are also likely to assimilate various small, reduced organic N compounds. The capability of microbes to use small, reduced organic nitrogen compounds, which are rarely measured, adds important information about adaptations of individual taxa to N limitation. However, DON assimilation has broader implications. When dissolved organic nitrogen was added to a Regional Ocean Model System (ROMS) of the mid-Atlantic Bight, phytoplankton biomass and primary productivity increased by 30%–300%, depending on the location, due to assimilation from regeneration (Druon et al., 2010). Similarly, utilization of DON likely increases chemoautotrophy rates and increases the growth of microbes using C1 metabolisms. In particular, this niche differentiation and use of dissolved organic N should allow a higher biomass of N cycling microbes and higher N transformation rates than a system competing for ammonia only. For example, Anammox bacteria are limited by ammonia in ocean ODZs (Bianchi et al., 2014), and competition for ammonia between Anammox and nitrite oxidizers is modeled to lead to oscillations in the volume of anoxia and amount of N loss (Penn et al., 2019). Additionally, other chemoautotrophs, such as S-oxidizing Thioglobacaea, might need to compete for this same ammonia. The use of small reduced organic N compounds expands the options for Anammox, nitrite oxidizers, and other chemoautotrophs beyond those typically considered in models, allowing for more niche differentiation and less competition, while also further decoupling Anammox from denitrification, a key source of ammonia in ODZs.

Data availability statement

The datasets presented in this study can be found in online repositories. The names of the repository/repositories and accession number(s) can be found here: NCBI SRA (https://www.ncbi.nlm.nih.gov/sra)- BioProject PRJNA704804, PRJNA350692 and PRJNA352737. The numerical results from this work are available in Supplementary Table S3.

Author contributions

PH-V: Conceptualization, Formal analysis, Funding acquisition, Visualization, Writing – original draft, Writing – review & editing. JC:

Supervision, Visualization, Writing – original draft, Writing – review & editing. CF: Conceptualization, Formal analysis, Methodology, Supervision, Visualization, Writing – original draft, Writing – review & editing.

Funding

The author(s) declare financial support was received for the research, authorship, and/or publication of this article. This work was funded by the Horn Point startup and student funds.

Acknowledgments

We thank Brittany Widner for providing numbers for cyanate concentrations from the ETSP. Sequencing of the five new metagenomes was paid by an award from the Isaac Walton League Mid-shore Chapter to PHV. We would like to acknowledge the captains and crews of the R/V *Thompson* and R/V *Nathaniel B. Palmer* and Chief Scientist Allan Devol. Cruises were funded by NSF OCE-1046017 for Allan Devol. This paper was a chapter of PHV's thesis. We appreciate the comments from her committee on the manuscript. This work is partially based on Hawaii Ocean Time Series observations supported by the US National Science Foundation under Award No. 1756517.

Conflict of interest

The authors declare that the research was conducted in the absence of any commercial or financial relationships that could be construed as a potential conflict of interest.

Publisher's note

All claims expressed in this article are solely those of the authors and do not necessarily represent those of their affiliated organizations, or those of the publisher, the editors and the reviewers. Any product that may be evaluated in this article, or claim that may be made by its manufacturer, is not guaranteed or endorsed by the publisher.

Supplementary material

The Supplementary Material for this article can be found online at: https://www.frontiersin.org/articles/10.3389/fmars.2024.1386686/full#supplementary-material

SUPPLEMENTARY TABLE S1
Metadata for metagenomes used in this study.

SUPPLEMENTARY TABLE S2
Sequence information for the new metagenomes from this paper.

SUPPLEMENTARY TABLE S3
The data published in this study, arranged by graph.

References

Ahlgren, N. A., Chen, Y., Needham, D. M., Parada, A. E., Sachdeva, R., Trinh, V., et al. (2017). Genome and epigenome of a novel marine Thaumarchaeota strain suggest viral infection, phosphorothioation DNA modification and multiple restriction systems. *Environ. Microbiol.* 19, 2434–2452. doi: 10.1111/1462-2920.13768

Ahlgren, N. A., Rocap, G., and Chisholm, S. W. (2006). Measurement of *Prochlorococcus* ecotypes using real-time polymerase chain reaction reveals different abundances of genotypes with similar light physiologies. *Environ. Microbiol.* 8, 441–454. doi: 10.1111/j.1462-2920.2005.00910.x

Aldunate, M., Henríquez-Castillo, C., Ji, Q., Lueders-Dumont, J., Mulholland, M. R., Ward, B. B., et al. (2020). Nitrogen assimilation in picocyanobacteria inhabiting the oxygen-deficient waters of the eastern tropical North and South Pacific. *Limnol. Oceanogr.* 65, 437–453. doi: 10.1002/lno.11315

Altschul, S. F., Madden, T. L., Schäffer, A. A., Zhang, J., Zhang, Z., Miller, W., et al. (1997). Gapped BLAST and PSI-BLAST: a new generation of protein database search programs. *Nucleic Acids Res.* 25, 3389–3402. doi: 10.1093/nar/25.17.3389

Babbin, A. R., Buchwald, C., Morel, F. M. M., Wankel, S. D., and Ward, B. B. (2020). Nitrite oxidation exceeds reduction and fixed nitrogen loss in anoxic Pacific waters. *Mar. Chem.* 224, 103814–103814. doi: 10.1016/j.marchem.2020.103814

Babbin, A. R., Keil, R. G., Devol, A. H., and Ward, B. B. (2014). Organic matter stoichiometry, flux, and oxygen control nitrogen loss in the ocean. *Science* 344, 406–408. doi: 10.1126/science.1248364

Babbin, A. R., Peters, B. D., Mordy, C. W., Widner, B., Casciotti, K. L., and Ward, B. B. (2017). Multiple metabolisms constrain the anaerobic nitrite budget in the Eastern Tropical South Pacific. *Global Biogeochem. Cycles* 31, 258–271. doi: 10.1002/2016GB005407

Barbera, P., Kozlov, A. M., Czech, L., Morel, B., Darriba, D., Flouri, T., et al. (2019). EPA-ng: massively parallel evolutionary placement of genetic sequences. *Systematic Biol.* 68, 365–369. doi: 10.1093/sysbio/syy054

Bayer, B., Saito, M. A., McIlvin, M. R., Lücker, S., Moran, D. M., Lankiewicz, T. S., et al. (2021). Metabolic versatility of the nitrite-oxidizing bacterium *Nitrospira marina* and its proteomic response to oxygen-limited conditions. *ISME J.* 15, 1025–1039. doi: 10.1038/s41396-020-00828-3

Berger, S. A., and Stamatakis, A. (2011). Aligning short reads to reference alignments and trees. *Bioinformatics* 27, 2068–2075. doi: 10.1093/bioinformatics/btr320

Berman, T., Béchemin, C., and Maestrini, S. (1999). Release of ammonium and urea from dissolved organic nitrogen in aquatic ecosystems. *Aquat. Microb. Ecol.* 16, 295–302. doi: 10.3354/ame016295

Berube, P. M., Biller, S. J., Hackl, T., Hogle, S. L., Satinsky, B. M., Becker, J. W., et al. (2018). Data descriptor: Single cell genomes of *Prochlorococcus, Synechococcus*, and sympatric microbes from diverse marine environments. *Sci. Data* 5, 180154–180154. doi: 10.1038/sdata.2018.154

Berube, P. M., Coe, A., Roggensack, S. E., and Chisholm, S. W. (2016). Temporal dynamics of *Prochlorococcus* cells with the potential for nitrate assimilation in the subtropical Atlantic and Pacific oceans. *Limnol. Oceanogr.* 61, 482–495. doi: 10.1002/lno.10226

Bianchi, D., Babbin, A. R., and Galbraith, E. D. (2014). Enhancement of anammox by the excretion of diel vertical migrators. *Proc. Natl. Acad. Sci.* 111, 15653–15658. doi: 10.1073/pnas.1410790111

Bolger, A. M., Lohse, M., and Usadel, B. (2014). Trimmomatic: a flexible trimmer for Illumina sequence data. *Bioinformatics* 30, 2114–2120.

Brown, S. A., Balmonte, J. P., Hoarfrost, A., Ghobrial, S., and Arnosti, C. (2022). Depth-related patterns in microbial community responses to complex organic matter in the western North Atlantic Ocean. *Biogeosciences* 19, 5617–5631. doi: 10.5194/bg-19-5617-2022

Callbeck, C. M., Lavik, G., Ferdelman, T. G., Fuchs, B., Gruber-Vodicka, H. R., Hach, P. F., et al. (2018). Oxygen minimum zone cryptic sulfur cycling sustained by offshore transport of key sulfur oxidizing bacteria. *Nat. Commun.* 9, 1729. doi: 10.1038/s41467-018-04041-x

Cepeda-Morales, J., Beier, J., Gaxiola-Castro, G., Lavin, M. F., and Godinez, V. M. (2009). Effect of the oxygen minimum zone on the second chlorophyll maximum in the Eastern Tropical Pacific off Mexico. *Cienc. Marinas* 35, 389–403. doi: 10.7773/cm.v35i4.1622

Cho, B., Park, M., Shim, J., and Azam, F. (1996). Significance of bacteria in urea dynamics in coastal surface waters. *Mar. Ecol. Prog. Ser.* 142, 19–26. doi: 10.3354/meps142019

Clifford, E. L., Hansell, D. A., Varela, M. M., Nieto-Cid, M., Herndl, G. J., and Sintes, E. (2017). Crustacean zooplankton release copious amounts of dissolved organic matter as taurine in the ocean. *Limnol. Oceanogr.* 62, 2745–2758. doi: 10.1002/lno.10603

Clifford, E. L., Varela, M. M., De Corte, D., Bode, A., Ortiz, V., Herndl, G. J., et al. (2019). Taurine is a major carbon and energy source for marine prokaryotes in the North atlantic ocean off the iberian peninsula. *Microbial. Ecol.* 78, 299–312. doi: 10.1007/s00248-019-01320-y

Connelly, T. L., Baer, S. E., Cooper, J. T., Bronk, D. A., and Wawrik, B. (2014). Urea uptake and carbon fixation by marine pelagic bacteria and archaea during the arctic summer and winter seasons. *Appl. Environ. Microbiol.* 80, 6013–6022. doi: 10.1128/AEM.01431-14

Czech, L., Barbera, P., and Stamatakis, A. (2020). Genesis and Gappa: processing, analyzing and visualizing phylogenetic (placement) data. *Bioinformatics* 36, 3263–3265. doi: 10.1093/bioinformatics/btaa070

Dalsgaard, T., Thamdrup, B., Farías, L., and Peter Revsbech, N. (2012). Anammox and denitrification in the oxygen minimum zone of the eastern South Pacific. *Limnol. Oceanogr.* 57, 1331–1346. doi: 10.4319/lo.2012.57.5.1331

Delmont, T. O., Pierella Karlusich, J. J., Veseli, I., Fuessel, J., Eren, A. M., Foster, R. A., et al. (2022). Heterotrophic bacterial diazotrophs are more abundant than their cyanobacterial counterparts in metagenomes covering most of the sunlit ocean. *ISME J.* 16, 927–936. doi: 10.1038/s41396-021-01135-1

Devol, A. H. (2003). Solution to a marine mystery. *Nature* 422, 575–575. doi: 10.1007/s00340-003-1120-z

DeVries, T., Deutsch, C., Rafter, P. A., and Primeau, F. (2013). Marine denitrification rates determined from a global 3-D inverse model. *Biogeosciences* 10, 2481–2496. doi: 10.5194/bg-10-2481-2013

Druon, J. N., Mannino, A., Signorini, S., McClain, C., Friedrichs, M., Wilkin, J., et al. (2010). Modeling the dynamics and export of dissolved organic matter in the Northeastern U.S. *continental shelf. Estuarine Coast. Shelf Sci.* 88, 488–507. doi: 10.1016/j.ecss.2010.05.010

Edgar, R. C. (2004). MUSCLE: multiple sequence alignment with high accuracy and high throughput. *Nucleic Acids Res.* 32, 1792–1797. doi: 10.1093/nar/gkh340

Fuchsman, C. A., Cherubini, L., and Hays, M. D. (2022). An Analysis of Protists in Pacific Oxygen Deficient Zones: Implications for *Prochlorococcus* and N_2 producing bacteria. *Environ. Microbiol.* 24, 1790–1804. doi: 10.1111/1462-2920.15893

Fuchsman, C. A., Devol, A. H., Casciotti, K. L., Buchwald, C., Chang, B. X., and Horak, R. E. A. (2018). An N isotopic mass balance of the Eastern Tropical North Pacific oxygen deficient zone. *Deep-Sea Res. Part II: Topical Stud. Oceanogr.* 156, 137–142. doi: 10.1016/j.dsr2.2017.12.013

Fuchsman, C. A., Devol, A. H., Saunders, J. K., McKay, C., and Rocap, G. (2017). Niche Partitioning of the N cycling microbial community of an offshore Oxygen Deficient Zone. *Front. Microbiol.* 8, 2384. doi: 10.3389/fmicb.2017.02384

Fuchsman, C. A., Garcia Prieto, D., Hays, M. D., and Cram, J. A. (2023). Associations between picocyanobacterial ecotypes and cyanophage host genes across ocean basins and depth. *PeerJ* 11, e14924. doi: 10.7717/peerj.14924

Fuchsman, C. A., and Hays, M. D. (2023). Increased cyanophage infection at the bottom of the euphotic zone, especially in the fall. *Environ. Microbiol.* 25, 3349–3363. doi: 10.1111/1462-2920.16525

Fuchsman, C. A., Palevsky, H. I., Widner, B., Duffy, M., Carlson, M. C. G., Neibauer, J. A., et al. (2019). Cyanobacteria and cyanophage contributions to carbon and nitrogen cycling in an oligotrophic oxygen-deficient zone. *ISME J.* 13, 2714–2726. doi: 10.1038/s41396-019-0452-6

Fuchsman, C. A., Staley, J. T., Oakley, B. B., Kirkpatrick, J. B., and Murray, J. W. (2012). Free-living and aggregate-associated planctomycetes in the black sea. *FEMS Microbiol. Ecol.* 80, 402–416. doi: 10.1111/fem.2012.80.issue-2

Ganesh, S., Bertagnolli, A. D., Bristow, L. A., Padilla, C. C., Blackwood, N., Aldunate, M., et al. (2018). Single cell genomic and transcriptomic evidence for the use of alternative nitrogen substrates by anammox bacteria. *ISME J.* 12, 2706–2722. doi: 10.1038/s41396-018-0223-9

Garcia, H. E., Weathers, K. W., Paver, C. R., Smolyar, I., Boyer, T. P., Locarnini, R. A., et al. (2019). *World Ocean Atlas 2018 Volume 3: Dissolved Oxygen, Apparent Oxygen Utilization, and Dissolved Oxygen Saturation* Vol. 83 (USA: NOAA National Centers for Environmental Information), 1–38.

Giovannoni, S. J., Halsey, K. H., Saw, J., Muslin, O., Suffridge, C. P., Sun, J., et al. (2019). A parasitic arsenic cycle that shuttles energy from phytoplankton to heterotrophic bacterioplankton. *mBio* 10, e00246-19. doi: 10.1128/mBio.00246-19

Giovannoni, S. J., Tripp, H. J., Givan, S., Podar, M., Vergin, K. L., Baptista, D., et al. (2005). Genome streamlining in a cosmopolitan oceanic bacterium. *Sci. (New York N.Y.)* 309, 1242–1245. doi: 10.1126/science.1114057

Glibert, P. M., Wilkerson, F. P., Dugdale, R. C., Raven, J. A., Dupont, C. L., Leavitt, P. R., et al. (2016). Pluses and minuses of ammonium and nitrate uptake and assimilation by phytoplankton and implications for productivity and community composition, with emphasis on nitrogen-enriched conditions. *Limnol. Oceanogr.* 61, 165–197. doi: 10.1002/lno.10203

Hausinger, R. P. (2004). Metabolic versatility of prokaryotes for urea decomposition. *J. Bacteriol.* 186, 2520–2522. doi: 10.1128/JB.186.9.2520-2522.2004

Horak, R. E. A., Ruef, W., Ward, B. B., and Devol, A. H. (2016). Expansion of denitrification and anoxia in the eastern tropical North Pacific from 1972 to 2012. *Geophysical Res. Lett.* 43, 5252–5260. doi: 10.1002/2016GL068871

Howe, K. L., Seitz, K. W., Campbell, L. G., Baker, B. J., Thrash, J. C., Rabalais, N. N., et al. (2023). Metagenomics and metatranscriptomics reveal broadly distributed, active, novel methanotrophs in the Gulf of Mexico hypoxic zone and in the marine water column. *FEMS Microbiol. Ecol.* 99, fiac153. doi: 10.1093/femsec/fiac153

Ito, T., Minobe, S., Long, M. C., and Deutsch, C. (2017). Upper ocean O_2 trends: 1958–2015. *Geophysical Res. Lett.* 44, 4214–4223. doi: 10.1002/2017GL073613

Johnson, W. V., and Anderson, P. M. (1987). Bicarbonate is a recycling substrate for cyanase. *J. Biol. Chem.* 262, 9021–9025. doi: 10.1016/S0021-9258(18)48040-4

Johnson, Z. I., Zinser, E. R., Coe, A., Mcnulty, N. P., Malcolm, E. S., Chisholm, S. W., et al. (2006). Partitioning among *prochlorococcus* ecotypes along environmental gradients. *Science* 311, 1737–1740. doi: 10.1126/science.1118052

Kamennaya, N. A., and Post, A. F. (2011). Characterization of cyanate metabolism in marine *synechococcus* and prochlorococcus spp. *Appl. Environ. Microbiol.* 77, 291–301. doi: 10.1128/AEM.01272-10

Keeling, P. J., Burki, F., Wilcox, H. M., Allam, B., Allen, E. E., Amaral-Zettler, L. A., et al. (2014). The marine microbial eukaryote transcriptome sequencing project (MMETSP): illuminating the functional diversity of eukaryotic life in the oceans through transcriptome sequencing. *PloS Biol.* 12, e1001889–e1001889. doi: 10.1371/journal.pbio.1001889

Kitzinger, K., Padilla, C. C., Marchant, H. K., Hach, P. F., Herbold, C. W., Kidane, A. T., et al. (2019). Cyanate and urea are substrates for nitrification by Thaumarchaeota in the marine environment. *Nat. Microbiol.* 4, 234–243. doi: 10.1038/s41564-018-0316-2

Kozlov, A. M., Darriba, D., Flouri, T., Morel, B., and Stramatakis, A. (2019). RAxML-ng: a fast, scalable and user-friendly tool for maximum likelihood phylogenetic inference. *Bioinformatics* 35, 4453–4455. doi: 10.1093/bioinformatics/btz305

Lam, P., Lavik, G., Jensen, M. M., Van De Vossenberg, J., Schmid, M., Woebken, D., et al. (2009). Revising the nitrogen cycle in the Peruvian oxygen minimum zone. *Proc. Natl. Acad. Sci. U.S.A.* 106, 4752–4757. doi: 10.1073/pnas.0812444106

Lanclos, V. C., Rasmussen, A. N., Kojima, C. Y., Cheng, C., Henson, M. W., Faircloth, B. C., et al. (2023). Ecophysiology and genomics of the brackish water adapted SAR11 subclade IIIa. *ISME J.* 17, 620–629. doi: 10.1038/s41396-023-01376-2

Lehmann, M. F., Carstens, D., Deek, A., McCarthy, M., Schubert, C. J., and Zopfi, J. (2020). Amino acid and amino sugar compositional changes during *in vitro* degradation of algal organic matter indicate rapid bacterial re-synthesis. *Geochimica Cosmochimica Acta* 283, 67–84. doi: 10.1016/j.gca.2020.05.025

Li, D., Liu, C. M., Luo, R., Sadakane, K., and Lam, T. W. (2015). MEGAHIT: An ultra-fast single-node solution for large and complex metagenomics assembly via succinct de Bruijn graph. *Bioinformatics* 31, 1674–1676.

Lücker, S., Nowka, B., Rattei, T., Spieck, E., and Daims, H. (2013). The genome of *Nitrospina gracilis* illuminates the metabolism and evolution of the major marine nitrite oxidizer. *Front. Microbiol.* 4. doi: 10.3389/fmicb.2013.00027

Luo, E., Eppley, J. M., Romano, A. E., Mende, D. R., and DeLong, E. F. (2020). Double-stranded DNA virioplankton dynamics and reproductive strategies in the oligotrophic open ocean water column. *ISME J.* 14, 1304–1315. doi: 10.1038/s41396-020-0604-8

Luo, H., Tolar, B. B., Swan, B. K., Zhang, C. L., Stepanauskas, R., Ann Moran, M., et al. (2014). Single-cell genomics shedding light on marine Thaumarchaeota diversification. *ISME J.* 8, 732–736. doi: 10.1038/ismej.2013.202

Maas, A. E., Frazar, S. L., Outram, D. M., Seibel, B. A., and Wishner, K. F. (2014). Fine-scale vertical distribution of macroplankton and micronekton in the Eastern Tropical North Pacific in association with an oxygen minimum zone. *J. Plankton Res.* 36, 1557–1575. doi: 10.1093/plankt/fbu077

Maas, A. E., Liu, S., Bolaños, L. M., Widner, B., Parsons, R., Kujawinski, E. B., et al. (2020). Migratory zooplankton excreta and its influence on prokaryotic communities. *Front. Mar. Sci.* 7. doi: 10.3389/fmars.2020.573268

Mao, X., Chen, J., van Oosterhout, C., Zhang, H., Liu, G., Zhuang, Y., et al. (2022). Diversity, prevalence, and expression of cyanase genes (*cynS*) in planktonic marine microorganisms. *ISME J.* 16, 602–605. doi: 10.1038/s41396-021-01081-y

Marshall, K. T., and Morris, R. M. (2013). Isolation of an aerobic sulfur oxidizer from the SUP05/Arctic96BD-19 clade. *ISME J.* 7, 452–455. doi: 10.1038/ismej.2012.78

Marshall, K. T., and Morris, R. M. (2015). Mixotroph from the SUP05 clade of marine gammaproteobacteria. *Genome Announcements* 3, e01155–e01115. doi: 10.1128/genomeA.01155-15

Martens-Habbena, W., Berube, P. M., Urakawa, H., de la Torre, J. R., and Stahl, D. A. (2009). Ammonia oxidation kinetics determine niche separation of nitrifying Archaea and Bacteria. *Nature* 461, 976–979. doi: 10.1038/nature08465

Martiny, A. C., Kathuria, S., and Berube, P. M. (2009). Widespread metabolic potential for nitrite and nitrate assimilation among *Prochlorococcus* ecotypes. *Proc. Natl. Acad. Sci. United States America* 106, 10787–10792. doi: 10.1073/pnas.0902532106

Mattes, T. E., Burke, S., Rocap, G., and Morris, R. M. (2022). Two metatranscriptomic profiles through low-dissolved-oxygen waters (DO, 0 to 33 μM) in the eastern tropical North pacific ocean. *Microbiol. Resource Announcements* 11, e01201–e01221. doi: 10.1128/mra.01201-21

Miller, C. A., and Glibert, P. M. (1998). Nitrogen excretion by the calanoid copepod *Acartia tonsa* : results of mesocosm experiments. *J. Plankton Res.* 20, 1767–1780. doi: 10.1093/plankt/20.9.1767

Morris, R. M., Rappe, M. S., Connon, S. A., Vergin, K. L., Siebold, W. A., Carlson, C. A., et al. (2002). SAR11 clade dominates ocean surface bacterioplankton communities. *Nature* 420, 806–810. doi: 10.1038/nature01281.1

Nixon, S. L., Daly, R. A., Borton, M. A., Solden, L. M., Welch, S. A., Cole, D. R., et al. (2019). Genome-resolved metagenomics extends the environmental distribution of the verrucomicrobia phylum to the deep terrestrial subsurface. *mSphere* 4, e00613-19. doi: 10.1128/mSphere.00613-19

Pachiadaki, M. G., Sintes, E., Bergauer, K., Brown, J. M., Record, N. R., Swan, B. K., et al. (2017). Major role of nitrite-oxidizing bacteria in dark ocean carbon fixation. *Science* 1051, 1046–1051. doi: 10.1126/science.aan8260

Painter, S., Sanders, R., Waldron, H., Lucas, M., and Torres-Valdes, S. (2008). Urea distribution and uptake in the Atlantic Ocean between 50°N and 50°S. *Mar. Ecol. Prog. Ser.* 368, 53–63. doi: 10.3354/meps07586

Palatinszky, M., Herbold, C., Jehmlich, N., Pogoda, M., Han, P., von Bergen, M., et al. (2015). Cyanate as an energy source for nitrifiers. *Nature* 524, 105–108. doi: 10.1038/nature14856

Parada, A. E., Wollard, J., Pett-ridge, J., Mayali, X., Weber, P. K., Santoro, A. E., et al. (2022). Constraining the composition and quantity of organic matter used by abundant marine Thaumarchaeota. *Environ. Microbiol.*, 25, 689–704. doi: 10.1111/1462-2920.16299

Penn, J. L., Weber, T., Chang, B. X., and Deutsch, C. (2019). Microbial ecosystem dynamics drive fluctuating nitrogen loss in marine anoxic zones. *Proc. Natl. Acad. Sci.* 116, 7220–7225. doi: 10.1073/pnas.1818014116

Peters, B., Horak, R., Devol, A. H., Fuchsman, C. A., Forbes, M., Mordy, C. W., et al. (2018). Estimating fixed nitrogen loss and associated isotope effects using concentration and isotope measurements of NO_3–, NO_2–, and N_2 from the Eastern Tropical South Pacific oxygen deficient zone. *Deep-Sea Res. Part II: Topical Stud. Oceanogr.* 156, 121–136. doi: 10.1016/j.dsr2.2018.02.011

Pitt, K. A., Welsh, D. T., and Condon, R. H. (2009). Influence of jellyfish blooms on carbon, nitrogen and phosphorus cycling and plankton production. *Hydrobiologia* 616, 133–149. doi: 10.1007/s10750-008-9584-9

Priddle, J., Whitehouse, M. J., Atkinson, A., Brierley, A. S., and Murphy, E. J. (1997). Diurnal changes in near-surface ammonium concentration—interplay between zooplankton and phytoplankton. *J. Plankton Res.* 19, 1305–1330. doi: 10.1093/plankt/19.9.1305

Qin, W., Amin, S. A., Martens-Habbena, W., Walker, C. B., Urakawa, H., Devol, A. H., et al. (2014). Marine ammonia-oxidizing archaeal isolates display obligate mixotrophy and wide ecotypic variation. *Proc. Natl. Acad. Sci. United States America* 111, 12504–12509. doi: 10.1073/pnas.1324115111

Qin, W., Wei, S. P., Zheng, Y., Choi, E., Li, X., Johnston, J., et al. (2014). Ammonia-oxidizing bacteria and archaea exhibit differential nitrogen source preferencesx. *Nat. Microbiol.* 9, 524–536.

Rappe, M. S., Connon, S. A., Vergin, K. L., and Giovannoni, S. J. (2002). Cultivation of the ubiquitous SAR11 marine bacterioplankton clade. *Nature* 418, 630–633. doi: 10.1038/nature00917

Revsbech, N. P., Larsen, L. H., Gundersen, J., Dalsgaard, T., Ulloa, O., and Thamdrup, B. (2009). Determination of ultra-low oxygen concentrations in oxygen minimum zones by the STOX sensor. *Limnol. Oceanogr.: Methods* 7, 371–381. doi: 10.4319/lom.2009.7.371

Rii, Y. M., Karl, D. M., and Church, M. J. (2016). Temporal and vertical variability in picophytoplankton primary productivity in the North Pacific Subtropical Gyre. *Mar. Ecol. Prog. Ser.* 562, 1–18. doi: 10.3354/meps11954

Rocap, G., Larimer, F. W., Lamerdin, J., Malfatti, S., Chain, P., Ahlgren, N. A., et al. (2003). Genome divergence in two *Prochlorococcus* ecotypes reflects oceanic niche differentiation. *Nature* 424, 1042–1047. doi: 10.1038/nature01947

Santoro, A. E., Dupont, C. L., Richter, R. A., Craig, M. T., Carini, P., McIlvin, M. R., et al. (2015). Genomic and proteomic characterization of "*Candidatus* Nitrosopelagicus brevis": An ammonia-oxidizing archaeon from the open ocean. *Proc. Natl. Acad. Sci.* 112, 1173–1178. doi: 10.1073/pnas.1416223112

Santoro, A. E., Saito, M. A., Goepfert, T. J., Lamborg, C. H., Dupont, C. L., and DiTullio, G. R. (2017). Thaumarchaeal ecotype distributions across the equatorial Pacific Ocean and their potential roles in nitrification and sinking flux attenuation. *Limnol. Oceanogr.* 62, 1984–2003. doi: 10.1002/lno.10547

Schmitz, R. A., Peeters, S. H., Versantvoort, W., Picone, N., Pol, A., Jetten, M. S. M., et al. (2021). Verrucomicrobial methanotrophs: ecophysiology of metabolically versatile acidophiles. *FEMS Microbiol. Rev.* 45, fuab007. doi: 10.1093/femsre/fuab007

Seemann, T. (2014). Prokka: rapid prokaryotic genome annotation. *Bioinformatics* 30, 2068–2069.

Shah, V., Chang, B. X., and Morris, R. M. (2017). Cultivation of a chemoautotroph from the SUP05 clade of marine bacteria that produces nitrite and consumes ammonium. *ISME J.* 11, 263–271. doi: 10.1038/ismej.2016.87

Shah, V., and Morris, R. M. (2015). Genome sequence of "*Candidatus* thioglobus autotrophica" Strain EF1, a chemoautotroph from the SUP05 clade of marine. *Genome Announcements* 3, e01156–e01115. doi: 10.1128/genomeA.01156-15.Copyright

Shah, V., Zhao, X., Lundeen, R. A., Ingalls, A. E., Nicastro, D., and Morris, R. M. (2019). Morphological plasticity in a sulfur-oxidizing marine bacterium from the SUP05 clade enhances dark carbon fixation. *mBio* 10, e00216–e00219. doi: 10.1128/mBio.00216-19

Shiozaki, T., Hashihama, F., Endo, H., Ijichi, M., Takeda, N., Makabe, A., et al. (2021). Assimilation and oxidation of urea-derived nitrogen in the summer Arctic Ocean. *Limnol. Oceanogr.* 66, 4159–4170. doi: 10.1002/lno.11950

Sieburth, J. N., Johnson, P. W., Eberhardt, M. A., Sieracki, M. E., Lidstrom, M., and Laux, D. (1987). The first methane-oxidizing bacterium from the upper mixing layer of the deep ocean: Methylomonas pelagica sp. nov. *Curr. Microbiol.* 14, 285–293. doi: 10.1007/BF01568138

Spieck, E., Keuter, S., Wenzel, T., Bock, E., and Ludwig, W. (2014). Characterization of a new marine nitrite oxidizing bacterium, Nitrospina watsonii sp. nov., a member of the newly proposed phylum "Nitrospinae. *Systematic Appl. Microbiol.* 37, 170–176. doi: 10.1016/j.syapm.2013.12.005

Stramma, L., Johnson, G. C., Sprintall, J., and Mohrholz, V. (2008). Expanding oxygen-minimum zones in the tropical oceans. *Science* 320, 655–658. doi: 10.1126/science.1153847

Sun, J., Steindler, L., Thrash, J. C., Halsey, K. H., Smith, D. P., Carter, A. E., et al. (2011). One carbon metabolism in SAR11 pelagic marine bacteria. *PloS One* 6, e23973–e23973. doi: 10.1371/journal.pone.0023973

Sun, X., and Ward, B. B. (2021). Novel metagenome-assembled genomes involved in the nitrogen cycle from a Pacific oxygen minimum zone. *ISME Commun.* 1, 26. doi: 10.1038/s43705-021-00030-2

Takeda, N., Hashihama, F., and Kanda, J. (2020). Automated colorimetric determination of nanomolar urea in seawater by gas-segmented continuous flow analysis using a liquid waveguide capillary cell. *Talanta* 208, 120371. doi: 10.1016/j.talanta.2019.120371

Thibodeau, P. S., Steinberg, D. K., and Maas, A. E. (2020). Effects of temperature and food concentration on pteropod metabolism along the Western Antarctic Peninsula. *J. Exp. Mar. Biol. Ecol.* 530–531, 151412–151412. doi: 10.1016/j.jembe.2020.151412

Tiano, L., Garcia-Robledo, E., Dalsgaard, T., Devol, A. H., Ward, B. B., Ulloa, O., et al. (2014). Oxygen distribution and aerobic respiration in the north and south eastern tropical Pacific oxygen minimum zones. *Deep Sea Res. Part I: Oceanographic Res. Papers* 94, 173–183. doi: 10.1016/j.dsr.2014.10.001

Tolar, B. B., Wallsgrove, N. J., Popp, B. N., and Hollibaugh, J. T. (2017). Oxidation of urea-derived nitrogen by thaumarchaeota-dominated marine nitrifying communities. *Environ. Microbiol.* 19, 4838–4850. doi: 10.1111/1462-2920.13457

Tripp, H. J. (2013). The unique metabolism of SAR11 aquatic bacteria. *J. Microbiol.* 51, 147–153. doi: 10.1007/s12275-013-2671-2

Tsementzi, D., Wu, J., Deutsch, S., Nath, S., Rodriguez-R, L. M., Burns, A. S., et al. (2016). SAR11 bacteria linked to ocean anoxia and nitrogen loss. *Nature* 536, 179–183. doi: 10.1038/nature19068

Ulloa, O., Henríquez-Castillo, C., Ramírez-Flandes, S., Plominsky, A. M., Murillo, A. A., Morgan-Lang, C., et al. (2021). The cyanobacterium *Prochlorococcus* has divergent light-harvesting antennae and may have evolved in a low-oxygen ocean. *Proc. Natl. Acad. Sci. United States America* 118, e2025638118–e2025638118. doi: 10.1073/pnas.2025638118

van de Vossenberg, J., Woebken, D., Maalcke, W. J., Wessels, H. J. C. T., Dutilh, B. E., Kartal, B., et al. (2013). The metagenome of the marine anammox bacterium '*Candidatus* Scalindua profunda' illustrates the versatility of this globally important nitrogen cycle bacterium. *Environ. Microbiol.* 15, 1275–1289. doi: 10.1111/j.1462-2920.2012.02774.x

Walsh, D. A., Zaikova, E., Howes, C. G., Song, Y. C., Wright, J. J., Tringe, S. G., et al. (2009). Metagenome of a versatile chemolithoautotroph from expanding oceanic dead zones. *Science* 326, 578–582. doi: 10.1126/science.1175309

Webb, K. L., and Johannes, R. E. (1967). Studies of the release of dissolved free amino acids by marine zooplankton. *Limnol. Oceanogr.* 12, 376–382. doi: 10.4319/lo.1967.12.3.0376

Widner, B., Fuchsman, C. A., Chang, B. X., Rocap, G., and Mulholland, M. R. (2018a). Utilization of urea and cyanate in waters overlying and within the eastern tropical north Pacific oxygen deficient zone. *FEMS Microbiol. Ecol.* 94, fiy138. doi: 10.1093/femsec/fiy138

Widner, B., Mordy, C. W., and Mulholland, M. R. (2018b). Cyanate distribution and uptake above and within the Eastern Tropical South Pacific oxygen deficient zone. *Limnol. Oceanogr.* 63, 177–192. doi: 10.1002/lno.10730

Widner, B., and Mulholland, M. R. (2017). Cyanate distribution and uptake in North Atlantic coastal waters. *Limnol. Oceanogr.* 62, 2538–2549. doi: 10.1002/lno.10588

Widner, B., Mulholland, M. R., and Mopper, K. (2013). Chromatographic determination of nanomolar cyanate concentrations in estuarine and sea waters by precolumn fluorescence derivatization. *Anal. Chem.* 85, 6661–6666. doi: 10.1021/ac400351c

Widner, B., Mulholland, M. R., and Mopper, K. (2016). Distribution, sources, and sinks of cyanate in the coastal North atlantic ocean. *Environ. Sci. Technol. Lett.* 3, 297–302. doi: 10.1021/acs.estlett.6b00165

Wishner, K. F., Seibel, B., and Outram, D. (2020). Ocean deoxygenation and copepods: Coping with oxygen minimum zone variability. *Biogeosciences* 17, 2315–2339. doi: 10.5194/bg-17-2315-2020

Wong, J. C. Y., Raven, J. A., Aldunate, M., Silva, S., Gaitán-Espitia, J. D., Vargas, C. A., et al. (2023). Do phytoplankton require oxygen to survive? A hypothesis and model synthesis from oxygen minimum zones. *Limnol. Oceanogr.* 68, 1417–1437. doi: 10.1002/lno.12367

Yamashita, Y., and Tanoue, E. (2003). Distribution and alteration of amino acids in bulk DOM along a transect from bay to oceanic waters. *Mar. Chem.* 82, 145–160. doi: 10.1016/S0304-4203(03)00049-5

Zhang, I. H., Fortin, S. G., Ward, B. B., and Babbin, A. R. (2023). Partitioning of the denitrification pathway and other nitrite metabolisms within global oxygen deficient zones. *ISME Commun.* 3, 76. doi: 10.1038/s43705-023-00284-y

Zinser, E. R., Johnson, Z. I., Coe, A., Karaca, E., Veneziano, D., and Chisholm, S. W. (2007). Influence of light and temperature on *Prochlorococcus* ecotype distributions in the Atlantic Ocean. *Limnol. Oceanogr.* 52, 2205–2220. doi: 10.4319/lo.2007.52.5.2205

Zubkov, M. V., Tarran, G. A., Mary, I., and Fuchs, B. M. (2008). Differential microbial uptake of dissolved amino acids and amino sugars in surface waters of the Atlantic Ocean. *J. Plankton Res.* 30, 211–220. doi: 10.1093/plankt/fbm091

Frontiers in Marine Science

Explores ocean-based solutions for emerging global challenges

The third most-cited marine and freshwater biology journal, advancing our understanding of marine systems and addressing global challenges including overfishing, pollution, and climate change.

Discover the latest Research Topics

See more →

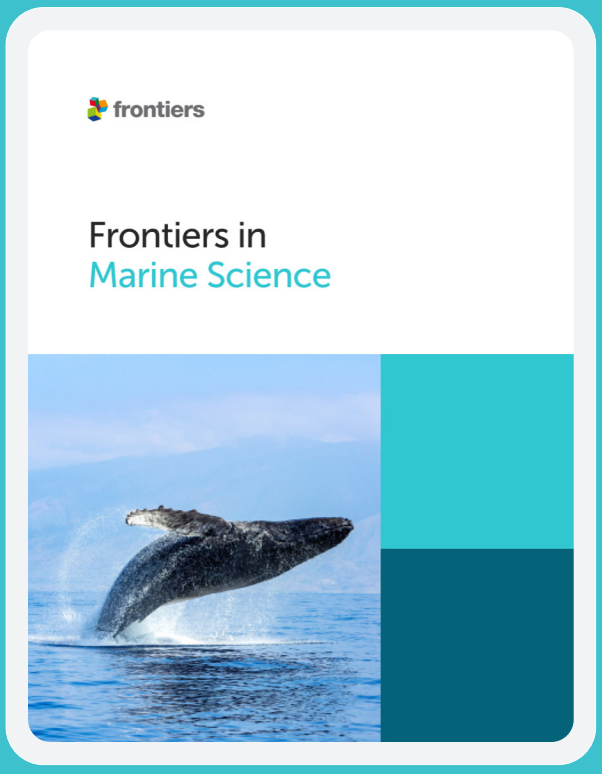

Frontiers

Avenue du Tribunal-Fédéral 34
1005 Lausanne, Switzerland
frontiersin.org

Contact us

+41 (0)21 510 17 00
frontiersin.org/about/contact